

New treatment strategies for canine intervertebral disc degeneration

Luc Smolders

New treatment strategies for canine intervertebral disc degeneration
Luc Smolders
PhD thesis, Utrecht University, the Netherlands

ISBN: 978-90-393-5902-0

Cover: Anjolieke Dertien en Luc Smolders
Layout and printing: Proefschrift-AIO, DPP Houten

Copyright © 2013 L.A. Smolders, all rights reserved. No part of this thesis may be reproduced or transmitted in any form or by any means, without the prior written permission of the author.

Correspondence and reprint requests: L.A.Smolders@gmail.com

New treatment strategies for canine intervertebral disc degeneration

Nieuwe behandelingsstrategieën voor tussenwervelschijfdegeneratie
bij de hond
(met een samenvatting in het Nederlands)

Proefschrift

ter verkrijging van de graad van doctor aan de Universiteit Utrecht op gezag
van de rector magnificus, prof. dr. G.J. van der Zwaan, ingevolge het besluit
van het college voor promoties in het openbaar te verdedigen
op donderdag 31 januari 2013 des middags te 12.45 uur

door

Lucas Adam Smolders

geboren op 28 januari 1986 te Geldrop

Promotor: Prof. dr. H.A.W. Hazewinkel

Co-promotoren: Dr. B.P. Meij
Dr. N. Bergknut
Dr. M.A. Tryfonidou

Publication of this thesis was financially supported by generous gifts of A. Menarini Diagnostics Benelux N.V., Anicur, AUV Groothandel, Boehringer Ingelheim, J.E. Jurriaanse Stichting, MSD Animal Health B.V., Novartis Consumer Health B.V, Pfizer Animal Health B.V., Royal Canin Nederland B.V., Scil animal care company, Stichting Anna Fonds, and Synthes B.V.

Contents

Chapter 1	Aims and scope of the thesis	11
Chapter 2.1	General introduction – Intervertebral disc degeneration and disease in the dog	21
Chapter 2.2	Soft tissue artifact in canine kinematic gait analysis	91
Chapter 3.1	Pedicle screw-rod fixation of the canine lumbosacral junction	109
Chapter 3.2	The performance of a hydrogel nucleus pulposus prosthesis in an ex vivo canine model	137
Chapter 3.3	Biomechanical evaluation of a novel nucleus pulposus prosthesis in canine cadaveric spines	153
Chapter 4	Biomechanical assessment of the effects of decompressive surgery in non-chondrodystrophic and chondrodystrophic canine multisegmented lumbar spines	169
Chapter 5.1	Optimal reference genes for quantitative polymerase chain reaction analysis of the nucleus pulposus	185
Chapter 5.2	Canonical Wnt signaling in the notochordal cell is upregulated in early intervertebral disc degeneration	203
Chapter 5.3	Gene expression profiling of early intervertebral disc degeneration	227
Chapter 5.4	Gene expression profiling of early intervertebral disc degeneration involves a down-regulation of canonical Wnt signaling and caveolin-1 expression: implications for development of regenerative strategies	273
Chapter 6	General discussion	335
Chapter 7	Summary	361
Chapter 8	Samenvatting	371
Addendum	Dankwoord	381
	Curriculum Vitae	389
	List of peer-reviewed publications	391

The studies described in this thesis were conducted at and financially supported by The Department of Clinical Sciences of Companion Animals, Faculty of Veterinary Medicine, Utrecht University, Utrecht, the Netherlands, the Faculty of Human Movement Sciences, VU University, Amsterdam, the Netherlands, and the Department of Clinical Sciences, Faculty of Veterinary Medicine and Animal Science, Swedish University of Agricultural Sciences, Uppsala, Sweden.

List of abbreviations

<i>actb</i>	<i>beta-actin</i>
ADAMTs	a disintegrin and metalloproteinase with thrombospondin motifs
AF	annulus fibrosus
AIBN	azobis-(isobutyronitrile)
AIC	akaike information criterion
AMA	allylmethacrylate
AR	axial rotation
<i>b2m</i>	<i>beta-2-microglobulin</i>
BMP	bone morphogenetic protein
<i>cav1</i>	<i>caveolin-1</i>
C	cervical
CD	chondrodystrophic
CI	confidence interval
<i>ck-8</i>	<i>cytokeratin-8</i>
CLC	chondrocyte-like cell
CS	chondroitin sulfate
CSM	cervical spondylomyelopathy
CT	computed tomography
DAB	diaminobenzidine
<i>dkk3</i>	<i>dickkopf homolog 3</i>
ECM	extracellular matrix
EDTA	ethylenediaminetetraacetic acid
EGF	epidermal growth factor
EP	endplate
DLL	dorsal longitudinal ligament
DLSS	degenerative lumbosacral stenosis
FDR	false discovery rate
FE	flexion/extension
FGF	fibroblast growth factor
<i>frzb</i>	<i>frizzled related protein</i>
FSU	functional spine unit
GAG	glycosaminoglycan
<i>gapdh</i>	<i>glyceraldehyde-3-phosphate dehydrogenase</i>
GEO	Gene Expression Omnibus
GSD	German Shepherd Dog
GSK3	glycogen synthase kinase 3
<i>gusb</i>	<i>glucuronidase, beta</i>
<i>fzd1</i>	<i>frizzled 1</i>
HA	hyaluronic acid
HEMA	hydroxethyl methacrylate
<i>hmb</i>	<i>hydroxymethylbilane synthase</i>

<i>hnrp</i>	<i>human nucleosome-assembly-protein-1</i>
<i>hprt</i>	<i>hypoxanthine-guanine phosphoribosyltransferase</i>
H&E	hematoxylin and eosin
IEMA	(iodobenzoyl)-oxo-ethyl methacrylate
IL	interleukin
<i>ilk</i>	<i>integrin-linked kinase</i>
IVD	intervertebral disc
KO	knock-out
KS	keratan sulfate
L	lumbar
LB	lateral bending
LBP	low back pain
LED	light-emitting diode
<i>lrp5</i>	<i>low density lipoprotein receptor-related protein 5</i>
LSJ	lumbosacral junction
LTVA	lumbosacral transitional vertebral anomaly
MAANOVA	microarray analysis of variance
MAPK	mitogen-activated protein kinase
MMP	matrix metalloproteinase
MRI	magnetic resonance imaging
MD	marker distance/motion direction
MSC	mesenchymal stromal cell
NC	notochordal cell
NCC	notochordal cell clusters
NCD	non-chondrodystrophic
NO	nitric oxide
NP	nucleus pulposus
NPP	nucleus pulposus prosthesis
NSAIDs	non-steroidal anti-inflammatory drugs
NVP	N-vinyl-2-pyrrolidinone
NZ	neutral zone
NZS	neutral zone stiffness
OA	osteoarthritis
OP	osteogenic protein
PBS	phosphate-buffered saline
PDN	prosthetic disc nucleus
PLAU	plasminogen activator-urokinase
PMMA	polymethyl methacrylate
PSRF	pedicle screw-rod fixation
P/S	penicillin/streptomycin
qPCR	quantitative polymerase chain reaction
RA	rheumatoid arthritis
<i>rpl13</i>	<i>ribosomal protein 113</i>
<i>rpl18</i>	<i>ribosomal protein 118</i>

<i>rps5</i>	<i>ribosomal protein s5</i>
<i>rps19</i>	<i>ribosomal protein s19</i>
<i>rspo3</i>	<i>r-spondin-3</i>
ROM	range of motion
S	sacral
SCB	subchondral bone
<i>sdha</i>	<i>succinate dehydrogenase complex subunit A</i>
SNC	single notochordal cells
<i>sprp</i>	<i>serine protease-like protein</i>
STA	soft tissue artifact
T	thoracic
tbp	tata box binding protein
TE	echo time
TGF	transforming growth factor
TIMP	tissue inhibitor of metalloproteinase
TNF	tumor necrosis factor
TR	repetition time
TWS	tussenwervelschijf
TZ	transition zone
<i>wif1</i>	<i>wnt inhibitory factor 1</i>
W/S	walking/standing ratio
Wmax/S	walk-maximum ratio
Wmin/S	walk-minimum ratio
<i>ywhaz</i>	<i>tryptophan 5-monooxygenase activation protein zeta</i>

AIMS AND SCOPE OF THE THESIS

Background

The dog is classified in the subphylum Vertebrata, also known as the vertebrates, which are defined by their spinal column¹. From head to tail, the spine is composed of individual vertebrae, separated by intervertebral discs (IVDs). As an essential component of the spine, the IVD simultaneously provides stability and mobility to the spinal column, characteristics that are vital for movement and spinal function²⁻⁴. The IVD is composed of three distinct, specialized structures: the central nucleus pulposus (NP), the outer annulus fibrosus (AF), and the cartilaginous endplates, which form the boundary between the NP/AF and the vertebral bodies⁵.

Degeneration of the IVD is a common problem in dogs and involves cellular changes within the IVD and concurrent degeneration of the IVD matrix⁶⁻¹⁵. IVD degeneration often occurs on a subclinical level, and can eventually result in bulging or herniation of the IVD with subsequent compression of the neural structures overlying the IVD and clinical manifestation of neurological deficits¹⁶⁻¹⁸. Common IVD diseases, i.e. diseases due to IVD degeneration, are cervical and thoracolumbar IVD herniation, cervical spondylomyelopathy, and degenerative lumbosacral stenosis¹⁶⁻¹⁸.

Treatment of IVD disease is conservative or surgical. Conservative therapy consists of anti-inflammatory drugs, exercise restriction, and physiotherapy¹⁶⁻¹⁸.

Surgical therapy is generally indicated in patients with moderate-to-severe neurological deficits and/or spinal pain refractory to conservative treatment. Surgical therapy alleviates mainly clinical end-stage IVD disease by means of decompression, such as ventral decompression (cervical disc disease), hemilaminectomy (thoracolumbar disc disease), or dorsal laminectomy (lumbosacral disc disease), usually combined with incision of the AF (annulotomy) or partial removal of the AF (annulectomy), and removal of the NP (nucleotomy or nucleotomy)¹⁶⁻¹⁸. However, therapies involving removal of the NP are far from optimal: disc height (distance endplate-IVD-endplate) and thereby the functionality of the IVD is not restored, and removal of the IVD may lead to loss of spinal stability and recurrence of clinical signs¹⁹⁻²². Therefore, novel treatment options, aimed at restoring spinal stability, are needed to improve the treatment of canine patients with IVD disease. One such salvage treatment is spinal fixation with pedicle screw-rod fixation enabling fusion of the affected spinal segment^{23,24}. However, a better scenario would be to interfere earlier in the degenerative process and to restore functionality (disc height and biomechanical stability) to the degenerated IVD. This could be achieved by replacing the diseased NP with an NP prosthesis (NPP)^{25,26}.

Another treatment strategy consists of regeneration of the IVD before clinical end-stage IVD degeneration has developed. With the aim of developing regenerative strategies for IVD degeneration, the dog is an intriguing species. The canine species can be divided into two types of breed, i.e. chondrodystrophic

breeds and non-chondrodystrophic breeds. Chondrodystrophic breeds, such as the Dachshund and the Beagle, are characterized by a disturbed endochondral ossification in the growth plates, resulting aberrant bone growth with disproportionately short extremities^{6,27}. These short limbs have been a trait favored in breeding programs of selected breeds^{28,29}; however, this characteristic is to a high extent linked to IVD degeneration^{6,29}. As a result, all chondrodystrophic breeds suffer from accelerated degeneration of the IVD, with histopathological signs of degeneration being found as early as 1 year of age and clinical manifestations occurring in the cervical and thoracolumbar spine as early as 3 years^{29,30}. In contrast, non-chondrodystrophic breeds exhibit normal bone growth and usually retain healthy IVDs throughout life. IVD degeneration and disease (cervical spondylomyelopathy, degenerative lumbosacral stenosis), if present, typically occur at an older age (> 6 years)^{29,30}. The fundamental difference between the IVD of these two breed groups is the perseverance of a certain cell type, the notochordal cell, within the NP of the IVD: in chondrodystrophic breeds, the notochordal cell is replaced by relatively small, chondrocyte-like cells before the age of 1 year, with a concurrent onset of IVD degeneration. In contrast, in non-chondrodystrophic breeds, the notochordal cell is retained throughout life and degeneration of the IVD is relatively uncommon^{6,15,29,31}. Therefore, the loss of notochordal cells is thought to play a fundamental role in the process of IVD degeneration in many species, including dogs and humans^{29,32,33}, and thus these cells are an interesting focus of research with a view to regenerating the degenerated IVD.

Aims and Hypotheses

The first aim of this thesis was to develop and test novel surgical techniques involving fixation of the degenerated spinal segment using pedicle screw-rod fixation. For this aim, the following hypothesis was tested:

Pedicle screw-rod fixation of the canine lumbosacral junction enables spinal fusion of L7-S1.

The second aim of this thesis was to investigate functional restoration of the degenerated IVD by insertion of an NPP, testing the following hypotheses:

Removal of the nucleus pulposus from the intervertebral disc (nuclectomy) results in a loss of disc height and loss of spinal stability.

Spinal stability can be restored by inserting a nucleus pulposus prosthesis (NPP) into the excavated intervertebral disc.

The third aim was to investigate the processes and effects of early IVD degeneration from a biomechanical and biomolecular perspective in order to

identify essential components of the degenerative process, thereby providing novel targets for treatment strategies aimed at regenerating the degenerated IVD at an early stage. For this aim, the following hypothesis was tested:

Significant loss of the notochordal cells from the nucleus pulposus results in significant alterations in biomolecular signaling pathways involved in intervertebral disc matrix health and degeneration.

The studies performed are described below.

Chapter 2.1 reviewed the current literature on canine IVD degeneration and IVD disease, in order to establish what is known about the degenerative process in dogs and currently used diagnostic methods and treatments. The study described in **Chapter 2.2** investigated the applicability of kinematic gait analysis in dogs, paying special attention to the soft tissue artifact. Kinematic gait analysis could be used as a tool for diagnosing and evaluating canine patients affected by IVD disease.

The aim of the study described in **Chapter 3.1** was to evaluate the applicability of surgical pedicle screw-rod fixation of the canine lumbosacral junction as a new surgical treatment of canine IVD disease. The surgical procedure and applicability of pedicle screw fixation were first assessed *ex vivo* in canine lumbosacral spines, followed by a pilot project *in vivo* involving three canine patients diagnosed with degenerative lumbosacral stenosis. The study described in **Chapter 3.2** tested implantation of an NPP, a new surgical treatment for canine IVD disease, using canine lumbosacral (L7-S1) segments *ex vivo*. A clinically-adapted mode for implanting the NPP in the nuclear cavity of the L7-S1 IVD was evaluated. The swelling and fit of the NPP *in situ* and the restoration of disc height were monitored by radiography, CT, and MRI. The study reported in **Chapter 3.3** investigated the NPP *in situ* under biomechanical loading to assess the potential of the NPP to restore the biomechanical function of the L2-L3 and L7-S1 IVD *ex vivo* in canine cadaveric spinal segments.

The aim of the study reported in **Chapter 4** was to investigate the biomechanical properties of the non-chondrodystrophic (healthy, notochordal cell-rich IVDs) and chondrodystrophic (degenerated, IVDs devoid of notochordal cells) spine, before and after spinal surgery, to assess the effects of IVD degeneration and breed type on spinal biomechanics.

The studies reported in **Chapter 5** involved experiments regarding the biomolecular processes that occur during early IVD degeneration. The aim of **Chapter 5.1** was to determine which reference genes are optimal for performing quantitative gene expression analysis in canine IVD tissue. The study described

1

in Chapter 5.2 investigated the role of Wnt/ β -catenin signaling in the notochordal cell *in vivo* and *in vitro*, and in the process of early IVD degeneration. With the aim to identify additional pathways and genes involved in the process of early IVD degeneration, **Chapter 5.3** investigated gene expression profiles of early IVD degeneration in both non-chondrodystrophic and chondrodystrophic dog breeds. The study reported in **Chapter 5.4** explored the differences between the non-chondrodystrophic and chondrodystrophic dogs with regard to Wnt/ β -catenin signaling in the notochordal cell and in early IVD degeneration. Furthermore, functional studies were performed highlighting the significance of caveolin-1 in the preservation of a healthy IVD.

The results of these studies are summarized and discussed in **Chapter 6**, and the English summary and Dutch summary are presented in **Chapter 7** and **Chapter 8**, respectively.

References

1. Paulson DR: The Phylum Chordata: Classification, External Anatomy, and Adaptive Radiation, in Wake MH (ed): Hyman's Comparative Vertebrate Anatomy (ed 3), Chicago, The University of Chicago Press, 1992, pp 7-56.
2. Bray JP, Burbidge HM: The canine intervertebral disk: part one: structure and function. *J Am Anim Hosp Assoc* 34:55-63, 1998.
3. White AA, 3rd, Panjabi MM: Clinical biomechanics of the spine. Philadelphia Toronto, J.B. Lippincott Company, 1978.
4. Zimmerman MC, Vuono-Hawkins M, Parsons JR, et al: The mechanical properties of the canine lumbar disc and motion segment. *Spine* 17:213-220, 1992.
5. Hukins DWL: Disc Structure and Function, in Ghosh P (ed): The Biology of the Intervertebral Disc (ed 1), Vol 1. Boca Raton, Florida, CRC Press, Inc., 1988, pp 1-38.
6. Braund KG, Ghosh P, Taylor TK, et al: Morphological studies of the canine intervertebral disc. The assignment of the beagle to the achondroplastic classification. *Res Vet Sci* 19:167-172, 1975.
7. Braund KG, Ghosh P, Taylor TK, et al: The qualitative assessment of glycosaminoglycans in the canine intervertebral disc using a critical electrolyte concentration staining technique. *Res Vet Sci* 21:314-317, 1976.
8. Braund KG, Taylor TK, Ghosh P, et al: Spinal mobility in the dog. A study in chondrodystrophoid and non-chondrodystrophoid animals. *Res Vet Sci* 22:78-82, 1977.
9. Cole TC, Burkhardt D, Frost L, et al: The proteoglycans of the canine intervertebral disc. *Biochim Biophys Acta* 839:127-138, 1985.
10. Cole TC, Ghosh P, Taylor TK: Variations of the proteoglycans of the canine intervertebral disc with ageing. *Biochim Biophys Acta* 880:209-219, 1986.
11. Ghosh P, Taylor TK, Braund KG: The variation of the glycosaminoglycans of the canine intervertebral disc with ageing. I. Chondrodystrophoid breed. *Gerontology* 23:87-98, 1977.
12. Ghosh P, Taylor TK, Braund KG: Variation of the glycosaminoglycans of the intervertebral disc with ageing. II. Non-chondrodystrophoid breed. *Gerontology* 23:99-109, 1977.
13. Ghosh P, Taylor TK, Braund KG, et al: The collagenous and non-collagenous protein of the canine intervertebral disc and their variation with age, spinal level and breed. *Gerontology* 22:124-134, 1976.
14. Ghosh P, Taylor TK, Braund KG, et al: A comparative chemical and histochemical study of the chondrodystrophoid and nonchondrodystrophoid canine intervertebral disc. *Vet Pathol* 13:414-427, 1976.
15. Ghosh P, Taylor TK, Yarroll JM: Genetic factors in the maturation of the canine intervertebral disc. *Res Vet Sci* 19:304-311, 1975.
16. Brisson BA: Intervertebral disc disease in dogs. *Vet Clin North Am Small Anim Pract* 40:829-858, 2010.
17. da Costa RC: Cervical spondylomyelopathy (wobbler syndrome) in dogs. *Vet Clin N Am Small Anim Pract* 40:881-913, 2010.
18. Meij BP, Bergknut N: Degenerative lumbosacral stenosis in dogs. *Vet Clin N Am Small Anim Pract* 40:983-1009, 2010.

19. Hill TP, Lubbe AM, Guthrie AJ: Lumbar spine stability following hemilaminectomy, pediclectomy, and fenestration. *Vet Comp Orthop Traumatol* 13:165-171, 2000.
20. Macy NB, Les CM, Stover SM, et al: Effect of disk fenestration on sagittal kinematics of the canine C5-C6 intervertebral space. *Vet Surg* 28:171-179, 1999.
21. Schulz KS, Waldron DR, Grant JW, et al: Biomechanics of the thoracolumbar vertebral column of dogs during lateral bending. *Am J Vet Res* 57:1228-1232, 1996.
22. Smith MEH, Bebczuk TN, Shmon CL, et al: An in vitro biomechanical study of the effects of surgical modification upon the canine lumbosacral spine. *Vet Comp Orthop Traumatol* 17:17-24, 2004.
23. Boos N, Webb JK: Pedicle screw fixation in spinal disorders: a European view. *Eur Spine J* 6:2-18, 1997.
24. Yahiro MA: Comprehensive literature review. Pedicle screw fixation devices. *Spine* 19:2274S-2278S, 1994.
25. Boelen EJ, van Hooy-Corstjens CS, Bulstra SK, et al: Intrinsically radiopaque hydrogels for nucleus pulposus replacement. *Biomaterials* 26:6674-6683, 2005.
26. Di Martino A, Vaccaro AR, Lee JY, et al: Nucleus pulposus replacement: basic science and indications for clinical use. *Spine* 30:S16-22, 2005.
27. Riser WH, Haskins ME, Jezyk PF, et al: Pseudoachondroplastic dysplasia in miniature poodles: clinical, radiologic, and pathologic features. *J Am Vet Med Assoc* 176:335-341, 1980.
28. Bray JP, Burbidge HM: The canine intervertebral disk. Part Two: Degenerative changes--nonchondrodystrophoid versus chondrodystrophoid disks. *J Am Anim Hosp Assoc* 34:135-144, 1998.
29. Hansen HJ: A pathologic-anatomical study on disc degeneration in dog, with special reference to the so-called enchondrosis intervertebralis. *Acta Orthop Scand Suppl* 11:1-117, 1952.
30. Hoerlein BF: Intervertebral disc protrusions in the dog. I. Incidence and pathological lesions. *Am J Vet Res* 14:260-269, 1953.
31. Cappello R, Bird JL, Pfeiffer D, et al: Notochordal cell produce and assemble extracellular matrix in a distinct manner, which may be responsible for the maintenance of healthy nucleus pulposus. *Spine (Phila Pa 1976)* 31:873-882, 2006.
32. Bergknut N, Rutges JP, Kranenburg HJ, et al: The dog as an animal model for intervertebral disc degeneration? *Spine (Phila Pa 1976)* 37:351-358, 2012.
33. Trout JJ, Buckwalter JA, Moore KC, et al: Ultrastructure of the human intervertebral disc. I. Changes in notochordal cells with age. *Tissue Cell* 14:359-369, 1982.

General introduction

Intervertebral disc degeneration and disease in the dog

Lucas A. Smolders ^a, Niklas Bergknut ^a, Guy C. M. Grinwis^c,
Anne-Sofie Lagerstedt^b, Herman A. W. Hazewinkel ^a,
Marianna A. Tryfonidou ^a, Björn P. Meij ^a

The Veterinary Journal 2012

doi: 10.1016/j.tvjl.2012.10.024 and 10.1016/j.tvjl.2012.10.01

Epub ahead of print

^a Department of Clinical Sciences of Companion Animals, Faculty of Veterinary Medicine, Utrecht University, Yalelaan 108, 3508 TD, Utrecht, The Netherlands

^b Department of Clinical Sciences, Division of Small Animals, Faculty of Veterinary Medicine and Animal Sciences, Swedish University of Agricultural Sciences, Ulls väg 12, Box 7040, 750 07 Uppsala, Sweden

^c Department of Pathobiology, Pathology Division, Faculty of Veterinary Medicine, Utrecht University, Utrecht, The Netherlands, Yalelaan 108, 3508 TD, Utrecht, The Netherlands

Introduction

Vertebrates are characterized by the evolution of the primitive axial skeleton (notochord) into a skull and spine ¹. The spine provides support, allows movement in all directions, and protects the spinal cord. Locomotion, and mobility are basic, but indispensable needs for all vertebrates. Differences in mobility between species are reflected by differences in the composition of the spine. In dogs, the spine consists of 7 cervical (C), 13 thoracic (T), 7 lumbar (L), 3 (fused) sacral (S), and a variable number of coccygeal vertebrae ^{2,3}. The vertebral bodies of C2-S1 and all coccygeal vertebrae are interconnected by an intervertebral disc (IVD) ^{2,4}. The IVD makes movement between the various vertebrae possible, provides stability to the spine, and enables forces to be transmitted between individual vertebrae ⁵. To fulfill this specialized function, the IVD is composed of four essentially different parts: a central nucleus pulposus (NP), an outer annulus fibrosus (AF), the transition zone (TZ) between the AF and NP, and cartilaginous endplates (EPs) between the IVD and the subchondral bone (Fig. 1).

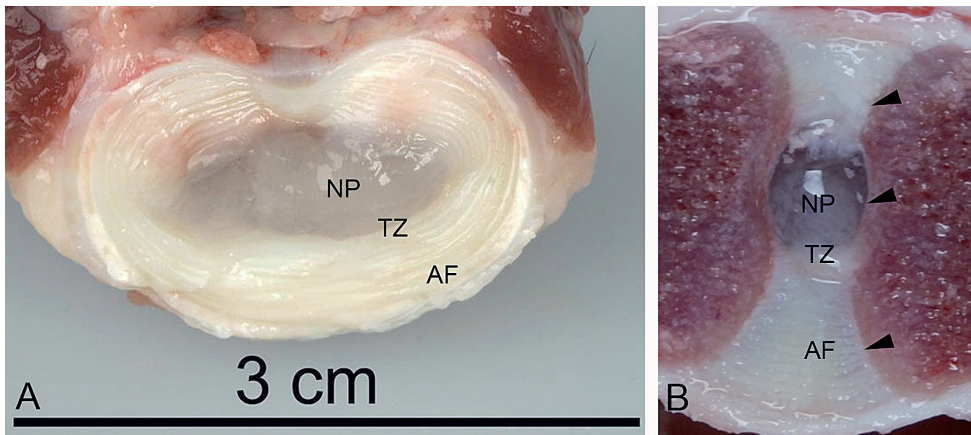


Figure 1. Transverse (A) and sagittal (B) section through the L5-L6 intervertebral disc of a mature, non-chondrodystrophic dog, showing the nucleus pulposus (NP), transition zone (TZ), annulus fibrosus (AF), and endplate (arrowheads).

The IVD has a key role in the posture and movement of the spine, and its malfunction gives rise to dysfunction and disease. The most important cause of neurological ailments in dogs is IVD-related disease ^{6,7}, which typically arises as a result of loss of functionality and quality of the IVD, a process also known as IVD degeneration ^{8,9}.

Degeneration of the IVD is a common phenomenon in dogs and can lead to IVD degenerative disease ⁸⁻¹⁰. IVD degeneration is known to predispose dogs to Hansen type I cervical and thoracolumbar disc herniation ³ and Hansen type

II disc herniation diseases, such as degenerative lumbosacral stenosis ¹¹ and cervical spondylomyelopathy ¹². However, IVD degeneration is also a common incidental finding in dogs without clinical signs of disease ^{3,12,13}.

2.1

The first case report of IVD degenerative disease in a dog was published in 1881 and involved a Dachshund with sudden onset of hind limb paralysis ¹⁴. The mass that compressed the spinal cord was described as a “chondroma located only to the epidural space”. Shortly thereafter, in 1896, a more comprehensive study was published on enchondrosis intervertebralis ¹⁵, a reactive inflammation in the epidural space, but it would take another 40 years before that disease was correctly described in the veterinary literature as the herniation of NP material from the IVD into the spinal canal, causing compression of the spinal cord ¹⁶. Pioneering studies of IVD degeneration in dogs were performed during the 1950s by the Swedish veterinarians Hansen and Olsson, in particular the study that led to the thesis by Hans-Jörgen Hansen in 1952 (Fig. 2) ^{3,17-20}. Since their studies, numerous publications have described the clinical aspects of IVD degenerative diseases, but few have revisited the fundamental aspects of IVD degeneration ²¹⁻³¹.

The aim of this chapter is to review the current literature on canine IVD degeneration and IVD degenerative diseases, with a view to improving our knowledge of these processes in dogs. Such knowledge is essential to our understanding of IVD degeneration and may help improve the treatment, and even prevention, of these degenerative diseases.

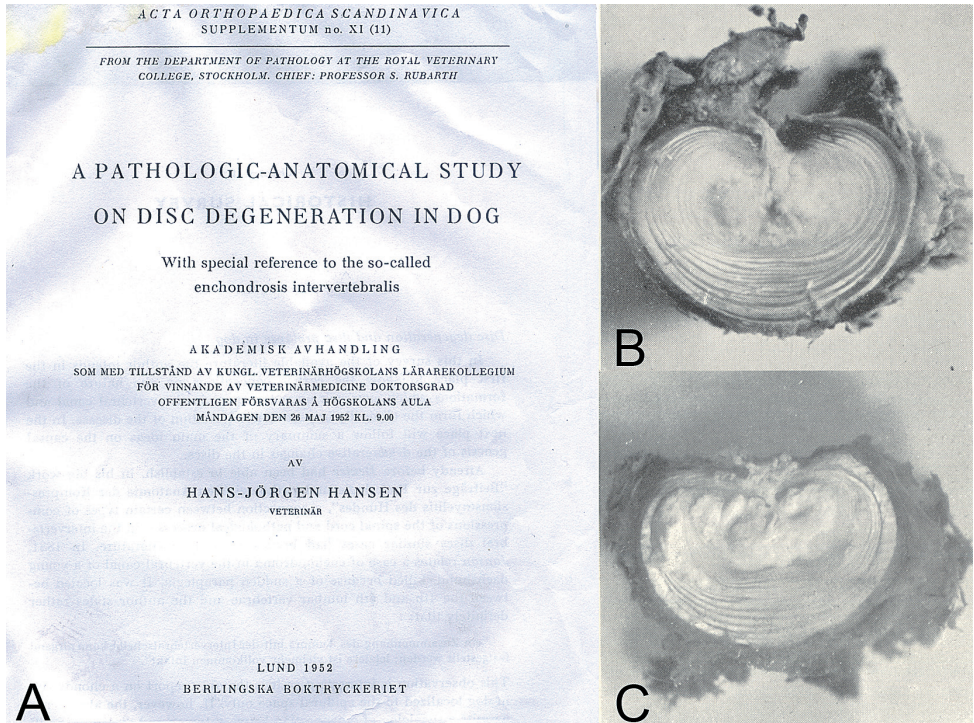


Figure 2. A) Title page of the thesis written by Hans-Jörgen Hansen in 1952, providing the first clear description of intervertebral disc degeneration and herniation in dogs, and the distinction between chondrodystrophic and non-chondrodystrophic breeds with regard to this process (discussed in part 2 of this review). B) Reproduction from Hansen's thesis (1952). The original figure legend reads as follows: "Dachshund, 6 years old. Disc 21 (L2-L3). Protrusion of type I. The picture shows the large dimensions of the protrusion and demonstrates clearly its origin from nucleus. The a.f. rupture is situated close to the right side of the lig. longituniale int. Nucleus is the site of a calcified necrosis and has lost its normal shape". C) Reproduction from Hansen's thesis (1952). The original figure legend reads as follows: "Dachshund, 4 years old. Disc 22 (L3-L4) with a calcified centre and a dorsomedian rupture of a.f. The protrusion is of type I with loose consistency and rough, uneven surface. An interlamellar dissection of calcified material is seen to the left of nucleus, emanating from a ventral rupture of the inner layer of a.f. This rupture, however, is not seen in this picture".

Embryology of the canine spine and IVD

Three somatic germ layers are formed early in mammalian embryogenesis: an outer ectodermal layer, a middle mesodermal layer, and an inner endodermal layer^{32,33}. A longitudinal column of mesoderm, the notochord, establishes the cranial/caudal and posterior/anterior axes of the developing embryo (Fig. 3)^{32,34,35}. Ectoderm directly posterior to the notochord gives rise to the neural

2.1 plate, which is composed of so-called neuroectoderm. The neural tube and neural crest cells (positioned dorsolateral to the neural tube) are formed from the neuroectoderm and give rise to the central nervous system and peripheral nervous system, respectively ^{32,35}.

During the development of the neural tube, mesoderm adjacent to the developing neural tube forms a thickened column of cells, the paraxial mesoderm. The paraxial mesoderm ultimately develops into discrete blocks, the somites, which form the axial skeleton, the associated musculature, and the overlying dermis. Each somite is divided into: 1) dermatome, which gives rise to dermis, 2) myotome, which gives rise to epaxial musculature, and 3) sclerotome, which gives rise to vertebral structures ^{32,35}. Sclerotomal cells form a continuous tube of mesenchymal cells, the perichordal tube, which completely surrounds the notochord ³⁶. An alternating series of dense and less dense accumulations of cells form along the perichordal tube, a process called resegmentation ^{36,37}. While the bodies of the vertebrae develop from the less dense accumulations, the dense accumulations form the AF and TZ of the IVD, intervertebral ligaments, vertebral arches, and vertebral processes, of which the latter two eventually fuse with their corresponding vertebral body ^{36,37}. The formation of the vertebral bodies results in segmentation of the notochord, which persists as separate portions in each intervertebral space. These separate portions of notochord expand, forming the NP of the individual IVDs ^{34,36-39}.

THE HEALTHY CANINE IVD

Anatomy and physiology of the IVD

The healthy IVD is composed of four distinct components, namely, the NP, AF, EP and TZ. The NP is a mucoïd, translucent, bean-shaped structure, mainly composed of water, located slightly eccentrically in the IVD ^{5,31,40,41}. The NP is surrounded by the AF, a dense network of multiple, organized, concentric fibrous lamellae. The ventral part of the AF is 2 to 3 times thicker than the dorsal part ^{3,42}. Near the center of the IVD, the AF becomes more cartilaginous and less fibrous ³⁻⁵.

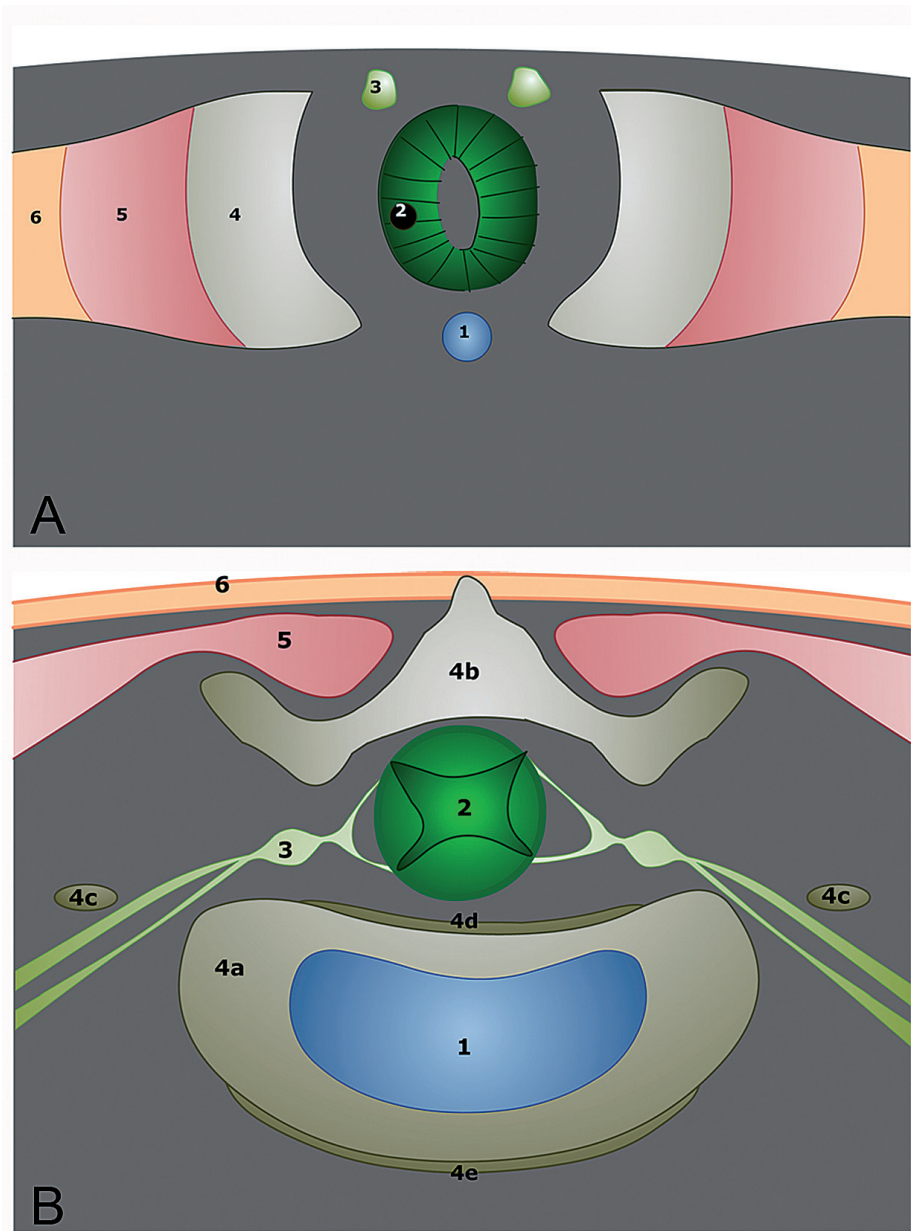


Figure 3 A and B. A) Schematic image of a transverse cross-section through the canine embryo, with the notochord (1), neural tube (2), neural crest cells (3), sclerotome (4), myotome (5), and dermatome (6). B) Schematic image of a transverse cross-section through the lumbar spine of a mature dog, with the nucleus pulposus (1), spinal cord (2), spinal nerves (3), annulus fibrosus (4a) and transition zone, dorsal vertebral lamina (4b), transverse spinal process (4c), dorsal longitudinal ligament (4d), ventral longitudinal ligament (4e), epaxial musculature (5), and skin (6). The colors of the structures of the mature animal correspond with the colors of their embryological origin.

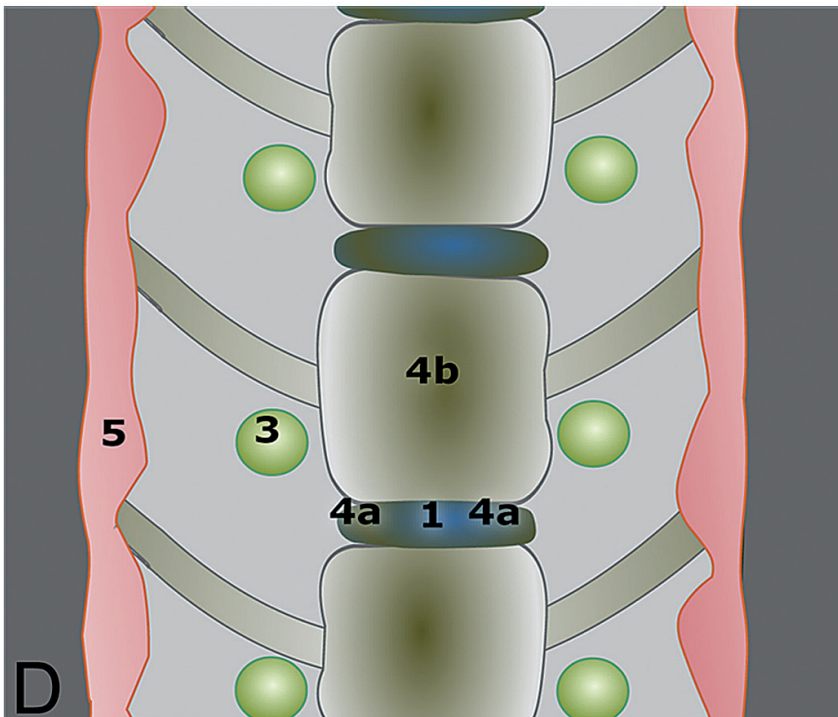
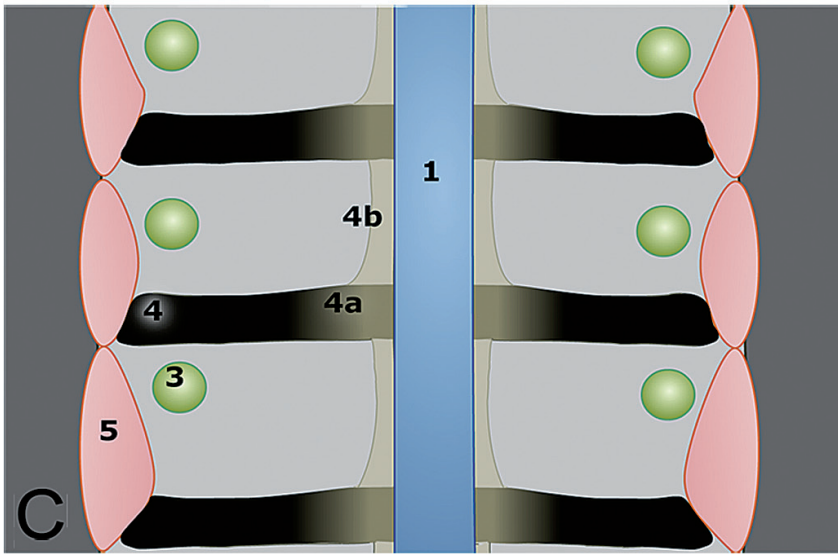


Figure 3C and D. C) Schematic image of a dorsal cross-section through the canine embryo, with the notochord (1), neural crest cells (3), sclerotome (4), and myotome (5). D) Schematic image of a dorsal cross-section through the lumbar spine of a mature dog, with the mature nucleus pulposus (1), spinal nerves (3), annulus fibrosus (4a) and vertebral body (4b), and epaxial musculature (5). The colors of the structures of the mature animal correspond with the colors of their embryological origin.

This transition from a fibrous to a more cartilaginous/mucoid structure, the TZ or the innermost AF, forms the interconnection between the NP and AF⁴³. The cranial and caudal borders of the IVD are formed by the cartilaginous EPs^{5,42,44}. The fibers of the inner AF are strongly connected with the EPs, whereas the fibers of the outer AF form connections with the bony vertebral body epiphyses (Sharpey's fibers)^{3,5,45}. The outer layers of the AF have a limited blood supply, but there is no direct blood supply to the inner layers of the AF or to the NP. However, terminal branches of the vertebral epiphyseal arteries give rise to a densely woven vascular network adjacent to the cartilaginous EPs^{46,47}. Innervation of the IVD tissue itself is sparse: nerve endings have only been found in the outer lamellae of the AF, and not in the inner AF, TZ, and NP^{3,48,49}. This is in contrast with the dorsal longitudinal ligament, which is densely innervated^{3,48}.

The EPs play an essential role in supplying the IVD with nutrients. Small molecules, such as oxygen and glucose, reach the cells of the NP, TZ, and AF through diffusion and osmosis from the capillary buds through the semipermeable EPs⁵⁰⁻⁵⁴. Additional nutrients and oxygen are supplied via the outer, vascularized parts of the AF^{50,52,53,55}. Larger molecules, such as albumin and enzymes, are transported by bulk fluid flow ('pumping mechanism') created by the physiological loading of the IVD and changes in posture^{50-52,54,55}.

Histology of the healthy IVD

In the healthy IVD, the main cell of the NP is the notochordal cell (Fig. 4C)^{3,23,43,56}. These large cells are characterized by cytoplasmic vesicles, the content and function of which are still debated^{3,57-60}, but there are indications that these vesicles are unique organelles, which have an osmoregulatory function, and that they are involved in the swelling and stretching of the embryonic notochord and in the regulation of osmotic stresses in the NP⁶¹. The notochordal cell has relatively few mitochondria and is therefore thought to rely mainly on anaerobic metabolism⁵⁷. Notochordal cells are found in clusters^{57,58,62} and produce an amorphous basophilic matrix rich in proteoglycans and collagen type II^{3,43,56,57,63,64}.

The TZ contains chondrocyte-like cells embedded in a loose, acidophilic fibrous matrix network^{3,21,23,44} and is distinct from the matrix surrounding the notochordal cells⁴³. Microscopically, the lamellae of the AF can be seen as separate fibrocartilaginous layers composed of eosinophilic fibrous bundles arranged in parallel (Fig. 4B, Fig. 5)^{3,23,43}. The cell population changes from fibrocyte-like cells in the outer layers of the AF to a mixed population of fibrocytes and chondrocyte-like cells in the inner layers^{3,23,43,44,65}. The canine EP (Fig. 4D) consists of cranio-caudally oriented layers of matrix and chondrocyte-like cells^{44,45}, on average 5 (3-8) cell layers thick and comprises 6% (3-11%) of the total width (intervertebral distance) of the canine IVD⁶⁶.

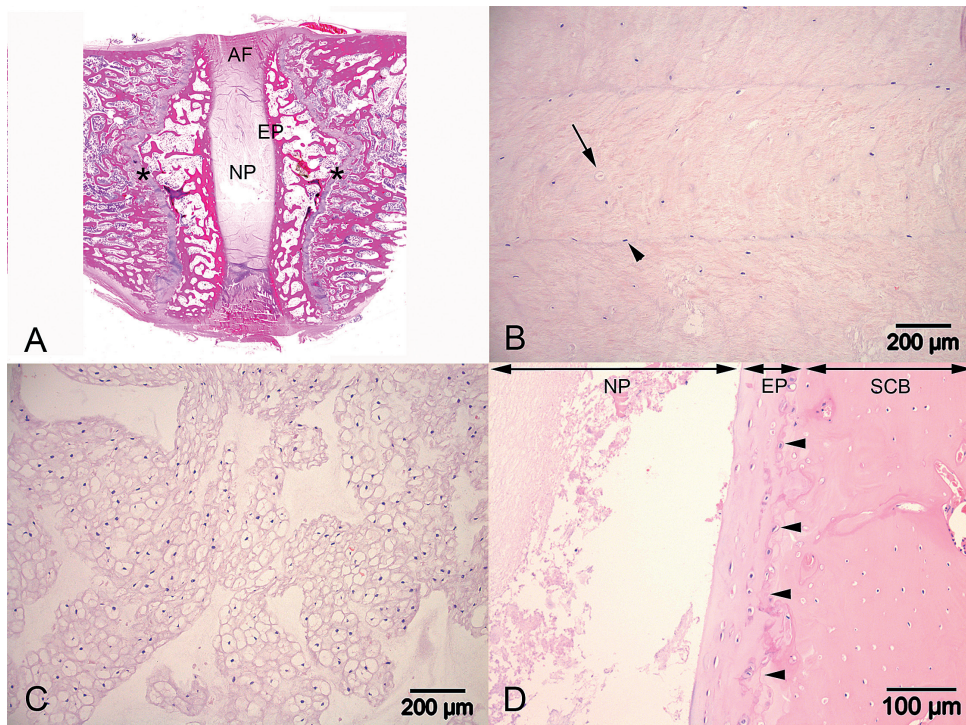


Figure 4. A) Mid-sagittal histological section (H&E) of a healthy, immature canine intervertebral disc, still with active growth plates in the vertebral bodies (). B) Annulus fibrosus (AF), showing the lamellar layers with fibrocyte-like cells (arrowhead) and chondrocyte-like cells (arrow). C) Nucleus pulposus (NP), showing clustered notochordal cells. D) Cartilaginous endplate (EP), showing chondrocyte-like cells in a hyaline-type matrix. The border between endplate (left) and subchondral bone (SCB) (right) is indicated with arrowheads.*

Biochemical structure of the healthy IVD

The healthy NP is composed of a complex network of negatively charged proteoglycans interwoven in a mesh of collagen fibers (mainly collagen type II)^{27,28}. The proteoglycan molecules consist of a protein backbone with negatively charged glycosaminoglycan (GAG) side chains. The most common side chains are chondroitin sulfate and keratan sulfate, which are covalently bound to the central core protein²⁵⁻²⁹. These negatively charged GAGs repel each other, giving the proteoglycans the appearance of a bottlebrush. The most common proteoglycan in the healthy IVD is aggrecan²⁹. The proteoglycans are in turn aggregated with hyaluronic acid, and these negatively charged large complexes create a strong osmotic gradient, attracting water into the NP. As a result, over 80% of the healthy NP is composed of water^{67,68}, creating a high intradiscal pressure^{25,26,28}.

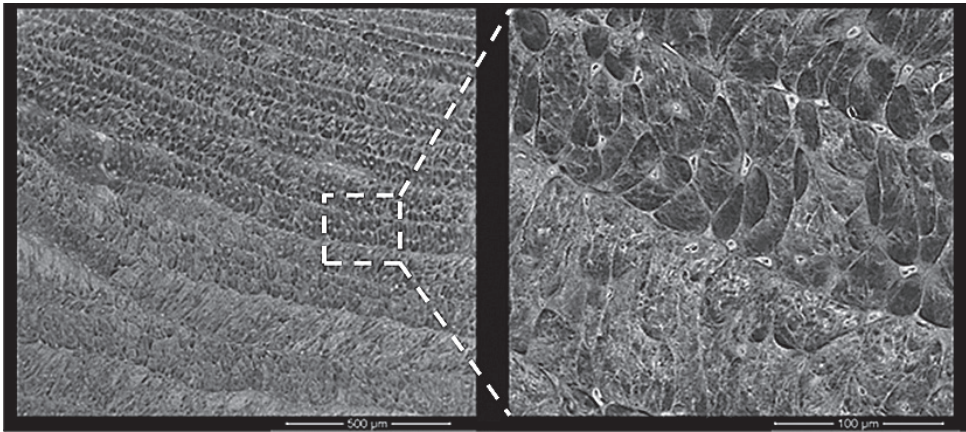


Figure 5. An electron microscopy image of the annulus fibrosus from a healthy canine, lumbar intervertebral disc. The overview to the left shows the well-organized lamellar layers. To the right, a higher resolution image showing the individual collagen bundles. Photos courtesy of Andrea Friedmann.

The lamellae of the AF are composed of collagen fibrils aggregated with elastic fibers and coated by proteoglycans^{28,29,69}. The outer part of the AF contains mostly collagen type I, whereas the inner part (TZ) contains predominantly collagen type II. The AF consists of 60% water^{67,68}.

The biochemical composition of the healthy EP is very similar to that of articular cartilage⁷⁰. The EP has a highly hydrated matrix (50-80%) composed of proteoglycans interconnected with hyaluronic acid and link proteins, and collagen (mainly type II)⁷⁰⁻⁷². The biochemistry of the EP is critical for maintaining the integrity of the IVD, since the proteoglycans in the matrix regulate the transport of solutes into and from the IVD⁷³.

The process of remodeling and breakdown of the extracellular matrix in the IVD is regulated by enzymes such as matrix metalloproteinases (MMPs) and A Disintegrin And Metalloproteinase with Thrombospondin Motifs (ADAMTs), produced by the cells of the IVD. While much is known about the activity of these regulatory enzymes in IVD remodeling in humans⁷⁴⁻⁷⁶, less is known about their activity in dogs⁷⁷⁻⁷⁹.

Biomechanical function of the healthy IVD

The biomechanical function of the IVD is to transmit compressive forces between vertebral bodies and to provide mobility as well as stability to the spinal segment^{80,81}. As in humans, the horizontally-positioned spine in dogs is loaded along its longitudinal axis, which is the result of contraction of the trunk muscles and the tension on structures such as the ligaments^{82,83}. Relatively

2.1

few biomechanical studies investigating the canine IVD have been performed. Therefore, human studies will be discussed as well. During motion, the canine IVD can be subjected to several motions/loading conditions, namely axial compression, shear, tension, bending, and torsion^{80,83}. The NP, AF, TZ, and EPs of the IVD work as a functional unit to resist these loads, with each component having a different specialized function^{5,74,84}. The NP is a highly hydrated structure that exerts swelling pressure inside the IVD. The EPs and AF function to contain the NP during loading. During axial compression, the majority of the compressive load is absorbed by the NP and the inner TZ. The surrounding AF protects the NP against shearing induced by the applied load and its own internal swelling pressure, thereby maintaining the disc circumference in spite of a decrease in disc height. It is thought that the alternating arrangement of the annular lamellae, combined with the oblique orientation of the lamellar fibres, enables the AF to cope with tensile forces generated during loading⁸¹. The IVD is rarely subjected to pure tensile loads, as the trunk muscles constantly act to keep the IVD compressed. The mechanism by which the IVD permits bending is essentially the same for flexion, lateral flexion, and extension. During flexion, the hydrostatic pressure in the NP increases, and the obliquely running fibres of the AF change their orientation. For example, in the transition from neutral position to dorsoflexion, the compressive stress within the NP increases on the dorsal side of the disc, the fibres of the ventral AF extend whereas those in the dorsal AF become compressed, resulting in bulging of the dorsal AF. The capacity of the IVD to resist bending is directly related to the volume of the NP: if the nuclear volume is increased (by saline injection), the resistance to bending increases. In comparison to bending motion, IVDs are stiffer in axial rotation/torsion⁸¹.

Vertebral motion has been shown to cause an outflow of fluid from the IVD, especially from the NP⁸⁵. Any outflow of fluid is reversed when the spine is unloaded. The diurnal cycle of load-induced fluid expression and regain seems to have important consequences for transport of large solutes and nutrients, because factors affecting diffusion, such as disc height (diffusion distance), are sensitive to hydration⁵⁴. This is further illustrated by the finding that spinal motion over a longer period of time it increases the aerobic metabolism of IVD cells, thereby decreasing the production of lactate⁸⁶.

THE DEGENERATING CANINE IVD

Degeneration of the IVD is a complex, multifactorial process that is characterized by changes in the composition of the cells and extracellular matrix of the NP, TZ, AF, and EPs. The pathophysiology of IVD degeneration in dogs has been largely unexplored. However, IVD degeneration in dogs is very similar to human IVD degeneration⁶⁶, and therefore the fundamental, pathophysiological

processes involved in human IVD degeneration will be briefly discussed.

IVD degeneration is described as an aberrant, cell-mediated response to progressive structural failure of the IVD and is associated with genetic predisposition, chronic physical-mechanical overload and trauma, inadequate metabolite and nutrient transport to and from the cells with the IVD matrix, cell senescence and death, altered levels of enzyme activity, changes in matrix macromolecules, and changes in water content (Fig. 6)^{87,88}. In the process of IVD degeneration, the GAG content of the IVD decreases, with a concurrent increase in collagen content. As a result, the matrix of the IVD becomes more rigid and loses its hydrostatic properties to function as a hydraulic cushion, rendering the IVD matrix suboptimal to fulfil its biomechanical function. Structural failure of the matrix results in a changed biomechanical environment of the IVD cells within the matrix. Also, because of the changes of the IVD matrix, diffusion of nutrients and the bulk fluid flow in and out of the disc become impaired, further deteriorating the health of the IVD cells and synthesis of healthy IVD matrix. The avascular and low cellular nature of the IVD, and the inferior biomechanical environment eventually impair the ability of IVD cells to adequately repair the matrix. The weakened IVD is vulnerable to damage by levels of stress that are considered physiological for the healthy IVD. Consequently, a vicious cycle of continued damage and inadequate repair and regeneration is triggered, resulting in degeneration rather than healing (Fig. 6). Structural failure of the IVD manifests itself in characteristic macroscopic changes of the IVD. As a result of dehydration of the IVD (especially the NP), the disc height (distance between two EPs) may decrease, and due to the decreased functionality of the NP, the AF, and EPs are loaded non-physiologically, eventually resulting in annular tears and EP fractures, respectively (further discussed below in “Biomechanical effects of IVD degeneration”). Structural failure of the IVD as a whole may also result in bulging or herniation of the IVD.

The changes seen in early IVD degeneration closely resemble those of physiological ageing of the disc. Although the definition proposed by Adams and Roughley (2006) may partially distinguish truly degenerative changes from age-related ones, it cannot be applied to the onset and early stages of IVD degeneration. Therefore, in this review, the term “IVD degeneration” is used to describe deterioration of the quality of the IVD matrix as a result of pathological and age-related changes and the associated structural changes of the disc, as described below.

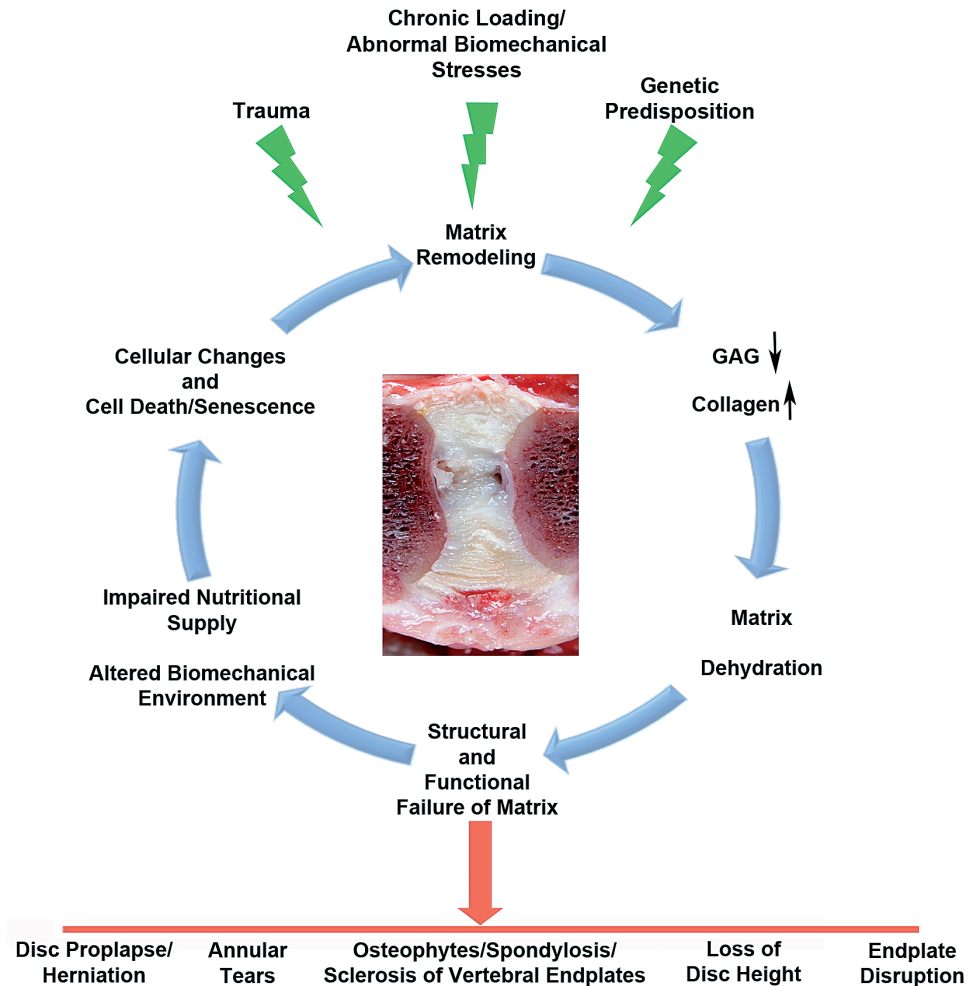


Figure 6. Generalized, schematic representation of the pathophysiology of intervertebral disc degeneration, illustrating the factors and the chain of events involved in the degenerative cascade as partly based on human literature. Intervertebral disc degeneration involves a vicious circle of repeated structural/functional failure and inadequate repair of the intervertebral disc matrix. Several factors (green symbols) may initiate or affect / accelerate the degenerative cycle, and structural/functional failure may result in various structural changes (red arrow) of the intervertebral disc and adjacent vertebral bodies.

Macroscopic and structural aspects of IVD degeneration

Degeneration of the IVD involves morphological changes of the NP, AF, EPs, and vertebral bodies (Fig. 7) ⁸⁹. Degeneration commonly starts in the mucoid NP, which changes color from shining translucent grey to dull, non-translucent white-grey or yellowish green-brown. These changes are accompanied by

cleft formation and ultimately collapse of the NP. As the NP degenerates, the lamellar structure of the AF buckles inwards and becomes disorganized. The TZ widens and becomes irregular, making it difficult to distinguish the AF from NP tissue^{3,21,23,56}. The cartilaginous EP thickens and becomes irregular and may fracture. New bone may be formed at the peripheral margins of the vertebral bodies, resulting in osteophytes and ventral spondylosis⁹⁰. Continued degeneration will lead to highly irregular and sometimes breached EPs and subchondral bone. As degeneration proceeds, the IVD space becomes smaller or may disappear completely in extreme cases, with bulging of the degenerated AF or even rupturing of the AF and herniation of the NP.

Degeneration of the NP, TZ, and AF may result in the compensatory thickening and crack formation of the EPs. Degeneration of the EPs involves loss of water and proteoglycans, and EP calcification and sclerosis, disturbing the physiological transport of solutes from and to the IVD^{73,91-94}. Thickening and irregularities of the subchondral bone, and vertebral bony proliferations, such as osteophytes and ventral spondylosis, start to develop mostly around the ventral aspect of the bony EPs, of the vertebral bodies^{90,95}.

Eventually, the degenerative process can result in bulging or herniation of the IVD, with partial or collapse of the IVD space³.

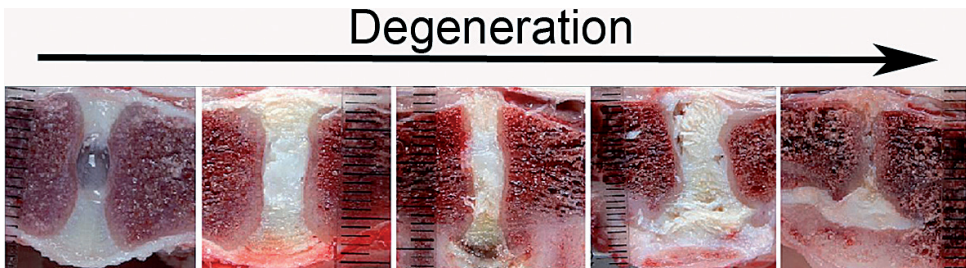


Figure 7. Sagittal sections through intervertebral discs showing stages of increasing degeneration, with macroscopic changes in the nucleus pulposus, annulus fibrosus, endplates, and vertebral bodies⁸⁹.

Histopathology of IVD degeneration

The early stage of degeneration is characterized by cellular changes within the NP. The large notochordal cell clusters are lost, resulting in smaller notochordal cell clusters or single notochordal cells (Fig. 8C). Concurrently, single or clusters of chondrocyte-like cells, surrounded by extracellular matrix, appear in the NP, dividing it into lobules, resulting in the gradual expansion of the TZ into the NP (Fig. 8D)^{3,65}. In essence, notochordal cells are replaced by chondrocyte-like cells and their associated extracellular matrix, which resembles hyaline cartilage and consists largely of disorganized collagen fibers. This process is referred to as *chondrification*^{3,21,23,56,58}. While chondrocyte-like cells may

2.1 migrate from the TZ into the NP, recent evidence suggest that it is more likely that they are of a differentiated notochordal cell lineage^{39,96-102}. Degeneration of the extracellular matrix of the NP can be observed as clefts and cracks, which are a result of the altered biochemical properties of the matrix (see below)¹⁰³.

Histologically, degeneration of the AF is characterized by the disorganization of the lamellar fibers and the ingrowth of chondrocyte-like cells from the TZ (Fig. 8B)^{3,65}. Cross-links between the annular fibers, which prevent lamellar movement in the AF, are more numerous in degenerated IVDs¹⁰⁴⁻¹⁰⁶. The inability of normal AF movement combined with NP degeneration and loss of IVD height may result in rupture or bulging of the AF, resulting in IVD herniation^{3,103}.

The EPs become thicker in the early stages of degeneration, and in later stages becomes increasingly irregular and may breach at several places (Fig. 8E). The breaches usually occur in the central parts of the EPs and can give rise to a “Schmorls node”, which is herniation of the NP into the vertebral body¹⁰⁷.

Biomechanical effects of IVD degeneration

The importance of the IVD as a stabilizing and mobilizing component is highlighted by biomechanical studies investigating the effects of IVD degeneration and surgical interventions on spinal biomechanics (presented below). Only a few such studies have been performed with canine material, but many studies have been performed human material. Although biomechanical loading of the spine is comparable in dogs and humans, the gravity load is generally considered to be greater in humans. However, the forces generated by contraction of the muscles of the trunk and the tension on structures such as the ligaments substantially add to axial loading on the quadruped spine, which is actually larger in quadrupeds than in bipeds^{82,83}. The canine spine is loaded along its long axis, as is the human spine^{82,108}, so results from human biomechanical spine studies can be extrapolated to dogs. Degeneration of the NP leads to a decrease in intradiscal pressure¹⁰⁹, resulting in increased stress and a compensatory increase in the functional size of the AF^{110,111}.

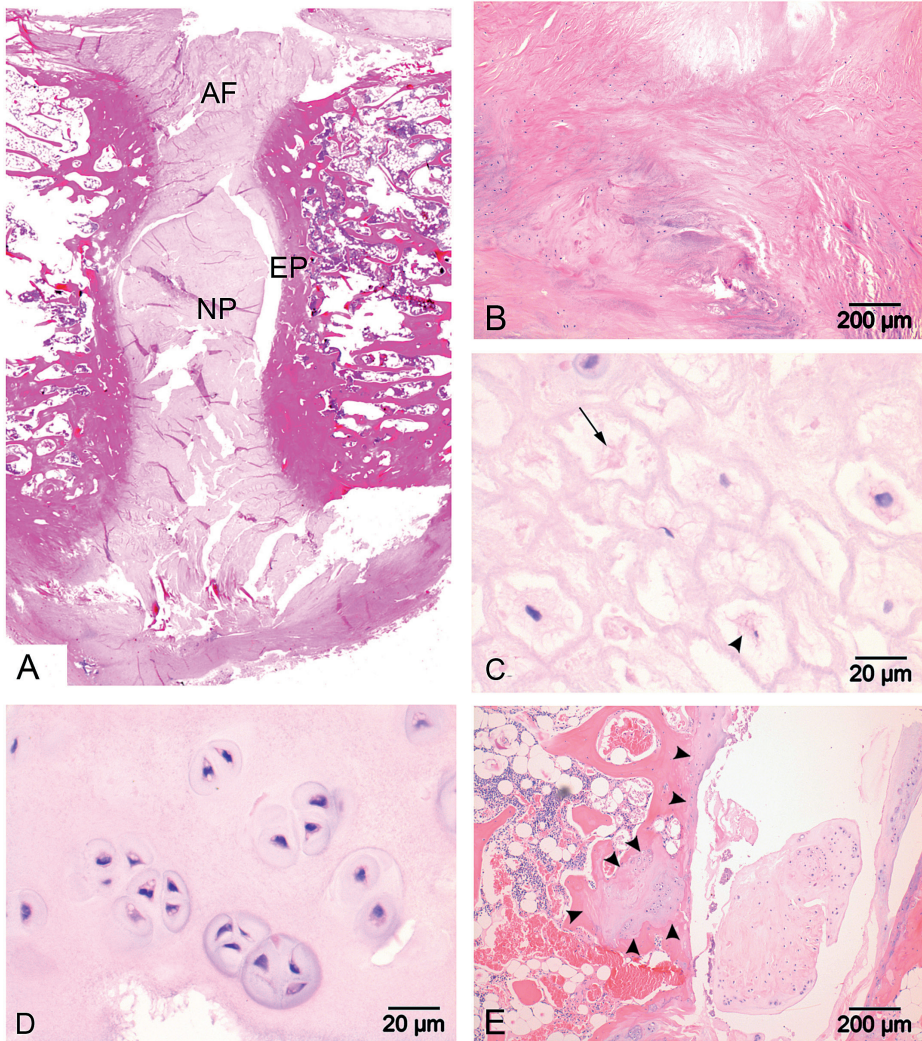


Figure 8A) Midsagittal histological section (H&E) of a degenerating, canine intervertebral disc. B) Annulus fibrosus (AF), showing disorganization of the lamellar structure and an increase in chondrocyte-like cells. C) Nucleus pulposus (NP), showing dead (arrow) and dying (arrowhead) notochordal cells. D) Nucleus pulposus, showing small groups of chondrocyte-like cells (cell-nests). E) Cartilaginous endplate (EP), showing endplate irregularities and damage. The irregular border between the endplate and the subchondral bone is marked with arrowheads.

Also, the loss of NP functionality leads to compressive loads being concentrated more peripherally, on the AF ^{111,112}. As a result, the loads on the AF are increased and altered, which can lead to annular tears and bulging and herniation of the IVD ¹¹³. Laboratory experiments with canine material have shown that removal

of the NP through an annular window, a procedure which resembles IVD herniation, causes spinal instability, indicating that AF and NP integrity are essential to the functionality of the spine¹¹⁴⁻¹¹⁷. Conversely, annular damage (fissures) can occur independently of NP degeneration and is likely to result in increased stress on the NP^{87,118,119}. It is still a matter of debate (IVD degeneration in humans and in non-chondrodystrophic dogs; see below) which of the IVD structures (NP or AF) is responsible for the initiation of the degenerative cascade⁸⁷. However, it should be noted that degeneration of the NP and AF can occur simultaneously and should be regarded as interacting processes, resulting in a vicious, degenerative cycle.

Degeneration of the NP and AF results in an uneven distribution of load on the EP¹²⁰, making it more susceptible to damage¹²¹. Although EPs are deformable when axially loaded¹²², they appear to be a weak link in the functional spinal unit and can develop cracks, disturbing the nutritional supply to the IVD relatively early in the degenerative cascade¹²³⁻¹²⁵.

As a component of the functional spinal unit, degeneration of the IVD affects not only the disc, but also other spinal components, such as ligaments, facet joints, and vertebral bodies^{5,80,87}. Decreased IVD function alters and increases facet joint loading^{126,127}, which can lead to secondary osteoarthritic changes. The altered loading pattern can also affect the adjacent vertebrae, leading to remodeling, sclerosis, and spondylosis of the vertebral bodies^{123,128}.

IVD degeneration, and subsequent degeneration of the functional spinal unit, results in a loss of spinal stiffness/stability, and increasing severity of degeneration results in an increased range of motion in different directions (i.e. flexion/extension, lateral bending, axial rotation). This increase in mobility is most apparent during axial rotation of the spine. In contrast, end-stage degeneration leads to decreased laxity and ‘restabilization’ of the spine due to the formation of osteophytes/spondylosis and the collapse of the IVD space^{125,129-132}. In addition, the degenerated IVD is less stiff and less resistant to axial compressive forces¹³³. The biomechanical effects of IVD degeneration on the canine spine have not been investigated and this is one of the topics investigated in the studies reported in this thesis.

Biomolecular and biochemical aspects of IVD degeneration

At a biomolecular level, several processes are involved in the degenerative cascade (Fig. 9). Initially, changes in cell population, involving the replacement of notochordal cells by chondrocyte-like cells, and later the formation of nests of chondrocyte-like cells, inevitably change the regulation of various biomolecular signaling pathways, leading to differences in the biochemical composition of the IVD^{64,100,134}. In humans, advanced stages of degeneration are associated with increased cell senescence, which is likely to result in decreased matrix anabolism^{135,136}. Changes in extracellular matrix (ECM) formation and remodeling occur, including changes in proteoglycan composition and

concentration, changes which are detrimental to the function of the NP matrix⁷⁴. The rate of synthesis of proteoglycans such as aggrecan and versican decreases^{74,137}. In addition, the proteoglycans that are produced are smaller¹³⁸⁻¹⁴⁰ and less aggregated¹³⁷, possibly because link-protein synthesis is decreased⁸⁸. In the GAG matrix, chondroitin sulfate side chains are replaced by shorter keratan sulfate side chains^{25,26}. The synthesis of collagen, another major constituent of the IVD ECM, also changes, with increased expression of collagen type I and decreased expression of collagen type II, which gives the NP a more fibrous, less gel-like character^{88,141,142}.

In addition, there are changes in the expression of mediators of matrix degradation and remodeling. For example, the expression of various matrix metalloproteinases (MMPs) and 'a disintegrin and metalloproteinase with thrombospondin motifs' (ADAMTs) is up-regulated^{87,143,144}, whereas the expression of tissue inhibitor of metalloproteinases (TIMPs), which inhibit MMP activity, is down-regulated^{87,143,144}. Increased concentrations of growth factors, such as TGF, have also been reported, which might reflect an attempt on the part of IVD cells to increase matrix synthesis and repair^{145,146}. The expression of the inflammatory mediators interleukin (IL)-1, tumor necrosis factor (TNF)- α , prostaglandin E2, and nitric oxide (NO) is increased in herniated IVD material, which may reflect the involvement of inflammatory mechanisms in the degenerative process¹⁴⁷. However, the biomolecular changes involved in the degenerative process are still largely unknown, especially the changes involved in the replacement of notochordal cells by chondrocyte-like cells.

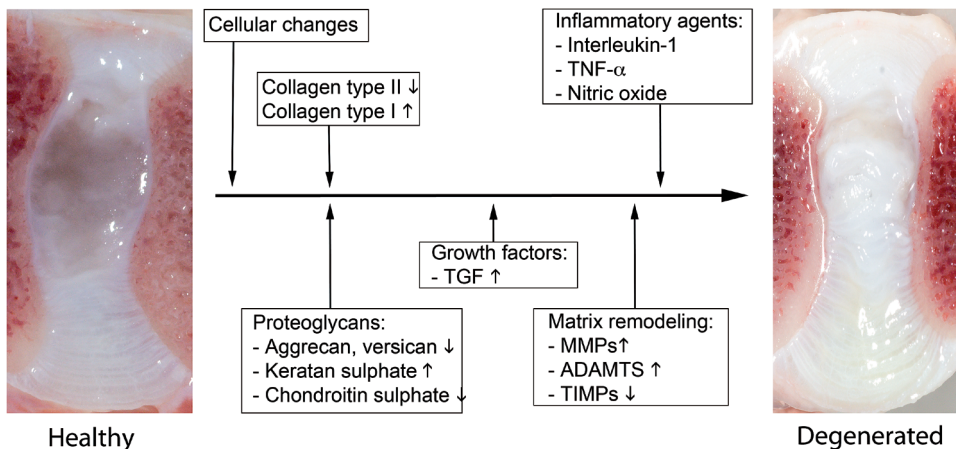


Figure 9. Biomolecular and biochemical changes involved in degeneration of the intervertebral disc. TGF: Transforming growth factor; TNF- α : tumor necrosis factor α ; MMPs: matrix metalloproteinases; ADAMTs; a disintegrin and metalloproteinases; TIMPs: tissue inhibitor of metalloproteinases.

IVD DEGENERATION: CHONDRODYSTROPHIC AND NON-CHONDRODYSTROPHIC DOG BREEDS

2.1

IVD degeneration can occur in all types of dog breeds. Dog breeds can be classified into two groups on the basis of predisposition to chondrodystrophy, i.e. chondrodystrophic (CD) dogs and non-chondrodystrophic (NCD) dogs. Apart from being distinctly different regarding the process of endochondral ossification, CD and NCD dogs are dissimilar with regard to the age of onset, frequency, and spinal location of IVD degeneration and IVD degenerative diseases, as first described by Hans-Jürgen Hansen (1952). IVD degeneration is more common in CD breeds, which are characterized by a disturbed endochondral ossification, primarily of the long bones, so that dogs of these breeds have disproportionately short limbs^{3,23,148}. Popular CD breeds include, among others, the (miniature) Dachshund, Basset Hound, French and English Bulldog, Shi Tzu, miniature Schnauzer, Pekingese, Beagle, Lhasa Apso, Bichon Frisé, Tibetan Spaniel, Cavalier King Charles Spaniel, Welsh Corgi, and the American Cocker Spaniel^{3,8,23,149-157}. It should be noted that in the work by Hansen (1952), which provides the basis for the distinction between CD and NCD dogs, only the Dachshund, Dachsbrache, Pekingese, Spaniel (unspecified), and French Bulldog were classified as CD breeds. As it has not been established which short-legged dog breeds show the typical ‘chondrodystrophy’-related characteristics of IVD degeneration, studies are often inconsistent about which dog breeds are classified as CD or NCD^{3,8,23,149-157}.

In CD breeds, IVD degenerative disease typically develops around 3-7 years of age, with the degenerative disease mainly occurring in the cervical or thoracolumbar spine^{3,8,149,153,154,156}.

In contrast, in NCD breeds IVD degenerative disease develops later, around 6–8 years of age, and mainly affects the caudal cervical or lumbosacral spine, although the thoracolumbar spine can also be affected^{3,8,9,158-160}. NCD breeds frequently affected by IVD degenerative disease include the German Shepherd Dog, Doberman, Rottweiler, the Labrador Retriever, the Dalmatian, and mixed breed dogs^{8,9,150,158-160}.

This part of the general introduction describes the similarities and differences in the histopathological and biochemical characteristics of IVD degeneration in CD and NCD dog breeds and discusses relevant etiological factors of IVD degeneration.

Pathological findings

Chondrodystrophic dogs

Histopathological differences between NCD and CD dogs can already be observed in the TZ of newborn dogs. Compared with the TZ of newborn NCD

dogs, the TZ of newborn CD dogs is relatively wide, occupying most of the AF, and its cells lack orientation^{3,23}. In new-born NCD dogs, the transition from AF to NP is more distinct and abrupt³.

IVD degeneration in CD breeds occurs earlier and faster than in NCD breeds³. In CD breeds, the change from a gelatinous, semi-fluid NP to a drier NP (Fig. 10) can already be observed at 3-4 months of age^{3,22,23,149}, and this transformation is complete in 75% of the cervical, 100%, of the thoracic, and 93.8% of the lumbar IVDs by 1 year of age. Ultimately, all IVDs are affected. In addition, the NP of CD dogs occupies a relatively small portion of the total transverse IVD surface and is located eccentrically to the dorsal side of the IVD^{3,31}. In contrast, the ventral TZ and AF are relatively wide compared to those of NCD dogs^{3,21,23,31}. These macroscopic differences in NP, TZ, and AF morphology decrease the functional size of the NP in IVDs from CD breeds^{110,111}.

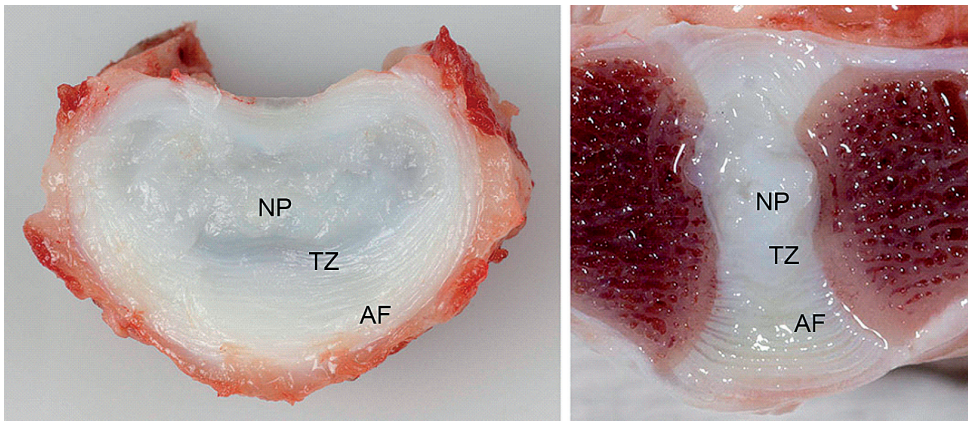


Figure 10. Transverse (left) and sagittal (right) sections through the L5-L6 intervertebral disc of a 2-year-old chondrodystrophic dog, showing a dorsally located, drier nucleus pulposus (NP), a widened transition zone (TZ), and a normal annulus fibrosus (AF). Compare with Figure 1.

In CD dogs, at 3 months of age the NP is gradually replaced by chondrocyte-like cells, embedded in a large amount of dense extracellular matrix^{3,21,23,31,56,57,65,66,161}. This chondroid metaplasia or chondrification of the NP tends to start in the periphery and spreads throughout the NP, and is completed in most IVDs by 1 year of age³. Notochordal cell remnants can however persist occasionally^{3,21,23,31,56,133}. Hansen (1952) termed this type of NP degeneration in CD breeds *chondroid metamorphosis*. The chondrocyte-like cells have a high rate of apoptosis, which increases with age¹⁶¹.

According to Hansen (1952), degeneration of the annulus fibrosus (AF) in CD dogs always occurs after NP degeneration, and not independently. Typically, AF degeneration tends to occur at one specific location within the AF, where it is more severe and acute, resulting in more pronounced disruption of the

original IVD structure. Degenerative changes in the AF consist of chondroid metaplasia and partial or complete rupture and separation of the annular lamellae. These changes are most often observed in the dorsal AF and rarely in the ventral AF^{3,65}. Apart from this localized defect within the dorsal or dorsolateral AF, the AF may appear completely healthy³.

IVD degeneration progresses rapidly in CD breeds and can result in dorsal herniation of the NP as early as 2 years of age^{3,156}. Herniation typically has sudden, explosive character, with complete rupture of the dorsomedian or dorsolateral AF, and dorsal longitudinal ligament, with extrusion of the degenerated NP into the vertebral canal³ (Fig. 11). This type of herniation, or Hansen type I herniation, usually occurs in the cervical and thoracolumbar spine^{3,8,17-19}, although Hansen type II herniation (discussed below) is also reported in CD breeds^{8,157,162,163}. The severity of chondrodystrophy seems to be associated with the risk of IVD herniation, as miniature Dachshunds are more frequently affected by IVD disease than normal-sized Dachshunds¹⁵⁰.

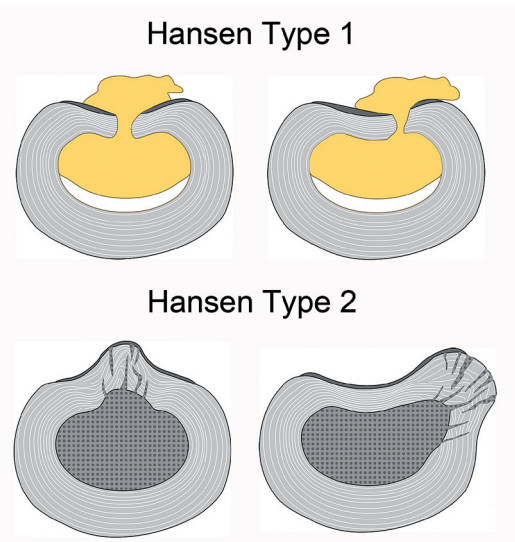
Non-chondrodystrophic dogs

In NCD dog breeds, the macroscopic changes of the NP are largely similar to those in CD dogs, but typically occur later in life (> 5 years)^{3,23}. The transition from gelatinous to fibrillar NP typically occurs in single IVDs and usually in the caudal cervical and lumbosacral spine^{3,9,12}. By 6-7 years of age, 50.0–68.7% of all NPs have undergone such changes (in a subset of dogs consisting of various Terrier Breeds, Toy breeds, Afganian, Alsatian, Boxer, Chow-Chow, Collie, Dalmatian, Dobermann pincher, Elkhound, Great Dane, Labrador, Maltese, Mongrel, New Foundland, Old English Sheepdog, Pointer, Poodle, Rottweiler, Russian Greyhound, Schnauzer, Setter, Spitz, St Bernhard, Swedish Hound, and Whippet), but not all IVDs undergo degenerative change^{3,20}.

In NCD dogs, the notochordal cell remains the predominant cell type of the NP throughout life^{3,20,23,31,56,161,164}, although age-related changes, which Hansen (1952) described as ‘slow maturation’ (Fig. 12A), may occur. In this maturation process, collagenous strands connected to the TZ appear within the notochordal cell-rich NP, dividing the NP into distinct lobules of notochordal cells. The notochordal cells may undergo degenerative changes, with a reduction in the size of the intracellular vesicles and apoptosis¹⁶⁵, and acquire a more fibrocyte-like morphology. Hansen (1952) termed these morphological changes and the production of intracellular collagen fibers ‘*fibroid metamorphosis*’ (Fig. 12A, C, E).

However, more recent research suggests that the NP degenerative changes seen in NCD breeds are similar to those seen in CD breeds, i.e. chondrification of the notochordal cell-rich NP^{65,66,157} rather than fibrosis of the NP (Fig. 12). The alleged distinction between “fibroid and chondroid metamorphosis” is discussed in greater detail below.

Figure 11. Schematic pictures of a type I and type II herniation of an intervertebral disc (IVD). Type I IVD herniation involves complete rupture of the dorsomedian (left) or dorsolateral (right) annulus fibrosus (AF, grey) and dorsal longitudinal ligament (DLL, dark grey) with extrusion of degenerated nucleus pulposus (NP) material (yellow). Type I IVD herniation is commonly observed in chondrodystrophic dog breeds. Type II IVD herniation involves partial ruptures and disorganization of the AF (grey), and bulging of NP, AF, and DLL towards the dorsomedian (left) or dorsolateral (right) side. Type II IVD herniation is commonly observed in non-chondrodystrophic dog breeds



The degenerative changes of the AF often occur concurrently with those of the NP³, but they may occur earlier, before substantial changes in the NP are seen³. Degeneration is gradual in NCD breeds and mainly consists of partial rupture of the AF fibers³, which can result in partial NP herniation through a defect in the AF, leading to intradiscal protrusions (migration of NP into the AF) and bulging of the IVD and dorsal longitudinal ligament. This type of herniation is referred to as Hansen type II herniation (Fig. 11) and mainly occurs in the caudal cervical and lumbosacral spine^{3,8,9,12,13,17,20}. However, Hansen I herniation can also occur in NCD dogs, and is then mainly seen in the cervical and thoracolumbar spine^{152,156,158,160}.

In addition to the classic Hansen type I and type II IVD herniations which involve degeneration of the IVD, a third type of disc extrusion, also referred to as traumatic acute, non-compressive disc prolapse or Hansen type III disc disease, has been described¹⁶⁶⁻¹⁶⁸. This herniation involves traumatic extrusion of non-degenerated NP material through the dorsal AF with consequent contusion of the spinal chord; however, spinal chord compression is subtle due to the resorption of the healthy NP by the epidural fat¹⁶⁶⁻¹⁶⁸. This type of herniation will not be further discussed in this thesis.

Chondroid vs. fibroid metamorphosis

The Hansen (1952) classification of ‘chondroid’ and ‘fibroid’ metamorphosis has been the accepted histopathological distinction between CD and NCD breeds for the past 60 years (Fig. 12)³. However, diligent investigation of Hansen’s thesis, more recent studies using macroscopic grading schemes for

IVD degeneration combined with histopathological grading suggest that the degenerative processes in CD and NCD dogs are more similar than previously assumed^{65,66,157}.

Although CD and NCD dogs were characterized by chondroid and fibroid metamorphosis of the NP, respectively, Hansen emphasized that NCD and CD dogs showed many similarities regarding the fundamental processes involved in the degenerative cascade. Also, Hansen described the fibroid metamorphosis of the NP in NCD dogs more as a process of maturation, rather than degeneration.

Recent studies have shown that more advanced stages of NP degeneration in NCD dogs involve replacement of notochordal cells by chondrocyte-like cells, similar to the changes observed in CD dogs (Fig. 12D, F)^{3,20,23,56-58,65,66,157,169}. This chondrification of the NP is also seen in other species. For example, studies on IVD degeneration in humans (naturally occurring) and mice (experimentally induced) showed the notochordal cell-rich NP to be sequentially transformed into a chondrocyte-like cell-rich NP with an increase in collagen II in the intercellular matrix^{60,66,170}.

Calcification

A process associated with IVD degeneration is calcification of the IVD, which is frequently observed in CD dogs, but rarely in NCD dogs (Fig. 13)^{3,20}. Although most frequently found in the thoracic spine, IVD calcification can be found at all spinal levels^{3,171-175} and can be seen as early as 5 months of age, and by 1 year of age 31.2% of cervical, 62.5% of thoracic, and 43.8% of lumbar IVDs in CD dogs show macroscopic signs of disc calcification (in a subset of dogs consisting of Dachshund, French Bulldog, Pekinese, Spaniel, and Dachsbrache)^{3,20}. Although the prevalence of disc calcification increases with age^{3,171,172,176}, it appears to reach a steady state or maximum at 24-27 months of age¹⁷².

Calcification mainly occurs at the periphery of the NP and occasionally in the AF^{3,175,177}, and can be observed before complete chondrification of the NP has occurred (Fig 13C, D). NP calcification is thought to be dystrophic in nature, secondary to tissue necrosis^{3,178-180}. It has been suggested that the mineral deposits found in the CD consist of hydroxyapatite¹⁷⁸; however, the actual composition of canine IVD mineralizations still needs to be elucidated. IVD calcification due to deposition of hydroxyapatite or calcium pyrophosphate dehydrate is also seen in humans (adults and rarely in children)¹⁸¹⁻¹⁸³.

IVD calcification might be associated with IVD herniation^{172,175-177,184-186}, with the total number of calcified discs in the spinal column being associated with the risk of developing IVD herniation at random spinal levels (not necessarily the calcified disc): the odds of IVD herniation occurring at any spinal location increases by 1.42 per calcified disk¹⁸⁴. Although IVD calcification can affect IVD integrity, and calcified discs can herniate, calcification occurs more often

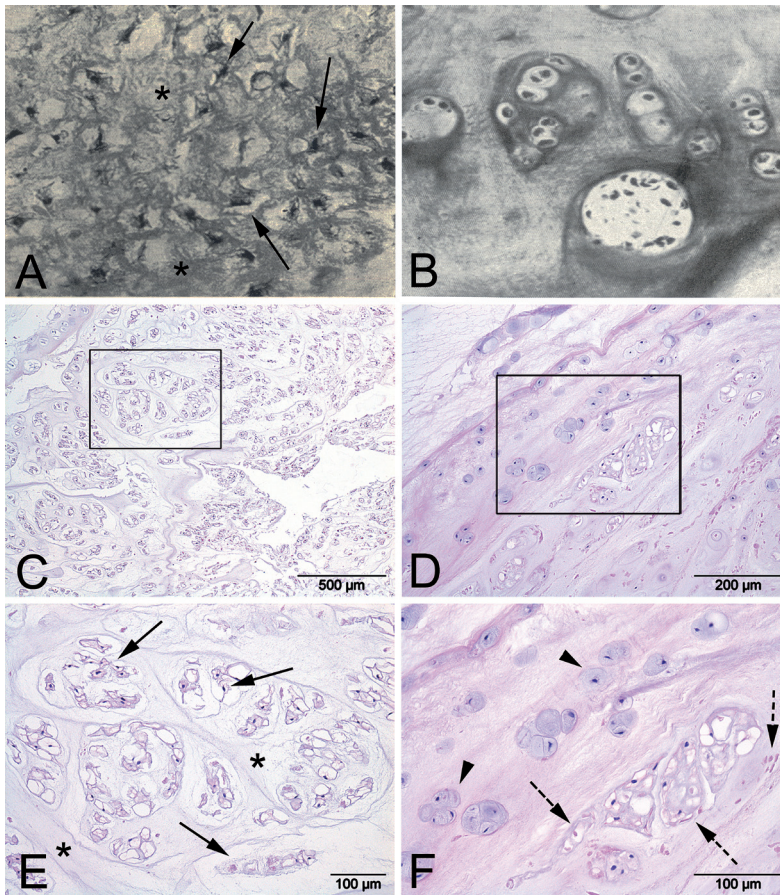


Figure 12. *A and B: Original pictures from the thesis by Hansen (1952), depicting fibroid (A) and chondroid (B) metamorphosis of the nucleus pulposus. Original legends from the thesis: A) Airedale terrier, 10 years old. Nucleus pulposus from disc 9 (T3-T4), showing vital cells with a certain similarity of fibrocytes (arrows) and an intercellular substance, rich in collagen fibers (asterisks). Van Gieson, 400X. B) Dachshund, 4 months old. Nucleus pulposus of disc 2 (C3-C4). Chondroid metamorphosis. The picture shows the definite cartilage-like cell pattern, except of one small group of a more original nuclear character. Van Gieson. 200X. C-F: Original comparable pictures: Haematoxylin & eosin (H&E) images of morphological changes in the nucleus pulposus (NP) of non-chondrodystrophic dogs. C and E show the so-called fibroid metamorphosis, the morphological picture of maturation or an early stage of degeneration of the NP, with an increase in fibrillar collagenous extracellular matrix (ECM, asterisks) dividing the NP into distinct islands of notochordal cells (NCs, arrows). The NCs decrease in size and show loss of intracellular vesicles and apoptosis. Note the morphological similarity of the cells in Hansen's fibroid metamorphosis in A (arrows) with the notochordal cells in C (arrows), while these latter cells lack the typical morphological characteristics of fibrocytes. D and F show a later stage of degeneration with characteristic chondroid metaplasia of the NP, characterized by chondrocyte-like cells (arrowheads) and degeneration/apoptosis of NCs (dashed arrows). E and F are magnifications of the squares in C and D, respectively.*

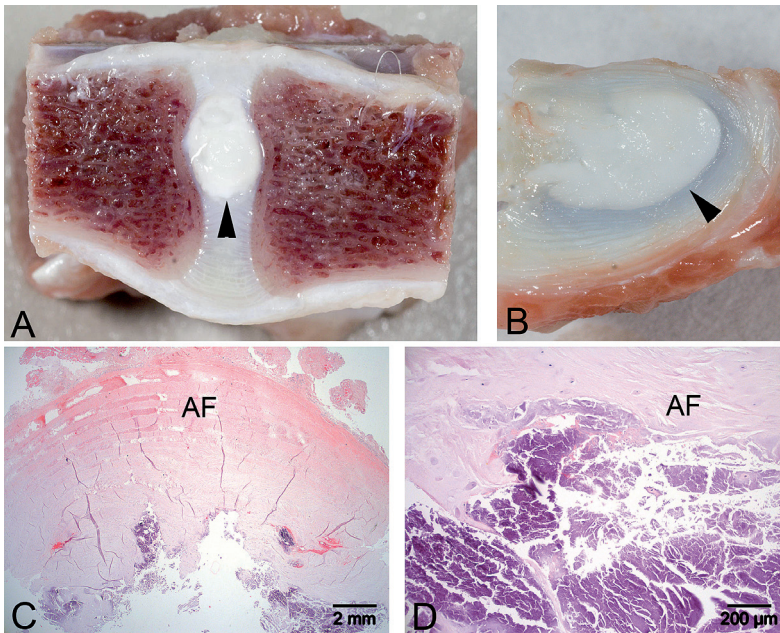


Figure 13. Mid-sagittal (A) and transverse (B) sections of an intervertebral disc from a 2-year-old chondrodystrophic dog with extensive mineralization of the nucleus pulposus (arrowhead). C) Transverse histological section (H&E) of the same intervertebral disc depicting the relatively normal structure of the ventral annulus fibrosus (AF) and a severely mineralized nucleus pulposus (purple). D) Close-up view of the mineral deposits (purple).

than IVD herniation. Moreover, disc extrusion can occur in IVDs without any radiographic evidence of calcification^{3,20,174}.

Partial or complete resolution of disc calcification has been reported^{171,172,186} and is common among CD dogs older than 3 years¹⁷². This might be because increased tension and tearing of the AF, with subsequent exposure of nuclear material to other tissues, may elicit an inflammatory response, with calcified material being removed by macrophage-like cells^{171,172}. Alternatively, pH changes in the IVD may lead to the dissolution of calcified material¹⁸⁷.

Biochemistry of the extracellular matrix of the IVD of CD and NCD dogs

Proteoglycans

Chondrification of the NP results in a significant decrease in its proteoglycan and hyaluronic acid content^{21,65}. At 9 months of age, the proteoglycan content of the NP is significantly higher in NCD dogs than in CD dogs (Fig. 14)²², whereas there are no differences in the proteoglycan content of the TZ and

AF. The main glycosaminoglycan (GAG) of the NP, TZ, and AF is chondroitin sulfate ²². At 30 months of age, the NP proteoglycan content decreases sharply in CD dogs, but remains constant throughout life in NCD dogs ^{25,26}. The proteoglycan content of the NP in particular changes in CD dogs around 1 year of age, with a decrease in chondroitin sulfate and an increase in keratan sulfate, which ultimately replaces chondroitin sulfate ²⁵. These changes also occur in NCD dogs, but after 30 months of age and less extensively ^{25,26}. Differences in the proteoglycan concentration in the TZ and AF between the two breeds groups are less pronounced ^{25,26}.

Collagen

Chondrification of the NP results in a significant increase in the collagen content ^{21,27,66}. Before 1 year of age, the NP at all spinal levels contains about 25% collagen in CD breeds but less than 5% in NCD breeds. The collagen content (percentage of total tissue) of the NP, AF and TZ in CD dogs is considerably greater than that in the NCD dog, and in CD dogs the collagen: non-collagenous protein ratio in the NP and AF increases sharply with age, starting before the 1 year of age in the NP and at 30 months in the AF ²⁷. In contrast, the collagen content and the collagen: non-collagenous protein ratio remain relatively constant over time in NCD dogs, increasing later in life (60 months and 124 months, respectively) at particular spinal levels, such as L7-S1. These changes are most probably due to chondrification/degeneration, with the NP of NCD breeds becoming more similar to that of CD breeds by 21-30 months of age ²⁷.

As the composition of the extracellular matrix depends on its constituent cells, and on notochordal cells in particular ^{56,79,164,188-191}, the observed differences in extracellular matrix composition in CD and NCD dogs probably reflect the chondrification of the NP, which occurs in all IVDs in CD dogs and in selected IVDs in NCD dogs, and give rise to rapid deterioration of the hydroelastic properties and, consequently, the hydraulic function of the IVD ^{22,25-27}.

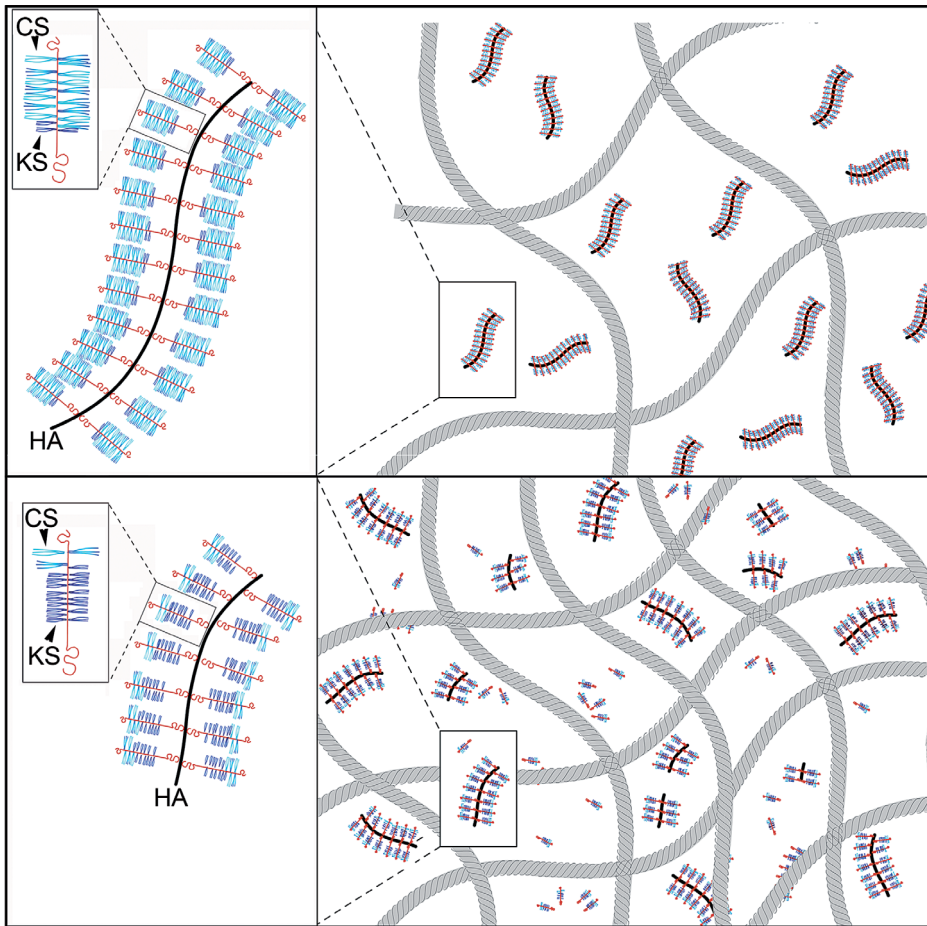


Figure 14. Schematic composition of the extracellular matrix of the nucleus pulposus in a 1-year-old non-chondrodystrophic (top) and chondrodystrophic (bottom) dog. The non-chondrodystrophic extracellular matrix contains long-chained proteoglycans rich in hyaluronic acid (HA; black line) and chondroitin sulfate (CS; light blue brushes), and it has a relatively low collagen content (grey bundles). The chondrodystrophic extracellular matrix contains significantly more collagen (grey bundles), proteoglycan molecules are shorter, and shorter keratan sulfate (KS; dark blue) side chains replace the chondroitin sulfate side chains.

Etiological factors for IVD degeneration

The etiology of IVD degeneration is multifactorial in both CD and NCD dogs; however, the early degeneration seen in CD, but not NCD, dogs suggests that there is a genetic component. Genes associated with the chondrodystrophic trait, and with IVD degeneration and calcification have recently been identified, which suggests that IVD degeneration has a multigenetic etiology^{3,23,149,177}. A locus on chromosome 12 has been shown to harbor genetic variations

associated with IVD calcification in the Dachshund¹⁹². In addition, the expression of a retrogene encoding *fibroblast growth factor 4* (*fgf4*) located on chromosome 18 is strongly associated with chondrodystrophy in several CD dog breeds, including the Dachshund, Corgi, and Basset hound¹⁵¹. However, *fgf4* retrogene expression was not found in several breeds commonly affected by accelerated IVD degeneration, such as the Beagle and American Cocker Spaniel¹⁵¹. Therefore, different genetic factors appear to be at play in different dog breeds, which requires further investigation.

The difference in the spinal location of IVD degeneration between CD and NCD breeds, with IVD degeneration occurring throughout the spine in CD, but not NCD breeds^{3,23,149}, suggests that biomechanical factors inherent to individual spinal levels seem to be of less importance to IVD degeneration in CD dogs. Although it would seem plausible that the disproportionately long spine relative to the short legs of CD breeds might predispose them to IVD degeneration, no association has been found between IVD degeneration and spine length or other body dimensions such as leg length^{3,185}. Moreover, the observation that degenerative changes of the IVD can already be found in newborn CD dogs supports the assumption that biomechanical factors are of minor importance in the development of IVD degeneration in CD dogs^{3,23}. CD dogs with a relatively shorter spine, a greater height at the withers, and a large pelvic circumference have been shown to be at higher risk of IVD herniation¹⁶³, but body dimensions are not associated with IVD calcification¹⁷³. The greater susceptibility of the cervical and thoracolumbar spine to herniation in CD breeds was thought to be due to the transition from the rigid, thoracic spine to the more flexible, lumbar spine; however, there is no convincing evidence to support this theory¹⁹³. The low risk of IVD displacement in the mid-thoracic spine (T1-T9) may be due to the presence of the intercapital ligaments, which may prevent dorsal and dorsolateral displacement of the IVD^{3,149}.

In NCD dogs, IVD degeneration commonly occurs at the caudal cervical and lumbosacral spine, and especially in large-breed dogs^{3,12,194-196}. The anatomical conformation of the cervical spine in most dogs does not permit considerable axial rotation within each functional spinal unit¹⁹⁷; however, the more concave shape of the facet joints of the caudal cervical spine in large-breed dogs compared with small-breed dogs^{198,199} allows considerable axial rotation, and may contribute to instability and misalignment of the facets^{198,199}, thereby increasing the workload and stresses on the cervical IVDs and promoting IVD degeneration²⁰⁰.

The L7-S1 junction of NCD dogs permits considerable mobility in flexion/extension and axial rotation^{3,201,202}. Also, the L7-S1 IVD in NCD dogs exhibits a low ventrodorsal shear stiffness, making it more susceptible for ventrodorsal subluxation/instability^{201,203,204}. Moreover, there is an imbalance between the dimensions of the lumbosacral contact area (IVD and facet joints) and the body weight in large-breed dogs compared with small-breed dog²⁰⁴, so that the L7-S1 junction in large-breed dogs may be subject to proportionally higher loads

²⁰⁴. These factors may predispose the L7-S1 IVD to a high degree of wear and tear, leading to IVD degeneration.

Of the NCD breeds, the German Shepherd Dog (GSD), especially the male working dog, is at the highest risk of developing IVD degeneration and disease at L7-S1 ^{9,11,187,205}. In the GSD, the facet joint angle of L7-S1 is more oblique (facet joint angle in the transverse plane) than those of L6-L7 and L5-L6 ^{195,196}, whereas in other large-breed dogs the facet joint angle is similar in L7-S1 and adjacent segments ^{195,196}. The oblique orientation of the L7-S1 facet joint in relation to adjacent spinal segments causes a disproportionately high workload on the L7-S1 IVD, predisposing the disc to degeneration, more so than in adjacent spinal segments ^{195,196,200}.

An additional predisposing factor is lumbosacral transitional vertebra anomaly (LTVA), which is strongly associated with lumbosacral IVD degeneration in large-breed dogs (e.g. the GSD) ²⁰⁶⁻²⁰⁸. Studies have shown that the mobility and distribution of force in the lumbosacral joints of dogs with LTVA is abnormal and that there is an increased translation in the IVD between the last lumbar vertebra and the LTVA ^{206,209}. These abnormal biomechanical characteristics may accelerate structural failure of the IVD ^{206,207}. Lastly, the GSD is predisposed to sacral osteochondrosis, which involves degeneration and fragmentation of the sacral EP ²¹⁰⁻²¹². The abnormal shape of the sacral EP may cause aberrant mechanical loading of the IVD, resulting in IVD degeneration. Alternatively, osteochondrosis of the sacral EP may impede the supply of nutrients to the disc, predisposing it to degeneration ²¹⁰⁻²¹².

Conclusion

The macroscopic, histopathological, and biochemical changes involved in IVD degeneration are largely similar in CD and NCD dogs, involving chondrification of the NP and structural failure of the IVD extracellular matrix. However, the age of onset, spinal level, progression of IVD degeneration, and the character of herniation are different, indicating that different etiological factors are at play in the two breed types.

In CD dogs, genetic factors related to the CD trait result in rapid IVD degeneration of all discs early in life, leading to progressive and then abrupt structural failure of the IVD, which in turn predisposes it to explosive type I herniation of NP material. In addition, calcification of the IVD is a common occurrence in CD dogs. In NCD dogs, IVD degeneration occurs relatively infrequently, only at selected spinal levels, and mostly in old age. As the NP matures, the notochordal cell population is preserved and although there are moderate histopathological changes, the extracellular matrix is healthy. At certain spinal levels, the IVD may be subjected to excessive stresses and loads, resulting in long-term “wear and tear” of the disc and subsequent IVD degeneration (chondroid metaplasia). This “wear and tear” process can result in structural failure and consequent bulging or type II herniation of the IVD.

CLINICAL MANIFESTATIONS OF IVD DEGENERATION

Degeneration of the IVD can ultimately lead to extrusion or protrusion of the IVD, which can cause compression of the overlying neural structures. IVD degeneration can lead to NP herniation, cervical spondylomyelopathy (CSM), and degenerative lumbosacral stenosis (DLSS). The clinical presentation of these diseases is discussed below, followed by a description of diagnostic and therapeutic approaches.

Hansen type I IVD herniation

Type I herniation of the IVD is characterized by local rupture of the dorsal AF and the dorsal longitudinal ligament, whereby NP tissue is extruded into the spinal canal³. This extrusion generally causes acute compression of neural structures and a sudden onset of clinical signs.

Type I IVD herniation occurs mainly in CD dogs (as discussed above), with the Dachshund being the most frequently affected breed: approximately 1 in 5 Dachshunds will display clinical signs of IVD herniation in their lifetime and this breed has been reported to be 12.6 times more likely to suffer from IVD herniation than the overall canine population^{150,153,154,213}. IVD herniation typically occurs in the cervical and thoracolumbar area, with C2-C3 and T12-T13/T13-L1 being the most commonly affected vertebrae in CD breeds^{3,8,152,214,215}. Type I IVD herniation in CD breeds generally becomes manifest between 3 and 7 years of age^{3,149,152-154}.

Clinical signs of type I IVD herniation are characterized by their acute onset, with acute cervical spinal pain, hyperesthesia of the neck region, muscle fasciculations or spasms, and guarding of the neck being common signs. Neurological deficits are less common with cervical IVD herniation than with thoracolumbar herniation, which is thought to be related to the relatively wide cervical vertebral canal²¹⁶⁻²¹⁸. Other clinical signs include unilateral or bilateral lameness caused by lower cervical nerve root compression, also known as nerve root signature, and occasionally ataxia with tetraparesis or tetraplegia²¹⁶⁻²¹⁸. Thoracolumbar IVD herniation usually manifests as back pain of varying severity and neurological deficits ranging from mild paraparesis to paraplegia, loss of bladder function, fecal incontinence, and loss of deep pain perception⁸.

Hansen type II IVD herniation

Hansen type II herniation is generally observed in NCD dogs and is caused by the synchronous degeneration of the NP and AF, resulting in bulging of the NP, AF, and dorsal longitudinal ligament (and not extrusion of NP material), which can result in compression of neural structures³. Breeds commonly affected by type II IVD herniation include the German shepherd dog, Labrador retriever, Doberman Pinscher, Rottweiler, and Dalmatian¹⁵⁸⁻¹⁶⁰. Type II IVD herniation

typically manifests between 6 and 8 years of age in NCD dogs^{3,149,152-154}. Similar to type I herniations, type II herniations can be observed in the cervical and thoracolumbar spine, with the C6-C7 and T13-L1/L1-L2/L2-L3 IVDs being the most commonly affected cervical and thoracolumbar segments, respectively^{3,8,152,214,215}.

Clinical signs associated with Hansen type II IVD herniation are generally milder in severity and less acute, with a more gradual onset than type I herniations. Common clinical signs of cervical type II IVD herniation include muscle fasciculations, guarding of the neck, cervical spinal pain, and hyperesthesia of the neck region. Other clinical signs include unilateral or bilateral lameness caused by lower cervical nerve root compression (nerve root signature)²¹⁶⁻²¹⁸. Thoracolumbar type II IVD herniation usually manifests as back pain of varying severity and paraparesis, but without the severe signs associated with type I herniation, such as loss of deep pain perception and paraplegia⁸.

Cervical spondylomyelopathy

IVD-related CSM involves the degeneration and Hansen type II herniation of one or more cervical IVDs, often in combination with stenosis of the cervical vertebral canal and/or interarcuate ligament hypertrophy. This combination of events results in compression of the cervical spinal cord^{10,219,220}.

Disc-related CSM is mainly seen in middle-aged, large-breed dogs, with a clear predisposition for Doberman Pinschers¹⁵⁰. This clear predisposition is thought to be related to a congenitally abnormal architecture of the spinal column, involving vertebral canal stenosis and asymmetry of the cervical vertebral bodies (mainly C5, C6, and C7)¹⁰. Another factor that predisposes Doberman Pinschers to CSM is the relatively large size of the IVD, which results in relatively larger bulging in the case of IVD herniation¹². However, subclinical degenerative abnormalities, such as IVD protrusion and foraminal stenosis, are also common in asymptomatic individuals. Moreover, 25% to 30% of clinically normal Doberman Pinschers were found to have clinically silent spinal cord compression on radiological/pathological investigation^{12,194}. A key mechanistic difference between clinically normal and CSM-affected Doberman Pinschers that explains the discrepancy between IVD degenerative changes and neurological signs is stenosis of the vertebral canal¹²: the diameter of the vertebral canal is consistently smaller throughout the entire length of the cervical spine in CSM-affected dogs, which increases the risk of neural compression if IVD bulging occurs, whereas the neural canal is relatively wider in clinically normal dogs, which prevents compression of neural structures¹². Another characteristic of CSM is dynamic compression of the spinal cord: dorsiflexion of the cervical spine often worsens the disc-associated compression, whereas ventroflexion alleviates the neural compression¹⁰. Other breeds affected by IVD-related CSM include the Weimaraner and

the Dalmatian, with the mean age of presentation being 7.9 years in all large breeds^{150,219-222}. The intervertebral spaces C6-C7, followed by C5-C6, are most commonly involved^{12,194,219,220}, which is due to the relatively low stiffness in axial rotation of the caudal cervical spine in large breed dogs^{198,199}.

Dogs affected by CSM commonly present with chronic and progressive clinical signs, although acute neck pain has also been reported. Neck pain occurs in about 50% of cases¹⁰. Other clinical signs include abduction of the elbows with internal rotation of the digits, proprioceptive ataxia, short-strided or spastic gait of the thoracic limbs (pseudohypermetria), and extreme flexion of the elbow joints with resulting “high” stepping of the thoracic limbs (hypermetria)¹⁰. Also, signs of nerve root signature affecting the thoracic limbs and uncoordinated gait with abduction of the pelvic limbs can be observed. Therefore, gait evaluation is a major component of the clinical investigation. Severely affected dogs may present with tetraparesis or tetraplegia. Evaluation of the spinal reflexes of the thoracic limbs usually shows a decreased withdrawal reflex (involvement of the musculocutaneous nerve originating from spinal cord segments C6 to C8), with normal to increased extensor tone suggestive of an upper motor neuron lesion. The pelvic limb reflexes are usually normal to increased¹⁰.

Degenerative lumbosacral stenosis

DLSS is a multifactorial degenerative disorder of the L6-L7 or L7-S1 spinal segment, involving stenosis of the spinal canal and compression of the cauda equina and/or its blood supply⁹. Cauda equina nerves include the sciatic nerve (L6-S1), pelvic nerve (S1-S3), pudendal nerve (S1-S3), and the caudal nerves (Cd1-Cd5). Factors involved in the degenerative process include:

- Degeneration and Hansen type II herniation of the L7-S1 IVD and ventral subluxation (spondylolisthesis) of S1 relative to L7 (lumbosacral instability)^{9,11,223,224};
- Sacral osteochondrosis of the dorsal rim of the sacral EP with fragmentation and disruption of the IVD^{212,225,226};
- Proliferation of the soft tissues surrounding the cauda equina, such as hypertrophy of the interarcuate ligament, the facet joint capsules, and epidural fibrosis^{224,227,228};
- Misalignment of the facet joints and congenital vertebral anomalies, such as symmetric or asymmetric transitional or extra vertebrae^{195,196,201,206,229-231}
- Vascular compromise of the blood supply to the spinal nerves^{228,232,233}.

It has been proposed that DLSS is initiated by degeneration of the L7-S1 IVD, which results in a loss of disc functionality and subsequent lumbosacral instability⁹. The IVD degeneration and resulting instability can cause dynamic impingement of the cauda equina, changes in the EPs with aberrant IVD nutrition, and reactive hypertrophy of the interarcuate ligament, epidural fibrosis, and thickening of the capsules of the articular processes⁹. These

degenerative changes form a vicious cycle, ultimately resulting in Hansen type II herniation (or less commonly Hansen type I herniation) and deterioration of vertebral canal stenosis and compression of the cauda equina. In addition, the inflammatory process may result in the ingrowth of nerves into the degenerated L7-S1 IVD, which contributes to the caudal lumbar pain²³⁴.

DLSS is seen in middle-aged (6-8 years), large breed dogs, with a predisposition for the German Shepherd Dog and male working dogs^{11,150,223,235-237}. Other breeds affected by DLSS include the Rottweiler, Doberman pinscher, Boxer, Bernese Mountain dog, Rhodesian Ridgeback, and Labrador Retriever^{11,150,223,235-237}.

Caudal lumbar pain is the predominant clinical sign in DLSS patients. Unilateral or bilateral pelvic limb lameness can be observed; unilateral pelvic limb lameness is the result of unilateral entrapment of spinal nerves, with radiating pain (nerve root signature). Other signs include difficulty standing up, sitting, or lying down, reluctance to jump or climb, dragging of toes, low carriage of the tail, posterior paresis, and in extreme cases urinary and/or fecal incontinence^{11,223,235-237}. The diagnosis of DLSS requires the use of specific clinical tests to evoke a caudal lumbar pain response, such as hyperextension of the caudal lumbar spine with lumbosacral pressure (lordosis test), tail hyperextension, the lumbosacral pressure test, or a combination of these tests. Profound neurological deficits are rare in dogs with DLSS and include lower motor neuron signs in the pelvic limbs, such as paresis, atrophy of muscles innervated by the sciatic nerve, hyporeflexia of the withdrawal reflex or cranial tibial reflex, or pseudo-hyperreflexia of the patellar reflex^{11,223,235-237}.

Diagnosing IVD disease

Diagnosing IVD degenerative disease requires a full diagnostic work-up to accurately determine the problem at hand. The signalment of the dog (CD or NCD breed and age) gives clear hints about the type of IVD degenerative disease to be expected. A good history is imperative to collect information about the onset and progression of clinical signs, such as spinal pain, that may have disappeared by time of presentation. The physical examination provides information about the overall health of the patient and the presence of systemic clinical signs that could be associated with IVD degenerative disease. Orthopedic examination provides information about musculoskeletal and joint disorders and should be performed to distinguish between neurological and orthopedic problems. Neurological examination is essential to assess neurological deficits and to localize the spinal lesion anatomically. After completion of these investigations, the combined information should be used to establish a neuro-anatomical localization of the lesion and to compile a list of likely differential diagnoses. Ancillary diagnostic tests are often required to confirm the final diagnosis²³⁸.

A diversity of diagnostic imaging tools can be used to diagnose IVD degenerative diseases, but it should be emphasized that the diagnosis of IVD

degenerative diseases is based on a combination of signalment, history, clinical signs, with diagnostic imaging and other diagnostic tools, such as blood (DNA) tests, being used for specific diseases or electrodiagnostics⁸⁻¹⁰. Diagnostic imaging can reveal the severity of spinal cord compression and/or damage, but it does not provide information about spinal cord function. The most reliable test to evaluate loss of neurological function is the neurological examination. Advanced imaging tools, such as computed tomography (CT) and magnetic resonance imaging (MRI), have the great benefit of visualizing the complex spinal anatomy on multiple planes. However, degenerative changes in dogs without clinical signs and discrepancies between clinical/surgical and CT/MRI findings have been reported, and therefore findings obtained using these advanced imaging techniques should be interpreted with caution^{12,216,239-241}.

Conventional radiography

Radiographic signs of IVD degenerative disease include narrowing of the IVD space, narrowing or increased opacity of the intervertebral foramen, the vacuum phenomenon (accumulated nitrogen gas in a ruptured, degenerated IVD; Fig. 19), and ventral spondylosis (Fig. 15)^{11,242-244}. Narrowing of the IVD space has been reported to be the most useful radiographic sign, but it has only a moderate sensitivity and predictive value, whereas the vacuum phenomenon is rare, but accurate in identifying the ruptured disc²⁴². Radiographic findings more specific for type I IVD herniation include the presence of mineralized disc material in the vertebral canal. Mineralization of the IVD itself is supportive of IVD degeneration, but not of IVD herniation^{172,175,245-247}. Radiographic findings seen in disc-associated CSM are primarily changes in the shape of the vertebral body, such as a triangular shape of affected vertebral bodies and stenosis of the vertebral canal²⁴⁴. Findings associated with DLSS include sclerosis of the vertebral EPs, elongation of the sacral lamina (“telescoping”) in the caudal aperture of L7, and lumbosacral step formation with ventral subluxation of S1. Stress radiography of the lumbosacral and cervical region, such as dynamic flexion/extension (CSM, DLSS) and linear traction (CSM), may worsen the spondylolisthesis or spinal compression and provide an indication of instability or compression^{10,248}. The limitation of conventional radiography is that normal radiographs do not exclude IVD degenerative disease, especially in case of type II IVD herniation^{248,249}. In addition, conventional radiography does not provide information on possible lateralization of the extrusion, or on the extent and severity of spinal cord compression.

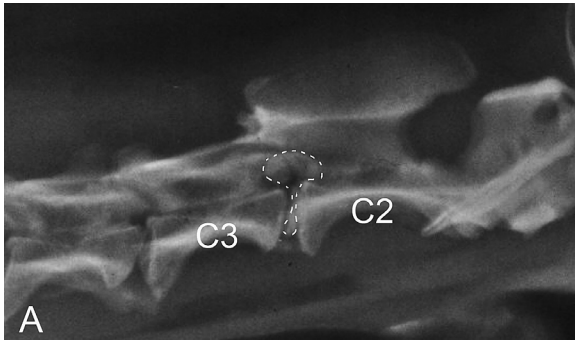


Figure 15A. Lateral radiographs of the cervical spine of a 5-year-old Beagle, showing extrusion of mineralized nucleus pulposus of the C2-C3 intervertebral disc (dotted line), and increased radiopacity of the C2-C3 intervertebral foramen.

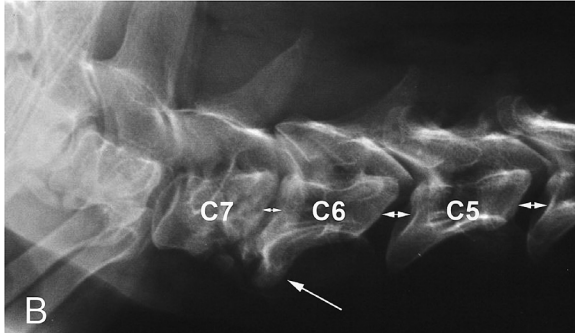


Figure 15B. Lateral radiograph of the caudal cervical spine of a 7-year-old Doberman Pinscher, showing a decreased disc height of the C6-C7 intervertebral space, and ventral spondylosis (arrow).

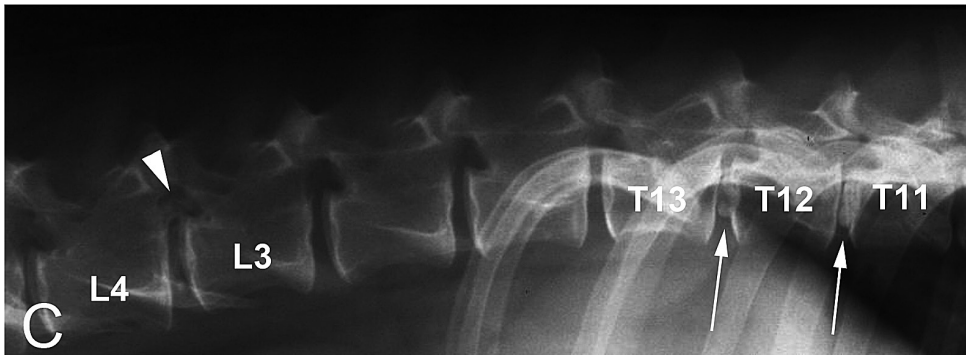


Figure 15C. Lateral radiograph of the thoracolumbar spine of a 4-year-old Dachshund, showing calcification of the T11-T13 intervertebral discs (arrows, and increased radiopacity of the L3-L4 intervertebral foramen, indicative of extrusion of the nucleus pulposus at L3-L4.

Myelography

Myelography has been the standard imaging modality for diagnosing IVD degenerative disease in dogs, but is gradually being replaced by MRI^{8,9,250,251}. Myelography is more sensitive than routine radiography, and myelographic findings of IVD degenerative disease include attenuation, thinning, or deviation of the contrast column suggestive of extradural compression (Fig. 16). Moreover, lateralization of IVD herniation can be detected on ventrodorsal

or oblique projections. The sensitivity of myelography can be increased by dynamic flexion/extension (CSM, DLSS) or linear traction (CSM) ^{244,250-252}. However, the usefulness of myelography for DLSS patients has been debated because it depends on the extension of the dural sac over the lumbosacral junction ⁹. In addition, as for conventional radiography, IVD degenerative disease (especially type II herniation) may be present without detectable abnormalities on myelography. ²⁵³ In addition, myelography may give rise to significant side effects, such as postmyelographic seizures and temporary deterioration of the patient's neurological status ^{9,10}.

Figure 16. Lateral (left) and dextroventral sinistrodorsal-oblique (right) myelograms of the thoracolumbar spine of a 5-year-old Dachshund, showing dorsolateral deviation of the spinal cord resulting from herniation of the L1-L2 intervertebral disc.

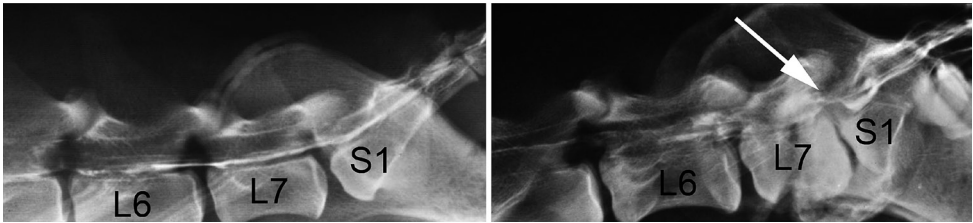
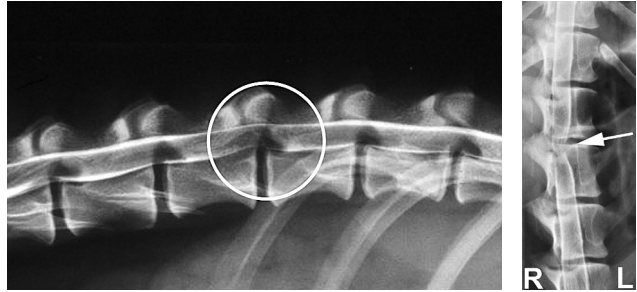


Figure 17. Epidurograms of a normal (left) and abnormal (right) canine lumbosacral junction. The abnormal epidurogram shows narrowing, deviation, and elevation of the epidural contrast line (arrow).

Epidurography and discography

Epidurography involves injection of contrast medium into the epidural space, and therefore this technique may be useful for DLSS patients. An epidurogram in dogs with DLSS may show narrowing, elevation, deviation, or obstruction of the epidural contrast-medium lines on lateral views, especially when combined with dynamic flexion/extension studies (Fig. 17) ²⁵⁴⁻²⁵⁶. For discography, contrast medium is injected into the NP through the AF ^{256,257}. Normally, no more than 0.1 mL contrast medium can be injected into a healthy L7-S1 NP and can be observed in the center of the NP on lateral radiographic views (Fig. 18). However, in case of a Hansen type II herniation, 1–2 mL contrast medium can be easily injected into L7-S1, and its

spread throughout the NP and AF can be seen on lateral radiographic views. However, discography can induce IVD degeneration^{258,259}, and the technique is considered controversial. Epidurography and discography have largely been replaced because of the increasing availability of CT and MRI⁹.

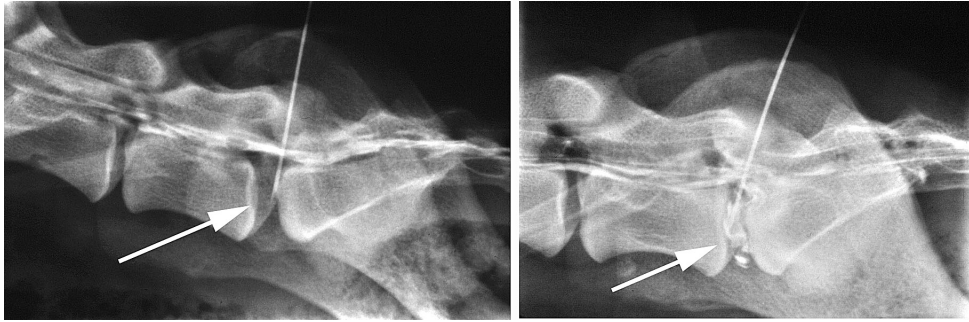


Figure 18. Lateral discograms of healthy (left) and degenerated (right) intervertebral disc, showing the absence of contrast in the healthy disc, whereas contrast is visible in the degenerated disc.

Computed tomography

Computed tomography (CT) is a sensitive and non-invasive diagnostic tool that can be used to provide information about the localization and lateralization of the IVD herniation and the about the severity of neural compression (Fig. 19). Moreover, three-dimensional digital reconstructions of multiple imaging planes can be created to improve the diagnostic process²⁶⁰⁻²⁶³. CT enables high-quality bone imaging and has a better soft-tissue contrast resolution (dural sac, interarcuate ligament) than conventional radiography, but is not considered the modality of choice to image soft tissue^{8,9,13,253,264,265}. CT is highly sensitive in detecting chronic disc lesions and disc mineralization^{260,261}. Transverse, parasagittal, and dorsoplanar views provide information on the intervertebral foramina²⁶⁶.

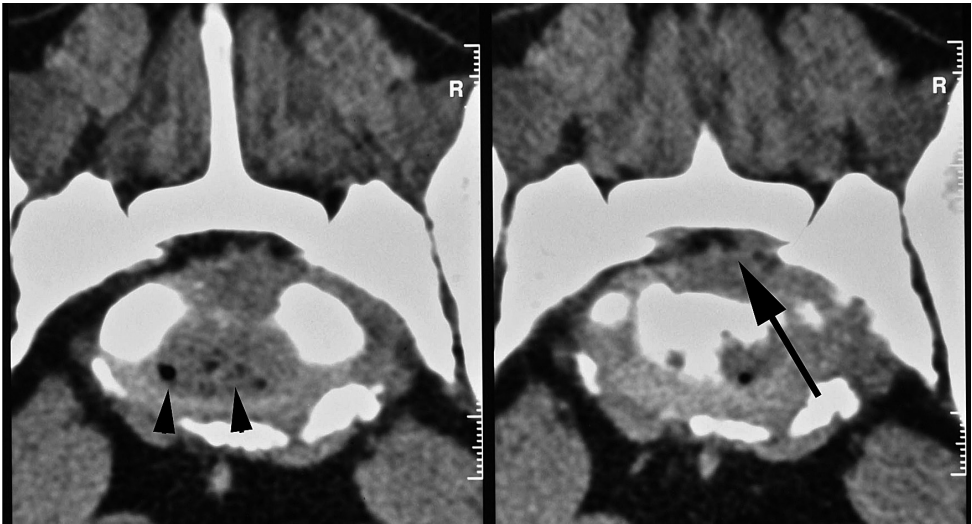


Figure 19. Transverse computed tomography images of the lumbosacral junction, showing vacuum phenomenon (arrowheads) resulting from IVD degeneration, and ventrodorsal compression of the dural sac by mid-centric dorsal protrusion of the L7-S1 intervertebral disc (arrow).

Magnetic resonance imaging

Magnetic resonance imaging (MRI) is considered the best diagnostic method for imaging the IVD and associated soft tissue structures^{8,267}. MRI is superior to other techniques for the early detection of IVD degeneration (characterized by a decreased T2 (water) signal^{268,269}), and a grading system for objective staging of IVD degeneration has recently been validated for dogs²⁷⁰. In addition, MRI allows assessment of the spinal cord parenchyma itself, thereby enabling visualization the disc-evoked compression of the cord and the integrity of the cord^{271,272}. MRI findings in IVD degenerative disease include changes in IVD signal intensity, narrowing and collapse of the IVD space, displacement or loss of epidural fat, and changes in the shape and integrity of the spinal cord^{8,267,270} (Fig. 20). Another advantage of MRI is that it is possible to visualize fibrocartilaginous thromboembolic myelopathy, which is a common differential diagnosis of Hansen type I disc herniation. Also foraminal stenosis and lateralization of herniated IVD material can be identified using MRI^{9,273,274}. In CSM patients, dynamic compression using traction MRI can be performed^{271,275} (although myelography or even CT myelography might be more suitable to detect dynamic spinal cord compression). In DLSS patients, MRI provides information about dural sac compression and cauda equine nerve root displacement^{9,273}.

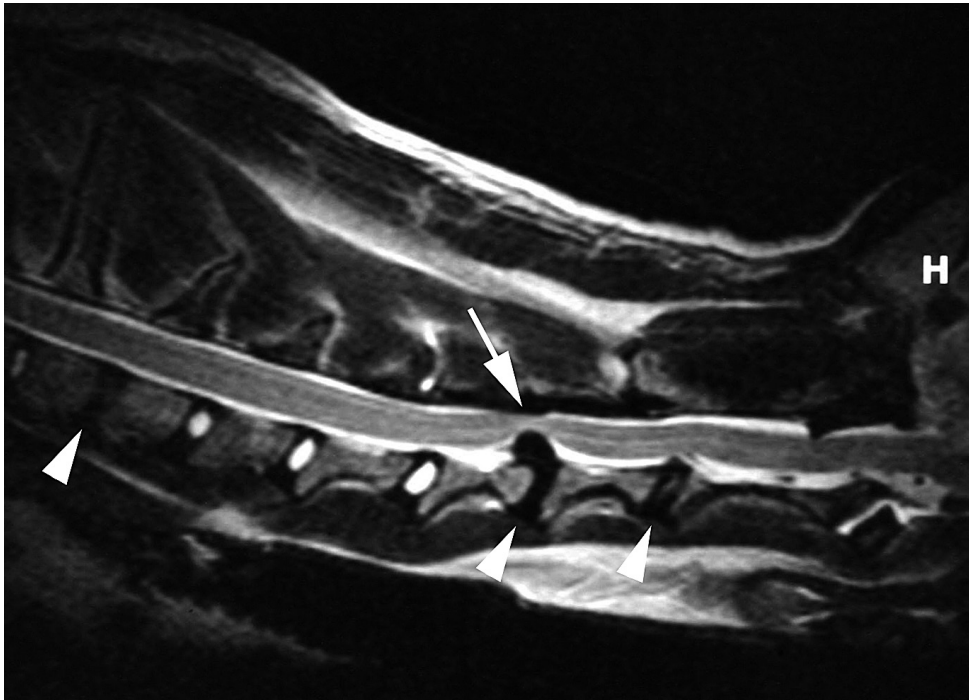


Figure 20. Preoperative mid-sagittal T2-weighted magnetic resonance image of the cervical spine of a 5-year-old Labrador Retriever, showing loss of the nucleus pulposus water signal of the C2-C3, C3-C4, C7-T1 intervertebral discs (arrowheads), dorsal extrusion (Type I herniation) of the nucleus pulposus at C3-C4, and spinal cord compression (arrow). H: Head.

Objective gait analysis

Kinesiology is the science of animal motion and includes kinetics (forces which effect motion) and kinematics (the temporal and geometric characteristics of motion). Interest in methods to objectively analyze the kinetics and kinematics of healthy and diseased canine gait has increased over the past 20 years²⁷⁶. In contrast to subjective evaluation, the assessment of canine gait using computer-assisted methods of analysis provides objective data. Moreover, a clinician is only able to perceive a few kinematic variables at a time, whereas computer-assisted analysis systems can capture, analyze, and store numerous observations per second. Kinetic and kinematic analysis allow accurate assessment of normal and abnormal gait, identification of characteristic features of specific gait abnormalities, and quantification of gait so that numeric comparisons can be made between different populations, thereby making it possible to objectively assess the effects of treatment^{276,277}.

Kinetics: force plate analysis

Force plate analysis involves quantification of the ground reaction forces involved in the stance phase of locomotion. The vertical (gravity), mediolateral, propulsive, and braking forces involved in paw placement (ground reaction forces) are objectively measured using a force plate mounted flush with the walking surface^{276,277}. Force plate analysis has been used in the assessment of various diseases, including DLSS: the propulsive forces of the pelvic limbs in DLSS patients are significantly lower than those of healthy dogs, reflecting impaired use of the pelvic limbs due to cauda equina compression^{278,279}. In addition, force plate analysis has been used to assess the effects of decompressive surgery. Results showed that DLSS patients that had undergone dorsal laminectomy and partial discectomy had an improved hind limb function up to 6 months after surgery; however, pelvic limb function deteriorated in the long term, which may be the result of lumbosacral instability induced by surgery or progressive IVD degeneration^{278,279}.

Kinematic gait analysis

Kinematic gait analysis involves the quantification of the positions, velocities, accelerations, and angles of anatomical points, segments, and joints in three-dimensional space. The aim of kinematic analysis is to provide information regarding the three-dimensional motion of the musculoskeletal system. Markers are attached to the skin, positioned at predefined anatomical landmarks on the dog, and the detection of these markers during the dog's gait cycle allows objective measurement of various factors involved in the canine gait, such as joint angles, stride length, and stride symmetry.

Kinematic gait analysis has been used to investigate gait in various diseases, including spinal abnormalities²⁸⁰, hip dysplasia^{281,282}, anterior cruciate ligament rupture^{24,283}, and restricted carpal motion²⁸⁴, and to evaluate the effects of surgical interventions^{24,285}. Kinematic gait analysis of dogs with IVD disease can provide valuable information about the consequences of IVD disease on gait. In addition, since the diagnosis of IVD degenerative disease can be considered troublesome due to the reported discrepancies between diagnostic imaging modalities and surgery, and between degenerative changes and clinical signs, kinematic gait analysis may serve as a valuable addition to the diagnostic work-up. However, the accuracy and sensitivity of kinematic gait analysis as a research tool to investigate new treatments and as a diagnostic tool for patients with IVD degenerative disease need to be investigated further.

Treatment of IVD disease

There are several strategies for treating IVD degenerative disease (Fig. 21). Currently, all treatments for canine IVD degenerative disease can be regarded as salvage procedures and involve conservative treatment, decompressive surgery, and/or surgical fixation of the affected spinal segment. A major improvement would be to restore functionality to the disc, and novel techniques to restore, or, even more ideally, regenerate IVD tissue may be appropriate in patients in which the IVD is not beyond repair, i.e. earlier in the degenerative cascade and before complete collapse of the IVD space.

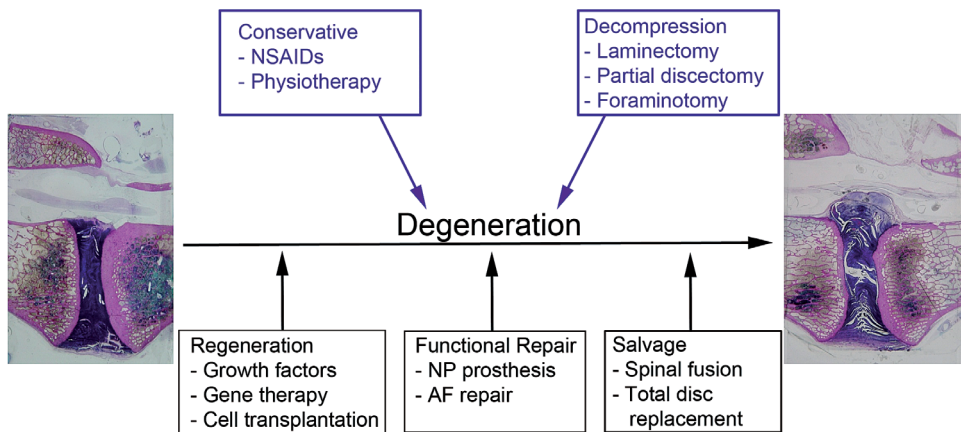


Figure 21. Current and new treatment strategies for intervertebral disc degeneration. Current strategies to treat intervertebral disc disease (purple boxes and letters) consist of conservative measures or surgical decompression. The new treatment strategies (black boxes and letters) can be applied at different stages of intervertebral disc degeneration, with salvage procedures being applied in late-stage degeneration/disease, functional repair being applied in intermediate-stage degeneration, and intervertebral disc regeneration being applied in early-stage degeneration. NP: Nucleus Pulposus; AF: Annulus Fibrosus.

Current Treatments

Conservative or medical treatment

Conservative treatment consists of providing analgesic support, often with non-steroidal anti-inflammatory drugs (NSAIDs) and opioids in the acute phase. Anti-inflammatory medication, consisting of corticosteroids or NSAIDs, is applied to counter the inflammatory response and to treat the spinal pain. NSAIDs are preferred to corticosteroids, because NSAIDs have similar analgesic and anti-inflammatory effects but significantly fewer side effects⁹. Controlled

and dosed exercise and physical therapy is also beneficial. Adjunct treatments, such as nutraceuticals and weight loss, are often used as well. Conservative treatment also consists of restricting activities that could exacerbate the neural compression, to prevent more NP material from herniating and to facilitate consolidation of the (partially) herniated disc. Extruded NP material is resorbed over a period of 4 to 6 weeks and the inflammation will settle, leading to resolution of the clinical signs. In addition, physical therapy can be started to prevent muscle atrophy due to disuse of muscles and to improve muscle tone, to maximize afferent sensory input in areas of deficit and to promote a normal range of movement, motion patterns, and function²⁸⁶. Conservative treatment is best suited for mild cases of IVD disease^{8,287,288}.

Surgical treatment

The decision to treat IVD patients surgically should be based on several factors, such as the severity of neurological signs, the severity of pain, the type and severity of compressive lesion(s), and the response to conservative therapy. General indications for surgery include clinical signs unresponsive to conservative treatment and the presence of neurological deficits⁸⁻¹⁰. The aim of surgery is to remove the compressive lesions and structures, such as the herniated IVD and hypertrophic ligaments, thereby alleviating neural compression. Once the decision has been made that surgery is the optimal treatment option, a wide array of surgical techniques are available to treat IVD-related compression. Direct decompressive procedures include ventral slot (cervical disc disease), inverted cone slot (CSM), dorsal laminectomy (DLSS), and hemilaminectomy (thoracolumbar disc disease), pediculotomy, corpectomy^{7-10,289}. Also, curettage or fenestration (nucleotomy) of the diseased disc or adjacent discs which may cause future disease is commonly performed⁸. Indirect decompressive techniques, such as distraction-stabilization/fusion, have also been described as treatment for CSM and DLSS^{9,10,290}. As decompression involves removing essential stabilizing structures, the decompressed segment can also be re-stabilized. A wide variety of techniques, including bone grafts, pins, screws, and cages, have been described for this purpose^{10,289-296}.

Ventral slot/inverted cone slot

In the case of ventral compression of the cervical spinal cord due to IVD herniation and CSM, a ventral approach is usually used. The degenerated IVD, including parts of the adjacent vertebrae, is removed by making a rectangular-shaped window/slot in the vertebrae and IVD (Fig. 22)^{10,289,297}. If necessary, the dorsal longitudinal ligament is excised to enable access to the vertebral canal, to allow the removal of extruded IVD material. However, the ventral approach allows limited removal of lateralized and dorsally located IVD material⁸.

Hemilaminectomy

Hemilaminectomy is the common procedure for decompression of the thoracolumbar spine^{8,152,298-300}. Hemilaminectomy is a technique similar to dorsal laminectomy; however, it involves a lateral approach and only the removal of the lamina on one side (Fig. 23). Hemilaminectomy is highly favored over dorsal laminectomy for treating thoracolumbar IVD patients, because it prevents removal of dorsal vertebral lamina resulting in less biomechanical instability of the thoracolumbar spine³⁰¹, it results in a significantly higher rate of postoperative neurologic improvement³⁰², and it involves a decreased risk of laminectomy membrane formation³⁰³. Positive clinical outcome has been associated with complete removal of the compressive disc material rather than simple vertebral canal decompression^{8,304}. Additional fenestration (nucleotomy) of the diseased IVD is commonly performed to prevent further extrusion of IVD material through the ruptured AF^{8,305}.

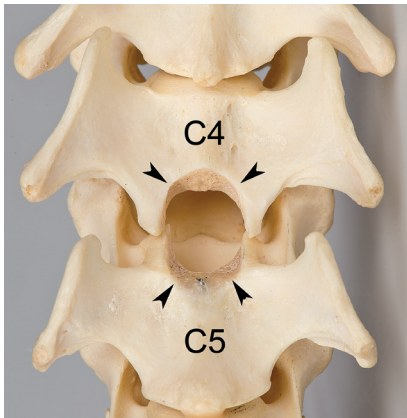


Figure 22. Ventral slot (arrowheads) of C4-C5, providing access to the cervical vertebral canal (asterisk).

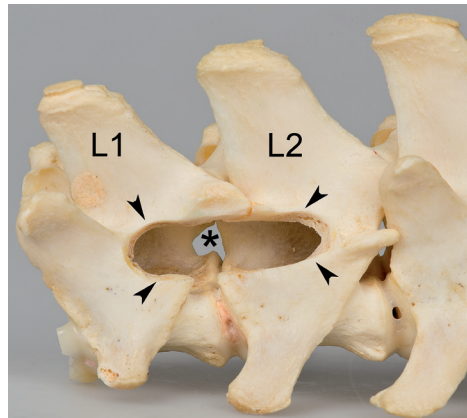


Figure 23. Left hemilaminectomy of L1-L2. After burring through the left lateral pedicle wall (arrowheads), disc material located in the vertebral canal (asterisk) can be removed.

IVD fenestration

Fenestration involves removal of degenerated NP material through a small incision in the AF. In CD patients, which usually show degeneration of multiple spinal segments, fenestration of thoracolumbar IVDs adjacent to the surgical lesion has been advocated to prevent future IVD herniation^{19,306-309}. The herniation recurrence rate after surgery without prophylactic fenestration is higher than after decompression with concurrent prophylactic fenestration of adjacent levels^{19,306-309}. However, degenerated IVDs still have a biomechanical function, and fenestration of the IVD has been shown to induce spinal instability

and increased postoperative morbidity¹¹⁴. Thus for the moment the value of prophylactic fenestration is debated.

Dorsal laminectomy

Dorsal laminectomy is the primary surgical procedure for DLSS (Fig. 24) and is commonly combined with partial discectomy, consisting of dorsal fenestration (dorsal annulectomy) and nuclear pulpectomy (nuclectomy), to adequately decompress the cauda equina nerve roots^{232,310-312}. In the case of nerve root compression, foraminotomy (widening of the intervertebral foramen) is applied to relieve spinal nerve compression^{232,310-312}. Foraminotomy without concurrent dorsal laminectomy has been reported in DLSS patients with nerve root compression without spinal canal stenosis²⁷³. In some cases, removal of the facet joints (facetectomy) can be performed; however, facetectomy should be avoided whenever possible as it increases lumbosacral instability¹¹⁷. The overall short-term prognosis after DLSS surgery is generally good to excellent, and improvement of clinical signs has been reported in 69% to 93% of surgically treated cases^{223,235,313,314}. However, in the long-term clinical signs recur in 3% to 37% of operated patients^{223,235,313,315}. Moreover, decompressive surgery does not completely restore hind limb propulsion in dogs with DLSS²⁴¹. These adverse outcomes may be due to lumbosacral instability after the decompressive procedure, with acceleration of degenerative changes in the lumbosacral spinal segment and recurrence of clinical signs^{223,235,313}.

Figure 24. Dorsal laminectomy of L7-S1, providing access to the vertebral canal and the L7-S1 intervertebral disc (asterisk).



Dorsal laminectomy of the cervical spine has been described for dorsal spinal cord compression associated with lamina malformation (so-called telescoping in the caudal apertura) and/or hypertrophy of the interarcuate ligament in dogs with CSM^{272,316}. However, dorsal laminectomy of the cervical spine is an

invasive procedure associated with postoperative pain and further neurological deterioration ³¹⁶.

Vertebral distraction/stabilization techniques

A wide variety of distraction/fusion techniques have been described for the treatment of CSM in particular, but also for the treatment of DLSS ^{10,289-296}. In CSM patients with a single dynamic compression, the affected spinal segment can be decompressed by a complete or partial ventral slot, after which the spinal segment is distracted and stabilized by ventral insertion of pins or screws into the vertebrae and fixation of the vertebrae with a polymethyl metacrylate (PMMA) bridge. The long-term success rate of this technique is 73% ³¹⁷; however, pin or screw placement is challenging and screw misplacement can result in penetration of the spinal cord or the foramina ³¹⁷⁻³¹⁹.

Another popular method of fixation of the cervical spine (specifically for Doberman Pinschers affected by CSM) involves distraction of the affected spinal segment and insertion of an intervertebral washer and transvertebral screw. After distraction of the vertebral bodies, a 5- or 7-mm metal washer is inserted into the IVD space. The spinal segment is further stabilized by drilling a transvertebral screw in a caudodorsal direction through the two adjacent vertebrae and through the washer ^{10,320}.

A third distraction technique described for the cervical spine involves drilling multiple holes into the cranial and caudal EPs of the affected spinal segment (after performing a ventral slot procedure). The segment is distracted and then PMMA is applied into the defect and into the excavated IVD, thereby stabilizing the operated spinal segment. The construct can be strengthened by applying a ventrally positioned cancellous bone graft over the vertebral bodies ^{10,289,321}.

In DLSS patients, stabilization of the lumbosacral junction is indicated if lumbosacral spondylolisthesis of S1 is present, or if it is necessary to correct or prevent progression of lumbosacral instability ⁹. Distraction-fusion of the lumbosacral junction involves enlarging the collapsed lumbosacral IVD space and foramina, thereby relieving the pressure on the nerve roots, and stabilizing the lumbosacral junction by inserting pins from the base of the L7 spinous process through the facet joints into the sacrum and the iliac wings ⁷. In addition, distraction of the lumbosacral junction, followed by removal of the articular cartilage of the facet joints and insertion of cortical bone screws ventrolaterally across the facets through the sacrum, has also been described ³¹. Although some clinical results of the above-described procedures have been reported, long-term follow-up information is not available.

A surgical procedure to adequately stabilize the lumbosacral spine has not been developed. In human medicine, surgical decompression combined with pedicle screw-rod fixation of the spinal segment has long been used to successfully

treat spinal stenosis, spinal instability, and degenerative disc disease ^{21,22}. The procedure may be valuable for treating DLSS patients, and therefore requires further evaluation (Fig. 25).

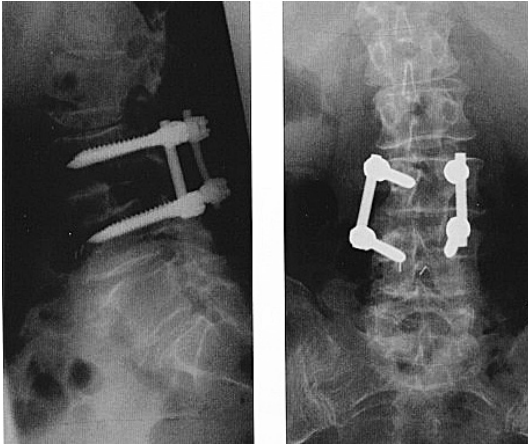


Figure 25. Lateral (left) and anteroposterior radiograph (right) of a human lumbar spine, stabilized using pedicle screw-rod fixation

Functional repair of the IVD

The above-described treatments can be regarded as salvage procedures: they are symptomatic and the compressive lesion is removed with or without stabilization of the spinal segment. However, the functionality of the IVD is not restored. Moreover, these surgical procedures all lead to altered biomechanics of the spinal segment: decompressive surgery without stabilization results in spinal instability, which may lead to recurrence of clinical signs ^{114,117}. While stabilization prevents degeneration of the decompressed spinal segment, it is associated with degeneration of the adjacent spinal segments, a phenomenon referred to as adjacent segment disease or the ‘domino effect’ ³²²⁻³²⁴. These complications have prompted interest in new technologies to restore the functionality of the IVD following decompression.

If IVD degeneration has not progressed beyond repair, the IVD may be repaired by replacing the diseased NP with a NP prosthesis (NPP) (Fig. 26) ^{325,326}. A novel, biocompatible, hydrogel NPP has recently been developed ^{325,327,328}. It is implanted in dry form, enabling insertion of the NPP through a small annular opening. After insertion, the prosthesis is allowed to expand *in situ* and reaches its final dimensions within 18 hours of placement. The prosthesis fills up the entire NP cavity created after nucleotomy (confinement), which is essential to achieve a physiological distribution of stress in the disc and to minimize the risk of implant migration. The NPP consists of an intrinsically radiopaque hydrogel, which makes it optimally visible on X-ray fluoroscopy, CT, and MRI ^{325,327,328}.

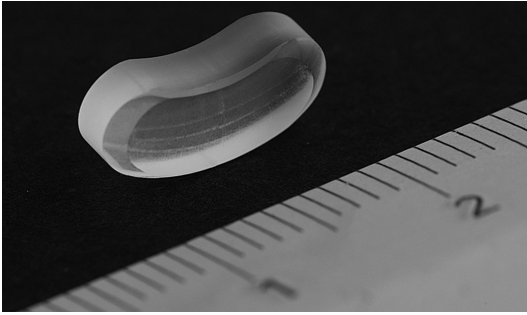


Figure 26. A hydrogel nucleus pulposus prosthesis, designed to mimic the dimensions and shape of the natural nucleus pulposus. The scale is in cm.

The physical-mechanical material properties of this NPP have been assessed by means of swelling and diffusion testing, static and dynamic mechanical testing, and creep and fatigue testing^{325,327,328}. However, before this technique can be used in canine IVD patients, the applicability of the surgical technique in the canine spine and the functionality of this concept need to be investigated.

Regeneration of the IVD

The optimal method for restoring IVD functionality would be to return the IVD to its healthy state, i.e. regeneration of the degenerated IVD tissue. Regeneration of the IVD involves the prevention, inhibition, and/or reversal of degenerative processes by concomitantly stimulating ECM synthesis and decreasing, and ideally reversing, ECM degradation^{329,330}. A prerequisite for IVD regeneration is that the IVD cells and environment still have the capability to produce, and thus restore, a healthy ECM³²⁹. Different strategies for biological repair of the degenerated IVD can be used, including the use of growth factors and anticatabolic agents, gene therapy, and cell-based strategies^{329,331-334}. Examples of such strategies include the application of tissue inhibitor of metalloproteinase (TIMP)-1 (anticatabolic) and bone morphogenetic protein (BMP)-7/osteogenic protein (OP)-1 (anabolic)^{329,331-334}. However, before any of these strategies can be used, it is important to consider the key steps in the degenerative process. A key factor initiating early degeneration, leading to the transformation of an optimal to a less optimal matrix, involves the disappearance of notochordal cells from the NP^{3,23,56}. Notochordal cells have been shown to positively influence the activity of surrounding chondrocyte-like cells and their homeostasis^{3,23,56,188} and have gained increased attention as a potential NP progenitor cell^{169,335,336}. In order to further characterize notochordal cells and their role in the degenerative process, it is important to investigate biomolecular signaling pathways involved in IVD degeneration.

In summary, the IVD is an essential stabilizing and mobilizing component of the spine. IVD degeneration is common and involves numerous cellular, biochemical, and biomechanical processes. IVD disease is a well-described phenomenon in veterinary medicine. The diagnosis and treatment of IVD

degenerative disease can be refined further, thereby facilitating early diagnosis and early treatment of IVD patients, which could lead to better outcomes and improved quality of life. However, much still needs to be learned about the fundamental processes involved in IVD degeneration, knowledge which may aid our understanding of the degenerative process and facilitate the development of novel strategies to regenerate the IVD.

References

1. Paulson DR: The Phylum Chordata: Classification, External Anatomy, and Adaptive Radiation, in Wake MH (ed): Hyman's Comparative Vertebrate Anatomy (ed 3), Chicago, The University of Chicago Press, 1992, pp 7-56.
2. Dyce KM, Sack WO, Wensing CJG: The Neck, Back, and Vertebral Column of the Dog and Cat, in Dyce KM, Sack WO, Wensing CJG (eds): Textbook of Veterinary Anatomy (ed 4), Vol. Philadelphia London New York St. Louis Sydney Toronto, Saunders Elsevier, 2010, pp 407-419.
3. Hansen HJ: A pathologic-anatomical study on disc degeneration in dog, with special reference to the so-called enchondrosis intervertebralis. *Acta Orthop Scand Suppl* 11:1-117, 1952.
4. Evans HE, Christensen GC: Joints and Ligaments, in Evans HE, Christensen GC (eds): Miller's Anatomy of the Dog (ed 2), Vol. Philadelphia London Toronto, W.B. Saunders Company, 1979, pp 225-268.
5. Hukins DWL: Disc Structure and Function, in Ghosh P (ed): The Biology of the Intervertebral Disc (ed 1), Vol 1. Boca Raton, Florida, CRC Press, Inc., 1988, pp 1-38.
6. Bray JP, Burbidge HM: The canine intervertebral disk: part one: structure and function. *J Am Anim Hosp Assoc* 34:55-63, 1998.
7. Sharp NJH, Wheeler SJ: Thoracolumbar and Lumbosacral disease, in Sharp NJH, Wheeler SJ (eds): Small Animal Spinal Disorders. Diagnosis and Surgery (ed 2), Vol. Edinburgh, Elsevier Mosby, 2005, pp 121-209.
8. Brisson BA: Intervertebral disc disease in dogs. *Vet Clin North Am Small Anim Pract* 40:829-858, 2010.
9. Meij BP, Bergknut N: Degenerative lumbosacral stenosis in dogs. *Vet Clin North Am Small Anim Pract* 40:983-1009, 2010.
10. da Costa RC: Cervical spondylomyelopathy (wobbler syndrome) in dogs. *Vet Clin North Am Small Anim Pract* 40:881-913, 2010.
11. Suwankong N, Meij BP, Voorhout G, et al: Review and retrospective analysis of degenerative lumbosacral stenosis in 156 dogs treated by dorsal laminectomy. *Vet Comp Orthop Traumatol* 21:285-293, 2008.
12. da Costa RC, Parent JM, Partlow G, et al: Morphologic and morphometric magnetic resonance imaging features of Doberman Pinschers with and without clinical signs of cervical spondylomyelopathy. *Am J Vet Res* 67:1601-1612, 2006.
13. Jones JC, Inzana KD: Subclinical CT abnormalities in the lumbosacral spine of older large-breed dogs. *Vet Radiol Ultrasound* 41:19-26, 2000.
14. Janson: *Schweizer Archiv für Tierheilk* 7:211, 1881.
15. Dexler H: *Zeitschriften für tierheilkunde* 7, 1896.
16. Tillmanns S: Beitrag zur enchondrosis intervertebralis und den dadurch bedingten Compression des Rückenmarks des Hundes. 1939.
17. Hansen HJ: A pathologic-anatomical interpretation of disc degeneration in dogs. *Acta Orthop Scand* 20:280-293, 1951.
18. Olsson SE, Hansen HJ: Cervical disc protrusions in the dog. *J Am Vet Med Assoc* 121:361-370, 1952.

19. Olsson SE: On disc protrusion in dog (enchondrosis intervertebralis); a study with special reference to roentgen diagnosis and to the value of disc fenestration. *Acta Orthop Scand Suppl* 8:1-95, 1951.
20. Hansen HJ: Comparative views of the pathology of disk degeneration in animals. *Laboratory investigation; a journal of technical methods and pathology* 8:1242-1265, 1959.
21. Ghosh P, Taylor TK, Yarroll JM: Genetic factors in the maturation of the canine intervertebral disc. *Res Vet Sci* 19:304-311, 1975.
22. Ghosh P, Taylor TK, Braund KG, et al: A comparative chemical and histochemical study of the chondrodystrophoid and nonchondrodystrophoid canine intervertebral disc. *Vet Pathol* 13:414-427, 1976.
23. Braund KG, Ghosh P, Taylor TK, et al: Morphological studies of the canine intervertebral disc. The assignment of the beagle to the achondroplastic classification. *Res Vet Sci* 19:167-172, 1975.
24. Braund KG, Ghosh P, Taylor TK, et al: The qualitative assessment of glycosaminoglycans in the canine intervertebral disc using a critical electrolyte concentration staining technique. *Res Vet Sci* 21:314-317, 1976.
25. Ghosh P, Taylor TK, Braund KG: The variation of the glycosaminoglycans of the canine intervertebral disc with ageing. I. Chondrodystrophoid breed. *Gerontology* 23:87-98, 1977.
26. Ghosh P, Taylor TK, Braund KG: Variation of the glycosaminoglycans of the intervertebral disc with ageing. II. Non-chondrodystrophoid breed. *Gerontology* 23:99-109, 1977.
27. Ghosh P, Taylor TK, Braund KG, et al: The collagenous and non-collagenous protein of the canine intervertebral disc and their variation with age, spinal level and breed. *Gerontology* 22:124-134, 1976.
28. Cole TC, Burkhardt D, Frost L, et al: The proteoglycans of the canine intervertebral disc. *Biochim Biophys Acta* 839:127-138, 1985.
29. Cole TC, Ghosh P, Taylor TK: Variations of the proteoglycans of the canine intervertebral disc with ageing. *Biochim Biophys Acta* 880:209-219, 1986.
30. Royal AB, Chigerwe M, Coates JR, et al: Cytologic and histopathologic evaluation of extruded canine degenerate disks. *Vet Surg* 38:798-802, 2009.
31. Johnson JA, da Costa RC, Allen MJ: Micromorphometry and cellular characteristics of the canine cervical intervertebral discs. *J Vet Intern Med* 24:1343-1349, 2010.
32. MacGeady TA, Quinn PJ, FitzPatrick ES: Establishment of the basic body plan, in MacGeady TA, Quinn PJ, FitzPatrick ES (eds): *Veterinary Embryology*, Oxford, Blackwell Publishing, 2006, pp 54-58.
33. Vejlsted M: Cellular and Molecular Mechanisms of Embryonic Development, in Hyttel P, Sinowatz F, Vejlsted M (eds): *Essentials of Domestic Animal Embryology* (ed 1), Edinburg London New York Oxford Philadelphia St. Louis Sydney Toronto, Saunders Elsevier, 2010, pp 13-24.
34. Stemple DL: Structure and function of the notochord: an essential organ for chordate development. *Development* 132:2503-2512, 2005.
35. Vejlsted M: Gastrulation, Body Folding and Coelum Formation, in Hyttel P, Sinowatz F, Vejlsted M (eds): *Essentials of Domestic Animal Embryology* (ed 1), Edinburg London New York Oxford Philadelphia St. Louis Sydney Toronto, Saunders Elsevier, 2010, pp 79-94.

36. MacGeady TA, Quinn PJ, FitzPatrick ES: Muscular and Skeletal Systems, in MacGeady TA, Quinn PJ, FitzPatrick ES (eds): *Veterinary Embryology*, Oxford, Blackwell Publishing, 2006, pp 184-204.
37. Sinowatz F: Musculo-skeletal System, in Hyttel P, Sinowatz F, Vejlsted M (eds): *Essentials of Domestic Animal Embryology* (ed 1), Edinburg London New York Oxford Philadelphia St. Louis Sydney Toronto, Saunders Elsevier, 2010, pp 286-316.
38. Smits P, Lefebvre V: Sox5 and Sox6 are required for notochord extracellular matrix sheath formation, notochord cell survival and development of the nucleus pulposus of intervertebral discs. *Development* 130:1135-1148, 2003.
39. McCann MR, Tamplin OJ, Rossant J, et al: Tracing notochord-derived cells using a Noto-cre mouse: implications for intervertebral disc development. *Dis Model Mech* 5: 73-82, 2012.
40. Urban JP, Maroudas A: Swelling of the intervertebral disc in vitro. *Connect Tissue Res* 9:1-10, 1981.
41. Hendry NG: The hydration of the nucleus pulposus and its relation to intervertebral disc derangement. *J Bone Joint Surg Br* 40-B:132-144, 1958.
42. Samuelson DA: Cartilage and Bone, in Samuelson DA (ed): *Textbook of Veterinary Histology*, St. Louis, Missouri, Saunders Elsevier, 2007, pp 100-129.
43. Butler WF: Comparative Anatomy and Development of the Mammalian Disc, in Ghosh P (ed): *The Biology of the Intervertebral Disc* (ed 1), Vol 1. Boca Raton, Florida, CRC Press, Inc., 1988, pp 83-108.
44. Eurell JA, van Sickle DC: Connective and Supportive Tissues, in Eurell JA, Frappier BL (eds): *Dellmann's Textbook of Veterinary Histology* (ed 6), Vol. Ames, Iowa, Blackwell Publishing, 2006, pp 31-60.
45. Inoue H: Three-dimensional architecture of lumbar intervertebral discs. *Spine (Phila Pa 1976)* 6:139-146, 1981.
46. Crock HV: The arterial supply and venous drainage of the vertebral column of the dog. *J Anat* 94:88-99, 1960.
47. Crock HV, Goldwasser M: Anatomic studies of the circulation in the region of the vertebral end-plate in adult Greyhound dogs. *Spine (Phila Pa 1976)* 9:702-706, 1984.
48. Forsythe WB, Ghoshal NG: Innervation of the canine thoracolumbar vertebral column. *Anat Rec* 208:57-63, 1984.
49. Willenegger S, Friess AE, Lang J, et al: Immunohistochemical demonstration of lumbar intervertebral disc innervation in the dog. *Anat Histol Embryol* 34:123-128, 2005.
50. Holm S, Selstam G, Nachemson A: Carbohydrate metabolism and concentration profiles of solutes in the canine lumbar intervertebral disc. *Acta Physiol Scand* 115:147-156, 1982.
51. Holm S, Maroudas A, Urban JP, et al: Nutrition of the intervertebral disc: solute transport and metabolism. *Connect Tissue Res* 8:101-119, 1981.
52. Urban JP, Holm S, Maroudas A: Diffusion of small solutes into the intervertebral disc: an in vivo study. *Biorheology* 15:203-221, 1978.
53. Urban JP, Holm S, Maroudas A, et al: Nutrition of the intervertebral disk. An in vivo study of solute transport. *Clin Orthop Relat Res*:101-114, 1977.
54. Urban JP, Smith S, Fairbank JC: Nutrition of the intervertebral disc. *Spine (Phila Pa 1976)* 29:2700-2709, 2004.

55. Maroudas A: Nutrition and Metabolism of the Intervertebral Disc, in Ghosh P (ed): The Biology of the Intervertebral Disc (ed 1), Vol 2. Boca Raton, Florida, CRC Press, Inc., 1988, pp 1-39.
56. Cappello R, Bird JL, Pfeiffer D, et al: Notochordal cells produce and assemble extracellular matrix in a distinct manner, which may be responsible for the maintenance of healthy nucleus pulposus. *Spine (Phila Pa 1976)* 31:873-882, 2006.
57. Hunter CJ, Matyas JR, Duncan NA: The three-dimensional architecture of the notochordal nucleus pulposus: novel observations on cell structures in the canine intervertebral disc. *J Anat* 202:279-291, 2003.
58. Hunter CJ, Matyas JR, Duncan NA: Cytomorphology of notochordal and chondrocytic cells from the nucleus pulposus: a species comparison. *J Anat* 205:357-362, 2004.
59. Hunter CJ, Matyas JR, Duncan NA: The functional significance of cell clusters in the notochordal nucleus pulposus: survival and signaling in the canine intervertebral disc. *Spine (Phila Pa 1976)* 29:1099-1104, 2004.
60. Trout JJ, Buckwalter JA, Moore KC, et al: Ultrastructure of the human intervertebral disc. I. Changes in notochordal cells with age. *Tissue Cell* 14:359-369, 1982.
61. Hunter CJ, Bianchi S, Cheng P, et al: Osmoregulatory function of large vacuoles found in notochordal cells of the intervertebral disc running title: an osmoregulatory vacuole. *Mol Cell Biomech* 4:227-237, 2007.
62. Guehring T, Urban JP, Cui Z, et al: Noninvasive 3D vital imaging and characterization of notochordal cells of the intervertebral disc by femtosecond near-infrared two-photon laser scanning microscopy and spatial-volume rendering. *Microsc Res Tech* 71:298-304, 2008.
63. Butler WF, Fujioka T: Fine structure of the nucleus pulposus of the intervertebral disc of the cat. *Anat Anz* 132:465-475, 1972.
64. Chen J, Yan W, Setton LA: Molecular phenotypes of notochordal cells purified from immature nucleus pulposus. *Eur Spine J* 15 Suppl 3:S303-311, 2006.
65. Bergknut N, Meij BP, Hagman R, et al: Intervertebral disc disease in dogs – Part 1: A new histological grading scheme for classification of intervertebral disc degeneration in dogs. *Vet J* 2012, July 10, Epub ahead of print.
66. Bergknut N, Rutges JP, Kranenburg HJ, et al: The dog as an animal model for intervertebral disc degeneration? *Spine* 37:351-358, 2012.
67. Holm S, Nachemson A: Nutritional changes in the canine intervertebral disc after spinal fusion. *Clin Orthop Relat Res*:243-258, 1982.
68. Holm S, Nachemson A: Variations in the nutrition of the canine intervertebral disc induced by motion. *Spine* 8:866-874, 1983.
69. Johnson EF, Caldwell RW, Berryman HE, et al: Elastic fibers in the anulus fibrosus of the dog intervertebral disc. *Acta Anat (Basel)* 118:238-242, 1984.
70. Roberts S, Menage J, Urban JP: Biochemical and structural properties of the cartilage endplate and its relation to the intervertebral disc. *Spine (Phila Pa 1976)* 14:166-174, 1989.
71. Antoniou J, Goudsouzian NM, Heathfield TF, et al: The human lumbar endplate. Evidence of changes in biosynthesis and denaturation of the extracellular matrix with growth, maturation, aging, and degeneration. *Spine (Phila Pa 1976)* 21:1153-1161, 1996.
72. Roughley PJ: Articular cartilage and changes in arthritis: noncollagenous proteins and proteoglycans in the extracellular matrix of cartilage. *Arthritis Res* 3:342-347, 2001.

73. Roberts S, McCall IW, Menage J, et al: Does the thickness of the vertebral subchondral bone reflect the composition of the intervertebral disc? *Eur Spine J* 6:385-389, 1997.
74. Roughley PJ: Biology of intervertebral disc aging and degeneration: involvement of the extracellular matrix. *Spine* 29:2691-2699, 2004.
75. Rutges J, Kummer J, Oner F, et al: Increased MMP-2 activity during intervertebral disc degeneration is correlated to MMP-14 levels. *J Pathol* 214:523-530, 2008.
76. Neidlinger-Wilke C, Wurtz K, Urban JP, et al: Regulation of gene expression in intervertebral disc cells by low and high hydrostatic pressure. *Eur Spine J* 15 Suppl 3:S372-378, 2006.
77. Melrose J, Taylor TK, Ghosh P: The serine proteinase inhibitory proteins of the chondrodystrophoid (beagle) and non-chondrodystrophoid (greyhound) canine intervertebral disc. *Electrophoresis* 18:1059-1063, 1997.
78. Melrose J, Taylor TK, Ghosh P: Variation in intervertebral disc serine proteinase inhibitory proteins with ageing in a chondrodystrophoid (beagle) and a non-chondrodystrophoid (greyhound) canine breed. *Gerontology* 42:322-329, 1996.
79. Erwin WM, Ashman K, O'Donnel P, et al: Nucleus pulposus notochord cells secrete connective tissue growth factor and up-regulate proteoglycan expression by intervertebral disc chondrocytes. *Arthritis Rheum* 54:3859-3867, 2006.
80. White AA, 3rd, Panjabi MM: Clinical biomechanics of the spine. Philadelphia Toronto, J.B. Lippincott Company, 1978.
81. Adams MA, Hutton WC: Mechanics of the Intervertebral Disc, in Ghosh P (ed): *The Biology of the Intervertebral Disc* (ed 1), Vol 2. Boca Raton, Florida, CRC Press, Inc., 1988, pp 39-73.
82. Smit TH: The use of a quadruped as an in vivo model for the study of the spine - biomechanical considerations. *Eur Spine J* 11:137-144, 2002.
83. Zimmerman MC, Vuono-Hawkins M, Parsons JR, et al: The mechanical properties of the canine lumbar disc and motion segment. *Spine* 17:213-220, 1992.
84. Setton LA, Chen J: Mechanobiology of the intervertebral disc and relevance to disc degeneration. *J Bone Joint Surg Am* 88 Suppl 2:52-57, 2006.
85. Adams MA, McMillan DW, Green TP, et al: Sustained loading generates stress concentrations in lumbar intervertebral discs. *Spine* 21:434-438, 1996.
86. Holm S, Nachemson A: Variations in the nutrition of the canine intervertebral disc induced by motion. *Spine (Phila Pa 1976)* 8:866-874, 1983.
87. Adams MA, Roughley PJ: What is intervertebral disc degeneration, and what causes it? *Spine (Philadelphia, Pa 1976)* 31:2151-2161, 2006.
88. Buckwalter JA: Aging and degeneration of the human intervertebral disc. *Spine* 20:1307-1314, 1995.
89. Bergknut N, Grinwis GCM, Pickee EB, et al: Reliability of macroscopic grading of intervertebral disk degeneration in dogs by use of the Thompson system and comparison with low-field magnetic resonance imaging findings. *Am J of Vet Res* 72:899-904, 2011.
90. Thompson JP, Pearce RH, Schechter MT, et al: Preliminary evaluation of a scheme for grading the gross morphology of the human intervertebral disc. *Spine* 15:411-415, 1990.
91. Aigner T, Gresk-otter KR, Fairbank JC, et al: Variation with age in the pattern of type X collagen expression in normal and scoliotic human intervertebral discs. *Calcif Tissue Int* 63:263-268, 1998.

92. Bernick S, Cailliet R: Vertebral end-plate changes with aging of human vertebrae. *Spine (Phila Pa 1976)* 7:97-102, 1982.
93. Roberts S, Urban JP, Evans H, et al: Transport properties of the human cartilage endplate in relation to its composition and calcification. *Spine (Phila Pa 1976)* 21:415-420, 1996.
94. Oda J, Tanaka H, Tsuzuki N: Intervertebral disc changes with aging of human cervical vertebra. From the neonate to the eighties. *Spine (Phila Pa 1976)* 13:1205-1211, 1988.
95. Meij BP, Bergknut N: Degenerative lumbosacral stenosis. *Vet Clin North Am Small Anim Pract* 40, 983-1009, 2010.
96. Kim KW, Kim YS, Ha KY, et al: An autocrine or paracrine Fas-mediated counterattack: a potential mechanism for apoptosis of notochordal cells in intact rat nucleus pulposus. *Spine* 30:1247-1251, 2005.
97. Kim KW, Lim TH, Kim JG, et al: The origin of chondrocytes in the nucleus pulposus and histologic findings associated with the transition of a notochordal nucleus pulposus to a fibrocartilaginous nucleus pulposus in intact rabbit intervertebral discs. *Spine (Phila Pa 1976)* 28:982-990, 2003.
98. Risbud MV, Schaer TP, Shapiro IM: Toward an understanding of the role of notochordal cells in the adult intervertebral disc: from discord to accord. *Dev Dyn* 239:2141-2148, 2010.
99. Erwin WM: The enigma that is the nucleus pulposus cell: the search goes on. *Arthritis Res Ther* 12:118, 2010.
100. Minogue BM, Richardson SM, Zeef LA, et al: Transcriptional profiling of bovine intervertebral disc cells: implications for identification of normal and degenerate human intervertebral disc cell phenotypes. *Arthritis Res Ther* 12:R22, 2010.
101. Shapiro IM, Risbud MV: Transcriptional profiling of the nucleus pulposus: say yes to notochord. *Arthritis Res Ther* 12:117, 2010.
102. Choi KS, Cohn MJ, Harfe BD: Identification of nucleus pulposus precursor cells and notochordal remnants in the mouse: implications for disk degeneration and chordoma formation. *Dev Dyn* 237:3953-3958, 2008.
103. Seiler G, Hani H, Scheidegger J, et al: Staging of lumbar intervertebral disc degeneration in nonchondrodystrophic dogs using low-field magnetic resonance imaging. *Vet Radiol Ultrasound* 44:179-184, 2003.
104. Puustjarvi K, Takala T, Wang W, et al: Enhanced prolylhydroxylase activity in the posterior annulus fibrosus of canine intervertebral discs following long-term running exercise. *Eur Spine J* 2:126-131, 1993.
105. Kaapa E, Zhang LQ, Muona P, et al: Expression of type I, III, and VI collagen mRNAs in experimentally injured porcine intervertebral disc. *Connect Tissue Res* 30:203-214, 1994.
106. Kaapa E, Wang W, Takala TE, et al: Elevated protein content and prolyl 4-hydroxylase activity in severely degenerated human annulus fibrosus. *Connect Tissue Res* 41:93-99, 2000.
107. Schmorl CG: Die pathologische Anatomie der Wirbelsäule. *Verhandlungen der Deutschen orthopädischen Gesellschaft* 21:3-41, 1926.
108. Alini M, Eisenstein SM, Ito K, et al: Are animal models useful for studying human disc disorders/degeneration? *Eur Spine J* 17:2-19, 2008.
109. Mitchell RA, Innes JF, McNally D: Pressure profilometry of the lumbosacral disk in dogs. *Am J Vet Res* 62:1734-1739, 2001.

110. Adams MA, McNally DS, Dolan P: 'Stress' distributions inside intervertebral discs. The effects of age and degeneration. *J Bone Joint Surg Br* 78:965-972, 1996.
111. McNally DS, Adams MA: Internal intervertebral disc mechanics as revealed by stress profilometry. *Spine (Phila Pa 1976)* 17:66-73, 1992.
112. McNally DS, Shackelford IM, Goodship AE, et al: In vivo stress measurement can predict pain on discography. *Spine (Phila Pa 1976)* 21:2580-2587, 1996.
113. Adams MA, Freeman BJ, Morrison HP, et al: Mechanical initiation of intervertebral disc degeneration. *Spine (Phila Pa 1976)* 25:1625-1636, 2000.
114. Macy NB, Les CM, Stover SM, et al: Effect of disk fenestration on sagittal kinematics of the canine C5-C6 intervertebral space. *Vet Surg* 28:171-179, 1999.
115. Hill TP, Lubbe AM, Guthrie AJ: Lumbar spine stability following hemilaminectomy, pediclectomy, and fenestration. *Vet Comp Orthop Traumatol* 13:165-171, 2000.
116. Schulz KS, Waldron DR, Grant JW, et al: Biomechanics of the thoracolumbar vertebral column of dogs during lateral bending. *Am J Vet Res* 57:1228-1232, 1996.
117. Smith MEH, Bebachuk TN, Shmon CL, et al: An in vitro biomechanical study of the effects of surgical modification upon the canine lumbosacral spine. *Vet Comp Orthop Traumatol* 17:17-24, 2004.
118. Osti OL, Fraser RD: MRI and discography of annular tears and intervertebral disc degeneration. A prospective clinical comparison. *J Bone Joint Surg Br* 74:431-435, 1992.
119. Osti OL, Vernon-Roberts B, Moore R, et al: Annular tears and disc degeneration in the lumbar spine. A post-mortem study of 135 discs. *J Bone Joint Surg Br* 74:678-682, 1992.
120. Horst M, Brinckmann P: 1980 Volvo award in biomechanics. Measurement of the distribution of axial stress on the end-plate of the vertebral body. *Spine (Phila Pa 1976)* 6:217-232, 1981.
121. Grant JP, Oxland TR, Dvorak MF, et al: The effects of bone density and disc degeneration on the structural property distributions in the lower lumbar vertebral endplates. *J Orthop Res* 20:1115-1120, 2002.
122. Brinckmann P, Frobin W, Hierholzer E, et al: Deformation of the vertebral end-plate under axial loading of the spine. *Spine (Phila Pa 1976)* 8:851-856, 1983.
123. Moore RJ, Vernon-Roberts B, Osti OL, et al: Remodeling of vertebral bone after outer anular injury in sheep. *Spine (Phila Pa 1976)* 21:936-940, 1996.
124. Natarajan RN, Ke JH, Andersson GB: A model to study the disc degeneration process. *Spine (Phila Pa 1976)* 19:259-265, 1994.
125. Tanaka M, Nakahara S, Inoue H: A pathologic study of discs in the elderly. Separation between the cartilaginous endplate and the vertebral body. *Spine (Phila Pa 1976)* 18:1456-1462, 1993.
126. Kahmann RD, Buttermann GR, Lewis JL, et al: Facet loads in the canine lumbar spine before and after disc alteration. *Spine (Phila Pa 1976)* 15:971-978, 1990.
127. Yang KH, King AI: Mechanism of facet load transmission as a hypothesis for low-back pain. *Spine (Phila Pa 1976)* 9:557-565, 1984.
128. Keller TS, Hansson TH, Abram AC, et al: Regional variations in the compressive properties of lumbar vertebral trabeculae. Effects of disc degeneration. *Spine (Phila Pa 1976)* 14:1012-1019, 1989.
129. Kirkaldy-Willis WH, Farfan HF: Instability of the lumbar spine. *Clin Orthop Relat Res*:110-123, 1982.

130. Mimura M, Panjabi MM, Oxland TR, et al: Disc degeneration affects the multidirectional flexibility of the lumbar spine. *Spine (Phila Pa 1976)* 19:1371-1380, 1994.
131. Haughton VM, Schmidt TA, Keele K, et al: Flexibility of lumbar spinal motion segments correlated to type of tears in the annulus fibrosus. *J Neurosurg* 92:81-86, 2000.
132. Fujiwara A, Lim TH, An HS, et al: The effect of disc degeneration and facet joint osteoarthritis on the segmental flexibility of the lumbar spine. *Spine (Phila Pa 1976)* 25:3036-3044, 2000.
133. Gillett NA, Gerlach R, Cassidy JJ, et al: Age-related changes in the beagle spine. *Acta Orthop Scand* 59:503-507, 1988.
134. Hunter CJ, Matyas JR, Duncan NA: The notochordal cell in the nucleus pulposus: a review in the context of tissue engineering. *Tissue Eng* 9:667-677, 2003.
135. Gruber HE, Ingram JA, Norton HJ, et al: Senescence in cells of the aging and degenerating intervertebral disc: immunolocalization of senescence-associated beta-galactosidase in human and sand rat discs. *Spine (Phila Pa 1976)* 32:321-327, 2007.
136. Roberts S, Evans EH, Kletsas D, et al: Senescence in human intervertebral discs. *Eur Spine J* 15 Suppl 3:S312-316, 2006.
137. Johnstone B, Bayliss MT: The large proteoglycans of the human intervertebral disc. Changes in their biosynthesis and structure with age, topography, and pathology. *Spine (Phila Pa 1976)* 20:674-684, 1995.
138. Adams P, Muir H: Qualitative changes with age of proteoglycans of human lumbar discs. *Ann Rheum Dis* 35:289-296, 1976.
139. Buckwalter JA, Pedrini-Mille A, Pedrini V, et al: Proteoglycans of human infant intervertebral disc. Electron microscopic and biochemical studies. *J Bone Joint Surg Am* 67:284-294, 1985.
140. Bushell GR, Ghosh P, Taylor TF, et al: Proteoglycan chemistry of the intervertebral disks. *Clin Orthop Relat Res*:115-123, 1977.
141. Deshmukh K, Kline WH: Characterization of collagen and its precursors synthesized by rabbit-articular-cartilage cells in various culture systems. *Eur J Biochem* 69:117-123, 1976.
142. Hadjipavlou AG, Tzermiadianos MN, Bogduk N, et al: The pathophysiology of disc degeneration: a critical review. *J Bone Joint Surg Br* 90:1261-1270, 2008.
143. Kanemoto M, Hukuda S, Komiya Y, et al: Immunohistochemical study of matrix metalloproteinase-3 and tissue inhibitor of metalloproteinase-1 human intervertebral discs. *Spine (Phila Pa 1976)* 21:1-8, 1996.
144. Kang JD, Georgescu HI, McIntyre-Larkin L, et al: Herniated lumbar intervertebral discs spontaneously produce matrix metalloproteinases, nitric oxide, interleukin-6, and prostaglandin E2. *Spine (Phila Pa 1976)* 21:271-277, 1996.
145. Doita M, Kanatani T, Harada T, et al: Immunohistologic study of the ruptured intervertebral disc of the lumbar spine. *Spine (Phila Pa 1976)* 21:235-241, 1996.
146. Peng B, Hao J, Hou S, et al: Possible pathogenesis of painful intervertebral disc degeneration. *Spine (Phila Pa 1976)* 31:560-566, 2006.
147. Kang JD, Stefanovic-Racic M, McIntyre LA, et al: Toward a biochemical understanding of human intervertebral disc degeneration and herniation. Contributions of nitric oxide, interleukins, prostaglandin E2, and matrix metalloproteinases. *Spine (Phila Pa 1976)* 22:1065-1073, 1997.

148. Riser WH, Haskins ME, Jezyk PF, et al: Pseudoachondroplastic dysplasia in miniature poodles: clinical, radiologic, and pathologic features. *J Am Vet Med Assoc* 176:335-341, 1980.
149. Hoerlein BF: Intervertebral disc protrusions in the dog. I. Incidence and pathological lesions. *Am J Vet Res* 14:260-269, 1953.
150. Bergknut N, Egenvall A, Hagman R, et al: Incidence and mortality of diseases related to intervertebral disc degeneration in a population of over 600,000 dogs. *J Am Vet Med Assoc* 240:1300-1309, 2012.
151. Parker HG, VonHoldt BM, Quignon P, et al: An expressed *fgf4* retrogene is associated with breed-defining chondrodysplasia in domestic dogs. *Science* 325:995-998, 2009.
152. Brown NO, Hephrey ML, Prata RG: Thoracolumbar disk disease in the dog: a retrospective analysis of 187 cases. *J Am Anim Hosp Assoc* 13:665-672, 1977
153. Goggin JE, Li AS, Franti CE: Canine intervertebral disk disease: characterization by age, sex, breed, and anatomic site of involvement. *Am J Vet Res* 31:1687-1692, 1970.
154. Priester WA: Canine intervertebral disc disease - occurrence by age, breed, and sex among 8,117 cases. *Theriogenology* 6:293-303, 1976.
155. Brisson BA, Moffatt SL, Swayne SL, et al: Recurrence of thoracolumbar intervertebral disk extrusion in chondrodystrophic dogs after surgical decompression with or without prophylactic fenestration: 265 cases (1995-1999). *J Am Vet Med Assoc* 224:1808-1814, 2004.
156. Olby N, Harris T, Burr J, et al: Recovery of pelvic limb function in dogs following acute intervertebral disc herniations. *J Neurotrauma* 21:49-59, 2004.
157. Kranenburg HC, Grinwis GCM, Bergknut N, et al: Intervertebral disc disease in dogs - Part 2: Comparison of clinical, magnetic resonance imaging, and histological findings in 74 surgically treated dogs. *Vet J* 2012, July 11, Epub ahead of print.
158. Cherrone KL, Dewey CW, Coates JR, et al: A retrospective comparison of cervical intervertebral disk disease in nonchondrodystrophic large dogs versus small dogs. *J Am Anim Hosp Assoc* 40:316-320, 2004.
159. Macias C, McKee WM, May C, et al: Thoracolumbar disc disease in large dogs: a study of 99 cases. *J Small Anim Pract* 43:439-446, 2002.
160. Cudia SP, Duval JM: Thoracolumbar intervertebral disk disease in large, nonchondrodystrophic dogs: a retrospective study. *J Am Anim Hosp Assoc* 33:456-460, 1997.
161. Klausner M, Forterre F, Doherr M, et al: Evaluation of apoptotic cell death in normal and chondrodystrophic canine intervertebral discs. *Vet Sci Dev* 2:20-24, 2012.
162. Besalti O, Pekcan Z, Sirin YS, et al: Magnetic resonance imaging findings in dogs with thoracolumbar intervertebral disk disease: 69 cases (1997-2005). *J Am Vet Med Assoc* 228:902-908, 2006.
163. Levine JM, Levine GJ, Kerwin SC, et al: Association between various physical factors and acute thoracolumbar intervertebral disk extrusion or protrusion in Dachshunds. *J Am Vet Med Assoc* 229:370-375, 2006.
164. Erwin WM: The Notochord, Notochordal cell and CTGF/CCN-2: ongoing activity from development through maturation. *J Cell Commun Signal* 2:59-65, 2008.

165. Kim KW, Kim YS, Ha KY, et al: An autocrine or paracrine Fas-mediated counterattack: a potential mechanism for apoptosis of notochordal cells in intact rat nucleus pulposus. *Spine (Phila Pa 1976)* 30:1247-1251, 2005.
166. Chang Y, Dennis R, Platt SR, et al: Magnetic resonance imaging of traumatic intervertebral disc extrusion in dogs. *Vet Rec* 160:795-799, 2007.
167. Griffiths IR: A syndrome produced by dorso-lateral "explosions" of the cervical intervertebral discs. *Vet Rec* 87:737-741, 1970.
168. De Risio L, Adams V, Dennis R, et al: Association of clinical and magnetic resonance imaging findings with outcome in dogs with presumptive acute noncompressive nucleus pulposus extrusion: 42 cases (2000-2007). *J Am Vet Med Assoc* 234:495-504, 2009.
169. Risbud MV, Schaer TP, Shapiro IM: Toward an understanding of the role of notochordal cells in the adult intervertebral disc: from discord to accord. *Dev Dyn* 239:2141-2148, 2010.
170. Yang F, Leung VY, Luk KD, et al: Injury-induced sequential transformation of notochordal nucleus pulposus to chondrogenic and fibrocartilaginous phenotype in the mouse. *J Pathol* 218:113-121, 2009.
171. Jensen VF: Asymptomatic radiographic disappearance of calcified intervertebral disc material in the Dachshund. *Veterinary Radiol & Ultrasound* 42:141-148, 2001.
172. Jensen VF, Arnbjerg J: Development of intervertebral disk calcification in the dachshund: a prospective longitudinal radiographic study. *J Am Anim Hosp Assoc* 37:274-282, 2001.
173. Jensen VF, Ersboll AK: Mechanical factors affecting the occurrence of intervertebral disc calcification in the dachshund--a population study. *J Vet Med A Physiol Pathol Clin Med* 47:283-296, 2000.
174. Rohdin C, Jeserevic J, Viitmaa R, et al: Prevalence of radiographic detectable intervertebral disc calcifications in Dachshunds surgically treated for disc extrusion. *Acta Vet Scand* 52:24, 2010.
175. Stigen O: Calcification of intervertebral discs in the dachshund. A radiographic study of 327 young dogs. *Acta Vet Scand* 32:197-203, 1991.
176. Stigen O: Calcification of intervertebral discs in the dachshund: a radiographic study of 21 stud-dogs. *Acta Vet Scand* 36:329-334, 1995.
177. Stigen O, Christensen K: Calcification of intervertebral discs in the dachshund: an estimation of heritability. *Acta Vet Scand* 34:357-361, 1993.
178. Melrose J, Burkhardt D, Taylor TK, et al: Calcification in the ovine intervertebral disc: a model of hydroxyapatite deposition disease. *Eur Spine J* 18:479-489, 2009.
179. Feinberg J, Boachie-Adjei O, Bullough PG, et al: The distribution of calcific deposits in intervertebral discs of the lumbosacral spine. *Clin Orthop Relat Res*:303-310, 1990.
180. Marcos JC, Arturi AS, Babini C, et al: Familial hydroxyapatite chondrocalcinosis with spondyloepiphyseal dysplasia: clinical course and absence of genetic linkage to the type II procollagen gene. *J Clin Rheumatol* 1:171-178, 1995.
181. Wong CC, Pereira B, Pho RW: Cervical disc calcification in children. A long-term review. *Spine* 17:139-144, 1992.
182. Dai LY, Ye H, Qian QR: The natural history of cervical disc calcification in children. *J Bone Joint Surg Am* 86-A:1467-1472, 2004.
183. Weinberger A, Myers AR: Intervertebral disc calcification in adults: a review. *Semin Arthritis Rheum* 8:69-75, 1978.

184. Jensen VF, Beck S, Christensen KA, et al: Quantification of the association between intervertebral disk calcification and disk herniation in Dachshunds. *J Am Vet Med Assoc* 233:1090-1095, 2008.
185. Jensen VF, Christensen KA: Inheritance of disc calcification in the dachshund. *J Vet Med A* 47:331-340, 2000.
186. Stigen O: Calcification of intervertebral discs in the dachshund: a radiographic study of 115 dogs at 1 and 5 years of age. *Acta Vet Scand* 37:229-237, 1996.
187. Bergknut N: Intervertebral Disc Degeneration in Dogs. PhD Doctoral Thesis, 2011.
188. Aguiar DJ, Johnson SL, Oegema TR: Notochordal cells interact with nucleus pulposus cells: regulation of proteoglycan synthesis. *Exp Cell Res* 246:129-137, 1999.
189. Erwin WM, Inman RD: Notochord cells regulate intervertebral disc chondrocyte proteoglycan production and cell proliferation. *Spine (Phila Pa 1976)* 31:1094-1099, 2006.
190. Erwin WM, Islam D, Inman RD, et al: Notochordal cells protect nucleus pulposus cells from degradation and apoptosis: implications for the mechanisms of intervertebral disc degeneration. *Arthritis Res Ther* 13:R215, 2011.
191. Erwin WM, Las Heras F, Islam D, et al: The regenerative capacity of the notochordal cell: tissue constructs generated in vitro under hypoxic conditions. *J Neurosurg Spine* 10:513-521, 2009.
192. Mogensen MS, Karlskov-Mortensen P, Proschowsky HF, et al: Genome-wide association study in Dachshund: identification of a major locus affecting intervertebral disc calcification. *J Hered* 102 Suppl 1:S81-86, 2011.
193. Braund KG, Taylor TK, Ghosh P, et al: Spinal mobility in the dog. A study in chondrodystrophoid and non--chondrodystrophoid animals. *Res Vet Sci* 22:78-82, 1977.
194. De Decker S, Gielen IM, Duchateau L, et al: Low-field magnetic resonance imaging findings of the caudal portion of the cervical region in clinically normal Doberman Pinschers and Foxhounds. *Am J Vet Res* 71:428-434, 2010.
195. Rossi F, Seiler G, Busato A, et al: Magnetic resonance imaging of articular process joint geometry and intervertebral disk degeneration in the caudal lumbar spine (L5-S1) of dogs with clinical signs of cauda equina compression. *Vet Radiol Ultrasound* 45:381-387, 2004.
196. Seiler GS, Háni H, Busato AR, et al: Facet joint geometry and intervertebral disc degeneration in the L5-S1 region of the vertebral column in German Shepherd Dogs. *Am J Vet Res* 63:86-90, 2002.
197. Penning L, Badoux DM: Radiological study of the movements of the cervical spine in the dog compared with those in man. *Anat Histol Embryol* 16:1-20, 1987.
198. Breit S, Kunzel W: Shape and orientation of articular facets of cervical vertebrae (C3-C7) in dogs denoting axial rotational ability: an osteological study. *Eur J Morphol* 40:43-51, 2002.
199. Johnson JA, da Costa RC, Bhattacharya S, et al: Kinematic motion patterns of the cranial and caudal canine cervical spine. *Vet Surg* 40:720-727, 2011.
200. Farfan HF, Cossette JW, Robertson GH, et al: The effects of torsion on the lumbar intervertebral joints: the role of torsion in the production of disc degeneration. *J Bone Joint Surg Am* 52:468-497, 1970.
201. Benninger MI, Seiler GS, Robinson LE, et al: Effects of anatomic conformation on three-dimensional motion of the caudal lumbar and lumbosacral portions of the vertebral column of dogs. *Am J Vet Res* 67:43-50, 2006.

202. Burger R, Lang J: [Kinetic study of the lumbar vertebrae and the lumbosacral passage in German shepherd dogs. 1. Functional anatomy and kinetic foundation]. *Schweiz Arch Tierheilkd* 134:411-416, 1992.
203. Benninger MI, Seiler GS, Robinson LE, et al: Three-dimensional motion pattern of the caudal lumbar and lumbosacral portions of the vertebral column of dogs. *Am J Vet Res* 65:544-551, 2004.
204. Breit S, Kunzel W: Breed specific osteological features of the canine lumbosacral junction. *Ann Anat* 183:151-157, 2001.
205. Danielsson F, Sjöström L: Surgical treatment of degenerative lumbosacral stenosis in dogs. *Vet Surg* 28:91-98, 1999.
206. Fluckiger MA, Damur-Djuric N, Hassig M, et al: A lumbosacral transitional vertebra in the dog predisposes to cauda equina syndrome. *Vet Radiol Ultrasound* 47:39-44, 2006.
207. Morgan JP, Bahr A, Franti CE, et al: Lumbosacral transitional vertebrae as a predisposing cause of cauda equina syndrome in German shepherd dogs: 161 cases (1987-1990). *J Am Vet Med Assoc* 202:1877-1882, 1993.
208. Lappalainen AK, Salomaa R, Junnila J, et al: Alternative classification and screening protocol for transitional lumbosacral vertebra in German shepherd dogs. *Acta Vet Scand* 54:27, 2012.
209. Geissbühler AD: Kinetische Studien am lumbosakralen Uebergang von Berner Sennenhunden und Deutschen Schäferhunden. Universität Bern, 1999.
210. Hanna FY: Lumbosacral osteochondrosis: radiological features and surgical management in 34 dogs. *J Small Anim Pract* 42:272-278, 2001.
211. Mathis KR, Havlicek M, Beck JB, et al: Sacral osteochondrosis in two German Shepherd Dogs. *Aust Vet J* 87:249-252, 2009.
212. Lang J, Hani H, P. S: A sacral lesion resembling osteochondrosis in the German Shepherd Dog. *Vet Radiol Ultrasound* 33:69-76, 1992.
213. Ball MU, McGuire JA, Swaim SF, et al: Patterns of occurrence of disk disease among registered dachshunds. *J Am Vet Med Assoc* 180:519-522, 1982.
214. Hoerlein BF: Intervertebral disc protrusions in the dog. II. Symptomatology and clinical diagnosis. *Am J Vet Res* 14:270-274, 1953.
215. Levine JM, Fosgate GT, Chen AV, et al: Magnetic resonance imaging in dogs with neurologic impairment due to acute thoracic and lumbar intervertebral disk herniation. *J Vet Intern Med* 23:1220-1226, 2009.
216. Ryan TM, Platt SR, Llabres-Diaz FJ, et al: Detection of spinal cord compression in dogs with cervical intervertebral disc disease by magnetic resonance imaging. *Vet Rec* 163:11-15, 2008.
217. Morgan PW, Parent J, Holmberg DL: Cervical pain secondary to intervertebral disc disease in dogs; radiographic findings and surgical implications. *Prog Vet Neurol* 4:76-80, 1993.
218. Takada T, Nishida K, Doita M, et al: Fas ligand exists on intervertebral disc cells: a potential molecular mechanism for immune privilege of the disc. *Spine* 27:1526-1530, 2002.
219. da Costa RC, Echandi RL, Beauchamp D: Computed tomographic findings in large and giant breed dogs with cervical spondylomyelopathy: 58 cases. *J Vet Intern Med* 23:709, 2009.
220. da Costa RC, Parent JM: Magnetic resonance imaging findings in 60 dogs with cervical spondylomyelopathy. *J Vet Intern Med* 23:740, 2009.

221. Lewis D: Cervical spondylomyelopathy ('wobbler' syndrome) in the dog: a study based on 224 cases. *J Small Anim Pract* 30:657-665, 1989.
222. McKee WM, Butterworth SJ, Scott HW: Management of cervical spondylopathy-associated intervertebral, disc protrusions using metal washers in 78 dogs. *J Small Anim Pract* 40:465-472, 1999.
223. De Risio L, Sharp NJ, Olby NJ, et al: Predictors of outcome after dorsal decompressive laminectomy for degenerative lumbosacral stenosis in dogs: 69 cases (1987-1997). *J Am Vet Med Assoc* 219:624-628, 2001.
224. Oliver JE, Jr., Selcer RR, Simpson S: Cauda equina compression from lumbosacral malarticulation and malformation in the dog. *J Am Vet Med Assoc* 173:207-214, 1978.
225. Hanna FY: Lumbosacral osteochondrosis: radiological features and surgical management in 34 dogs. *J Small Anim Pract* 42:272-278, 2001.
226. Mathis KR, Havlicek M, Beck JB, et al: Sacral osteochondrosis in two German Shepherd Dogs. *Aust Vet J* 87:249-252, 2009.
227. Palmer RH, Chambers JN: Canine Lumbosacral Diseases. Part I. Anatomy, Pathophysiology, and Clinical Presentation. *Compend Contin Educ Pract Vet* 13:61-69, 1991.
228. Tarvin G, Prata RG: Lumbosacral stenosis in dogs. *J Am Vet Med Assoc* 177:154-159, 1980.
229. Aihara T, Takahashi K, Ogasawara A, et al: Intervertebral disc degeneration associated with lumbosacral transitional vertebrae: a clinical and anatomical study. *J Bone Joint Surg Br* 87:687-691, 2005.
230. Damur-Djuric N, Steffen F, Hassig M, et al: Lumbosacral transitional vertebrae in dogs: classification, prevalence, and association with sacroiliac morphology. *Vet Radiol Ultrasound* 47:32-38, 2006.
231. Morgan JP: Transitional lumbosacral vertebral anomaly in the dog: a radiographic study. *J Small Anim Pract* 40:167-172, 1999.
232. Sharp NJH, Wheeler SJ: Lumbosacral disease, in Sharp NJH, Wheeler SJ (eds): *Small Animal Spinal Disorders. Diagnosis and Surgery* (ed 2), Edinburgh, Elsevier Mosby, 2005, pp 181-209.
233. Sugawara O, Atsuta Y, Iwahara T, et al: The effects of mechanical compression and hypoxia on nerve root and dorsal root ganglia. An analysis of ectopic firing using an in vitro model. *Spine (Phila Pa 1976)* 21:2089-2094, 1996.
234. Freemont AJ, Peacock TE, Goupille P, et al: Nerve ingrowth into diseased intervertebral disc in chronic back pain. *Lancet* 350:178-181, 1997.
235. Danielsson F, Sjoström L: Surgical treatment of degenerative lumbosacral stenosis in dogs. *Vet Surg* 28:91-98, 1999.
236. Moore GE, Burkman KD, Carter MN, et al: Causes of death or reasons for euthanasia in military working dogs: 927 cases (1993-1996). *J Am Vet Med Assoc* 219:209-214, 2001.
237. Indrieri RJ: Lumbosacral stenosis and injury of the cauda equina. *Vet Clin North Am Small Anim Pract* 18:697-710, 1988.
238. Parent J: Clinical approach and lesion localization in patients with spinal diseases. *Vet Clin North Am Small Anim Pract* 40:733-753, 2010.
239. Jones JC, Banfield CM, Ward DL: Association between postoperative outcome and results of magnetic resonance imaging and computed tomography in working dogs with degenerative lumbosacral stenosis. *J Am Vet Med Assoc* 216:1769-1774, 2000.

240. Mayhew PD, Kapatkin AS, Wortman JA, et al: Association of cauda equina compression on magnetic resonance images and clinical signs in dogs with degenerative lumbosacral stenosis. *J Am Anim Hosp Assoc* 38:555-562, 2002.
241. Suwankong N, Voorhout G, Hazewinkel HA, et al: Agreement between computed tomography, magnetic resonance imaging, and surgical findings in dogs with degenerative lumbosacral stenosis. *J Am Vet Med Assoc* 229:1924-1929, 2006.
242. Lamb CR, Nicholls A, Targett M, et al: Accuracy of survey radiographic diagnosis of intervertebral disc protrusion in dogs. *Vet Radiol Ultrasound* 43:222-228, 2002.
243. Burk RL: Problems in the radiographic interpretation of intervertebral disc disease in the dog. *Probl Vet Med* 1:381-401, 1989.
244. Sharp NJ, Wheeler SJ, Cofone M: Radiological evaluation of 'wobbler' syndrome—caudal cervical spondylomyelopathy. *J Small Anim Pract* 33:491-499, 1992.
245. Jensen VF: Asymptomatic radiographic disappearance of calcified intervertebral disc material in the Dachshund. *Vet Radiol Ultrasound* 42:141-148, 2001.
246. Stigen O: Calcification of intervertebral discs in the dachshund: a radiographic study of 21 stud-dogs. *Acta Vet Scand* 36:329-334, 1995.
247. Jensen VF, Beck S, Christensen KA, et al: Quantification of the association between intervertebral disk calcification and disk herniation in Dachshunds. *J Am Vet Med Assoc* 233:1090-1095, 2008.
248. Scharf G, Steffen F, Grunenfelder F, et al: The lumbosacral junction in working German shepherd dogs -- neurological and radiological evaluation. *J Vet Med A Physiol Pathol Clin Med* 51:27-32, 2004.
249. Steffen F, Hunold K, Scharf G, et al: A follow-up study of neurologic and radiographic findings in working German Shepherd Dogs with and without degenerative lumbosacral stenosis. *J Am Vet Med Assoc* 231:1529-1533, 2007.
250. Kirberger R, Roos C, Lubbe A: The radiological diagnosis of thoracolumbar disc disease in the Dachshund. *Vet Radiol Ultrasound* 33:255-261, 1992.
251. Olby N, Dyce J, Houlton J: Correlation of plain radiographic and lumbar myelographic findings in thoracolumbar disc disease. *J Small Anim Pract* 35:345, 1994
252. Seim HB, Withrow SJ: Pathophysiology and diagnosis of caudal cervical spondylomyelopathy with emphasis on the Doberman Pinscher. *J Am Anim Hosp Assoc* 18:241-245, 1982.
253. Ramirez O, 3rd, Thrall DE: A review of imaging techniques for canine cauda equina syndrome. *Vet Radiol Ultrasound* 39:283-296, 1998.
254. Robert RE, Selcer BA: Diagnostic imaging: myelography and epidurography. *Vet Clin North Am Small Anim Pract* 23:307-329, 1993.
255. Sisson AF, LeCouteur RA, Ingram JT, et al: Diagnosis of cauda equina abnormalities by using electromyography, discography, and epidurography in dogs. *J Vet Intern Med* 6:253-263, 1992.
256. Barthez PY, Morgan JP, Lipsitz D: Discography and epidurography for evaluation of the lumbosacral junction in dogs with cauda equina syndrome. *Vet Radiol Ultrasound* 35:152-157, 1994.
257. Morgan JP, Bailey CS: Cauda equina syndrome in the dog: radiographic evaluation. *J Small Anim Pract* 34:69-77, 1990.

258. Masuda K, Aota Y, Muehleman C, et al: A novel rabbit model of mild, reproducible disc degeneration by an annulus needle puncture: correlation between the degree of disc injury and radiological and histological appearances of disc degeneration. *Spine (Phila Pa 1976)* 30:5-14, 2005.
259. Sobajima S, Kompel JF, Kim JS, et al: A slowly progressive and reproducible animal model of intervertebral disc degeneration characterized by MRI, X-ray, and histology. *Spine (Phila Pa 1976)* 30:15-24, 2005.
260. Hecht S, Thomas WB, Marioni-Henry K, et al: Myelography vs. computed tomography in the evaluation of acute thoracolumbar intervertebral disk extrusion in chondrodystrophic dogs. *Vet Radiol Ultrasound* 50:353-359, 2009.
261. Israel SK, Levine JM, Kerwin SC, et al: The relative sensitivity of computed tomography and myelography for identification of thoracolumbar intervertebral disk herniations in dogs. *Vet Radiol Ultrasound* 50:247-252, 2009.
262. Olby NJ, Munana KR, Sharp NJ, et al: The computed tomographic appearance of acute thoracolumbar intervertebral disc herniations in dogs. *Vet Radiol Ultrasound* 41:396-402, 2000.
263. King JB, Jones JC, Rossmeisl JH, Jr., et al: Effect of multi-planar CT image reformatting on surgeon diagnostic performance for localizing thoracolumbar disc extrusions in dogs. *J Vet Sci* 10:225-232, 2009.
264. Jones JC, Wilson ME, Bartels JE: A review of high resolution computed tomography and a proposed technique for regional examination of the canine lumbosacral spine. *Vet Radiol Ultrasound* 35 339-346, 1994.
265. Sande RD: Radiography, myelography, computed tomography, and magnetic resonance imaging of the spine. *Vet Clin North Am Small Anim Pract* 22:811-831, 1992.
266. Wood BC, Lanz OI, Jones JC, et al: Endoscopic-assisted lumbosacral foraminotomy in the dog. *Vet Surg* 33:221-231, 2004.
267. Levitski RE, Lipsitz D, Chauvet AE: Magnetic resonance imaging of the cervical spine in 27 dogs. *Vet Radiol Ultrasound* 40:332-341, 1999.
268. Adams WH, Daniel GB, Pardo AD, et al: Magnetic resonance imaging of the caudal lumbar and lumbosacral spine in 13 dogs (1990-1993). *Vet Radiol Ultrasound* 36:3-13, 1995.
269. de Haan JJ, Shelton SB, Ackerman N: Magnetic resonance imaging in the diagnosis of degenerative lumbosacral stenosis in four dogs. *Vet Surg* 22:1-4, 1993.
270. Bergknot N, Auriemma E, Wijsman SJCM, et al: Evaluation of intervertebral disk degeneration in chondrodystrophic and nonchondrodystrophic dogs by use of Pfirrmann grading of images obtained with low-field magnetic resonance imaging. *Am J Vet Res* 72:893-898, 2011.
271. da Costa RC, Parent J, Dobson H, et al: Comparison of magnetic resonance imaging and myelography in 18 Doberman pinscher dogs with cervical spondylomyelopathy. *Vet Radiol Ultrasound* 47:523-531, 2006.
272. Lipsitz D, Levitski RE, Chauvet AE, et al: Magnetic resonance imaging features of cervical stenotic myelopathy in 21 dogs. *Vet Radiol Ultrasound* 42:20-27, 2001.
273. Godde T, Steffen F: Surgical treatment of lumbosacral foraminal stenosis using a lateral approach in twenty dogs with degenerative lumbosacral stenosis. *Vet Surg* 36:705-713, 2007.
274. Chambers JN, Selcer BA, Sullivan SA, et al: Diagnosis of lateralized lumbosacral disk herniation with magnetic resonance imaging. *J Am Anim Hosp Assoc* 33:296-299, 1997.

275. Penderis J, Dennis R: Use of traction during magnetic resonance imaging of caudal cervical spondylomyelopathy (“wobbler syndrome”) in the dog. *Vet Radiol Ultrasound* 45:216-219, 2004.
276. Gillette RL, Angle TC: Recent developments in canine locomotor analysis: A review. *Vet J*, 2008.
277. McLaughlin RM: Kinetic and kinematic gait analysis in dogs. *Vet Clin North Am Small Anim Pract* 31:193-201, 2001.
278. Suwankong N, Meij BP, Van Klaveren NJ, et al: Assessment of decompressive surgery in dogs with degenerative lumbosacral stenosis using force plate analysis and questionnaires. *Vet Surg* 36:423-431, 2007.
279. van Klaveren NJ, Suwankong N, De Boer S, et al: Force plate analysis before and after dorsal decompression for treatment of degenerative lumbosacral stenosis in dogs. *Vet Surg* 34:450-456, 2005.
280. Gradner G, Bockstahler B, Peham C, et al: Kinematic study of back movement in clinically sound malinois dogs with consideration of the effect of radiographic changes in the lumbosacral junction. *Vet Surg* 36:472-481, 2007.
281. Adler JH, Schoenbaum M, Silberberg R: Early onset of disk degeneration and spondylosis in sand rats (*Psammomys obesus*). *Vet Pathol* 20:13-22, 1983.
282. Poy NS, DeCamp CE, Bennett RL, et al: Additional kinematic variables to describe differences in the trot between clinically normal dogs and dogs with hip dysplasia. *Am J Vet Res* 61:974-978, 2000.
283. Tashman S, Anderst W, Kolowich P, et al: Kinematics of the ACL-deficient canine knee during gait: serial changes over two years. *J Orthop Res* 22:931-941, 2004.
284. Eward C, Gillette RL, Eward W: Effects of unilaterally restricted carpal range of motion on kinematic gait analysis of the dog. *Vet Comp Orthop Traumatol* 16:158-163, 2003.
285. Lee JY, Kim G, Kim JH, et al: Kinematic gait analysis of the hind limb after tibial plateau levelling osteotomy and cranial tibial wedge osteotomy in ten dogs. *J Vet Med A Physiol Pathol Clin Med* 54:579-584, 2007.
286. da Costa RC, Parent JM, Holmberg DL, et al: Outcome of medical and surgical treatment in dogs with cervical spondylomyelopathy: 104 cases (1988-2004). *J Am Vet Med Assoc* 233:1284-1290, 2008.
287. Levine JM, Levine GJ, Johnson SI, et al: Evaluation of the success of medical management for presumptive cervical intervertebral disk herniation in dogs. *Vet Surg* 36:492-499, 2007.
288. Levine JM, Levine GJ, Johnson SI, et al: Evaluation of the success of medical management for presumptive thoracolumbar intervertebral disk herniation in dogs. *Vet Surg* 36:482-491, 2007.
289. Sharp NJ, Wheeler SJ: Cervical spondylomyelopathy, in Sharp NJH, Wheeler SJ (eds): *Small animal spinal disorders diagnosis and surgery*. (ed 2nd). Philadelphia, Elsevier Mosby 2005, pp 211–246.
290. Slocum B, Devine T: L7-S1 fixation-fusion for treatment of cauda equina compression in the dog. *J Am Vet Med Assoc* 188:31-35, 1986.
291. Trotter EJ: Cervical spine locking plate fixation for treatment of cervical spondylotic myelopathy in large breed dogs. *Vet Surg* 38:705-718, 2009.

292. Denny HR, Gibbs C, Gaskell CJ: Cervical spondylopathy in the dog--a review of thirty-five cases. *J Small Anim Pract* 18:117-132, 1977.
293. Meij BP, Suwankong N, Van der Veen AJ, et al: Biomechanical flexion-extension forces in normal canine lumbosacral cadaver specimens before and after dorsal laminectomy-discectomy and pedicle screw-rod fixation. *Vet Surg* 36:742-751, 2007.
294. Ullman SL, Boudrieau RJ: Internal skeletal fixation using a Kirschner apparatus for stabilization of fracture/luxations of the lumbosacral joint in six dogs. A modification of the transilial pin technique. *Vet Surg* 22:11-17, 1993.
295. Méheust P: Une nouvelle technique de stabilisation lombosacrée : l'arthrodèse par vissage pédiculaire, étude clinique de 5 cas. *Prat Med Chir Anim Comp* 35:201-207, 2000.
296. Méheust P, Mallet C, Marouze C: Une nouvelle technique de stabilisation lombosacrée: l'arthrodèse par vissage pédiculaire considérations anatomiques *Prat Med Chir Anim Comp* 35:193-199, 2000.
297. Swaim SF: Ventral decompression of the cervical spinal cord in the dog. *J Am Vet Med Assoc* 164:491-495, 1974.
298. Funkquist B: Decompressive laminectomy in thoraco-lumbar disc protrusion with paraplegia in the dog. *J Small Anim Pract* 11:445-451, 1970.
299. Sukhiani HR, Parent JM, Atilola MA, et al: Intervertebral disk disease in dogs with signs of back pain alone: 25 cases (1986-1993). *J Am Vet Med Assoc* 209:1275-1279, 1996.
300. Sharp NJH, Wheeler SJ: Thoracolumbar disc disease, in Sharp NJH, Wheeler SJ (eds): *Small Animal Spinal Disorders. Diagnosis and Surgery* (ed 2), Edinburgh, Elsevier Mosby, 2005, pp 121-159.
301. Smith GK, Walter MC: Spinal decompressive procedures and dorsal compartment injuries: comparative biomechanical study in canine cadavers. *Am J Vet Res* 49:266-273, 1988.
302. Muir P, Johnson KA, Manley PA, et al: Comparison of hemilaminectomy and dorsal laminectomy for thoracolumbar intervertebral disc extrusion in dachshunds. *J Small Anim Pract* 36:360-367, 1995.
303. Gage ED, Hoerlein BF: Hemilaminectomy and dorsal laminectomy for relieving compressions of the spinal cord in the dog. *J Am Vet Med Assoc* 152:351-359, 1968.
304. McKee WM: A comparison of hemilaminectomy (with concomitant disc fenestration) and dorsal laminectomy for the treatment of thoracolumbar disc protrusion in dogs. *Vet Rec* 130:296-300, 1992.
305. Scott HW: Hemilaminectomy for the treatment of thoracolumbar disc disease in the dog: a follow-up study of 40 cases. *J Small Anim Pract* 38:488-494, 1997.
306. Davies JV, Sharp NJ: A comparison of conservative treatment and fenestration for thoracolumbar intervertebral disc disease in the dog *J Small Anim Pract* 24:721-729, 1983.
307. Olsson SE: Observations concerning disc fenestration in dogs. *Acta Orthop Scand* 20:349-356, 1951.
308. Funkquist B: Investigations of the therapeutic and prophylactic effects of disc evacuation in cases of thoraco-lumbar herniated discs in dogs. *Acta Vet Scand* 19:441-457, 1978.
309. Levine SH, Caywood DD: Recurrence of neurological deficits in dogs treated for thoracolumbar disk disease. *J Am Anim Hosp Assoc* 20:889-894, 1984.
310. Chambers JN, Selcer BA, Oliver JE, Jr.: Results of Treatment of Degenerative Lumbosacral Stenosis in Dogs by Exploration and Excision. *Vet Comp Orthop Traumatol* 3:130-133, 1988.

311. Denny HR, Gibbs C, Holt PE: The diagnosis and treatment of cauda equina lesions in the dog. *J Small Anim Pract* 23:425-443, 1982.
312. Lenehan TM: Canine Cauda Equina Syndrome. *Compend Contin Educ Pract Vet* 5:941-950, 1983.
313. Janssens LAA, Moens Y, Coppens P, et al: Lumbosacral Degenerative Stenosis in the Dog. *Vet Comp Orthop Traumatol* 13:97-103, 2000.
314. Ness M: Degenerative lumbosacral Stenosis in the dog: a review of 30 cases. *J Small Anim Pract* 35:185-190, 1994.
315. Linn LL, Bartels KE, Rochat MC, et al: Lumbosacral stenosis in 29 military working dogs: epidemiologic findings and outcome after surgical intervention (1990-1999). *Vet Surg* 32:21-29, 2003.
316. De Risio L, Munana K, Murray M, et al: Dorsal laminectomy for caudal cervical spondylomyelopathy: postoperative recovery and long-term follow-up in 20 dogs. *Vet Surg* 31:418-427, 2002.
317. Bruecker KA, Seim HB, Blass CE: Caudal cervical spondylomyelopathy: decompression by linear traction and stabilization with Steinmann pins and polymethyl methacrylate. *J Am Anim Hosp Assoc* 25:677-683, 1989.
318. Koehler CL, Stover SM, LeCouteur RA, et al: Effect of a ventral slot procedure and of smooth or positive-profile threaded pins with polymethylmethacrylate fixation on intervertebral biomechanics at treated and adjacent canine cervical vertebral motion units. *Am J Vet Res* 66:678-687, 2005.
319. Corlazzoli D: Bicortical implant insertion in caudal cervical spondylomyelopathy: a computed tomography simulation in affected Doberman Pinschers. *Vet Surg* 37:178-185, 2008.
320. McKee WM, Butterworth SJ, Scott HW: Management of cervical spondylopathy-associated intervertebral, disc protrusions using metal washers in 78 dogs. *J Small Anim Pract* 40:465-472, 1999.
321. Dixon BC, Tomlinson JL, Kraus KH: Modified distraction-stabilization technique using an interbody polymethyl methacrylate plug in dogs with caudal cervical spondylomyelopathy. *J Am Vet Med Assoc* 208:61-68, 1996.
322. Lee CK: Accelerated degeneration of the segment adjacent to a lumbar fusion. *Spine* 13:375-377, 1988.
323. MacDougall J, Perra J, Pinto M: Incidence of adjacent segment degeneration at ten years after lumbar spine fusion. *Spine J* 3:675, 2003.
324. Schlegel JD, Smith JA, Schleusener RL: Lumbar motion segment pathology adjacent to thoracolumbar, lumbar, and lumbosacral fusions. *Spine* 21:970-981, 1996.
325. Boelen EJ, van Hooy-Corstjens CS, Bulstra SK, et al: Intrinsically radiopaque hydrogels for nucleus pulposus replacement. *Biomaterials* 26:6674-6683, 2005.
326. Goins ML, Wimberley DW, Yuan PS, et al: Nucleus pulposus replacement: an emerging technology. *Spine J* 5:317S-324S, 2005.
327. Boelen EJ, Koole LH, van Rhijn LW, et al: Towards a functional radiopaque hydrogel for nucleus pulposus replacement. *J Biomed Mater Res B Appl Biomater* 83:440-450, 2007.

- 2.1
328. Boelen EJH, van Hooy-Corstjens CSJ, Gijbels MJJ, et al: Preliminary evaluation of new intrinsically radiopaque hydrogels for replacing the nucleus pulposus. *Journal of Materials Chemistry* 16:824-828, 2006.
 329. Tow BP, Hsu WK, Wang JC: Disc regeneration: a glimpse of the future. *Clin Neurosurg* 54:122-128, 2007.
 330. Yoon ST: Molecular therapy of the intervertebral disc. *Spine J* 5:280S-286S, 2005.
 331. An HS, Masuda K: Relevance of in vitro and in vivo models for intervertebral disc degeneration. *J Bone Joint Surg Am* 88 Suppl 2:88-94, 2006.
 332. Masuda K: Biological repair of the degenerated intervertebral disc by the injection of growth factors. *Eur Spine J* 17 Suppl 4:441-451, 2008.
 333. Sakai D: Future perspectives of cell-based therapy for intervertebral disc disease. *Eur Spine J* 17 Suppl 4:452-458, 2008.
 334. Tow BP, Hsu WK, Wang JC: Disc regeneration: a glimpse of the future. *Clin Neurosurg* 54:122-128, 2007.
 335. Henriksson H, Thornemo M, Karlsson C, et al: Identification of cell proliferation zones, progenitor cells and a potential stem cell niche in the intervertebral disc region: a study in four species. *Spine (Phila Pa 1976)* 34:2278-2287, 2009.
 336. Risbud MV, Schipani E, Shapiro IM: Hypoxic regulation of nucleus pulposus cell survival: from niche to notch. *Am J Pathol* 176:1577-1583, 2010.

Soft tissue artifact in canine kinematic gait analysis

Monique Schwencke^a, Lucas A. Smolders^a, Niklas Bergknut^{a,b},
Pia Gustås^b, Bjorn P. Meij^a, Herman. A. W. Hazewinkel^a

Veterinary Surgery 41(7):829-837, 2012

^a Department of Clinical Sciences of Companion Animals, Faculty of Veterinary Medicine, Utrecht University, Utrecht, the Netherlands.

^b Department of Clinical Sciences, Division of Small Animals, Faculty of Veterinary Medicine and Animal Sciences, Swedish University of Agricultural Sciences, Sweden

Abstract

Objective: To investigate, noninvasively, the soft tissue artifact (STA) in canine kinematic gait analysis.

Methods: 4 Labrador retriever dogs were used. Kinematic study: Reflective markers were glued to the skin over bony landmarks, with the distance between 2 markers representing the length of the underlying scapula, humerus, ulna, femur, and crus. The distance between these markers (marker distance) was measured with infrared cameras while the dogs stood still or walked on a treadmill. Fluoroscopy study: Radiopaque markers were glued on the skin over the spinous process of the L6 vertebra and the stifle to allow fluoroscopic observation of the markers and underlying skeletal segments while the dogs walked on the treadmill. The position of the markers was compared with the position of the underlying skeletal segments during different phases of the step cycle.

Results: Kinematic study: Significant differences were found between marker distance during standing and walking for all bones investigated. Mean percentage differences in marker distance ranged from -18% to +6%. Fluoroscopy study: Significant displacements relative to the bony landmarks were found ranging from 0.4 - 1.2 cm.

Conclusions: Analysis of the motion of skeletal structures with the use of markers attached to the skin showed that the skin moves relative to underlying skeletal structures. When working with a 3-D motion-capture system using skin markers, researchers should be aware that the soft tissue artifact could significantly influence their results.

Key words: kinematics; gait analysis; dog; soft tissue artifact

Introduction

Lameness in small animals is usually evaluated subjectively by visual observation, but this method is inadequate for clinical and research purposes, for which objective methods are needed^{1,2}. Several methods are in use, such as kinetic (analysis of ground reaction forces by force plate analysis) and kinematic gait analysis. Kinematic gait analysis has proven useful for analysis of movement in dogs³ and has been used to evaluate orthopedic abnormalities⁴⁻⁶ and the effects of surgical intervention^{7,8}. Most studies of kinematic gait analysis in dogs have used skin markers positioned over bony prominences on the extremities^{9,10}. However, studies of horses and people have shown that the use of skin markers introduces error because the movement of skin is recorded rather than the movement of underlying skeletal structures. This soft tissue artifact (STA) is a common source of error in human and equine gait analysis and has been investigated using different techniques, such as percutaneous tracking markers, often combined with digital video fluoroscopy¹¹⁻¹⁶.

Quantification of the STA and ways to counteract it have been described to improve the accuracy of human and equine kinematics^{11,15-20}. Although it is assumed that there is an STA in canine kinematic gait analysis^{21,22}, to the authors' knowledge there has been only one preliminary report on the STA in dogs²³. Therefore, our purpose was to investigate in more detail the STA during gait analysis in the dog, using noninvasive kinematic and fluoroscopic techniques. Since there may be breed differences, we studied one breed, i.e., the Labrador retriever. In the kinematic study, we hypothesized that the distance between 2 markers fixed to the skin overlying a long bone measured in the standing dog would not be different from that in the walking dog, and that there would be no significant difference between marker movement on the left and right sides. In the fluoroscopy study, we hypothesized that the position of markers attached to the skin relative to the underlying bone would remain the same during different phases of the step cycle.

Materials and methods

Animals

Four clinically sound, adult Labrador retrievers were used in this study (1 male, 3 females). Mean age was 6.3 years (range, 4–9 years), mean body weight was 25.9 kg (range, 20.2-29.6 kg) and all dogs had a body condition score of 3 on a 5-point scale²⁴. Dogs were trained to walk on the treadmill, to ensure a consistent, repeatable gait during the experiments.

Kinematics

In canine kinematic gait analysis, skin markers are generally placed over the center of rotation of each joint under investigation^{3,9,10}. Because the purpose of this study was to investigate the movement of skin markers relative to the underlying skeletal structures, an alternative marker placement was used. The markers were placed at the most proximal and distal bony landmark of each long bone. On the assumption that the actual bones of interest do not change in length during movement, measurement of the marker distances representing the underlying long bones reflects the movement of the overlying skin. If the measured marker distances change during movement, the skin moves relative to the underlying long bones.

Spherical, retroreflective markers (Qualisys, Gothenburg, Sweden), 12 mm in diameter, were glued to the skin on both sides of the dog at defined anatomical sites. For the scapula, markers were placed over the dorsal border of the scapula (cartilago scapulae) and over the acromion; for the humerus, markers were placed over the greater tubercle of the humerus and over the lateral epicondyle of the humerus; for the ulna, markers were placed over the olecranon and over the styloid process of the ulna; for the femur, markers were placed over the greater trochanter of the femur and over the lateral epicondyle of the femur; for the crus, markers were placed over the fibular head and over the lateral fibular malleolus (Fig. 1). The hair over the anatomic sites was clipped to facilitate marker placement and to reduce displacements caused by fur. All markers were glued (Karlsons klister®, UHU, Stockholm, Sweden) in position by the same person while the dog was standing squarely with its head in a neutral, forward position. For data collection, 6 infrared cameras (Proreflex®, Qualisys, Gothenburg, Sweden) were placed around the treadmill to record the three-dimensional marker positions, with a frame rate of 100 Hz. Data were processed and analyzed with track manager software (Qualisys Track Manager software). Marker positions were recorded in each dog during two 60-s periods.

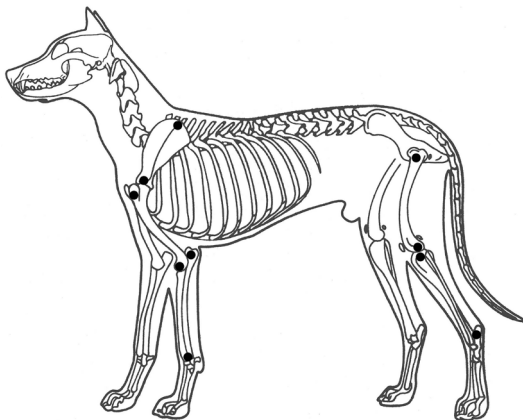


Figure 1. Markers were attached to the skin overlying the dorsal border of the scapula, the acromion, the greater tubercle of the humerus, the lateral epicondyle of the humerus, the olecranon, the styloid process of the ulna, the greater trochanter of the femur, the lateral epicondyle of the femur, the fibular head, and the lateral fibular malleolus. The marker distance (MD) was measured for the scapula (a), humerus (b), ulna (c), femur (d), and crus (e) by measuring the distance between the 2 markers.

During the first 60s the dog was standing squarely at rest, in the same position as when the markers were placed (the standing period), and in the next recording session the dog was walking on the treadmill at a constant speed of 1.4 m/s (the walking period).

Fluoroscopy

For this study, 2 markers containing lead were glued to the skin while the dog was standing squarely. One marker was placed dorsally over the spinous process of L6 (L6 marker) and one marker was placed laterally over the lateral epicondyle of the left femur (stifle marker). Because of technical limitations and the radiation hazard associated with the use of fluoroscopy, only 2 markers were used. A fluoroscopy system (6 Hz, Philips, Eindhoven, the Netherlands) was placed perpendicular to the treadmill. A video camera (24 Hz) was placed in an oblique position in such a way that the entire hind limb could be recorded. The dog was placed on the treadmill and walked at a constant speed of 0.83 m/s, during which the L6 marker and underlying skeletal structures were visualized with fluoroscopy and simultaneously video recorded. The same procedure was performed for the stifle marker. After completion of registration, the video and fluoroscopy recordings were synchronized and 13 consecutive step cycles were selected per dog ($n = 4$) for each marker.

Data Analysis

Kinematics. The three-dimensional distance between 2 individual markers placed over one bone, now referred to as marker distance (MD), was calculated for each bone using the track manager software. The left and right sides were analyzed separately, resulting in 2 MD/bone/dog, yielding 8 MD/bone ($n=4$). The distance between markers was calculated when the dog stood squarely and when the dog walked with constant gait on the treadmill during a 12-s period of sequential gait cycles. For each gait cycle, both the minimum and maximum MDs were isolated and based on these extremes average maximum and minimum MDs were calculated for each bone. To enable comparison between recordings during standing and walking, we calculated the walking/standing ratios (W/S) for separate bones. The walk-minimum ratio (Wmin/S) was defined as the ratio between the average minimum MD during walking and the average MD of the same markers during standing. The walk-maximum MD ratio (Wmax/S) was defined as the ratio between the average maximum MD during walking and the average MD of the same markers during standing. The data obtained from the left and right side of the 4 individual dogs were grouped and the ratios were used for statistical analysis.

Statistical analyses were performed using R statistical software (R version 2.10.0 (2009-10-26) Copyright (C) 2009 The R Foundation for Statistical Computing ISBN 3-900051-07-0). The Shapiro-Wilk normality test was used to

confirm the normal distribution of data. Comparisons were then made by using a linear mixed model containing both fixed and random effects. The factors incorporated in the fixed part were ‘side’ (left and right side), ‘condition’ (three levels: standing measurement, walk-maximum MD, walk-minimum MD), ‘bone’ (5 bones), and the interaction between these factors. The factors incorporated in the random part were ‘bone’ (5 bones) within ‘dog’ (4 dogs) in order to take the correlation within each dog into account. P values and confidence intervals (CIs) were calculated to compare the standing measurement with the walk-maximum MD (Wmax/S) and walk-minimum MD (Wmin/S) for each bone. The Benjamini and Hochberg False Discovery Rate procedure was used to correct for multiple testing²⁵. $P < 0.05$ was considered as statistically significant and 95% CIs were calculated for each comparison.

Fluoroscopy. Four video-film frames were selected by visual assessment from each step cycle: frame 1 (‘90° stifle’, defined as the zero starting position of the knee, in which the tibial axis was positioned at a right angle to the femoral axis²⁶), frame 2 (toe off), frame 3 (maximal flexion of the stifle joint), and frame 4 (initial ground contact). The marker position was measured in the two-dimensional images in each frame. The position of the markers was calculated as follows:

L6 marker: A line a was drawn parallel to the ventral side of vertebrae L5, L6, and L7, and a line b was drawn perpendicular to line a, touching the cranial border of L6. Then a line c was drawn from the center of the marker to line b, parallel to line a (Fig. 2A). The position of the L6 marker was measured in craniocaudal direction (length of line c in cm).

Stifle marker: A line d was drawn parallel to the shaft of the femur, and a line e was drawn perpendicular to line d, touching the distal end of the femur. Then a line f was drawn between the center of the marker and line d, parallel to line e, and a line g was drawn between the center of the marker and line e, parallel to line d (Fig. 2B). The position of the stifle marker was measured in 2 directions: in craniocaudal direction (length of line f in cm) and in proximodistal direction (length of line g in cm).

Data obtained for individual dogs were grouped and used for statistical analysis. The three parameters (lengths of lines c, f, and g) were analyzed separately. The positions of the L6 marker and the stifle marker at 90° stifle were chosen as references. The position at 90° stifle was considered the ‘neutral’ position of the hind limb, where the marker was assumed to be positioned closest to the skeletal structure of interest. The positions of the L6 marker and the stifle marker obtained from frame 1 (90° stifle) of each step cycle were used as reference values, in such a way that the marker positions in frames 2, 3, and 4 were displayed as positions relative to frame 1 to illustrate the displacement of the marker during each step cycle. Displacement of the marker cranial and/or distal to the position of the marker in frame 1 was defined as negative displacement, whereas displacement in caudal and/or proximal directions was

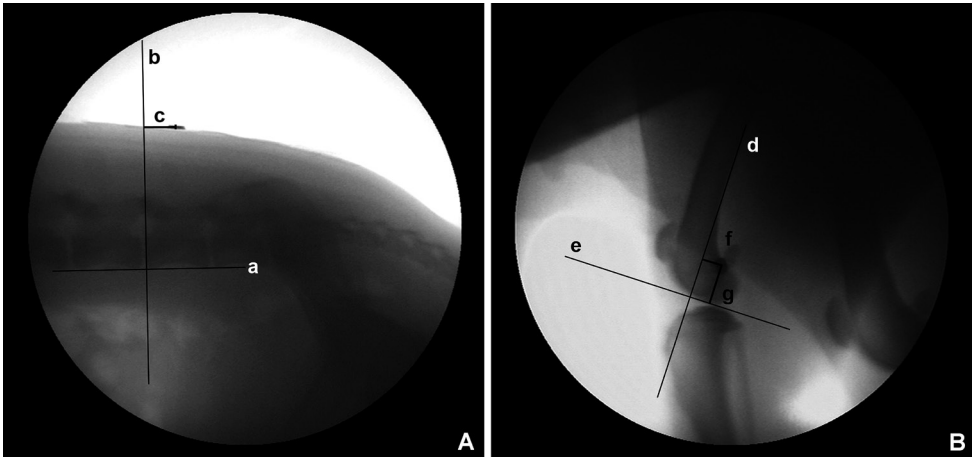


Figure 2. Line a-g were drawn in the images selected from the fluoroscopy film and the length of line c, f, and g was measured in cm. Craniocaudal direction was considered as positive and caudocranial was considered as negative. Distoproximal was considered as positive and proximodistal was considered as negative.

defined as positive displacement. Comparisons were made with the use of a linear mixed model, containing both fixed and random effects. The factor incorporated in the fixed part was 'step cycle point' (4 frames). The factor incorporated in the random part was 'dog' (4 dogs) to take the correlation within each dog into account. The Shapiro-Wilk normality test was used to confirm the normal distribution of the data, and when necessary, extreme residuals were removed to obtain normal distribution of the data. P values and CIs were calculated to determine the differences between step cycle point 1 and step cycle points 2, 3, and 4. The Benjamini and Hochberg False Discovery Rate procedure was used to correct for multiple testing²⁵. $P < 0.05$ was considered as statistically significant and 95% CIs were calculated for each comparison.

Results

Kinematics

Statistical modeling showed that the factor 'side' did not have a significant effect ($P=0.449$), indicating that there was no significant difference between measurements for the left and right sides, and therefore the data for the 2 sides were pooled.

The MD was constant for each bone when the dogs stood, but changed in an apparently repetitive pattern when the dogs walked, which seemed to be synchronous with the dog's step cycle (Table 1, Fig. 3). The mean minimum and maximum lengths of the scapula segment during walking were both smaller

than the lengths measured during standing, whereas for all other bones the mean maximum MD during walking exceeded the value during standing. This was also evidenced by the W_{max}/S , which was <1 for the scapula during walking but was >1 for the other bones (Fig. 4 and Table 2). The MD of the scapula during standing was significantly larger than both the minimum MD (-9%, $P=0.003$) and the maximum MD (-4%, $P=0.025$) during walking. The MD of the humerus during standing was significantly different from both the minimum MD (-18%, $P=0.010$) and the maximum MD (+4%, $P=0.036$) during walking. The MD of the ulna during standing was significantly different from both the minimum MD (-6%, $P=0.002$) and the maximum MD (+6%, $P=0.001$) during walking. The MD of the femur during standing was not significantly different from the minimum MD during walking ($P=0.102$), but was significantly different from the maximum MD during walking (+6%, $P=0.003$). The MD of the crus during standing was significantly different from both the minimum MD (-10%, $P=0.005$) and the maximum MD (+6%, $P=0.002$) during walking.

Bone	Standing period	Walk-min	Walk-max
Scapula	16.2 ± 1.7	14.8 ± 2.1	15.7 ± 1.9
Humerus	15.0 ± 1.2	12.2 ± 1.0	15.5 ± 1.3
Ulna	18.6 ± 1.8	17.5 ± 1.7	19.6 ± 1.9
Femur	16.0 ± 1.7	15.6 ± 1.8	17.0 ± 1.7
Crus	16.2 ± 1.2	14.7 ± 1.7	17.2 ± 1.5

Table 1. The means ± standard deviation (SD) of the marker distance (MD) in cm during standing, and the mean minimal and maximal MD during walking in kinematic gait analysis of 4 Labrador retrievers.

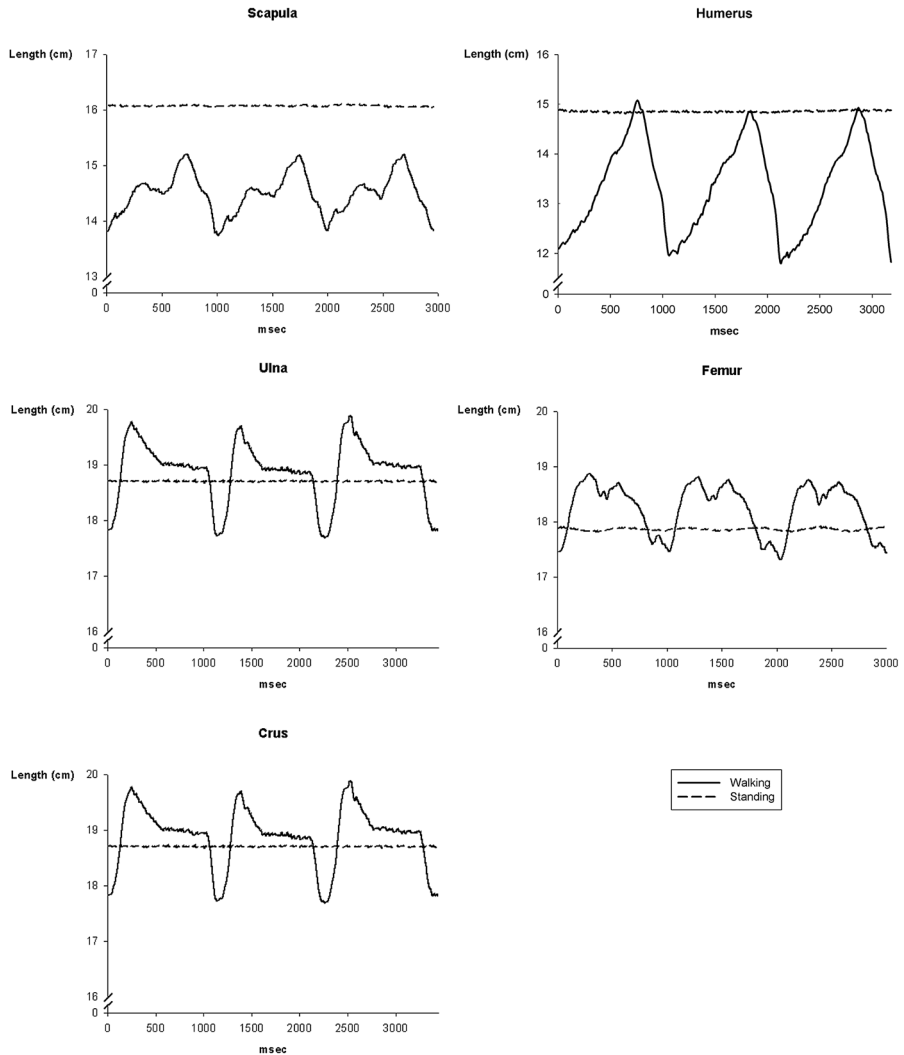


Figure 3. The distance between 2 markers attached to the skin overlying the scapula, humerus, ulna, femur, and crus during kinematic gait analysis when the dog stood and walked (three step cycles).

Ratios (Walking/Standing)

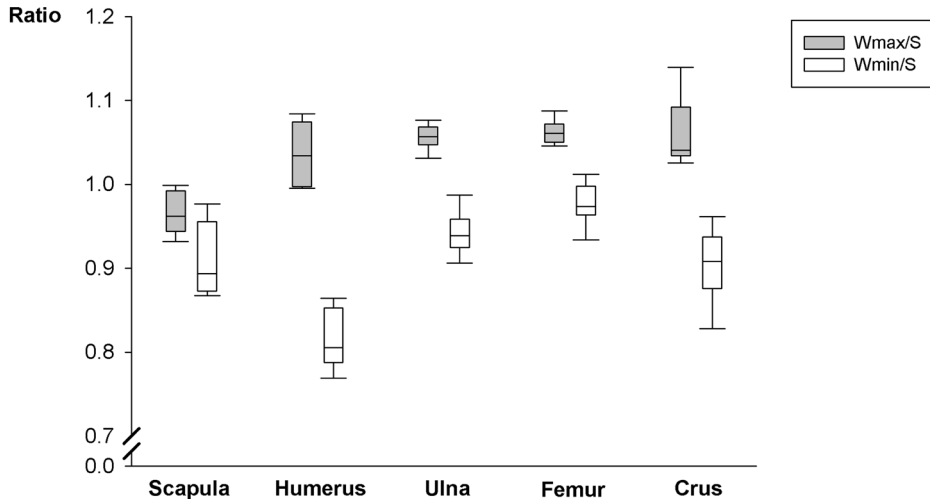


Figure 4. Boxplots of the walking/standing ratios (W/S) of marker distance representing the scapula, humerus, ulna, femur, and crus obtained from 4 Labrador Retrievers during kinematic gait analysis. W_{max}/S = ratio between the mean maximum MD during walking and the mean MD of the same markers during standing. W_{min}/S = the ratio between the mean minimum MD during walking and the mean MD of the same markers during standing.

	W_{min}/S^a			W_{max}/S^b		
	Mean	P value	CI	Mean	P value	CI
Scapula	0.91	0.003	0.88 - 0.94	0.97	0.025	0.94 - 0.99
Humerus	0.82	0.010	0.79 - 0.84	1.04	0.036	1.01 - 1.06
Ulna	0.94	0.002	0.92 - 0.97	1.06	0.001	1.03 - 1.08
Femur	0.98	0.102	0.95 - 1.00	1.06	0.003	1.04 - 1.09
Crus	0.90	0.005	0.88 - 0.99	1.06	0.002	1.04 - 1.09

Table 2. The means, P values, and 95% confidence intervals (CI) of W_{min}/S and W_{max}/S ratios in kinematic analysis in 4 Labrador retrievers. $P < 0.05$ was considered as statistically significant. *a* The walk-minimum MD ratio (W_{min}/S) = the ratio between the average minimum MD during walking and the average MD of the same markers during standing. *b* The walk-maximum MD ratio (W_{max}/S) = the ratio between the average maximum MD during walking and the average MD of the same markers during standing.

Fluoroscopy

For both markers, frame 1 (90° stifle) was used as a reference point and was compared with the values obtained in frames 2 (toe off), 3 (maximal flexion of the stifle), and 4 (initial contact). Both markers (L6 marker and stifle marker) moved in a constant pattern relative to the underlying skeletal structures (Fig. 5, Table 3). The stifle marker moved in craniocaudal and proximodistal direction at the same time. The combined displacement of the stifle marker relative to the underlying skeletal structures can be described as follows: from 90° stifle to toe off, the marker moved in a cranioproximal direction; from toe-off to maximal flexion of the stifle, the marker moved in a caudodistal direction; from maximal flexion of the stifle to initial contact, the marker moved in a cranioproximal direction; from initial contact to 90° stifle, the marker moved in a craniodistal direction.

During one step cycle, the L6 marker moved caudally compared with the position at 90° stifle, with a significant mean difference of 0.4 cm ($P<0.001$) and 0.7 cm ($P<0.001$) at toe off and initial contact, respectively (Table 4). No significant displacement was found at maximal flexion of the stifle ($P=0.408$). The stifle marker showed significant displacements in the craniocaudal plane relative to the 90° stifle phase of 1.2 cm ($P<0.001$) in the cranial direction at toe-off, and 0.9 cm ($P<0.001$) in the caudal direction at maximal flexion of the stifle, giving a maximum stifle marker displacement of 2.1 cm in the craniocaudal plane during one step cycle. No significant relative marker displacement was found at initial contact ($P=0.531$). The stifle marker showed a significant displacement in the proximodistal plane relative to the 90° stifle phase of 0.7 cm ($P<0.001$) in the proximal direction at toe off. No significant marker displacements were found at maximal flexion of the stifle ($P=0.132$) and initial contact ($P=0.879$).

Frame	L6 marker Craniocaudal (line C)		Stifle marker Craniocaudal (line F)		Stifle marker Proximodistal (line G)	
	Mean	SD	Mean	SD	Mean	SD
90° stifle	1.6	1.4	1.9	0.8	3.5	0.9
Toe off	2.0	1.3	0.8	0.6	4.2	0.9
Max flexion stifle	1.7	1.4	2.8	0.7	3.3	1.1
Initial contact	2.3	1.6	2.0	0.5	3.5	1.2

Table 3. Fluoroscopic measurements of distances (mean \pm SD) in cm between markers and predefined lines on L6 (Fig. 2A) and the stifle joint (Fig. 2B) during 13 steps in 4 walking Labrador retriever dogs each.

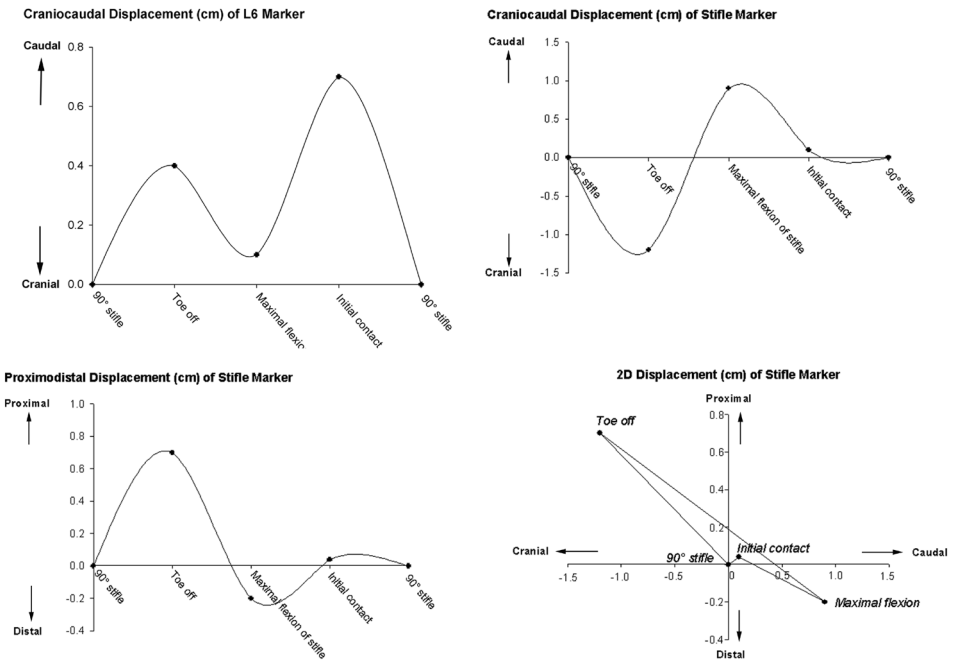


Figure 5. A) Craniocaudal displacement of the L6 marker; B) craniocaudal displacement of the stifle marker; C) proximodistal displacement of the stifle marker; and D) combined craniocaudal and proximodistal displacement of the stifle marker during fluoroscopy obtained from frame 1 (90° stifle), frame 2 (toe off), frame 3 (maximal flexion of the stifle), and frame 4 (initial contact). Displacement is displayed in values relative to frame 1. Curve fitting was applied in figures A, B, and C.

	L6 marker			Stifle marker			Stifle marker		
	Line C (craniocaudal)			Line F (craniocaudal)			Line G (proximodistal)		
	Mean	P	CI	Mean	P	CI	Mean	P	CI
F 1	1.6	-	0.7 - 2.4	1.9	-	1.6 - 2.3	3.5	-	3.2 - 3.8
F 1 - 2	0.4	<0.001	0.3 - 0.6	-1.2	<0.001	-1.4 - -0.9	0.7	<0.001	0.4 - 1.0
F 1 - 3	0.1	0.408	-0.1 - 0.3	0.9	<0.001	0.6 - 1.1	-0.2	0.132	-0.5 - 0.1
F 1 - 4	0.7	<0.001	0.6 - 0.9	0.1	0.531	-0.2 - 0.4	0.04	0.879	-0.3 - -0.4

Table 4. The means, P values, and 95% confidence intervals (CI) in cm of line C, F, and G (see Fig. 2) during fluoroscopy at frame (F) 1 (90° stifle), and comparisons with frame 2 (toe off), 3 (maximal flexion of the stifle), and 4 (initial contact). P<0.05 was considered statistically significant.

Discussion

Kinematic gait analysis is an attractive method to evaluate gait since it allows objective and precise measurement of movement in three dimensions. Kinematic gait analysis has been frequently used to assess three-dimensional motion patterns in several species, such as humans^{13,17,18}, horses^{15,27}, and dogs⁴⁻⁸. However, one confounder that needs to be addressed is the soft tissue artifact, which occurs when markers are attached to the skin to monitor the motion of underlying skeletal structures in a noninvasive manner. In human and horse kinematics, the STA significantly affects kinematic measurements^{11,15-17}. In this study, the STA was investigated in canine kinematic gait analysis by calculating both variations in marker distances (kinematic study) and individual marker displacements (fluoroscopy study). Despite the small sample population (4 Labrador retrievers), both the variations in marker distances and individual marker displacements were significant.

The aim of kinematic gait analysis using markers glued to the skin is to objectively investigate the motion of skeletal structures. Accurate and reproducible marker placement is a prerequisite for reliable results in longitudinal and comparative kinematic gait analysis. In the present study, accurate and reproducible marker placement was troublesome, because it required the dog to stand perfectly still in a square position, with its head held still in a neutral position, and its weight spread equally over all 4 limbs. The reliability of marker placement needs to be investigated further in future dog studies to determine the effects of variations caused by inaccurate or inconsistent marker placement.

The results obtained from the kinematic study indicate that the MD during walking significantly differed from the MD during standing for all bone segments investigated. The MD changed in a constant pattern during walking. The maximum MD of the humerus, ulna, femur, and crus during walking was significantly larger than the MD of these bones during standing, while the minimum MD of the scapula, humerus, ulna, and crus during walking was significantly smaller than the MD of these bones during standing. In addition, the maximum MD of the scapula during walking was significantly smaller than the MD of this bone found during standing. This latter finding can be explained by the difference in posture when a dog stands or walks: when the dog stands square, its head is held up and forward in a neutral position, resulting in a relatively long MD for the scapula; however, when the dog walks, it lowers its head, and the skin overlying the cartilago scapulae and the corresponding marker move craniodistally, resulting in a relatively shorter MD.

The 95% confidence intervals calculated for the Wmin/S and the Wmax/S indicate that, when comparing the standing dog with the walking dog, considerable variations regarding the MD are possible. These results demonstrate that, even in a uniform sample population, the skin can displace in an unpredictable fashion relative to the underlying long bones, potentially

resulting in erroneous data when conducting kinematic gait analysis.

The fluoroscopy study showed that individual skin markers move in various directions relative to the underlying skeletal structures. The L6 marker showed significant displacements in caudal direction, and the stifle marker showed significant displacements in both craniocaudal and proximal direction. However, these findings are limited by the method used to obtain them: while the skin markers move in three dimensions, fluoroscopy provides two-dimensional images of the skin markers. In addition, since visual examination was used to select the 4 frames of each step cycle in combination with a relatively low measurement frequency, it is questionable whether the exact same predefined points were selected within each dog and between different dogs. Although the results should be interpreted with caution, they do show the presence of the STA.

The STA of the left and the right side of the dogs were not significantly different, indicating that these 4 Labrador retrievers displayed a homogenous, bilateral, motion pattern of the skin when walking. We trained the dogs to walk on a treadmill prior to measurements to ensure a consistent, repeatable gait²⁸, although some investigators suggested that this is not necessary to obtain reliable data²⁹. The absence of significant differences between the left and right side suggest that joint angle measurements based on skin markers are equally affected on each side. Since most clinical gait evaluations using kinematics depend on the detection of asymmetry in joint motion, kinematic assessment of canine gait may still be possible.

The present study had limitations. In the kinematic study, the distance between 2 markers was calculated. Using the marker distance as a parameter, the contribution of the individual markers to the STA cannot be specified. However, on the assumption that the 2 markers representing a long bone move in a similar direction during each step cycle due to the skin's elasticity, although not necessarily to the same extent, the influence of an individual marker on the STA may well be larger than the combined influence measured. The fluoroscopy study was performed to investigate the contribution of the individual markers to the STA; however, only 2 markers were used because of technical problems and concern about radiation hazard. Secondly, the marker position at 90° stifle was considered the 'neutral' position of the hind limb, where the marker was assumed to be positioned closest to the skeletal structure of interest. The marker position at 90° stifle was chosen as a reference to describe the relative displacement of the marker during one step cycle. However, the actual position in which the marker is closest to the anatomical landmark of interest is during the marker placement, when the dog stands squarely. Therefore, although the described range of marker displacement is accurate, the 90° stifle point may not necessarily be the actual starting point of the marker displacement curve. Thirdly, the curves describing the 2-dimensional marker displacement were based on 4 well-defined frames within each gait cycle. Although these curves provide an informative view of the marker displacement, the precise

marker displacement in between these frames and consequently, the exact marker displacement throughout the complete gait cycle, are not described. Future research should focus on the STA of individual skin markers throughout the complete gait cycle and how the STA is influenced by breed differences, age, and body height, weight and condition.

The joint angles and changes in these angles are parameters commonly evaluated with kinematic gait analysis^{3,9,10}. In the present study, the MDs on separate bones were evaluated and no direct conclusions regarding kinematic joint angle measurements can be drawn. However, the combined results obtained from the kinematic and fluoroscopy study provide sufficient evidence for future evaluation of the soft tissue artifact in joint angle kinematics.

The aim of this study was to investigate the STA in canine kinematic gait analysis in a non-invasive manner. The STA may be significantly affected by factors such as breed, age, body height, weight, and condition. In veterinary medicine, correction algorithms have been proposed to correct for the STA in horses^{19,20}. Correction algorithms designed specifically for dogs may also be valuable to correct for the STA in dogs. The kinematic and fluoroscopic techniques applied in this study are the first steps to address the STA in dogs. In order to develop accurate correction algorithms for the STA of specific dog breeds and sizes, more invasive techniques may include insertion of percutaneous tracking markers¹¹⁻¹⁶.

In this study, a soft tissue artifact was demonstrated during kinematic and fluoroscopic gait analysis in 4 Labrador retrievers. In the kinematic study, the MD remained constant during standing but changed in a constant pattern during walking. It was similar between the right and left side of the dogs. In the fluoroscopy images, a discrepancy was found between the position of the marker and the underlying bony prominences during one step cycle, indicating that marker movement does not accurately reflect the movement of the underlying skeletal structures. It is concluded that the STA needs to be taken into account when conducting kinematic gait analysis.

Acknowledgments

We thank Hans Vernooij (Utrecht University) for assistance in statistical analysis, Jane Sykes for language corrections, and the Department of Diagnostic Imaging of the Faculty of Veterinary Medicine, Utrecht University, for technical assistance.

References

1. Burton NJ, Owen MR, Colborne GR, et al: Can owners and clinicians assess outcome in dogs with fragmented medial coronoid process? *Vet Comp Orthop Traumatol* 22:183-189, 2009.
2. Waxman AS, Robinson DA, Evans RB, et al: Relationship between objective and subjective assessment of limb function in normal dogs with an experimentally induced lameness. *Vet Surg* 37:241-246, 2008.
3. DeCamp CE: Kinetic and kinematic gait analysis and the assessment of lameness in the dog. *Vet Clin North Am Small Anim Pract* 27:825-840, 1997.
4. Tashman S, Anderst W, Kolowich P, et al: Kinematics of the ACL-deficient canine knee during gait: serial changes over two years. *J Orthop Res* 22:931-941, 2004.
5. Bockstahler BA, Henninger W, Muller M, et al: Influence of borderline hip dysplasia on joint kinematics of clinically sound Belgian Shepherd dogs. *Am J Vet Res* 68:271-276, 2007.
6. Burton NJ, Dobney JA, Owen MR, et al: Joint angle, moment and power compensations in dogs with fragmented medial coronoid process. *Vet Comp Orthop Traumatol* 21:110-118, 2008.
7. Lee JY, Kim G, Kim JH, et al: Kinematic gait analysis of the hind limb after tibial plateau leveling osteotomy and cranial tibial wedge osteotomy in ten dogs. *J Vet Med A Physiol Pathol Clin Med* 54:579-584, 2007.
8. Marsolais GS, McLean S, Derrick T, et al: Kinematic analysis of the hind limb during swimming and walking in healthy dogs and dogs with surgically corrected cranial cruciate ligament rupture. *J Am Vet Med Assoc* 222:739-743, 2003.
9. Clements DN, Owen MR, Carmichael S, et al: Kinematic analysis of the gait of 10 labrador retrievers during treadmill locomotion. *Vet Rec* 156:478-481, 2005.
10. Gillette RL, Angle TC: Recent developments in canine locomotor analysis: a review. *Vet J* 178:165-176, 2008.
11. Leardini A, Chiari L, Della Croce U, et al: Human movement analysis using stereophotogrammetry. Part 3. Soft tissue artifact assessment and compensation. *Gait Posture* 21:212-225, 2005.
12. Cappozzo A, Catani F, Leardini A, et al: Position and orientation in space of bones during movement: experimental artefacts. *Clin Biomech (Bristol, Avon)* 11:90-100, 1996.
13. Reinschmidt C, van den Bogert AJ, Nigg BM, et al: Effect of skin movement on the analysis of skeletal knee joint motion during running. *J Biomech* 30:729-732, 1997.
14. Taylor WR, Ehrig RM, Duda GN, et al: On the influence of soft tissue coverage in the determination of bone kinematics using skin markers. *J Orthop Res* 23:726-734, 2005.
15. van Weeren PR, van den Bogert AJ, Barneveld A: Quantification of skin displacement in the proximal parts of the limbs of the walking horse. *Equine Vet J* 22:110-118, 1990.
16. Lanovaz JL, Khumsap S, Clayton HM: Quantification of three-dimensional skin displacement artefacts on the equine tibia and third metatarsus. *Equine Comp Exerc Physiol* 1:141-150, 2004.
17. Andriacchi TP, Alexander EJ: Studies of human locomotion: past, present and future. *J Biomech* 33:1217-1224, 2000.
18. Alexander EJ, Andriacchi TP: Correcting for deformation in skin-based marker systems. *J Biomech* 34:355-361, 2001.

19. van den Bogert AJ, van Weeren PR, Schamhardt HC: Correction for skin displacement errors in movement analysis of the horse. *J Biomech* 23:97-101, 1990.
20. van Weeren PR, van den Bogert AJ, Barneveld A: Correction models for skin displacement in equine kinematic gait analysis. *J Equine Vet Sc* 12:178-192, 1990.
21. Gradner G, Bockstahler B, Peham C, et al: Kinematic study of back movement in clinically sound malinois dogs with consideration of the effect of radiographic changes in the lumbosacral junction. *Vet Surg* 36:472-481, 2007.
22. Bockstahler BB, Gesky R, Mueller M, et al: Correlation of surface electromyography of the vastus lateralis muscle in dogs at a walk with joint kinematics and ground reaction forces. *Vet Surg* 38:754-761, 2009.
23. Kim SY, Kim JY, Hayashi K, et al: Effect of skin movement over the stifle joint on kinematic analysis of the hind limb during trot on a treadmill in dogs. *Proc 36th Annual Conference of the Veterinary Orthopedic Society. Vet Comp Orthop Traumatol* 3, 2009. (abstr).
24. Edney AT, Smith PM: Study of obesity in dogs visiting veterinary practices in the United Kingdom. *Vet Rec* 118:391-396, 1986.
25. Benjamini Y, Hochberg Y: Controlling the false discovery rate: a practical and powerful approach to multiple testing. *J Royal Stat Soc B* 57:289-300, 1995.
26. Newton CD: Normal Joint Range of Motion in the Dog and Cat Appendix B, in Nunamaker DM, Newton CD (eds): *Textbook of Small Animal Orthopaedics* (ed 1). Philadelphia, J.B. Lippincott Company, 1985, pp 1101-1106.
27. Faber M, Schamhardt H, van Weeren R, et al: Basic three-dimensional kinematics of the vertebral column of horses walking on a treadmill. *Am J Vet Res* 61:399-406, 2000.
28. Fanchon L, Grandjean D: Habituation of healthy dogs to treadmill trotting: repeatability assessment of vertical ground reaction force. *Res Vet Sci* 87:135-139, 2009.
29. Bockstahler BA, Skalicky M, Peham C, et al: Reliability of ground reaction forces measured on a treadmill system in healthy dogs. *Vet J* 173:373-378, 2007.

Pedicle screw-rod fixation of the canine lumbosacral junction

Lucas A. Smolders ^a, George Voorhout, Renée van de Ven ^a,
Niklas Bergknut ^{a,c}, Guy C. M. Grinwis ^d, Herman A. W. Hazewinkel ^a,
Björn P. Meij ^a,

Veterinary Surgery 41(6): 720-732, 2012

^a Department of Clinical Sciences of Companion Animals, Faculty of Veterinary Medicine, Utrecht University, Utrecht, The Netherlands

^b Division of Diagnostic Imaging, Faculty of Veterinary Medicine, Utrecht University, The Netherlands

^c Department of Clinical Sciences, Division of Small Animals, Faculty of Veterinary Medicine and Animal Sciences, Swedish University of Agricultural Sciences, Sweden

^d Department of Pathobiology, Pathology Division, Faculty of Veterinary Medicine, Utrecht University, Utrecht, The Netherlands

Abstract

Objective: To assess pedicle screw-rod fixation (PSRF) of the canine lumbosacral junction (LSJ) *ex vivo* and *in vivo*.

Methods: *Ex vivo* study: PSRF of the LSJ was performed in six spinal specimens using predefined guidelines and was evaluated with radiography, computed tomography and magnetic resonance imaging. *In vivo* study: Three Greyhounds diagnosed with DLSS underwent dorsal laminectomy and partial discectomy combined with PSRF of the LSJ. Curettage of the endplates with insertion of an autologous cancellous bone graft was performed to promote spinal fusion. During the 18-month follow-up, the dogs were monitored by means of clinical evaluation, diagnostic imaging, and force plate analysis. The dogs were euthanized for reasons unrelated to the PSRF or their lumbosacral disease, and post-mortem imaging and histopathological investigations of the LSJ were performed.

Results: *Ex vivo* study: Sixteen of 24 inserted screws had an acceptable placement. *In vivo* study: Ten of 12 inserted screws had an acceptable placement. Clinical signs of ‘lower’ back pain resolved at 4 weeks after surgery. Diagnostic imaging and histopathology showed no bony spinal fusion of the LSJ. Force plate analysis revealed a trend toward improved pelvic limb function relative to the preoperative function.

Conclusions: PSRF of the LSJ of large breed dogs is technically possible. Improvement to the surgical technique to induce spinal fusion and assessment in a larger sample size are required before it can be recommended. PSRF may become a valuable addition to decompressive surgery in patients with DLSS but further work is necessary before this can be substantiated.

Key words: pedicle screw fixation; canine; lumbosacral junction; degenerative lumbosacral stenosis; laminectomy; discectomy

Introduction

Degenerative lumbosacral stenosis (DLSS) is a common cause of lumbosacral disease in dogs^{1,2}. DLSS is mostly seen in middle-aged (7-8 years), middle to large breed dogs, with a clear predisposition for the German Shepherd dog²⁻⁵. Repetitive physical overload of the lumbosacral intervertebral disc (IVD) and/or genetic predisposition may induce disc degeneration and subsequent lumbosacral instability. This instability results in degenerative changes in adjacent bony and soft tissue structures, such as facet joints, ligaments, L7 and S1 vertebrae, and endplates. These changes may contribute to spinal stenosis and cauda equina compression^{2,3,5,6}. Clinical signs include caudal lumbar pain, pain upon pressure on the LSJ, pelvic limb lameness, reluctance to perform certain exercises and activities, such as standing up and jumping, hyperesthesia, automutilation, posterior paresis, proprioceptive deficits, tail hypotonia, and urinary and fecal incontinence²⁻⁸. The diagnosis of DLSS can be challenging and should be made by combining history, clinical signs, imaging and electrodiagnostic findings⁹. Advanced imaging, such as computed tomography (CT) and magnetic resonance imaging (MRI), has the great benefit of visualizing the complex lumbosacral anatomy on multiple planes. However, degenerative lumbosacral changes in dogs without clinical signs and discrepancies between clinical/surgical and CT/MRI findings have been reported and therefore, findings obtained using these advanced imaging techniques should be interpreted with caution¹⁰⁻¹². Considerable degenerative changes in the spine of asymptomatic humans have also been reported^{13,14}.

Treatment of DLSS can be conservative or surgical. Conservative treatment is recommended when pain is the main clinical sign and consists of weight loss, physiotherapy, administration of anti-inflammatory drugs, and medication for neuropathic pain, such as gabapentin^{4,15-17}. Surgical treatment is indicated when the pain is severe and non-responsive to medical treatment, and/or when motor or sensory deficits are present^{2-5,16}. Surgical treatment consists of dorsal laminectomy, if necessary combined with partial discectomy, and is aimed at alleviating the compression of the cauda equina. Additional unilateral or bilateral facetectomy and foraminotomy (possible via lateral approach)¹⁸ may be indicated if stenosis of the intervertebral foramina is present^{3-5,18,19}. Distraction-fusion of the LSJ with pins through the L7 spinous process, facet joints, sacrum and iliac wings, has also been described⁷.

The overall short-term prognosis is generally good to excellent, and improvement of clinical signs has been reported in 69% to 93% of surgically treated cases^{2-4,15}. However, in the long-term clinical signs recur in 3% to 37% of the operated patients^{3,4,15,20}. Moreover, decompressive surgery does not completely restore hind limb propulsion in dogs with DLSS¹⁶. These adverse outcomes may be due to lumbosacral instability after the decompressive procedure with acceleration of degenerative changes and recurrence of clinical signs^{3,4,15}.

In human medicine, surgical decompression combined with pedicle screw-rod fixation (PSRF) of the spinal segment has long been used to successfully treat spinal stenosis, spinal instability, and degenerative disc disease^{21,22}. The aim of PSRF is to facilitate bony fusion of one or multiple spinal segments, thereby stabilizing the decompressed spinal segment and preventing further degenerative changes^{22,23}. In the veterinary literature, PSRF has been biomechanically evaluated in canine cadaveric spines and has been shown to effectively stabilize the canine LSJ after decompressive surgery²⁴. PSRF of the canine lumbosacral spine *in vivo* was reported for the first time by Méheust et al. (2000)^{25,26}. A similar technique used in dogs consisted of dorsal insertion of screws in the pedicles of L7 and S1 and fixation of the screw heads in a cement bridge¹⁹. However, limited clinical experience with PSRF in dogs and its long-term clinical results warrants further evaluation of this surgical procedure. To this end, the aims of this study were to 1) investigate the safe corridors for pedicle screw insertion into the canine L7 and S1 vertebrae *ex vivo* in canine cadaveric spines, and 2) assess the effect of insertion of pedicle screws in the canine lumbosacral spine *in vivo* in a pilot study involving three dogs with DLSS.

Materials and Methods

Implantation corridor definitions and parameters

The pedicle is defined as the structure connecting the vertebral lamina with the vertebral body²⁷. Two LSJs (L7-S1, including the surrounding soft tissue structures) were isolated from one adult Golden Retriever dog (age, 6 years; weight, 25.1 kg) and one mixed-breed dog (age, 2 years; body weight, 21.0 kg). One spinal specimen was used for histological examination. The LSJ was isolated from the frozen spinal segment and cut into transverse histological sections (thickness: 25 μ m). The slices were fixed in 10% neutral buffered formalin, routinely stained with hematoxylin and eosin (H&E). The other spinal specimen was sawn in the parasagittal plane, through the middle of the L7 and S1 pedicle, with the use of a water-cooled diamond saw (Exact Standard precision saw 300 CL, \varnothing 1mm, Klinipath, Duiven, the Netherlands). On the basis of evaluation of the transverse and sagittal sections, the following implantation corridor definitions and parameters were defined:

- *The pedicle screw entry point* (EP). For L7, the EP was defined as the intersection between the line crossing the caudal border of the facet joint and the cranio-caudal line crossing the base of the transverse process (Fig. 1). For S1, the EP was situated halfway between the caudal border of the cranial articular process and the intermediate sacral crest²⁴.
- *The optimal implantation corridor* runs in a dorso-caudo-lateral to ventro-cranio-medial oblique direction from the dorsal cortex of the lamina to the

ventral cortex of the vertebral body, without perforating the ventral cortex, the medial pedicle wall, or the lateral pedicle wall²⁴. Optimal screw anchorage is achieved by involving, but not perforating, as many cortices as possible.

- The *transverse insertion angle* (α) was defined as the angle between the optimal implantation corridor and the sagittal plane (Fig. 2).
- The *sagittal insertion angle* (β) was defined as the angle between the line drawn parallel to the cranial endplate and the optimal implantation corridor, with a dorsocaudal to ventrocranial screw direction (Fig. 3).
- The *length of the implantation corridor* (L) was used to determine the optimal length of the pedicle screws to achieve optimal screw anchorage.
- The *minimal pedicle width* (W) was used to determine the optimal screw width to achieve maximum screw anchorage.

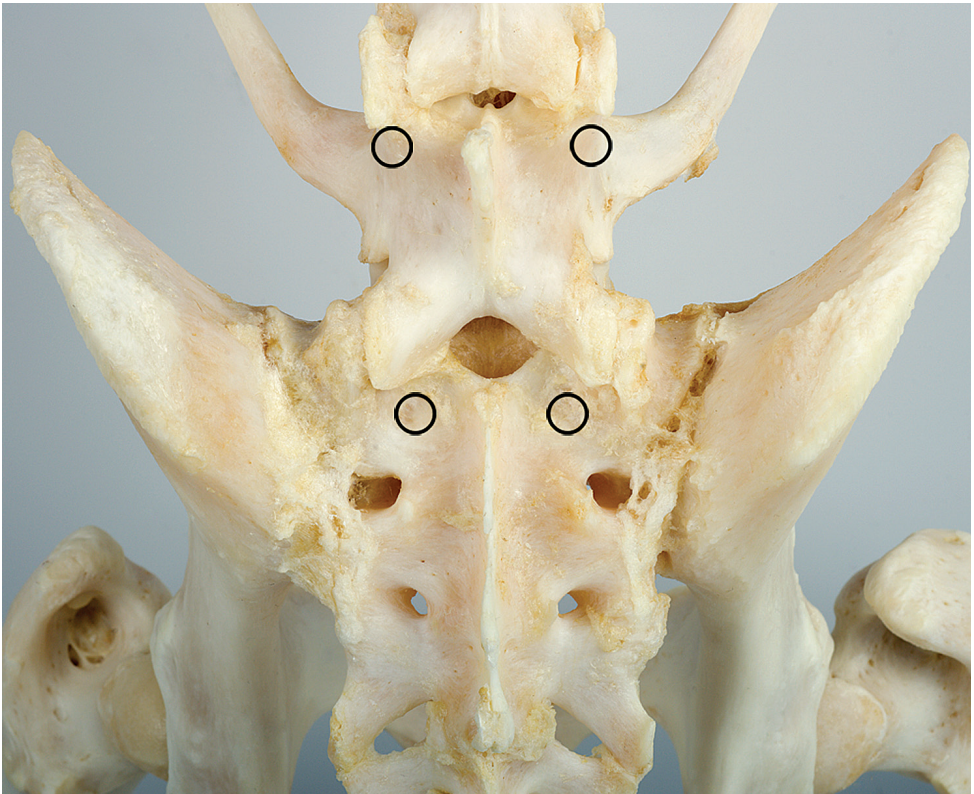


Figure 1. Dorsal view of the skeletal structures of the canine lumbosacral spine, showing the pedicle screw entry points into L7 (top two circles) and S1 (bottom two circles) vertebrae.

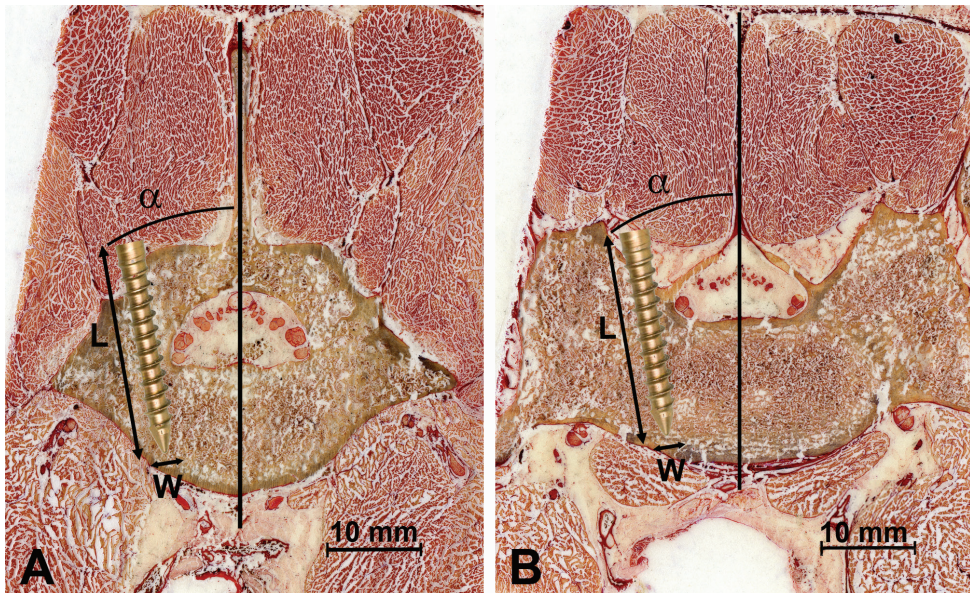


Figure 2. Transverse histological sections through the pedicle of L7 (A) and S1 (B), showing the optimal implantation corridor and the corresponding length of the implantation corridor (L), the minimum pedicle width (W), and the transverse insertion angle (α). H&E stain.

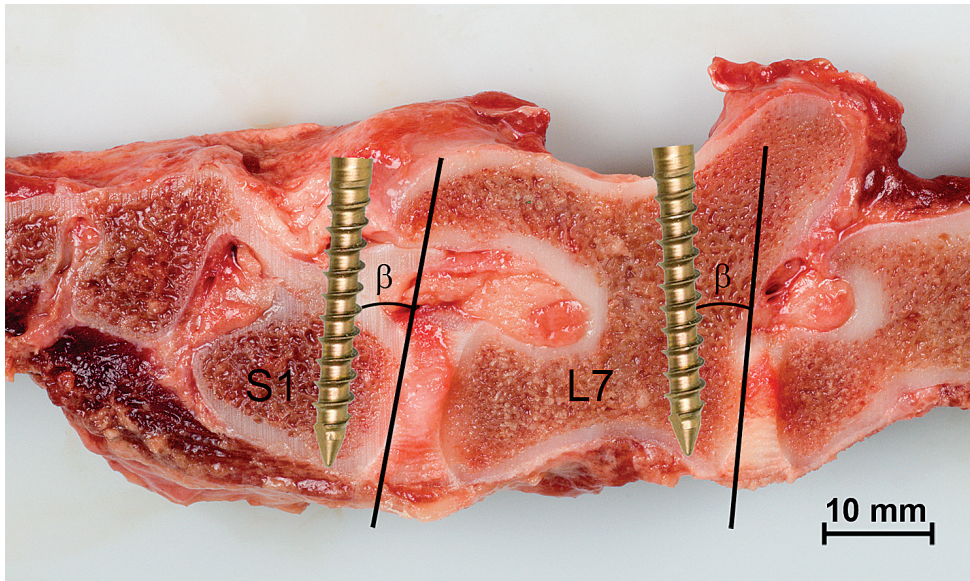


Figure 3. Parasagittal section through the pedicles of L7 and S1 of a canine lumbar spine specimen, showing the optimal implantation corridors and the corresponding sagittal insertion angle (β).

Ex vivo cadaver study

Specimens

Six spinal specimens were isolated from six healthy, adult Labrador Retriever dogs (three males and three females). All dogs were euthanized in unrelated experiments at 20 to 39 months of age (weight range, 28 to 32 kg). During their life span, the dogs had had a normal level of activity and had no known history of spinal problems. The specimens were harvested immediately after death. Each specimen included the L3-L7 spine, the sacrum with the pelvis attached, the tail base with the first coccygeal vertebra, and the surrounding soft tissue structures. The specimens were wrapped in saline-soaked towels to prevent specimen dehydration and were subsequently frozen at -20°C . Specimens were thawed at 4°C for 1 day before use.

Imaging

Survey radiography: ventrodorsal, lateral, left-ventral to right-dorsal oblique, and right-ventral to left-dorsal oblique radiographs of the LSJ were made.

CT: Contiguous 2 mm thick slices with 1 mm overlap were obtained from the caudal half of L6 to S2 using a single slice spiral CT scanner (Philips Secura, Philips, NV, Eindhoven, the Netherlands) was used with exposure settings of 120 kV and 260 mA, a pitch of 0.5, and a scan time of 1 sec per rotation. Transverse images and reconstructed sagittal images were analyzed with the use of CT computer software (Philips CT Secura, Philips Medical Systems, Eindhoven, the Netherlands).

MRI: Images were obtained with a 0.2 Tesla open magnet (Magnetom Open Viva, Siemens AG, Germany). T1-weighted images (repetition time (TR), 510 to 624 ms; echo time (TE), 26 ms) and T2-weighted images (TR, 3835 to 4455 ms; TE, 117 ms) were made in sagittal, transverse and dorsal planes. T2-weighted images were obtained with a repetition time of 3835.0 to 4455.0 ms with an echo time of 117.0 ms in sagittal and transverse planes. Contiguous 3 mm thick slices were obtained. Additionally, flash 3D compositions (TR, 34 ms; TE, 12 ms) were made for the 3D assessment of each inserted screw with a slice thickness of 1.4 mm.

Implantation corridor parameters

The guideline values for the implantation corridor parameters L, W, and α were calculated based on the transverse CT images, and the β was calculated based on the reconstructed sagittal CT images. For each spinal specimen, the implantation corridor parameters were calculated for all CT slices in which a reliable calculation was possible using CT computer software (Philips CT Secura, Philips Medical Systems, Eindhoven, the Netherlands). Means \pm SD were calculated for each parameter.

Surgical procedure

PSRF of the LSJ was performed in the six spinal specimens, using the calculated implantation corridor parameters. All surgical procedures were performed by an experienced veterinary neurosurgeon (BPM). Pedicle screw insertion was performed as described by Meij et al. (2007)²⁴. Briefly, a dorsal midline incision, ranging from the spinous process of L6 to S1, was made. The EPs were identified and pedicle screw entry holes were prepared with an awl. Both α and β were used to determine the exact angle of screw insertion. The pedicle screw corridors were prepared in the cancellous bone within the pedicle with a pedicle probe (Synthes®, Zeist, the Netherlands). Once the ventral cortex was reached, the corridor length was measured and the pedicle probe was removed from the screw corridor. To facilitate screw anchorage in the ventral vertebral cortex, predrilling of the dorsal part of the ventral cortex was performed with a K-pin (1.2 mm) without perforating the ventral cortex.

On the basis of the guideline values for L and W, four 25-mm long, 4-mm wide titanium pedicle screws (USS Small Stature, Synthes®, Zeist, the Netherlands) were selected (Fig. 4). The pedicle screws (two into L7; two into S1) were inserted into the pedicle and vertebral body, using the depth measurements as a reference. Approximately 50-80% of the total screw length was inserted into the vertebral body, leaving 20-50% of each screw protruding from the vertebra. Two 5-cm long, 5-mm wide titanium rods were used to connect the L7 pedicle screws with the respective ipsilateral S1 pedicle screws. This particular PSRF construct has been designed specifically for fixation of the pediatric human spine and is currently the smallest option available. The rod was slightly adjusted with a rod bender to acquire a proper fit on both screw heads. Once a snug fit was obtained, the sleeves and nuts were applied and tightened.



Figure 4. The components of the titanium pedicle screw and rod fixation construct, with the nut (top left), the sleeve (top right), the pedicle screw (middle), and the interconnecting rod (bottom).

Postsurgical evaluation

Survey radiography was used to assess the overall position of each screw. CT and MRI (as described for the presurgical evaluation) were used to evaluate pedicle screw placement. The extent of pedicle wall penetration and ventral cortex penetration were determined for each screw based on the CT images, using the criteria described by Schizas et al. (2006)²⁸. Penetration was classified as cortical encroachment if either the lateral or medial pedicle cortex could not be visualized and if bone in excess of 2 mm was visible on the opposite side. Penetration was classified as frank penetration when both the cortex was invisible and when the screw trajectory was clearly outside the pedicle boundaries²⁸. The MR images were assessed for soft tissue damage, i.e. the IVD, the cauda equina, and the vessels situated ventrally to the ventral cortex of the vertebral body. Pedicle screw placement was classified as optimal, acceptable, or unacceptable based on our own developed criteria partly based on previous studies (Table 1)^{28,29}.

Classification	Criteria
Optimal	-in the center of the pedicle -involvement of the ventral cortex -involvement of both the medial and lateral pedicle wall
Acceptable	-cortical encroachment of medial or lateral pedicle wall -minor (< 7.0 mm ²⁹) penetration of the ventral cortex -no involvement of the ventral cortex

Table 1. Classification criteria for the assessment of pedicle screw placement. IVD= intervertebral disc.

In vivo study

Animals

Three adult Greyhound dogs (two males, one female; age range, 8-9 years; weight, 24-33kg), of the Department's colony, used for education of veterinary students and as blood donors, were diagnosed with DLSS. The dogs were housed individually (1.5 x 1.8 m indoor kennel and 1.5 x 5.0 m outdoor kennel; 20 hours/day) and in groups (outside kennel: 7.5 x 5.0 m; 4 hours/day). The daily exercise level of the dogs before surgery consisted of 1-hour leash walks and running in the large outside kennel for 4 hours. The dogs showed unilateral pelvic limb lameness, reluctance to rise, and a positive lumbosacral pressure test, and were painful upon extension of the LSJ. Diagnostic imaging (as described for the ex vivo study), with the LSJ of the dogs in extended

position, revealed stenosis of the lumbosacral vertebral canal due to protrusion of the L7-S1 IVD, grade III IVD degeneration according to the Pfirrmann scale (inhomogeneous IVD structure with decreased signal intensity, unclear distinction between the nucleus pulposus and annulus fibrosus, and slightly decreased disc height)³⁰ with moderate ventral spondylosis of the LSJ (Fig. 5). There was no overt lateralized disc protrusion that could explain the lateralized pelvic limb lameness. Significant foraminal stenosis was not observed with CT/MRI. The history and clinical signs of the dogs, and findings on clinical examination in combination with radiographic, MR, and CT imaging on multiple planes, led to the diagnosis DLSS. After initial diagnosis of DLSS, the dogs were treated conservatively with anti-inflammatory drugs (carprofen, 2 mg/kg, twice daily, PO) during multiple 2-week periods, for a total of 6 weeks. Although clinical signs temporarily resolved, recurrence of lumbosacral pain was noted in all dogs up to a point that the dogs could not be used for blood donation or educational purposes. Therefore, surgical therapy was elected to permanently resolve the clinical signs.

Surgical procedure

The dogs underwent general anesthesia and decompressive surgery combined with PSRF of the LSJ. Decompressive surgery consisted of dorsal laminectomy combined with partial discectomy as described by Sharp and Wheeler (2005).¹⁹ Subsequently, curettage of the endplates was performed without broaching. In dog 1, an autologous cancellous bone graft, obtained from the spinous processes and dorsal lamina, was inserted into the L7-S1 disc space to promote spinal fusion. In dogs 2 and 3, the autologous cancellous bone graft was first mixed with biocompatible β -tricalcium phosphate (chronOS, Synthes, Zeist, The Netherlands) before insertion. A free autologous fat graft was placed around the cauda equina, a ventral fat sling was placed between the annular defect and the cauda equina, and a larger fat graft was positioned in the laminar defect dorsal to the cauda equine⁹.

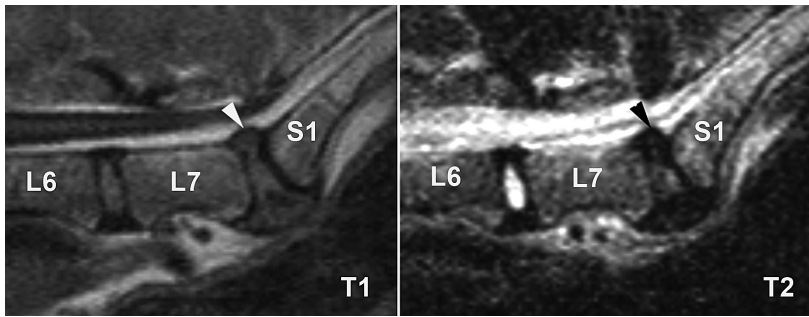


Figure 5A. Pre-operative mid-sagittal T1- and T2-weighted MR images of dog 1 showing loss of the nucleus pulposus water signal, dorsal protrusion of the intervertebral disc (arrowhead), and stenosis of the lumbosacral vertebral canal.

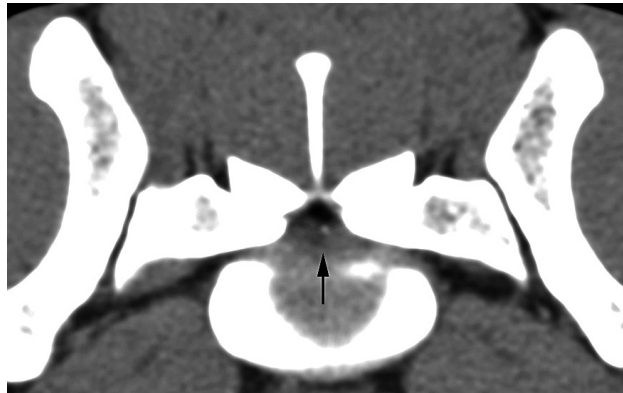


Figure 5B. Pre-operative transverse computed tomography image of dog 3 showing stenosis of the lumbosacral vertebral canal by midcentric dorsal protrusion of the L7-S1 intervertebral disc (arrow).

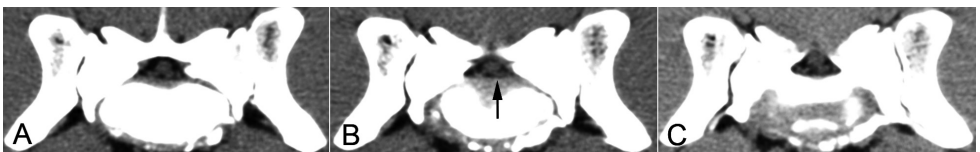


Figure 5C. Pre-operative serial transverse computed tomography images (from cranial (A) to caudal (C)) of dog 1 showing ventro-dorsal compression of the dural sac by midcentric dorsal protrusion of the L7-S1 intervertebral disc (arrow).

After decompressive surgery, the LSJ was stabilized with the use of PSRF, as described for the *ex vivo* cadaver study (Fig. 6). Intra-operative fluoroscopy was used to confirm the position of each screw. In dog 3, additional β -tricalcium phosphate (chronOS, Synthes, Zeist) and autologous bone graft were applied onto the lateral sides of the titanium rods to stimulate spinal fusion. The overlying muscle, fascia, subcutaneous and skin layers were apposed and closed in routine fashion.

Post surgical treatment consisted of 6 weeks of cage rest followed by 6 weeks of leash restraint. Thereafter, dogs had similar exercise levels as preoperatively. The dogs received buprenorphine (10 μ g/kg, SC) for 3 days, carprofen (2 mg/kg twice daily, PO) for 10 days and amoxicillin-clavulate (12.5 mg/kg twice daily, PO) for 10 days.

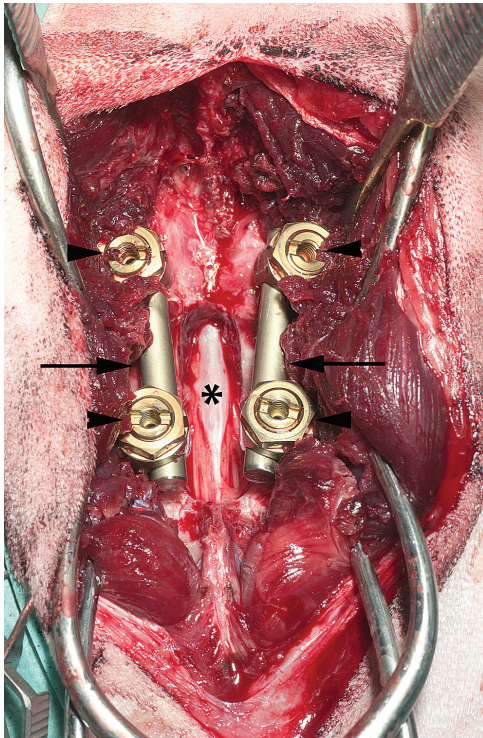


Figure 6. Dorsal view of the lumbosacral junction after decompressive surgery and pedicle screw and rod fixation, showing the laminectomy defect (asterisk), the lumbar (top arrow heads) and sacral (bottom arrow heads) pedicle screws, and the interconnecting rods (arrows).

Clinical examination

Each dog was observed daily and was clinically examined at 1 day, 1 week, 1 month, 6 months, 12 months, and 18 months after surgery. Clinical examination consisted of a complete general physical, orthopedic, and neurological examination. The lumbosacral spine was not manipulated until 1 week after surgery. Follow-up was discontinued after 18 months due to old age of the dogs.

Diagnostic imaging

Imaging was repeated at 3 and 12 months after surgery and post-mortem. The pedicle screw placement and the degree of fusion between the L7 and S1 vertebrae were assessed. Placement of the screws was assessed with the use of the classification criteria described for the *ex vivo* study.

Force plate analysis

Force plate analysis of each dog was performed as reported previously¹⁶, 1 day before surgery and 1 week, and 1, 6, 12, and 18 months after surgery. The vertical (Fz) and craniocaudal (Fy) forces, associated with paw placement, were recorded for all four limbs. The average of at least 10 recordings per limb was used for data processing.

The peak vertical force (Fz), the peak braking force (Fy+), and the peak propulsive force (Fy-) were calculated for each limb.¹⁶ Ratios reflecting the distribution of forces over all four limbs were calculated separately for each dog. The pelvic/thoracic limb ratio (P/T) for Fz (P/T Fz) was defined as the ratio between the sum of the peak Fz for the pelvic limbs and the sum of the peak Fz for the thoracic limbs, and describes the distribution of weight over the thoracic and pelvic limbs. The P/T Fy+ was defined as the ratio between the sum of the peak Fy+ for the pelvic limbs and the sum of the peak Fy+ for the thoracic limbs, and describes the distribution of the braking force over the thoracic and pelvic limbs. The P/T Fy- was defined as the ratio between the sum of the peak Fy- for the pelvic limbs and the sum of the peak Fy- for the thoracic limbs and describes the distribution of the propulsive force over the thoracic and pelvic limbs.

Histopathology

Dogs 1, 2, and 3 were euthanized at 28, 23, and 31 months after surgery, respectively, for reasons unrelated to this study. At this time, dogs 1, 2, and 3 were 12 years and 1 month, 11 years and 7 months, and 11 years and 5 months of age, respectively. After euthanasia, the spinal specimens were isolated from the dogs. Paramedian sections through the lumbosacral segments were cut with a diamond saw (Exact Standard precision saw 300 CL, \varnothing 1mm, Klinipath, Duiven, the Netherlands), fixed in 10% neutral buffered formalin, decalcified in EDTA for 3 months, and embedded in paraffin. The specimens were cut into 4 μ m sections and routinely stained with hematoxylin and eosin (H&E) for histopathological examination.

Results

Ex vivo study

Implantation corridor parameters

Guideline values for insertion of the pedicle screws into the spinal specimens were derived from the implantation corridor parameters in the six cadaveric spinal specimens (Table 2). For L7, the mean guideline values for α and β were 8.7° and 13.3° , respectively; for S1, the mean guideline values for α and β were 8.2° and 19.7° , respectively.

Parameter	L7 pedicle	S1 pedicle
L (mm)	19.7 ± 1.4	14.4 ± 1.2
W (mm)	6.0 ± 0.7	10.8 ± 1.6
α ($^\circ$)	8.7 ± 0.8	8.2 ± 1.4
β ($^\circ$)	13.3 ± 3.4	19.7 ± 2.2

Table 2. Means \pm SD for guideline values for screw insertion into the L7 and S1 pedicle. The measurements were calculated from the computed tomography images of six spinal specimens from adult Labrador Retrievers. L= length of optimal implantation corridor; W= minimum width of implantation corridor; α = transverse insertion angle; β = sagittal insertion angle.

Screw Placement

On the basis of the postoperative radiographs, CT images, and MR images of the six spinal specimens, the placement of 16 of the 24 screws inserted (66.7%) was acceptable. The tip of 2 screws (8.3%) did not reach into the ventral cortex, the tip of 2 screws (8.3%) contacted the ventral vertebral cortex without perforating it, and the tip of 12 screws (50.0%) penetrated the ventral cortex (penetration ranging from 2-5 mm). Cortical encroachment of the medial pedicle wall was observed with 11 screws (45.8%) of the inserted screws; these placements were classified as acceptable.

The placement of 8 screws (33.3%) was unacceptable: 4 screws (16.7%) showed frank penetration of the medial pedicle wall, causing displacement of the cauda equina nerve roots. Three screws (12.5%) penetrated into the IVD space and 4 screws (16.7%) penetrated into the ventral cortex by more 7 mm, but MRI showed no visible damage to ventral soft tissue structures.

In vivo study

Clinical examination

All dogs were able to walk, trot, and run without signs of lameness or pain during the entire 18-month-follow-up period. No proprioceptive deficits were noted and all dogs were able to urinate and defecate without any signs of discomfort. Dog 1 developed discospondylitis of L7-S1 with caudal lumbar pain at 24 months after surgery (after follow-up period), which was diagnosed based on clinical examination, survey radiography, CT, and MR imaging. The discospondylitis was managed successfully with antimicrobial therapy. Dog 2 had a stiff gait at 6, 12, and 18 months after surgery. The stiff gait observed in dog 2 was investigated by general and orthopedic examination and was mainly attributed to old age of the dog. The dog remained active and showed no signs of discomfort. Dog 3 developed lumbar back pain 1 year after surgery and was treated with carprofen (20 mg, PO twice daily). The pain subsided after 7 days of treatment.

Diagnostic imaging

Of the 12 screws inserted, 4 (33.3%) had an optimal placement, 6 (50.0%) an acceptable placement, and 2 (16.7%) an unacceptable placement (Fig. 7). Cortical encroachment of the medial pedicle wall was observed with 7 screws (58.3%) and frank penetration was found with 1 screw (8.3%). Implant failure was observed with 1 screw (8.3%). One screw (8.3%) penetrated into the ventral cortex (5 mm). There was no bony fusion of the L7 and S1 vertebral bodies in any of the dogs. At 3 months after surgery, diagnostic imaging showed an irregular caudal endplate of L7 and increased signal intensity on T2-weighted images at the L7 endplate in all three dogs. Imaging at 12 months after surgery and post-mortem examination showed that the endplate remained irregular in dogs 2 and 3. However, in dog 1 the post-mortem imaging revealed extensive sclerosis of the caudal endplate of L7 and the cranial endplate of S1, and a vacuum phenomenon of the L7-S1 IVD space. The latter findings were attributed to the development of discospondylitis of the L7-S1 IVD in this dog 24 months after surgery, which was managed with antimicrobial therapy at the time and was not a deciding factor for euthanasia.

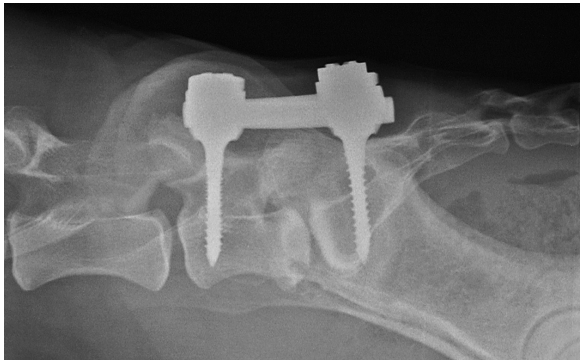


Figure 7A. Lateral radiograph of the lumbo-sacral junction in dog 1, 1 year after surgery. Both the lumbar and sacral screws appear to be positioned well. There is no bony fusion of the lumbo-sacral junction.

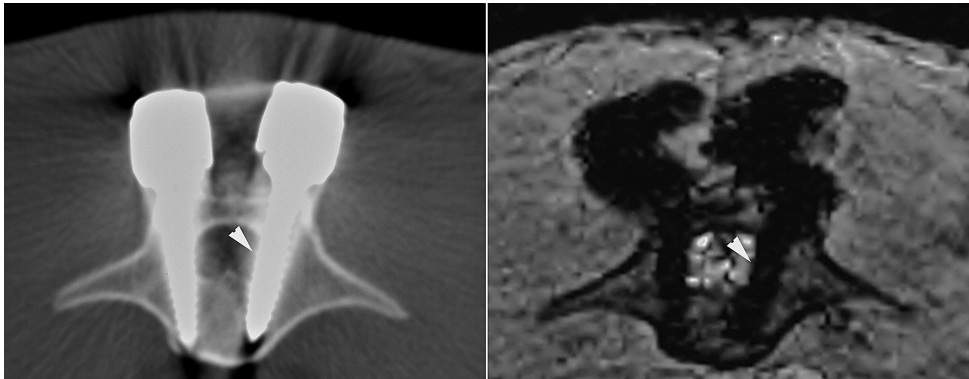


Figure 7B. Transverse computed tomography (left) and magnetic resonance (right) images through the L7 pedicle screws in dog 2, 1 year after surgery. The placement of the left screw was classified as acceptable due to the cortical encroachment of the medial pedicle wall, while the right screw was classified as unacceptable due to the frank penetration of the medial pedicle wall (arrowhead). Both screws reach into the ventral cortex.



Figure 7C. Transverse computed tomography (left) and magnetic resonance (right) images through the S1 pedicle screws in dog 2, 1 year after surgery. The left screw was classified as acceptable due to the cortical encroachment (arrowhead) of the medial pedicle wall, while the right screw was classified as optimal. Both screws reach into the ventral cortex.

Force plate analysis

P/T Fz (vertical force): One month after surgery, all three dogs had a reduced P/T Fz (Fig. 8). Despite a decrease at 12 months after surgery in dog 1, the P/T Fz gradually increased in dogs 1 and 3 during follow-up, being higher at 6 and 12 months after surgery than before surgery, respectively. Dog 2 showed a fluctuating pattern, with the P/T Fz reaching the preoperative value at 3 months after surgery, declining up to 12 months, and increasing thereafter.

P/T Fy+ (braking force): In dog 1, the P/T Fy+ values fluctuated over the 18-month follow-up. In dog 2, the P/T Fy+ had decreased relative to the preoperative value 1 month after surgery, whereas in dog 3 it had increased. The P/T Fy+ had increased 3, 6, and 12 months after surgery in dogs 2 and 3. In all three dogs, the P/T Fy+ was lower 18 months after surgery than before surgery.

P/T Fy- (propulsive force): After an initial decrease in the P/T Fy- 1 month after surgery, the P/T Fy- increased up to 12 months after surgery in dogs 1 and 2. In dog 3, the P/T Fy- was lower 1 month after surgery than before surgery; it was higher at 3 months, but was lower at 6 months. In all three dogs, the P/T Fy- was higher at 12 months and 18 months after surgery than before surgery.

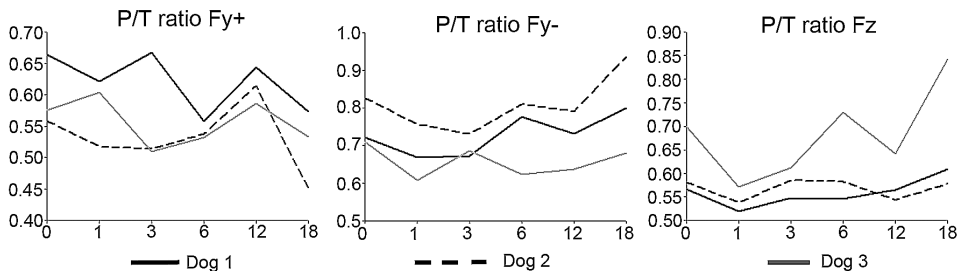


Figure 8. Line curves of the P/T Fy+, P/T Fy-, and P/T Fy- in three Greyhounds with degenerative lumbosacral stenosis after pedicle screw and rod fixation over a follow-up period of 18 months.

Histopathology

In all three dogs, the IVD was mainly composed of fibrous and chondroid tissue (Fig. 9). The ventral and lateral annulus fibrosus showed a lamellar configuration of fibrous tissue. The lumbosacral segments in dogs 1 and 2 showed moderate to marked irregularity of the L7 endplate with loss of compact bone and proliferation of cell-poor fibrovascular granulation tissue, extending into the bone marrow of the adjacent vertebral body. In dog 1, multifocal depositions of slightly granular proteinaceous material surrounded by moderate to high numbers of macrophages were observed. In the same animal, multiple dilated lymph vessels and multifocal plasmacytic and histiocytic infiltrates were found in the dorsal part of the annulus fibrosus, which were attributed to the

development of discospondylitis of the L7-S1 IVD 24 months after surgery. Spinal bony fusion of the endplates was not observed in any of the dogs.

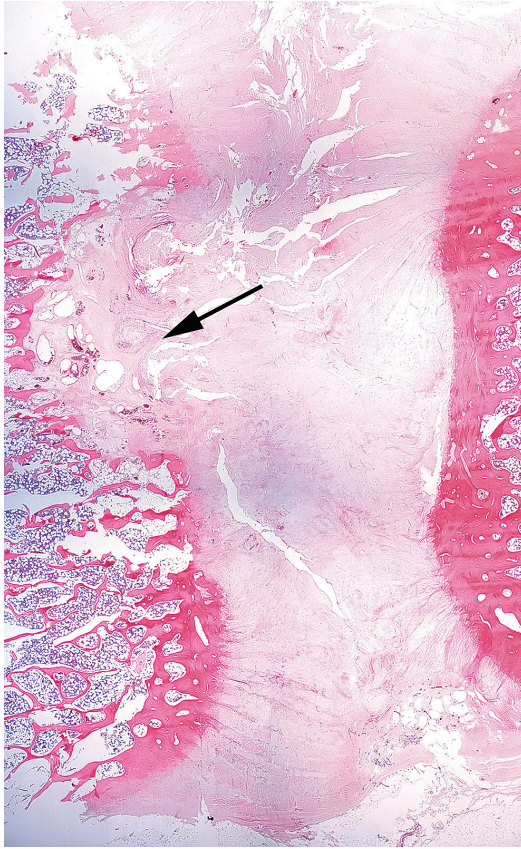


Figure 9. Histopathological section of the L7-S1 IVD of dog 1, illustrating the absence of osseous fusion of the lumbar and sacral vertebrae. Note the unilateral marked irregularity of the endplate with loss of compact bone and proliferation of cell-poor granulation tissue extending into the bone marrow of the adjacent vertebral body of L7. A multifocal granulomatous reaction is present in this area (arrow). H&E stain.

Discussion

Surgical fixation of the LSJ is not a common procedure in veterinary medicine. Several lumbosacral fixation techniques have been described in the veterinary literature,^{5,7,19,20,25,26,32} some of which have been evaluated in a clinical setting over an adequate follow-up period^{1,7,26,32}. Slocum et al. (1986) described a distraction-fusion technique, which consisted of enlarging the collapsed lumbosacral IVD space and foramina, relieving the pressure on the nerve roots, and stabilizing the LSJ by inserting pins from the base of the L7 spinous process, through the facet joints and into the sacrum and the iliac wings⁷. Ullman et al. (1993) described a modified transilial pin technique to repair and fix fracture/luxation of the LSJ in six dogs³². Bagley (2003) described distraction of the LSJ, followed by removal of the articular cartilage of the facet joints and insertion of cortical bone screws ventrolaterally across the facets through the sacrum³¹.

Although some clinical results of the above described procedures have been reported, long-term follow-up information is not available.

In human medicine, decompression followed by spinal fusion (either instrumented or non-instrumented) is the most common procedure for surgical treatment of degenerative disc disease^{33,34}. Numerous spinal instrumentation techniques have been described and applied.³⁵ Instrumented spinal fixation significantly contributes to the rate of complete bony fusion compared with spinal fusion without instrumentation³⁶⁻³⁸, and biomechanical studies have shown that pedicle screw fixation is superior to other methods for stabilizing the lumbar spinal segment^{39,40}. Pedicle screw fixation is generally regarded as a relatively demanding technique with a clear learning curve and carries several potential risks, such as damage to neurological structures caused by screw misplacement^{21,28,41}. Therefore, in order to customize this surgical technique for the canine LSJ, we defined entry points and guideline values for safe pedicle screw insertion into the canine L7 and S1 vertebrae. Other reports describing guideline values for optimal pedicle screw corridors in the canine LSJ defined screw insertion corridors directed either parallel to or divergent from the sagittal plane (screw corridors directed from dorsomedial to ventrolateral)^{25,26,29}. We chose to use a converging screw insertion pattern in a triangular fashion (screw corridors directed from dorsolateral to ventromedial), which is the preferred method in the human spine⁴². This screw orientation has been shown to significantly improve the pull-out strength and stabilizing function of the implants compared with a parallel screw orientation^{43,44}.

Although survey radiography is a common method for general postoperative assessment of screw position, it gives no three-dimensional information and screw misplacement can be easily overlooked⁴⁵. CT imaging is generally regarded as the gold standard for imaging the vertebral morphometry⁴⁶ and has been reported to be 10 times more sensitive in detecting medial pedicle perforations than survey radiography^{45,47}. MRI is a valid method to assess the three-dimensional position of MRI-compatible titanium screws; it is inferior to CT for visualizing cortical bone structures⁴⁵, but superior for visualizing soft tissue structures. Although relatively expensive, titanium screws considerably reduce artifacts on MR imaging; consequently, the use of titanium pedicle screws facilitates the surgeon's ability to accurately evaluate the position of the pedicle screw^{41,48,49}. The combined use of CT and MRI may be the optimal method for assessing pedicle screw position.

Pedicle screw insertion into the canine cadaveric lumbosacral spine resulted in unacceptable screw placement in 33.3%. Unacceptable screw placement was defined as frank penetration of the medial pedicle wall, greater than 7 mm penetration of the ventral vertebral cortex, and/or penetration of the IVD. Studies evaluating the safety of pedicle screw insertion in human cadaveric spinal specimens have reported misplacement rates of 5.5-24%^{50,51}. Discrepancies between the results obtained in the present study and in the human studies may be explained by several factors, such as differences in pedicle dimensions

between species, operation of different spinal levels, the relatively high level of experience of spine surgeons working with human patients, the use of technical aids to facilitate screw insertion⁵¹, and differences in evaluation methods.

There are few reports of pedicle screw fixation of the canine LSJ *in vivo* in the veterinary literature. Sharp et al. (2005) described pedicle screw insertion into the L7 and S1 pedicles, followed by placement of a cement bridge between L7 and S1¹⁹. Méheust (2000) described pedicle screw fixation of the LSJ in five dogs diagnosed with cauda equina syndrome²⁶; however, procedures to induce fusion were not used. Fixation of the LSJ resulted in a complication- and pain-free recovery with excellent tolerance of the inserted material during a 6-month-follow-up²⁶. In the present study, all 3 dogs recovered without pain and complications after surgery. However, although clinical and orthopedic examination revealed no back pain in Dog 2, the stiff gait observed at 6, 12, and 18 months after surgery may have been associated with surgery of the caudal lumbar spine. Imaging and histopathology showed changes caused by surgery in all three dogs. The histopathological changes observed in the post-mortem specimen of dog 1 can be explained by discospondylitis that occurred 24 months after surgery. Although discospondylitis was not a deciding factor for euthanasia, degeneration and surgery of the IVD may predispose for infection of the IVD. The 3 Greyhounds in the present study were mildly affected with lumbosacral disease; further evaluation of PSRF in dogs with more severe lumbosacral disease is necessary to assess whether PSRF has a similarly successful outcome in these patients.

Force plate analysis is an accepted method to objectively and accurately assess canine locomotion⁵². In the present study, P/T ratios for Fz, Fy+ and Fy- were calculated. An increase in a P/T ratio is indicative of a relative shift of force towards the pelvic limbs, whereas a decrease is indicative of a relative shift of force towards the thoracic limbs. Force plate analysis of clinically sound dogs indicates that the greater part of the braking function is provided by the thoracic limbs, whereas the pelvic limbs contribute more to propulsion⁵³. Dogs diagnosed with DLSS have less propulsive force in their pelvic limbs than clinically sound dogs⁵⁴. Decompressive surgery alone resulted in initial improvement of the propulsive force P/T Fy- at 6 months after surgery, but propulsive force deteriorated again at 18 months after surgery^{16,54}. In the present study, it was decided to treat the 3 Greyhounds with decompressive surgery in combination with PSRF, aimed at fully restoring the propulsive function of the hind limbs in the long term. Force plate analysis of the operated dogs showed a long-term trend towards a relative shift of the braking force towards the thoracic limbs, of the propulsive force towards the hind limbs, and of the weight bearing towards the hind limbs compared with the preoperative state. Our findings indicate that PSRF may provide a better pelvic limb function than decompressive surgery alone in the long term. However, there are some limitations regarding the force plate analysis in this study: statistical analysis was not performed due to the small sample size, and a follow-up period longer

than 18 months after surgery would have given more insight into the long term outcome, but the dogs in this pilot study could not be reliably followed for longer because of their old age.

Diagnostic imaging and histopathology showed that bony interbody fusion of the LSJ was not achieved. Moreover, the histopathological findings were similar to those observed after nucleotomy alone⁵⁵. In humans, spinal fusion is promoted by bilaterally broaching both endplates and placing a cancellous bone graft into the disc space.⁵⁶ In canine experimental studies, similar methods resulted in bony fusion in 57-82%^{38,57}. In the present study, the endplates were curetted, but not broached, and a cancellous bone graft was placed into the intervertebral space. None of the LSJs fused, which may have resulted in suboptimal clinical results. Therefore, in the future the surgical techniques should include more thorough debridement of the vertebral endplates.

Common complications associated with PSRF in humans are screw misplacement and implant failure, which can result in neurologic deficits and early loosening and failure of the construct^{22,28,42}. In the present study, unacceptable screw placement was found in two (16.7%) of the inserted screws, one case being the consequence of implant failure (8.3%). In human medicine, pedicle screw misplacement percentages of 18-39.8% have been reported^{45,50,58}. The small sample size used in this study, and differences between the operated spinal levels and between human and canine vertebral dimensions may explain the differences between the latter studies and the present one. Because surgery for pedicle screw insertion has a considerable learning curve, screw placement may improve when a larger sample size is used⁵⁸. In addition, the accuracy and safety of pedicle screw insertion can be increased by using intraoperative imaging with fluoroscopy or neuronavigation with CT or MRI data^{49,59,60}. Although the medial pedicle wall was penetrated in each operated dog, this did not result in neurological deficits. This could be explained by the mobility of the nerve roots inside the spinal canal and the distance between the inner pedicular wall and the nerve roots⁵⁸. Similar findings regarding the relation between screw placement and neurologic dysfunction have been reported in human studies^{23,39,47}. A long-term complication of PSRF concerns the altered biomechanical functionality of the adjacent L6-L7 spinal segment. Although fixation of the LSJ provides additional stabilization of the decompressed spinal segment, it does reduce the mobility of the L7-S1 spinal segment²⁴. Consequently, the workload of the adjacent L6-L7 IVD and facet joints is increased, which in turn may lead to degenerative changes in the L6-L7 spinal segment⁶¹⁻⁶³.

Strict adherence to the guideline values for the screw insertion does not guarantee safe screw placement. In addition, the guidelines values proposed in the present study were based on 6 spinal specimens from one dog breed and therefore, may not apply to other dog breeds. Moreover, a considerable inter-individual and inter-breed variation exists regarding the spatial dimensions of the vertebrae and the surrounding soft tissue structures²⁹; consequently, standardized guideline values are not generally applicable. Therefore, accurate

CT- and MRI-based evaluation of the vertebral dimensions of both L7 and S1 and their surrounding soft tissue structures is required to obtain insight into the optimal screw insertion corridors for individual patients.

PSRF may be a future treatment for selected DLSS patients, aimed at stabilizing the decompressed LSJ, concurrently improving the propulsive function of the hind limbs in the long term. The dogs that would benefit the most from combined decompressive surgery and PSRF may well be the dogs with neurological deficits due to severe instability of the LSJ on dynamic imaging. Also, dogs with lumbosacral discospondylitis and concurrent instability that do not respond to medical therapy may be suitable surgical candidates for PSRF.

In conclusion, PSRF of the canine LSJ may be a valuable addition to current surgical treatments for dogs with DLSS and LSJ instability. This study suggests that PSRF provides adequate stability, is well-tolerated, and may lead to an improvement of hind limb function as quantified by force plate analysis; however, further studies are necessary before this can be sustained. Detailed knowledge of the pedicle anatomy and dimensions of individual patients is required to optimize the accuracy and safety of screw insertion. Meticulous preparation of the vertebral endplates and the use of primary cancellous autograft material or osteo-inductive compounds are essential to achieve bony fusion of the spinal segment. Evaluation of the surgical procedure in a larger canine sample size and in dogs with severe lumbosacral disease is required to draw valid conclusions regarding the safety, outcome and complications of PSRF.

Acknowledgments

The authors wish to thank Mr. Arie Doornenbal, Mw. Ank van Wees, and Mr. J. Fama for their technical assistance.

References

1. Watt PR: Degenerative lumbosacral stenosis in 18 dogs. *J Small Anim Pract* 32:125-134, 1991.
2. Ness M: Degenerative lumbosacral Stenosis in the dog: a review of 30 cases *J Small Anim Pract* 35:185-190, 1994.
3. Danielsson F, Sjostrom L: Surgical treatment of degenerative lumbosacral stenosis in dogs. *Vet Surg* 28:91-98, 1999.
4. De Risio L, Sharp NJ, Olby NJ, et al: Predictors of outcome after dorsal decompressive laminectomy for degenerative lumbosacral stenosis in dogs: 69 cases (1987-1997). *J Am Vet Med Assoc* 219:624-628, 2001.
5. De Risio L, Thomas WB, Sharp NJ: Degenerative lumbosacral stenosis. *Vet Clin North Am Small Anim Pract* 30:111-132, vi, 2000.
6. Wheeler SJ: Lumbosacral disease. *Vet Clin North Am Small Anim Pract* 22:937-950, 1992.
7. Slocum B, Devine T: L7-S1 fixation-fusion for treatment of cauda equina compression in the dog. *J Am Vet Med Assoc* 188:31-35, 1986.
8. Suwankong N, Meij BP, Voorhout G, et al: Review and retrospective analysis of degenerative lumbosacral stenosis in 156 dogs treated by dorsal laminectomy. *Vet Comp Orthop Traumatol* 21:285-293, 2008.
9. Meij BP, Bergknut N: Degenerative lumbosacral stenosis. *Vet Clin North Am Small Anim Pract* 40:983-1009, 2010.
10. Jones JC, Inzana KD: Subclinical CT abnormalities in the lumbosacral spine of older large-breed dogs. *Vet Radiol Ultrasound* 41:19-26, 2000.
11. Mayhew PD, Kapatkin AS, Wortman JA, et al: Association of cauda equina compression on magnetic resonance images and clinical signs in dogs with degenerative lumbosacral stenosis. *J Am Anim Hosp Assoc* 38:555-562, 2002.
12. Suwankong N, Voorhout G, Hazewinkel HA, et al: Agreement between computed tomography, magnetic resonance imaging, and surgical findings in dogs with degenerative lumbosacral stenosis. *J Am Vet Med Assoc* 229:1924-1929, 2006.
13. Boden SD, Davis DO, Dina TS, et al: Abnormal magnetic-resonance scans of the lumbar spine in asymptomatic subjects. A prospective investigation. *J Bone Joint Surg Am* 72:403-408, 1990.
14. Jensen MC, Brant-Zawadzki MN, Obuchowski N, et al: Magnetic resonance imaging of the lumbar spine in people without back pain. *N Engl J Med* 331:69-73, 1994.
15. Janssens LAA, Moens Y, Coppens P, et al: Lumbosacral Degenerative Stenosis in the Dog. *Vet Comp Orthop Traumatol* 13:97-103, 2000.
16. Suwankong N, Meij BP, Van Klaveren NJ, et al: Assessment of decompressive surgery in dogs with degenerative lumbosacral stenosis using force plate analysis and questionnaires. *Vet Surg* 36:423-431, 2007.
17. Lamont LA: Adjunctive analgesic therapy in veterinary medicine. *Vet Clin North Am Small Anim Pract* 38:1187-1203, 2008.
18. Gödde T, Steffen F: Surgical treatment of lumbosacral foraminal stenosis using a lateral approach in twenty dogs with degenerative lumbosacral stenosis. *Vet Surg*, 36:705-713, 2007.

19. Sharp NJH, Wheeler SJ: Lumbosacral disease, in Sharp NJH, Wheeler SJ (eds): *Small Animal Spinal Disorders. Diagnosis and Surgery* (ed 2), Vol. Edinburgh, Elsevier Mosby, 2005, pp 181-209.
20. Linn LL, Bartels KE, Rochat MC, et al: Lumbosacral stenosis in 29 military working dogs: epidemiologic findings and outcome after surgical intervention (1990-1999). *Vet Surg* 32:21-29, 2003.
21. Yahiro MA: Comprehensive literature review. Pedicle screw fixation devices. *Spine* 19:2274S-2278S, 1994.
22. Boos N, Webb JK: Pedicle screw fixation in spinal disorders: a European view. *Eur Spine J* 6:2-18, 1997.
23. Davne SH, Myers DL: Complications of lumbar spinal fusion with transpedicular instrumentation. *Spine (Phila Pa 1976)* 17:S184-189, 1992.
24. Meij BP, Suwankong N, Van der Veen AJ, et al: Biomechanical flexion-extension forces in normal canine lumbosacral cadaver specimens before and after dorsal laminectomy-discectomy and pedicle screw-rod fixation. *Vet Surg* 36:742-751, 2007.
25. Méheust P, Mallet C, Marouze C: Une nouvelle technique de stabilisation lombosacrée: l'arthrodèse par vissage pédiculaire considérations anatomiques *Prat Med Chir Anim Comp* 35:193-199, 2000.
26. Méheust P: Une nouvelle technique de stabilisation lombosacrée : l'arthrodèse par vissage pédiculaire, étude clinique de 5 cas. *Prat Med Chir Anim Comp* 35:201-207, 2000.
27. Bell GR: Anatomy of the Lumbar Spine: Developmental to Normal Adult Anatomy, in Wiesel SW, Weinstein JN, Herkowitz H, et al (eds): *The Lumbar Spine*, Vol 1. Philadelphia, W.B. Saunders Company, 1996, pp 43-52.
28. Schizas C, Michel J, Kosmopoulos V, et al: Computer tomography assessment of pedicle screw insertion in percutaneous posterior transpedicular stabilization. *Eur Spine J* 16:613-617, 2007.
29. Watine S, Cabassu JP, Catheland S, et al: Computed tomography study of implantation corridors in canine vertebrae. *J Small Anim Pract* 47:651-657, 2006.
30. Bergknut N, Auriemma E, Wijsman SJCM, et al: Evaluation of intervertebral disk degeneration in chondrodystrophic and non-chondrodystrophic dogs by use of Pfirrmann grading of images obtained with low-field magnetic resonance imaging. *Am J Vet Res* 72: 893-898, 2011.
31. Bagley RS: Surgical Stabilization of the Lumbosacral Joint, in Slatter D (ed): *Textbook of small animal surgery* (ed 3rd), Vol. Philadelphia, Saunders, 2003, pp 1238-1243.
32. Ullman SL, Boudrieau RJ: Internal skeletal fixation using a Kirschner apparatus for stabilization of fracture/luxations of the lumbosacral joint in six dogs. A modification of the transilial pin technique. *Vet Surg* 22:11-17, 1993.
33. Gibson JN, Waddell G: Surgical interventions for lumbar disc prolapse: updated Cochrane Review. *Spine (Phila Pa 1976)* 32:1735-1747, 2007.
34. Hanley EN, Jr., David SM: Lumbar arthrodesis for the treatment of back pain. *J Bone Joint Surg Am* 81:716-730, 1999.
35. Bridwell KH, DeWald RL: *The Textbook of Spinal Surgery* (ed 2nd). Philadelphia, Lippincott-Raven, 1997.

36. Lorenz M, Zindrick M, Schwaegler P, et al: A comparison of single-level fusions with and without hardware. *Spine (Phila Pa 1976)* 16:S455-458, 1991.
37. Zdeblick TA: A prospective, randomized study of lumbar fusion. Preliminary results. *Spine (Phila Pa 1976)* 18:983-991, 1993.
38. McAfee PC, Farey ID, Sutterlin CE, et al: 1989 Volvo Award in basic science. Device-related osteoporosis with spinal instrumentation. *Spine (Phila Pa 1976)* 14:919-926, 1989.
39. Ferguson RL, Tencer AF, Woodard P, et al: Biomechanical comparisons of spinal fracture models and the stabilizing effects of posterior instrumentations. *Spine (Phila Pa 1976)* 13:453-460, 1988.
40. Gurr KR, McAfee PC, Shih CM: Biomechanical analysis of posterior instrumentation systems after decompressive laminectomy. An unstable calf-spine model. *J Bone Joint Surg Am* 70:680-691, 1988.
41. Matsuzaki H, Tokuhashi Y, Matsumoto F, et al: Problems and solutions of pedicle screw plate fixation of lumbar spine. *Spine (Phila Pa 1976)* 15:1159-1165, 1990.
42. Gaines RW, Jr.: The use of pedicle-screw internal fixation for the operative treatment of spinal disorders. *J Bone Joint Surg Am* 82-A:1458-1476, 2000.
43. Barber JW, Boden SD, Ganey T, et al: Biomechanical study of lumbar pedicle screws: does convergence affect axial pullout strength? *J Spinal Disord* 11:215-220, 1998.
44. Carson WL, Duffield RC, Arendt M, et al: Internal forces and moments in transpedicular spine instrumentation. The effect of pedicle screw angle and transfixation--the 4R-4bar linkage concept. *Spine (Phila Pa 1976)* 15:893-901, 1990.
45. Laine T, Makitalo K, Schlenzka D, et al: Accuracy of pedicle screw insertion: a prospective CT study in 30 low back patients. *Eur Spine J* 6:402-405, 1997.
46. Ofiram E, Polly DW, Gilbert TJ, Jr., et al: Is it safer to place pedicle screws in the lower thoracic spine than in the upper lumbar spine? *Spine (Phila Pa 1976)* 32:49-54, 2007.
47. Farber GL, Place HM, Mazur RA, et al: Accuracy of pedicle screw placement in lumbar fusions by plain radiographs and computed tomography. *Spine (Phila Pa 1976)* 20:1494-1499, 1995.
48. Yoo JU, Ghanayem A, Petersilge C, et al: Accuracy of using computed tomography to identify pedicle screw placement in cadaveric human lumbar spine. *Spine (Phila Pa 1976)* 22:2668-2671, 1997.
49. Laine T, Lund T, Ylikoski M, et al: Accuracy of pedicle screw insertion with and without computer assistance: a randomised controlled clinical study in 100 consecutive patients. *Eur Spine J* 9:235-240, 2000.
50. Castro WH, Halm H, Jerosch J, et al: Accuracy of pedicle screw placement in lumbar vertebrae. *Spine (Phila Pa 1976)* 21:1320-1324, 1996.
51. Steinmann JC, Herkowitz HN, el-Kommos H, et al: Spinal pedicle fixation. Confirmation of an image-based technique for screw placement. *Spine (Phila Pa 1976)* 18:1856-1861, 1993.
52. McLaughlin RM: Kinetic and kinematic gait analysis in dogs. *Vet Clin North Am Small Anim Pract* 31:193-201, 2001.
53. Budsberg SC, Verstraete MC, Soutas-Little RW: Force plate analysis of the walking gait in healthy dogs. *Am J Vet Res* 48:915-918, 1987.

54. van Klaveren NJ, Suwankong N, De Boer S, et al: Force plate analysis before and after dorsal decompression for treatment of degenerative lumbosacral stenosis in dogs. *Vet Surg* 34:450-456, 2005.
55. Wagner SD, Ferguson HR, Leipold H, et al: Radiographic and histologic changes after thoracolumbar disc curettage. *Vet Surg* 16:65-69, 1987.
56. Lenke LG: Basic Techniques of Posterior Segmental Spine Internal Fixation, in Bridwell KH, DeWald RL (eds): *The Textbook of Spinal Surgery*, Vol 1. Philadelphia, Lippincott-Raven, 1997, pp 121-138.
57. Thomas I, Kirkaldy-Willis WH, Singh S, et al: Experimental spinal fusion in guinea pigs and dogs: the effect of immobilization. *Clin Orthop Relat Res*:363-375, 1975.
58. Gertzbein SD, Robbins SE: Accuracy of pedicular screw placement in vivo. *Spine (Phila Pa 1976)* 15:11-14, 1990.
59. Haberland N, Ebmeier K, Hliscs R, et al: Neuronavigation in surgery of intracranial and spinal tumors. *J Cancer Res Clin Oncol* 126:529-541, 2000.
60. Meij BP, Suwankong N, van den Brom WE, et al: Tibial nerve somatosensory evoked potentials in dogs with degenerative lumbosacral stenosis. *Vet Surg* 35:168-175, 2006.
61. Eck JC, Humphreys SC, Hodges SD: Adjacent-segment degeneration after lumbar fusion: a review of clinical, biomechanical, and radiologic studies. *Am J Orthop* 28:336-340, 1999.
62. Lee CK: Accelerated degeneration of the segment adjacent to a lumbar fusion. *Spine* 13:375-377, 1988.
63. MacDougall J, Perra J, Pinto M: Incidence of adjacent segment degeneration at ten years after lumbar spine fusion. *Spine J* 3:675, 2003.

The performance of a hydrogel nucleus pulposus prosthesis in an ex vivo canine model

Niklas Bergknut ^{a,b}, Lucas A. Smolders ^a, Leo H. Koole ^c, George Voorhout ^d, Ragnvi Hagman ^b, Anne-Sofie Lagerstedt ^b, Keti Saralidze ^c, Herman A. W. Hazewinkel ^a, Albert van der Veen ^e, Björn P. Meij ^a

Biomaterials 31(26):6782-8, 2010

^a Department of Clinical Sciences of Companion Animals, Faculty of Veterinary Medicine, Utrecht University, The Netherlands

^b Department of Clinical Sciences, Faculty of Veterinary Medicine and Animal Sciences, Swedish University of Agricultural Sciences, Uppsala, Sweden

^c Department of Biomedical Engineering/Biomaterials Science, Faculty of Health, Medicine and Life Sciences, Maastricht University, The Netherlands

^d Division of Diagnostic Imaging, Faculty of Veterinary Medicine, Utrecht University, The Netherlands

^e VU University Medical Center, Department of Physics and Medical Technology, Amsterdam, The Netherlands

This research forms part of the Project P2.01 IDiDAS of the research program of the BioMedical Materials institute co-funded by the Dutch Ministry of Economic Affairs.

Abstract

Objective: A nucleus pulposus prosthesis (NPP) made of the hydrogel N-vinyl-2-pyrrolidinone copolymerized with 2-(4'-iodobenzoyl)-oxo-ethyl methacrylate has recently been developed. The objectives of this study were to investigate the special features of this NPP, i.e. intrinsic radiopacity, and its ability to swell *in situ* to fill the nucleus cavity and restore disc height, *ex-vivo* in canine spinal specimens.

3.2 *Methods:* L7-S1 intervertebral discs were isolated from three canine spinal specimens, and the dimensions of the nuclei pulposi were measured. Based on these averaged measurements, the NPP prototype was made and inserted in its dry form (xerogel) into a canine cadaveric spinal segment and allowed to swell overnight at 38 °C. The integrity of the NPP and the filling of the nucleus cavity were assessed before and after swelling, using radiography, computed tomography, and magnetic resonance imaging. The ability of the NPP to restore disc height was assessed on radiographs of 10 spinal specimens. Thereafter the NPP was macroscopically assessed *in situ* by dissection of the spinal specimen.

Results: Both on imaging and macroscopically, 9/10 NPPs appeared to have a near perfect fit and disc height was restored in 8/10 spinal segments.

Conclusions: The NPP may be an acceptable treatment option for low back patients meeting the requirements for NPP treatment.

Key words: intervertebral disc; spinal surgery; radiopacity; hydrogel

Introduction

Low back pain (LBP) is a major health problem in the Western world ^{1,2}, and its incidence has increased dramatically over the last two decades ³. The most common cause of back pain is believed to be intervertebral disc (IVD) degeneration ^{4,5}. IVD degeneration can apart from discogenic pain also lead to spinal instability and stenosis of the spinal canal causing severe clinical symptoms. Most patients suffering from IVD degeneration responds well to conservative and medical treatment. Surgical treatment is preserved for patients refractory to medical treatment. The most common surgical treatment of these patients is decompressive surgery combined with spinal fusion. The primary aim of this procedure is to reduce pain. It does however leave the patients with altered biomechanical properties of the spine, which can lead to adjacent segment degeneration ^{6,7}. For patients with IVD degeneration at a single level, without spinal canal stenosis, total disc replacement can be a treatment option. Total disc replacement, contrary to spinal fusion, preserves near normal biomechanical functionality of the spinal segment. However, severe complications such as implant migration and failure may occur ^{8,9}.

New treatments aim at being minimally invasive and at intervening earlier in the degenerative process by restoring the nucleus pulposus (NP) function and/or supporting regeneration of the IVD. Regenerative treatments have been investigated but in experimental settings only ¹⁰⁻¹², and although minimally invasive surgical procedures coagulating the NP or the posterior annulus are currently used, they are considered controversial ^{13,14}. One drawback is that they reduce IVD height and do not restore the normal biomechanical function of the NP, leading to further degeneration of the spinal segment ¹⁵. Another treatment option is implantation of an NP prosthesis (NPP) after nucleotomy of the degenerated disc, but this procedure requires that the annulus fibrosus is intact. The Prosthetic Disc Nucleus (PDN, Raymedica, Inc., Bloomington, MN), which is commercially available, has been implanted in over 5500 human patients worldwide ^{16,17}. Criteria for the use of any NPP are: 1) disc degeneration manifest by morphologic changes in the NP, 2) a competent annulus fibrosus, and 3) a minimal IVD height of 5 mm ^{18,19}. These requirements mean that the implant is suitable for only a small group of patients with low back pain, but in these patients implantation will restore disc height and mobility of the spinal segment, thereby relieving pain and may also prevent further degeneration of the spinal segment ²⁰⁻²³ as well as adjacent segment degeneration, which is a common problem after spinal fusion ^{6,7}. Although preclinical and preliminary clinical data show promising results ^{16,17,24}, long-term clinical studies are still lacking.

However, most commercial NPPs are not designed to completely fill the nuclear cavity. Complete filling of the nuclear cavity and even distribution of the load over the endplates can halt further degeneration of the annulus fibrosus, whereas incomplete filling is likely to lead to incorrect biomechanical

loading and to progression of annular degeneration or even implant migration²⁰⁻²². Boelen *et al.* proposed applying custom-made synthetic hydrogel NPP implants designed to precisely fill the nuclear cavity²⁵. The NPP is made of a radiopaque synthetic hydrogel biomaterial in its water-free state, taking into account the increase in size due to three-dimensional swelling of the material *in situ*. The NPP is implanted in its dry state, so that only a small annular opening is needed, and then absorbs fluid from the surrounding tissue and swells to fill the nucleotomy cavity and thus restore disc height. The radiopacity of the implant enables imaging by radiography or computed tomography (CT), and the absorbed fluid makes magnetic resonance imaging (MRI) possible.

The aim of this study was to test this NPP *ex-vivo* in canine lumbosacral segments (L7-S1). A clinically adapted mode of implantation of the NPP in the nuclear cavity of the L7-S1 intervertebral disc is reported. Swelling, fit, and restoration of disc height of the NPP *in situ* were monitored by radiography, CT, and MR imaging.

Materials and methods

Manufacturing of the nucleus pulpous prosthesis

The NPPs were made in a bean-shaped form, to copy the shape of the normal NP. The biomaterial is a chemically cross-linked hydrogel that is synthesized through a free-radical polymerization reaction from four reactive vinyl-type monomers: N-vinyl-2-pyrrolidinone (NVP), 2-hydroxyethyl methacrylate (HEMA), 2-(4'-iodobenzoyl)-oxo-ethyl methacrylate (4-IEMA), and allylmethacrylate (AMA). NVP and HEMA are responsible for the hydrophilic nature of the material, 4-IEMA provides intrinsic radiopacity to the NPPs as the material contains covalently linked iodine, and AMA results in chemical cross-linking¹⁸. The NPPs were manufactured in two steps: (i) polymerization and (ii) computer-controlled machining of the hydrogel in its dry state.

All chemicals were purchased from Acros (Landsmeer, the Netherlands). NVP and HEMA were distilled under reduced pressure to remove inhibitory additives. The monomer 4-IEMA was synthesized from HEMA and 4-iodobenzoylchloride as described previously. AMA and 2,2'-Azobis(isobutyronitrile) (AIBN) were used as received. NVP, HEMA, 4IEMA, and AMA were weighed into a 500-mL round-bottom flask in the molar ratio 71.8 : 20.4 : 5.8 : 2. The total mass was about 200 g. AIBN (0.03 mole %) was added and completely dissolved in the monomer mixture. The reaction mixture was divided over a number of Teflon tubes (inner diameter 15 mm, wall thickness 1 mm, length 300 mm), which were closed with a stopper at one end. The tubes were filled to maximally 60%. The monomer-filled tubes were partially immersed in a thermostated oil bath and a computer-controlled time/temperature profile was run as follows:

(i), constant temperature at 40 °C for 1 h; (ii) slow heating to 50 °C over 1 h; (iii), constant temperature at 50 °C for 6 h; (iv), slow heating to 60°C over 1h; (v) constant temperature at 60 °C for 6 h; (vi) slow heating to 80 °C over 1 h; (vii), constant temperature at 80 °C for 4 h; (viii), slow heating to 100 °C over 1 h; (ix), constant temperature at 100 °C for 4 h; (x) slow heating to 130 °C over 1 h; (xi), constant temperature at 130 °C for 2 h; (xii) slow cooling to ambient temperature (over 8 h). The procedure yielded transparent, glassy rods, which were removed from the Teflon tubes. NPPs were machined from the polymer rods, using a five-axes computer-controlled lathe/milling system. As the material is a hydrogel, cooling with water had to be avoided, which meant that the machining process was performed slowly.

Determining the size of the implants

Four lumbosacral spines were isolated from the cadavers of healthy mixed-breed dogs (weight range 22.9-24.0 kg; age range 15-22 months) euthanized in an unrelated experiment. Three spines were used to determine the dimensions of the implants and the fourth spine was used for the implantation of the NPP (see below). MRI was performed using a 0.2 T open magnet (Magnetom Open Viva, Siemens AG, Utrecht, the Netherlands). For optimal resolution of the IVDs, a mixed signal sequence was used (DESS - Dual Echo Steady State) with a repetition time of 41 ms, an echo time of 12 ms, and a slice thickness of 1.194 mm. The MR images were obtained and assessed on standard computer screens using the software Web1000 5.1 (Clinical Review Station, Agfa Gevaert, N.V.). MRI showed the L7-S1 IVDs to be normal. The IVDs were then isolated by careful dissection for measurement of the width, height, and thickness of the NPs with a Vernier caliper (accuracy 0.05 mm). The NPPs were made on the basis of the mean dimensions of these three lumbosacral IVDs. Based upon our experience during pilot studies, the implants were made 20% smaller to compensate for residual NP material after nucleotomy. A swelling factor of 1.3 in each dimension was taken into account when making the implants, representing a volume swelling factor of 2.2 (1.3^3)^{18,25}. The custom-made NPPs measured (width x height x thickness) 10.4 x 4.5 x 2.4 mm in the unswollen state, and 13.5 x 5.9 x 3.1 mm in the swollen state (Fig. 1).

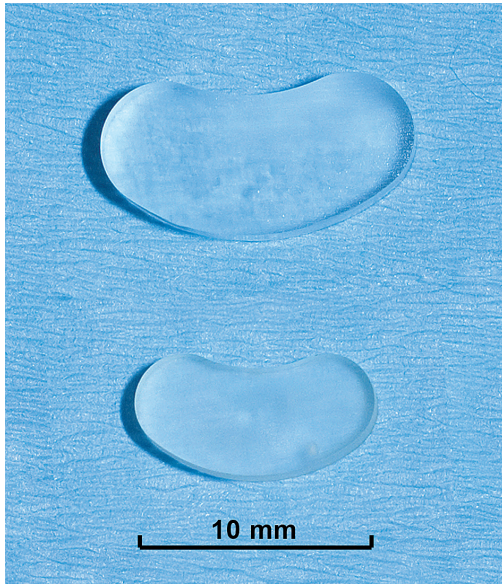


Figure 1. The nucleus pulposus prosthesis: dry state/xerogel (bottom) and hydrated/swollen (top).

Surgical implantation and imaging of the NPP in situ

Implantation of the custom-made NPP was studied using the spine from the fourth healthy mixed-breed dog. A dorsal (posterior approach) laminectomy was performed over the lumbosacral region of the cadaveric spinal segment, followed by nucleotomy of the L7-S1 disc. The NPP was inserted into the nuclear cavity through a 5-mm transverse incision in the dorsal (posterior) annulus fibrosus (Fig. 2), and 5 mL phosphate-buffered saline (PBS) was subsequently injected into the cavity and surrounding tissue to initiate implant hydration^{18,25}.

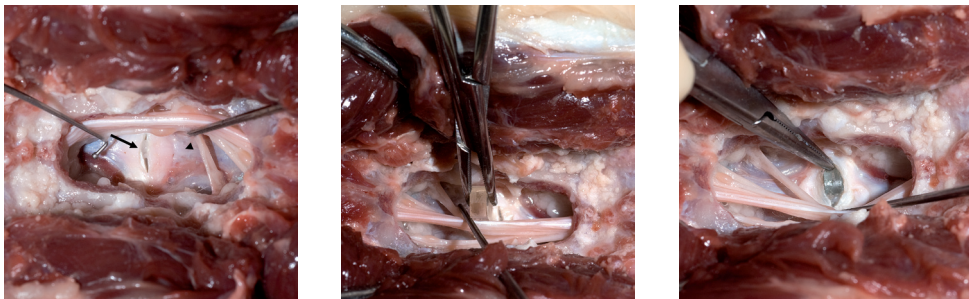


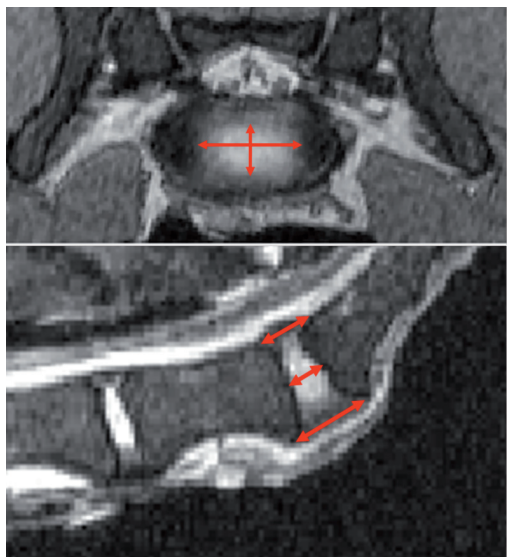
Figure 2. A) Dorsal view of the canine L7-S1 intervertebral disc (IVD) prepared for implantation of a nucleus pulposus prosthesis (NPP). Access to the IVD is gained via dorsal laminectomy followed by transverse incision of the dorsal annulus fibrosus (arrow). The gelatinous nucleus pulposus is removed. The cauda equina is gently retracted (arrow head). B) The NPP is carefully inserted through the incision in the dorsal annulus fibrosus. C) The NPP just before being pushed beyond the annulus fibrosus into the nuclear cavity.

The annular incision was closed with a mattress suture (Polydioxanone 2-0, Johnson & Johnson, New Jersey, USA), and reinforced with tissue glue (Dermabond, Johnson & Johnson, New Jersey, USA). Lastly, a piece of polypropylene mesh⁵ (1.0 x 1.5 cm; Johnson & Johnson, New Jersey, USA) was glued over the annular defect. The spinal segment was wrapped in PBS-soaked gauzes and placed in a plastic bag to prevent implant and specimen dehydration. To achieve complete swelling of the implant, the spinal segment was incubated at 38°C (i.e., the normal canine body temperature) for 18 h. Imaging was performed using digital radiography (Philips bucky Diagnost, Philips, NV, Eindhoven, the Netherlands), CT (Philips Secura, Single slice spiral scanner, Philips, NV, Eindhoven, the Netherlands), and MRI (Magnetom Open Viva, Siemens AG, Utrecht, the Netherlands) to monitor the positioning, swelling, and fit of the NPP *in situ*.

Assessment of the accuracy of IVD dimensions measured by MRI versus in situ with calipers

The following dimensions of the lumbosacral spine were measured on MR images and *in situ* with a Vernier caliper: annulus fibrosus width (left to right, at widest point), annulus fibrosus height (ventral [anterior] to dorsal [posterior], at widest point), NP width (left to right, at widest point), NP height (ventral to dorsal, at widest point), thickness of the disc (cranial-caudal [superior-inferior]) on the dorsal side, and thickness of the disc (cranial-caudal) on the ventral side. The dimensions were measured on mid-sagittal and transverse, mixed signal (DESS) images, using the automated settings and measurement tool provided by the software Web1000 5.1 (Clinical Review Station, Agfa Gevaert N.V.) (Fig. 3).

Fig. 3 A) Transverse, mixed signal (DESS) MR-image, used to measure the width and height of the nucleus pulposus (red arrows) and annulus fibrosus. B) Mid-sagittal, mixed signal (DESS) MR-image, used to measure the thickness of the disc in the middle, on the dorsal (posterior) and ventral (anterior) side (red arrows).



Assessment of IVD height

Canine cadaveric spine segments (L5-Cd1) from 10 healthy female mixed-breed dogs (weight range 16.1-20.4 kg; age range 26-44 months), euthanized in an unrelated experiment, were used. Dorsoventral and lateral radiographs were taken using digital radiography (Digital vet Premium, Sedecal, Madrid, Spain) to assure that no congenital or acquired anomalies were present. The spinal specimens were subjected to the same procedures described above and radiographs were made in: 1) the native spine, 2) after dorsal laminectomy and nucleotomy, and 3) after implantation and swelling of the NPP. The radiographs were subsequently blinded and the L7-S1 IVD height was measured by three independent observers on standard computer screens, using the software Sante Dicom viewer (Santesoft, Athens, Greece) and the same settings and magnification for all three observers. A single line, perpendicular to the endplates, positioned in the center of the IVD was used to measure IVD height.

Data and statistical analysis

MRI and caliper measurements were compared using a paired Student's *t*-test. The linear correlation between these two sets of measurements was also evaluated, using Pearson's correlation. The mean disc height \pm standard deviation (SD) on radiographs was calculated for the three conditions and a linear mixed model was used to compare them. "Observer" (three levels: observer 1-3) was set as a fixed effect, whereas "spine" (10 levels: specimen 1-10) was assigned to random effects. "Condition" (three levels: condition 1-3) was used both as a fixed and a random effect. A Bonferroni correction was applied to compensate for the multiple comparisons. The level for statistical significance was set to $P < 0.05$.

Results

Surgical implantation and imaging of the NPP in situ

The dorsal (posterior) approach, which is routinely used in canine lumbosacral IVD surgery, enabled accurate insertion of the NPP. The implant was visualized before and after swelling by radiography (Fig. 4), CT (Fig. 5), and MRI (Fig. 6). No artifacts were observed on CT or MR imaging. The NPP conformed to fill the nuclear cavity, as was also seen after isolation of the implant from the IVD at the end of the experiment (Fig. 7).



Figure 4. Lateral radiograph of the canine lumbosacral region with a swollen nucleus pulposus prosthesis indicated by an arrow.

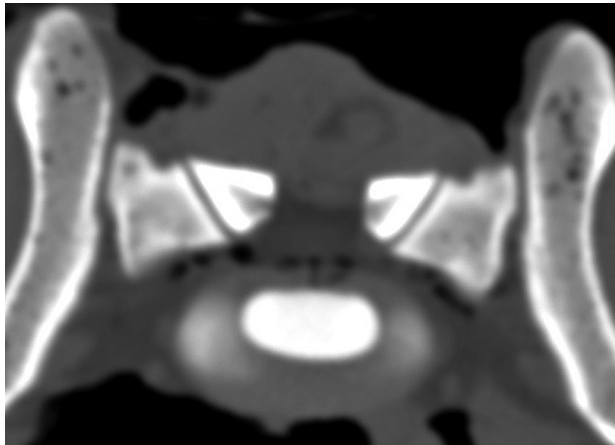


Figure 5. Transverse CT images of the L7-S1 intervertebral disc with a swollen nucleus pulposus prosthesis in the center of the figure.

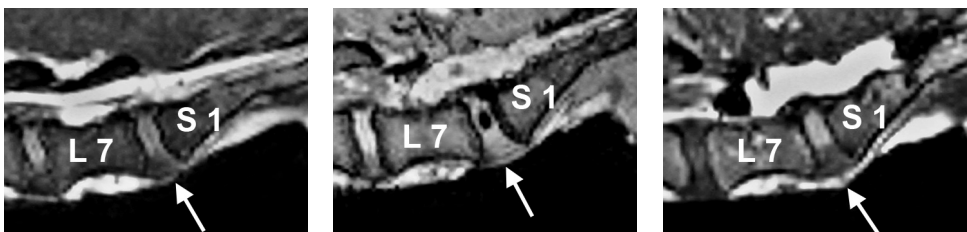


Figure 6. T2-weighted, sagittal magnetic resonance image of the canine lumbosacral segment. A) The native spinal segment with a normal L7-S1 intervertebral disc (IVD). B) After dorsal laminectomy, nucleotomy, and insertion of the nucleus pulposus prosthesis (NPP). The NPP before swelling (arrow). C) The same spinal segment after incubation at 38°C for 18 h, showing the swollen NPP (arrow).

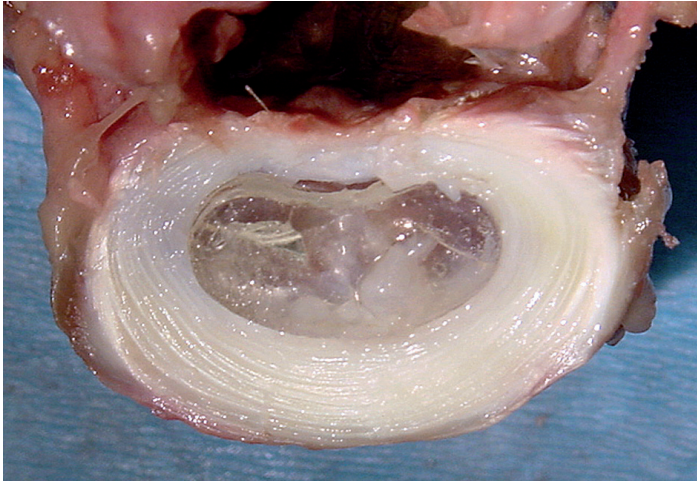


Figure 7. Transverse section of a canine L7-S1 intervertebral disc with the hydrated nucleus pulposus prosthesis (NPP) in place. The insertion tunnel through the dorsal annulus can still be visualized. Minor damage was caused to the top right corner of the NPP during surgical extraction.

Assessment of the accuracy of IVD measured by MRI versus in situ by caliper

The MRI and caliper measurements of the IVD dimensions were not significantly different (Student's *t*-test) and were linearly correlated ($r = 0.965$; $P = 0.001$) (Fig. 8).

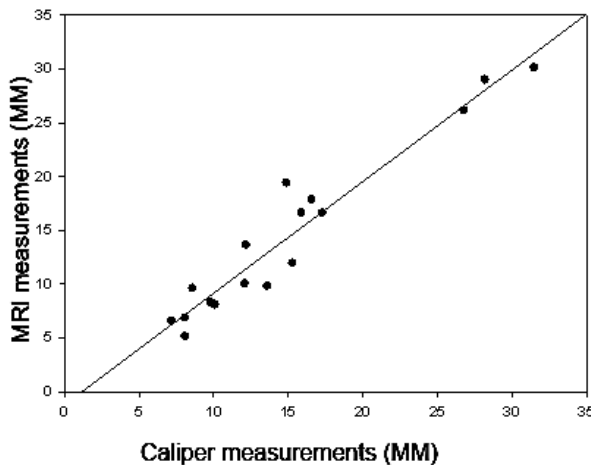


Figure 8. Scatter diagram showing the linear relationship between MRI and caliper measurements of the dimensions of canine L7-S1 intervertebral discs.

Assessment of IVD height

In 8 of 10 spinal segments IVD height was restored after swelling of the NPP. In 1 of the other 2 spinal segments, the NPP was fractured and herniated through the annular incision; no explanation could be found for the failure to restore IVD height in the second segment. The mean (\pm SD) disc height for the spines in the native state, after nucleotomy, and after implantation and swelling of the NPP was 6.08 ± 0.59 mm, 5.44 ± 0.67 mm, and 6.29 ± 0.58 mm, respectively. There was a significant difference between the mean disc height in the native spine and that after nucleotomy, and also between the mean disc height after nucleotomy and that after implantation and swelling of the NPP. No significant difference was found between the mean disc height in the native spine and that after implantation and swelling of the NPP (Fig. 9).

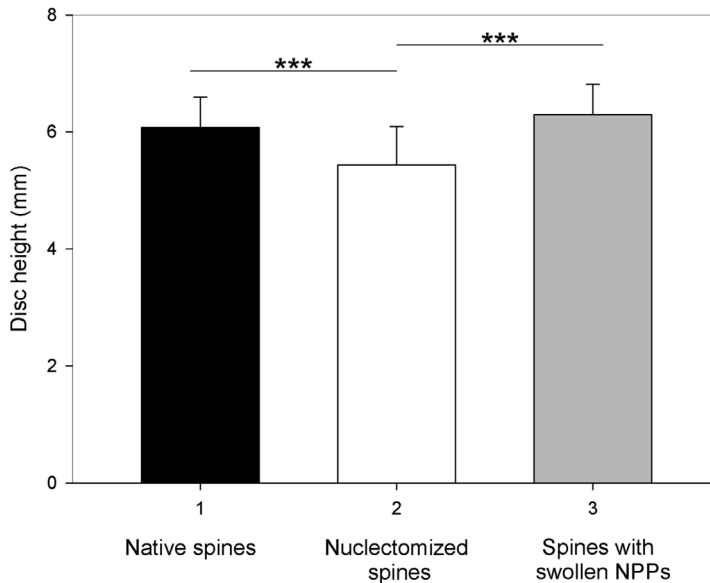


Figure 9. The mean canine lumbosacral intervertebral disc height in 1) the native spine, 2) after laminectomy and nucleotomy, and 3) after implantation and swelling of the nucleus pulposus prosthesis (NPP). *** = $P \leq 0.001$.

Discussion

We found that the NPP conforms well to fill the nuclear cavity, as reported previously¹⁸. An adequate fit with complete filling of the nuclear cavity is required to provide an even pressure over the endplates, which may prevent further degeneration of the IVD²⁰⁻²³. Because it is unlikely that surgeons can completely remove the remaining NP tissue from the IVD, to leave a nuclear cavity with smooth edges, it is essential that the nuclear implant should be able to conform to fill the space provided. In practice, the implant should be somewhat smaller than the NP, to prevent stress points along its margins.

The NPP is, due to its intrinsic radiopacity and fluid absorbing capacity, easy to visualize using radiography, CT, and MRI, which facilitates optimal positioning of the implant intraoperatively (radiography) and enables postoperative monitoring of in the implant to detect whether structural changes occur with time (CT and MRI). Low-field 0.2 Tesla MRI provides low-resolution images, but these were sufficient to allow accurate measurement of the IVD dimensions, as evidenced by the strong linear correlation between MRI and caliper measurements. High-field MRI using magnets with 1.5 Tesla or higher, which are commonly available in human hospitals, provide high-resolution MR images, which should make it possible to measure the actual size of the NP of patients *in vivo* in order to make customized NPPs. No NPP-induced artifacts were observed on the MR images. Such artifacts sometimes occur with NP implants containing metallic markers for radiographic localization^{26,27}.

The fact that the NPP is inserted in its dehydrated (xerogel) state facilitates its insertion in the annular incision of the lumbosacral IVD. When the implant absorbs water it swells and locks itself in place between the vertebrae, decreasing the risk of implant migration. However, fragmentation and implant migration occurred of one NPP in this study. To prevent herniation the authors recommend improving the annular-closing technique further and also to improve the physical-mechanical characteristics of the biomaterial to prevent fragmentation.

Although the NPPs in this study were all inserted via a dorsal (posterior approach) laminectomy, the authors have also successfully implanted a number of NPPs via an anterior-lateral approach in canine cadaveric lumbar IVDs other than the L7-S1. This is likely to be the approach used for implantation of NPPs in humans.

In general, IVD height was significantly restored by the swollen NPP and even a trend towards overcompensation was noted. Although this difference was not significant, this could imply that the implants may have been too large. This could be because of the difference in the body weight between the 3 dogs, used to obtain the dimensions for the NPP, and the body weight of the 10 dogs used to assess IVD height. The reason that IVD height was not restored in two of the specimens could be explained by fragmentation and migration of part of the implant in one case, but in the other case the implant was retrieved intact

and no satisfactory explanation could be found.

The results indicate that an NPP made from cross-linked NVP/HEMA/4-IEMA/AMA hydrogel has promising qualities. Previous studies have demonstrated the biocompatible nature of the material¹⁸, the implants can restore IVD height, and the intrinsic characteristics of the NPP facilitate imaging by radiography, CT, and MRI. Interestingly, the NPP concept may not only be applicable to treat human patients but may also be used for companion animals (dogs) suffering from low back pain. This opens the possibility to evaluate the experimental implant not only in an animal model, but also in animal patients.

Conclusions

A NPP made from cross-linked NVP/HEMA/4-IEMA/AMA has clinically valuable characteristics, i.e., intrinsic radiopacity and the ability to swell *in situ* to fit the space provided. The dry-state xerogel implant can be inserted through a small annular opening and when it swells (2.2-times volume) it locks into place between the adjacent vertebral bodies and is contained by the annular ring, thereby restoring the height of the nucleotomized lumbosacral IVD. These properties make the NPP potentially suitable for clinical use in early stages of IVD degeneration. However, before *in vivo* testing occurs, physical-mechanical improvements to the hydrogel are needed to prevent fragmentation, and an annular closure technique has to be developed to prevent implant migration.

Acknowledgments

This research forms part of the Project P2.01 IDiDAS of the research program of the BioMedical 254 Materials institute, co-funded by the Dutch Ministry of Economic Affairs. The authors would like to thank Jane Sykes for language corrections and Hans Vernooij (Utrecht University) for statistical analysis.

References

1. Frymoyer JW, Cats-Baril WL: An overview of the incidences and costs of low back pain. *Orthop Clin North Am* 22:263-271, 1991.
2. Maniadakis N, Gray A: The economic burden of back pain in the UK. *Pain* 84:95-103, 2000.
3. Freburger JK, Holmes GM, Agans RP, et al: The rising prevalence of chronic low back pain. *Arch Intern Med* 169:251-258, 2009.
4. Cheung KM, Karppinen J, Chan D, et al: Prevalence and pattern of lumbar magnetic resonance imaging changes in a population study of one thousand forty-three individuals. *Spine (Phila Pa 1976)* 34:934-940, 2009.
5. Adams MA: Biomechanics of back pain. *Acupunct Med* 22:178-188, 2004.
6. Min JH, Jang JS, Jung BJ, et al: The clinical characteristics and risk factors for the adjacent segment degeneration in instrumented lumbar fusion. *J Spinal Disord Tech* 21:305-309, 2008.
7. Yang JY, Lee JK, Song HS: The impact of adjacent segment degeneration on the clinical outcome after lumbar spinal fusion. *Spine* 33:503-507, 2008.
8. van Ooij A, Schurink GW, Oner FC, et al: [Findings in 67 patients with recurrent or persistent symptoms after implantation of a disc prosthesis for low back pain.] *Ned Tijdschr Geneesk* 151:1577-1584, 2007.
9. Resnick DK, Watters WC: Lumbar disc arthroplasty: a critical review. *Clin Neurosurg* 54:83-87, 2007.
10. Hiyama A, Mochida J, Iwashina T, et al: Transplantation of mesenchymal stem cells in a canine disc degeneration model. *J Orthop Res* 26:589-600, 2008.
11. Ganey T, Libera J, Moos V, et al: Disc chondrocyte transplantation in a canine model: a treatment for degenerated or damaged intervertebral disc. *Spine* 28:2609-2260, 2003.
12. Masuda K, Imai Y, Okuma M, et al: Osteogenic protein-1 injection into a degenerated disc induces the restoration of disc height and structural changes in the rabbit anular puncture model. *Spine* 31:742-754, 2006.
13. Raj PP: Intervertebral disc: anatomy-physiology-pathophysiology-treatment. *Pain Pract* 8:18-44, 2008.
14. Felder-Puig R, Gyimesi M, Mittermayr T, et al: [Chemonucleolysis and intradiscal electrothermal therapy: what is the current evidence?]. *Rofo* 181:936-944, 2009.
15. Putzier M, Schneider SV, Funk JF, et al: The surgical treatment of the lumbar disc prolapse: nucleotomy with additional transpedicular dynamic stabilization versus nucleotomy alone. *Spine (Phila Pa 1976)* 30:E109-114, 2005.
16. Coric D, Mummaneni PV: Nucleus replacement technologies. *J Neurosurg Spine* 8:115-120, 2008.
17. Shim CS, Lee SH, Park CW, et al: Partial disc replacement with the PDN prosthetic disc nucleus device: early clinical results. *J Spinal Disord Tech* 16:324-330, 2003.
18. Boelen EJH, van Hooy-Corstjens CSJ, Gijbels MJJ, et al: Preliminary evaluation of new intrinsically radiopaque hydrogels for replacing the nucleus pulposus. *J Mater Chem*: 824 - 828, 2006.
19. Guyer RD, Ohnmeiss DD: Intervertebral disc prostheses. *Spine (Phila Pa 1976)* 28:S15-23, 2003.

20. Meakin JR: Replacing the nucleus pulposus of the intervertebral disk: prediction of suitable properties of a replacement material using finite element analysis. *J Mater Sci Mater Med* 12:207-213, 2001.
21. Meakin JR, Reid JE, Hukins DW: Replacing the nucleus pulposus of the intervertebral disc. *Clin Biomech (Bristol, Avon)* 16:560-565, 2001.
22. Di Martino A, Vaccaro AR, Lee JY, et al: Nucleus pulposus replacement: basic science and indications for clinical use. *Spine (Phila Pa 1976)* 30:S16-22, 2005.
23. Berlemann U, Schwarzenbach O: An injectable nucleus replacement as an adjunct to microdiscectomy: 2 year follow-up in a pilot clinical study. *Eur Spine J* 18:1706-1712, 2009.
24. Jin D, Qu D, Zhao L, et al: Prosthetic disc nucleus (PDN) replacement for lumbar disc herniation: preliminary report with six months' follow-up. *J Spinal Disord Tech* 16:331-337, 2003.
25. Boelen EJ, Koole LH, van Rhijn LW, et al: Towards a functional radiopaque hydrogel for nucleus pulposus replacement. *J Biomed Mater Res B Appl Biomater* 83:440-450, 2007.
26. Yang CW, Liu L, Wang J, et al: Magnetic resonance imaging of artificial lumbar disks: safety and metal artifacts. *Chin Med J (Engl)* 122:911-916, 2009.
27. Rupp R, Ebraheim NA, Savolaine ER, et al: Magnetic resonance imaging evaluation of the spine with metal implants. General safety and superior imaging with titanium. *Spine (Phila Pa 1976)* 18:379-385, 1993.

Biomechanical evaluation of a novel nucleus pulposus prosthesis in canine cadaveric spines

Lucas A. Smolders ^a, Niklas Bergknut ^{a,b}, Idsart Kingma ^c,
Albert J. van der Veen ^d, Theo H. Smit ^e, Leo H. Koole ^f,
Herman A.W. Hazewinkel ^a, Björn P. Meij ^a

The Veterinary Journal, 192(2):199-205, 2012

^a Department of Clinical Sciences of Companion Animals, Faculty of Veterinary Medicine, Utrecht University, The Netherlands

^b Department of Clinical Sciences, Division of Small Animals, Faculty of Veterinary Medicine and Animal Sciences, Swedish University of Agricultural Sciences, Uppsala, Sweden

^c Research institute MOVE, Faculty of Human Movement Sciences, VU University, Amsterdam, The Netherlands

^d Research Institute MOVE, VU University Medical Center, Department of Orthopedic Surgery, Amsterdam, The Netherlands

^e Research Institute MOVE, VU University Medical Center, Department of Physics and Medical Technology, Amsterdam, The Netherlands

^f Department of Biomedical Engineering/Biomaterials Science, Faculty of Health, Medicine and Life Sciences, Maastricht University, Maastricht, The Netherlands

This research forms part of the Project P2.01 IDiDAS of the research program of the BioMedical Materials institute co-funded by the Dutch Ministry of Economic Affairs.

Abstract

Objective: Partial disc replacement is a new surgical technique aimed at restoring functionality to degenerated intervertebral discs (IVDs). The aim of the present study was to assess biomechanically the behaviour of a novel nucleus pulposus prosthesis (NPP) in situ and its ability to restore functionality to the canine IVD after nucleotomy alone or after combined dorsal laminectomy and nucleotomy.

Methods: Nine canine T13-L5 specimens (L2L3 group) and 10 L5-Cd1 specimens (LS group) were tested biomechanically in the native state, after nucleotomy (L2L3 group) or after combined dorsal laminectomy and nucleotomy (LS group), and after insertion of the NPP. Range of motion (ROM), neutral zone (NZ), and neutral zone stiffness (Nzs) were determined in flexion/extension, lateral bending, and axial rotation.

Results: Nucleotomy alone and combined dorsal laminectomy and nucleotomy caused significant instability in all motion directions. Implantation of the NPP resulted in significant restoration of the parameters (ROM, NZ, and Nzs) towards the native state; however, fragmentation/herniation of the NPP occurred in 47% of the cases.

Conclusions: The NPP has the ability to improve functionality of the nucleotomized canine IVD. The high rate of NPP failure requires modifications directed at the integrity of the NPP and its confinement to the nuclear cavity.

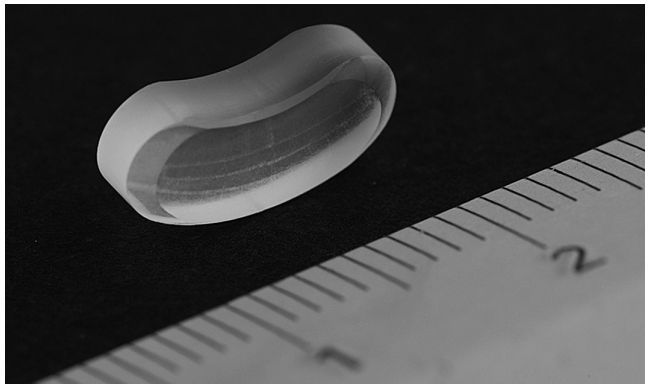
Key words: intervertebral disc; biomechanics; laminectomy; nucleotomy; nucleus pulposus prosthesis

Introduction

Intervertebral disc (IVD)-related diseases in dogs include cervical spondylomyelopathy, thoracolumbar disc disease, and degenerative lumbosacral stenosis, and are highly associated with IVD degeneration¹⁻³. Surgical therapy for IVD-related disease consists of decompressive procedures, such as ventral decompression and hemi- or dorsal laminectomy, usually including partial discectomy, and sometimes vertebral stabilization¹⁻³. Prophylactic fenestration of the IVD has been advocated to prevent potential future disc-associated disease^{1,4}. Although these surgical procedures are clinically effective in relieving symptoms in the short term, they involve removal of the nucleus pulposus (NP) without restoration of IVD function. Partial discectomy/nuclectomy has been shown to result in significant instability of the spine⁵⁻⁸ and vertebral stabilization significantly increases the stiffness of the spine^{9,10}. Hence, these surgical techniques result in altered spinal biomechanics, increasing the risk of recurrence of clinical signs at the site of operation and of the development of pathologies in the adjacent segments¹¹⁻¹⁴.

New technologies aimed at restoring IVD function in humans may also be of benefit to veterinary species. Replacement of the NP with a nucleus pulposus prosthesis (NPP) is aimed at restoring normal IVD function to avoid complications caused by decompressive procedures and/or stabilization¹⁵. Recently, a novel, preformed, biocompatible, radiopaque hydrogel has been developed to adequately replace a diseased NP (Fig. 1)¹⁶⁻¹⁹. This NPP is implanted in dry form (xerogel), enabling insertion of the NPP through a small annular opening. After insertion, the prosthesis expands in situ, reaching its final dimensions within 18 h of placement.

Figure 1. The dry hydrogel nucleus pulposus prosthesis custom-made for insertion into the nuclear cavity of the L2-L3 canine intervertebral disc. The scale is in cm.



The physico-mechanical properties of the material, surgical insertion, positioning, imaging characteristics, and ability of the NPP to restore disc height after nuclectomy have been evaluated¹⁶⁻¹⁹. However, its behaviour in situ under biomechanical loading has not been tested, nor has its ability to restore

functionality to the IVD after nucleotomy. The aim of this study was to assess the behaviour of this novel NPP in situ and to evaluate its ability to restore functionality to the canine IVD after nucleotomy.

Materials and methods

Nine T13-L5 and ten L5-Cd1 canine spine specimens (pelvis removed), isolated from 10 healthy, female mongrel dogs, were used. All dogs were euthanased when approximately 2 years of age (weight range, 16.1-20.4 kg) in an unrelated experiment (approved by the Ethics Committee on Animal Experimentation of Utrecht University: DEC 06.06.053). During their life span, the dogs had had a normal level of activity and no known history of back pathology. Dorsoventral and lateral radiographs were taken to exclude spinal specimens demonstrating anomalies or signs of pathology.

Specimen preparation and testing

The specimens were divided into two groups, with group 1 containing all nine T13-L5 spinal specimens (referred to as the L2L3 group) and group 2 containing all 10 L5-Cd1 spinal specimens (referred to as the LS group).

Immediately after euthanasia, the spinal specimens were harvested and frozen at -20°C . Prior to testing, each frozen specimen was thawed at 4°C (24 h) and cleared of all soft tissue, except for the ligamentous tissues and IVDs. The cranial and caudal segment ends were embedded in two metal cups, using heated cerro-low147 (alloy consisting of 48% bismuth, 25.6% lead, 12.8% tin, 9.5% cadmium, 4% indium; Cerro Metal Products Co). During preparation and testing, the specimens were kept moist by regularly spraying them with saline solution (0.9% NaCl).

The embedded spinal specimens were inserted into a four-point bending device. Load was applied with a hydraulic materials testing machine (Instron Model 8872, Instron Corporation IST), attached to the four-point bending device. L-shaped flags, each containing three light-emitting diodes (LEDs), were attached to the ventral side of each vertebral body (L1, L2, and L3 in the L2L3 group; L6, L7, and S1 in the LS group). The movement of each flag was recorded at 50 samples/s with an optoelectronic 3D movement registration system with one array of three cameras (Optotrak 3020, Northern Digital Inc.). The 3D resolution of the system is 0.02 mm. The sampling rate for both the load and the displacement measurements was 50 samples/s.

Each specimen was deformed at a constant loading rate of $1.0^{\circ}/\text{s}$ and was subjected to a cyclic bending moment (back and forth from -2 Nm to $+2\text{ Nm}$), applied in the region of T13 to L5 (L2L3 group) or L5 to Cd1 (LS group). Each specimen was tested in flexion/extension (FE), lateral bending (LB), and axial rotation (AR). During axial rotation, the metal cup at the caudal side of the spine was restrained in all directions. The metal cup at the cranial side was

free to move in axial rotation. The torsional load was applied by a displacement controlled movement at the cranial side of the spine at a constant loading rate of $1.0^{\circ}/s$. Load was applied with the materials testing machine by pulling a steel wire, which was winded around the metal cup at the cranial side of the spine, thereby creating a rotational movement along the longitudinal axis of the spine. The specimen was subjected to three loading cycles per motion direction.

Preparation of the NPP

To obtain accurate NPP measurements for this study, three canine lumbar spines, isolated from three healthy mongrel dogs (weight range, 22.9-24.0 kg; age range, 15-22 months; euthanased in an unrelated experiment approved by the Ethics Committee on Animal Experimentation of Utrecht University: DEC 06.06.053) were used. The complete L2-L3 and L7-S1 IVDs (NP and annulus fibrosus) were isolated by cutting directly adjacent to the cranial and caudal endplates using a #11 surgical blade. In this manner, the IVD was isolated in one piece while maintaining the integrity of the NP and annulus fibrosus. The width, height, and thickness of the NP were measured with a Vernier caliper (accuracy 0.05 mm). The thickness of the NP was measured at its thickest middle region without compressing the NP. The width, height, and thickness of the L2-L3 and L7-S1 NPs obtained from the three spines were averaged, and the NPPs were made on the basis of these measurements, taking into account a material swelling factor of 1.3. The custom-made NPPs measured $7.7 \times 3.6 \times 1.8$ mm (width x height x thickness) for the L2-L3 IVD and $10.4 \times 4.5 \times 2.4$ mm for the L7-S1 IVD in the dry state, and $10.0 \times 4.7 \times 2.4$ mm for the L2-L3 IVD and $13.5 \times 5.9 \times 3.1$ mm for the L7-S1 IVD in the swollen, hydrated state.

Testing steps

Each specimen was tested in the following sequence:

1. Native spinal specimen (Condition 1).
2. Spinal specimen after nucleotomy (Condition 2). In the L2L3 group, a nucleotomy was performed on the L2-L3 IVD via a left lateral approach. A small stab incision (length x width: 4×2 mm) was made into the middle of the IVD with a #11 surgical blade, parallel to the fibres of the outer annular ring. All NP material was removed through the annular incision with the use of a ball-tipped probe and grasping forceps. The L1-L2 IVD was left intact and served as a control. In the LS group, surgery was performed on the lumbosacral (L7-S1) junction via a dorsal approach. A dorsal laminectomy was performed, as described previously⁹. Subsequently, nucleotomy of the L7-S1 IVD was performed as described for the L2L3 group, but through a dorsal annular incision (4.5×3 mm). The L6-L7 IVD was left intact and served as a control.

3. Spinal specimen after insertion of the NPP (Condition 3). The annular incision was carefully widened with grasping forceps. The non-hydrated NPP was inserted into the nuclear cavity through the annular incision, using the closed end of grasping forceps and manual manipulation. Phosphate-buffered saline (PBS) was injected into the cavity to initiate implant hydration. The annular incision was closed with a combination of one cruciate suture (Polydioxanone 2-0) through the outer annular layer and 2-octyl cyanoacrylate glue (Dermabond, Ethicon INC). Polypropylene mesh (1.0 x 1.5 cm) was glued over the closed annular defect. Proper positioning of the NPP in all spinal specimens was confirmed by radiography in lateral and dorsoventral views (Fig. 2). Each specimen was wrapped in PBS-soaked surgical gauze and placed in a plastic bag to prevent implant and specimen dehydration. Each specimen was incubated for 18 h at 38 °C to allow complete hydration of the NPP.

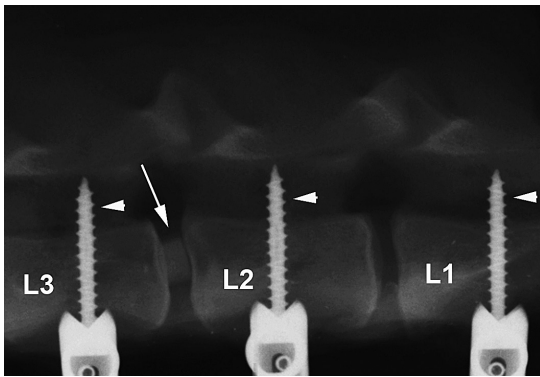


Figure 2. Lateral view of a canine lumbar spinal specimen after insertion of the novel, radiopaque nucleus pulposus prosthesis (arrow) into the L2-L3 intervertebral disc. Screws, which serve as anchor points for the L-shaped flags containing the light emitting diodes, have been inserted into the L1, L2, and L3 vertebrae (arrowheads).

After biomechanical testing, the NPP was retrieved through an incision in the ventral annulus fibrosus. The overall condition of the prosthesis and the annular closure were examined.

Data analysis

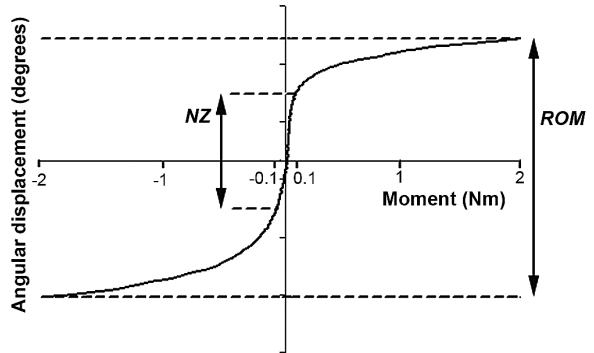
Angular displacement of the L1-L2, L2-L3 (L2L3 group) and of the L6-L7, L7-S1 (LS group) intervertebral junctions was calculated using spatial data of the LED markers collected by the camera system. Only data for the third loading cycle of each motion series were used. The following parameters were determined for all three conditions:

Range of motion (ROM): the range of angular displacement between minimum (-2 Nm) and maximum (+2 Nm) applied moments (Fig. 3).

Neutral zone (NZ): the range over which the specimen moves essentially free of applied loading. NZ was determined by calculating the angular displacement found between - 0.1 Nm and +0.1 Nm of applied moment.

Neutral zone stiffness (NZS): the quotient of loading and angular displacement in the NZ. NZS was calculated from the upward slope of the load-displacement curve ²⁰.

Figure 3. Load-displacement curve showing the neutral zone (NZ, angular displacement in degrees between -0.1 Nm and $+0.1$ Nm of applied moment) and the range of motion (ROM, angular displacement in degrees between -2.0 Nm and $+2.0$ Nm of applied moment)



The ROM, NZ, and NZS were calculated for FE (ROM_{FE} , NZ_{FE} and NZS_{FE} , respectively), LB (ROM_{LB} , NZ_{LB} and NZS_{LB} , respectively), and AR (ROM_{AR} , NZ_{AR} and NZS_{AR} , respectively).

Statistics

The Shapiro-Wilk normality test was used to confirm the normal distribution of the data. Means \pm SD were calculated for all parameters. Repeated measures ANOVAs were applied to ROM, NZ, and NZS with the within-subject factors 'condition' (three levels: native specimen, nuclectomized specimen, NPP specimen) and 'motion direction' (three levels: FE, LB, AR) and the between-subject factor 'status' (NPP intact or fragmented after testing). When significant interactions between factors were found, post-hoc repeated measures ANOVAs were applied. For all main effects of condition, t-tests for paired samples were conducted to specify which conditions differed from one another. Bonferroni adjustment for multiple comparisons was applied. $P < 0.05$ was considered statistically significant.

Results

L2L3 group

Compared with the native state, nuclectomy caused a significant increase (mean percentual difference) in the ROM_{FE} (+32.7%), ROM_{LB} (+10.8%), ROM_{AR} (+44.2%), NZ_{FE} (+247.1%), NZ_{LB} (+95.9%) and NZ_{AR} (+103.8%), whereas the NZS_{FE} (-75.4%), NZS_{LB} (-49.8%) and NZS_{AR} (-48.2%) were significantly decreased (Fig. 4).

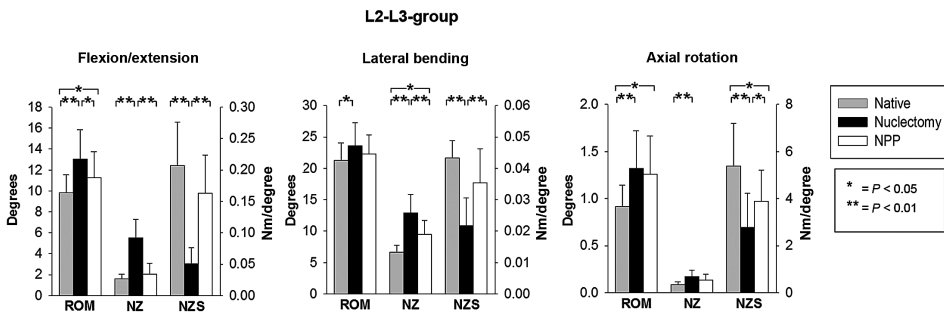


Figure 4. Means \pm SD for the range of motion (ROM), neutral zone (NZ), and neutral zone stiffness (NZS) in flexion/extension, lateral bending, and axial rotation for the native spinal specimen, the nuclectomy specimen, and the specimen after insertion of the nucleus pulposus prosthesis (NPP) in the L2-L3 group. The left vertical axes apply to the ROM and NZ, while the right vertical axes apply to the NZS.

An intact NPP induced significant restoration of stability (Fig. 5). Compared with the nuclectomized state, prosthesis insertion led to a significant decrease in the ROM_{FE} (-13.6%), NZ_{FE} (-63.2%) and NZ_{LB} (-26.4%), but not in the ROM_{LB} , ROM_{AR} , and NZ_{AR} . Significant differences from the native state were found for the ROM_{FE} (+14.7%), ROM_{AR} (+37.3%), and NZ_{LB} (+44.1%), but not for the ROM_{LB} , NZ_{FE} , and NZ_{AR} . Compared with the nuclectomized state, prosthesis insertion resulted in a significant increase in the NZS_{FE} (+221.2%) and NZS_{LB} (+63.2%) to levels not significantly different from those in the native state. The NZS_{AR} was significantly increased (+39.5%), but was still significantly different from the native state (-27.8%).

Four of nine (44.4%) NPPs retrieved from the tested spinal specimens showed considerable damage. In one specimen the annular incision had ruptured, causing parts of the prosthesis to herniate through the annular defect. To assess whether the state of the NPP significantly affected the parameter values obtained in Condition 3, a distinction was made between ‘intact prosthesis specimens’ and ‘fragmented prosthesis specimens’. This was realized by incorporating a between-subject factor (factor ‘status’) in the statistical model. No significant effects were found for the factor ‘status’.

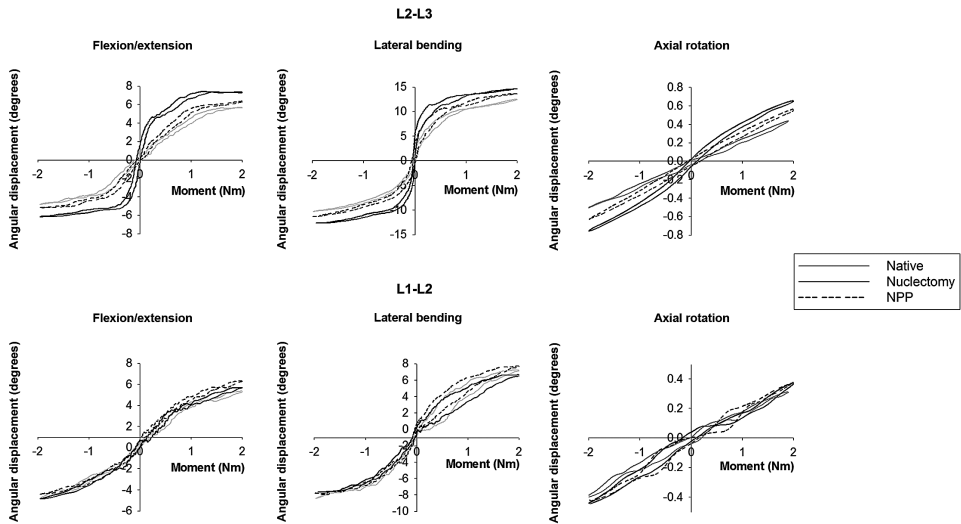


Figure 5. Typical examples of load-displacement curves for flexion/extension, lateral bending, and axial rotation for the L2-L3 (surgery) and L1-L2 (control) intervertebral junction. An intact nucleus pulposus prosthesis (NPP) was isolated from this particular specimen. Only the third loading cycles are displayed.

LS group

Relative to the native state, dorsal laminectomy and nuclectomy caused significant changes for the ROM_{FE} (+28.7%), ROM_{LB} (+26.2%), ROM_{AR} (+139.4%), NZ_{FE} (+128.1%), NZ_{LB} (266.9%), NZ_{AR} (+203.5%), NZS_{FE} (-64.9%), NZS_{LB} (-79.9%), and NZS_{AR} (-71.1%) (Fig. 6). An intact NPP induced significant restoration of stability (Fig. 7). Compared with the nuclectomized state, insertion of the NPP led to a significant decrease in the ROM_{FE} (-8.8%), ROM_{AR} (-16.8%), NZ_{FE} (-25.8%), NZ_{LB} (-30.8%) and NZ_{AR} (-35.0%) but not in the ROM_{LB} . After NPP insertion, the NZS_{FE} (+63.8%), NZS_{LB} (+107.0%) and NZS_{AR} (+59.0%) were significantly increased. Compared with the native state, significant differences were found for the ROM_{FE} (+17.3%), ROM_{LB} (+19.1%), ROM_{AR} (+99.3%), NZ_{FE} (+69.0%), NZ_{LB} (+153.8%), NZ_{AR} (+97.3%), NZS_{FE} (-42.6%), NZS_{LB} (-58.5%) and NZS_{AR} (-54.0%).

Five of ten (50%) NPPs retrieved from the tested spinal specimens were damaged, with rupture of the annular incision resulting in herniation of NPP material. To assess the effect of the state of the prosthesis on the parameter values in Condition 3, a between-subject factor 'status' was used as described for the L2L3 group. A significant interaction between factor 'status' and factor 'condition' was found for all parameters, except for the NZ_{AR} and NZS_{AR} . Thus, the prosthesis integrity had a significant effect on the parameter values obtained in Condition 3. Comparison of the values found for 'intact prosthesis

specimens' ($n = 5$) with those found for 'fragmented prosthesis specimens' ($n = 5$) in Condition 3 showed that the NZ_{FE} and NZ_{LB} were significantly lower with an intact prosthesis ($P = 0.007$ and $P = 0.007$, respectively) and that the NZS_{FE} and NZS_{LB} were significantly higher ($P = 0.001$ and $P = 0.002$, respectively) (Fig. 8).

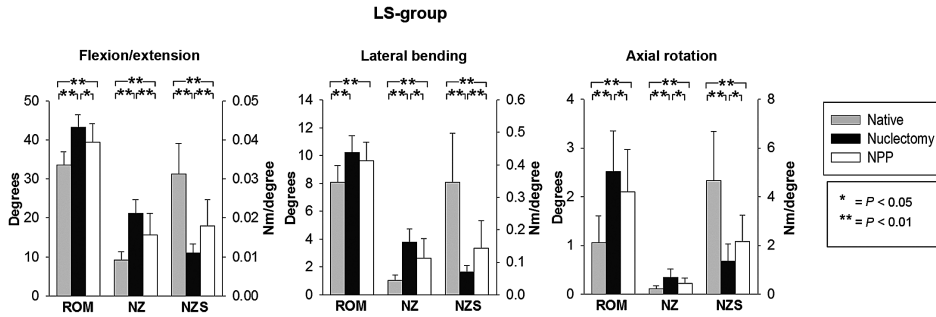


Figure 6. Means \pm SD for the range of motion (ROM), neutral zone (NZ), and neutral zone stiffness (NZS) in flexion/extension, lateral bending, and axial rotation for the native spinal specimen, the nuclectomy specimen, and the specimen after insertion of the nucleus pulposus prosthesis (NPP) in the LS group. The left vertical axes apply to the ROM and NZ, while the right vertical axes apply to the NZS.

Control segments

For the control segments L1-L2 and L6-L7, no significant changes were found between the native state, the nuclectomized state, and the NPP state (data not shown).

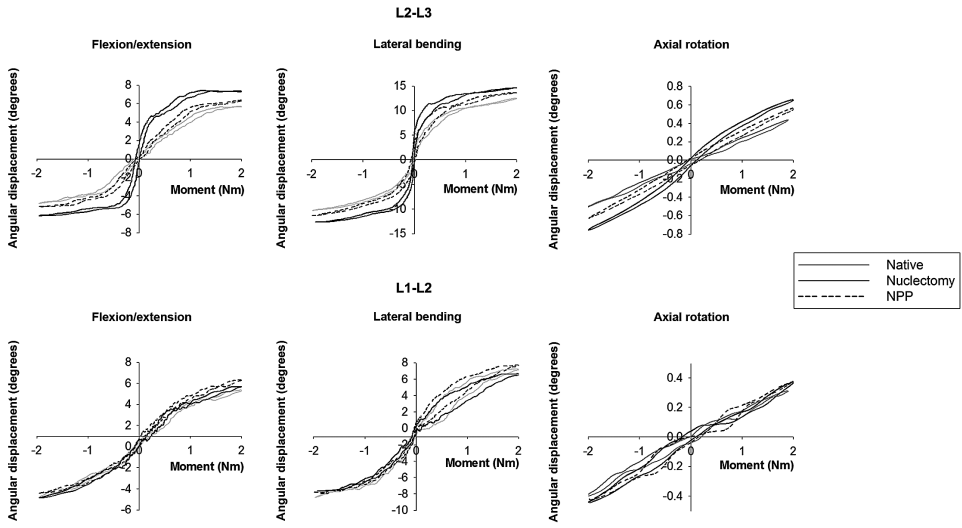


Figure 7. Typical examples of load-displacement curves for flexion/extension, lateral bending, and axial rotation for the L7-S1 (surgery) and L6-L7 (control) intervertebral junction. An intact nucleus pulposus prosthesis (NPP) was isolated from this particular spinal specimen. Only the third loading cycles are displayed.

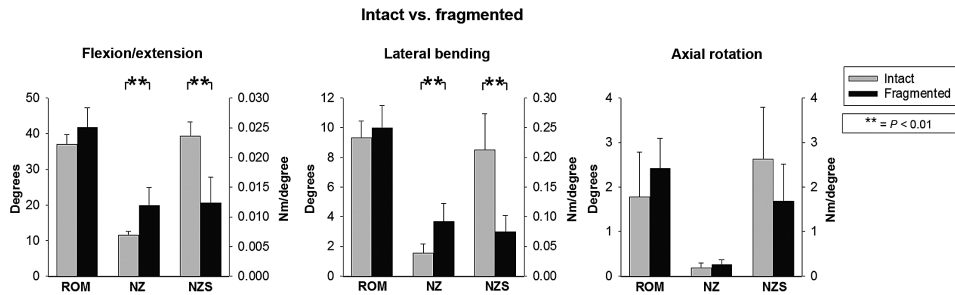


Figure 8. Comparison of spinal specimens with intact ($n = 5$) and fragmented ($n = 5$) nucleus pulposus prostheses (Condition 3) in flexion/extension, lateral bending, and axial rotation in the LS group. The left vertical axes apply to the range of motion (ROM) and neutral zone (NZ), while the right vertical axes apply to the neutral zone stiffness (NZS).

Discussion

The present study involved three-dimensional motion analysis of individual spinal segments in multisegmented specimens, as has been described for other recent canine biomechanical studies²¹⁻²³. Nuclectomy of a lumbar/lumbosacral IVD resulted in significant spinal instability, which is in accordance with previous studies⁵⁻⁸. These results support the rationale to restore function to the spinal segment after nuclectomy.

Replacement of the NP may be a solution for dogs affected by disc degeneration and for which conservative therapy has failed and functional repair of the annulus is still feasible^{19,24}. The NPP tested in this study distinguishes itself from other NPP designs: it consists of an intrinsically radiopaque hydrogel, which makes it optimally visible on imaging; after insertion it expands *in situ* to completely fill the nuclear cavity and prevent implant migration¹⁶⁻¹⁹. Our findings indicate that the NPP has the ability to improve functionality of the nuclectomized IVD; however, not all variables returned to levels found in the native state, most likely because NPP fragmentation was observed in a large fraction of the tested specimens. Even though the NPPs were subjected to short-term cyclic loading (3 loading cycles), fragmentation of the NPP was observed with 44.4% and 50% of the L2L3 and LS group cases, respectively. The state of the prosthesis significantly affected parameters measured only in the LS group, which may be because herniation of the prosthesis material occurred in all damaged LS group prostheses, but in only one of the four damaged L2L3 group prostheses. The significant differences in the results obtained for ‘fragmented prosthesis specimens’ and ‘intact prosthesis specimens’ in the LS group highlight the importance of NPP integrity for its functionality.

There are several possible explanations for the fragmentation and herniation of the NPP. First, the physico-mechanical properties of the NPP material may be inadequate to withstand the forces generated by physiological spinal motion. However, the results obtained from *in vitro* biomechanical tests of the NPP biomaterial do not explain the observed NPP fragmentation¹⁷⁻¹⁹. A possible explanation may be that the NPP material is less deformable, more rigid, than the natural NP, and while the NPP biomaterial can withstand extreme compressive strains¹⁷, it may have a relatively small resistance to tensile forces. In addition, biomechanical loading, and thereby physiological motion, of the spinal segment is likely to result in a form of ‘wedging’ of the IVD, with one side of the IVD being compressed and the other side being opened. This wedging may promote migration of the NPP within the nucleus cavity toward the ‘open side’, resulting in increased pressure against the repaired annulus fibrosus. The NPP has been designed to function optimally in a confined space and a suboptimal fit of the NPP due to wedging may create intolerable biomechanical stresses on the implant. In addition, this wedging may create shear forces within the implant material, which may result in fragmentation of the NPP.

Second, the technique used to close the annular incision may have

contributed to NPP fragmentation. The annular closure method used provides durable closure²⁵, but only closes the outer layer of the annulus fibrosus. This means that the original NP cavity may become enlarged, so that the custom-made prosthesis cannot completely fill the space, allowing the NPP to migrate inside the cavity. This might expose the NPP to unexpected compressive and tensile forces, resulting in prosthesis damage. The annular closure method consisting of a suture combined with cyanoacrylate glue and polypropylene mesh may be safely applied when using a lateral approach for nucleotomy. However, this method is not appropriate for closure of the dorsal annulus fibrosus (L7-S1) in an *in vivo* situation because of the close proximity of the cauda equina nerve roots. Therefore, further modifications to the described annular closure technique or the development of a specialized annular closure technique/device²⁶ are required for optimal and safe application of this nucleus replacement procedure in dogs.

Third, the prosthesis may have been damaged during insertion. Several insertion devices have been developed to facilitate the insertion of other NPP designs²⁷⁻²⁹. The annular incision was kept as small as possible to reduce the chance of implant extrusion but consequently, considerable force was required to insert the NPP through the annular opening. However, assessment of NPP integrity prior to biomechanical testing by way of radiography, computed tomography, magnetic resonance imaging, and macroscopic examination revealed no NPP damage/fragmentation¹⁶. These results suggest that the methods for insertion of the NPP and closure of the annulus fibrosus are adequate in this experimental setting and are unlikely to be the cause for NPP fragmentation. This, NPP fragmentation is likely the result of biomechanical loading of the NPP *in situ*. While implant extrusion is a common complication of NP replacement^{24,30-32}, we found extrusion of NPP material only when the prosthesis was damaged and not when the prosthesis was intact.

Conclusions

This study demonstrates that the novel NPP, when *in situ* and intact, is able to improve the functionality and stability of the lumbar/lumbosacral IVD after nucleotomy. The NPP requires significant alterations to function as a long-term partial disc replacement. Prosthesis integrity and its confinement to the nuclear cavity are essential conditions for the safety and functionality of this concept. Improvements of this NPP concept are prerequisites for safe, future applications of the NPP *in vivo*.

Conflict of interest statement

None of the authors has any financial or personal relationships that could inappropriately influence or bias the content of the paper.

References

1. Brisson BA: Intervertebral disc disease in dogs. *Vet Clin North Am Small Anim Pract* 40:829-858, 2010.
2. da Costa RC: Cervical spondylomyelopathy (wobbler syndrome) in dogs. *Vet Clin North Am Small Anim Pract* 40:881-913, 2010.
3. Meij BP, Bergknut N: Degenerative lumbosacral stenosis in dogs. *Vet Clin North Am Small Anim Pract* 40:983-1009, 2010.
4. Brisson BA, Moffatt SL, Swayne SL, et al: Recurrence of thoracolumbar intervertebral disk extrusion in chondrodystrophic dogs after surgical decompression with or without prophylactic fenestration: 265 cases (1995-1999). *J Am Vet Med Assoc* 224:1808-1814, 2004.
5. Hill TP, Lubbe AM, Guthrie AJ: Lumbar spine stability following hemilaminectomy, pediculectomy, and fenestration. *Vet Comp Orthop Traumatol* 13:165-171, 2000.
6. Macy NB, Les CM, Stover SM, et al: Effect of disk fenestration on sagittal kinematics of the canine C5-C6 intervertebral space. *Vet Surg* 28:171-179, 1999.
7. Schulz KS, Waldron DR, Grant JW, et al: Biomechanics of the thoracolumbar vertebral column of dogs during lateral bending. *Am J Vet Res* 57:1228-1232, 1996.
8. Smith MEH, Bebchuk TN, Shmon CL, et al: An in vitro biomechanical study of the effects of surgical modification upon the canine lumbosacral spine. *Vet Comp Orthop Traumatol* 17:17-24, 2004.
9. Meij BP, Suwankong N, Van der Veen AJ, et al: Biomechanical flexion-extension forces in normal canine lumbosacral cadaver specimens before and after dorsal laminectomy-discectomy and pedicle screw-rod fixation. *Vet Surg* 36:742-751, 2007.
10. Walker TM, Pierce WA, Welch RD: External fixation of the lumbar spine in a canine model. *Vet Surg* 31:181-188, 2002.
11. Danielsson F, Sjoström L: Surgical treatment of degenerative lumbosacral stenosis in dogs. *Vet Surg* 28:91-98, 1999.
12. De Risio L, Sharp NJ, Olby NJ, et al: Predictors of outcome after dorsal decompressive laminectomy for degenerative lumbosacral stenosis in dogs: 69 cases (1987-1997). *J Am Vet Med Assoc* 219:624-628, 2001.
13. Eck JC, Humphreys SC, Hodges SD: Adjacent-segment degeneration after lumbar fusion: a review of clinical, biomechanical, and radiologic studies. *Am J Orthop* 28:336-340, 1999.
14. Frei H, Oxland TR, Rathonyi GC, et al: The effect of nucleotomy on lumbar spine mechanics in compression and shear loading. *Spine* 26:2080-2089, 2001.
15. Di Martino A, Vaccaro AR, Lee JY, et al: Nucleus pulposus replacement: basic science and indications for clinical use. *Spine* 30:S16-22, 2005.
16. Bergknut N, Smolders LA, Koole LH, et al: The performance of a hydrogel nucleus pulposus prosthesis in an ex vivo canine model. *Biomaterials* 31:6782-6788, 2010.
17. Boelen EJ, Koole LH, van Rhijn LW, et al: Towards a functional radiopaque hydrogel for nucleus pulposus replacement. *J Biomed Mater Res B Appl Biomater* 83:440-450, 2007.
18. Boelen EJ, van Hooy-Corstjens CS, Bulstra SK, et al: Intrinsically radiopaque hydrogels for nucleus pulposus replacement. *Biomaterials* 26:6674-6683, 2005.

19. Boelen EJH, van Hooy-Corstjens CSJ, Gijbels MJJ, et al: Preliminary evaluation of new intrinsically radiopaque hydrogels for replacing the nucleus pulposus. *J Mater Chem* 16:824-828, 2006.
20. Wilke HJ, Wenger K, Claes L: Testing criteria for spinal implants: recommendations for the standardization of in vitro stability testing of spinal implants. *Eur Spine J* 7:148-154, 1998.
21. Benninger MI, Seiler GS, Robinson LE, et al: Three-dimensional motion pattern of the caudal lumbar and lumbosacral portions of the vertebral column of dogs. *Am J Vet Res* 65:544-551, 2004.
22. Benninger MI, Seiler GS, Robinson LE, et al: Effects of anatomic conformation on three-dimensional motion of the caudal lumbar and lumbosacral portions of the vertebral column of dogs. *Am J Vet Res* 67:43-50, 2006.
23. Hediger KU, Ferguson SJ, Gedet P, et al: Biomechanical analysis of torsion and shear forces in lumbar and lumbosacral spine segments of nonchondrodystrophic dogs. *Vet Surg* 38:874-880, 2009.
24. Coric D, Mummaneni PV: Nucleus replacement technologies. *J Neurosurg Spine* 8:115-120, 2008.
25. Heuer F, Ulrich S, Claes L, et al: Biomechanical evaluation of conventional anulus fibrosus closure methods required for nucleus replacement. Laboratory investigation. *J Neurosurg Spine* 9:307-313, 2008.
26. Bron JL, Helder MN, Meisel HJ, et al: Repair, regenerative and supportive therapies of the annulus fibrosus: achievements and challenges. *Eur Spine J* 18:301-313, 2009.
27. Allen MJ, Schoonmaker JE, Bauer TW, et al: Preclinical evaluation of a poly (vinyl alcohol) hydrogel implant as a replacement for the nucleus pulposus. *Spine* 29:515-523, 2004.
28. Bertagnoli R: Disc surgery in motion. *SpineLine* 6:23-28, 2004.
29. Husson JL, Korge A, Polard JL, et al: A memory coiling spiral as nucleus pulposus prosthesis: concept, specifications, bench testing, and first clinical results. *J Spinal Disord Tech* 16:405-411, 2003.
30. Jin D, Qu D, Zhao L, et al: Prosthetic disc nucleus (PDN) replacement for lumbar disc herniation: preliminary report with six months' follow-up. *J Spinal Disord Tech* 16:331-337, 2003.
31. Klara PM, Ray CD: Artificial nucleus replacement: clinical experience. *Spine* 27:1374-1377, 2002.
32. Wilke HJ, Heuer F, Neidlinger-Wilke C, et al: Is a collagen scaffold for a tissue engineered nucleus replacement capable of restoring disc height and stability in an animal model? *Eur Spine J* 15 Suppl 3:S433-438, 2006.

**Biomechanical assessment of the effects
of decompressive surgery in non-
chondrodystrophic and chondrodystrophic
canine multisegmented lumbar spines**

Lucas A. Smolders ^a, Idsart Kingma ^b, Niklas Bergknut ^{a,c},
Albert J. van der Veen ^d, Wouter J.A. Dhert ^{a,e}, Herman A.W. Hazewinkel ^a,
Jaap H. van Dieën ^b, Björn P. Meij

European Spine Journal 21(9): 1692-1699, 2012

^a Department of Clinical Sciences of Companion Animals, Faculty of Veterinary Medicine,
Utrecht University, Yalelaan 108, 3508 TD Utrecht, The Netherlands

^b Research institute MOVE, Faculty of Human Movement Sciences, VU University, Van der
Boechorststraat 9, 1081 BT Amsterdam, The Netherlands

^c Department of Clinical Sciences, Division of Small Animals, Faculty of Veterinary Medicine
and Animal Sciences, Swedish University of Agricultural Sciences, Ulls väg 12, Box 7040,
750 07 Uppsala, Sweden

^d Research Institute MOVE, VU University Medical Center, Department of Orthopedic Surgery,
De Boelelaan 1117, 1007 MB Amsterdam, The Netherlands

^e Department of Orthopaedics, Division of Surgical Specialties, University Medical Center
Utrecht, Heidelberglaan 100, 3584 CX Utrecht, The Netherlands

Abstract

Purpose: Dogs are often used as an animal model in spinal research, but consideration should be given to the breed used as chondrodystrophic (CD) dog breeds always develop IVD degeneration at an early age, whereas non-chondrodystrophic (NCD) dog breeds may develop IVD degeneration, but only later in life. The aim of this study was to provide a mechanical characterization of the NCD (non-degenerated intervertebral discs (IVDs), rich in notochordal cells) and CD (degenerated IVDs, rich in chondrocyte-like cells) canine spine before and after decompressive surgery (nucleotomy).

Methods: The biomechanical properties of multisegmented lumbar spine specimens (T13-L5 and L5-Cd1) from 2-year old NCD dogs (healthy) and CD dogs (early degeneration) were investigated in flexion/extension (FE), lateral bending (LB), and axial rotation (AR), in the native state and after nucleotomy of L2-L3 or dorsal laminectomy and nucleotomy of L7-S1. The range of motion (ROM), neutral zone (NZ), and NZ stiffness (Nzs) of L1-L2, L2-L3, L6-L7, and L7-S1 were calculated.

Results: In native spines in both dog groups, the greatest mobility in FE was found at L7-S1, and the greatest mobility in LB at L2-L3. Surgery significantly increased the ROM and NZ, and significantly decreased the Nzs in FE, LB, and AR in both breed groups. However, surgery at L2-L3 resulted in a significantly larger increase in NZ and decrease in Nzs in the CD spines compared with the NCD spines, whereas surgery at L7-S1 induced a significantly larger increase in ROM and decrease in Nzs in the NCD spines compared with the CD spines.

Conclusions: Spinal biomechanics significantly differ between NCD and CD dogs and researchers should consider this aspect when using the dog as a model for spinal research.

Key words: biomechanics; lumbar spine; intervertebral disc degeneration; canine model; nucleotomy

Introduction

Low back pain is a common ailment with a considerable socioeconomic impact^{1,2}. A major cause of low back pain is degeneration of the intervertebral disc (IVD)^{3,4}. IVD degeneration is also an important cause of back problems in dogs, and the underlying processes show many similarities in dogs and humans⁵. For these reasons, dogs are often used to study spinal biomechanics and strategies to reverse or ameliorate IVD degeneration^{6,7}. However, it should be borne in mind that various dog breeds are not uniformly susceptible to developing IVD degeneration. With regard to IVD degeneration, dogs can be divided into chondrodystrophic (CD) (e.g., Beagle) and non-chondrodystrophic (NCD) dog breeds (e.g., mongrel dog). The CD dogs are characterized by abnormal growth of the long bones due to a genetic disorder, resulting in short limbs relative to the length of the spine, whereas the NCD dogs exhibit a normal growth of the long bones. CD dogs develop IVD degeneration at about 1 year of age. In contrast, in NCD dogs, signs of IVD degeneration are generally seen later in life, at 6 to 8 years of age⁸. Moreover, significant differences in the cell population (NCD: rich in notochordal cells; CD: rich in chondrocyte-like cells), matrix composition, and morphology of the nucleus pulposus (NP) can be seen at an early age in the two types of dog⁸⁻¹⁰.

The aim of surgery for IVD degeneration-related diseases is to relieve the compression of neural structures and may consist of removal of the NP (nucleotomy) alone or combined with partial removal of the vertebral roof (laminectomy)¹¹. Decompressive surgery results in spinal instability in humans¹²; however, the effects of decompressive surgery in either NCD or CD dogs separately have not been investigated. A biomechanical investigation of the NCD and CD multisegmented spine before and after decompressive surgery may provide insight into the effects of IVD degeneration and surgical interventions on spinal biomechanics. This knowledge should be taken into account when using the dog as a model in future spinal research.

Materials and Methods

Eighteen T13-L7-Sacrum-Cd1 spinal specimens were isolated from nine healthy, female mongrel dogs (NCD; mean weight, 17.4 kg, range, 16.1-20.4 kg) and nine healthy, female Beagle dogs (CD; mean weight, 14.3 kg, range, 13.0-17.2 kg). All dogs were euthanized at approximately 2 years of age in unrelated experiments approved by the Ethics Committee on Animal Experimentation of Utrecht University. During their life, the dogs had a normal level of activity. Dorsoventral and lateral radiographs were taken to exclude spinal pathology other than IVD degeneration.

Specimen Preparation and Testing

Specimens were prepared and tested as described previously¹³. Immediately after euthanasia, the spinal specimens were harvested. The pelvis was removed and each specimen was sawn in the transverse plane halfway through the L5 vertebra, creating nine T13-L5 and nine L5-Cd1 specimens (note that the canine spine has 13 thoracic and 7 lumbar vertebrae) for both the NCD and CD dog group. The specimens were stored at -20°C and prior to biomechanical testing each specimen was thawed at 4°C (24 hours) and cleaned of all soft tissue, except for the ligamentous tissues and IVDs. The cranial and caudal segment ends were fixed in neutral orientation in two metal cups, using an alloy with a low melting point (cerro-low147, consisting of 48% bismuth, 25.6% lead, 12.8% tin, 9.5% cadmium, 4% indium; Cerro Metal Products Co., Bellefonte, PA, USA). During preparation and testing, the specimens were kept moist by regularly spraying them with saline solution (0.9% NaCl). The fixed spinal specimens were inserted into a four-point bending device¹³. Load was applied with a hydraulic materials-testing machine (Instron Model 8872, Instron Corporation IST, Toronto, Ontario, Canada) attached to the four-point bending device. L-shaped flags, each containing three light-emitting diodes (LEDs), were attached to the ventral side of each vertebral body (L1, L2, and L3 in T13-L5 specimens; L6, L7, and S1 in the L5-Cd1 specimens). The movement of each LED was recorded with an optoelectronic 3D movement registration system (resolution: 0.02mm) with one array of three cameras (Optotrak 3020, Northern Digital Inc, Waterloo, Ontario, Canada). The sampling rate for both the load and the displacement measurements was 50 samples/s. Each specimen was deformed at a constant displacement rate of $1.0^{\circ}/\text{s}$ and was subjected to a cyclic bending moment (back and forth from -2Nm to $+2\text{Nm}$; a bending moment of 2 Nm was determined to result in physiological displacement of the tested canine specimens), applied in the region of T13 to L5 or L5 to Cd1. Specimens were tested in the following sequence: 1) flexion/extension (FE), 2) lateral bending (LB), 3) axial rotation (AR); specimens were subjected to three loading cycles per motion direction.

Testing Steps

Each specimen was tested in the native state and after surgery. In the T13-L5 specimens, surgery was performed on the L2-L3 IVD. Via a left lateral approach, a small, transverse stab incision was made into the middle of the IVD with a #11 surgical blade. All NP material was removed (nucleotomy) through the annular incision, using a ball-tipped probe and grasping forceps. The L1-L2 IVD was left intact and served as a control. In the L5-Cd1 specimens, surgery was performed on the lumbosacral (L7-S1) junction via a dorsal approach. The dorsal vertebral arch was removed (dorsal laminectomy; Fig. 1a)) as described previously¹³, leaving the articular facets intact.

Subsequently, nucleotomy of the L7-S1 IVD was performed as described for the L2-L3 IVD, but through a dorsal annular incision (Fig. 1b). The L6-L7 IVD was left intact and served as a control. The structural composition of all surgically removed NPs was examined macroscopically. The NP taken from the NCD discs was gel-like, similar to the NP seen in Thompson grade I IVDs, whereas the NP from the CD discs had a fibrocartilaginous appearance, similar to the NP seen in Thompson grade II IVDs (Fig. 2) ¹⁴.

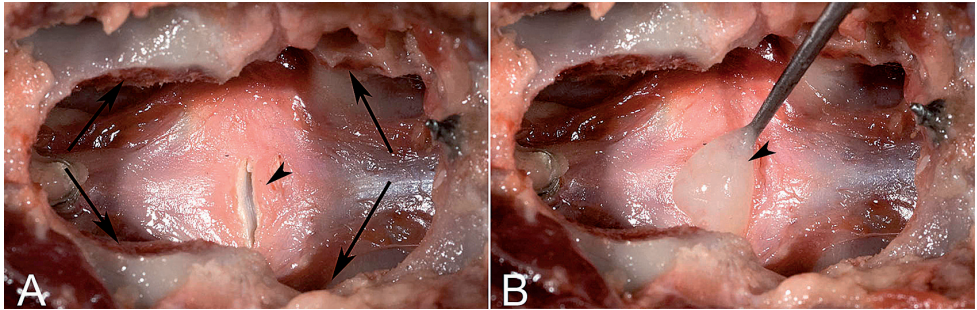


Figure 1. Dorsal view of the L7-S1 segment from a non-chondrodystrophic spine after dorsal laminectomy, showing the laminectomy defect (arrows) and the incision in the dorsal annulus fibrosus (arrowhead) (A). The mucoïd nucleus pulposus (arrowhead) was removed (nucleotomy) from the nuclear cavity using a ball-tipped probe (B).

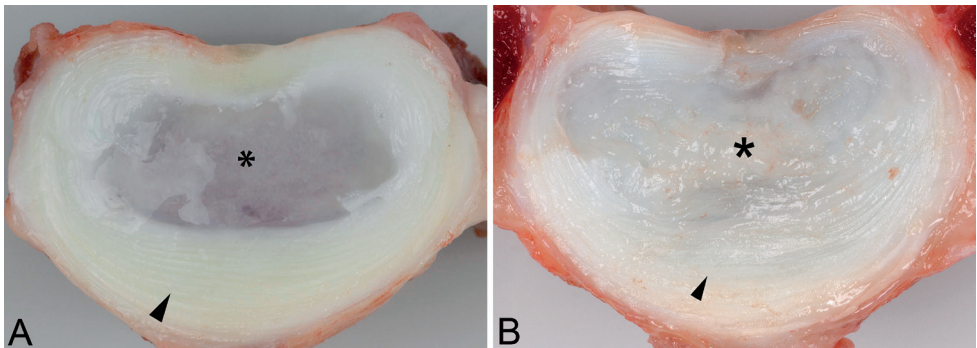


Figure 2. Transverse section of an L2-L3 intervertebral disc obtained from a 2-year-old non-chondrodystrophic dog (A) and a 2-year-old chondrodystrophic (B) dog, showing the central nucleus pulposus (NP) (asterisk) and the outer annulus fibrosus (arrowhead).

Data Analysis

Angular displacement of the L1-L2, L2-L3 (T13-L5 specimens) and of the L6-L7, L7-S1 (L5-Cd1 specimens) intervertebral junctions was calculated using the spatial measurements obtained by means of the LED markers, collected with the Optotrak system. Only the data obtained during the third loading cycle of each motion series were analyzed. The following parameters were calculated before and after surgery: *Range of motion (ROM)*, the range of angular displacement between minimum (-2Nm) and maximum (+2Nm) applied moments¹⁵; *Neutral zone (NZ)*, the range over which the specimen moves essentially free of applied loading; NZ was determined by calculating the angular displacement found between -0.1Nm and +0.1Nm of applied moment; *Neutral zone stiffness (Nzs)*, the quotient of loading and angular displacement in the NZ. Nzs was calculated from the upward slope of the load-displacement curve. The ROM, NZ, and Nzs were calculated for FE (ROM_{FE} , NZ_{FE} , Nzs_{FE}), LB (ROM_{LB} , NZ_{LB} , Nzs_{LB}), and AR (ROM_{AR} , NZ_{AR} , Nzs_{AR}).

Statistics

Statistical analyses were performed using R statistical software¹⁶. The parameters ROM, NZ, Nzs were analyzed using a linear mixed model containing both fixed and random effects¹⁷. The Akaike Information Criterion (AIC) was used for model selection. The factors incorporated in the fixed part were 'motion direction' (FE, LB, AR), 'condition' (native spine, operated spine), 'dog type' (NCD, CD), and the 2- and 3-way interactions between these factors. A random intercept for 'dog' (18 spinal segments) was added to take the correlation within each dog into account. Normal distribution of the response variables within each model was assessed with PP and QQ plots. In the case of significant interactions between factors, post-hoc T-tests were used to calculate the P values for specific effects of interest. The Benjamini and Hochberg False Discovery Rate procedure was used to correct for multiple testing¹⁸. $P < 0.05$ was considered statistically significant.

Results

The biomechanics of the native spine at different levels were markedly different in both the NCD and CD spines: in both groups the L7-S1 spinal segment had the highest ROM_{FE} , approximately 3 times higher than that of L1-L2, L2-L3, and L6-L7 (Table 1). The highest ROM_{LB} was found at L2-L3, followed by L1-L2, L6-L7, and L7-S1. The ROM_{AR} was relatively small at all spinal levels and showed little variation between segment levels, but was highest at L7-S1. A similar but more pronounced intersegmental pattern was found for the NZ. The Nzs showed a similar, but opposite, pattern compared with that of

the ROM and NZ.

No significant differences were found between the native state and the operated state for the control segments L1-L2 and L6-L7 in both groups (data not shown); however, the ROM, NZ, and NZS were markedly different in the

		ROM		NZ		NZS	
		NCD	CD	NCD	CD	NCD	CD
FE	L1-L2	10.1 ± 1.72	11.9 ± 1.41	1.41 ± 0.38	1.47 ± 0.42	0.23 ± 0.08	0.15 ± 0.04
	L2-L3	9.80 ± 1.72	11.4 ± 1.31	1.59 ± 0.47	1.45 ± 0.52	0.21 ± 0.07	0.16 ± 0.06
	L2-L3*	13.0 ± 2.85	14.0 ± 1.78	5.51 ± 1.77	5.93 ± 1.41	0.05 ± 0.03	0.03 ± 0.01
	L6-L7	13.7 ± 2.71	14.4 ± 2.64	2.04 ± 0.37	1.89 ± 0.56	0.14 ± 0.02	0.12 ± 0.07
	L7-S1	33.6 ± 3.36	38.2 ± 4.07	9.25 ± 2.14	9.93 ± 3.88	0.03 ± 0.01	0.02 ± 0.01
	L7-S1*	43.4 ± 3.50	44.8 ± 6.58	21.2 ± 3.83	16.8 ± 3.93	0.01 ± 0.01	0.01 ± 0.01
LB	L1-L2	15.3 ± 2.18	17.6 ± 1.36	4.07 ± 1.17	3.39 ± 0.57	0.08 ± 0.04	0.06 ± 0.01
	L2-L3	21.2 ± 2.77	17.7 ± 2.15	6.59 ± 1.19	3.69 ± 0.89	0.04 ± 0.01	0.06 ± 0.01
	L2-L3*	23.5 ± 2.30	22.9 ± 3.60	12.9 ± 2.92	10.3 ± 2.74	0.02 ± 0.01	0.02 ± 0.01
	L6-L7	10.6 ± 3.69	9.93 ± 3.38	1.82 ± 0.37	1.20 ± 0.53	0.16 ± 0.04	0.19 ± 0.07
	L7-S1	8.10 ± 1.16	10.6 ± 1.66	1.02 ± 0.37	1.36 ± 0.47	0.35 ± 0.15	0.17 ± 0.07
	L7-S1*	10.3 ± 1.25	12.2 ± 2.78	3.74 ± 1.03	3.66 ± 1.84	0.07 ± 0.02	0.06 ± 0.03
AR	L1-L2	0.70 ± 0.14	1.28 ± 0.45	0.07 ± 0.04	0.07 ± 0.07	7.61 ± 3.40	5.10 ± 4.51
	L2-L3	0.92 ± 0.23	1.29 ± 0.34	0.08 ± 0.03	0.06 ± 0.05	5.37 ± 1.83	3.62 ± 1.23
	L2-L3*	1.32 ± 0.40	2.12 ± 0.49	0.17 ± 0.07	0.24 ± 0.26	2.78 ± 1.45	1.39 ± 0.82
	L6-L7	0.74 ± 0.38	1.28 ± 0.52	0.07 ± 0.07	0.07 ± 0.03	8.25 ± 3.70	4.27 ± 3.63
	L7-S1	1.05 ± 0.55	1.81 ± 0.60	0.11 ± 0.06	0.10 ± 0.08	4.67 ± 2.00	2.56 ± 1.61
	L7-S1*	2.56 ± 0.88	3.00 ± 0.87	0.35 ± 0.18	0.24 ± 0.10	1.35 ± 0.74	1.01 ± 0.46

Table 1. Parameter values of native non-chondrodystrophic and chondrodystrophic spines. Means ± SD for the parameters range of motion (ROM; degrees), neutral zone (NZ; degrees), and neutral zone stiffness (NZS; Nm/degree) for flexion/extension (FE), lateral bending (LB), and axial rotation (AR) for L1-L2, L2-L3, L6-L7, and L7-S1 of native non-chondrodystrophic (NCD) and chondrodystrophic (CD) spines. L2-L3* (nuclectomy) and L7-S1* (dorsal laminectomy and nuclectomy) depict the parameter values after spinal surgery.

spinal segments L2-L3 and L7-S1, which had undergone nuclectomy (Table 2). Nuclectomy at L2-L3 significantly increased the ROM_{FE}, ROM_{LB}, and ROM_{AR} to a similar extent in NCD and CD spines (Figs. 3 and 4). Nuclectomy significantly increased the NZ_{FE}, NZ_{LB}, and NZ_{AR}, and significantly decreased the NZS_{FE}, NZS_{LB}, and NZS_{AR}, with a significantly larger increase in NZ and significantly larger decrease in NZS in the CD spines than in the NCD spines in all directions of motion.

Dorsal laminectomy and nuclectomy of L7-S1 significantly increased the ROM_{FE}, ROM_{LB}, and ROM_{AR}, with a significantly larger increase in the NCD spines than in the CD spines in all directions of motion. Surgery resulted in a

significant increase in NZ_{FE} , NZ_{LB} , and NZ_{AR} , with no significant differences between the NCD and CD spines. Dorsal laminectomy and nucleotomy significantly decreased the NZS_{FE} , NZS_{LB} , and NZS_{AR} , with a significantly larger decrease in the NCD spines than in the CD spines in all directions of motion.

	<i>L2-L3</i>			<i>L7-S1</i>		
	ROM	NZ	NZS	ROM	NZ	NZS
condition	<0.001	<0.001	<0.001	<0.001	<0.001	<0.001
dog type	<0.001	0.001	0.003	<0.001	<0.001	<0.001
MD	<0.001	<0.001	<0.001	<0.001	<0.001	<0.001
condition x dog type	0.120	0.017	0.043	0.002	0.447	0.004
condition x MD	<0.001	0.047	0.106	<0.001	0.038	0.004
condition x dog type x MD	0.1161	0.087	0.293	0.2954	0.353	0.584
<i>Condition per MD</i>						
FE	<0.001	<0.001	<0.001	<0.001	<0.001	<0.001
LB	<0.001	<0.001	<0.001	<0.001	<0.001	<0.001
AR	<0.001	<0.001	<0.001	<0.001	0.001	<0.001
<i>Condition per dog type</i>						
NCD	-	<0.001	<0.001	<0.001 [^]	-	<0.001 [^]
CD	-	<0.001 [#]	<0.001 [#]	<0.001	-	<0.001

Table 2. Statistical analyses results. *P* values for range of motion (ROM), neutral zone (NZ), and neutral zone stiffness (NZS) for the factors 'condition' (native or operated), 'dog type' (non-chondrodystrophic (NCD) and chondrodystrophic (CD) dogs), 'motion direction (MD)' (flexion/extension (FE), lateral bending (LB), and axial rotation (AR)), and their interactions in L2-L3 and L7-S1. In case of significant interactions, *P* values for condition per MD and condition per dog type were calculated. *P*<0.05 was considered statistically significant. # indicates a significantly higher effect of the factor condition in CD spines compared with NCD spines; ^ indicates a significantly higher effect of the factor condition in NCD spines compared with CD spines.

Discussion

The biomechanical properties of two types of dog spines, which differed regarding the state of IVD degeneration, were investigated in the native state and after decompressive surgery. The dog offers an interesting model to study the effects of IVD degeneration, with the CD and NCD dogs showing early and late spontaneous degeneration, respectively. The tested specimens were subjected to a cyclic bending moment of -2Nm to 2Nm . Although this bending moment is considerably smaller than the moment applied when biomechanically testing human lumbar spinal specimens ($\pm 7.5\text{ Nm}^{15}$), this applied moment was assessed to be physiological for the relatively small canine specimens. Using the bending moment of -2Nm to 2Nm , the specimens were moved over their complete physiological range of motion without being damaged. In both the NCD and CD spines, the caudal lumbar segments, especially L7-S1, were most

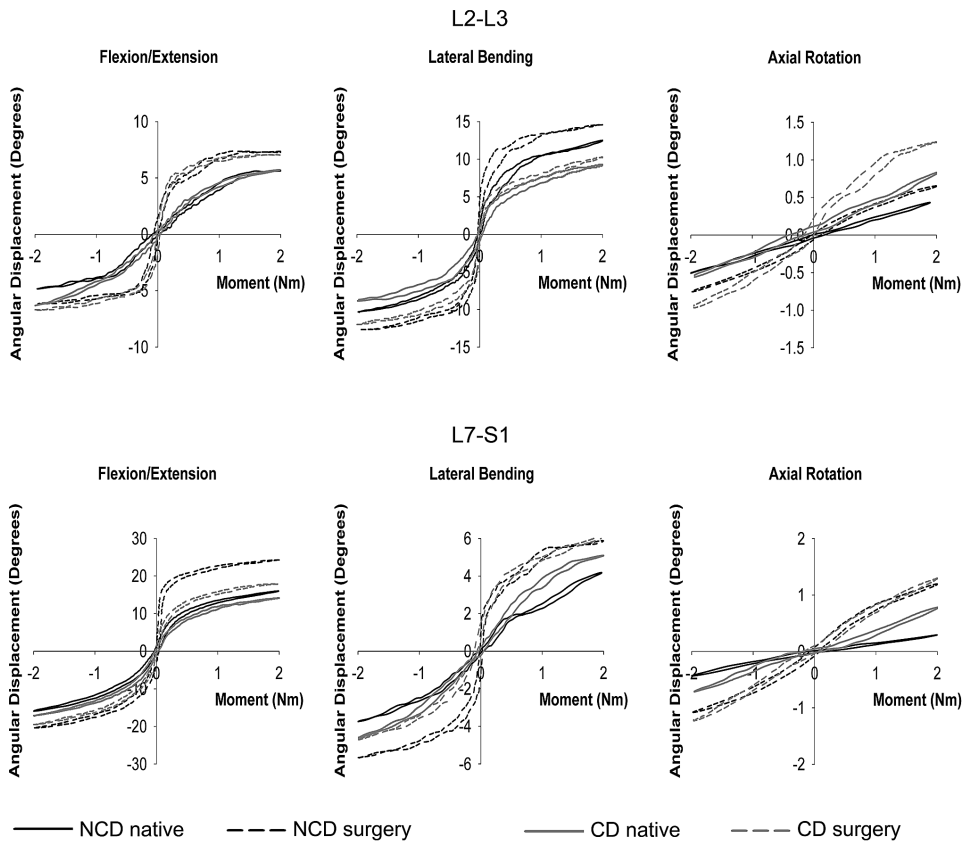


Figure 3. Representative load-displacement curves for non-chondrodystrophic (NCD) and chondrodystrophic (CD) spines in flexion/extension, lateral bending, and axial rotation for the L2-L3 and L7-S1 spinal segment in the native state and after nucleotomy (L2-L3) or dorsal laminectomy and nucleotomy (L7-S1). Only the third loading cycles are displayed.

mobile in FE, whereas the cranial lumbar segments were more mobile in LB; all segments were relatively stiff in AR, with L7-S1 being the most mobile. It is not possible to directly compare our data for dog spines with those for human spines because of differences in test set-up. However, several similarities and differences can be observed. One notable difference is that normal dog spines have 7 lumbar vertebrae, whereas normal human spines only have 5. The intersegment differences in FE, LB, and AR found in the present study are also seen in the human spine. The absolute mobility of the L1-L2 and L2-L3 segments in FE appears to be comparable in canine and human spines, whereas the canine spine is more mobile in LB. The mobility of the L6-L7 segment in FE and LB in dogs is comparable to that of the L4-L5 segment in humans.

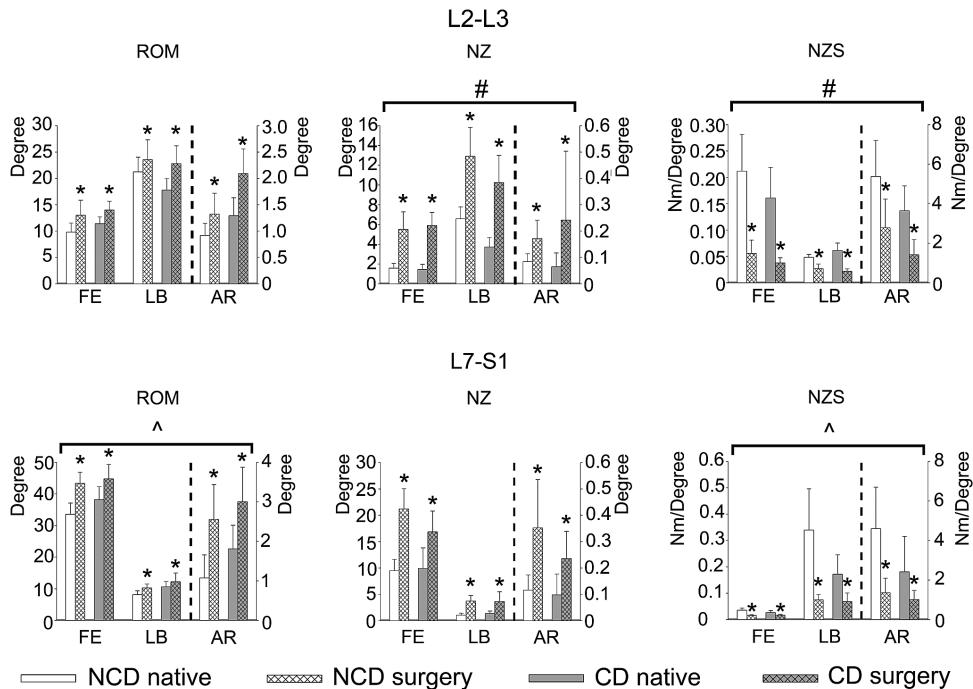


Figure 4. Mean \pm SD of the range of motion (ROM), neutral zone (NZ), and neutral zone stiffness (NZS) of the segments L2-L3 (nuclectomy) and L7-S1 (dorsal laminectomy and nuclectomy) in flexion/extension (FE), lateral bending (LB), and axial rotation (AR) for the native state and after surgery in spines from non-chondrodystrophic (NCD) dogs and chondrodystrophic (CD) dogs. The left vertical axes apply to FE and LB, and the right one to AR (indicated by dashed line). * indicates significant ($P < 0.05$) effect of surgery; # and ^ indicate significantly greater effect of surgery on CD and NCD spines, respectively.

Although the mobility of the L7-S1 segment in dogs in LB is similar to that of the L5-S1 segment in humans, it is considerably more mobile in FE; in addition, the canine lumbar spine is considerably stiffer than the human spine in AR¹⁹.

All in all, the canine lumbar spine resembles the human spine biomechanically, but caution is warranted regarding the absolute mobility of the individual spinal segments.

When using the dog as a model for spinal research, both CD and NCD dogs have their specific qualities. CD dogs show degeneration of all IVDs before 2 years of age, allowing biomechanical research into the degenerated IVD and novel strategies for treating the degenerated IVD^{5,8,9}. In NCD dogs, IVDs remain healthy and rich in notochordal cells until late in life^{5,8-10}. Therefore, NCD dogs allow biomechanical research into the healthy, notochordal cell-rich IVD.

In the present study, the NP of all NCD spines was gelatinous (Thompson grade I), whereas the NP of all CD spines was fibrocartilaginous (Thompson grade II). In the human spine, an increasing grade of IVD degeneration is associated with an increase in segmental ROM, especially in AR^{20,21}. Therefore, comparison of the native spine from CD dogs and NCD dogs could provide novel insights into the effects of IVD degeneration and could be used to assess the validity of the dog as a model of spontaneous IVD degeneration. We initially aimed to make this comparison, using a correction factor for size differences between the NCD and CD dogs based on the transverse area and height of the IVDs in both types of dog. This analysis indicated that the degenerated CD spine exhibited a larger ROM in AR (in line with human studies^{20,21}) and that the NCD, notochordal cell-rich IVD exhibited a larger NZ (data not shown). However, comparison of the NCD spine with the smaller CD spine, using such a correction factor, is problematic because of the non-linearity of the load-displacement behavior of the spines, and differences in the geometry of the facet joints and other spinal structures between the two types of dog. We therefore focused on the effects of decompressive surgery on the biomechanical properties of NCD and CD spines, using each spine as an intrinsic control. Decompressive surgery resulted in an increased ROM and NZ, and decreased NZS in all directions of motion in both groups of dogs, as has been reported in humans^{12,22}. However, nucleotomy of L2-L3 resulted in a significantly larger increase in NZ and decrease in NZS in FE, LB, and AR in the CD spines than in the NCD spines, whereas dorsal laminectomy and nucleotomy of L7-S1 resulted in relatively greater increases in the ROM and greater decreases in NZS in FE, LB, and AR in the NCD spines than in the CD spines. These differences indicate that there are substantial biomechanical differences between NCD and CD spines. Apart from differences in the state of IVD degeneration, these differences may be caused by differences in the size/weight of the types of dog, IVD height and size relative to the size of the dog, the facet joint orientation and conformation, and other spinal characteristics²³. These differences require further investigation.

The present study had some limitations. Although the Beagle dog and mongrel dog spines were of the CD and NCD types, respectively, they represent one group/breed of dogs. Therefore, because several other dog breeds can be

classified as NCD or CD, the data obtained cannot be generalized to all NCD and CD dogs.

In conclusion, the biomechanics of the native canine spine differ by spinal level, and in both NCD and CD dogs spinal surgery results in a significant decrease in stiffness similar to that seen in the human spine after decompressive surgery. In view of using the dog as a model for biomechanical research of the spine, NCD dogs can serve as an appropriate model for studying the healthy, notochordal cell-rich IVD, while CD dogs are appropriate for studying degenerated IVDs. Spinal biomechanics and the effects of spinal surgery significantly differ between NCD and CD dogs as a result of existing IVD degeneration in CD dogs. This knowledge should be taken into account when using the dog as a model for spinal research.

Acknowledgments

The authors would like to thank Jane Sykes for language corrections and Hans Vernooij (Utrecht University) for statistical analysis.

References

1. Andersson GB: Epidemiological features of chronic low-back pain. *Lancet* 354:581-585, 1999.
2. Druss BG, Marcus SC, Olfson M, et al: The most expensive medical conditions in America. *Health Aff (Millwood)* 21:105-111, 2002.
3. Adams MA, Roughley PJ: What is intervertebral disc degeneration, and what causes it? *Spine (Philadelphia, Pa 1976)* 31:2151-2161, 2006.
4. Luoma K, Riihimaki H, Luukkonen R, et al: Low back pain in relation to lumbar disc degeneration. *Spine* 25:487-492, 2000.
5. Bergknut N, Rutges JP, Kranenburg HJ, et al: The dog as an animal model for intervertebral disc degeneration? *Spine* 37:351-358, 2012.
6. Ganey T, Hutton WC, Moseley T, et al: Intervertebral disc repair using adipose tissue-derived stem and regenerative cells: experiments in a canine model. *Spine (Phila Pa 1976)* 34:2297-2304, 2009.
7. Smith GK, Walter MC: Spinal decompressive procedures and dorsal compartment injuries: comparative biomechanical study in canine cadavers. *Am J Vet Res* 49:266-273, 1988.
8. Hansen HJ: A pathologic-anatomical study on disc degeneration in dog, with special reference to the so-called enchondrosis intervertebralis. *Acta Orthop Scand Suppl* 11:1-117, 1952.
9. Bray JP, Burbidge HM: The canine intervertebral disk. Part Two: Degenerative changes--nonchondrodystrophoid versus chondrodystrophoid disks. *J Am Anim Hosp Assoc* 34:135-144, 1998.
10. Cappello R, Bird JL, Pfeiffer D, et al: Notochordal cell produce and assemble extracellular matrix in a distinct manner, which may be responsible for the maintenance of healthy nucleus pulposus. *Spine (Phila Pa 1976)* 31:873-882, 2006.
11. Gibson JN, Waddell G: Surgical interventions for lumbar disc prolapse: updated Cochrane Review. *Spine (Phila Pa 1976)* 32:1735-1747, 2007.
12. Goel VK, Nishiyama K, Weinstein JN, et al: Mechanical properties of lumbar spinal motion segments as affected by partial disc removal. *Spine* 11:1008-1012, 1986.
13. Meij BP, Suwankong N, Van der Veen AJ, et al: Biomechanical flexion-extension forces in normal canine lumbosacral cadaver specimens before and after dorsal laminectomy-discectomy and pedicle screw-rod fixation. *Vet Surg* 36:742-751, 2007.
14. Thompson JP, Pearce RH, Schechter MT, et al: Preliminary evaluation of a scheme for grading the gross morphology of the human intervertebral disc. *Spine (Phila Pa 1976)* 15:411-415, 1990.
15. Wilke HJ, Wenger K, Claes L: Testing criteria for spinal implants: recommendations for the standardization of in vitro stability testing of spinal implants. *Eur Spine J* 7:148-154, 1998.
16. R Development Core Team: R: A language and environment for statistical computing. R Foundation for Statistical Computing. Vienna, Austria, 2010.
17. Pinheiro J, Bates D, DebRoy S, et al: nlme: linear and nonlinear mixed effects models. R package version 3:1-96, 2009.
18. Benjamini Y, Hochberg Y: Controlling the false discovery rate: a practical and powerful approach to multiple testing. *Journal of the Royal Statistical Society B* 57:289-300, 1995.

19. Panjabi MM, Oxland TR, Yamamoto I, et al: Mechanical behavior of the human lumbar and lumbosacral spine as shown by three-dimensional load-displacement curves. *J Bone Joint Surg Am* 76:413-424, 1994.
20. Fujiwara A, Lim TH, An HS, et al: The effect of disc degeneration and facet joint osteoarthritis on the segmental flexibility of the lumbar spine. *Spine (Phila Pa 1976)* 25:3036-3044, 2000.
21. Tanaka N, An HS, Lim TH, et al: The relationship between disc degeneration and flexibility of the lumbar spine. *Spine J* 1:47-56, 2001.
22. Strauss PJ, Novotny JE, Wilder DG, et al: Multidirectional stability of the Graf system. *Spine* 19:965-972, 1994.
23. Benninger MI, Seiler GS, Robinson LE, et al: Effects of anatomic conformation on three-dimensional motion of the caudal lumbar and lumbosacral portions of the vertebral column of dogs. *Am J Vet Res* 67:43-50, 2006.

**Optimal reference genes for quantitative
polymerase chain reaction analysis
of the nucleus pulposus**

Lucas A. Smolders^a, Frank M. Riemers^a, Douwe Heuvel^a, Bjorn P. Meij^a,
Niklas Bergknut^{a,b}, Herman A.W. Hazewinkel^a, Marianna A. Tryfonidou^a,
Louis C. Penning^a

^a Department of Clinical Sciences of Companion Animals, Faculty of Veterinary Medicine,
Utrecht University, Yalelaan 108, 3508 TD, Utrecht, The Netherlands

^b Department of Clinical Sciences, Division of Small Animals, Faculty of Veterinary Medicine
and Animal Sciences, Swedish University of Agricultural Sciences, Sweden

Abstract

Objective: Degeneration of the nucleus pulposus (NP) is a fundamental component of intervertebral disc degeneration, which is a major cause of back problems in dogs. Interest in regenerative strategies for stopping or reversing the degenerative process is increasing, but the development of such strategies needs a thorough understanding of the biomolecular processes involved in the degenerative process. Quantitative reverse-transcriptase polymerase chain reaction (qPCR) analysis is an accurate and quantitative method to analyse the relative expression of genes of interest, provided that there is a set of stable reference genes for normalization. The aim of this study was to identify a set of stable reference genes for qPCR analysis of NP tissue.

Methods: Healthy and mildly degenerated NPs (Thompson grade I and II) were collected from adult Beagle dogs (a chondrodystrophic breed), young Labrador retriever dogs (a non-chondrodystrophic breed), and adult mixed-breed dogs (non-chondrodystrophic breeds). The expression of 15 commonly used reference genes was analysed in all dogs and in each group of dogs, using GeNorm and NormFinder analysis. The optimal number of reference genes was investigated in all dogs and in each group of dogs using GeNorm analysis.

Results: For dogs overall (three breeds combined), *rps19*, *rps5*, *rpl13*, *sprp*, and *hprt* were the most stable reference genes using GeNorm analysis, and *ywhaz*, *actb*, *hprt*, *sprp*, and *rps19* were the most stable using NormFinder analysis. Other stable reference genes in the individual dog groups were *rpl8* and *sdha*. The expression stability of the evaluated reference genes differed considerably between different dog groups and between the two analytical methods. On the basis of GeNorm analysis, 2 to 3 reference genes would be sufficient for reliable normalization in any type of dog.

Conclusions: For the healthy and mildly degenerated NP, the use of 2 to 3 reference genes would seem sufficient for accurate normalization in dogs. However, the expression stability of commonly used reference genes can differ by type of breed and animal age, which means that the ideal set of reference genes needs to be determined in each individual experiment.

Key words: intervertebral disc; degeneration; nucleus pulposus; reference genes; housekeeping genes; qPCR; dog

Introduction

Degeneration of the intervertebral disc (IVD) causes spinal diseases in both humans and dogs. In humans, degeneration of the IVD is a main cause of low back pain, a major health problem in the Western world^{1,2}. In dogs, diseases originating from IVD degeneration include cervical spondylomyelopathy, cervical and thoracolumbar disc disease, and degenerative lumbosacral stenosis^{3,4}. IVD disease can be treated non-surgically with anti-inflammatory medication, exercise restraint, and physiotherapy, and surgically by decompression with partial discectomy (removal of the diseased IVD tissue). Additional stabilization and fusion of the operated segment can be performed⁵⁻⁹. Although these surgical therapies are generally successful, they are accompanied by various complications, such as spinal instability and adjacent segment degeneration, and implant failure¹⁰⁻¹⁷. Moreover, the physiological function of the IVD is not restored. This has prompted interest in regenerative strategies, such as the administration of growth factors, gene therapy, and/or mesenchymal stromal cells or progenitor cells¹⁸⁻²⁴, aimed at restoring the health and function of the IVD. One of the most characteristic features of IVD degeneration is structural failure of the nucleus pulposus (NP), which can lead to defects in the annulus fibrosus and endplates, and consequently disc prolapse or extrusion of NP material^{25,26}. Therefore, many regenerative strategies are aimed at halting or reversing the degenerative process within the NP¹⁸⁻²⁴, but such strategies require knowledge of the fundamental biomolecular signalling pathways involved. In this regard, several studies have investigated the relative expression of gene products in IVD disease, in an attempt to identify and investigate the pathways involved²⁷⁻²⁹.

In quantitative reverse-transcriptase polymerase chain reaction (qPCR), the main method used for measuring relative gene expression, the expression of target genes is expressed relative to, or normalized to, that of a reference gene or multiple reference genes³⁰. Accurate normalization using a stably expressed reference gene transcript is therefore essential for obtaining reliable results. Most studies investigating the biomolecular processes of IVD degeneration used a single reference gene (commonly *glyceraldehyde-3-phosphate dehydrogenase (gapdh)*)^{27,28,31-38}, but this can result in unreliable results^{39,40}, because a single internal control gene is often not expressed at stable levels in different tissues or cells⁴¹. For this reason, multiple reference genes, forming an optimal reference gene set, should be used for reliable normalization of gene expression data. However, little information is available about an optimal reference gene set specifically for the NP of the IVD. The aim of this study was to identify an optimal set of reference genes for biomolecular investigation of the NP in dogs. Two or 3 reference genes were found to be sufficient for accurate normalization in dogs; however, the expression of commonly used reference genes differed considerably by type of breed and animal age.

Materials and methods

Sample collection

Material was collected from chondrodystrophic (n=9, median age: 2 years) and non-chondrodystrophic dogs (young, n=4; adult; n=12; median age: 1.5 years) euthanized in other, unrelated experiments approved by the Ethics Committee on Animal Experimentation of Utrecht University (DEC 2007.II.01.029, 2007.III.08.110, and 2009.III.05.037) (Table 1). NPs were collected from the cervical, thoracic, and lumbar spine, snap frozen in liquid nitrogen, and stored at -70 °C until further processing.

Breed	Breed type	Age (years)	Sex	Level	Grade
Beagle	CD	3	F	C3-C4	2
Beagle	CD	2	M	C6-C7	2
Beagle	CD	3	F	T10-T11	1
Beagle	CD	2	M	T13-L1	2
Beagle	CD	2	M	L1-L2	2
Beagle	CD	2	M	L4-L5	2
Beagle	CD	2	M	L6-L7	2
Beagle	CD	2	M	L6-L7	2
Beagle	CD	3	F	L7-S1	2
Labrador	NCD	0.4	M	C5-C6	1
Labrador	NCD	0.4	M	T12-T13	1
Labrador	NCD	0.4	M	L3-L4	1
Labrador	NCD	0.4	M	L7-S1	1
Mixed breed	NCD	1.5	F	C3-C4	1
Mixed breed	NCD	1	F	C4-C5	1
Mixed breed	NCD	1	F	C4-C5	1
Mixed breed	NCD	1.5	F	C6-C7	1
Mixed breed	NCD	1.5	M	C6-C7	1
Mixed breed	NCD	1.5	M	C7-T1	1
Mixed breed	NCD	1.5	F	T1-T2	1
Mixed breed	NCD	3.5	F	T10-T11	1
Mixed breed	NCD	4	M	T13-L1	1
Mixed breed	NCD	1.5	F	L5-L6	1
Mixed breed	NCD	1.5	F	L5-L6	1
Mixed breed	NCD	2	M	L5-L6	2

Table 1. Material used for analyzing reference genes for qPCR analysis of the nucleus pulposus, showing dog breed, breed type (chondrodystrophic (CD) or non-chondrodystrophic (NCD)), age, sex (female (F) or male (M)), spinal level, and degeneration grade according to Thompson⁴².

RNA isolation, reverse transcription and qPCR

Total tissue RNA was isolated using the RNeasy Fibrous Tissue Mini Kit (Qiagen, Leusden, the Netherlands) according to the manufacturer's instructions. The RNA samples were treated on column with DNase-I (Qiagen RNase-free DNase kit), and RNA was quantified spectrophotometrically using Nanodrop ND-1000 (Isogen Life Science, De Meern, the Netherlands). Reverse transcriptase PCR was performed with 50 ng of total RNA in a total volume of 20 μ l using iScript™ cDNA Synthesis Kit (Biorad, Veenendaal, the Netherlands) containing a mix of both random hexamer and oligo-dT primers.

After cDNA synthesis, a standard sample was made by pooling 5 μ l of each sample, and then this sample was serially diluted to calculate a standard line used to determine PCR efficiency; the remaining cDNA was diluted five fold. For all dilutions, ultra-pure water as used (Millipore-purified, Amsterdam, the Netherlands).

QPCR was performed in duplicate using a MyIQ thermal cycler and IQ SYBRGreen SuperMix (BioRad, Veenendaal, the Netherlands) and 1 μ l of template. Reactions further contained 1.0 μ l of 5 x diluted cDNA, 12.5 μ l IQ SYBRGreen SuperMix (BioRad, Veenendaal, the Netherlands) and 400 nM of each primer (Eurogentec, Maastricht, the Netherlands, Table 2) in a reaction volume of 25 μ l. Primers were designed for the target genes *beta-actin* (*actb*), *beta-2-microglobulin* (*b2m*), *glyceraldehyde-3-phosphate dehydrogenase* (*gapdh*), *glucuronidase*, *beta* (*gusb*), *hydroxymethylbilane synthase* (*hmbs*), *human nucleosome-assembly-protein-I* (*hnrp*), *hypoxanthine-guanine phosphoribosyltransferase* (*hprt*), *ribosomal protein l13* (*rpl13*), *ribosomal protein l18* (*rpl18*), *ribosomal protein s5* (*rps5*), *ribosomal protein s19* (*rps19*), *succinate dehydrogenase complex subunit A* (*sdha*), *serine protease-like protein* (*sprp*), *tata box binding protein* (*tbp*), and *tyrosine 3-monooxygenase/tryptophan 5-monooxygenase activation protein zeta* (*ywhaz*). Sequencing confirmed the specificity of the amplicons.

Cycling conditions for qPCR were as follows: first 3 min at 95 °C, followed by 45 cycles with denaturing template for 20 s at 95 °C, followed by 30 s at room temperature and elongation for 30 s at 72 °C. For a T_m greater than 57 °C, the elongation at 72 °C was omitted and extension took place at T_a . Finally, a melt curve was generated starting at 65 °C and increasing to 99 °C by 1 °C each cycle for 30 s. The amplification efficiencies were always between 90% and 110%. The contamination of RNA with genomic DNA was verified with minus reverse transcriptase (RT) controls, and no-template controls were included to test for other contamination.

Gene	Forward primer 5'→3'	Exon	Reverse primer 5'→3'	Exon	Amplicon Size	Temp (°C)	Accession #
<i>actb</i> ⁴³	GATATCGCTGGCTTGTGGTC	1	GGCTGGGGTGTGAAAGTCTC	3	383	58	NM_001195845
<i>b2m</i>	TCCTCATCTCCTCGCT	1	TTCTCTGCTGGGTGTCG	2	85	61.2	XM_535458
<i>gapdh</i>	TGTCCCAACCCCAATGATC	2	CTCCGATGCCTGCTTCACTACCTT	2	100	58	NM_001003142
<i>gusb</i>	AGACGCTTCCAAGTACCCC	4	AGGTGTGGTGTAGAGGAGCAC	5	103	62	NM_001003191
<i>hmbs</i>	TCACCATCGGAGCCATCT	6	GTTCCACCCAGCTCTTCT	6/7	112	61	XM_546491
<i>hnrp</i>	CTCACTATGATCCACCACG	5	TAGCCTCCATAAACCTCCAC	5/6	151	61.2	XM_538576
<i>hprt</i>	AGCTTGTGGTGAAGAAGGAC	5/6	TTATAGTCAAAGGCATATCC	7	104	56	AY283372
<i>rpl8</i>	CCATGAATCCTGTGGAGC	4/5	GTAGAGGGTTTGCCGATG	5	64	55	XM_532360
<i>rpl13</i> ⁴³	GCCGGAAGGTTGTAGTCGT	3	GGAGGAAGGCCAGGTAATTC	4	87	61	XM_003432726
<i>rps5</i>	TCACTGGTGAGAACCCCT	2/3	CCTGATTCACACGGCGTAG	3	141	62.5	XM_533568
<i>rps19</i>	CCTTCCTCAAAAAGTCTGGG	2/3	GTTCTCATCGTAGGGAGCAAG	3	95	61	XM_533657
<i>sdha</i> ⁴³	GCCTTGGATCTTTGATGGA	6	TTCTTGGCTCTTATGCGATG	6	92	61	XM_535807
<i>sprp</i>	GCTTCAGGATCTGGACTGC	7	GTTCCCTTGGTAGCACTGG	7/8	81	61.2	XM_546411
<i>tbp43</i>	CTATTTCTTGGTGTGCAITGAGG	5	CCTCGGCAITCAGTCTTTTC	5	96	57	XM_849432
<i>ywhaz</i> ⁴³	CGAAGTTGCTGCTGGTGA	2	TTGCATTTCCTTTTTGCTGA	2/3	94	58	XM_533072

Table 2. Primers used for quantitative PCR of the target genes beta-actin (*actb*), beta-2-microglobulin (*b2m*), glyceraldehyde-3-phosphate dehydrogenase (*gapdh*), glucuronidase, beta (*gusb*), hydroxymethylbilane synthase (*hmbs*), human nucleosome-assembly-protein-1 (*hnrp*), hypoxanthine-guanine phosphoribosyltransferase (*hprt*), ribosomal protein 113 (*rpl13*), ribosomal protein 118 (*rpl8*), ribosomal protein s5 (*rps5*), ribosomal protein s19 (*rps19*), succinate dehydrogenase complex, subunit A (*sdha*), serine protease-like protein (*sprp*), tata box binding protein (*tbp*), and tyrosine 3-monooxygenase/tryptophan 5-monooxygenase activation protein, zeta (*ywhaz*). Primers not indicated by ⁴³ are in-house design.

Data analysis

Two different analysis methods were used to determine the optimal reference gene set, i.e. GeNorm⁴⁰ and NormFinder³⁹. GeNorm calculates a gene stability measure, based on the principle that the ratio of expression of two ideal reference genes is identical in all samples and conditions. In this way, variation in the expression ratios of two reference genes reflects whether one or both of these genes is not constantly expressed, resulting in a decreased expression stability. For each reference gene, the pairwise variation with all other evaluated reference genes is calculated. The average pairwise variation of a particular gene compared with all other reference genes is calculated, which is defined as the internal control gene-stability measure M (the gene with the lowest M has the highest expression stability).

GeNorm can subsequently be used to determine the optimal number of reference genes. Using the three most stably expressed reference genes, a normalization factor (NF_n ; $n=3$) is calculated. Then, stepwise inclusion of more control genes is performed until the $(n+1)$ th reference gene does not significantly improve the newly calculated normalization factor (NF_{n+1}). The pairwise variation $V_{n/n+1}$ is calculated between two sequential normalization factors NF_n and N_{Fn+1} as a measure of the expression stability of a combination of genes. A cut-off value of 0.15 for the pairwise variation was chosen⁴⁰, indicating that the use of a set of reference genes with a pairwise variation < 0.15 results in valid normalization. The average expression stability M and the pairwise variation were calculated with the statistical environment R, using the SLqPCR package^{44,45} with implementation of the GeNorm method⁴⁰.

NormFinder analysis consists of a model-based approach, by which the overall variation in expression within sample groups of interest (intra-group variation) and the variation across the sample population groups (inter-group variation) are calculated for each evaluated reference gene. The combination of the two variation parameters results in a stability value, which represents a practical measure of the systematic error that will be introduced when using a particular reference gene. NormFinder calculations were done using the NormFinder plug-in for Microsoft Excel⁴⁶.

Results

For dogs overall (three dog groups combined), GeNorm analysis revealed that *rps19*, *rps5*, *rpl13*, *sprp*, and *hprt* were the most stable reference genes (Fig. 1, Table 3), and 2 to 3 reference genes were found to be sufficient for reliable normalization in any type of dog (Fig. 2). When using NormFinder, *ywhaz*, *actb*, *hprt*, *sprp*, and *rps19* were the most stable reference genes for dogs overall.

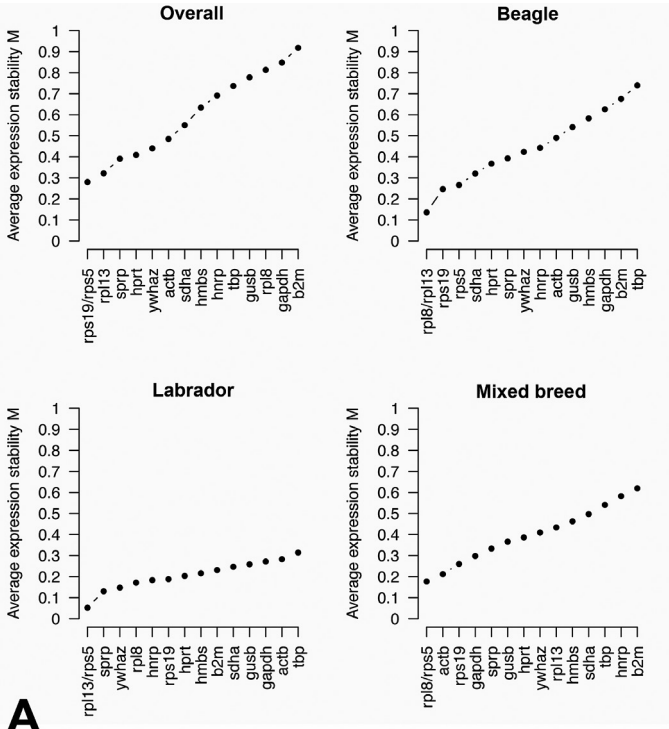
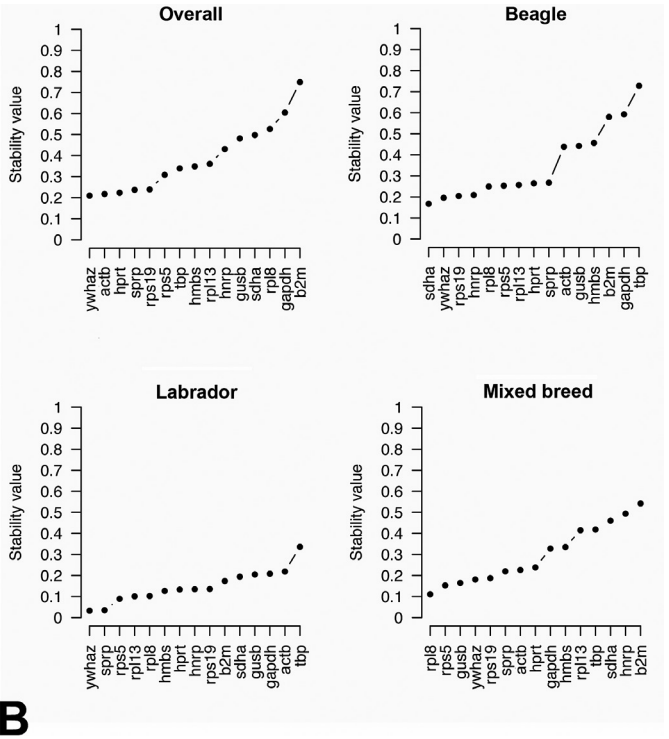


Figure 1. Expression stability of reference genes in canine nucleus pulposus tissue. Ranking of expression stability obtained with GeNorm (A) and NormFinder (B) for the various reference genes evaluated in dogs overall, Beagle dogs, Labrador retriever dogs, and mixed breed dogs.



5.1

Rank	Overall		Beagle		Labrador		Mixed breed	
	G	N	G	N	G	N	G	N
1	<i>rps19</i>	<i>ywhaz</i>	<i>rpl8</i>	<i>sdha</i>	<i>rpl13</i>	<i>ywhaz</i>	<i>rpl8</i>	<i>rpl8</i>
2	<i>rps5</i>	<i>actb</i>	<i>rpl13</i>	<i>ywhaz</i>	<i>rps5</i>	<i>sprp</i>	<i>rps5</i>	<i>rps5</i>
3	<i>rpl13</i>	<i>hprt</i>	<i>rps19</i>	<i>rps19</i>	<i>sprp</i>	<i>sprs5</i>	<i>actb</i>	<i>gusb</i>
4	<i>sprp</i>	<i>sprp</i>	<i>rps5</i>	<i>hnrp</i>	<i>ywhaz</i>	<i>rpl13</i>	<i>rps19</i>	<i>ywhaz</i>
5	<i>hprt</i>	<i>rps19</i>	<i>sdha</i>	<i>rpl8</i>	<i>rpl8</i>	<i>rpl8</i>	<i>gapdh</i>	<i>rps19</i>
6	<i>ywhaz</i>	<i>rps5</i>	<i>hprt</i>	<i>rps5</i>	<i>hnrp</i>	<i>hmbs</i>	<i>sprp</i>	<i>sprp</i>
7	<i>actb</i>	<i>tbp</i>	<i>sprp</i>	<i>rpl13</i>	<i>rps19</i>	<i>hprt</i>	<i>gusb</i>	<i>actb</i>
8	<i>sdha</i>	<i>hmbs</i>	<i>ywhaz</i>	<i>hprt</i>	<i>hprt</i>	<i>hnrp</i>	<i>hprt</i>	<i>hprt</i>
9	<i>hmbs</i>	<i>rpl13</i>	<i>hnrp</i>	<i>sprp</i>	<i>hmbs</i>	<i>rps19</i>	<i>ywhaz</i>	<i>gadh</i>
10	<i>hnrp</i>	<i>hnrp</i>	<i>actb</i>	<i>actb</i>	<i>b2m</i>	<i>b2m</i>	<i>rpl13</i>	<i>hmbs</i>
11	<i>tbp</i>	<i>gusb</i>	<i>gusb</i>	<i>gusb</i>	<i>sdha</i>	<i>sdha</i>	<i>hmbs</i>	<i>rpl13</i>
12	<i>gusb</i>	<i>sdha</i>	<i>hmbs</i>	<i>hmbs</i>	<i>gusb</i>	<i>gusb</i>	<i>sdha</i>	<i>tbp</i>
13	<i>rpl8</i>	<i>rpl8</i>	<i>gapdh</i>	<i>b2m</i>	<i>gapdh</i>	<i>gapdh</i>	<i>tbp</i>	<i>sdha</i>
14	<i>gapdh</i>	<i>gapdh</i>	<i>b2m</i>	<i>gadph</i>	<i>actb</i>	<i>actb</i>	<i>hnrp</i>	<i>hnrp</i>
15	<i>b2m</i>	<i>b2m</i>	<i>tbp</i>	<i>tbp</i>	<i>tbp</i>	<i>tbp</i>	<i>b2m</i>	<i>b2m</i>

Table 3. Ranking of expression stability of reference genes in canine nucleus pulposus tissue. Ranking of expression stability of reference genes based on GeNorm (G) and Normfinder (N) analysis in dogs overall, Beagle dogs, Labrador Retriever dogs, mixed breed dogs.

In adult chondrodystrophic Beagle dogs, *rpl8*, *rpl13*, *rps19*, *rps5*, and *sdha* were the most stable reference genes on GeNorm analysis and *sdha*, *ywhaz*, *rps19*, *hnrp*, and *rpl8* on NormFinder analysis. In young non-chondrodystrophic Labrador retriever dogs, *rpl13*, *rps5*, *sprp*, *ywhaz*, and *rpl8* were the most stable reference genes on GeNorm analysis and *ywhaz*, *sprp*, *rps5*, *rpl13*, and *rpl8* on NormFinder analysis. In non-chondrodystrophic, mixed breed dogs, *rpl8*, *rps5*, *actb*, *rps19*, and *gapdh* were the most stable reference genes on GeNorm analysis and *rpl8*, *rps5*, *gusb*, *ywhaz*, and *rps19* on NormFinder analysis.

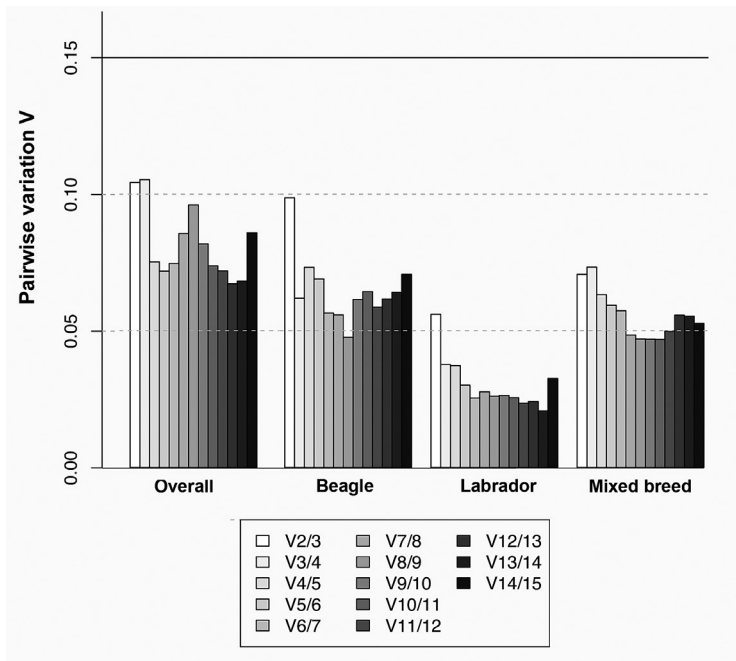


Figure 2. GeNorm analysis of pairwise variation (V) in gene expression between normalization based on the most stably expressed reference genes (x) and stepwise inclusion of an additional reference gene ($x+1$) to determine the optimal number of control genes required for accurate normalization in dogs overall, Beagle dogs, Labrador Retriever dogs, and mixed breed dogs.

Discussion

The aim of this study was to identify an optimal set of reference genes for the NP of different types of dog breed. The cell composition of the NP changes with age and is different in different (chondrodystrophic and non chondrodystrophic) types of dog breed^{26,47-53}. The NP of all young dogs is rich in notochordal cells, which produce a high quality extracellular matrix^{26,47-49}. However, in chondrodystrophic dogs, the native notochordal cells of the NP are replaced by chondrocyte-like cells before 1 year of age, resembling the NP cell population changes seen in early intervertebral disc degeneration^{26,47-49}. In non-chondrodystrophic dogs, notochordal cells are retained throughout most of life, but the NP undergoes significant histopathological changes (fibroid metamorphosis)²⁶ usually later in life, ultimately leading to intervertebral disc degeneration. These changes in NP composition involve changes in the expression of various genes and proteins^{26,47-53}. Therefore, when investigating biomolecular signalling pathways in the canine NP using qPCR analysis, it is essential to use a reliable reference gene set to enable accurate normalization of gene expression.

The use of a single reference gene for normalization, which is commonly

applied in the literature^{27,28,31-38}, is not a valid method for accurate normalization, because no single gene has a constant level of expression across all tissues, cells, experimental treatments, etc.⁴⁰. For instance, a recent study showed that normalization of gene expression on the basis of one gene was not a valid approach in in-bred rat and rabbit IVD organ cultures⁵⁴. In contrast, the combination of a group of consistently expressed genes can provide the expression stability necessary for accurate relative gene expression analysis^{39,40}.

The present study evaluated the stability of expression of commonly used reference genes in different types of dog, i.e. the adult chondrodystrophic Beagle, the young non-chondrodystrophic Labrador retriever, and the adult non-chondrodystrophic mixed breed dog. For dogs overall, the reference genes *rps19*, *hprt*, and *sprp* were among the top 5 most stable reference genes in both the GeNorm and NormFinder analyses. The expression stability of the tested reference genes varied little within each breed type, as inclusion or exclusion of additional reference genes did not result in excessive changes in pairwise variation V. Moreover, the most commonly used reference genes *gapdh* and *actb* were not the most stably expressed genes, illustrating the need for analysis-based selection of reference genes, as recently advocated⁵⁵. In addition, both methods of analysis found different rankings of reference genes between different types of dog and different ages, indicating there is no universally optimal reference gene set for the expression analysis of the NP in dogs. Moreover, the ranking of gene expression stability appeared to vary depending on the method used, which is probably due to differences in the methods of analysis used in the respective software programs. GeNorm analysis involves the selection of two genes with a low intra-group variation to calculate a pairwise variation, and uses this parameter to rank the genes according to the similarity of their expression profiles⁴⁰. In contrast, NormFinder analysis consists of a model-based approach and calculates the overall expression variation within sample groups of interest (intra-group variation) and the variation across the sample population groups (inter-group variation). The combination of the two variation parameters results in a stability value, which represents a practical measure of the systematic error that will be introduced when using a particular reference gene³⁹. Both methods have their drawbacks. With GeNorm analysis, the evaluated reference genes are ranked according to the similarity of their expression profiles. However, this can be problematic if co-regulated genes are potential reference genes, as these will inadvertently have a tendency to show similar expression profiles and thus, independent of their expression stability, tend to be ranked the highest. In this study, this co-regulation was illustrated by the observed ranking of the genes coding for ribosomal proteins, such as *rpl8*, *rpl13*, *rps19*, and *rps5*, which were all top ranked genes in the GeNorm analysis. This potentially erroneous selection of reference genes can be avoided by selecting one of these reference genes, and including independent reference genes such as *hprt*, *ywhaz*, and *sprp*, which also ranked high in the NormFinder analysis.

A drawback of NormFinder is that it does not allow easy and quick selection of an optimal number of reference genes. Apart from the fact that GeNorm is more commonly used, determination of the optimal number of reference genes is relatively easy when using this program.

A potential limitation of this study is that NP material from relatively healthy dogs showing mild IVD degeneration (Thompson grade I and II ⁴²) was used. It is conceivable that the degenerative process involves changes in the regulation of various genes, including those used for normalization. This highlights the need for analysis of reference gene stability in all stages of IVD degeneration in both chondrodystrophic and non-chondrodystrophic dogs. Also, potential effects of age, breed type, and degeneration stage necessitate that each study investigating NP degeneration needs to involve reference gene stability analysis to identify a study-specific reference gene set.

Conclusions

Two or 3 reference genes are sufficient for accurate normalization of gene expression in healthy and mildly degenerated NP tissue from chondrodystrophic and non-chondrodystrophic dog breeds. However, the stability of expression of commonly used reference genes varies by breed type, age, and stage of IVD degeneration, so that experiment-specific analysis of the optimal reference gene set is advised. Once such an evaluation has been performed, accurate normalization is possible, which makes it possible to compare the results of different publications using qPCR analysis.

Acknowledgements

The authors would like to thank Ms. Jane Sykes for language corrections.

References

1. Cheung KM, Karppinen J, Chan D, et al: Prevalence and pattern of lumbar magnetic resonance imaging changes in a population study of one thousand forty-three individuals. *Spine (Phila Pa 1976)* 34:934-940, 2009.
2. Druss BG, Marcus SC, Olfson M, et al: The most expensive medical conditions in America. *Health Aff (Millwood)* 21:105-111, 2002.
3. Bray JP, Burbidge HM: The canine intervertebral disk: part one: structure and function. *J Am Anim Hosp Assoc* 34:55-63, 1998.
4. Sharp NJH, Wheeler SJ: Thoracolumbar and Lumbosacral disease, in Sharp NJH, Wheeler SJ (eds): *Small Animal Spinal Disorders. Diagnosis and Surgery (ed 2)*, Edinburgh, Elsevier Mosby, 2005, pp 121-209.
5. Meij BP, Bergknut N: Degenerative lumbosacral stenosis in dogs. *Vet Clin North Am Small Anim Pract* 40:983-1009, 2010.
6. da Costa RC: Cervical spondylomyelopathy (wobbler syndrome) in dogs. *Vet Clin North Am Small Anim Pract* 40:881-913, 2010.
7. Brisson BA: Intervertebral disc disease in dogs. *Vet Clin North Am Small Anim Pract* 40:829-858, 2010.
8. Bono CM, Lee CK: Critical analysis of trends in fusion for degenerative disc disease over the past 20 years: influence of technique on fusion rate and clinical outcome. *Spine (Phila Pa 1976)* 29:455-463, 2004.
9. Gibson JN, Waddell G: Surgical interventions for lumbar disc prolapse: updated Cochrane Review. *Spine (Phila Pa 1976)* 32:1735-1747, 2007.
10. Brinckmann P, Grootenboer H: Change of disc height, radial disc bulge, and intradiscal pressure from discectomy. An in vitro investigation on human lumbar discs. *Spine* 16:641-646, 1991.
11. Eck JC, Humphreys SC, Hodges SD: Adjacent-segment degeneration after lumbar fusion: a review of clinical, biomechanical, and radiologic studies. *Am J Orthop* 28:336-340, 1999.
12. Frei H, Oxland TR, Rathonyi GC, et al: The effect of nucleotomy on lumbar spine mechanics in compression and shear loading. *Spine* 26:2080-2089, 2001.
13. Goel VK, Nishiyama K, Weinstein JN, et al: Mechanical properties of lumbar spinal motion segments as affected by partial disc removal. *Spine* 11:1008-1012, 1986.
14. Lee CK: Accelerated degeneration of the segment adjacent to a lumbar fusion. *Spine* 13:375-377, 1988.
15. MacDougall J, Perra J, Pinto M: Incidence of adjacent segment degeneration at ten years after lumbar spine fusion. *Spine J* 3:675, 2003.
16. Macy NB, Les CM, Stover SM, et al: Effect of disk fenestration on sagittal kinematics of the canine C5-C6 intervertebral space. *Vet Surg* 28:171-179, 1999.
17. Smith MEH, Bebhuk TN, Shmon CL, et al: An in vitro biomechanical study of the effects of surgical modification upon the canine lumbosacral spine. *Vet Comp Orthop Traumatol* 17:17-24, 2004.
18. Ganey T, Hutton WC, Moseley T, et al: Intervertebral disc repair using adipose tissue-derived stem and regenerative cells: experiments in a canine model. *Spine (Phila Pa 1976)* 34:2297-2304, 2009.

19. Tow BP, Hsu WK, Wang JC: Disc regeneration: a glimpse of the future. *Clin Neurosurg* 54:122-128, 2007.
20. An HS, Thonar EJ, Masuda K: Biological repair of intervertebral disc. *Spine (Phila Pa 1976)* 28:S86-92, 2003.
21. Masuda K, Oegema TR, Jr., An HS: Growth factors and treatment of intervertebral disc degeneration. *Spine (Phila Pa 1976)* 29:2757-2769, 2004.
22. Hiyama A, Mochida J, Iwashina T, et al: Transplantation of mesenchymal stem cells in a canine disc degeneration model. *J Orthop Res* 26:589-600, 2008.
23. Ruan DK, Xin H, Zhang C, et al: Experimental intervertebral disc regeneration with tissue-engineered composite in a canine model. *Tissue Eng Part A* 16:2381-2389, 2010.
24. Sakai D: Future perspectives of cell-based therapy for intervertebral disc disease. *Eur Spine J* 17 Suppl 4:452-458, 2008.
25. Adams MA, Roughley PJ: What is intervertebral disc degeneration, and what causes it? *Spine (Philadelphia, Pa 1976)* 31:2151-2161, 2006.
26. Hansen HJ: A pathologic-anatomical study on disc degeneration in dog, with special reference to the so-called enchondrosis intervertebralis. *Acta Orthop Scand Suppl* 11:1-117, 1952.
27. Minogue BM, Richardson SM, Zeef LA, et al: Transcriptional profiling of bovine intervertebral disc cells: implications for identification of normal and degenerate human intervertebral disc cell phenotypes. *Arthritis Res Ther* 12:R22, 2010.
28. Minogue BM, Richardson SM, Zeef LA, et al: Characterization of the human nucleus pulposus cell phenotype and evaluation of novel marker gene expression to define adult stem cell differentiation. *Arthritis Rheum* 62:3695-3705, 2010.
29. Sakai D, Nakai T, Mochida J, et al: Differential phenotype of intervertebral disc cells: microarray and immunohistochemical analysis of canine nucleus pulposus and anulus fibrosus. *Spine (Phila Pa 1976)* 34:1448-1456, 2009.
30. Pfaffl MW: A new mathematical model for relative quantification in real-time RT-PCR. *Nucleic Acids Res* 29:e45, 2001.
31. Huang M, Wang HQ, Zhang Q, et al: Alterations of ADAMTSs and TIMP-3 in human nucleus pulposus cells subjected to compressive load: Implications in the pathogenesis of human intervertebral disc degeneration. *J Orthop Res* 30:267-273, 2012.
32. Mwale F, Masuda K, Pichika R, et al: The efficacy of Link N as a mediator of repair in a rabbit model of intervertebral disc degeneration. *Arthritis Res Ther* 13:R120, 2011.
33. Li S, Jia X, Duance VC, et al: The effects of cyclic tensile strain on the organisation and expression of cytoskeletal elements in bovine intervertebral disc cells: an in vitro study. *Eur Cells Mater* 21:508-522, 2011.
34. Sowa G, Coelho P, Vo N, et al: Determination of annulus fibrosus cell response to tensile strain as a function of duration, magnitude, and frequency. *J Orthop Res* 29:1275-1283, 2011.
35. Wang F, Zhu Y: Aquaporin-1: a potential membrane channel for facilitating the adaptability of rabbit nucleus pulposus cells to an extracellular matrix environment. *J Orthop Sci* 16:304-312, 2011.

36. Strassburg S, Richardson SM, Freemont AJ, et al: Co-culture induces mesenchymal stem cell differentiation and modulation of the degenerate human nucleus pulposus cell phenotype. *Regen Med* 5:701-711, 2010.
37. Niu CC, Yuan LJ, Chen LH, et al: Beneficial effects of hyperbaric oxygen on human degenerated intervertebral disk cells via suppression of IL-1beta and p38 MAPK signal. *J Orthop Res* 29:14-19, 2011.
38. Niu CC, Yuan LJ, Lin SS, et al: Mesenchymal stem cell and nucleus pulposus cell coculture modulates cell profile. *Clin Orthop Relat R* 467:3263-3272, 2009.
39. Andersen CL, Jensen JL, Orntoft TF: Normalization of real-time quantitative reverse transcription-PCR data: a model-based variance estimation approach to identify genes suited for normalization, applied to bladder and colon cancer data sets. *Cancer Res* 64:5245-5250, 2004.
40. Vandesompele J, De Preter K, Pattyn F: Accurate normalization of realtime quantitative RT-PCR data by geometric averaging of multiple internal control genes. 2002. *Genome Biol* 3:research 0034.0031-0034.0011, 2002.
41. Fundel K, Haag J, Gebhard PM, et al: Normalization strategies for mRNA expression data in cartilage research. *Osteoarthr Cartilage* 16:947-955, 2008.
42. Thompson JP, Pearce RH, Schechter MT, et al: Preliminary evaluation of a scheme for grading the gross morphology of the human intervertebral disc. *Spine (Phila Pa 1976)* 15:411-415, 1990.
43. Peters IR, Peeters D, Helps CR, et al: Development and application of multiple internal reference (housekeeper) gene assays for accurate normalisation of canine gene expression studies. *Vet Immunol Immunopathol* 117:55-66, 2007.
44. Kohl M: SLqPCR: Functions for analysis of real-time quantitative PCR data at SIRS-Lab GmbH. R package. Jena, SIRS-Lab GmbH, 2007.
45. R Development Team: R: A language and environment for statistical computing. R Foundation for Statistical Computing. Vienna, Austria, 2010.
46. NormFinder plug-in for Microsoft Excel. Available from: (<http://www.mdl.dk/publicationsnormfinder.htm>).
47. Bergknut N, Rutges JP, Kranenburg HJ, et al: The dog as an animal model for intervertebral disc degeneration? *Spine*, 2011.
48. Braund KG, Ghosh P, Taylor TK, et al: Morphological studies of the canine intervertebral disc. The assignment of the beagle to the achondroplastic classification. *Res Vet Sci* 19:167-172, 1975.
49. Cappello R, Bird JL, Pfeiffer D, et al: Notochordal cell produce and assemble extracellular matrix in a distinct manner, which may be responsible for the maintenance of healthy nucleus pulposus. *Spine (Phila Pa 1976)* 31:873-882, 2006.
50. Ghosh P, Taylor TK, Braund KG: The variation of the glycosaminoglycans of the canine intervertebral disc with ageing. I. Chondrodystrophoid breed. *Gerontology* 23:87-98, 1977.
51. Ghosh P, Taylor TK, Braund KG: Variation of the glycosaminoglycans of the intervertebral disc with ageing. II. Non-chondrodystrophoid breed. *Gerontology* 23:99-109, 1977.
52. Ghosh P, Taylor TK, Braund KG, et al: The collagenous and non-collagenous protein of the canine intervertebral disc and their variation with age, spinal level and breed. *Gerontology* 22:124-134, 1976.

53. Ghosh P, Taylor TK, Braund KG, et al: A comparative chemical and histochemical study of the chondrodystrophoid and nonchondrodystrophoid canine intervertebral disc. *Vet Pathol* 13:414-427, 1976.
54. Seol D, Choe H, Zheng H, et al: Selection of reference genes for normalization of quantitative real-time PCR in organ culture of the rat and rabbit intervertebral disc. *BMC Res Notes* 4:162, 2011.
55. Bustin SA, Beaulieu JF, Huggett J, et al: MIQE precis: Practical implementation of minimum standard guidelines for fluorescence-based quantitative real-time PCR experiments. *BMC Mol Biol* 11:74, 2010.

**Canonical Wnt signaling
in the notochordal cell is upregulated in
early intervertebral disc degeneration**

Lucas A. Smolders ^a, Björn P. Meij ^a, Frank M. Riemers ^a, Ruud Licht ^b,
Richard Wubbolts ^c, Douwe Heuvel ^a, Guy C.M. Grinwis ^d,
Hans C.M. Vernooij ^e, Herman A.W. Hazewinkel ^a, Louis C. Penning ^a,
Marianna A. Tryfonidou ^a

Journal of Orthopaedic Research 30(6):950-957, 2012

^a Department of Clinical Sciences of Companion Animals, Faculty of Veterinary Medicine, Utrecht University, Yalelaan 108, 3508 TD, Utrecht, The Netherlands

^b Department of Orthopaedics, Division of Surgical Specialties, University Medical Center Utrecht, Heidelberglaan 100, 3584 CX Utrecht, The Netherlands

^c Department of Biochemistry and Cell Biology, Faculty of Veterinary Medicine, Utrecht University, Yalelaan 1, 3584 CL, Utrecht, the Netherlands

^d Department of Pathobiology, Pathology Division, Faculty of Veterinary Medicine, Utrecht University, Utrecht, The Netherlands

^e Department of Biostatistics (Farm Animal Health), Faculty of Veterinary Medicine, Utrecht University, Yalelaan 7, 3584 CL, Utrecht, the Netherlands

Abstract

Objective: The notochordal cell (NC) of the nucleus pulposus (NP) is considered a potential NP progenitor cell, and early intervertebral disc (IVD) degeneration involves replacement of NCs by chondrocyte-like cells (CLCs). Wnt/ β -catenin signaling plays a crucial role in maintaining the notochordal fate during embryogenesis, but is also involved in tissue degeneration and regeneration. The canine species, which can be subdivided into non-chondrodystrophic and chondrodystrophic breeds, is characterized by differential maintenance of the NC: in non-chondrodystrophic dogs, the NC remains the predominant cell type during the majority of life, with IVD degeneration only occurring at old age; conversely, in chondrodystrophic dogs the NC is lost early in life, with concurrent degeneration of all IVDs. This study investigated Wnt/ β -catenin signaling in the healthy, NC-rich NP and early degenerated, CLC-rich NP of both breed types.

Methods: β -catenin protein expression and relative gene expression of *brachyury* and *cytokeratin 8* (notochordal markers) and Wnt targets *axin2*, *cyclin D1*, and *c-myc* were investigated in the healthy, NC-rich NP and early degenerated, CLC-rich NP of both breed types. Also, the same targets were investigated in NCs *in vitro*.

Results: Both NCs and CLCs showed nuclear and cytoplasmic β -catenin protein expression and *axin2* gene expression, but β -catenin signal intensity and Wnt target gene expression were higher in the CLC-rich NP. Primary NCs in monolayer culture (normoxic conditions) showed Wnt/ β -catenin signaling comparable to the *in vivo* situation, with increased *cyclin D1* and *c-myc* gene expression.

Conclusions: Wnt/ β -catenin signaling activity in the NC within the NC-rich NP and in culture supports the role of this cell as a potential progenitor cell; increased Wnt/ β -catenin signaling activity in early IVD degeneration may be a reflection of its dual role.

Key words: notochordal cell; intervertebral disc degeneration; Wnt/ β -catenin signaling; canine

Introduction

Back pain caused by degeneration of the intervertebral disc (IVD) has considerable socioeconomic consequences^{1,2}. Current regenerative strategies for IVD degeneration aim at restoring the physiological function of the IVD, using adult stem or progenitor cells, growth factors, and/or gene therapy³. However, much remains enigmatic about IVD progenitor cells and the pathways involved in degeneration^{4,5}.

The center of the IVD, the nucleus pulposus (NP), is derived from the notochord⁶, and notochordal cells (NCs) are considered potential NP progenitor cells^{4,5}. In young humans and in many other species, NCs are the predominant cell type in the NP; however, in some species, such as dogs and humans, the NCs are eventually replaced by smaller, chondrocyte-like cells (CLCs)^{4,7,8}. Dogs suffer from spontaneous IVD degeneration, and the degenerative process involves macroscopic, histopathological, and biochemical changes similar to humans⁹. However, the dog is a unique species with regard to NC maintenance and IVD degeneration: chondrodystrophic dog breeds (with disproportionately short limbs relative to the length of the spine) are predisposed to early-onset IVD degeneration. In this dog type, NCs are replaced by or differentiate into CLCs before 1 year of age, an age at which IVD degeneration starts. In contrast, in non-chondrodystrophic breeds, the NC is the predominant cell type of the NP until late in life and IVD degeneration develops only around 6–8 years of age (Fig. 1)^{4,7,10}. Thus, the disappearance of NCs accompanied by the appearance of the CLCs seems to be associated with IVD degeneration^{7,10}.

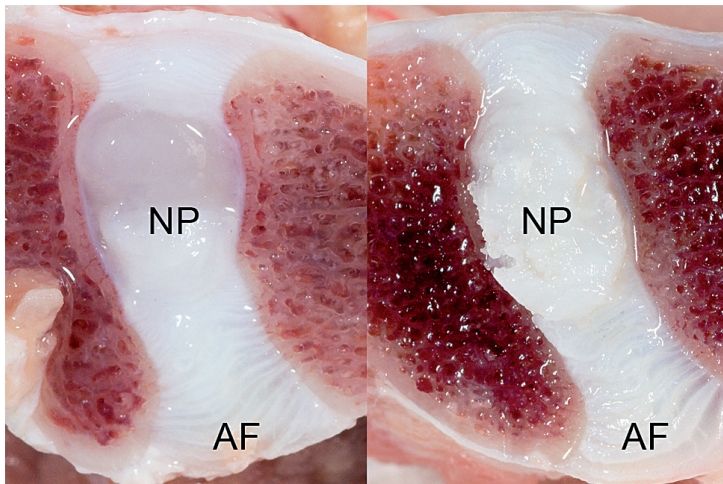


Figure 1. Typical example of a sagittal section through the intervertebral disc from a 2-year-old non-chondrodystrophic (left) and chondrodystrophic (right) dog, with the central nucleus pulposus (NP) and surrounding annulus fibrosus (AF). The healthy, non-chondrodystrophic NP has a mucoid, semitranslucent character, whereas the chondrodystrophic, early degenerated NP has a fibrocartilaginous appearance.

Canonical Wnt signaling plays a critical role in promoting the differentiation or maintenance of stem cells in a self-renewing state ¹¹, and sustained Wnt/ β -catenin signaling is required to maintain the notochord fate of progenitor cells throughout embryogenesis ¹². Also, development of the IVD in mice is regulated by Wnt/ β -catenin signaling ¹³. However, Wnt/ β -catenin signaling has also been associated with degenerative joint disease and matrix degeneration ¹⁴⁻¹⁶. The role of Wnt/ β -catenin signaling in both degenerative and regenerative processes prompted us to investigate its role in early IVD degeneration, i.e. the replacement of NCs by CLCs in chondrodystrophic and non-chondrodystrophic dogs, a naturally occurring animal model representing differential NC survival and onset of IVD degeneration ^{7,9}.

Materials and methods

Canonical Wnt signaling in dogs with naturally occurring IVD degeneration

5.2

All animals included in this study were euthanized in other, unrelated experiments approved by the Ethics Committee on Animal Experimentation of Utrecht University.

Cervical (C2-T1) and thoracolumbar (T10-S1) spines were collected from six mongrel dogs (non-chondrodystrophic, 13-60 months, weighing 26.6-32.1 kg) and six Beagle dogs (chondrodystrophic, 25-36 months, weighing 13.6-16.0 kg). The single functional spinal units (endplate-IVD-endplate) were cut in the sagittal plane into two equal parts: the NP from one half was snap frozen and stored at -70 °C, and the other half was fixed, decalcified in 10% EDTA for 3 months, and embedded in paraffin.

Histopathological classification

Mid-sagittal sections (4 μ m) were mounted on Microscope KP+ slides (Klinipath B.V) and stained with hematoxylin and eosin (H&E). Composite raw images of each IVD were made using a Colorview IIIU digital camera (Olympus) mounted to a BX-40 microscope (Olympus). The images were scaled and the following parameters were measured: 1) Proportion (%) of NP surface area and pericellular matrix consisting of NCs: NCs were identified based on morphologic characteristics ^{8,17}, dead NCs were distinguished from viable NCs by karyopyknosis and increased cytoplasmic eosinophilia; 2) Proportion of NP surface area consisting of CLCs and fibrocartilagenous matrix. Each section was classified by an experienced veterinary pathologist as follows (Fig. 2):

- Notochordal cell-rich (NC-rich) group: >90% of surface area consisting of NCs.
- Mixed group: cell population consisting of both NCs and CLCs in ratios between 10-90%.
- Chondrocyte-like cell-rich (CLC-rich) group: > 90% of surface area consisting of CLCs and corresponding matrix.

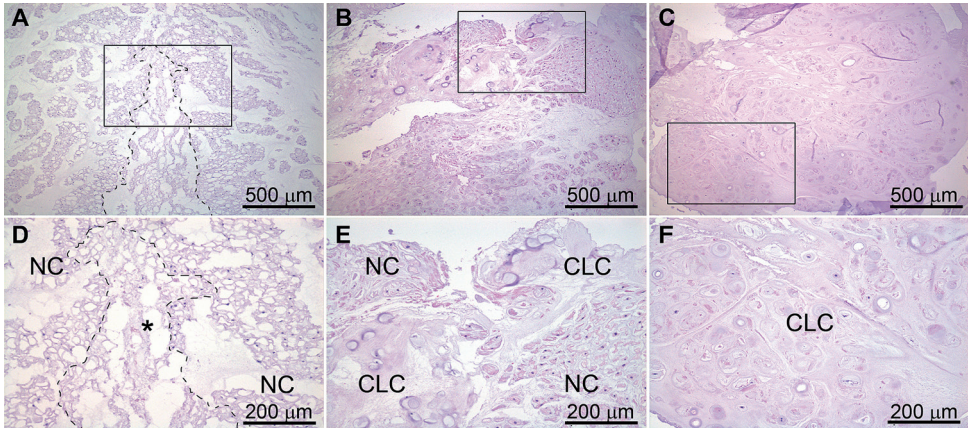


Figure 2. Typical H&E-images of the notochordal cell (NC)-rich group (A, D) containing NCs with a viable morphology organized in clusters and centrally localized dead NCs (separated by dotted line, *); the mixed-group (B, E) containing both NCs and chondrocyte-like cells (CLC); and the CLC-rich group (C, F) containing solely CLCs embedded in a dense matrix. D, E, and F are magnifications of the squares in A, B, and C, respectively.

Immunohistochemistry

β -catenin protein expression was evaluated in NPs from 5 non-chondrodystrophic and 5 chondrodystrophic dog sections for each group (NC-rich, Mixed, CLC-rich; n=10 per group). These sections were routinely processed and subjected to antigen retrieval in 10 mM citrate buffer (pH 6.0), followed by blocking of endogenous peroxidase activity¹⁸. Nonspecific background staining was minimized by pre-incubation with blocking buffer containing 10% normal goat serum (Sigma-Aldrich) / 0.025% Triton-X (Triton® X-100, Sigma-Aldrich) in phosphate-buffered saline (PBS) for 30 min, and an overnight incubation at 4°C with the primary antibody rabbit anti- β -catenin (Abcam, ab6302, 1:50 in PBS supplemented with 1% bovine serum albumin). After sections were washed in PBS buffer/0.025% Triton X, β -catenin was visualized with the goat anti-rabbit Envision System and the liquid diaminobenzidine (DAB) chromogen system (Dako). Sections were counterstained with hematoxylin (Hematoxylin QS, Vector Laboratories Inc.). In negative control sections, the primary antibody was omitted or replaced with its respective serum.

Morphometrical quantification of β -catenin expression

The total NP surface was measured by defining the perimeter of the NP, excluding the transition zone. A custom-made color range selection optimized for β -catenin specific staining was used to calculate the proportion of the NP surface area that stained for β -catenin, as well as the mean gray value (staining intensity) and integrated density (mean gray value times positive surface area).

Quantitative PCR (qPCR)

Six NPs representing the NC-rich group (from 6 non-chondrodystrophic dogs) and 6 NPs representing the CLC-rich group (from 6 chondrodystrophic dogs) were studied. The cellular composition of each NP was assessed through histopathological evaluation by a board-certified veterinary pathologist; qPCR samples corresponded with samples used for immunohistochemistry. In addition, the applied classification was further assessed by investigating the gene expression of the notochordal markers *brachyury*⁵ *cytokeratin 8*¹⁹ in both groups. Total RNA was isolated using the RNeasy Fibrous Tissue Mini Kit (Qiagen) according to the manufacturer's instructions. After on-column DNase-I treatment (Qiagen RNase-free DNase kit), RNA was quantified spectrophotometrically using Nanodrop ND-1000 (Isogen Life Science). Reverse transcriptase-PCR was performed with 100 ng of total RNA in a total volume of 40 μ L, using iScript™ cDNA Synthesis Kit (Biorad) with a mix of random hexamer and oligo-dT primers. qPCR was performed in duplicate using a MyIQ thermal cycler, IQ SYBRGreen SuperMix (BioRad) and dogs-specific primers were designed for genes involved in Wnt-signaling: *axin2*, *cyclin D1*, and *c-myc* (Eurogentec, Table 1)²⁰⁻²².

Conditions for the qPCR experiments were carefully validated. The amplification efficiency was between 90% and 110%. For all reference genes and groups (NC-rich and CLC-rich), the average expression stability (M) and the pair-wise variation were calculated with the statistical environment R²³, using the SLqPCR package²⁴, with implementation of the GENORM method²⁵ to determine an optimal reference gene set for valuable normalization²⁶. The optimal reference gene set as determined by the GENORM analysis included glyceraldehyde 3-phosphate dehydrogenase (*gapdh*), hypoxanthine-guanine phosphoribosyltransferase (*hprt*), beta-actin, ribosomal protein S19 (*rps19*), signal recognition particle receptor (*srpr*), beta-2-microglobulin (*b2m*), ribosomal protein L13 (*rpl13*), succinate dehydrogenase complex, subunit A, flavoprotein (*sdha*), tyrosine 3-monooxygenase/tryptophan 5-monooxygenase activation protein, zeta (*ywhaz*), and TATA box binding protein (*tbp*). For each experimental sample, the expression of reference genes was determined to control the template quality/quantity to normalize expression²⁶.

Protein	Forward Sequence 5'→3'	EXON	Reverse Sequence 5'→3'	EXON	Amplicon Size	Annealing temp (°C)	Accession no.
Target Genes							
<i>brachyury</i>	AGACAGCCAGCAATCTG	5	TGGAGGGAAGTGAGAGG	6	115	53	NM_001003092.1
<i>axin2</i>	GGACAAATCGTGGATACCT	1	TGCTTGGAGACAATGCTGTT	1	128	60	XM_548025
<i>cyclinD1</i>	GCCTCGAAGATGAAGGAGAC	2	CAGTTTGTTCACCAAGGAGCA	3	117	60	NM_001005757
<i>c-myc</i>	GCCGGGCCCCAGCGAGGATA	1	GCGACTGCGACGTAGGAGGGCGAGC	1	108	61	NM_001003246
Reference Genes							
<i>gapdh</i>	TGTCCCAACCCCAATGTATC	2	CTCCGATGCCCTGCTTCACTACCTT	2	100	58	NM_001003142
<i>hprt</i>	AGCTTGTGGTGAATAAGGAC	5/6	TTATAGTCAAGGGCATAATCC	7	104	56	NM_001003357
<i>β-actin (L)</i>	GATATCGCTGCGCTTGTGGTC	1	GGCTGGGGTGTGAAAAGTCTC	3	384	58	NM_001195845
<i>rps19</i>	CCTTCCCAAAAAGTCTGGG	2/3	GTTCTCATCGTAGGGAGCAAG	3	95	61	XM_533657
<i>sprpr</i>	GCTTCAGGATCTGGACTGC	7	GTTCCCTTGGTAGCACTGG	7/8	81	61	XM_546411
<i>b2m</i>	TCCTCATCCCTCGCT	1	TTCTCTGCTGGGTGTCG	2	85	61	XM_535458
<i>rpl13</i> ²⁷	GCCGGAAGTTGTAGTCTGT		GGAGAAAGCCAGGTAATTC		87	61	AJ388525
<i>sdha</i> ²⁷	GCCTTGGATCTTTGATGGA	6	TTCTTGGCTCTTATGCGATG	6	92	61	XM_535807
<i>ywhaz</i> ²⁷	CGAAGTTGCTGCTGGTGA	2	TTGCAITTCCTTTTGTGCTGA	2/3	94	58	XM_533072
<i>Tbp</i> ²⁷	CTAITTCCTTGGTGTGCAATGAGG	5	CCTCGGCAITTCAGTCTTTTC	5	96	57	XM_849432

Table 1. Primers used for quantitative PCR. Primers not indicated by²⁷ were designed in-house.

Relative expression was calculated by the efficiency corrected delta-delta Ct ($\Delta\Delta Ct$) method²⁸.

For each experimental sample, the expression of reference genes was determined to control the template quality/quantity to normalize expression²⁶. Relative expression was calculated by the efficiency corrected delta-delta Ct ($\Delta\Delta Ct$) method²⁸.

Canonical Wnt signaling of NCs in vitro

Cervical (C2-T1) and lumbar (L1-S1) spines from six mongrel dogs (non-chondrodystrophic, aged 16-18 months and weighing 16-24 kg) were removed en bloc. Based on the dog type and age of the selected dogs, as well as the macroscopic appearance of the IVDs, the NPs of all IVDs were assumed to be rich in NCs¹⁰. In addition, to assess the notochordal phenotype of the NPs used for culture, the relative gene expression levels of *brachyury* and *cytokeratin 8* were determined. Ten NPs were collected from each dog and NCs were cultured both in their original cluster-like conformation and as single cells²⁹ as follows. All NPs from one dog were pooled and pre-digested in 0.1% Pronase (Roche Diagnostics) for 45 minutes. Tissue/cells were collected by filtering through a 40- μ m filter (BD Biosciences) putting the cell strainer upside down, and flushing with 1% penicillin/streptomycin (P/S) and 10% fetal calf serum (FCS) supplemented DMEM-F12. Tissue/cells were further processed by overnight digestion in 0.05% collagenase type II (Worthington). Clusters of NCs retained on the filter were harvested. Half of the sample was used to create single NCs by incubation with 0.2% Pronase +0.0004% DNase (Qiagen) for 2 hours. The digest was centrifuged at 1500 RPM (room temperature) for 5 minutes and the cell pellet was dissolved in P/S-FCS-DMEM-F12. The average cell yield was 1.5×10^6 cells per dog. The NC clusters and the single NCs were plated out on six 6-well plates (Falcon Multiwell Primaria, Becton Dickinson) and cultured in P/S-FCS-DMEM-F12 under normoxic conditions (5% CO₂) at 37 °C. At days 0, 2, 4, 6, 8 and 10 photographs were taken at 20x and 40x magnification using a Leica DM IRB microscope.

Immunofluorescent labeling of β -catenin

Cells were fixed at days 0, 2, 4, 6, 8 and 10 and were subjected to immunofluorescent labeling of β -catenin. Cells cultured on coverslips placed in the wells and adhered by day 4 in culture. On days 0 and 2, cells were mounted on positively charged slides (Klinipath), using a Shandon Cytospin 4 (Therma Scientific). On days 4, 6, 8, and 10, the adherent cells on coverslips were washed once with Hank's balance salt solution (PAA Laboratories), fixed in 4% paraformaldehyde (Sigma-Aldrich), and stored at -20 °C until further processing. Immunofluorescent labeling of β -catenin was performed as

described above, but using the primary antibody at a dilution of 1:100 and 1:100 donkey anti-rabbit antibodies conjugated to Alexa488 (Invitrogen) and nuclear staining with Topro-3 iodide (Invitrogen, T3605) for visualization. The cells were mounted with Fluorsave (Calbiochem). Images at 5 random locations in each sample were acquired by a sequentially recording procedure on a multiphoton imaging station (MP2100, Zeiss, Herfordshire, UK). Images were analyzed with ImageJ software package (Rasband NIH, Bethesda, ML, USA), and using a customized macro in which masks were generated from the cell nuclei using the Topro-3 images (nuclear staining) and cells using the β -catenin images. These masks were used to calculate the integrated intensity of nuclear and cytoplasmic β -catenin protein expression after the subtraction of background. The integrated density per cell, integrated density of the nucleus per cell, integrated density of the cytoplasm per cell, and the ratio of the integrated density of the nucleus to cytoplasm were calculated using Microsoft Office Excel 2007 (Microsoft Corporation).

Quantitative PCR

Non-adhered cells at days 0 and 2 were collected by centrifuging the medium at 1500 RPM at 4°C for 1 minute and washing the wells with RNase-free Hank's solution. On days 4, 6, 8, and 10, medium was removed and wells were washed with RNase-free Hank's solution. The relative gene expression of *brachyury* and *cytokeratin 8* (notochordal markers), and *axin2*, *cyclinD1*, and *c-myc* was determined as described above.

Data Analysis and Statistics

Statistical analyses were performed using R statistical software²³. Linear mixed models³⁰, containing both fixed and random effects, were used to analyze the described parameters separately for the immunohistochemistry, qPCR of tissue samples, immunofluorescence, and qPCR of culture samples. The Akaike Information Criterion (AIC) was used for model selection. A random intercept for each dog was added to each model to take the correlation of the observations within a dog into account. If necessary, models were optimized by applying a correction for unequal variances and/or for autoregressive correlation. Conditions for the use of mixed models, including normal distribution of the data, were assessed by analyzing the residuals (PP- and QQ plots) of the acquired models; no violations of these conditions were observed. P values were calculated per parameter or target gene to analyze differences of interest between groups/time points. Relative gene expression data from all target genes for both the *in vivo* and *in vitro* studies were analyzed as one outcome variable due to the potential inter-gene correlations within the canonical Wnt-signaling pathway. For the immunofluorescence analysis, the data obtained from the 5 images for all measured parameters for each time point per cell

fraction per dog were averaged and used for data analysis. Values obtained for the immunofluorescent parameters were analyzed as one outcome variable due to the correlation between these parameters.

For each model, the Benjamini Hochberg correction was used to correct for multiple comparisons. $P < 0.05$ was considered statistically significant.

Results

Cell type distribution in relation to histopathological classification

Histopathological evaluation of the NP of both chondrodystrophic and non-chondrodystrophic dogs revealed distinct differences in its cellular composition (Table 2): The NP surface of the NC-rich group consisted almost entirely (>90% NCs) of NCs embedded in a modest matrix. A clear distinction could be made between dead NCs, which were in the central part of the NP, and viable NCs at the periphery of the NP (Fig. 2). In the Mixed group, 10-90% of the NP surface consisted of dead and viable NCs. The NP surface of the CLC-rich group consisted of 100% CLCs and matrix; no NCs were found in any of the CLC-rich samples.

	Dead NCs	Viable NCs	Total NCs	CLCs
NC-rich	66.4-30.4%	69.6-33.6%	100.0-90.6%	9.4-0.0%
Mixed	24.6-0.0%	37.1-10.3%	39.0-10.3%	89.7-61.0%
CLC-rich	0.0%	0.0%	0.0%	100.0%

Table 2. Cell type distribution in the nucleus pulposus (NP) expressed as % of the total NP surface area in the notochordal cell (NC) rich, Mixed, and chondrocyte-like cell (CLC) rich groups.

Protein expression of β -catenin and qPCR analysis of Wnt target genes

Nuclear and cytoplasmic β -catenin staining was seen in all histopathological groups of both non-chondrodystrophic and chondrodystrophic dogs, but only in viable NCs and in part of the CLC population (Fig. 3). The proportion of the NP surface area staining positive for β -catenin and the integrated density for the β -catenin staining were highest in the NC-rich group, followed by the Mixed group, and were lowest in the CLC-rich group (Fig. 4, Table 3). The CLC-rich group exhibited the highest intensity (mean gray value) of β -catenin staining, followed by the Mixed group, and was lowest in the NC-rich group. For the immunohistochemical parameters, no significant differences were found between non-chondrodystrophic and chondrodystrophic dogs within the NC-rich, Mixed, and CLC-rich group.

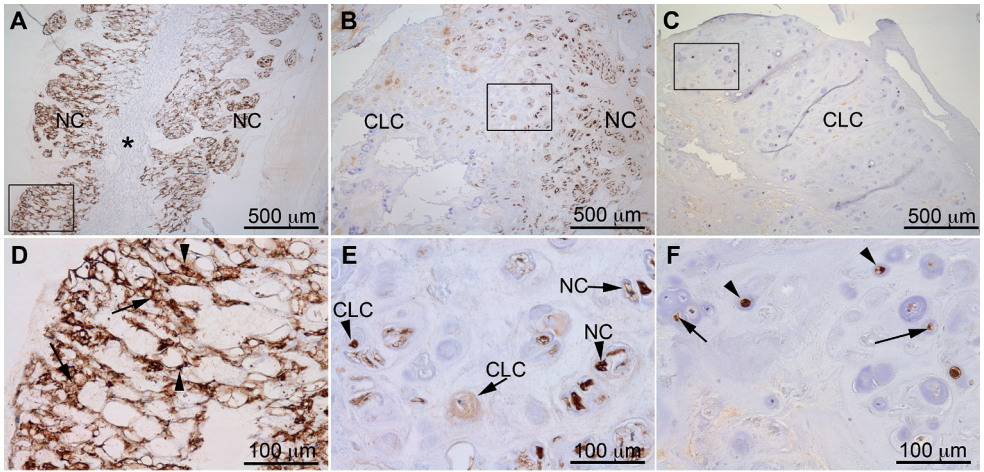


Figure 3. Nucleus pulposus (NP) sections stained for β -catenin, showing notochordal cell-rich NP (A, D) with a viable morphology (NC) and dead notochordal cells (*); mixed cell population NP with notochordal cells (NC) and chondrocyte-like cells (CLCs) (B, E); CLC-rich NP (C, F). In each group nuclear (arrowhead) and cytoplasmic (arrow) staining can be observed. D, E, and F are magnifications of the squares in A, B, and C, respectively.

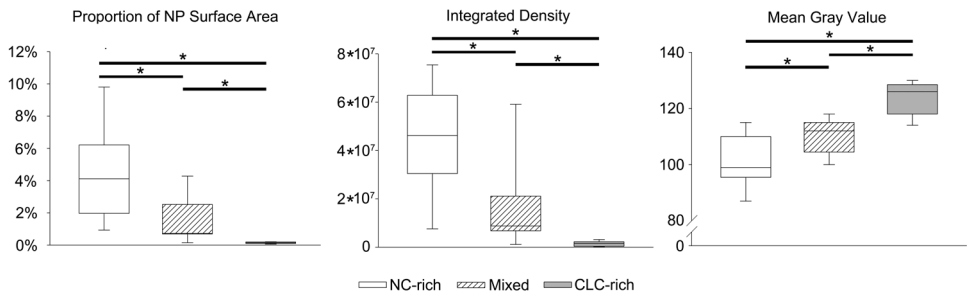


Figure 4. Boxplots of the proportion of surface area, integrated density, and median gray value of β -catenin in the nucleus pulposus (NP) for the notochordal cell-rich (NC-rich) NP, mixed population of notochordal cells and chondrocyte-like cells (Mixed) NP, and chondrocyte-like cell-rich NP (CLC-rich). * indicates significant differences ($P < 0.05$) between the NC-rich, Mixed, and CLC-rich groups. For the NC-rich, Mixed, and CLC-rich NP, no significant differences were found between the non-chondrodystrophic and chondrodystrophic groups.

Parameter	Immunohistochemistry			Quantitative PCR	
	Group	Breed	Group*Breed	Gene	
Surface Area %	<0.001	0.964	0.305	Gene	<0.001
Integrated Density	<0.001	0.354	0.609	Group	<0.001
Mean Grey Value	<0.001	0.074	0.846	Gene * Group	<0.001
	<i>Inter-group comparison per parameter</i>			<i>Inter-group comparison per target gene</i>	
	NCR-MX	NCR- CLCR	MX-CLCR	<i>brachyury/ck-8</i>	<0.001
Surface Area %	0.001	<0.001	<0.001	<i>axin2</i>	<0.001
Integrated Density	0.007	<0.001	<0.001	<i>c-myc</i>	<0.001
Mean Grey Value	0.013	<0.001	<0.001	<i>cyclin D1</i>	<0.001

Table 3. Linear mixed model results for the immunohistochemistry and qPCR analyses of healthy vs. early-degenerated nuclei pulposi. *P* values for the mixed model explanatory factors ‘Gene (*brachyury*, *cytokeratin 8 (ck-8)*, *axin2*, *cyclin D1*, *c-myc*), ‘Group’ (Immunohistochemistry: *notochordal cell rich (NCR)*, *mixed population (MX)*, *chondrocyte-like cell rich (CLCR)*; qPCR: *NCR* and *CLCR*), ‘Breed’ (*non-chondrodystrophic* or *chondrodystrophic* dog), and their interactions. *P* values for comparisons between groups per parameter (immunohistochemistry) and groups per gene (qPCR) were calculated. $P < 0.05$ was considered statistically significant.

Therefore, qPCR analysis was performed on NC-rich samples from non-chondrodystrophic dogs (healthy NP) and compared to CLC-rich samples from chondrodystrophic dogs (degenerated NP). The notochordal markers *brachyury* and *cytokeratin 8* showed a significantly higher (mean \pm SD of N-fold change) gene expression (8.3 ± 0.1 and 25.3 ± 1.9 , respectively) in the healthy, non-chondrodystrophic, NC-rich NP compared with the degenerated, chondrodystrophic, CLC-rich NP. Compared with the healthy, non-chondrodystrophic, NC-rich NP (reference, set at 1), the relative gene expression of *axin2* (2.8 ± 0.2), *cyclin D1* (152.1 ± 12.8), and *c-myc* (4.4 ± 0.3) was significantly higher in the degenerated, chondrodystrophic, CLC-rich NP (Fig. 5).

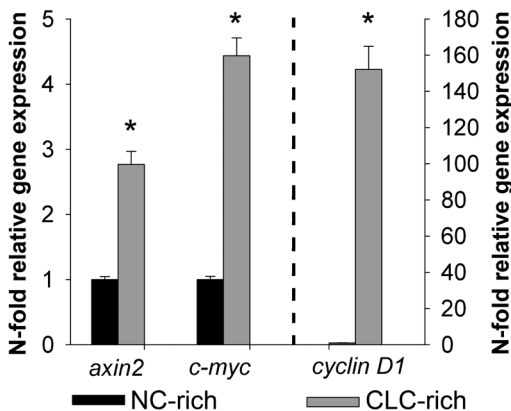
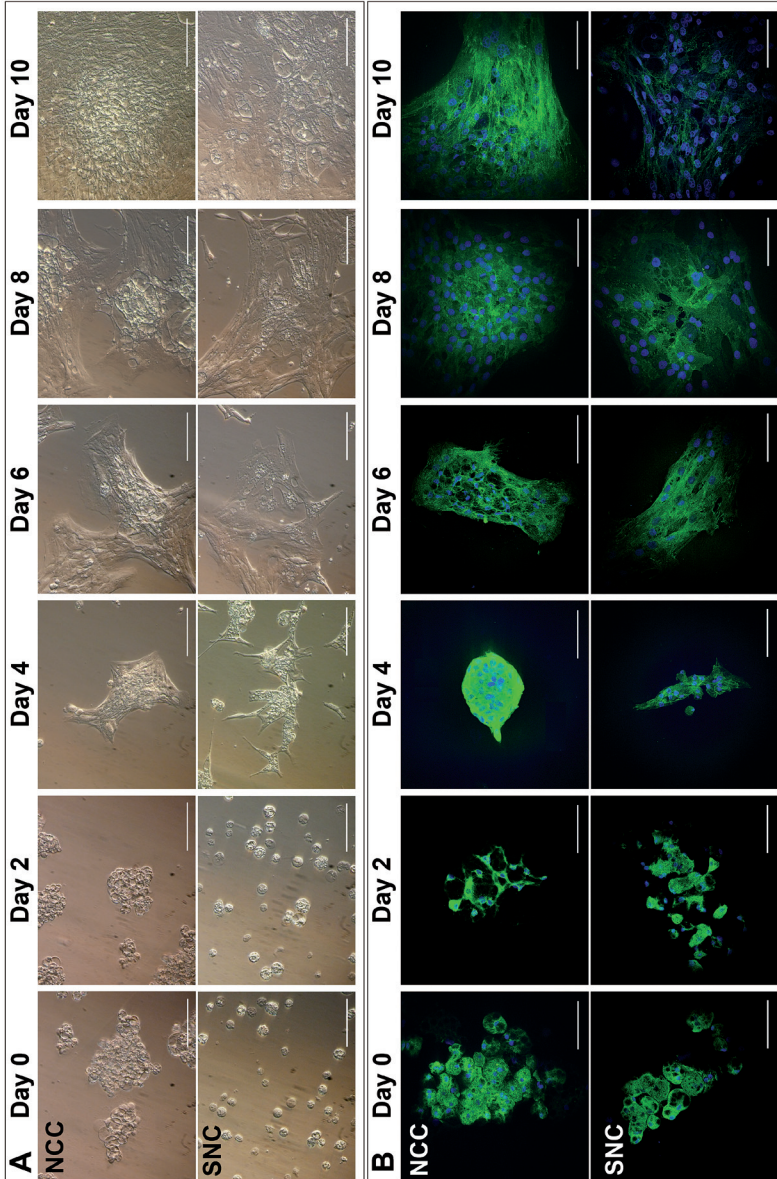


Figure 5. Relative gene expression of *axin2*, *cyclin D1*, and *c-myc* in chondrocyte-like cell rich (CLC-rich) group versus the notochordal cell rich (NC-rich) group (reference, set at 1). The left vertical axis applies to *axin2* and *c-myc*, and the right axis to *cyclin D1*. * $P < 0.05$.

In vitro culture of NCs

All NP samples used for the culture study had a relative *brachyury* and *cytokeratin 8* gene expression comparable to the NC-rich samples employed in the tissue study. All NC clusters and 3 out of 6 single NC samples had adhered by day 4 (Fig. 6). After adherence, the cells became more ovoid-shaped, but retained their cytoplasmic vesicles during the entire culture period (Fig.6). Once single NCs had adhered, they migrated toward each other and formed cellular extensions toward neighboring cells. Non-adhered single NC samples were analyzed separately. NCs in culture showed a significantly lower gene expression of *brachyury* and *cytokeratin 8* at all time points compared with the NC-rich NP tissue (Fig. 7).

Figure 6. Phase contrast light microscopy (A) and immunofluorescence (B) images of the notochordal cell clusters (NCC) and single notochordal cells (SNC) on days 0, 2, 4, 6, 8, and 10 in culture. Scale bar: A: 100 μm ; B: 50 μm . Once SNCs had adhered, they migrated towards each other and formed cellular extensions towards neighboring cells (A, SNC day 4). In the immunofluorescent images, nuclear staining (Topro-3) and β -catenin staining are depicted in blue and green, respectively. Note: as a result of the cytospin at days 0 and 2 for the immunofluorescence analysis, single cells appear as grouped cells.



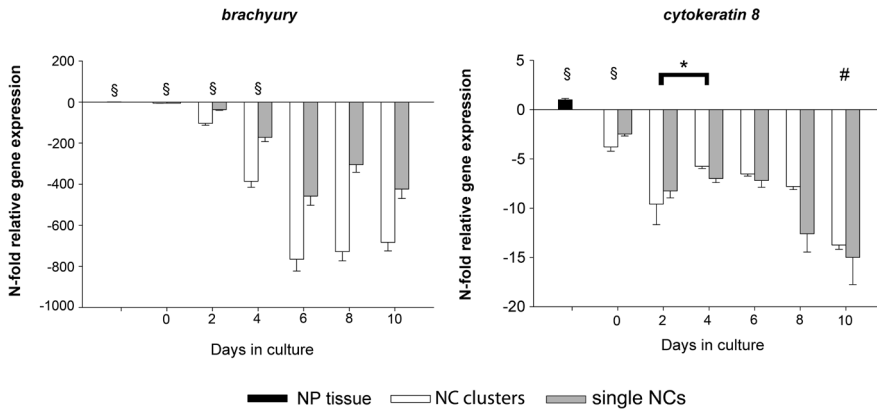


Figure 7. Relative gene expression of *brachyury* and *cytokeratin 8* in the notochordal cell (NC) clusters (white bars) and single NCs (gray bars) on different days in culture. NC-rich NP tissue served as a reference (black bar, set at 1). §: indicates significant difference with all subsequent time points in culture; # indicates significant difference with all previous time points in culture; * indicates significant difference between two time points. No significant differences were found between the NC cluster and single NC groups.

Evaluation of β -catenin protein expression

β -Catenin protein expression, as indicated by the total integrated density per cell, nuclear integrated density per cell, cytoplasmic integrated density per cell, and nucleus/cytoplasm ratio, was not significantly different between NC clusters and single NCs in culture (Fig. 8, Table 4). The total integrated density for β -catenin expression was significantly higher on days 6 and 8 than on day 0 in culture (Fig. 9). The nuclear integrated density per cell was significantly higher on days 2, 4, and 6 in culture than on day 0, with no significant differences on days 8 and 10. Cytoplasmic integrated density per cell was significantly higher on day 8 compared with days 0 and 4 in culture. The nucleus/cytoplasm ratio was highest on day 4, and significantly decreased later on. β -Catenin expression was significantly lower in non-adherent than in adherent cells.

Quantitative PCR of target genes of *Wnt*/ β -catenin signaling during P0 NC culture

The relative gene expression of *axin2* was significantly higher in NC clusters and single NCs after plating out than in the NC-rich NP tissue *ex vivo*, but thereafter *axin2* gene expression decreased significantly in NC clusters and NCs (Fig. 10). The relative gene expression of *axin2* was significantly higher in single NCs than in NC clusters at all time points. The relative gene expression of *cyclin D1* in NCs in culture was significantly higher on days 2, 4, 6, 8 and 10 than on day 0 or in the NC-rich NP tissue *ex vivo*, and was also significantly

higher in NC clusters than in NC single cells at all time points. The relative gene expression of *c-myc* was significantly higher in NC clusters and single cells than in the NC-rich NP tissue ex vivo at all time points, but decreased significantly on day 6 and remained thereafter. The relative expression of *c-myc* was significantly higher in single NCs than in NC clusters.

β -Catenin Protein Expression

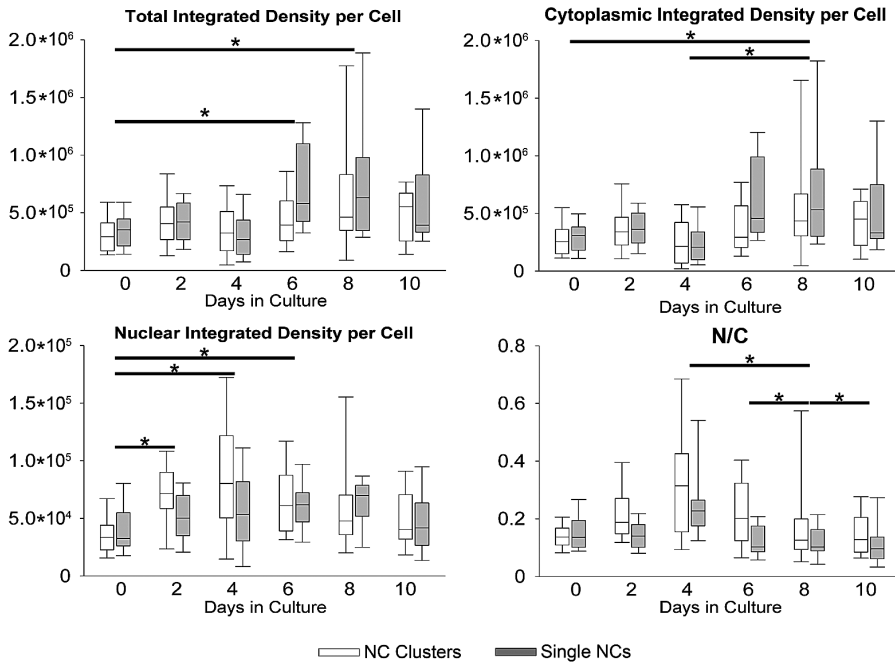


Figure 8. Boxplots of β -catenin protein expression as indicated by the total integrated density per cell, nuclear integrated density per cell, cytoplasmic integrated density per cell, and the nuclear/cytoplasmic integrated density ratio per cell (N/C) for the notochordal cell (NC) clusters (white bars) and single NCs (gray bars; solely adhered cells) on day 0, 2, 4, 6, 8, and 10 in culture. * indicates differences ($P < 0.05$) between different time points in culture.

Table 4. Linear mixed model results for the immunofluorescence and qPCR analyses of in vitro culture of notochordal cells (NCs). values for the mixed model explanatory variables 'Parameter' (total integrated density per cell (TID), nuclear integrated density per cell (NID), cytoplasmic integrated density per cell (CID), immunofluorescence nuclear/cytoplasmic signal ratio (N/C)), 'Gene' (qPCR: *brachyury*, *cytokeratin 8*, *axin2*, *cyclin D1*, *c-myc*), 'Time Point' (days 0, 2, 4, 6, 8 and 10 in culture), 'Cell Culture Condition (CCC)' (notochordal cell clusters (NCC), notochordal single cells (NSC)), 'Cell adherence' (yes or no), and their interactions. In case of significant interactions, P values for comparisons between time points per parameter/gene, cell adherence per parameter, and culture method per gene were calculated. $P < 0.05$ was considered statistically significant (highlighted in bold text).

Immunofluorescence					Quantitative PCR				
Parameter				<0.001	Gene				<0.001
Time Point				0.013	Time Point				<0.001
CCC				0.174	CCC				<0.001
Cell Adherence				<0.001	Cell Adherence				0.042
Parameter * Time Point				0.004	Gene*Time Point				<0.001
Parameter * CCC				0.092	Gene * CCC				<0.001
Parameter*Cell Adherence				<0.001	Gene*Cell Adherence				<0.001
Time Point*CCC				0.063	Time Point * Culture Method				0.258
Parameter*Time Point*CCC				0.194	Gene* time Point* CCC				0.210
<i>Time Point comparison per Parameter</i>					<i>Time Point Comparison per Gene</i>				
	TID	NID	CID	N/C	<i>brachy</i>	<i>ctk 8</i>	<i>axin-2</i>	<i>cyclin DI</i>	<i>c-myc</i>
NP - day 0	-	-	-	-	<0.001	<0.001	<0.001	0.637	0.033
NP - day 2	-	-	-	-	<0.001	<0.001	0.067	<0.001	0.001
NP - day 4	-	-	-	-	<0.001	<0.001	0.946	<0.001	0.001
NP - day 6	-	-	-	-	<0.001	<0.001	0.044	<0.001	0.003
NP - day 8	-	-	-	-	<0.001	<0.001	0.676	<0.001	0.008
NP - day 10	-	-	-	-	<0.001	<0.001	0.696	<0.001	0.021
Day 0-2	0.249	0.046	0.312	0.875	<0.001	<0.001	<0.001	<0.001	0.001
Day 0-4	0.425	0.006	0.617	0.335	<0.001	<0.001	<0.001	<0.001	0.032
Day 0-6	0.044	0.023	0.056	0.757	<0.001	<0.001	<0.001	<0.001	0.397
Day 0-8	0.009	0.114	0.010	0.112	<0.001	<0.001	<0.001	<0.001	0.542
Day 0-10	0.072	0.118	0.091	0.521	<0.001	<0.001	<0.001	<0.001	0.698
Day 2-4	0.760	0.293	0.598	0.323	<0.001	0.026	0.013	0.009	0.324
Day 2-6	0.349	0.653	0.346	0.814	<0.001	0.096	<0.001	0.002	0.022
Day 2-8	0.158	0.842	0.120	0.093	<0.001	0.173	0.006	0.004	0.012
Day 2-10	0.497	0.750	0.488	0.605	<0.001	0.084	0.014	0.008	0.008
Day 4-6	0.152	0.519	0.099	0.416	0.001	0.569	<0.001	0.676	0.261
Day 4-8	0.077	0.242	0.031	0.007	0.015	0.377	0.494	0.815	0.158
Day 4-10	0.330	0.153	0.239	0.695	0.002	<0.001	0.540	0.903	0.091
Day 6-8	0.583	0.505	0.495	0.025	0.401	0.756	0.011	0.862	0.838
Day 6-10	0.759	0.426	0.756	0.757	0.759	0.001	0.021	0.753	0.668
Day 8-10	0.393	0.835	0.330	0.010	0.648	0.003	0.955	0.855	0.834
<i>Cell adherence per Parameter</i>					<i>NCC vs NSC and cell adherence per Gene</i>				
	TID	NID	CID	N/C	<i>brachy- yury</i>	<i>ctk 8</i>	<i>axin2</i>	<i>cyclin DI</i>	<i>c-myc</i>
NCC vs. NSC	-	-	-	-	0.223	0.498	<0.001	<0.001	0.001
Cell Adherence	0.013	0.012	0.007	0.334	0.147	0.687	0.074	<0.001	0.159

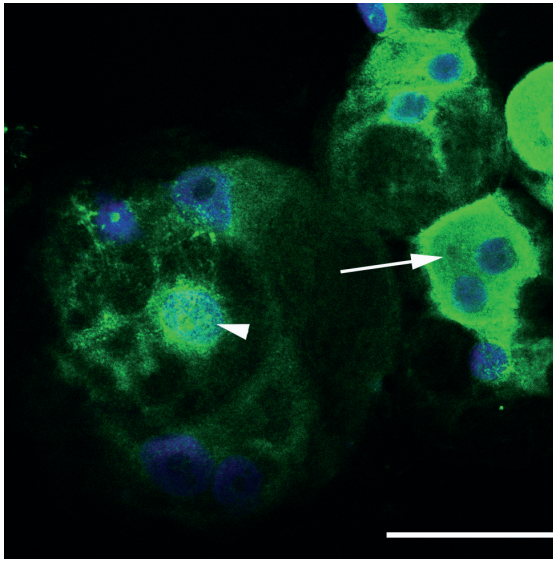


Figure 9. Typical immunofluorescence image of notochordal cells in culture labelled for β -catenin, showing nuclear (arrowhead) and cytoplasmic (arrow) localisation of β -catenin protein expression. Scale bar: 20 μ m.

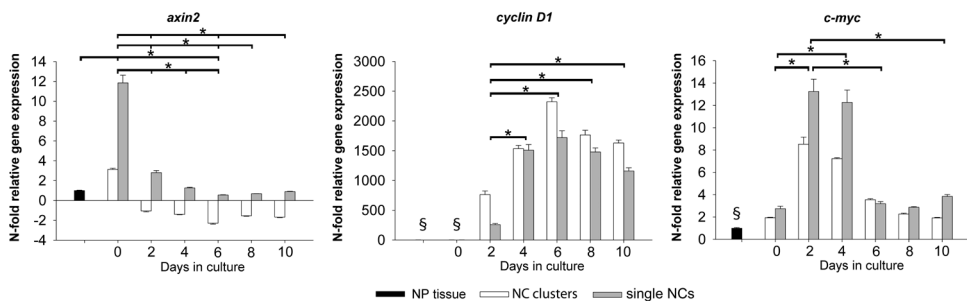


Figure 10. Relative gene expression of *axin2*, *cyclin D1*, and *c-myc* in the notochordal cell (NC) clusters (white bars) and single NCs (gray bars) on different days in culture. NC-rich NP tissue served as a reference (black bar; set at 1).

* indicates significant differences between different time points in culture ($P < 0.05$).

§: indicates significant difference with all subsequent time points in culture.

Discussion

The present study investigated canonical Wnt signaling in NP tissue from non-chondrodystrophic and chondrodystrophic dogs, which, in view of investigating the NC and IVD degeneration and regeneration, represent an intriguing, large animal model: in non-chondrodystrophic dogs, the NC remains the predominant cell type of the NP during the majority of life, with IVD degeneration only occurring at old age; conversely, in chondrodystrophic dogs the NC is lost early in life, with concurrent degeneration of all IVDs^{9,31}. Classification of the NP samples was performed and confirmed by assessing the macroscopic and histopathological appearance, and relative gene expression of *brachyury* and *cytokeratin 8*, and canonical Wnt signaling was evaluated in the healthy, NC-rich IVD and compared with the onset of degeneration, represented by the Mixed group, and with early degeneration, represented by the CLC-rich group.

NCs express canonical Wnt signaling in the adult healthy IVD.

In the healthy, NC-rich NP, nuclear and cytoplasmic β -catenin protein expression (both non-chondrodystrophic and chondrodystrophic NP) and *axin2* gene expression were detected, indicating that Wnt/ β -catenin signaling is active in NCs *in vivo*³². The relatively high integrated density in the NC-rich group can be attributed to the larger size of NCs relative to CLCs and the high NP cell/matrix ratio in the NC-rich group compared with the CLC-rich group. These results showing Wnt signaling in NCs are consistent with those of studies reporting nuclear β -catenin expression in embryonic and neonatal rat NCs¹⁵, and robust Wnt signaling activity in notochord progenitor cells, which is considered essential for the maintenance of notochord identity and fate¹². Altogether, these data support the role of the NC as a putative NP progenitor cell, also in the adult NP.

Early IVD degeneration involves increased canonical Wnt signaling.

Canonical Wnt signaling increased during IVD degeneration, based on the significantly higher β -catenin staining intensity (mean gray value) in the CLC-rich group, compared with the Mixed group and the NC-rich group of both non-chondrodystrophic and non-chondrodystrophic dogs. Moreover, the gene expression of *axin2*, *c-myc*, and *cyclin D1* was also significantly higher in the chondrodystrophic, CLC-rich, degenerated NP than in the non-chondrodystrophic, NC-rich healthy NP. *Axin2* serves as a gene expression read out specific for canonical Wnt signaling²¹, whereas cell cycle regulators, such as *c-myc* and *cyclin D1*, are induced, but not exclusively, by Wnt/ β -catenin activation^{20,22}. Taken together, these results might suggest that activation of canonical Wnt signaling supports the proliferation of cells within the degenerating IVD³³, possibly in an attempt to restore IVD health. In line with these findings, activation of Wnt/ β -catenin signaling in rat NP cells resulted in, amongst others, increased expression of MMP-9 and -10, both indicative for IVD degeneration¹⁵. However, stimulation of canonical Wnt signaling also increased cell senescence and induced down-regulation of *cyclin D1* and *c-myc*

gene expression¹⁶. This discrepancy may be the result of differences in the cell types examined, *in vivo* versus *in vitro* cell investigation, and the effects of LiCl on the cell cycle^{15,16}. Whether canonical Wnt-activation acts directly on CLCs within the degenerated IVD or indirectly by modifying the niches of NCs that have been also shown to present in late stages of degeneration^{19,34} remains to be elucidated.

Canonical Wnt signaling is initially activated in NCs in culture.

NCs were cultured in clusters, maintaining their original multi-cellular conformation^{10,29,35,36}, and as single cells^{36,37}. After adhesion, both NCs in clusters and single cells formed complex cell networks, with single NCs migrating toward each other and forming intercellular connections, mimicking the cellular organization seen in the NC clusters (see Fig. 6A, single NCs day 4). Attached NCs became more ovoid in appearance, but retained their intracytoplasmic vesicles during the entire culture period, which is in accordance with previous studies³⁵. Gene expression of *brachyury* and *cytokeratin 8* was significantly decreased at all time points in culture compared with NC-rich NP tissue, indicating a loss of notochordal phenotype and potential de-differentiation of NCs in monolayer culture under normoxic conditions³⁸. NCs have been shown to thrive in three-dimensional culture under hypoxic conditions³⁸, and therefore we cannot exclude that the culture conditions applied may have been a possible confounding factor. Primary NCs (both clusters and single cells) showed active Wnt/ β -catenin signaling with nuclear and cytoplasmic β -catenin expression. *Axin2* gene expression was significantly higher on days 0 and 2 in culture, than thereafter, when levels were comparable to those seen in the NC-rich NP tissue *ex vivo*. There was no evidence that activation of the canonical Wnt signaling pathways led to initiation of a ‘degenerative process’¹⁵: in the current study, levels of *mmp9* gene expression were significantly lower than in NC-rich NP tissue *ex vivo* (data not shown). The gene expression of *cyclin D1* and *c-myc* increased during most of the culture period, indicating increased proliferation, which was confirmed by an increase in total DNA content (data not shown). Interestingly, *axin2* gene expression and β -catenin protein expression were only increased during the first few days of culture, perhaps indicating that Wnt/ β -catenin signaling is involved in the initiation of a regenerative process.

Although the culture conditions for clustered or single NCs were to a large extent comparable, there were some important differences. While all NC cluster samples had adhered by day 4, as described before^{35,36}, only 50% of the single NC samples had adhered, and non-adherent cells showed a significantly lower β -catenin protein expression, and hence lower Wnt/ β -catenin signaling activity, than adherent cells. Isolated NCs showed significantly higher *axin2* and *c-myc*, and lower *cyclin D1* gene expression than the NC clusters. It is tempting to postulate that single NCs exhibit greater Wnt/ β -catenin signaling activation, reflecting a regenerative process as a response to the disruption of the physiological cluster-like conformation. Thus NC clusters reflect the *in vivo* situation better than isolated cells based on β -catenin expression.

In conclusion, the present study investigated canonical Wnt signaling in the NC and in the process of early IVD degeneration. NCs *ex vivo* and in culture express active Wnt/ β -catenin signaling as shown by nuclear and cytoplasmic β -catenin protein expression and *axin2* gene expression, supporting their role as a putative progenitor cell of the NP^{4,5,11}. Moreover, expression of Wnt target genes *axin2*, *c-myc*, and *cyclin D1* and β -catenin protein expression were upregulated in the CLC-rich, degenerated NP, suggesting increased Wnt/ β -catenin activity in early IVD degeneration, possibly reflecting a regenerative response.

Acknowledgements

The authors would like to thank Ms. Jane Sykes for language corrections and the Multimedia Department of the Faculty of Veterinary Medicine for technical assistance.

References

1. Andersson GB: Epidemiological features of chronic low-back pain. *Lancet* 354:581-585, 1999.
2. Luoma K, Riihimaki H, Luukkonen R, et al: Low back pain in relation to lumbar disc degeneration. *Spine* 25:487-492, 2000.
3. Tow BP, Hsu WK, Wang JC: Disc regeneration: a glimpse of the future. *Clin Neurosurg* 54:122-128, 2007.
4. Erwin WM: The enigma that is the nucleus pulposus cell: the search goes on. *Arthritis Res Ther* 12:118, 2010.
5. Risbud MV, Schaer TP, Shapiro IM: Toward an understanding of the role of notochordal cells in the adult intervertebral disc: from discord to accord. *Dev Dyn* 239:2141-2148, 2010.
6. Choi KS, Cohn MJ, Harfe BD: Identification of nucleus pulposus precursor cells and notochordal remnants in the mouse: implications for disk degeneration and chordoma formation. *Dev Dyn* 237:3953-3958, 2008.
7. Hansen HJ: A pathologic-anatomical study on disc degeneration in dog, with special reference to the so-called enchondrosis intervertebralis. *Acta Orthop Scand Suppl* 11:1-117, 1952.
8. Trout JJ, Buckwalter JA, Moore KC, et al: Ultrastructure of the human intervertebral disc. I. Changes in notochordal cells with age. *Tissue Cell* 14:359-369, 1982.
9. Bergknot N, Rutges JP, Kranenburg HJ, et al: The dog as an animal model for intervertebral disc degeneration? *Spine* 37: 351-358, 2012.
10. Cappello R, Bird JL, Pfeiffer D, et al: Notochordal cell produce and assemble extracellular matrix in a distinct manner, which may be responsible for the maintenance of healthy nucleus pulposus. *Spine (Phila Pa 1976)* 31:873-882, 2006.
11. Reya T, Clevers H: Wnt signalling in stem cells and cancer. *Nature* 434:843-850, 2005.
12. Ukita K, Hirahara S, Oshima N, et al: Wnt signaling maintains the notochord fate for progenitor cells and supports the posterior extension of the notochord. *Mech Dev* 126:791-803, 2009.

13. Kondo N, Yuasa T, Shimono K, et al: Intervertebral Disc Development Is Regulated by Wnt/beta-catenin Signaling. *Spine (Phila Pa 1976)* 36: E513-518, 2011.
14. Corr M: Wnt-beta-catenin signaling in the pathogenesis of osteoarthritis. *Nat Clin Pract Rheumatol* 4:550-556, 2008.
15. Hiyama A, Sakai D, Risbud MV, et al: Enhancement of intervertebral disc cell senescence by WNT/beta-catenin signaling-induced matrix metalloproteinase expression. *Arthritis Rheum* 62:3036-3047, 2010.
16. Hiyama A, Sakai D, Tanaka M, et al: The relationship between the Wnt/beta-catenin and TGF-beta/BMP signals in the intervertebral disc cell. *J Cell Physiol*, 2010.
17. Hunter CJ, Matyas JR, Duncan NA: The three-dimensional architecture of the notochordal nucleus pulposus: novel observations on cell structures in the canine intervertebral disc. *J Anat* 202:279-291, 2003.
18. Tryfonidou MA, Hazewinkel HA, Riemers FM, et al: Intraspecies disparity in growth rate is associated with differences in expression of local growth plate regulators. *Am J Physiol Endocrinol Metab* 299:E1044-1052, 2010.
19. Gilson A, Dreger M, Urban JP: Differential expression level of cytokeratin 8 in cells of the bovine nucleus pulposus complicates the search for specific intervertebral disc cell markers. *Arthritis Res Ther* 12:R24, 2010.
20. He TC, Sparks AB, Rago C, et al: Identification of c-MYC as a target of the APC pathway. *Science* 281:1509-1512, 1998.
21. Jho EH, Zhang T, Domon C, et al: Wnt/beta-catenin/Tcf signaling induces the transcription of Axin2, a negative regulator of the signaling pathway. *Mol Cell Biol* 22:1172-1183, 2002.
22. Shtutman M, Zhurinsky J, Simcha I, et al: The cyclin D1 gene is a target of the beta-catenin/LEF-1 pathway. *Proc Natl Acad Sci U S A* 96:5522-5527, 1999.
23. R Development Core Team: R: A language and environment for statistical computing. R Foundation for Statistical Computing. Vienna, Austria, 2010.
24. Kohl M: SLqPCR: Functions for analysis of real-time quantitative PCR data at SIRS-Lab GmbH. R package. Jena, SIRS-Lab GmbH, 2007.
25. Vandesompele J, De Preter K, Pattyn F: Accurate normalization of realtime quantitative RT-PCR data by geometric averaging of multiple internal control genes. 2002. *Genome Biol* 3:research 0034.0031-0034.0011, 2002.
26. Brinkhof B, Spee B, Rothuizen J, et al: Development and evaluation of canine reference genes for accurate quantification of gene expression. *Anal Biochem* 356:36-43, 2006.
27. Peters IR, Peeters D, Helps CR, et al: Development and application of multiple internal reference (housekeeper) gene assays for accurate normalisation of canine gene expression studies. *Vet Immunol Immunopathol* 117:55-66, 2007.
28. Pfaffl MW: A new mathematical model for relative quantification in real-time RT-PCR. *Nucleic Acids Res* 29:e45, 2001.
29. Hunter CJ, Matyas JR, Duncan NA: The functional significance of cell clusters in the notochordal nucleus pulposus: survival and signaling in the canine intervertebral disc. *Spine (Phila Pa 1976)* 29:1099-1104, 2004.
30. Pinheiro J, Bates D, DebRoy S, et al: nlme: linear and nonlinear mixed effects models. R package version 3:1-96, 2009.

31. Erwin WM: The Notochord, Notochordal cell and CTGF/CCN-2: ongoing activity from development through maturation. *J Cell Commun Signal* 2:59-65, 2008.
32. MacDonald BT, Tamai K, He X: Wnt/beta-catenin signaling: components, mechanisms, and diseases. *Dev Cell* 17:9-26, 2009.
33. Johnson WE, Eisenstein SM, Roberts S: Cell cluster formation in degenerate lumbar intervertebral discs is associated with increased disc cell proliferation. *Connective Tissue Research* 42:197-207, 2001.
34. Minogue BM, Richardson SM, Zeef LA, et al: Transcriptional profiling of bovine intervertebral disc cells: implications for identification of normal and degenerate human intervertebral disc cell phenotypes. *Arthritis Res Ther* 12:R22, 2010.
35. Erwin WM, Inman RD: Notochord cells regulate intervertebral disc chondrocyte proteoglycan production and cell proliferation. *Spine (Phila Pa 1976)* 31:1094-1099, 2006.
36. Kim JH, Deasy BM, Seo HY, et al: Differentiation of intervertebral notochordal cells through live automated cell imaging system in vitro. *Spine (Phila Pa 1976)* 34:2486-2493, 2009.
37. Chen J, Yan W, Setton LA: Molecular phenotypes of notochordal cells purified from immature nucleus pulposus. *Eur Spine J* 15 Suppl 3:S303-311, 2006.
38. Erwin WM, Las Heras F, Islam D, et al: The regenerative capacity of the notochordal cell: tissue constructs generated in vitro under hypoxic conditions. *J Neurosurg Spine* 10:513-521, 2009.

Gene expression profiling of early intervertebral disc degeneration

Lucas A. Smolders ^a, Frank M. Riemers ^a, Louis C. Penning ^a,
Niklas Bergknut ^{a,b}, Hendrik-jan C. Kranenburg ^a,
Herman A.W. Hazewinkel ^a, Guy C. M. Grinwis ^c,
Marian J. A. Groot-Koerkamp ^d, Björn P. Meij ^a, Marianna A. Tryfonidou ^a

Preliminary report

^a Department of Clinical Sciences of Companion Animals, Faculty of Veterinary Medicine, Utrecht University, Yalelaan 108, 3508 TD, Utrecht, The Netherlands

^b Department of Clinical Sciences, Division of Small Animals, Faculty of Veterinary Medicine and Animal Sciences, Swedish University of Agricultural Sciences, Sweden

^c Department of Pathobiology, Pathology Division, Faculty of Veterinary Medicine, Utrecht University, Yalelaan 108, 3508 TD, Utrecht, The Netherlands

^d Department of Physiological Chemistry, University Medical Center Utrecht, Utrecht, the Netherlands.

Abstract

Objective: Early degeneration of the intervertebral disc (IVD) is associated with a change in the nucleus pulposus (NP) cell population, with the native notochordal cell (NC) population being replaced by or differentiating into chondrocyte-like cells (CLCs). In this respect, the NC could be a NP progenitor cell and a target for disc regeneration strategies. As little is known about the biomolecular processes involved in early degeneration, this study investigated gene expression profiles in the healthy, NC-rich NP, the NP containing both NCs and CLCs, and the early degenerated, CLC-rich NP from dogs of both chondrodystrophic and non-chondrodystrophic breeds.

Methods: A two-color cDNA-microarray with a reference design experiment was performed to analyze the regulation of gene expression and the biomolecular pathways involved in early NP degeneration.

Results: Gene expression profiling revealed numerous pathways that were significantly up- or down-regulated, five of which were investigated further: 1) extracellular matrix remodeling, which revealed the expected modulation of different types of collagen, proteoglycans, and extracellular matrix enzymes during degeneration; 2) plasmin signaling and 3) plasminogen activator urokinase (PLAU) signaling, which together revealed decreased plasmin activity during degeneration; 4) Wnt-signaling and cytoskeleton remodeling, which revealed significant changes in Wnt-associated genes and actin/myosin expression; and 5) bone morphogenetic protein (BMP) signaling, which revealed increased BMP expression and associated BMP-signaling activity.

Conclusions: Biomolecular pathways involved in extracellular matrix synthesis, cell-matrix interactions, and cytoskeletal remodeling are altered during early IVD degeneration. These data are preliminary, and further investigations (reported in Chapter 5.4 of this thesis) are needed before valid conclusions can be drawn about the involvement of the various biomolecular pathways in the process of IVD degeneration.

Key words: intervertebral disc degeneration; notochordal cell; microarray; dog

Introduction

The spine is a fundamental structure in all vertebrates, providing flexibility, stability and durability. These characteristics are realized by the composition of the spine, with the individual vertebrae being interposed by fibrous, cushion-like structures, the intervertebral discs (IVDs) ¹⁻⁴. In both dogs and humans, degeneration of the IVD is considered the most important cause of spinal diseases, including cervical spondylomyelopathy, cervical and thoracolumbar disc disease, and degenerative lumbosacral stenosis ^{5,6}. In humans, degeneration of the IVD is one of the major causes of low back pain, a major health problem in the Western world ⁷⁻¹⁰. IVD disease can be treated conservatively with anti-inflammatory medication and physical therapy, and/or surgically with decompression by laminectomy combined with nucleotomy (removal of the diseased nucleus pulposus). Additional stabilization/fusion of the operated segment or restoration of spinal functionality can be achieved with IVD arthroplasty ¹¹⁻¹⁶. Although these surgical therapies are generally successful, they are associated with various complications, such as spinal instability, adjacent segment degeneration, and implant failure ¹⁷⁻²⁴. Moreover, the physiological function of the IVD is not restored. This has prompted interest in regenerative strategies aimed at restoring the health and function of the IVD. Regeneration of the IVD can be approached through several strategies, including the application of mesenchymal stromal cells or progenitor cells, growth factors, and/or gene therapy ²⁵⁻³¹.

Although the knowledge regarding cellular processes and biomolecular pathways involved in degeneration is increasing, there are still gaps in our knowledge ³²⁻³⁴. Regardless of the species, macroscopically the degenerative process appears to commence in the center of the IVD, i.e. in the nucleus pulposus (NP) ^{35,36}. Embryologically, the NP is derived from the notochord ³⁷, and in young individuals the predominant cell type of the NP is the notochordal cell (NC). NCs are characterized by their morphology, i.e. size, cytoplasmatic vesicles, and their organization in multicellular clusters ³⁸⁻⁴⁰, and by the expression of notochord-associated genes including *brachyury* and *cytokeratin 8* ^{32,41}. During maturation in some species, including humans, the NC is replaced by or differentiates into a smaller, chondrocyte-like cell (CLC), and this marks the onset of NP degeneration ⁴²⁻⁴⁵. Whether this is a physical replacement or differentiation of NCs into CLCs remains uncertain. The dog is unique in that two main types of breed can be distinguished in relation to the degenerative process, i.e. chondrodystrophic and non-chondrodystrophic dog breeds. The chondrodystrophic dog breeds, such as the Dachshund and the Beagle, are characterized by disproportionally short limbs relative to the length of the spine due to aberrant growth of the long bones ^{46,47}; conversely, the non-chondrodystrophic dog breeds, such as the German Shepherd Dog and the Dobermann, exhibit normal limb length. These two types of dog breed differ regarding the cell population of the NP and the onset and location of IVD

degeneration. In chondrodystrophic breeds, NCs are replaced by or differentiate into CLCs before the age of 1 year; in these breeds IVD degeneration starts before the age of 1 year and can be found throughout the entire spine. In contrast, in non-chondrodystrophic breeds, the NCs remain the predominant cell type of the NP throughout most of the lifespan; in these breeds, IVD degeneration develops later in life (6-8 years) and at spinal levels subjected to high workloads. Thus, NCs appear to maintain NP matrix health, and the disappearance of NCs accompanied by the simultaneous appearance of CLCs is strongly linked to the onset of IVD degeneration^{42,46,48,49}. Moreover, degeneration appears to have a mainly genetic cause in chondrodystrophic dogs and a physical cause, likely “wear and tear”, in non-chondrodystrophic dogs. Study of the gene expression patterns involved in the transition from a NC to a CLC population in the NP may provide insight into the pathways involved in early IVD degeneration and identify new targets for strategies to interfere or reverse the degenerative process in both canine and human patients. In the current preliminary report, we analyzed gene expression profiles in chondrodystrophic and non-chondrodystrophic dogs, concentrating on the processes involved in early IVD degeneration.

Materials and methods

Ethics statement

All materials used in this study were collected from animals euthanized in other, unrelated experiments approved by the Ethics Committee on Animal Experimentation (DEC) of Utrecht University. Canine IVD tissue was collected from dogs euthanized in studies investigating osteoarthritis (Experiment numbers DEC 2007.III.08.110 and DEC 2009.III.05.037; euthanasia performed by way of an intravenous overdose of pentobarbital)⁵⁰⁻⁵² and cardiovascular disease (Experiment number DEC 2007.II.01.029; euthanasia performed under general anesthesia by way of fibrillation and subsequent excision of the heart)⁵³ (and other, unpublished work). All experimental procedures were performed strictly according the guidelines set by the Ethics Committee of Utrecht University. The Ethics Committee of Utrecht University approved post-mortem harvesting of the IVD tissue employed in the present study.

Sample collection

Cervical (C2-T1) and thoracolumbar (T10-S1) spines were collected from five mongrel dogs (non-chondrodystrophic group; age range, 13-60 months; body weight range, 26.6-32.1 kg) and six Beagle dogs (chondrodystrophic group; age range 25-36 months, weight range, 13.6-16.0 kg). Spines were resected *en bloc* and cut into single functional spinal units (FSUs; endplate-IVD-endplate). Each FSU was cut in the sagittal plane into two equal parts. The NP was collected from one part, snap frozen in liquid nitrogen, and stored at -70 °C.

The other part was fixed in 4% neutral buffered formaldehyde, decalcified in 10% ethylenediaminetetraacetic acid (EDTA) for 3 months at room temperature, and embedded in paraffin.

Histopathological classification

To optimally investigate mRNA expression patterns associated with NC maintenance and replacement of NCs by CLCs, histopathological classification was performed as described previously⁵⁴. Mid-sagittal sections (4 μ m) were mounted on Microscope KP+ slides (Klinipath B.V) and stained with hematoxylin and eosin (H&E). Composite raw images of each IVD were made using a Colorview IIIU digital camera (Olympus) mounted to a BX-40 microscope (Olympus). The images were scaled and the following parameters were measured for the NP: 1) Proportion (%) of NP surface area and pericellular matrix consisting of NCs: NCs were identified based on morphologic characteristics^{39,45}; 2) Proportion of NP surface area consisting of CLCs and fibrocartilaginous matrix. Samples were classified by a board certified veterinary pathologist into a notochordal cell-rich (NC-rich) group (> 90% of surface area consisting of NCs), a Mixed group (cell population consisting of both NCs and CLCs, with 10-90% of surface area consisting of NCs), and a chondrocyte-like cell-rich (CLC-rich) group (> 90% of surface area consisting of CLCs and corresponding matrix) (Fig. 1).

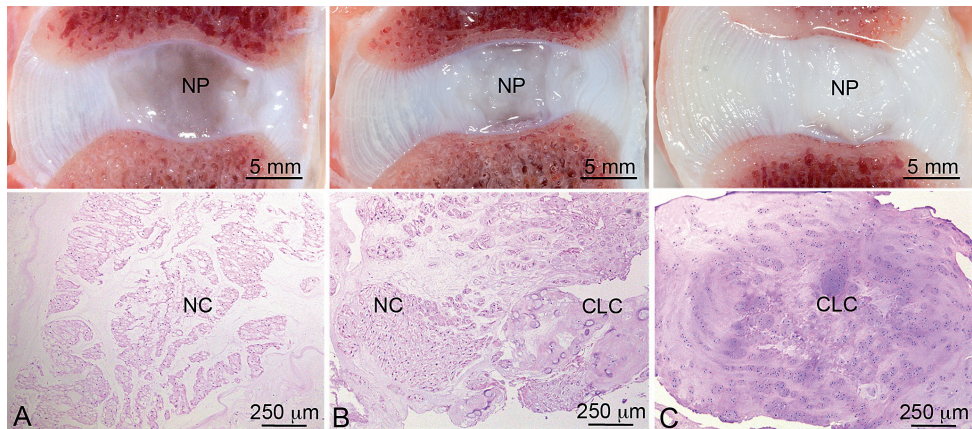


Figure 1. Typical macroscopic pictures and corresponding H&E sections of the applied classification. The notochordal cell (NC)-rich nucleus pulposus (NP) (A) contains NCs with a viable morphology organized in clusters; the Mixed group (B) contains both NCs and chondrocyte-like cells (CLC); and the CLC-rich group (C) contains solely CLCs embedded in a dense matrix.

To further assess the cellular phenomenon involving the transition from NC-rich to CLC-rich NP, and thus the applied classification, the gene expression of the notochordal markers *brachyury*^{32,55} and *cytokeratin 8*^{41,56} was investigated in all groups (by way of qPCR analysis; see Chapter 5.4 of this thesis).

DNA microarray analysis

Four NPs from the three histopathological groups for each breed type were randomly selected and used to isolate total RNA, using the RNeasy Fibrous Tissue Mini Kit (Qiagen) according to the manufacturer's instructions. After on-column DNase-I treatment (Qiagen RNase-free DNase kit), RNA was quantified spectrophotometrically using Nanodrop ND-1000 (Isogen Life Science) and RNA integrity was determined using a Bioanalyzer 2100 (Agilent Technologies). RNA integrity numbers of the samples varied from 4.5 to 7.4.

A two-color DNA microarray with a reference experiment design was performed on 44 k Canine Gene Expression Microarrays V1 (G2519F, Agilent Technologies)⁵⁷. Double round RNA amplification and labeling were performed as described before⁵⁸ on an automated system (Caliper Life Sciences) with 10-50 ng total RNA input from each sample. The common RNA reference pool consisted of a multitude of canine organs, including liver, spleen, kidney, lung, heart, intestine, and bone. Hybridizations were performed on an HS4800PRO system with QuadChambers (Tecan Benelux B.V.B.A.), using 300-500 ng labeled cRNA per channel as described previously⁵⁹. From each group two samples were labeled with Cy5 and hybridized against the common reference cRNA (Cy3) on dual channel arrays, and two samples was hybridized in dye swap. Hybridized slides were scanned on an Agilent scanner (G2565BA) at 100% laser power, 100% PMT. After automated data extraction using Imagene 8.0 (BioDiscovery), printtip Loess normalization was performed⁶⁰ on mean spot intensities. Dye bias was corrected based on a within-set estimate⁶¹.

Patterns of gene expression were compared between the three stages of IVD degeneration (NC-rich, Mixed, CLC-rich NP) within each breed type and between the two breed types. Data were analyzed using microarray analysis of variance (MAANOVA)⁶². In a fixed effect analysis, sample, array, and dye effects were modeled. P values were determined with a permutation F2-test, in which residuals were shuffled 5000 times globally. Genes with $P < 0.05$ after a Benjamini-Hochberg determination of false discovery rate (FDR) were considered significantly changed; a change cutoff value of 1.3-fold was applied.

Differentially expressed genes were converted to their human homologues, the following array comparisons were included in functional pathway analysis using the GeneGo MetaCore platform⁶³: 1) NC-rich group vs. Mixed group, Mixed group vs. CLC-rich group, and NC-rich group vs. CLC-rich group in both chondrodystrophic and non-chondrodystrophic dogs; 2) non-chondrodystrophic vs. chondrodystrophic breeds: NC-rich group, Mixed group, and CLC-rich group.

Results

Cell type distribution in relation to histopathological classification

In NPs from non-chondrodystrophic dogs, the NC-rich, Mixed, and CLC-rich groups consisted of 100.0% NCs, 45.4%-87.0% NCs, and 100.0% CLCs, respectively; in NPs from chondrodystrophic dogs, these proportions were 93.9%-100.0% NCs, 39.7%-89.9% NCs, and 100.0% CLCs, respectively. Therefore, the applied histopathological classification resulted in the NC-rich, Mixed, and CLC-rich groups being comparable between chondrodystrophic and non-chondrodystrophic dogs, allowing reliable investigation of early IVD degeneration within both types of breed, and comparison between the two types of breed.

In chondrodystrophic dogs, gene expression of *brachyury* and *cytokeratin-8* was significantly down-regulated in the CLC-rich compared with the NC-rich and Mixed groups. In non-chondrodystrophic dogs, qPCR analysis of the notochordal markers *brachyury* and *cytokeratin-8* showed no significant differences between the different stages of degeneration in non-chondrodystrophic dogs. *Brachyury* and *cytokeratin-8* gene expression was significantly lower in the chondrodystrophic, CLC-rich NP than in the non-chondrodystrophic, CLC-rich NP (for additional information and figures: see Chapter 5.4 of this thesis).

Gene expression regulation

Comparison of gene expression patterns in the three histological groups and the chondrodystrophic and non-chondrodystrophic groups revealed several genes that were significantly up-regulated and down-regulated (after Benjamini-Hochberg false discovery rate correction). In the chondrodystrophic group, 712 genes were significantly down-regulated and 570 genes were up-regulated in the Mixed group compared with the NC-rich group, and 1741 genes were significantly down-regulated and 1178 genes were up-regulated in the CLC-rich group compared with the NC-rich group; 1173 genes were down-regulated and 1121 genes were up-regulated in the CLC-rich group compared with the Mixed group.

In the non-chondrodystrophic group, 11 genes were down-regulated and 11 genes were up-regulated in the Mixed group compared with the NC-rich group, and 2 genes were down-regulated and no genes were up-regulated in the CLC-rich group compared with the NC-rich group; there were no differences between the CLC-rich and the Mixed groups.

Compared with the non-chondrodystrophic group, in the chondrodystrophic group 562, 248, and 6 genes were significantly down-regulated in the NC-rich, Mixed, and CLC-rich groups, respectively, and 1241, 604, and 6 genes were significantly up-regulated, respectively.

Genego pathway map analysis

Intra-breed comparisons in the non-chondrodystrophic breed group were not included in the pathway analysis because relatively few genes were down-or up-regulated in this breed group.

The following pathways were selected on the basis of significance and common involvement in pathways/signaling events of the performed arrays:

- Cell adhesion: extracellular matrix (ECM) remodeling.
- Cell adhesion: plasmin signaling.
- Cell adhesion: plasminogen activator urokinase (PLAU) signaling.
- Wnt signaling and cytoskeletal remodeling.
- Bone morphogenetic protein (BMP) signaling.

Cell adhesion: extracellular matrix remodeling

The gene expression of *collagen I*, *versican*, and *laminin subunit beta 1 (lamb1)* was significantly down-regulated and the gene expression of *laminin subunit beta 2 (lamb2)* and *kallikrein-related peptidase 1* was significantly up-regulated in the Mixed group compared with the NC-rich group (Table 1). The gene expression of *laminin subunit alfa 4 (lama4)*, *lamb2*, *laminin subunit gamma 1 (lamc1)*, and *kallikrein-related peptidase 1* was significantly down-regulated and the gene expression of *collagen I*, *collagen III*, *collagen IV*, *versican*, *tissue inhibitor of metalloprotease 2 (timp2)*, *matrix metalloprotease (mmp) 12*, and *syndecan 2* was significantly up-regulated in the CLC-rich group compared with the Mixed group. The gene expression of *collagen II*, *lama4*, *lamb2*, *kallikrein peptidase 1*, *alfa-1beta-1 integrin*, and *ezrin* was significantly down-regulated and the gene expression of *collagen III*, *collagen IV*, *osteonectin*, *versican*, *laminin subunit alfa 1 (lama1)*, *tissue inhibitor of metalloprotease 1 (timp1)*, *mmp9*, *mmp12*, and *syndecan 2* gene expression was significantly up-regulated in the CLC-rich group compared with the NC-rich group.

In the NC-rich group, the gene expression of *collagen II*, *collagen III*, *versican*, *lamb1*, and *ezrin* was significantly higher and the gene expression of *lama4*, *lamc1*, *kallikrein peptidase 1*, and *interleukin-8 (il-8)* was significantly lower in the chondrodystrophic group than in the non-chondrodystrophic group (Table 2), and in the Mixed group the gene expression of *lam1* and *lama4* was significantly higher and the gene expression of *collagen IV* was significantly lower in the chondrodystrophic group than in the non-chondrodystrophic group. There were no differences in gene expression in the CLC-rich group between the non-chondrodystrophic and the chondrodystrophic groups.

Cell adhesion: extracellular matrix remodeling								
Gene	Function/action in pathway	NC-rich vs.		Mixed vs.		NC-rich vs.		
		Mixed		CLC-rich		CLC-rich		
		N	P	N	P	N	P	
E	<i>collagen I</i>	Extracellular matrix protein	-1.75	0.007	2.31	0.029	--	--
	<i>collagen II</i>	Extracellular matrix protein	--	--	--	--	-2.04	0.002
	<i>collagen III</i>	Extracellular matrix protein	--	--	4.75	<0.001	2.38	<0.001
	<i>collagen IV</i>	Extracellular matrix protein	--	--	1.93	0.015	1.87	0.009
	<i>osteonectin</i>	Extracellular matrix protein	--	--	--	--	1.49	0.011
	<i>versican</i>	Extracellular matrix proteoglycan; activates CD44 transmembrane receptor	-2.73	<0.001	1.84	0.006	2.14	0.018
	<i>laminin subunit alfa 1 (lama1)</i>	Extracellular matrix protein	--	--	--	--	0.82	<0.001
	<i>laminin subunit alfa 4 (lama4)</i>	Activates syndecan 2 receptor	--	--	-2.75	<0.001	-1.52	0.002
	<i>laminin subunit beta 1 (lamb1)</i>	Extracellular matrix protein	-1.58	0.030	--	--	--	--
	<i>laminin subunit beta 2 (lamb2)</i>	Extracellular matrix protein	1.30	0.019	-2.13	<0.001	-1.58	0.005
	<i>laminin subunit gamma 1 (lamc1)</i>	Extracellular matrix protein	--	--	-1.52	0.032	--	--
	<i>tissue inhibitor of matrix metalloproteinase 2</i>	Inhibits matrix metalloproteinase (MMP) 1 and 13	--	--	--	--	1.84	0.003
	<i>(timp 1)</i>							
	<i>tissue inhibitor of matrix metalloproteinase 2</i>	Inhibits matrix metalloproteinase (MMP) 13	--	--	1.52	0.020	--	--
	<i>(timp 2)</i>							
	<i>matrix metalloproteinase (mmp) 9</i>	Cleaves versican, collagen I, collagen III, and collagen IV	--	--	--	--	1.78	0.044
	<i>matrix metalloproteinase (mmp) 12</i>	Cleaves vitronectin and laminin 1	--	--	2.14	0.007	1.78	0.022
	<i>kallikrein related peptidase 1</i>	Activates matrix metalloproteinase 9	1.47	0.003	-1.1	<0.001	-1.78	0.048
M	<i>syndecan 2</i>	Activates ezrin	--	--	5.70	0.004	2.12	<0.001
	<i>alfa-1 beta-1 integrin</i>	Involved in integrin outside-in signaling	--	--	--	--	-2.43	0.004
C	<i>ezrin</i>	Plasma membrane-actin skeleton intermediate	--	--	--	--	-1.53	0.048

Table 1: *N*-fold changes (*N*) and *P*-values (*P*) for significant up- and down-regulation of gene expression involved in the Cell adhesion: extracellular matrix remodeling pathway for the comparisons between notochordal cell (NC)-rich group, Mixed group, and chondrocyte-like cell (CLC)-rich group within the chondrodystrophic breed group. In each comparison, gene regulation is expressed relative to the least degenerated group (reference). E = extracellular protein; M= membranous protein; C = cytoplasmic; -- = no significant regulation.

Cell adhesion: extracellular matrix remodeling									
Chondrodystrophic vs. non-chondrodystrophic									
Gene	Function/action in pathway	NC-rich		Mixed		CLC-rich			
		N	P	N	P	N	P		
E	<i>collagen II</i>	Extracellular matrix protein	1.82	0.002	--	--	--	--	
	<i>collagen III</i>	Extracellular matrix protein	2.68	0.024	--	--	--	--	
	<i>collagen IV</i>	Extracellular matrix protein	--	--	-1.55	<0.001	--	--	
	<i>laminin 1 (lam1)</i>	Extracellular matrix protein	--	--	1.61	0.030	--	--	
	<i>versican</i>	Activates CD44 transmembrane receptor	2.60	0.009	--	--	--	--	
	<i>laminin subunit alfa 4 (lama4)</i>	Activates syndecan 2 receptor	-1.75	0.003	2.20	0.004	--	--	
	<i>laminin subunit b1 (lamb1)</i>	Extracellular matrix protein	1.61	0.005	--	--	--	--	
	<i>laminin subunit gamma 1 (lamc1)</i>	Extracellular matrix protein	-1.55	0.019	--	--	--	--	
	<i>kallikrein related peptidase 1</i>	Activates matrix metalloprotease 9	-1.62	0.004	--	--	--	--	
	C	<i>ezrin</i>	Cell plasma membrane-- actin skeleton intermediate, activates CD44 receptor	1.78	0.007	--	--	--	--

Table 2: *N*-fold changes (*N*) and *P*-values (*P*) for significant differences between the chondrodystrophic dog and the non-chondrodystrophic dog (reference) in gene expression involved in the cell adhesion: extracellular matrix remodeling pathway for the notochordal cell (NC) -rich group, Mixed group, and chondrocyte-like cell (CLC) -rich group. E = extracellular protein; C = cytoplasmic protein; -- = no significant regulation.

Plasmin signaling

		<i>Chondrodystrophic NC-rich — Mixed— CLC-rich</i>						
Gene	Function/action in pathway	NC-rich vs. Mixed		Mixed vs. CLC-rich		NC-rich vs. CLC-rich		
		N	P	N	P	N	P	
E	<i>c1 inhibitor</i>	Inhibits plasmin	--	--	5.94	0.003	5.06	<0.001
	<i>neuroserpin</i>	Inhibits plasmin	--	--	2.55	0.013	--	--
	<i>vascular endothelial growth factor a (vegfa)</i>	Activates vascular endothelial growth factor a receptor→ AKT signaling	--	--	-1.99	0.023	--	--
M	<i>laminin a1 (lama1)</i>	Cell-matrix interaction	--	--	--	--	-1.77	0.011
	<i>laminin b1 (lamb1)</i>	Cell-matrix interaction	-1.58	0.030	--	--	--	--
	<i>laminin b2 (lamb2)</i>	Cell-matrix interaction	1.30	0.044	-2.04	<0.001	-1.58	0.005
	<i>laminin c1 (lamc1)</i>	Cell-matrix interaction	--	--	-1.52	0.032	--	--
	<i>collagen IV</i>	Cell-matrix interaction	--	--	1.93	0.015	1.88	0.009
	<i>fibrinogen</i>	Cleavage of fibrinogen by MMP13 → fibrinolysis	-1.48	0.030	3.58	0.008	--	--
C	<i>phosphatidylinositol 3-kinase subgroup 1A, regulatory subunit (pi3k reg1a)</i>	Activates phosphatidylinositol 3-kinase subgroup 1A, catalytic subunit (P13Kcat 1A)	--	--	-1.66	0.032	-1.87	0.007
	<i>transforming growth factor-beta-activated kinase 1 (tak1/map3k7)</i>	Promotes mitogen-activated protein kinase p38 gamma (p38/MAPK)-signaling	--	--	--	--	-1.43	0.033

Table 3: N-fold changes (N) and P-values (P) for significant up- and down-regulation of gene expression involved in the plasmin signaling pathway for the comparisons between notochordal cell (NC)-rich group, Mixed group, and chondrocyte-like cell (CLC)-rich group within the chondrodystrophic breed group. In each comparison, gene regulation is expressed relative to the least degenerated group (reference). E = extracellular protein; M=membranous protein; C= cytoplasmic protein; -- = no significant regulation.

Plasmin signaling

The gene expression of *lamb1*, and *fibrinogen* gene expression was significantly down-regulated and that of *laminin b2 (lamb2)* was significantly up-regulated in the Mixed group compared with the NC-rich group (Table 3). The expression of *vascular endothelial growth factor a (vegfa)*, *lamb2*, *lamc1*, and *phosphatidylinositol 3-kinase subgroup 1a regulatory subunit (pi3kreg1a)* was significantly down-regulated and the gene expression of *c1 inhibitor*, *neuroserpin*, *collagen IV*, and *fibrinogen* was significantly up-regulated in the CLC-rich group compared with the Mixed group. The gene expression of *lamal*, *lamb2*, *p13kreg1a*, and *transforming growth factor-beta-activated kinase 1 (tak1)* was significantly down-regulated and the gene expression of *c1 inhibitor* and *collagen IV* was significantly up-regulated in the CLC-rich group compared with the NC-rich group.

In the NC-rich group, the gene expression of *neuroserpin*, *vegfa*, *lamb1*, *phosphatidylinositol-3-kinase subgroup 1a catalytic subunit (pi3kcat1a)*, and *tak1* was significantly higher and the gene expression of *plat*, *transforming growth factor beta 1 (tgf- β 1)*, and *tgf- β receptor III* was significantly lower in the chondrodystrophic group than in the non-chondrodystrophic group (Table 4). In the Mixed group, the gene expression of *vegfa* and *tak1* was significantly higher and the gene expression of *fibrinogen*, *collagen IV* and *pi3kreg1a* was significantly lower in the chondrodystrophic group than in the non-chondrodystrophic group. In the CLC-rich group, the gene expression of *neuroserpin* was significantly higher in the chondrodystrophic group than in the non-chondrodystrophic group.

Table 4: *N-fold change (N) and P-values (P) for significant differences between the chondrodystrophic dog compared with the non-chondrodystrophic dog (reference) in gene expression involved in the plasmin signaling pathway for the notochordal cell (NC)-rich group, Mixed group, and chondrocyte-like cell (CLC)-rich group. -- = no significant regulation.*

Plasmin signaling

Chondrodystrophic vs. non-chondrodystrophic

Gene	Function/action in pathway	NC-rich		Mixed		CLC-rich	
		N	P	N	P	N	P
E <i>plasminogen activator (plat)</i>	Converts plasminogen to plasmin	-1.36	0.044	--	--	--	--
<i>neuroserpin</i>	Inhibits plasmin	3.36	<0.001	--	--	5.17	<0.001
<i>transforming growth factor beta (tgf-β)-1</i>	Activates transforming growth factor receptor I and II	-1.34	0.043	--	--	--	--
<i>vascular endothelial growth factor a (vegfa)</i>	Activates vascular endothelial growth factor a receptor→ AKT signaling	2.71	<0.001	2.08	0.004	--	--
M <i>transforming growth factor beta receptor III (betaglycan)</i>	Activates transforming growth factor beta-1 and transforming growth factor receptor Type I	-1.56	0.029	--	--	--	--
<i>laminin b1(lamb1)</i>	Cell-matrix interaction	1.61	0.005	--	--	--	--
<i>fibrinogen</i>	Cleavage of fibrinogen by MMP13 → fibrinolysis	--	--	-1.80	0.015	--	--
<i>collagen IV</i>	Cell-matrix interaction	--	--	-2.93	<0.001	--	--
C <i>phosphatidylinositol 3-kinase subgroup 1A, regulatory subunit (pi3kreg1a)</i>	Activates Phosphatidylinositol 3-kinase subgroup 1A, catalytic subunit (P13K cat 1A)	--	--	-1.60	0.011	-	-
<i>phosphatidylinositol 3-kinase subgroup 1a, catalytic subunit (p13k cat 1a)</i>	Involved in v-akt murine thymoma viral oncogene homolog 2 (AKT) – signaling→ regulates cell cycle progression and apoptosis	1.44	0.015	--	--	--	--
<i>transforming growth factor-beta-activated kinase 1 (tak1/map3k7)</i>	Promotes mitogen-activated protein kinase p38 gamma (p38/ MAPK)- signaling	1.56	0.016	1.51	0.046	--	--

PLAU signaling

The gene expression of *casein-linked kinase II alpha chains* was significantly down-regulated and the gene expression of *pai1* and *epidermal growth factor receptor (egfr)* was significantly up-regulated in the Mixed group compared with the NC-rich group (Table 5). The gene expression of *pai1*, *epidermal growth factor (egf)*, *egfr*, *hepatocyte growth factor receptor (hgfr)*, *casein-linked kinase II alpha chains*, *pi3kreg1a*, and *growth factor receptor bound protein 2-associated protein 1 (gab1)* was significantly down-regulated and the expression of *protein c inhibitor* and *pai2* was significantly up-regulated in the CLC-rich group compared with the Mixed group. The gene expression of *egf*, *casein-linked kinase II alpha chains*, *casein-linked kinase II beta chain*, *pi3reg1a*, *gab1*, and *integrin linked kinase 1 (ilk1)* was significantly down-regulated and the gene expression of *protein c inhibitor*, *pai2*, and *egfr* was significantly up-regulated in the CLC-rich group compared with the NC-rich group.

In the NC-rich group, the gene expression of *pai2*, *casein-linked kinase alpha chains*, *egfr*, *pi3kcat1a*, *gab1*, and *janus kinase 1 (jak1)* was significantly higher and the gene expression of *plat* and *pai1* was significantly lower in the chondrodystrophic group than in the non-chondrodystrophic group (Table 6). In the Mixed group, the gene expression of *egfr* and *gab1* was significantly higher and the gene expression of *pi3kreg1a* was significantly lower in the chondrodystrophic group than in the non-chondrodystrophic group. In the CLC-rich group, there were no differences in gene expression between the chondrodystrophic and the non-chondrodystrophic groups.

Table 5: *N*-fold changes (*N*) and *P*-values (*P*) for significant up- and down-regulation of gene expression involved in the PLAU signaling pathway for the comparisons between notochordal cell (NC)-rich group, Mixed group, and chondrocyte-like cell (CLC)-rich group within the chondrodystrophic breed group. In each comparison, gene regulation is expressed relative to the least degenerated group (reference). E = extracellular protein; M = membranous protein; C = cytoplasmic protein; -- = no significant regulation.

PLAU signaling

Chondrodystrophic: NC-rich – Mixed – CLC-rich

Gene	Function/action in pathway	NC-rich vs. Mixed		Mixed vs. CLC-rich		NC-rich vs. CLC-rich	
		N	P	N	P	N	P
E <i>protein C inhibitor</i>	Inhibits plasminogen activator, urokinase (PLAU)	--	--	3.23	0.010	4.96	<0.001
<i>plasminogen activator (pai) 1</i>	Inhibits plasminogen activator, urokinase (PLAU)	1.42	0.008	-3.63	0.049	--	--
<i>plasminogen activator inhibitor 2 (pai2/serpin2)</i>	Inhibits plasminogen activator, urokinase (PLAU)	--	--	1.75	0.022	2.30	0.027
<i>epidermal growth factor (egf)</i>	Activates epidermal growth factor receptor (EGFR)	--	--	-1.53	0.040	-1.57	0.017
M <i>epidermal growth factor receptor (egfr)</i>	Activates focal adhesion kinase 1, proto oncogen s-SCR, and SRC transforming protein 1	1.53	<0.001	-1.28	0.001	1.60	0.001
<i>hepatocyte growth factor receptor (met) (hgfr)</i>	Activates phosphatidylinositol 3-kinase subgroup 1A, regulatory subunit (pi3kreg1A)--Akt signaling	--	--	-1.42	0.03	--	--
<i>casein linked kinase II alpha chains</i>	Activates nucleolin en vitronectin	-1.68	0.006	-1.79	0.032	-1.87	0.02
<i>casein linked kinase beta chains</i>	Activates casein linked kinase alpha	--	--	--	--	-1.99	0.028
C <i>phosphatidylinositol 3-kinase subgroup 1A, regulatory subunit (pi3k reg1A)</i>	Activates Phosphatidylinositol 3-kinase subgroup 1A, catalytic subunit (P13Kcat1A)	--	--	-1.60	0.032	-1.87	0.007
<i>growth factor receptor bound protein 2-associated protein 1 (gab1)</i>	Activates Phosphatidylinositol 3-kinase subgroup 1A, regulatory subunit (PI3Kreg1A)	--	--	-1.45	0.023	-1.48	0.010
<i>integrin linked kinase1 (ilk1)</i>	Activates v-akt murine thymoma viral oncogene homolog 2 (AKT)	--	--	--	--	-1.61	0.048

PLAU signaling

Chondrodystrophic vs. non-chondrodystrophic

Gene	Function/action in pathway	NC-rich vs.		Mixed vs.		NC-rich vs.	
		Mixed		CLC-rich		CLC-rich	
		N	P	N	P	N	P
E <i>plasminogen activator (plat)</i>	converts plasminogen to plasmin (promotes fibrinolysis through mmps)	-0.44	0.044	--	--	--	--
	<i>plasminogen activator inhibitor 1 (pai-1/serpin 1)</i>	-0.54	0.024	--	--	--	--
	<i>plasminogen activator inhibitor 2 (pai-2/serpin 2)</i>	2.36	0.002	--	--	--	--
	<i>casein linked kinase alpha chains</i>	1.87	0.010	--	--	--	--
M <i>epidermal growth factor receptor(egfr)</i>	Activates Focal Adhesion Kinase 1, proto oncogen s-SCR, and SRC transforming protein 1	1.69	0.001	1.95	<0.001	--	--
	<i>phosphatidylinositol 3-kinase subgroup 1A, regulatory subunit (pi3kreg1a)</i>	--	--	-1.60	0.011	--	--
	<i>phosphatidylinositol 3-kinase subgroup 1A, catalytic subunit (pi3k cat1A)</i>	1.44	0.015	--	--	--	--
	<i>growth factor receptor bound protein 2-associated protein 1 (gab1)</i>	2.14	0.003	2.06	<0.001	--	--
	<i>janus kinase 1 (jak1)</i>	1.34	0.043	--	--	--	--
C <i>growth factor receptor bound protein 2-associated protein 1 (gab1)</i>	Activates signal inducer and activator of transcription 1 (STAT1)	--	--	-1.45	0.023	-1.48	0.010
	Activates Phosphatidylinositol 3-kinase subgroup 1A, regulatory subunit (PI3Kreg1A)	--	--	--	--	-1.61	0.048
	Activates v-akt murine thymoma viral oncogene homolog 2 (AKT)	--	--	--	--	--	--

Table 6: *N*-fold changes (*N*) and *P*-values (*P*) for significant differences between the chondrodystrophic dog compared with the non-chondrodystrophic dog (reference) in gene expression involved in the PLAU signaling pathway for the notochordal cell (NC)-rich group, Mixed group, and chondrocyte-like cell (CLC)-rich group. E = extracellular protein; M = membranous protein; C = cytoplasmic protein -- = no significant regulation.

Wnt signaling and cytoskeletal remodeling

The gene expression of *tal**in*, *destrin*, *ras-related c3 botulinum toxin substrate 1*, and *alpha actinin* was significantly down-regulated and the gene expression of *wnt7b*, *wnt10b*, *lim kinase 2 (limk2)*, and *myosin II light chain (melc)* was significantly up-regulated in the Mixed group compared with the NC-rich group (Table 7). The gene expression of *low-density lipoprotein receptor-related protein 5 (lrp5)*, *p13kreg1a*, *dedicator of cytokinesis 1 (dock1)*, *p21-activated kinase 1 (pak1)*, *actin beta/cytoskeletal*, *melc*, and *myosin regulatory light chain (mrlc)* was significantly down-regulated and the gene expression of *wnt inhibitory factor 1 (wif1)*, *limk2*, *actin-related protein 2/3 complex (arp2/3)*, and *myosin phosphatase target subunit 1 (mlcp reg)* was significantly up-regulated in the CLC-rich group compared with the Mixed group. The gene expression of *lrp5*, *caveolin-1*, *ilk*, *tak1*, *pi3kreg1a*, *tal**in*, *alpha actinin*, *arp2/3*, *actin beta/cytoskeletal*, *dock1*, *pak1*, and *mrlc* was significantly down-regulated and the gene expression of *wnt10b*, *limk2*, *mlcp (reg)*, *melc*, and *cellular tumor antigen p53 (p53)* was significantly up-regulated in the CLC-rich group compared with the NC-rich group.

Wnt signaling and cytoskeletal remodeling

Chondrodystrophic NC-rich – Mixed – CLC-rich

Gene	Function/action in pathway	NC-rich vs.		Mixed vs.		NC-rich vs.	
		Mixed		CLC-rich		CLC-rich	
		N	P	N	P	N	P
E <i>wnt 7b</i>	Activates low density lipoprotein receptor related protein 5 (LRP5) and frizzled receptors	1.43	0.027	--	--	--	--
<i>wnt 10b</i>	Activates low density lipoprotein receptor related protein 5 (LRP5) and frizzled receptors	2.55	0.016	--	--	2.07	0.010
<i>wnt inhibitory factor (wif) 1</i>	Inhibits wnt ligands	--	--	3.65	0.030	--	--
M <i>low density lipoprotein receptor related protein 5 (lrp5)</i>	Binding of Wnt ligand→ Wnt signaling activation	--	--	-3.65	0.005	-2.73	0.001
C <i>caveolin-1</i>	Activates integrin linked kinase (ILK)	--	--	-1.76	0.015	-2.01	0.006
<i>integrin-linked kinase (ilk)</i>	Inhibits GSK-3-beta→ activates Wnt signaling.	--	--	--	--	-1.61	0.049
<i>transforming growth factor-beta-activated kinase 1 (tak1)</i>	Activates nemo like kinase (NLK)→ inhibits Wnt signaling	--	--	--	--	-1.43	0.033
<i>Phosphatidylinositol 3-kinase subgroup 1A, catalytic subunit (pi3kreg1a)</i>	Activates phosphatidylinositol 3-kinase subgroup 1A, catalytic subunit (P13Kcat 1A)	--	--	-1.66	0.032	-1.88	0.007
<i>talin</i>	Promotes ATP signaling	-1.42	0.020	--	--	-1.67	0.002
<i>destrin</i>	Inhibits actin-beta	-1.59	0.025	--	--	--	--
<i>lim kinase 2 (limk2)</i>	Activates destrin	1.51	0.026	1.45	0.048	1.61	0.019
<i>actin related protein 2/3 complex (arp2/3)</i>	Activates actin, cytoskeletal	--	--	1.51	0.017	-1.51	0.016
<i>alpha actinin</i>	Activates actin, beta	-1.99	<0.001	--	--	-1.75	0.004
<i>actin,beta/ Actin, cytoskeletal</i>	Involved in cell motility, structure, and integrity.	--	--	-2.69	0.007	-2.69	0.004

<i>myosin phosphatase target subunit 1 (mlcp reg)</i>	Activates myosin light chain phosphatase (MLCP)→ induces mysosin light chain (MELC and MRLC) inhibition	--	--	1.62	0.002	1.62	0.005
<i>dedicator of cytokinesis protein (dock)-1</i>	Activates ras-related C3 botulinum toxin substrate 1 (Rac-1) →activates p21 activated kinase	--	--	-2.14	0.018	-2.62	0.004
<i>p21 activated kinase (pak)-1</i>	Activates myosin regulatory light chain (MELC)	--	--	-2.71	0.004	-2.58	0.003
<i>myosin II light chain (melc)</i>	Cytoskeletal component	1.44	0.049	-2.18	0.032	2.00	<0.001
<i>myosin regulatory light chain (mrlc)</i>	Cytoskeleton regulation	--	--	-7.21	0.02	-2.10	<0.001
<i>cellular tumor antigen p53 (p53)</i>	Regulates target genes that induce cell cycle arrest, apoptosis, senescence, DNA repair.	--	--	--	--	1.39	0.023

Table 7: *N*-fold changes (*N*) and *P*-values (*P*) for significant up- and down-regulation of gene expression involved in the *Wnt*, and cytoskeletal remodeling pathway for the comparisons between notochordal cell (NC)-rich group, Mixed group, and chondrocyte-like cell (CLC)-rich group within the chondrodystrophic breed group. In each comparison, gene regulation is expressed relative to the least degenerated group (reference). *E* = extracellular protein; *M* = membranous protein; *C* = cytoplasmic protein; -- = no significant regulation.

In the NC-rich group, the gene expression of *pi3kcat1a*, *tak1*, *nemo-like kinase (nlk)*, *dextrin*, *arp2/3*, *alpha actinin*, and *mrlc* was significantly higher and that of *wnt10b*, *talin*, and *melc* was significantly lower in the chondrodystrophic group than in the non-chondrodystrophic group (Table 8). In the Mixed group, the gene expression of *tak1*, *actin beta/cytoskeleton*, *melc* was significantly higher and the gene expression of *pi3kreg1a*, *myosin light chain kinases (mylk and mlck)* was significantly lower in chondrodystrophic group than in the non-chondrodystrophic group. In the CLC-rich group, there were no significant differences in gene expression between the chondrodystrophic group and the non-chondrodystrophic group.

BMP signaling

No significant differences in gene expression were found between the NC-rich group and Mixed group for this pathway (Table 9). Early NP degeneration involved significant down-regulation of gene expression of *mothers against decapentaplegic homolog 6 (smad6)* and *tak1* (only for NC-rich vs CLC-rich),

and significant up-regulation of gene expression of *bmp2*, *bmp4* (only for Mixed vs CLC-rich), *bmp6*, *transducer of erb-2 (tob1)*, and *smad specific E3 ubiquitin protein ligase 2 (smurf2)*.

In the NC-rich group, the gene expression of *gremlin*, *bmp6*, *activin a receptor 2 (alk2)*, *tak1*, and *tob1* was significantly higher in the chondrodystrophic group than in the non-chondrodystrophic group (Table 10). In the Mixed group, the gene expression of *gremlin*, *bmp6*, *alk2* and *tak1* was significantly higher and that of *bmp2* was significantly lower in the chondrodystrophic group than in the non-chondrodystrophic group. In the CLC-rich group, the gene expression of *tob1* was significantly higher in the chondrodystrophic group than in the non-chondrodystrophic group.

Discussion

In order to develop new strategies for disrupting or reversing the processes involved in IVD degeneration, we analyzed the gene expression profile of healthy, NC-rich NP tissue and compared it with that of NP tissue in the early stages of IVD degeneration. Typically, healthy canine NP mainly consists of NCs, both in chondrodystrophic and non-chondrodystrophic breeds. The chondrification of the NP is regarded as an initiating step in the process of IVD degeneration, involving the replacement of the native NC population by CLCs⁴²; the Mixed and CLC groups identified in this study represent early and progressive phases of IVD degeneration, respectively

Wnt Signaling and cytoskeletal remodeling

Chondrodystrophic vs. non-chondrodystrophic

Gene	Function/action in pathway	NC-rich		Mixed		CLC-rich	
		N	P	N	P	N	P
E wnt10b	Activates low density lipoprotein receptor related protein 5 (LRP5) and frizzled receptors	-2.06	0.023	--	--	--	--
C phosphatidylinositol 3-kinase subgroup 1A, regulatory subunit (pi3kreg1a)	Activates phosphatidylinositol 3-kinase subgroup 1A, catalytic subunit (P13K cat 1A)	--	--	-1.60	0.011	--	--
phosphatidylinositol 3-kinase subgroup 1a, catalytic subunit (p13k cat1a)	Involved in ATP signaling	1.44	0.015	--	--	--	--
talin	Promotes ATP signaling	-1.44	0.031	--	--	--	--
transforming growth factor-beta-activated kinase 1 (tak1)	Activates nemo like kinase (NLK)	1.59	0.016	1.51	0.046	--	--
nemo like kinase (nlk)	Inhibits Tcf(Lef) (Wnt signaling)	1.49	0.017	--	--	--	--
destrin	Inhibits actin-beta	1.39	0.020	--	--	--	--
actin related protein 2/3 complex (arp2/3)	Activates cytoskeletal actin	1.68	0.006	--	--	--	--
alpha actinin	Activates actin, beta	1.73	0.037	--	--	--	--
actin,beta/ actin, cytoskeletal	Involved in cell motility, structure, and integrity.	--	--	0.95	0.019	--	--
myosin light chain kinase (mylk and mlck)	Activates mitogen-activated protein kinase, MRLC, and MELC	--	--	-1.78	0.013	--	--
myosin II light chain (melc)	Cytoskeletal protein	-1.64	<0.001	2.29	<0.001	--	--
myosin regulatory light chain (mrlc)	Cytoskeletal protein	2.31	<0.001	--	--	--	--

Table 8: *N*-fold changes (*N*) and *P*-values (*P*) for significant differences between the non-chondrodystrophic dog (reference) and chondrodystrophic dog in gene expression involved in the Wnt signaling and cytoskeletal remodeling pathway for the notochordal cell (NC)-rich group, Mixed group, and chondrocyte-like cell (CLC)-rich group. E = extracellular protein; C = cytoplasmic protein; -- = no significant regulation.

BMP signaling

Chondrodystrophic: NC-rich – Mixed – CLC-rich

Gene	Function/action in pathway	NC-rich vs. Mixed		Mixed vs. CLC-rich		NC-rich vs. CLC-rich		
		N	P	N	P	N	P	
E	<i>bone morphogenetic protein (bmp) 2</i>	Activates activin a receptor (ALK2) and bone morphometric protein receptors 1a, 1b, and 2	--	--	2.95	0.004	2.39	0.008
	<i>bone morphogenetic protein (bmp) 4</i>	Activates activin a receptor (ALK2) and bone morphometric protein receptors 1a and 1b	--	--	1.47	0.006	--	--
	<i>bone morphogenetic protein (bmp) 6</i>	Activates activin a receptor (ALK2) and bone morphometric protein receptors 1a, 1b, and 2	--	--	5.17	0.005	3.12	0.029
C	<i>tissue growth factor beta activated kinase 1 (tak1)</i>	Activates mitogen activated protein kinases 3 and 6→ promotion of p38 mediated apoptosis and ATF-2 mediated stem cell differentiation	--	--	--	--	-1.43	0.033
N	<i>mothers against decapentaplegic 6 (smad6)</i>	Inhibits SMAD-1 and TAK1/p38 mediated apoptosis	--	--	-1.65	0.028	-1.87	0.009
	<i>transducer of erb-2 1 (tob1)</i>	Inhibits SMAD-1 and 9; Activates SMAD-6	--	--	1.77	0.048	1.35	0.019
	<i>smad specific E3</i>	Inhibits SMAD-1	--	--	1.31	0.048	1.37	0.012

Table 9: N-fold changes (N) and P-values (P) for significant up- and down-regulation of gene expression involved in the 'BMP signaling' pathway for the comparisons between notochordal cell (NC)-rich group, Mixed group, and chondrocyte-like cell (CLC)-rich group within the chondrodystrophic breed group. In each comparison, gene regulation is expressed relative to the least degenerated group (reference). E = extracellular protein; C = cytoplasmic protein; N = nuclear protein; -- = no significant regulation.

In this preliminary report, we found differences between chondrodystrophic and non-chondrodystrophic breeds in the expression of numerous genes involved in various cell processes, including intracellular transcription activity, and the synthesis and remodeling of the extracellular matrix (ECM) and cytoskeletal components.

BMP signaling

Chondrodystrophic vs. non-chondrodystrophic

Gene	Function/action in pathway	NC-rich		Mixed		CLC-rich	
		N	P	N	P	N	P
E <i>gremlin</i>	Inhibits bone morphogenetic protein 2, 4, and 7	2.73	0.030	1.89	0.042	--	--
<i>bone morphometric protein (bmp) 2</i>	Activates activin a receptor (ALK2) and bone morphometric protein receptors 1a, 1b, and 2	--	--	-1.71	0.006	--	--
<i>bone morphometric protein (bmp) 6</i>	Activates activin a receptor (ALK2) and bone morphometric protein receptors 1a, 1b, and 2	2.56	0.032	--	--	--	--
M <i>activin A receptor (alk2)</i>	Activates smad1, 2, and 9, and bone morphometric protein receptor 2	1.64	0.023	1.53	0.040	--	--
C <i>tissue growth factor beta activated kinase 1 (tak1)</i>	Activates mitogen activated protein kinases 3 and 6→ promotion of p38 mediated apoptosis and ATF-2 mediated stem cell differentiation	1.43	0.016	1.51	0.046	--	--
N <i>transducer of erb-2 1 (tob1)</i>	Inhibits SMAD-1 and 9; Activates SMAD-6	2.20	<0.001	--	--	2.17	<0.001

Table 10: N-fold changes (N) and P-values (P) for significant differences between the chondrodystrophic dog compared with the non-chondrodystrophic dog (reference) in gene expression involved in the BMP signaling pathway for the notochordal cell (NC)-rich group, Mixed group, and chondrocyte-like cell (CLC)-rich group. E = extracellular protein; M = membranous protein; C = cytoplasmic protein; N = nuclear protein; = no significant regulation.

The combined analysis of multiple arrays revealed several pathways that appear to be significantly involved in the early degenerative process within chondrodystrophic dog, as well as differences between the chondrodystrophic and non-chondrodystrophic dog breeds.

Microarray has its limitations. It is a semi-quantitative method for measuring gene expression, and thus is not accurate for detecting absolute RNA expression. In addition, it is limited by sensitivity issues, such that the expression of certain genes can only be measured if the gene is expressed

well above the sensitivity threshold, and this may result in a reduced ability to detect changes in the expression of specific individual genes with relatively few expression copies per cell⁶⁴. In order to draw accurate and valid conclusions regarding the exact expression of certain genes of interest, further studies require the use of quantitative techniques, such as quantitative PCR, protein expression analyses (Western blotting, especially on activated protein levels; immunohistochemistry), and functional studies, such as *in vitro* culture of NP cells and eventually gene knock-in or knock-out studies. Therefore, the results discussed below should be regarded as preliminary, but the array yielded intriguing data regarding the events of IVD degeneration, which may provide opportunities for developing novel strategies for IVD regeneration.

Early IVD degeneration appears to involve an increase in ECM anabolism and remodeling. The transition for the NC-rich to CLC-rich NP of chondrodystrophic dogs involved significant changes in the regulation of ECM components, matrix enzymes, and cell/matrix signaling molecules (Fig. 2 and 3). These findings are in line with other studies showing an increase in the overall protein content of the IVD during degeneration in dogs⁶⁵. However, with regard to collagen type II in particular, which is the primary collagen of the NP⁶⁶, there were discrepancies between the findings of this and other studies: in the present study, early IVD degeneration was accompanied by down-regulation of *collagen II* gene expression, whereas other studies, mainly involving induced IVD degeneration in rabbits, showed an increase in the expression of type II collagen gene and protein⁶⁷⁻⁶⁹. This discrepancy might be explained by differences in the nature of IVD degeneration – spontaneous in this study and induced in other studies. With regard to the proteoglycans of the NP, the expression of *versican* was down-regulated in the Mixed group compared with the NC-rich group, but was up-regulated in the CLC-rich group. *Versican* is a large ECM proteoglycan similar to aggrecan⁷⁰, and versican production by CLCs has been reported to increase after stimulation with NC-derived medium⁷¹. However, this finding seems contradictory to the observed up-regulation of *versican* gene expression that accompanied the disappearance of NCs from the NP in the present study. Therefore, factors other than the positive influence of NCs on CLC matrix production appear to have significant influence. IVD degeneration in humans is associated with a decrease in versican gene and protein expression⁷². This apparent contradiction may be the result of differences in the histological stage of degeneration investigated: the present study investigated early IVD degeneration with NC loss from the NP, whereas most human studies focus on the later stages of IVD degeneration, with degradation of the matrix of the CLC-rich NP. The expression of *osteonectin* was also up-regulated in the CLC-rich group compared with the NC-rich group. Osteonectin is a matricellular protein involved in cell–matrix interactions⁷³ and is associated with a mesenchymal stromal cell phenotype⁷⁴. In addition, the expression of osteonectin protein is decreased during IVD degeneration in

humans, which suggests that this protein is important to matrix health ⁷⁵.

Significant changes in the expression of genes for extracellular enzymes were also found. The gene expression of *kallikrein 1* (activates MMP-9 ⁷⁶) was significantly regulated and that of *mmp9* (cleaves collagen I, II, III and versican ⁷⁷⁻⁸⁰), *mmp12* (cleaves vitronectin and laminin1 ^{81,82}) and regulatory proteins *timp1* (inhibits MMP-1 and MMP-13 ^{83,84}) and *timp2* (inhibits MMP-13 ⁸⁵) was up-regulated. These changes might reflect increased matrix remodeling, with increased activity of MMP-9 and 12, and inactivation of MMP-1 and -13 reflecting an initial regenerative response (NC-rich vs Mixed), after which the NP is characterized by the production and remodeling of an abundant ECM. These findings are in agreement with the histopathological and morphological changes observed in early IVD degeneration, which involve a higher matrix:cell ratio in the CLC-rich NP compared with the NC-rich NP, and the transition from a mucoid, semi-fluid NP to a more fibrous, collagenous NP ^{39,42,86-88}.

It is tempting to postulate that the NCs produce a small amount of relatively high quality matrix containing highly hydrophilic molecules that is well-suited to meet the biomechanical requirements of the healthy NP, and that the loss of NCs involves a compensatory, CLC-mediated production and anabolism of a relatively larger amount of inferior quality matrix.

C	Description
1	notochordal cell-rich group (reference) vs. mixed group in the chondrodystrophic dog
2	mixed group (reference) vs. chondrocyte-like cell rich group in the chondrodystrophic dog
3	notochordal cell-rich group (reference) vs. chondrocyte-like cell rich group in the chondrodystrophic dog
4	non-chondrodystrophic dog (reference) vs. chondrodystrophic group for the notochordal cell-rich group
5	non-chondrodystrophic dog (reference) vs. chondrodystrophic group for the mixed group
6	non-chondrodystrophic dog (reference) vs. chondrodystrophic group for the chondrocyte-like cell rich group

Table 11. Descriptions corresponding with the array comparisons (C) depicted in Figures 2-7.

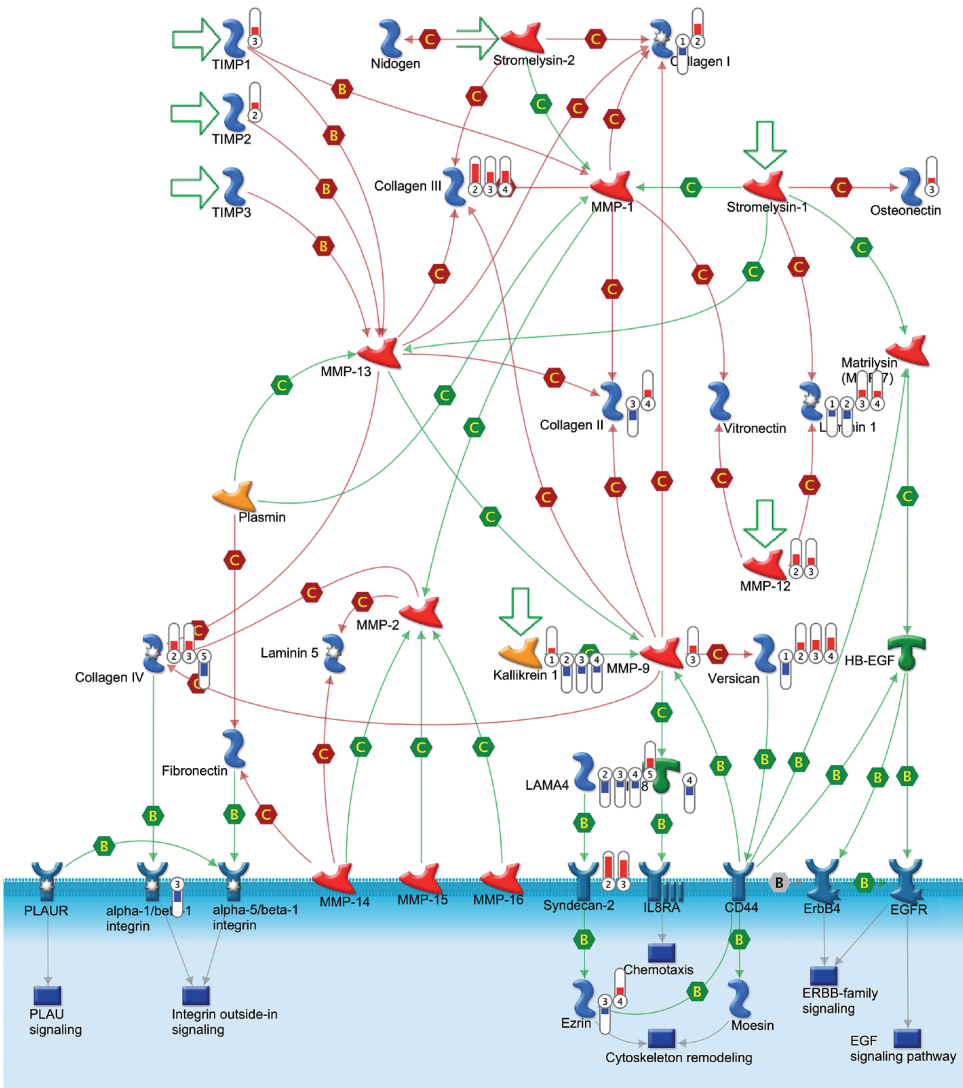


Figure 2. Gene expression regulations of the components involved in the cell adhesion: Extracellular matrix remodeling pathway, showing relative down-regulations (blue bars) and up-regulations (red bars) of specific genes in specific array comparisons (numbered 1-6, comparisons described in Table 11), suggesting an increase in extracellular matrix anabolism and remodelling. Green and red hexagons between protein symbols represent activation and inhibition, respectively.

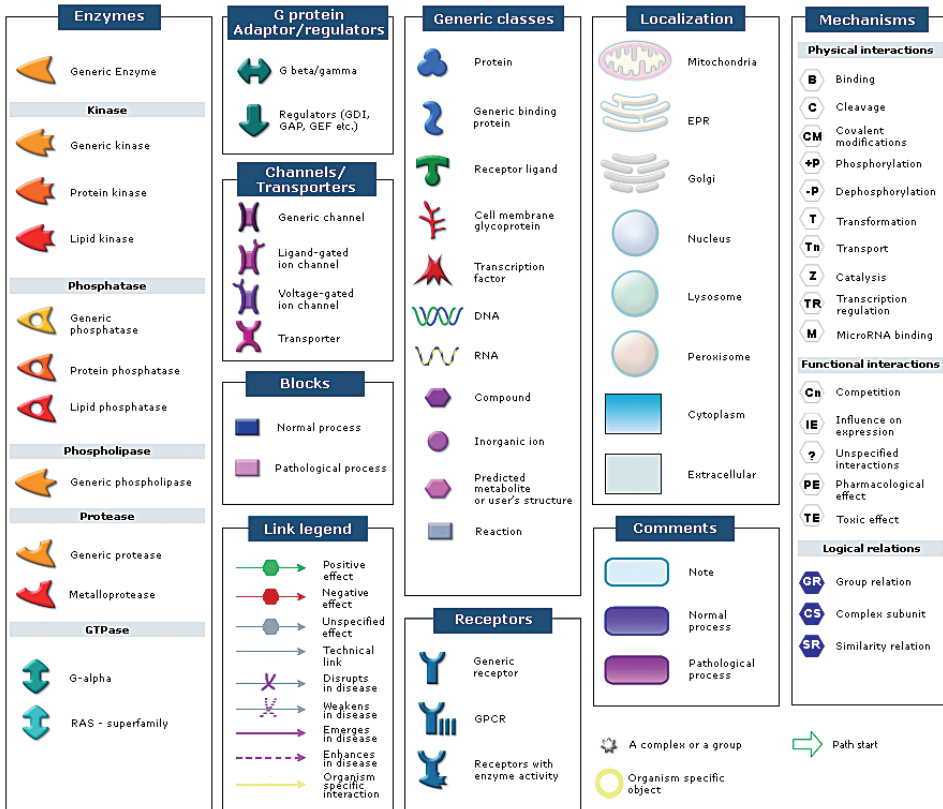


Figure 3: Legend for symbols used in figures 2, 4, 5, 6 and 7.

NCs and CLC appear to significantly differ regarding cell-matrix interactions. The expression of the genes for several laminin subunits was also altered. The laminins are a family of glycoproteins that form an integral part of the basement membrane⁸⁹, and they are involved in cell differentiation, changes in cell shape and movement, and cell survival⁸⁹. During the course of degeneration, changes in matrix/receptor signaling involve a reduced gene expression of *lama4* and *ezrin*, and an increased gene expression of *syndecan2*, which is suggestive of a different cell-matrix/actin cytoskeleton interaction in NCs and CLCs^{90,91}. The down-regulation of the expression of *alfa1beta1*, a class of cell adhesion molecules that regulate interactions between the cell and its surrounding matrix (collagen, fibronectin, laminin), in the CLC-rich NP compared with NC-rich NP further supports the variation in cell-matrix interactions between NCs and CLCs⁹². However, additional studies will be required to characterize the interactions of the laminin and integrin subunits with specific matrix constituents as well as their functional role in the biomechanical properties of the matrix.

Early IVD degeneration may involve decreased plasmin activity and associated fibrolysis and laminin breakdown. The synthesis of matrix components during the transition from NC-rich to CLC-rich NP is further supported by the decrease in plasmin activity and fibrolysis seen in the Mixed and CLC-rich group vs. the NC-rich group (Fig. 4). In contrast, a high expression of plasmin protein has been associated with IVD degeneration⁹³. Therefore, during early IVD degeneration the inhibition of plasmin activity and associated fibrolysis that accompanies the appearance of CLCs most probably reflects increased matrix synthesis, instead of matrix degradation.

Furthermore, during degeneration variations in the gene expression of various membranous laminin subunits (influence on cellular growth, survival, morphology, differentiation, and motility⁸⁹) and up-regulation of membranous collagen (involved in cell-matrix interactions⁹⁴) were noted. In particular, laminin has the ability to stimulate cell movement^{95,96}, and thus the changes in laminin subunit gene expression and the relative reduction in plasmin activity and consequent laminin breakdown may be associated with the appearance/migration of CLCs throughout the NP⁹⁷ and with the different cell-matrix interactions seen in NCs and CLCs.

Early NP degeneration involves alterations in TGF- β /MAPK/p38 signaling.

Plasmin activity also promotes TGF- β signaling through the mitogen-activated protein kinase/p38 (MAPK/p38) signaling pathway. Therefore, a decrease in plasmin activity, resulting from the increased gene expression of *neuroserpin* and *clnhibitor*, in combination with the 1.43-fold decrease in *tak1/mapk3k7* gene expression may point to reduced TGF- β /MAPK/p38 signaling during the replacement of NCs by CLCs at the onset of IVD degeneration. TGF- β signaling regulates cell growth and matrix formation⁹⁸ and is considered an anabolic signaling pathway in articular cartilage⁹⁹⁻¹⁰¹. The exact role of TGF- β in IVD degeneration is unclear²⁸. Human herniated disc material expresses low levels of TGF- β and TGF receptor proteins, suggesting that the low expression of anabolic growth factors may be involved in IVD degeneration¹⁰². In addition, the expression of TGF- β , TGF-receptor, and TGF-related proteoglycan is reduced in IVDs from old rats¹⁰³.

However, in humans the expression of TGF- β and TGF receptor is increased in samples from herniated IVDs compared with control IVDs¹⁰⁴, and it is suggested that this increased expression is involved with the inflammation/neovascularization that accompanies the resorption of herniated IVDs²⁸. MAPK/p38 signaling is activated in inflammation, apoptosis, cell cycle progression, and cell differentiation¹⁰⁵. In the IVD, MAPK/p38- signaling regulates aggrecan expression^{106,107} and is associated with the differentiation of mesenchymal stromal cells into chondrocyte-like cells¹⁰⁸. Inhibition of MAPK/p38 signaling in cytokine-activated IVD cells inhibits the production

of factors associated with degeneration, such as IL1- β , IL6, and PGE2¹⁰⁹. Taken together, the relevance of TGF- β /MAPK/p38 signaling in the transition from NC-rich to CLC-rich NP observed in the present study is unclear.

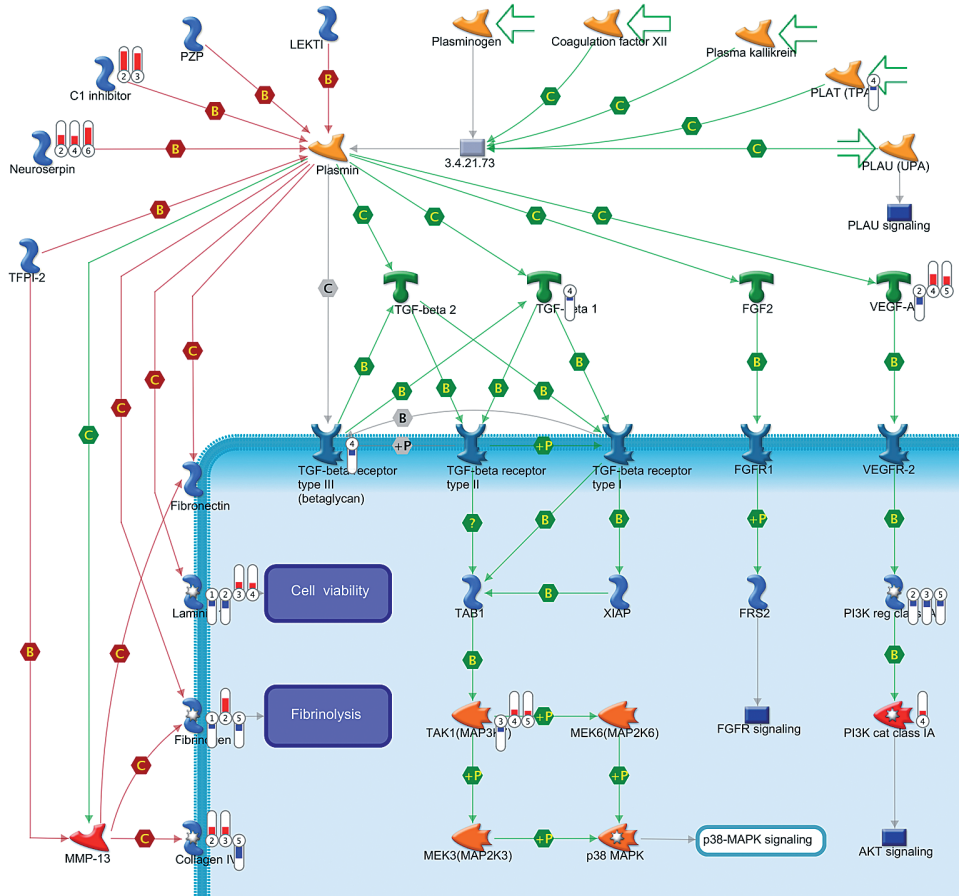


Figure 4. Gene expression regulations of the components involved in the Plasmin signaling pathway, showing relative down-regulations (blue bars) and up-regulations (red bars) of specific genes in specific array comparisons (numbered 1-6; described in Table 11), suggesting that early IVD degeneration may involve decreased plasmin activity and associated fibrolysis and laminin breakdown. Green and red hexagons between protein symbols represent activation and inhibition, respectively.

Replacement of NCs by CLCs may be associated with a reduced plasmin/VEGF/Akt signaling activity. Plasmin activity is also linked to VEGF and associated Akt signaling, which are associated with angiogenesis ¹¹⁰. Akt is a serine/threonine protein kinase that is activated by a number of growth factors and cytokines in a phosphatidylinositol-3 kinase-dependent manner ¹¹¹. Akt signaling regulates glucose metabolism and protein synthesis, but also has anti-apoptotic actions ¹¹¹. In the present study, the expression of *vegf* was lower in the CLC-rich group than in the Mixed group, and the expression of *pi3kregclas1a* was lower in the CLC-rich group than in the NC-rich and Mixed groups, indicating that plasmin/VEGF/AKT signaling is decreased during the replacement/loss of NCs from the NP. Hypoxic conditions have been shown to result in the up-regulation of VEGF and in the activation of Akt signaling in NCs, and the loss of NCs from the NP is accompanied by a decrease in VEGF protein expression ^{112,113}. Akt is important for the maintenance of Glut-1 transcriptional activity and, therefore, for the anaerobic delivery of glucose to cells ¹¹². Moreover, PI3K/Akt signaling has been shown to regulate the survival of rat NCs under hypoxic conditions, with a linked inactivation of glycogen synthase kinase 3 (GSK3), an effector protein involved in the regulation of apoptosis ¹¹⁴. In conclusion, the current data support the notion that plasmin/VEGF/Akt signaling is active in the NC-rich NP and that the loss of this signal is involved in the transition from NC-rich NP to CLC-rich NP accompanied by NC apoptosis, which may be linked to a decreased anaerobic delivery of glucose to the metabolically active NCs ¹¹⁵.

Early IVD degeneration appears to involve reduced PLAU/Akt signaling activity. The activity of urokinase plasminogen activator (PLAU) is linked to several intracellular pathways, including Akt signaling (Fig. 5). Early IVD degeneration involved significant up-regulation of *pai1* (only NC-rich compared to Mixed), *pai2*, and *protein c inhibitor* expression, which is indicative of increased inhibition of PLAU. PLAU inactivation results in decreased plasmin activity (see Plasmin signaling). Indeed, decreased PLAU activity in combination with down-regulation of the gene expression of *casein kinase II beta chain* and *casein kinase alpha chains* was observed in the CLC-rich group compared with the NC-rich group, indicating that early IVD degeneration may involve inactivation of Akt signaling via two pathways:

1) the HGF/PI3KregClass1A pathway, as indicated by the down-regulation of *hgf receptor*, *p13kregclass1a*, and *gab1* expression in the CLC group. The expression of *hgf* has not been reported in the IVD, but it has been reported in joint cartilage, with elevated levels in rheumatoid arthritis and osteoarthritis ^{116,117}. HGF has been suggested to facilitate cartilage matrix repair ^{118,119}, and the potential involvement of HGF signaling in IVD degeneration with putative effects on matrix health may be an interesting topic for further research.

2) the $\alpha 8/\beta 1$ integrin receptor/Akt signaling pathway, as indicated by the down-regulation of *ilk* gene expression. Since Akt is considered a pathway

for the anaerobic delivery of glucose to cells 112, it is tempting to suggest that the down-regulation of this pathway is linked to the decreased metabolic demands of CLCs compared with NCs. Epidermal growth factor (EGF) signaling is also involved in the depicted PLAU signaling pathway (Fig. 5). Early IVD degeneration involved decreased *egf* gene expression but increased *egfr* gene expression. The stimulation of EGFR by EGF has been shown to increase proteoglycan production and cell proliferation in NP tissue culture ¹²⁰. In addition, herniated IVD material has been shown to express low levels of EGF and EGFR, which may induce matrix anabolism preserve matrix health

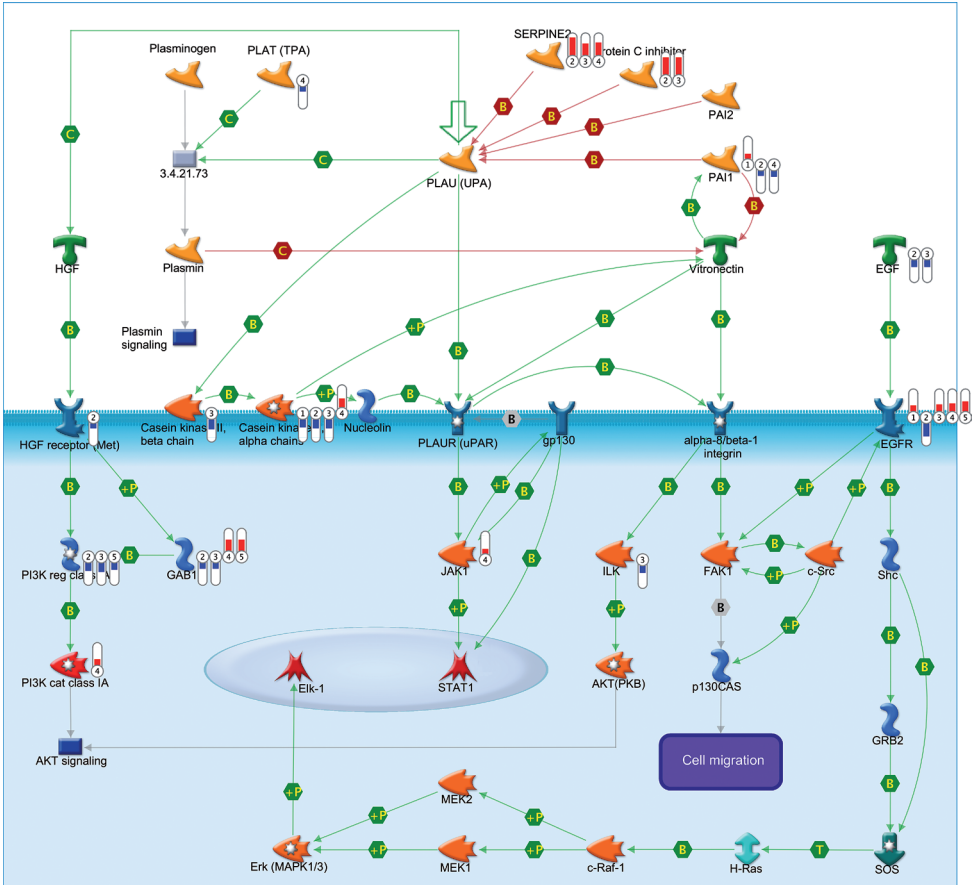


Figure 5. Gene expression regulations of the components involved in the plasminogen activator, urokinase (PLAU)-signaling pathway, showing relative down-regulations (blue bars) and up-regulations (red bars) of specific genes in specific array comparisons (numbered 1-6; described in Table 11), suggesting that early IVD degeneration involves reduced PLAU/Akt signaling activity. Green and red hexagons between protein symbols represent activation and inhibition, respectively.

¹⁰². In early IVD degeneration there seem to be alterations in EGF signaling, but clear conclusions regarding EGF signaling are difficult to draw because the down-regulation of EGF may be counteracted by the relative upregulation of EGF receptor.

Early IVD degeneration may involve reduced Wnt/ β -catenin signaling activity. Canonical Wnt signaling is involved in the regulation, self-renewal, proliferation, and differentiation of various stem cells and tissues ¹²¹. While Wnt signaling maintains the notochordal fate of NCs throughout embryogenesis ¹²², it has also been associated with the deterioration and breakdown of joint cartilage in degenerative joint disease and with IVD degeneration ¹²³⁻¹²⁷. Wnt signaling was recently found to be at basal levels in canine NCs ⁵⁴. Accordingly, the present study shows the involvement of *wnt7b* and *wnt10b*, which activates canonical Wnt signaling through both the frizzled and LRP5 receptors ¹²⁸ (Fig. 6). Also, decreased *caveolin* and *ilk* gene expression were found. Taken together, these results suggest that Wnt/ β -catenin signaling activity was decreased in the CLC-rich group compared with the NC-rich group. These results will be further investigated in Chapter 5.4 of this thesis.

NCs and CLCs exhibit significant differences in cytoskeletal remodeling. Transformation of the NP cell population from NC-rich to CLC-rich involved complex changes in the regulation of the expression of genes involved in cytoskeletal remodeling. Significant differences in gene expression of cytoskeletal components between the canine NP and annulus fibrosus have been reported ³¹. Actin is an important NP cell cytoskeleton component ^{39,129,130}, whereas relatively little is known about myosin. Actin–cytoskeleton function would appear to be different in the CLC-rich NP compared with the NC-rich NP, as suggested by the significantly lower expression of *actin* (cytoskeleton), *arp2/3*, *α -actinin*, and *talin*, and the significantly higher expression of *limk2*. The difference in cytoskeletal functionality between NCs and CLCs is most likely related to the size, conformation, and functional intracellular vesicles characteristic of the NC ^{38,39,131}, and these findings highlight the importance of the actin cytoskeleton in the NC. In addition, the change from NC-rich to CLC-rich NP involved a shift from a relatively high *mrlc* expression to a high *melc* expression combined with decreased activation of *mrlc* through Dock1/Rac1/PAK1 in the CLC-rich NP. The changes in gene expression may reflect an altered cytoskeletal composition in the NC compared with the CLC. Moreover, an increased expression of *mlcp(reg)* and decreased inactivation of *MLCP (reg)* through RhoA-regulated ROCK activation (Figure 6) may reflect an increase in MLCP (cat) activity with consequent *melc/mrlc* cleavage and cytoskeletal remodeling ¹³².

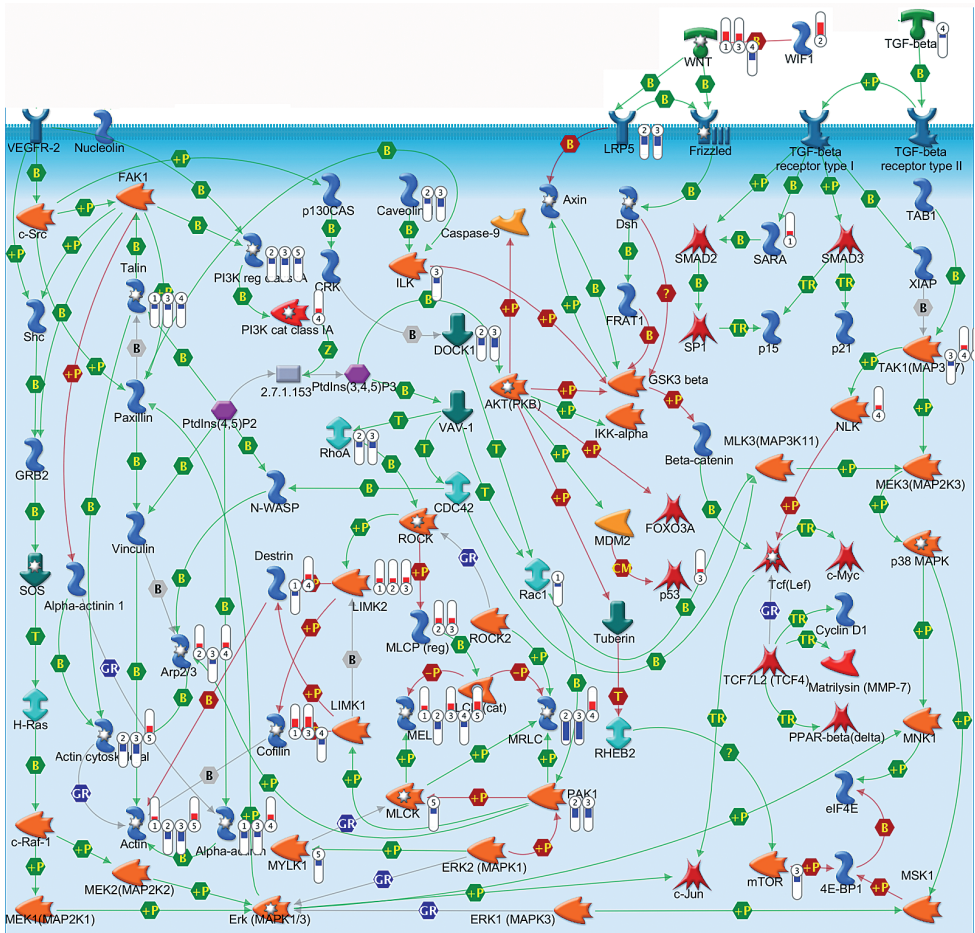


Figure 6. Gene expression regulations of the components involved in the Wnt signaling and cytoskeletal remodeling pathway, showing relative down-regulations (blue bars) and up-regulations (red bars) of specific genes in specific array comparisons (numbered 1-6; described in Table 11), suggesting that early IVD degeneration may involve reduced Wnt/ β -catenin signaling activity. Green, red, and blue hexagons between protein symbols represent activation, inhibition, and unspecified action, respectively.

Early IVD degeneration may involve increased BMP/SMAD signaling activity. The BMPs signaling molecules belong to the TGF family, which regulates transcription through the intracellular SMAD family of proteins¹³³. The SMAD family contains receptor-regulated SMADs (SMAD1, 2, 5, and 8), one cooperative SMAD (SMAD4), and two inhibitory SMADs (SMAD6 and 7)¹³³. SMAD1, 5, and 8 are activated by stimulation through BMPs, while SMAD6 selectively inhibits BMP signals¹³³. The transition from NC-rich to CLC-rich NP in chondrodystrophic dogs involved the up-regulation of *bmp2*, *bmp4*, and *bmp6*, and the down-regulation of *smad6* expression, which may

indicate activation of SMAD1, 5, and 8 in early IVD degeneration (Fig. 7). Active BMP/SMAD signaling may reflect increased matrix synthesis in the transition from the NC-rich to the CLC-rich NP, which is supported by the observed histological changes (NC-rich: little matrix, many cells; CLC-rich: abundant matrix with few cells (Fig. 1). The BMP family has received considerable attention as a potential target for IVD regeneration strategies (BMP2 and 7 are food and drug administration (FDA)-approved products^{134,135}) because these molecules promote ECM anabolism²⁸. Specific effects of BMP-2 on IVD cells include increased gene and protein expression of aggrecan and collagen type I and II¹³⁶⁻¹³⁹. However, the transition from NC-rich to CLC-rich NP also involved an increased gene expression of *tob1* and *smurf2*, which inhibits SMAD1 and SMAD9 activity, thereby inhibiting the BMP-induced activation of SMAD¹³³. Further evaluation of BMP/SMAD-related gene and protein expression is needed to draw conclusions about its role in early IVD degeneration.

Chondrodystrophic vs. non-chondrodystrophic degeneration

Significant differences in gene expression were found between the non-chondrodystrophic and chondrodystrophic dog breeds regarding the discussed pathways.

Cell adhesion/ECM remodeling. The gene expression for several collagens (collagen I and II) and proteoglycans (versican) was up-regulated in chondrodystrophic dogs vs non-chondrodystrophic dogs, changes which were also observed in the transition from NC-rich to CLC-rich NP. **This difference between chondrodystrophic and non-chondrodystrophic dog breeds may highlight the accelerated degeneration and disappearance of NCs, and the compensatory increase in matrix production in chondrodystrophic dog breeds.** However, some findings are inconsistent with this theory, including the down-regulation of *collagen IV* and the up-regulation of *lama4* gene expression in chondrodystrophic dogs compared with non-chondrodystrophic dogs. Also, the expression of *il8*, which is associated with macrophage chemotaxis¹⁴⁰, in the NC-rich NP was significantly higher in chondrodystrophic dogs than in non-chondrodystrophic dogs. However, the expression of IL8 has been reported in both healthy and degenerated/herniated IVDs¹⁴⁰ and the exact role of IL8 in the process of early IVD degeneration still has to be determined.

Plasmin/PLAU signaling. The expression of *tgfbeta1* and *tgfbetaIII* was significantly lower and the expression of *map3k7* was significantly higher in the NC-rich NP from chondrodystrophic dogs than in the NC-rich NP from non-chondrodystrophic dogs. The few significantly regulated genes involved in combination with the inconclusive involvement of this pathway in IVD degeneration hamper a clear interpretation of the differences between chondrodystrophic and non-chondrodystrophic dogs. With regard to VEGF-Akt signaling, the expression of *vegfa* and *pi3catclass1a*, *gab1*, *serpine2*, *casein kinase alpha chains* was higher and that of *pail* was lower in the NC-rich

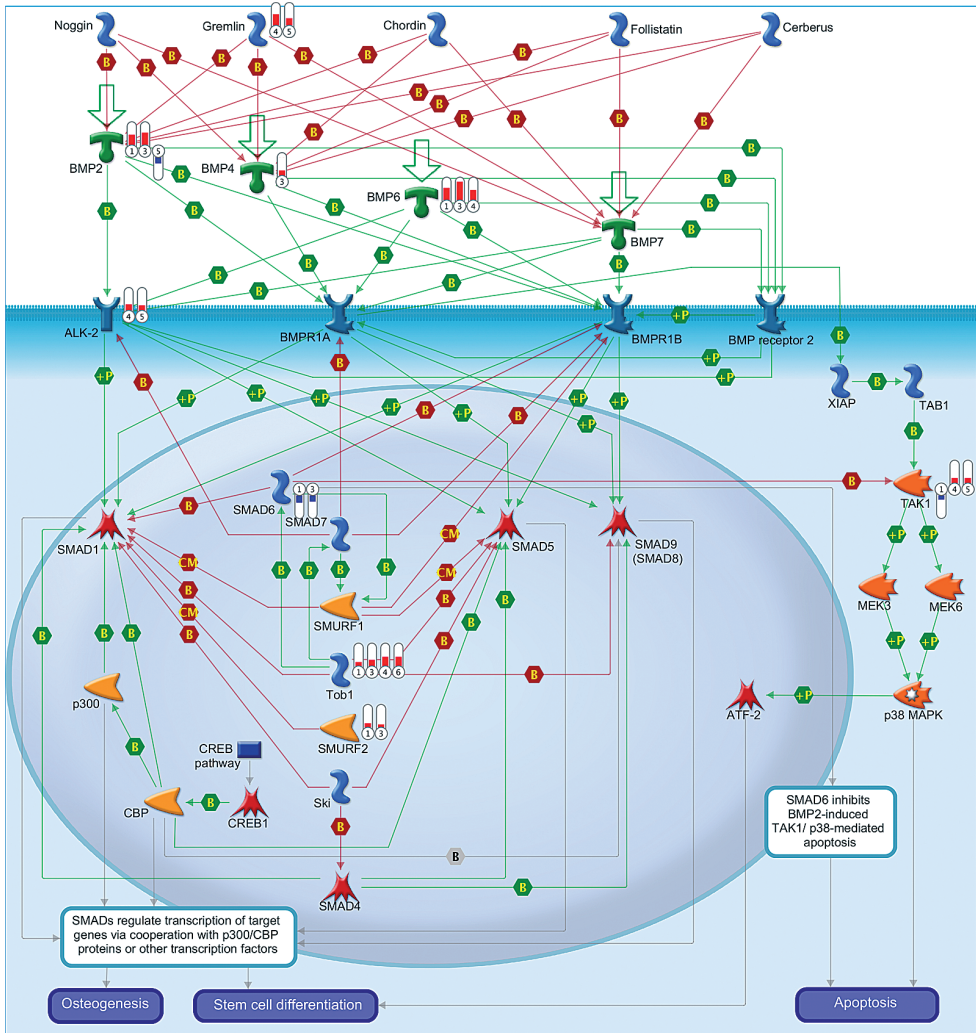


Figure 7. Gene expression regulations of the components involved in the bone morphogenetic protein (BMP)-signaling pathway, showing relative down-regulations (blue bars) and up-regulations (red bars) of specific genes in specific array comparisons (numbered 1-6, described in Table 11), suggesting that early IVD degeneration may involve increased BMP/SMAD signaling activity. Green and red hexagons between protein symbols represent activation and inhibition, respectively.

NP from chondrodystrophic dogs, indicating increased VEGF-Akt signaling. In relation to the up-regulation of VEGF expression in NC cells as a response to hypoxia ¹¹³ and the importance of Akt signaling in the anaerobic delivery of glucose to the NC ¹¹², the NP may be subjected to a higher degree of hypoxia and metabolic demand in chondrodystrophic dogs, which may predispose the NP to accelerated degeneration. Also the NC-rich NP and Mixed NP from

chondrodystrophic dogs had a significantly higher *egfr* expression than that of the NC-rich NP and Mixed NP from non-chondrodystrophic dogs, which may indicate that proteoglycan expression and cell migration are increased in the NP of chondrodystrophic dogs^{94, 113}.

Wnt signaling. The expression of *wnt10b* was lower, and that of *nlk* (NC-rich group) and *map3k7* (NC-rich and Mixed-group) was higher in chondrodystrophic dogs than in non-chondrodystrophic dogs. This may reflect decreased canonical Wnt signaling activity in the chondrodystrophic NC-rich NP, which, in view of the potential decrease in canonical Wnt signaling in early IVD degeneration as proposed above, may be related to the accelerated character of NP degeneration in this breed type.

Cytoskeleton remodeling. Comparison of the samples from chondrodystrophic and non-chondrodystrophic dogs revealed various alterations in the expression of genes for actin and myosin cytoskeletal components, with an overall higher actin expression and activation, and a relatively higher *melc* and lower *mrlc* gene expression in the NC-rich NP from chondrodystrophic dogs. Although these findings are inconclusive, **they may reflect a change in cytoskeletal behavior in NCs from chondrodystrophic dogs due to the accelerated nature of IVD degeneration observed in this breed group.**

BMP signaling. The expression of *bmp2* was lower and that of *gremlin* (inhibits BMPs 2,4, and 7^{141,142}), *bmp6*, *alk2* and *tob1* was higher in chondrodystrophic dogs. Although the gene expression of *bmp6* and the BMP receptor *alk2* was higher in these dogs, the changes (up-regulation and down-regulation of various components) in the expression of genes of the BMP signaling pathway make it difficult to draw a conclusion regarding the absolute difference in BMP/SMAD signaling activation between chondrodystrophic and non-chondrodystrophic dog breeds.

Limitations and considerations of the study

The present study had some limitations apart from the limitations associated with micro-array studies specifically as mentioned earlier. Firstly, although multiple microarray analysis revealed differences in the pathways involved in IVD degeneration in chondrodystrophic and non-chondrodystrophic dog breeds, it must be emphasized that analysis of individual arrays may reveal many more pathways of interest, which could lead to novel insights into the degenerative process and potential mechanisms to regenerate degenerated IVDs. For example, individual analysis of the array comparing the NC-rich NP and Mixed NP may reveal pathways explicitly involved in the disappearance of NCs from the NP during IVD degeneration. Secondly, as described above, microarray analysis has certain limitations that make it impossible to acquire quantitative results. Therefore, the results discussed above should be considered preliminary and require further validation. Thirdly, microarray analysis revealed few significant differences in the regulation of gene expression between the NC-rich, Mixed,

and CLC-rich NP in non-chondrodystrophic dogs, which may be explained by the high genetic variation in this group: the chondrodystrophic dogs were Beagle dogs of the same age, whereas the non-chondrodystrophic dogs were mongrels of different age. This may have resulted in a relatively high genetic variation in the non-chondrodystrophic dog samples and consequently few significant differences in gene expression in the non-chondrodystrophic group. Lastly, in the present study only the NP of the IVD was analyzed. However, as the IVD is composed of the NP, annulus fibrosus, and endplates, and because IVD degeneration affects these components as well, similar microarray analyses of the annulus fibrosus and endplates of the IVD are required to fully elucidate the fundamental processes involved in IVDD.

Conclusions

In conclusion, early IVD degeneration, i.e., the replacement transition from the NC-rich to CLC-rich NP, involves an altered regulation of various genes for different signaling pathways, many of which are largely unexplored in the IVD. Although the obtained data require additional analysis, they provide new insights into IVD degeneration, which can eventually be used to develop new strategies to regenerate the degenerated IVD.

References

1. Adams MA, Hutton WC: Mechanics of the Intervertebral Disc, in Ghosh P (ed): *The Biology of the Intervertebral Disc* (ed 1), Vol 2. Boca Raton, Florida, CRC Press, Inc.1988, pp 39-73.
2. Dyce KM, Sack WO, Wensing CJG: *The Neck, Back, and Vertebral Column of the Dog and Cat*, in Dyce KM, Sack WO, Wensing CJG (eds): *Textbook of Veterinary Anatomy* (ed 4), Vol. Philadelphia London New York St. Louis Sydney Toronto, Saunders Elsevier, 2010, pp 407-419.
3. Evans HE, Christensen GC: Joints and Ligaments, in Evans HE, Christensen GC (eds): *Miller's Anatomy of the Dog* (ed 2), Vol. Philadelphia London Toronto, W.B. Saunders Company, 1979, pp 225-268.
4. White AA, 3rd, Panjabi MM: *Clinical biomechanics of the spine*. Philadelphia Toronto, J.B. Lippincott Company, 1978.
5. Bray JP, Burbidge HM: The canine intervertebral disk: part one: structure and function. *J Am Anim Hosp Assoc* 34:55-63, 1998.
6. Sharp NJH, Wheeler SJ: Thoracolumbar and Lumbosacral disease, in Sharp NJH, Wheeler SJ (eds): *Small Animal Spinal Disorders. Diagnosis and Surgery* (ed 2), Edinburgh, Elsevier Mosby, 2005, pp 121-209.
7. Cheung KM, Karppinen J, Chan D, et al: Prevalence and pattern of lumbar magnetic resonance imaging changes in a population study of one thousand forty-three individuals. *Spine (Phila Pa 1976)* 34:934-940, 2009.
8. Andersson GB: Epidemiological features of chronic low-back pain. *Lancet* 354:581-585, 1999.
9. Druss BG, Marcus SC, Olfson M, et al: The most expensive medical conditions in America. *Health Aff (Millwood)* 21:105-111, 2002.
10. Maniadakis N, Gray A: The economic burden of back pain in the UK. *Pain* 84:95-103, 2000.
11. Anderson PA, Rouleau JP: Intervertebral disc arthroplasty. *Spine* 29:2779-2786, 2004.
12. Meij BP, Bergknut N: Degenerative lumbosacral stenosis in dogs. *Vet Clin North Am Small Anim Pract* 40:983-1009, 2010.
13. da Costa RC: Cervical spondylomyelopathy (wobbler syndrome) in dogs. *Vet Clin North Am Small Anim Pract* 40:881-913, 2010.
14. Brisson BA: Intervertebral disc disease in dogs. *Vet Clin North Am Small Anim Pract* 40:829-858, 2010.
15. Bono CM, Lee CK: Critical analysis of trends in fusion for degenerative disc disease over the past 20 years: influence of technique on fusion rate and clinical outcome. *Spine (Phila Pa 1976)* 29:455-463; discussion Z455, 2004.
16. Gibson JN, Waddell G: Surgical interventions for lumbar disc prolapse: updated Cochrane Review. *Spine (Phila Pa 1976)* 32:1735-1747, 2007.
17. Brinckmann P, Grootenboer H: Change of disc height, radial disc bulge, and intradiscal pressure from discectomy. An in vitro investigation on human lumbar discs. *Spine* 16:641-646, 1991.
18. Eck JC, Humphreys SC, Hodges SD: Adjacent-segment degeneration after lumbar fusion: a review of clinical, biomechanical, and radiologic studies. *Am J Orthop* 28:336-340, 1999.

19. Frei H, Oxland TR, Rathonyi GC, et al: The effect of nucleotomy on lumbar spine mechanics in compression and shear loading. *Spine* 26:2080-2089, 2001.
20. Goel VK, Nishiyama K, Weinstein JN, et al: Mechanical properties of lumbar spinal motion segments as affected by partial disc removal. *Spine* 11:1008-1012, 1986.
21. Lee CK: Accelerated degeneration of the segment adjacent to a lumbar fusion. *Spine* 13:375-377, 1988.
22. MacDougall J, Perra J, Pinto M: Incidence of adjacent segment degeneration at ten years after lumbar spine fusion. *Spine J* 3:675, 2003.
23. Macy NB, Les CM, Stover SM, et al: Effect of disk fenestration on sagittal kinematics of the canine C5-C6 intervertebral space. *Vet Surg* 28:171-179, 1999.
24. Smith MEH, Bebachuk TN, Shmon CL, et al: An in vitro biomechanical study of the effects of surgical modification upon the canine lumbosacral spine. *Vet Comp Orthop Traumatol* 17:17-24, 2004.
25. Ganey T, Hutton WC, Moseley T, et al: Intervertebral disc repair using adipose tissue-derived stem and regenerative cells: experiments in a canine model. *Spine (Phila Pa 1976)* 34:2297-2304, 2009.
26. Tow BP, Hsu WK, Wang JC: Disc regeneration: a glimpse of the future. *Clin Neurosurg* 54:122-128, 2007.
27. An HS, Thonar EJ, Masuda K: Biological repair of intervertebral disc. *Spine (Phila Pa 1976)* 28:S86-92, 2003.
28. Masuda K, Oegema TR, Jr., An HS: Growth factors and treatment of intervertebral disc degeneration. *Spine (Phila Pa 1976)* 29:2757-2769, 2004.
29. Hiyama A, Mochida J, Iwashina T, et al: Transplantation of mesenchymal stem cells in a canine disc degeneration model. *J Orthop Res* 26:589-600, 2008.
30. Ruan DK, Xin H, Zhang C, et al: Experimental intervertebral disc regeneration with tissue-engineered composite in a canine model. *Tissue Eng Part A* 16:2381-2389, 2010.
31. Sakai D: Future perspectives of cell-based therapy for intervertebral disc disease. *Eur Spine J* 17 Suppl 4:452-458, 2008.
32. Risbud MV, Schaer TP, Shapiro IM: Toward an understanding of the role of notochordal cells in the adult intervertebral disc: from discord to accord. *Dev Dyn* 239:2141-2148, 2010.
33. Erwin WM: The Notochord, Notochordal cell and CTGF/CCN-2: ongoing activity from development through maturation. *J Cell Commun Signal* 2:59-65, 2008.
34. Hadjipavlou AG, Tzermiadianos MN, Bogduk N, et al: The pathophysiology of disc degeneration: a critical review. *J Bone Joint Surg Br* 90:1261-1270, 2008.
35. Thompson JP, Pearce RH, Schechter MT, et al: Preliminary evaluation of a scheme for grading the gross morphology of the human intervertebral disc. *Spine (Phila Pa 1976)* 15:411-415, 1990.
36. Bergknut N, Grinwis GCM, Pickee EB, et al: Reliability of macroscopic grading of canine intervertebral disc degeneration according to Thompson and comparison with low-field magnetic resonance imaging findings. *Am J Vet Res* In press 72:899-904, 2011.
37. Choi KS, Cohn MJ, Harfe BD: Identification of nucleus pulposus precursor cells and notochordal remnants in the mouse: implications for disk degeneration and chordoma formation. *Dev Dyn* 237:3953-3958, 2008.

38. Hunter CJ, Bianchi S, Cheng P, et al: Osmoregulatory function of large vacuoles found in notochordal cells of the intervertebral disc running title: an osmoregulatory vacuole. *Mol Cell Biomech* 4:227-237, 2007.
39. Hunter CJ, Matyas JR, Duncan NA: The three-dimensional architecture of the notochordal nucleus pulposus: novel observations on cell structures in the canine intervertebral disc. *J Anat* 202:279-291, 2003.
40. Guehring T, Urban JP, Cui Z, et al: Noninvasive 3D vital imaging and characterization of notochordal cells of the intervertebral disc by femtosecond near-infrared two-photon laser scanning microscopy and spatial-volume rendering. *Microsc Res Tech* 71:298-304, 2008.
41. Gilson A, Dreger M, Urban JP: Differential expression level of cytokeratin 8 in cells of the bovine nucleus pulposus complicates the search for specific intervertebral disc cell markers. *Arth Res Ther* 12:R24, 2010.
42. Hansen HJ: A pathologic-anatomical study on disc degeneration in dog, with special reference to the so-called enchondrosis intervertebralis. *Acta Orthop Scand Suppl* 11:1-117, 1952.
43. Hunter CJ, Matyas JR, Duncan NA: Cytomorphology of notochordal and chondrocytic cells from the nucleus pulposus: a species comparison. *J Anat* 205:357-362, 2004.
44. Trout JJ, Buckwalter JA, Moore KC: Ultrastructure of the human intervertebral disc: II. Cells of the nucleus pulposus. *Anat Rec* 204:307-314, 1982.
45. Trout JJ, Buckwalter JA, Moore KC, et al: Ultrastructure of the human intervertebral disc. I. Changes in notochordal cells with age. *Tissue Cell* 14:359-369, 1982.
46. Braund KG, Ghosh P, Taylor TK, et al: Morphological studies of the canine intervertebral disc. The assignment of the beagle to the achondroplastic classification. *Res Vet Sci* 19:167-172, 1975.
47. Riser WH, Haskins ME, Jezyk PF, et al: Pseudoachondroplastic dysplasia in miniature poodles: clinical, radiologic, and pathologic features. *J Am Vet Med Assoc* 176:335-341, 1980.
48. Aguiar DJ, Johnson SL, Oegema TR: Notochordal cells interact with nucleus pulposus cells: regulation of proteoglycan synthesis. *Exp Cell Res* 246:129-137, 1999.
49. Cappello R, Bird JL, Pfeiffer D, et al: Notochordal cell produce and assemble extracellular matrix in a distinct manner, which may be responsible for the maintenance of healthy nucleus pulposus. *Spine (Phila Pa 1976)* 31:873-882, 2006.
50. Vos P, Interma F, van El B, et al: Does loading influence the severity of cartilage degeneration in the canine Groove-model of OA? *J Orthop Res* 27:1332-1338, 2009.
51. Vos PA, Degroot J, Barten-van Rijbroek AD, et al: Elevation of cartilage AGEs does not accelerate initiation of canine experimental osteoarthritis upon mild surgical damage. *J Orthop Res*, accepted for publication, 2012.
52. Van Meegeren MER, Roosendaal G, Barten-van Rijbroek AD, et al: Coagulation aggravates blood-induced joint damage. *Arthritis Rheum*, accepted for publication, 2012.
53. van Horssen P, Siebes M, Hofer I, et al: Improved detection of fluorescently labeled microspheres and vessel architecture with an imaging cryomicrotome. *Med Biol Eng Comput* 48:735-744, 2010.
54. Smolders LA, Meij BP, Riemers FM, et al: Canonical Wnt signaling in the notochordal cell is upregulated in early intervertebral disk degeneration. *J Orthop Res* 30:950-957, 2012.

55. Herrmann BG, Kispert A: The T genes in embryogenesis. *Trends Genet* 10:280-286, 1994.
56. Gotz W, Kasper M, Fischer G, et al: Intermediate filament typing of the human embryonic and fetal notochord. *Cell Tissue Res* 280:455-462, 1995.
57. Holstege Lab, Microarray. Utrecht, (<http://microarrays.holstegelab.nl/modx/index.php>), 2011.
58. Roepman P, de Koning E, van Leenen D, et al: Dissection of a metastatic gene expression signature into distinct components. *Genome Biol* 7:R117, 2006.
59. van de Peppel J, Kemmeren P, van Bakel H, et al: Monitoring global messenger RNA changes in externally controlled microarray experiments. *EMBO Rep* 4:387-393, 2003.
60. Yang YH, Dudoit S, Luu P, et al: Normalization for cDNA microarray data: a robust composite method addressing single and multiple slide systematic variation. *Nucleic Acids Res* 30:e15, 2002.
61. Margaritis T, Lijnzaad P, van Leenen D, et al: Adaptable gene-specific dye bias correction for two-channel DNA microarrays. *Mol Syst Biol* 5:266, 2009.
62. Wu H, Kerr MK, Cui X, et al: MAANOVA: a software package for the analysis of spotted cDNA microarray experiments. *The analysis of gene expression data: methods and software*, 2002.
63. Ekins S, Nikolsky Y, Bugrim A, et al: Pathway mapping tools for analysis of high content data. *Meth Mol Biol* 356:319-350, 2007.
64. Draghici S, Khatri P, Eklund AC, et al: Reliability and reproducibility issues in DNA microarray measurements. *Trends Genet* 22:101-109, 2006.
65. Ghosh P, Taylor TK, Braund KG, et al: The collagenous and non-collagenous protein of the canine intervertebral disc and their variation with age, spinal level and breed. *Gerontology* 22:124-134, 1976.
66. Roughley PJ: Biology of intervertebral disc aging and degeneration: involvement of the extracellular matrix. *Spine* 29:2691-2699, 2004.
67. Takaishi H, Nemoto O, Shiota M, et al: Type-II collagen gene expression is transiently upregulated in experimentally induced degeneration of rabbit intervertebral disc. *J Orthop Res* 15:528-538, 1997.
68. Anderson DG, Izzo MW, Hall DJ, et al: Comparative gene expression profiling of normal and degenerative discs: analysis of a rabbit annular laceration model. *Spine (Phila Pa 1976)* 27:1291-1296, 2002.
69. Omlor GW, Lorenz H, Engelleiter K, et al: Changes in gene expression and protein distribution at different stages of mechanically induced disc degeneration--an in vivo study on the New Zealand white rabbit. *J Orthop Res* 24:385-392, 2006.
70. Schwartz N: Biosynthesis and regulation of expression of proteoglycans. *Front Biosci* 5:D649-655, 2000.
71. Erwin WM, Inman RD: Notochord cells regulate intervertebral disc chondrocyte proteoglycan production and cell proliferation. *Spine (Phila Pa 1976)* 31:1094-1099, 2006.
72. Cs-Szabo G, Ragasa-San Juan D, Turumella V, et al: Changes in mRNA and protein levels of proteoglycans of the annulus fibrosus and nucleus pulposus during intervertebral disc degeneration. *Spine (Phila Pa 1976)* 27:2212-2219, 2002.
73. Sodek J, Zhu B, Huynh MH, et al: Novel functions of the matricellular proteins osteopontin and osteonectin/SPARC. *Connect Tissue Res* 43:308-319, 2002.

74. Steck E, Bertram H, Abel R, et al: Induction of intervertebral disc-like cells from adult mesenchymal stem cells. *Stem Cells* 23:403-411, 2005.
75. Gruber HE, Ingram JA, Leslie K, et al: Cellular, but not matrix, immunolocalization of SPARC in the human intervertebral disc: decreasing localization with aging and disc degeneration. *Spine (Phila Pa 1976)* 29:2223-2228, 2004.
76. Tschesche H, Michaelis J, Kohnert U, et al: Tissue kallikrein effectively activates latent matrix degrading metalloenzymes. *Adv Exp Med Biol* 247A:545-548, 1989.
77. Christiansen VJ, Jackson KW, Lee KN, et al: Effect of fibroblast activation protein and alpha2-antiplasmin cleaving enzyme on collagen types I, III, and IV. *Arch Biochem Biophys* 457:177-186, 2007.
78. Bigg HF, Rowan AD, Barker MD, et al: Activity of matrix metalloproteinase-9 against native collagen types I and III. *FEBS J* 274:1246-1255, 2007.
79. Zhen EY, Brittain IJ, Laska DA, et al: Characterization of metalloprotease cleavage products of human articular cartilage. *Arthritis Rheum* 58:2420-2431, 2008.
80. Passi A, Negrini D, Albertini R, et al: The sensitivity of versican from rabbit lung to gelatinase A (MMP-2) and B (MMP-9) and its involvement in the development of hydraulic lung edema. *FEBS Lett* 456:93-96, 1999.
81. Roy R, Zhang B, Moses MA: Making the cut: protease-mediated regulation of angiogenesis. *Exp Cell Res* 312:608-622, 2006.
82. Chandler S, Cossins J, Lury J, et al: Macrophage metalloelastase degrades matrix and myelin proteins and processes a tumour necrosis factor-alpha fusion protein. *Biochem Biophys Res Commun* 228:421-429, 1996.
83. Bouwmeester T, Bauch A, Ruffner H, et al: A physical and functional map of the human TNF-alpha/NF-kappa B signal transduction pathway. *Nat Cell Biol* 6:97-105, 2004.
84. Knauper V, Cowell S, Smith B, et al: The role of the C-terminal domain of human collagenase-3 (MMP-13) in the activation of procollagenase-3, substrate specificity, and tissue inhibitor of metalloproteinase interaction. *J Biol Chem* 272:7608-7616, 1997.
85. Knauper V, Lopez-Otin C, Smith B, et al: Biochemical characterization of human collagenase-3. *J Biol Chem* 271:1544-1550, 1996.
86. Butler WF: Comparative Anatomy and Development of the Mammalian Disc, in Ghosh P (ed): *The Biology of the Intervertebral Disc* (ed 1), Vol 1. Boca Raton, Florida, CRC Press, Inc. 1988, pp 83-108.
87. Butler WF, Fujioka T: Fine structure of the nucleus pulposus of the intervertebral disc of the cat. *Anat Anz* 132:465-475, 1972.
88. Bergknut N, Grinwis GCM, Pickee EB, et al: Reliability of macroscopic grading of canine intervertebral disc degeneration according to Thompson and comparison with low-field magnetic resonance imaging findings. *Am J Vet Res In press* 72:899-904, 2011.
89. Colognato H, Yurchenco PD: Form and function: the laminin family of heterotrimers. *Dev Dyn* 218:213-234, 2000.
90. Granes F, Urena JM, Rocamora N, et al: Ezrin links syndecan-2 to the cytoskeleton. *J Cell Sci* 113 (Pt 7):1267-1276, 2000.
91. Woods A: Syndecans: transmembrane modulators of adhesion and matrix assembly. *J Clin Invest* 107:935-941, 2001.

92. Nettles DL, Richardson WJ, Setton LA: Integrin expression in cells of the intervertebral disc. *J Anat* 204:515-520, 2004.
93. Salo J, Mackiewicz Z, Indahl A, et al: Plasmin-matrix metalloproteinase cascades in spinal response to an experimental disc lesion in pig. *Spine (Phila Pa 1976)* 33:839-844, 2008.
94. Kuhn K: Basement membrane (type IV) collagen. *Matrix Biol* 14:439-445, 1995.
95. McCarthy JB, Furcht LT: Laminin and fibronectin promote the haptotactic migration of B16 mouse melanoma cells in vitro. *J Cell Biol* 98:1474-1480, 1984.
96. McCarthy JB, Palm SL, Furcht LT: Migration by haptotaxis of a Schwann cell tumor line to the basement membrane glycoprotein laminin. *J Cell Biol* 97:772-777, 1983.
97. Kim KW, Lim TH, Kim JG, et al: The origin of chondrocytes in the nucleus pulposus and histologic findings associated with the transition of a notochordal nucleus pulposus to a fibrocartilaginous nucleus pulposus in intact rabbit intervertebral discs. *Spine (Phila Pa 1976)* 28:982-990, 2003.
98. Favoni RE, de Cupis A: The role of polypeptide growth factors in human carcinomas: new targets for a novel pharmacological approach. *Pharmacol Rev* 52:179-206, 2000.
99. Lafeber FP, Vander Kraan PM, Huber-Bruning O, et al: Osteoarthritic human cartilage is more sensitive to transforming growth factor beta than is normal cartilage. *Br J Rheumatol* 32:281-286, 1993.
100. Morales TI, Roberts AB: Transforming growth factor beta regulates the metabolism of proteoglycans in bovine cartilage organ cultures. *J Biol Chem* 263:12828-12831, 1988.
101. O'Keefe RJ, Puzas JE, Brand JS, et al: Effects of transforming growth factor-beta on matrix synthesis by chick growth plate chondrocytes. *Endocrinology* 122:2953-2961, 1988.
102. Kontinen YT, Kempainen P, Li TF, et al: Transforming and epidermal growth factors in degenerated intervertebral discs. *J Bone Joint Surg Br* 81:1058-1063, 1999.
103. Matsunaga S, Nagano S, Onishi T, et al: Age-related changes in expression of transforming growth factor-beta and receptors in cells of intervertebral discs. *J Neurosurg* 98:63-67, 2003.
104. Tolonen J, Gronblad M, Virri J, et al: Transforming growth factor beta receptor induction in herniated intervertebral disc tissue: an immunohistochemical study. *Eur Spine J* 10:172-176, 2001.
105. Ono K, Han J: The p38 signal transduction pathway: activation and function. *Cell Signal* 12:1-13, 2000.
106. Tsai TT, Guttapalli A, Agrawal A, et al: MEK/ERK signaling controls osmoregulation of nucleus pulposus cells of the intervertebral disc by transactivation of TonEBP/OREBP. *J Bone Miner Res* 22:965-974, 2007.
107. Watanabe H, de Caestecker MP, Yamada Y: Transcriptional cross-talk between Smad, ERK1/2, and p38 mitogen-activated protein kinase pathways regulates transforming growth factor-beta-induced aggrecan gene expression in chondrogenic ATDC5 cells. *J Biol Chem* 276:14466-14473, 2001.
108. Risbud MV, Albert TJ, Guttapalli A, et al: Differentiation of mesenchymal stem cells towards a nucleus pulposus-like phenotype in vitro: implications for cell-based transplantation therapy. *Spine (Phila Pa 1976)* 29:2627-2632, 2004.
109. Studer RK, Aboka AM, Gilbertson LG, et al: p38 MAPK inhibition in nucleus pulposus cells: a potential target for treating intervertebral disc degeneration. *Spine (Phila Pa 1976)* 32:2827-2833, 2007.

110. Ferrara N, Gerber HP, LeCouter J: The biology of VEGF and its receptors. *Nat Med* 9:669-676, 2003.
111. Shiojima I, Walsh K: Role of Akt signaling in vascular homeostasis and angiogenesis. *Circ Res* 90:1243-1250, 2002.
112. Erwin WM, Las Heras F, Islam D, et al: The regenerative capacity of the notochordal cell: tissue constructs generated in vitro under hypoxic conditions. *J Neurosurg Spine* 10:513-521, 2009.
113. Fujita N, Imai J, Suzuki T, et al: Vascular endothelial growth factor-A is a survival factor for nucleus pulposus cells in the intervertebral disc. *Biochem Biophys Res Commun* 372:367-372, 2008.
114. Risbud MV, Fertala J, Vresilovic EJ, et al: Nucleus pulposus cells upregulate PI3K/Akt and MEK/ERK signaling pathways under hypoxic conditions and resist apoptosis induced by serum withdrawal. *Spine (Phila Pa 1976)* 30:882-889, 2005.
115. Guehring T, Wilde G, Sumner M, et al: Notochordal intervertebral disc cells: sensitivity to nutrient deprivation. *Arthritis Rheum* 60:1026-1034, 2009.
116. Feuerherm AJ, Borset M, Seidel C, et al: Elevated levels of osteoprotegerin (OPG) and hepatocyte growth factor (HGF) in rheumatoid arthritis. *Scand J Rheumatol* 30:229-234, 2001.
117. Pfander D, Cramer T, Weseloh G, et al: Hepatocyte growth factor in human osteoarthritic cartilage. *Osteoarth Cartilage* 7:548-559, 1999.
118. Wakitani S, Imoto K, Kimura T, et al: Hepatocyte growth factor facilitates cartilage repair. Full thickness articular cartilage defect studied in rabbit knees. *Acta Orthop Scand* 68:474-480, 1997.
119. Martel-Pelletier J, Boileau C, Pelletier JP, et al: Cartilage in normal and osteoarthritis conditions. *Best Pract Res Clin Rheumatol* 22:351-384, 2008.
120. Thompson JP, Oegema TR, Jr., Bradford DS: Stimulation of mature canine intervertebral disc by growth factors. *Spine (Phila Pa 1976)* 16:253-260, 1991.
121. Reya T, Clevers H: Wnt signalling in stem cells and cancer. *Nature* 434:843-850, 2005.
122. Ukita K, Hirahara S, Oshima N, et al: Wnt signaling maintains the notochord fate for progenitor cells and supports the posterior extension of the notochord. *Mech Dev* 126:791-803, 2009.
123. Dell'Accio F, De Bari C, Eltawil NM, et al: Identification of the molecular response of articular cartilage to injury, by microarray screening: Wnt-16 expression and signaling after injury and in osteoarthritis. *Arthritis Rheum* 58:1410-1421, 2008.
124. Sen M: Wnt signalling in rheumatoid arthritis. *Rheumatology (Oxford)* 44:708-713, 2005.
125. Yuasa T, Otani T, Koike T, et al: Wnt/beta-catenin signaling stimulates matrix catabolic genes and activity in articular chondrocytes: its possible role in joint degeneration. *Lab Invest* 88:264-274, 2008.
126. Hiyama A, Sakai D, Risbud MV, et al: Enhancement of intervertebral disc cell senescence by WNT/beta-catenin signaling-induced matrix metalloproteinase expression. *Arthritis Rheum* 62:3036-3047, 2010.
127. Hiyama A, Sakai D, Tanaka M, et al: The relationship between the Wnt/beta-catenin and TGF-beta/BMP signals in the intervertebral disc cell. *J Cell Physiol*, 2010.

128. Wang Z, Shu W, Lu MM, et al: Wnt7b activates canonical signaling in epithelial and vascular smooth muscle cells through interactions with Fzd1, Fzd10, and LRP5. *Mol Cell Biol* 25:5022-5030, 2005.
129. Errington RJ, Puustjarvi K, White IR, et al: Characterisation of cytoplasm-filled processes in cells of the intervertebral disc. *J Anat* 192 (Pt 3):369-378, 1998.
130. Hayes AJ, Benjamin M, Ralphs JR: Role of actin stress fibres in the development of the intervertebral disc: cytoskeletal control of extracellular matrix assembly. *Dev Dyn* 215:179-189, 1999.
131. Hunter CJ, Matyas JR, Duncan NA: The notochordal cell in the nucleus pulposus: a review in the context of tissue engineering. *Tissue Eng* 9:667-677, 2003.
132. Ito M, Nakano T, Erdodi F, et al: Myosin phosphatase: structure, regulation and function. *Mol Cell Biochem* 259:197-209, 2004.
133. Itoh S, Itoh F, Goumans MJ, et al: Signaling of transforming growth factor-beta family members through Smad proteins. *Eur J Biochem* 267:6954-6967, 2000.
134. Infuse FDA Approval letter. (<http://www.fda.gov/cdrh/mda/docs/p000058.html>), 2007.
135. OP-1 FDA letter Humanitarian Device Exemption. (<http://www.fda.gov/cdrh/MDA/DOCS/h020008.html>), 2007.
136. Kim DJ, Moon SH, Kim H, et al: Bone morphogenetic protein-2 facilitates expression of chondrogenic, not osteogenic, phenotype of human intervertebral disc cells. *Spine (Phila Pa 1976)* 28:2679-2684, 2003.
137. Li J, Yoon ST, Hutton WC: Effect of bone morphogenetic protein-2 (BMP-2) on matrix production, other BMPs, and BMP receptors in rat intervertebral disc cells. *J Spinal Disord Tech* 17:423-428, 2004.
138. Tim Yoon S, Su Kim K, Li J, et al: The effect of bone morphogenetic protein-2 on rat intervertebral disc cells in vitro. *Spine (Phila Pa 1976)* 28:1773-1780, 2003.
139. Yoon ST, Park JS, Kim KS, et al: ISSLS prize winner: LMP-1 upregulates intervertebral disc cell production of proteoglycans and BMPs in vitro and in vivo. *Spine (Phila Pa 1976)* 29:2603-2611, 2004.
140. Burke JG, Watson RW, McCormack D, et al: Spontaneous production of monocyte chemoattractant protein-1 and interleukin-8 by the human lumbar intervertebral disc. *Spine (Phila Pa 1976)* 27:1402-1407, 2002.
141. Balemans W, Van Hul W: Extracellular regulation of BMP signaling in vertebrates: a cocktail of modulators. *Dev Biol* 250:231-250, 2002.
142. Hsu DR, Economides AN, Wang X, et al: The *Xenopus* dorsalizing factor Gremlin identifies a novel family of secreted proteins that antagonize BMP activities. *Mol Cell* 1:673-683, 1998.

Gene expression profiling of early intervertebral disc degeneration reveals a down-regulation of canonical Wnt signaling and caveolin-1 expression: implications for development of regenerative strategies

Lucas A. Smolders ^a, Björn P. Meij ^a, David Onis ^a, Frank M. Riemers ^a,
Niklas Bergknut ^{a,b}, Richard Wubbolts ^c, Guy C.M. Grinwis ^d,
Martin Houweling ^e, Marian J.A. Groot Koerkamp ^f, Dik van Leenen ^f,
Frank C. P. Holstege ^f, Herman A.W. Hazewinkel ^a, Laura B. Creemers ^g,
Louis C. Penning ^a, Marianna A. Tryfonidou ^a

*Pending acceptance, resubmitted after revision to
Arthritis Research & Therapy*

^a: Department of Clinical Sciences of Companion Animals, Faculty of Veterinary Medicine, Utrecht University, Yalelaan 108, 3508 TD, Utrecht, The Netherlands.

^b: Department of Clinical Sciences, Division of Small Animals, Faculty of Veterinary Medicine and Animal Sciences, Swedish University of Agricultural Sciences, Sweden.

^c: Department of Biochemistry and Cell Biology, Faculty of Veterinary Medicine, Utrecht University, Yalelaan 1, 3584 CL, Utrecht, the Netherlands

^d: Department of Pathobiology, Pathology Division, Faculty of Veterinary Medicine, Utrecht University, Utrecht, The Netherlands

^e: Department of Biochemistry and Cell Biology, Faculty of Veterinary Medicine, Utrecht University, Yalelaan 2, 3584 CL, Utrecht, the Netherlands.

^f: Molecular Cancer Research, University Medical Center Utrecht, Heidelberglaan 100, 3584 CX, Utrecht, The Netherlands.

^g: Department of Orthopedics, University Medical Center Utrecht, Heidelberglaan 100, 3584 CX, Utrecht, The Netherlands.

Abstract

Introduction: Early degeneration of the intervertebral disc (IVD) involves a change in cellular differentiation from notochordal cells (NCs) in the nucleus pulposus (NP) to chondrocyte-like cells (CLCs). The purpose of this study was to investigate the gene expression profiles involved in this process using NP tissue from non-chondrodystrophic and chondrodystrophic dogs, a species with naturally occurring IVD degeneration.

Methods: Dual channel DNA microarrays were used to compare 1) healthy NP tissue containing only NCs (NC-rich), 2) NP tissue with a mixed population of NCs and CLCs (Mixed), and 3) NP tissue containing solely CLCs (CLC-rich) in both non-chondrodystrophic and chondrodystrophic dogs. Based on previous reports and the findings of the microarray analyses, canonical Wnt signaling was further evaluated using qPCR of relevant Wnt target genes. We hypothesized that caveolin-1, a regulator of Wnt signaling that showed significant changes in gene expression in the microarray analyses, played a significant role in early IVD degeneration. Caveolin-1 expression was investigated in IVD tissue sections and in cultured NCs. To investigate the significance of caveolin-1 in IVD health and degeneration, the NP of 3-month-old caveolin-1 knock-out mice was histopathologically evaluated and compared with the NP of wild-type mice of the same age.

Results: Early IVD degeneration involved significant changes in numerous pathways, including Wnt/ β -catenin signaling. With regard to Wnt/ β -catenin signaling, *axin2* gene expression was significantly higher in chondrodystrophic dogs compared with non-chondrodystrophic dogs. IVD degeneration involved significant down-regulation of *axin2* gene expression. IVD degeneration involved significant down-regulation in caveolin-1 gene and protein expression. NCs showed abundant caveolin-1 expression *in vivo* and *in vitro*, whereas CLCs did not. The NP of wild-type mice was rich in viable NCs, whereas the NP of caveolin-1 knock-out mice contained chondroid-like matrix with mainly apoptotic, small, rounded cells.

Conclusions: Early IVD degeneration involves down-regulation of canonical Wnt signaling and caveolin-1 expression, which appears to be essential to the physiology and preservation of NCs. Therefore, caveolin-1 may be regarded an exciting target for developing strategies for IVD regeneration.

Key words: Intervertebral disc degeneration; back pain; microarray; Wnt signaling; caveolin-1; notochordal cell; regeneration; canine; chondrodystrophic; non-chondrodystrophic

Introduction

Degeneration of the intervertebral disc (IVD) is a major cause of low back pain, a major health problem in the Western world ¹. Low back pain resulting from IVD degeneration may be treated medically in combination with physiotherapy. Surgical therapies include decompression with partial discectomy (removal of the diseased IVD tissue), spinal fusion of the affected segment, or by partial or total artificial IVD replacement ^{2,3}. Although these surgical therapies are generally successful, they are suboptimal since they are not curative and are associated with various complications: decompression/partial discectomy results in spinal instability, spinal fusion can result in adjacent segment degeneration, and IVD replacements/prostheses are associated with failure of the surgical implants ⁴⁻⁹. Therefore, within the field of regenerative medicine the focus has been on strategies concentrating on biological repair of the degenerating disc using adult stem or progenitor cells, growth factors, and/or gene therapy ¹⁰. However, the biomolecular events involved in IVD degeneration remain largely unexplored ¹¹⁻¹³.

Like humans, dogs suffer from spontaneous IVD degeneration that involves similar macroscopic (e.g. dehydration of the nucleus pulposus, decrease in disc height), histopathological (e.g. chondrocyte proliferation, disorganization of the annulus fibrosus), and biochemical changes (e.g. decrease in proteoglycan content, increase in MMP activity) ¹⁴. In humans and dogs, the juvenile, healthy nucleus pulposus (NP) of the IVD consists of a dense population of notochordal cells (NCs) embedded in a modest amount of extracellular matrix ^{15,16}. The NC has restorative capacity upon other cells, such as chondrocyte-like cells and mesenchymal stem cells, with significant regenerative potential, and thus is an interesting focus for regenerative strategies ^{13,17-21}. In humans and dogs, aging and early degeneration of the IVD involves chondroid metaplasia of the NP, which is characterized by the replacement of NCs by chondrocyte-like cells (CLCs) ^{11,16,22}. With regard to this cellular phenomenon, the dog is a unique species, because two subspecies can be distinguished, namely, chondrodystrophic and non-chondrodystrophic dog breeds ^{22,23}. Chondrodystrophic breeds are characterized by a disturbed endochondral ossification, resulting in disproportionally short limbs relative to the length of the spine. In these breeds, replacement of NCs by CLCs occurs before 1 year of age, with a concurrent onset of IVD degeneration at all spinal levels ²². In contrast, non-chondrodystrophic breeds show a normal growth of the long bones, and in these dogs the NC remains the predominant cell type of the NP until middle or old age. In non-chondrodystrophic dogs, IVD degeneration generally occurs at older age compared with chondrodystrophic dogs (>4-5 years of age), and mainly at selected locations (caudal cervical and lumbosacral spine), probably due to a high workload at these spinal levels ^{22,24-29}.

Therefore, these two dog types reflect a naturally occurring animal model for IVD degeneration, representing differential maintenance of the NC with

differential causative factors^{14,30}. Hence, the dog can be considered a unique model for studying the (patho)physiology of the NC and associated early IVD degeneration.

Although the process of early IVD degeneration has been described histopathologically^{14,16,22}, biomolecular signaling pathways involved in the transition from the NP rich in NCs to the NP rich in CLCs (i.e. early IVD degeneration) require further investigation. The aim of this study was to investigate the biomolecular signaling profiles associated with NC maintenance and replacement of NCs by CLCs in non-chondrodystrophic and chondrodystrophic dogs to identify possible targets for IVD regeneration. In the present study, apart from expected biomolecular signaling pathways involved in early IVD degeneration, including Wnt/ β -catenin signaling, new pathways were identified. In particular, caveolin-1, a regulator of Wnt/ β -catenin signaling, was found to be a crucial factor in the maintenance of NC health and physiology, and in the initiation of IVD degeneration, being significantly different between the two canine subspecies. These results indicate that caveolin-1 is a exciting target for further studies.

Materials and methods

Ethics statement

All materials used in this study were collected from animals euthanized in other, unrelated experiments approved by the Ethics Committee on Animal Experimentation (DEC) of Utrecht University. Canine IVD tissue was collected from dogs euthanized in studies investigating osteoarthritis (Experiment numbers DEC 2007.III.08.110 and DEC 2009.III.05.037; euthanasia performed by way of an intravenous overdose of pentobarbital)³¹⁻³³ and cardiovascular disease (Experiment number DEC 2007.II.01.029; euthanasia performed under general anesthesia by way of fibrillation and subsequent excision of the heart)

³⁴.

Murine IVD tissue was collected from mice euthanized for studies investigating the role of caveolin-1 in liver regeneration (Experiment number DEC 2008.III.01.001; euthanasia performed by way of exsanguination under isoflurane anesthesia; work not yet published). In these unrelated experiments, the animals were sacrificed for the collection of tissue other than IVD. All experimental procedures were performed strictly according the guidelines set by the Ethics Committee of Utrecht University. The Ethics Committee of Utrecht University approved post-mortem harvesting of the IVD tissue employed in the present study.

Sample collection

Cervical (C2-T1) and thoracolumbar (T10-S1) spines were collected from five mongrel dogs (non-chondrodystrophic group; age range, 13-60 months; body weight range, 26.6-32.1 kg) and six Beagle dogs (chondrodystrophic group; age range 25-36 months, weight range, 13.6-16.0 kg). Spines were processed, NP tissue was collected for RNA isolation, and paraffin-embedded slides of the IVDs were created as described in Chapter 5.3.

Histopathological grading of IVD samples.

To optimally investigate mRNA expression patterns associated with NC maintenance and replacement of NCs by CLCs, histopathological grading was performed as described previously³⁵. Mid-sagittal sections (4 µm) were mounted on Microscope KP+ slides (Klinipath B.V) and stained with hematoxylin and eosin (H&E). Composite raw images of each IVD were made using a Colorview IIIU digital camera (Olympus) mounted to a BX-40 microscope (Olympus). The images were scaled and the following parameters were measured for the NP: 1) Proportion (%) of NP surface area and pericellular matrix consisting of NCs: NCs were identified based on morphologic characteristics (cell size, intracytoplasmic vesicles, typical NC clusters)^{16,36}; 2) Proportion of NP surface area consisting of CLCs and fibrocartilaginous matrix. By combining these parameters for each IVD sample, samples were assigned by a board certified veterinary pathologist to one of three groups, i.e. 1) a notochordal cell-rich (NC-rich) group (> 90% of NP surface area consisting of NCs), 2) a Mixed group (cell population consisting of both NCs and CLCs, with 10-90% of NP surface area consisting of NCs), and a chondrocyte-like cell-rich (CLC-rich) group (> 90% of NP surface area consisting of CLCs and corresponding matrix) (Fig. 1).

To further assess the cellular phenomenon involving the transition from NC-rich to CLC-rich NP, and thus the applied histopathological grading, the gene expression of the notochordal markers *brachyury*^{12,37} and *cytokeratin 8*^{38,39} was investigated in all groups (qPCR analysis, see below).

DNA microarray analysis

Four NPs from the three histopathological groups for each breed type were randomly selected and used to isolate total RNA, using the RNeasy Fibrous Tissue Mini Kit (Qiagen) according to the manufacturer's instructions. After on-column DNase-I treatment (Qiagen RNase-free DNase kit), RNA was quantified spectrophotometrically using Nanodrop ND-1000 (Isogen Life Science) and RNA integrity was determined using a Bioanalyzer 2100 (Agilent Technologies). RNA integrity numbers of the samples varied from 4.5 to 7.4,

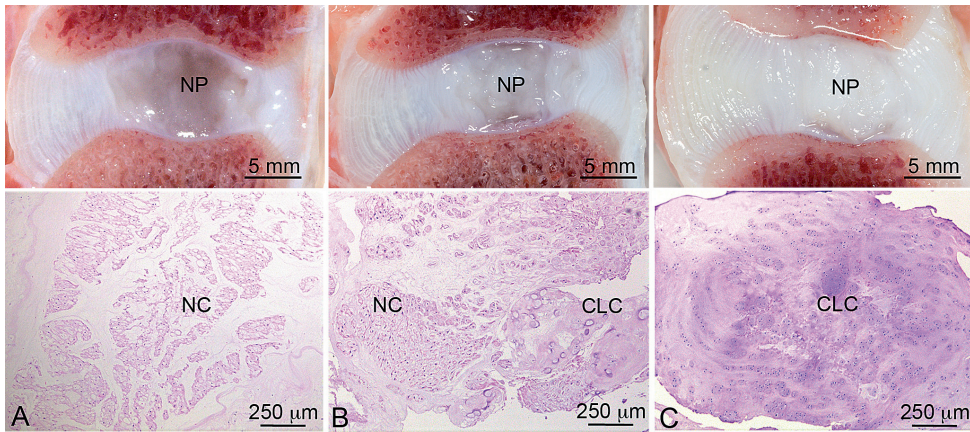


Figure 1. Typical macroscopic pictures and corresponding H&E sections of the applied classification. The notochordal cell (NC)-rich nucleus pulposus (NP) (A) contains NCs with a viable morphology organized in clusters; the Mixed group (B) contains both NCs and chondrocyte-like cells (CLC); and the CLC-rich group (C) contains solely CLCs embedded in a dense matrix.

(mean \pm SD: 6.2 ± 0.7), indicating that these samples could be used to perform valid gene expression analysis⁴⁰.

A two-color DNA microarray with a reference experiment design was performed as described in Chapter 5.3 of this thesis.

Differentially expressed genes were converted to their human homologues, and the following array comparisons were included in functional pathway analysis using the GeneGo MetaCore platform⁴¹: 1) NC-rich group vs. Mixed group, Mixed group vs. CLC-rich group, and NC-rich group vs. CLC-rich group in both chondrodystrophic and non-chondrodystrophic dogs; 2) non-chondrodystrophic vs. chondrodystrophic breeds: NC-rich group, Mixed group, and CLC-rich group. Pathways showing significant changes in gene expression were selected and analyzed further as described below.

Quantitative PCR (qPCR)

Six NPs from the three histopathological groups for each breed type were analyzed (cDNA samples used for microarray and additional, similarly processed samples). Unlabeled microarray cDNA from the first round of amplification was used. For the additional samples, cRNA was synthesized by extracting RNA as described for the microarray, followed by one round of amplification using *in vitro* transcription⁴², assuring similar pre-PCR treatment of both cRNA sources.

For all samples, cDNA was synthesized using the iScript™ cDNA Synthesis Kit (Biorad). qPCR was performed in duplicate using a MyIQ thermal cycler, IQ SYBRGreen SuperMix (BioRad) and dog-specific primers (Eurogentec; Table 1). Each sample was treated as an individual sample, and samples from different histopathological grades and subspecies were analyzed separately (in

technical duplicates). Primers were designed for the notochordal marker genes *brachyury* and *cytokeratin 8*, and based on the microarray analyses primers were designed for the following *Wnt target genes*: *wnt3a*, *wnt7b*, *wnt inhibitory factor 1 (wif1)*, *frizzled 1 (fzd1)*, *low density lipoprotein receptor-related protein 5 (lrp5)*, *dickkopf homolog 3 (dkk3)*, *integrin-linked kinase (ilk)*, *caveolin-1 (cav1)* and *axin2*⁴³⁻⁵¹. Conditions for the qPCR experiments were carefully validated as described previously³⁵. The amplification efficiency was between 90% and 110%. Relative expression was calculated by the efficiency corrected delta-delta Ct ($\Delta\Delta Ct$) method⁵² using a set of 5 reference genes (Table 1). For statistical analysis, see below.

β -Catenin protein expression

To validate differences in Wnt/ β -catenin signaling between non-chondrodystrophic and chondrodystrophic dogs, immunohistochemistry of β -catenin was performed as described before³⁵ and analyzed focussing on differences between non-chondrodystrophic and chondrodystrophic dogs. The parameter ‘integrated density for β -catenin staining of the NP’ was corrected for the surface area of the NP positively stained for β -catenin in order to correct for the difference in disc size between the two breed groups. Furthermore, total protein was extracted from lumbar CLC-rich NP from non-chondrodystrophic and chondrodystrophic dogs using RIPA buffer; protein concentration was determined with a Lowry assay. Aliquots of protein were subjected to 10% SDS-PAGE (15 μ g/lane). Protein (5 μ g) from a human insulinoma CM celline⁵³ served as positive control. The proteins were electroblotted onto a Hybond-C nitrocellulose membrane (Amersham Biosciences, RPN203C). After blocking with 4% non-fat dry milk in Tris-buffered saline containing 0.1% Tween20 (TBST0.1), the membrane was incubated overnight at 4°C with β -catenin antibody (Ab6302, Abcam, 1:500 in 4% bovine serum albumin (BSA) in TBST0.1). After three 5 minute washes in TBST0.1, the membrane was incubated for 90 minutes with anti-rabbit horseradish peroxidase (HRP)-conjugated secondary antibody (R&D HAF008, 1:20.000 in TBST0.1). Protein expression was detected using an enhanced chemiluminescence substrate (ECL Advance, Amersham RPN2135) in a ChemiDoc XRS System (Bio-Rad Laboratories). Control experiments were included by omitting the primary antibodies. After completing the western blot for β -catenin, the membranes were washed in TBST0.1 and re-used to determine α -tubulin protein expression. For this purpose, all steps as described above were performed except for the antibody incubations: the membrane was incubated with primary antibody for α -tubulin (Sigma T6199, 1:750) for 2 hours at room temperature, followed by secondary anti-mouse HRP-conjugated antibody (R&D HAF007, 1:20000). All experiments were performed in triplicate.

Gene name	Forward sequence 5'→3'	Exon	Reverse primer	Exon	Size	Temp (°C)	Accession no.
Target Genes							
<i>t</i>	AGACAGCCAGCAATCTG	5	TGGAGGGAAGTGAGAGG	6	115	53	NM_001003092.1
<i>kpr8</i>	CCTTAGGGGGTCTCTCGTA	9	GGGAAAGCTGGTGTCTGAGTC				
		149	63	XM_543639.4			
<i>wnt3a</i>	TCCCTGCGTTTCCGAAG	5	GGACCGAACTTGGAGATGC	5/6	89	64.5	XM_539327
<i>wnt7b</i>	AACACGCACCAAGTACACCAA	4	CACCTTGCAGGTGAAGACCTC	4	110	60	XM_539327
<i>wif1</i>	CCGAAATGGAGGCTTTTGTA	5	ATGCAGAAACCCAGGAGTGAC				
		6	61.5	XM_538269.3			
<i>fzd1</i>	GGCGCAGGGCACCAAGAAG	1	GAGCGACAGAATCACCCACCAGA	1	97	63	XM_539411
<i>lrp5</i>	GATCCTTGTGTCCGAIGACC	8	ACTCGAATTTGGGGTTTCC	9	104	53	XM_003432415
<i>dkk3</i>	CATCCAGTCCAGTGCTCTCA	3'UTR	GGGCCAGGATTGTAAGTGAA				
		3'UTR	58	XM_534060			
<i>ilk</i>	AAAGCAGGGACTTCAAATGAGGA	7	ACTTCACAGCTTGGCTCTGG	8	197	64	XM_858003
<i>cav1</i>	CGCACACCAAGGAAATCG	1	AAATCAATCTTGACCCACGTCTG				
		2	60	NM_001003296			
<i>axin2</i>	GGACAAAATGCGTGGATACCT	1	TGCTTGGAGACAATGCTGTT				
		1	60	XM_548025			
Reference							
Genes							
<i>hprt</i>	AGCTTGCTGGTGAAAAAGGAC	5/6	TTATAGTCAAGGGCATAATCC	7	104	56	NM_001003357
<i>rps19</i>	CCTTCCTCAAAAAAGTCTGGG	2/3	GTTCTCATCGTAGGGAGCAAG	3	95	61	XM_533657
<i>srpr</i>	GCTTCAGGATCTGGACTGC	7	GTTCCCTTGGTAGCACTGG	7/8	81	61	XM_546411
<i>rp113⁴¹</i>	GCCGGAAGGTTGTAGTCGT	3	GGAGGAAAGCCAGGTAATTC	4	87	61	XM_003432726
<i>ywhaz⁴¹</i>	CGAAGTTGCTGCTGGTGA	2	TTGCATTTCTCTTTTGTGCTGA	2/3	94	58	XM_533072

Table 1. Primers used for qPCR analysis. Primers (in-house design, except for 54) used for qPCR analysis of brachyury (*t*), cytokeratin 8 (*krt8*), *wnt3a*, *wnt7b*, *wnt* inhibitory factor 1 (*wif1*), *frizzled 1* (*fzd1*), low density lipoprotein receptor-related protein 5 (*lrp5*), integrin-linked kinase (*ilk*), *dickkopf* homolog 3 (*dkk3*), *caveolin-1* (*cav1*), and *axin2*, and reference genes hypoxanthine-guanine phosphoribosyltransferase (*hppt*), ribosomal protein S19 (*rps19*), signal recognition particle receptor (*srpr*), ribosomal protein L13 (*rpl13*), and tyrosine 3-monooxygenase/tryptophan 5-monooxygenase activation protein, zeta (*ywhaz*).

UTR = untranslated region.

Caveolin-1 immunohistochemistry

Paraffin-embedded IVD (as described above) sections from 5 non-chondrodystrophic and 5 chondrodystrophic dogs for each group (NC-rich, Mixed, CLC-rich; n=10 per group) were subjected to antigen retrieval in 10 mM citrate buffer (pH 6.0), followed by blocking of endogenous peroxidase activity³⁵. Nonspecific background staining was minimized by pre-incubation with blocking buffer containing 10% normal goat serum (Sigma-Aldrich) / 0.1% Tween-20 (Tween-20, Boom BV) in phosphate-buffered saline (PBS) for 30 min, and an overnight incubation at 4 °C with the primary antibody monoclonal mouse anti-caveolin-1 (Transduction Laboratories, mAb2297, 2.5 µg/ml, 1:100 in PBS with 0.1% Tween-20). After sections were washed in PBS buffer/0.025% Triton X, caveolin-1 was visualized with the goat anti-mouse Envision System and the liquid diaminobenzidine (DAB) chromogen system (Dako) and counterstained with hematoxylin (Hematoxylin QS, Vector Laboratories Inc.). In negative control sections, the primary antibody was omitted or replaced with its respective serum. All sections were stained in the same session.

Detailed overview images of each stained slide were made using a Colorview IIIU digital camera (Olympus) mounted to a BX-40 microscope (Olympus). The total NP surface of each sample was measured by defining the perimeter of the NP, excluding the transition zone. A custom-made color range selection optimized for caveolin-1 specific staining was used to calculate 'the proportion of the NP surface area that stained for caveolin-1' and the mean gray value (staining intensity) for caveolin-1 staining in each sample (as described previously³⁵). For statistical analysis, see below.

To investigate the relationship between caveolin-1 and canonical Wnt signaling in the NP, their co-localization was investigated by way of simultaneous immunofluorescence analysis of both proteins. Paraffin-embedded IVD slides were used for immunofluorescent labeling of caveolin-1 as described above, except that the slides were incubated overnight with a combination of primary antibodies monoclonal mouse anti-caveolin-1 (Transduction Laboratories, mAb2297, 2.5 µg/ml, 1:100 in PBS with 0.1% Tween-20) and polyclonal rabbit anti-β-catenin (Abcam, ab6302, 1:50 in PBS with 0.1% Tween-20).

The secondary antibodies used were 1:100 goat anti-mouse antibody conjugated to Alexa488 (2.5 µg/ml; Invitrogen) and 1:100 goat anti-rabbit antibody conjugated to Alexa568 (2.5 µg/ml; Invitrogen). Topro-3 iodide (2 µg/ml; Invitrogen, T3605) was used to stain the nucleus.

To outline proximity of the fluorescently-marked caveolin-1 and β -catenin proteins, profile intensity plots were generated in LAS-AF imaging software (Leica microsystems, Wetzlar, Germany). Straight lines were drawn across representative cell bodies and intensity profiles were extracted from the channels visualizing and measuring the fluorescence of caveolin-1, β -catenin, and Topro-3. The data were subsequently exported to Microsoft Excel (Microsoft Corporation) and plotted.

Caveolin-1 expression in NCs in vitro

On the basis of the previous analyses, caveolin-1 was investigated in NCs *in vitro*. NCs were isolated from the NPs of cervical (C2-T1) and lumbar (L1-S1) IVDs from six, young-adult, mongrel dogs (non-chondrodystrophic, aged 16-18 months and weighing 16-24 kg). The NCs were cultured in their original cluster-like conformation as described previously³⁵ on coverslips in 6-well plates (Falcon Multiwell Primaria, Becton Dickinson) in penicillin/streptomycin (P/S)-fetal calf serum (FCS, 10%)-DMEM-F12 under normoxic conditions (5% CO₂) at 37 °C for 10 days.

For RNA isolation, non-adherent cells at days 0 and 2 (NCs first adhered on day 4) were collected by centrifuging the medium at 1500 RPM at 4 °C for 1 minute; on days 4, 6, 8, and 10, the medium was removed, the wells were washed with RNase-free Hank's solution, and the adherent cells were lysed and used for analysis. For all time points, total cellular RNA was isolated using the RNeasy Mini Kit (Qiagen) according to the manufacturer's instructions. The relative gene expression of *caveolin-1* was analyzed as described above.

Non-adhered cells on days 0 and 2 were cells were collected from the culture medium and mounted on positively charged slides (Klinipath) using a Shandon Cytospin 4 (Therma Scientific). Cells were fixed on days 0, 2, 4, 6, 8, and 10 were used for immunofluorescent labeling of caveolin-1 as described above, except that the secondary antibody used was 1:100 donkey anti-mouse antibody conjugated to Alexa488 (2.5 µg/ml; Invitrogen). Topro-3 iodide (2 µg/ml; Invitrogen, T3605) was used to stain the nucleus. The cells were mounted with Fluorsave (Calbiochem). Images at 5 random locations in each sample were acquired by a sequential recording procedure on a multiphoton imaging station (MP2100, Zeiss, Herfordshire, UK). Immunofluorescent images of the cells were analyzed with CellProfiler 2.0 software package (Massachusetts Institute of Technology, Massachusetts, USA), with cell nuclei being detected on the Topro-3 images (nuclear staining) and the caveolin-1 expression signal on the caveolin-1 images. For each image, the total number of cells and the total caveolin-1 signal were measured, and the estimated mean intensity of caveolin-1

protein staining per cell was calculated by dividing the total caveolin-1 signal, after subtraction of background, by the total number of cells.

For statistical analysis, see below.

Data analysis and statistics for qPCR and immunohistochemistry/immunofluorescence

Statistical analyses were performed using R statistical software⁵⁵. Linear mixed models⁵⁶, containing both fixed and random effects, were used to analyze the described parameters separately for the qPCR of tissue samples, immunohistochemistry, qPCR of culture samples, and immunofluorescence. The Akaike Information Criterion (AIC) was used for model selection. A random intercept for each dog was added to each model to take the correlation of the observations within a dog into account. If necessary, models were optimized by correcting for unequal variances and/or for autoregressive correlation. Conditions for the use of mixed models, including normal distribution of the data, were assessed by analyzing the residuals (PP- and QQ plots) of the acquired models; no violations of these conditions were observed. For all the below-described models, the Benjamini-Hochberg correction was used to correct for multiple comparisons⁵⁷. $P < 0.05$ was considered statistically significant.

In the qPCR analysis of tissue samples, the Δ CT for individual target genes was used as parameter value; relative gene expression data from all target genes were analyzed as one outcome variable because there were potential inter-gene correlations within the canonical Wnt-signaling pathway. The explanatory factors for the linear mixed model were ‘target gene’ (*brachyury*, *cytokeratin 8*, *wnt7b*, *wnt inhibitory factor 1 (wif1)*, *frizzled 1 (fzd1)*, *low density lipoprotein receptor-related protein 5 (lrp5)*, *dickkopf homolog 3 (dkk3)*, *integrin-linked kinase (ilk)*, *caveolin-1 (cav1)* and *axin2*), ‘degeneration stage’ (NC-rich, Mixed, CLC-rich), breed type (non-chondrodystrophic and chondrodystrophic), and the interaction between these factors. P values were calculated per target gene to analyze differences between groups and degeneration stages.

In the immunohistochemistry study, ‘integrated density’ and ‘mean gray value’ were calculated. The explanatory factors for the linear mixed model were ‘Group’ (NC-rich, Mixed, CLC-rich), ‘Breed’ (non-chondrodystrophic and chondrodystrophic), and the interaction between these factors. P values were calculated per parameter to analyze differences between groups and degeneration stages.

In the NC culture study, the parameter values used for qPCR and immunofluorescence of *caveolin-1* were Δ CT for caveolin-1 gene expression and caveolin-1 protein expression per cell, respectively. For the immunofluorescence analysis, the data obtained from 5 images for each time point per dog were used for data analysis. The fixed factor in the linear mixed models used for both parameters was ‘time point in culture’ (days 0, 2, 4, 6, 8 and 10). P values were

calculated to analyze differences in caveolin-1 gene and protein expression between time points in culture.

NP in caveolin-1 knock-out (KO) mice

To further assess the role of caveolin-1 in NC preservation and early IVD degeneration, spines were collected from 3-month-old caveolin-1 KO-mice (Cav^{tm1Mls}, JAX®, the Jackson Laboratory, Maine, USA) and wild-type mice (strain B6129SF2, JAX®). Spines were fixed in 4% neutral buffered formalin, decalcified (7 days in EDTA at 4 °C), and embedded in paraffin. Mid-sagittal sections (4 µm) were mounted on Microscope KP+ slides (Klinipath B.V.) and stained with H&E and Alcian Blue/Picosirius Red, the latter highlighting proteoglycan (blue) and collagen content (red)⁵⁸. Multiple sections of the NP of multiple cervical and lumbar IVDs (n= 4) from each mouse were histopathologically evaluated.

Results

Microarray: changes in gene expression

In NPs from non-chondrodystrophic dogs, the NC-rich, Mixed, and CLC-rich groups consisted of 100.0% NCs, 45.4%-87.0% NCs, and 100.0% CLCs, respectively; in NPs from chondrodystrophic dogs, these proportions were 93.9%-100.0% NCs, 39.7%-89.9% NCs, and 100.0% CLCs, respectively. Therefore, the applied histopathological classification resulted in the NC-rich, Mixed, and CLC-rich groups being comparable between chondrodystrophic and non-chondrodystrophic dogs, allowing reliable investigation of early IVD degeneration within both types of breed, and comparison between the two types of breed.

qPCR analysis revealed no significant differences in the expression of the notochordal markers *brachyury* and *cytokeratin 8* in the different histopathological stages in non-chondrodystrophic dogs, indicating that the expression of NC marker genes was preserved in all histopathological stages despite significant changes in IVD morphology (Fig. 2; Table 2). However, in chondrodystrophic dogs, *brachyury* and *cytokeratin 8* gene expression was significantly down-regulated in the CLC-rich group compared with the NC-rich and Mixed groups; *brachyury* and *cytokeratin 8* gene expression was significantly lower in CLC-rich NP from chondrodystrophic dogs than CLC-rich NP from non-chondrodystrophic dogs. These results suggest that in chondrodystrophic dogs the transition from NC-rich to CLC-rich NP involves a significant down-regulation in NC marker gene expression. These results were sustained by the microarray results, showing decreased gene expression in the CLC-rich group compared with the NC-rich group of notochordal markers *cytokeratin 8* and¹⁹

Numerous up- and down-regulated genes were found in the performed microarrays (Table 3; Appendix I; the microarray data discussed in this manuscript have been deposited in NCBI's Gene Expression Omnibus (GEO) ⁶¹ and are accessible through GEO Series accession number GSE 35717; the following link can be used: <http://www.ncbi.nlm.nih.gov/geo/query/acc.cgi?to ken=phonhywsqeosgra&acc=GSE35717>).

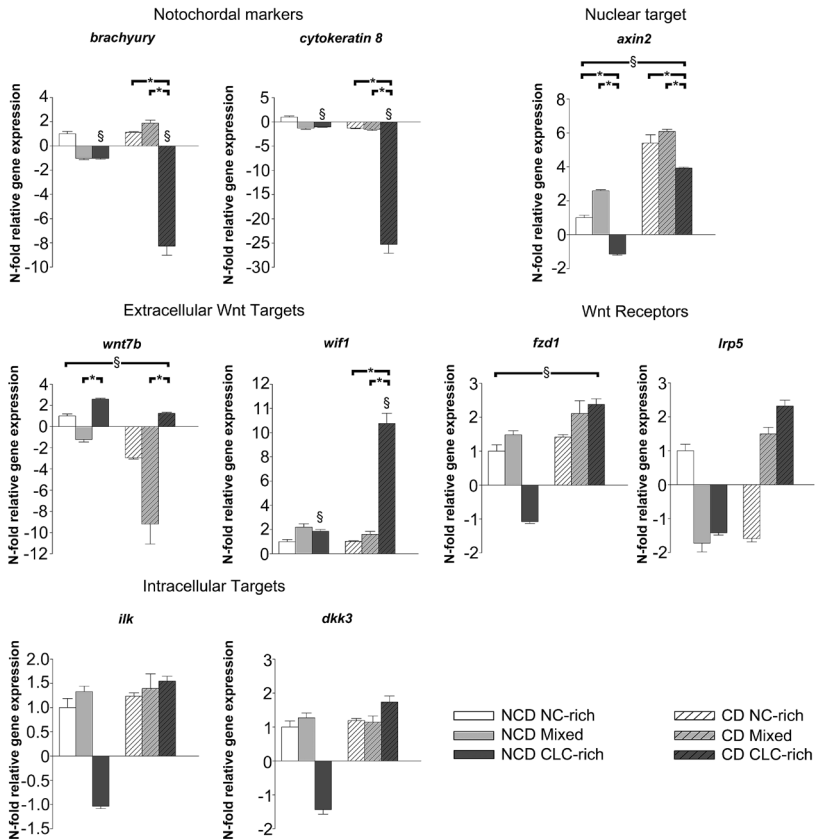


Figure 2. Relative gene expression of relevant target genes. Relative gene expression of *brachyury*, *cytokeratin 8*, *axin2*, *frizzled 1 (fzd1)*, *low density lipoprotein receptor-related protein 5 (lrp5)*, *wnt7b*, *wnt inhibitory factor 1 (wif1)*, *integrin linked kinase (ilk)*, and *dickkopf homolog 3 (dkk3)* in the notochordal cell rich (NC-rich), Mixed, and chondrocyte-like cell rich (CLC-rich) NP from non-chondrodystrophic (NCD) and chondrodystrophic (CD) dogs (NCD, NC-rich NP was used as reference, set at 1). * indicates significant difference between NC-rich, Mixed, and CLC-rich NP; § indicates significant difference between NCD and CD dogs.

	Non-chondro dystrophic											
	NC-rich vs. Mixed				Mixed vs. CLC-rich				NC-rich vs. CLC-rich			
	Array	P	qPCR	P	Array	P	qPCR	P	Array	P	qPCR	P
<i>t</i>	-1.87		-1.02		1.31		1.00		-1.43		-1.02	
<i>krt8</i>	-1.66		-1.27		-1.95		1.23		-3.24		-1.04	
<i>wnt7b</i>	-1.16		-1.21		1.10		3.11	0.017	-1.05		2.57	
<i>wnt10b</i>	1.09				-1.08				1.01			
<i>wif1</i>	1.17		2.20		1.81		-1.19		2.11		1.85	
<i>rspo3</i>	-2.41				1.40				-1.73			
<i>fzd1</i>	-1.07		1.48		-1.00		-1.60		-1.07		-1.08	
<i>frzb</i>	6.16				-1.17				5.28			
<i>lrp2</i>	-1.38				1.16				1.16			
<i>lrp5</i>	-1.29		-1.73		1.24		1.22		-1.03		-1.42	
<i>ilk</i>	-1.36		1.33		-0.81		-1.38		-1.11		-1.04	
<i>dkk3</i>	-1.03		1.27		-1.02		-1.82		-1.05		-1.44	
<i>cav1</i>	-1.37		-1.18		-1.08		-1.01		-1.47		-1.20	
<i>cav2</i>	-1.63	0.041			1.46				-1.12			
<i>cav3</i>	1.45				1.26				1.83			
<i>axin2</i>	1.08		2.58		-1.01		-2.95	0.025	1.07		-1.14	0.047

	Chondro dystrophic											
	NC-rich vs. Mixed				Mixed vs. CLC-rich				NC-rich vs. CLC-rich			
	Array	P	qPCR	P	Array	P	qPCR	P	Array	P	qPCR	P
<i>t</i>	1.53	0.028	1.67		-3.89	0.001	-10.51	0.004	-2.54	0.017	-9.30	0.019
<i>krt8</i>	-1.21		-1.16		-4.90	0.031	-22.83	0.023	-5.94	0.026	-23.49	0.001
<i>wnt7b</i>	1.43	0.027	-3.13		-1.19		11.41	0.017	1.21		3.65	
<i>wnt10b</i>	2.54	0.000			-1.23				2.07	0.002		
<i>wif1</i>	-2.63		1.57		3.64	0.030	6.73	0.048	1.38		10.54	0.043
<i>rspo3</i>	1.48				-5.14	0.000			-3.48	0.001		
<i>fzd1</i>	1.26		1.49		-1.08		1.13		1.16		1.68	
<i>frzb</i>	-1.95				14.18	0.009			7.26	0.004		
<i>lrp2</i>	1.42				-2.58	0.005			-1.82			
<i>lrp5</i>	-1.11		2.38		-2.46	0.005	-1.43		-2.74	0.001	1.66	
<i>ilk</i>	-1.11		1.13		-1.45	0.056	1.11		-1.61	0.049	1.25	
<i>dkk3</i>	1.08		-1.05		-1.07		1.53		1.02		1.46	
<i>cav1</i>	-1.14		1.12		-1.77	0.017	-1.98	0.002	-2.02	0.011	-1.76	0.006
<i>cav2</i>	1.16				-2.12	0.009			-1.83	0.006		
<i>cav3</i>	2.34	0.007			1.67	0.045			3.92	0.001		
<i>axin2</i>	1.08		1.13		-1.10		-1.77	0.025	-1.02		-1.57	0.047

Non-chondrodystrophic vs. chondrodystrophic												
	NC-rich				Mixed				CLC-rich			
	Array	P	qPCR	P	Array	P	qPCR	P	Array	P	qPCR	P
<i>t</i>	-1.14		1.12	0.983	2.52	0.007	1.92		-2.01		-8.09	0.024
<i>krt8</i>	1.05		-1.30	0.687	1.44		-1.18		-1.75		-24.37	0.003
<i>wnt7b</i>	-1.43		-2.94	0.018	1.17		-7.62	0.018	-1.12		-2.08	0.018
<i>wnt10b</i>	-2.05	0.007			1.13				-1.00			
<i>wif1</i>	2.10		1.02	0.584	-1.47		-1.37		1.38		5.81	0.039
<i>rspo3</i>	-1.44				2.47				-2.90			
<i>fzd1</i>	-1.13		1.41	0.042	1.20		1.42	0.042	1.10		2.56	0.042
<i>frzb</i>	5.56				-2.16				7.64			
<i>lrp2</i>	1.51				2.96	0.004			-1.01			
<i>lrp5</i>	1.30		-1.59	0.458	1.50		2.58		-2.04		1.48	
<i>ilk</i>	1.00		1.23	0.051	1.23		1.05		-1.45		1.60	
<i>dkk3</i>	-1.15		1.19	0.444	-1.03		-1.12		-1.08		2.49	
<i>cav1</i>	1.02		-1.21	0.680	1.23		1.09		-1.34		-1.79	
<i>cav2</i>	-1.01				1.87	0.046			-1.65			
<i>cav3</i>	-1.93				-1.20				1.11			
<i>axin2</i>	1.29		5.40	0.009	1.29		2.36	0.009	1.18		3.92	0.009

Table 2. N-fold changes and P values for microarray and qPCR analysis.

N-fold changes and P values (in case of significance, highlighted in bold text) for microarray analysis of brachyury (*t*), cytokeratin 8 (*krt8*), and Wnt-associated gene targets *wnt7b*, *wnt10b*, *wnt* inhibitory factor 1 (*wif1*), *r*-spondin-3 (*rspo3*), *frizzled* 1 (*fzd1*), *frizzled*-related protein (*frzb*), low density lipoprotein receptor-related protein-2 (*lrp2*), low density lipoprotein receptor-related protein 5 (*lrp5*), *integrin*-linked kinase (*ilk*), *dickkopf* homolog 3 (*dkk3*), *caveolin*-1 (*cav1*), *caveolin*-2 (*cav2*), *caveolin*-3 (*cav3*), and *axin2*, and qPCR of selected gene targets. N-fold changes are displayed for the comparisons between the Notochordal cell (NC)-rich nucleus pulposus (NP), the Mixed NP, and the chondrocyte-like cell (CLC)-rich NP, and between non-chondrodystrophic dogs and chondrodystrophic dogs for the three histological NP stage

Chondrodystrophic dogs: NC-rich NP vs. CLC-rich NP

Gene symbol	Description	Total up-regulated genes: 1178		Total down-regulated genes: 1741	
		GO term: Biological Process	Ensemble Gene ID	N-fold Change	P-value
CPE	Carboxypeptidase E	Protein modification process	ENSG00000109472	8.65	8.65E-05
TF	Transferrin	Transferrin transport	ENSG00000091513	8.58	1.56E-02
CP	Ceruloplasmin (ferroxidase)	Cellular iron ion homeostasis	ENSG00000047457	7.34	2.02E-03
FRZB	Frizzled-related protein	Negative regulation of canonical Wnt receptor signaling pathway	ENSG00000162998	7.26	4.24E-03
DCN	Decorin	Peptide cross-linking via chondroitin 4-sulfate glycosaminoglycan	ENSG00000011465	7.11	2.00E-02
COMP	Cartilage oligomeric matrix protein	Anti-apoptosis	ENSG00000105664	7.08	6.69E-05
SRGN	Serglycin	Negative regulation of bone mineralization	ENSG00000122862	6.97	9.64E-03
LUM	Lumican	Collagen fibril organization	ENSG00000139329	6.88	1.39E-02
Not annotated	Not annotated	Not annotated	Not annotated	6.66	1.15E-02
MT2A	Metallothionein 2A	Cellular response to erythropoietin	ENSG00000125148	6.60	5.33E-03
RANBP3L	RAN binding protein 3-like	Intracellular transport	ENSG00000164188	6.54	4.71E-02
RBP4	Retinol binding protein 4, plasma	Protein complex assembly	ENSG00000138207	6.40	6.79E-04
CDO1	Cysteine dioxygenase, type 1	Response to glucagon stimulus	ENSG00000129596	6.30	1.36E-02
ADCY2	Adenylate cyclase 2	Activation of adenylate cyclase activity by G-protein signaling pathway	ENSG00000078295	5.97	3.94E-04
TSPAN13	Tetraspanin 13	Not available	ENSG00000106537	5.88	1.95E-02
MFAP5	Microfibrillar associated protein 5	Not available	ENSG00000197614	5.75	1.17E-04
PRG4	Proteoglycan 4	Cell proliferation	ENSG00000116690	5.61	3.00E-03
S100A12	S100 calcium binding protein A12	Inflammatory response	ENSG00000163221	5.59	1.15E-02

Table 3, continued

PID1	Phosphotyrosine interaction domain containing 1	Not available	ENSG00000153823	5.57	8.41E-05
NPNT	Nephronectin	Cell differentiation	ENSG00000168743	5.54	2.76E-04
LYZ	Lysozyme	Cell wall macromolecule catabolic process	ENSG00000090382	5.47	2.42E-02
SPARCL1	SPARC-like 1 (hevin)	Signal transduction	ENSG00000152583	5.34	2.85E-02
G25L	Glycoprotein 25L	Not available	Not available	5.27	5.84E-04
SER-PING1	Serpin peptidase inhibitor, clade G (C1 inhibitor), member 1	Regulation of proteolysis	ENSG00000149131	5.08	6.92E-04
SMPDL3A	Sphingomyelin phosphodiesterase, acid-like 3A	Sphingomyelin catabolic process	ENSG00000172594	5.01	1.16E-02
SER-PINA5	Serpin peptidase inhibitor, clade A (alpha-1 antiprotease, antitrypsin), member 5	Regulation of proteolysis	ENSG00000188488	4.94	1.28E-03
BBOX1	Butyrobetaine (gamma), 2-oxoglutarate dioxygenase (gamma-butyrobetaine hydroxylase) 1	Cellular nitrogen compound metabolic process	ENSG00000129151	4.83	2.82E-03
MT1	Metallothionein 1	Not available	ENSG00000205360	4.82	6.04E-04
ARH-GEF10	Rho guanine nucleotide exchange factor (GEF) 10	Regulation of Rho protein signal transduction	ENSG00000104728	4.55	< 1.0E-06
S100A9	S100 calcium binding protein A9	Chemotaxis	ENSG00000163220	4.50	1.07E-02
PMEPA1	Prostate transmembrane protein, androgen induced 1	Androgen receptor signaling pathway	ENSG00000124225	4.45	1.03E-04

Table 3, continued

SCRG1	Stimulator of chondrogenesis 1	Nervous system development	ENSG00000164106	4.43	3.24E-03
SDC2	Syndecan 2	Response to hypoxia	ENSG00000169439	4.34	5.78E-04
ATP2B1	ATPase, Ca ⁺⁺ transporting, plasma membrane 1	ATP biosynthetic process	ENSG00000070961	4.21	1.31E-03
EPSTI1	Epithelial stromal interaction 1	Not available	ENSG00000133106	4.21	1.62E-04
SPSB2	SplA/ryanodine receptor domain and SOCS box containing 2	Intracellular signal transduction	ENSG00000111671	4.18	1.0E-06
NT5E	5'-nucleotidase, ecto (CD73)	Nucleotide catabolic process	ENSG00000135318	4.14	4.17E-03
SMOC2	SPARC related modular calcium binding 2	Signal transduction	ENSG00000112562	4.10	6.04E-04
CCL23	Chemokine (C-C motif) ligand 23	Cellular calcium ion homeostasis	ENSG00000167236	4.09	1.67E-02
SLC5A3	Solute carrier family 5 (sodium/myo-inositol cotransporter), member 3	Transmembrane transport	ENSG00000198743	3.96	1.66E-02
NDUFA7	NADH dehydrogenase (ubiquinone) 1 alpha subcomplex	Oxidation-reduction process	ENSG00000167774	3.93	3.42E-04
CAV3	Caveolin 3	Negative regulation of cardiac muscle hypertrophy	ENSG00000182533	3.92	7.98E-04
PLBD1	Phospholipase B domain containing 1	Lipid catabolic process	ENSG00000121316	3.87	1.20E-02
BCAT1	Branched chain amino-acid transaminase 1, cytosolic	Branched chain family amino acid biosynthetic process	ENSG00000060982	3.87	2.12E-02
S100A8	S100 calcium binding protein A8	Chemotaxis	ENSG00000143546	3.85	8.49E-03
CAMP	Cathelicidin antimicrobial peptide	Defense response to bacterium	ENSG00000164047	3.81	4.99E-02
CLIC6	Chloride intracellular channel 6	Ion transport	ENSG00000159212	3.80	3.70E-04

Table 3, continued

PLCL1	Phospholipase C-like 1	Lipid metabolic process	ENSG00000115896	-7.40	9.48E-03
DSC3	Desmocollin 3	Cell adhesion	ENSG00000134762	-7.05	1.40E-03
MYL9	Myosin, light chain 9, regulatory	Regulation of muscle contraction	ENSG00000101335	-6.84	1.64E-02
MRPS27	Mitochondrial ribosomal protein S27	Not available	ENSG00000113048	-6.76	4.96E-04
ENPP2	Ectonucleotide pyrophosphatase/phosphodiesterase 2	Regulation of cell migration	ENSG00000136960	-6.41	9.38E-03
KRT19	Keratin 19	Cell differentiation involved in embryonic placenta development	ENSG00000171345	-6.32	6.00E-03
PKP2	Plakophilin 2	Carbohydrate metabolic process	ENSG00000057294	-6.13	6.02E-04
TSPAN7	Tetraspanin 7	Interspecies interaction between organisms	ENSG00000156298	-6.01	3.00E-03
KRT8	Keratin 8	Cytoskeleton organization	ENSG00000170421	-5.94	2.60E-02
NAP1L1	Nucleosome assembly protein 1-like 1	DNA replication	ENSG00000187109	-5.92	1.40E-03
RAB20	RAB20, member RAS oncogene family	Small GTPase mediated signal transduction	ENSG00000139832	-5.79	2.91E-03
CALD1	Caldesmon 1	Positive regulation of protein binding	ENSG00000122786	-5.68	3.60E-03
KCNS3	Potassium voltage-gated channel, delayed-rectifier, subfamily S, member 3	Synaptic transmission	ENSG00000170745	-5.64	4.46E-03
APLN	Apelin	Positive regulation of phosphorylation	ENSG00000171388	-5.59	7.66E-03
SORBS2	Sorbin and SH3 domain containing 2	Biological process	ENSG00000154556	-5.42	3.39E-03
PCTP	Phosphatidylcholine transfer protein	Cholesterol metabolic process	ENSG00000141179	-5.37	1.30E-03
KCNIP1	Kv channel interacting protein 1	Synaptic transmission	ENSG00000182132	-5.14	1.0E-06

Table 3, continued

CA2	Carbonic anhydrase II	Carbon utilization	ENSG00000104267	-5.07	2.57E-02
THY1	Thy-1 cell surface antigen	Cytoskeleton organization	ENSG00000154096	-4.74	1.10E-02
RAB38	RAB38, member RAS oncogene family	GTP catabolic process	ENSG00000123892	-4.71	5.79E-04
SEMA3C	Sema domain, immunoglobulin domain (Ig), short basic domain, secreted, (semaphorin) 3C	Neural tube development	ENSG00000075223	-4.58	1.01E-04
DSC2	Desmocollin 2	Cell adhesion	ENSG00000134755	-4.48	9.91E-03
PHACTR1	Phosphatase and actin regulator 1	Regulation of transcription, DNA-dependent	ENSG00000112137	-4.48	3.17E-04
SCRN1	Secernin 1	Exocytosis	ENSG00000136193	-4.48	2.71E-02
SLC24A5	Solute carrier family 24, member 5	Ion transport	ENSG00000188467	-4.46	3.18E-03
CA3	Carbonic anhydrase III, muscle specific	Response to oxidative stress	ENSG00000164879	-4.46	2.63E-03
TUBB2A	Tubulin, beta 2A	Microtubule-based movement	ENSG00000137267	-4.42	1.40E-02
BRAF	V-raf murine sarcoma viral oncogene homolog B1	Negative regulation of apoptosis	ENSG00000157764	-4.39	8.65E-05
YIPF2	Yip1 domain family, member 2	Not available	ENSG00000130733	-4.35	3.12E-05
SLC12A2	Solute carrier family 12 (sodium/potassium/chloride transporters), member 2	Ion transport	ENSG00000064651	-4.34	1.10E-02
LGALS1	Lectin, galactoside-binding, soluble, 1	Positive regulation of I-kappaB kinase/NF-kappaB cascade	ENSG00000100097	-4.30	2.82E-03
C10orf137	Chromosome 10 open reading frame 137	Regulation of transcription, DNA-dependent	ENSG00000107938	-4.26	2.30E-02
LYST	Lysosomal trafficking regulator	Endosome to lysosome transport	ENSG00000143669	-4.25	5.73E-03

Table 3, continued

ODAM	Odontogenic, ameloblast associated	Biomineral tissue development	ENSG00000109205	-4.25	< 1.0E-06
PEX5L	Peroxisomal biogenesis factor 5-like	Protein import into peroxisome matrix	ENSG00000114757	-4.13	1.01E-04
PCDH7	Protocadherin 7	Cell adhesion	ENSG00000169851	-4.12	2.32E-03
EML2	Echinoderm microtubule associated protein like 2	Sensory perception	ENSG00000125746	-4.07	8.98E-03
PCDH15	Protocadherin-related 15	Cell adhesion	ENSG00000150275	-4.07	4.16E-03
KIAA0368	KIAA0368	ER-associated protein catabolic process	ENSG00000136813	-4.05	2.43E-05
VCAN	Versican	Cell adhesion	ENSG00000038427	-4.01	< 1.0E-06
STX8	Syntaxin 8	Transport	ENSG00000170310	-3.99	8.47E-04
LRRC4	Leucine rich repeat containing 4	Not available	ENSG00000128594	-3.99	1.20E-03
C3orf49	Chromosome 3 open reading frame 49	Not available	ENSG00000163632	-3.98	6.41E-04
LAMB4	Laminin, beta 4	Cell adhesion	ENSG00000091128	-3.97	1.58E-04
Ehd3	EH-domain containing 3	Endocytic recycling	ENSG00000013016	-3.95	3.97E-02

Table 3. Top 50 up- and down-regulated genes for the microarray comparison ‘notochordal cell (NC)-rich nucleus pulposus (NP) (reference) vs. chondrocyte-like cell-(CLC)-rich NP’ in chondrodystrophic dogs. This specific comparison was chosen to illustrate the overall trend in gene regulations observed in early IVD degeneration. For up- and down-regulations in the other microarray analyses: see Appendix I. For brevity, only one Gene Ontology (GO)-term is given for each gene (obtained with bioDBnet⁶²).

Metacore pathway map analysis showed that several signaling pathways were up-regulated or down-regulated in the transition from NC-rich to CLC-rich NP from chondrodystrophic dogs, such as extracellular matrix remodeling, plasmin signaling, plasminogen activator-urokinase (PLAU)-signaling, bone morphogenetic protein signaling, and Wnt signaling/cytoskeletal remodeling (Table 4).

Metacore pathway map analysis could not be performed on the gene regulation results from non-chondrodystrophic dogs, because relatively too few genes were down-or up-regulated in this breed group (Appendix I).

Wnt/ β -catenin signaling was analyzed further because it is involved in both the regeneration and the degeneration of various tissues⁶³. The expression of the *wnt7b* (Wnt ligand), *wif1* (inhibits by binding to Wnt ligands), *ilk* (inhibits glycogen synthase kinase 3- β), and *lrp5* (Wnt co-receptor) genes was significantly changed and these Wnt/ β -catenin targets genes were analyzed

further by qPCR, as were additional targets involved in canonical Wnt signaling: *wnt3a* (Wnt ligand), *fzd1* (Wnt receptor), *dkk3* (negative regulator of Wnt), and *axin2* (Wnt read-out) (Table 2).

Pathway	P value
Cytoskeleton remodeling: TGF, Wnt and cytoskeleton remodeling	2.63e-7
Cell adhesion: extracellular matrix (ECM) remodeling	8.22e-5
Cell adhesion: plasmin signaling.	1.58e-4
Cell adhesion: plasminogen activator urokinase (PLAU) signaling.	6.96e-4
Bone Morphogenic Protein (BMP) signaling	1.16e-2

Table 4. Top 5 most significantly regulated pathways on the basis of all performed microarray comparisons using Metacore pathway analysis ⁴¹.

Quantitative PCR of canonical Wnt signaling pathway and β -catenin protein expression

The relative gene expression of *axin2*, which is a highly reliable read-out for the activity of Wnt/ β -catenin signaling ⁶⁴⁻⁶⁶, was significantly lower in the CLC-rich group than in the NC-rich and Mixed groups in both non-chondrodystrophic and chondrodystrophic dogs (Fig. 2). In chondrodystrophic dogs, this decrease in *axin2* gene expression may be related to the gene expression of *wif1* (inhibits Wnt ligands), which was significantly up-regulated in the CLC-rich group compared with the NC-rich and Mixed groups. In non-chondrodystrophic dogs, no significant changes in *wif1* gene expression were found. However, gene expression of the Wnt ligand *wnt7b*, which activates canonical Wnt signaling through interactions with Fzd and LRP5 ⁶⁷, was significantly higher in the CLC-rich group compared with the Mixed group in both non-chondrodystrophic and chondrodystrophic dogs.

Compared with non-chondrodystrophic dogs, *axin2* gene expression was significantly higher in chondrodystrophic dogs in all histopathological groups, indicating an overall higher Wnt signaling activity in chondrodystrophic dogs. Accordingly, the integrated density of β -catenin corrected for the NP surface area positively stained was significantly higher in the CLC-rich NP of chondrodystrophic dogs compared with non-chondrodystrophic dogs (Fig. 3A and B).

Due to the abundance of matrix protein in the native CLC-rich NP tissue, western blot analysis of active β -catenin expression was cumbersome and quantification of the data was not reliable. The chondrodystrophic CLC-rich NP appeared, though, to have less degraded β -catenin compared to non-chondrodystrophic dogs (Fig. 3C). These findings are sustained by investigation of the gene expression of Wnt receptor *fzd1*, which was significantly higher in chondrodystrophic dogs than in non-chondrodystrophic dogs for all three histopathological stages. Gene expression of *wnt7b* was significantly higher

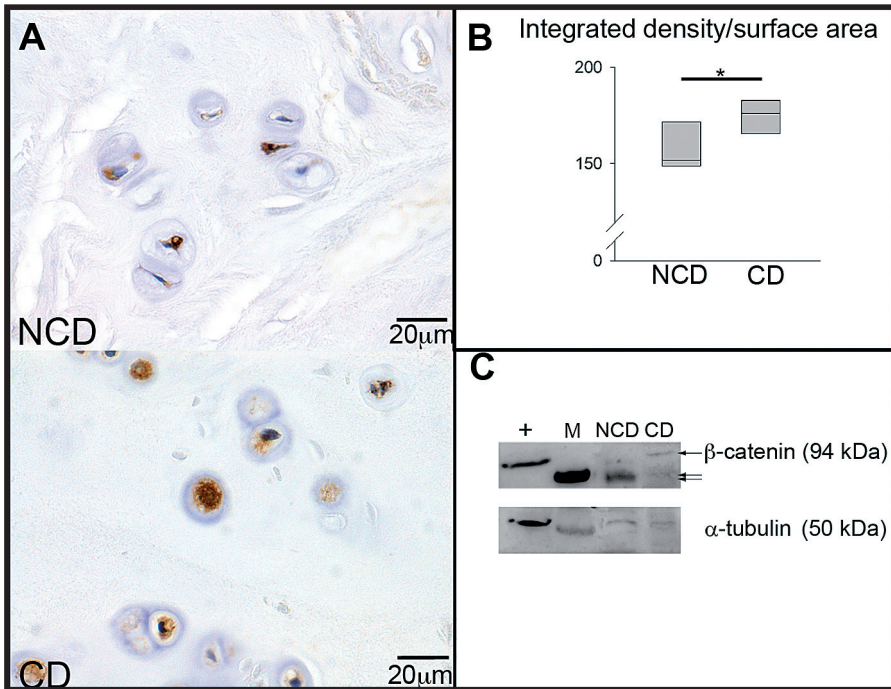


Figure 3. β -Catenin protein expression in the chondrocyte-like cell (CLC)-rich nucleus pulposus (NP) of non-chondrodystrophic and chondrodystrophic dogs. A) Typical examples of immunohistochemistry for β -catenin in the chondrocyte-like cell (CLC)-rich nucleus pulposus (NP) from non-chondrodystrophic (NCD) and chondrodystrophic (CD) dogs, showing a stronger staining intensity for β -catenin in CLCs of CD dogs. B) Boxplots for the integrated density/surface area of β -catenin staining for the CLC-rich NP of NCD and CD dogs. The asterisk indicates a significant difference between NCD and CD dogs. C) Western blot for β -catenin in the CLC-rich NP from NCD and CD dogs. Typically, in CD dogs β -catenin antibody identified the whole β -catenin (94 kDa; single arrow), whereas in NCD dogs a wider band of ~ 70 kDa (double arrow) was identified, most probably representing phosphorylated β -catenin subjected to degradation⁶⁸. Protein extracted from the human insulinoma CM cell-line was used as positive control (+). Note that 5 μ g protein of the CM cell-line was sufficient to generate a clear signal of β -catenin and α -tubulin, whereas 15 μ g protein of NP extract gave a weak signal (also for α -tubulin) due to the relative abundance of matrix proteins within the CLC-rich NP.

in non-chondrodystrophic dogs compared with chondrodystrophic dogs in all histopathological stages.

The relative gene expression of *lrp5*, *ilk*, and *dkk3* remained unchanged in both non-chondrodystrophic and chondrodystrophic dogs. Gene expression of the *wnt3a* was undetectable in all groups in both breed types.

Caveolin-1 expression

The microarray analyses showed significant changes in *caveolin-1*, -2 and -3. Early IVD degeneration involved significant down-regulation of *caveolin-1* and -2, and significant up-regulation of *caveolin-3* (Table 2, Appendix 1). Given the role of caveolin-1 in the regulation of canonical Wnt signaling^{49,50,69} and the reported upregulation of *caveolin-1* in degenerated human IVDs⁷⁰, its gene and protein expression were further investigated by way of qPCR and immunohistochemistry.

In chondrodystrophic dogs, the gene expression of *caveolin-1* was significantly down-regulated in the CLC-rich group compared with the NC-rich and Mixed groups (Fig. 4); no significant changes were found in non-chondrodystrophic dogs. The gene expression of *caveolin-1* in the CLC-rich NP was significantly lower in chondrodystrophic dogs than in non-chondrodystrophic dogs.

Caveolin-1 protein was predominantly located in the cell membranes of NCs, and occasionally in their cytoplasm; caveolin-1 protein was seldom observed in CLCs. The ‘proportion of the NP surface area that stained for caveolin-1’ was significantly lower in the CLC-rich NP than in the NC-rich and Mixed NP in both non-chondrodystrophic and chondrodystrophic dogs, indicating decreased caveolin-1 protein expression (Table 5). No significant differences were found in the mean gray value (staining intensity) between the NC-rich, Mixed, and CLC-rich groups in both non-chondrodystrophic and chondrodystrophic dogs. The intensity of caveolin-1 staining in all three histopathological groups was significantly higher in non-chondrodystrophic dogs than in chondrodystrophic dogs.

To further assess the relationship between caveolin-1 and canonical wnt signaling in the NP, co-immunofluorescence of caveolin-1 and β -catenin was performed. Profile intensity plots (Fig. 4D) showed clear signal peaks of β -catenin expression within the cell nucleus of NCs, indicative of active canonical Wnt signaling. Also, clear protein expression of caveolin-1/ β -catenin were co-localized at the cell membrane of NCs, which is supportive of interaction of these proteins within the NC-rich NP. In CLCs, caveolin-1 and β -catenin protein expression was rarely observed, which are indicative of less active canonical Wnt signaling and no co-localization and potential protein interaction.

To verify the possible role of caveolin-1 in NCs, its expression and intracellular distribution in primary NCs was investigated. The relative gene expression of *caveolin-1* in primary NCs on day 0 in culture was comparable to that in NC-rich NP tissue *ex vivo*, but thereafter increased significantly on days 2, 4, and 6 and remained stable on days 8 and 10 (Fig. 5; Table 6). Caveolin-1 protein was located in intracellular membranes, as suggested by the inhomogeneous appearance of the immunolabeled membrane-embedded marker, and in the

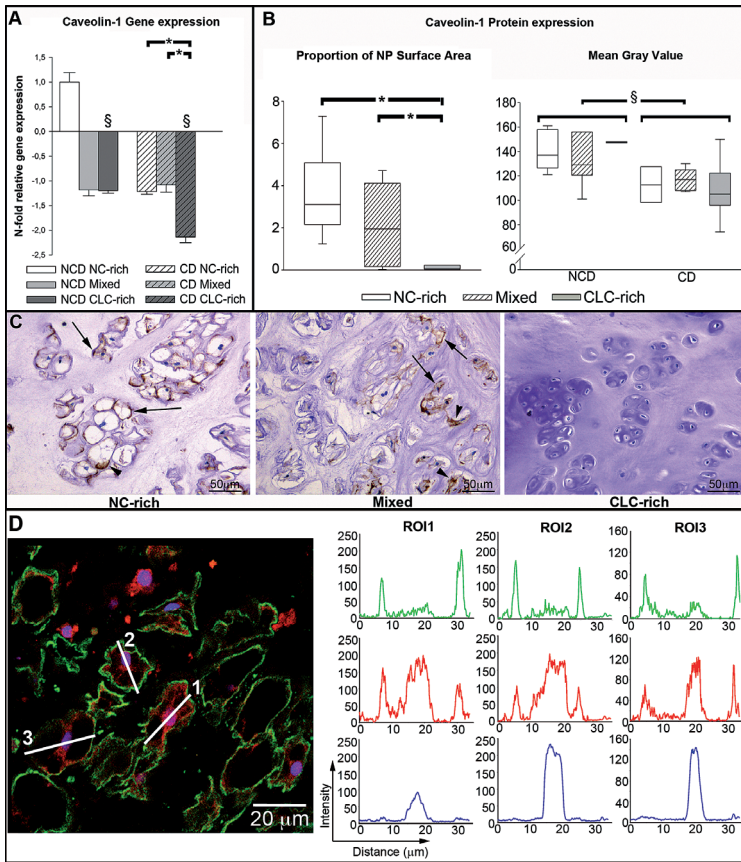


Figure 4. Caveolin-1 expression in the course of early intervertebral disc degeneration. A) Caveolin-1 gene expression and B) 'the proportion of the NP surface area that stained for caveolin-1' and mean gray value for caveolin-1 protein expression in the notochordal cell (NC)-rich, Mixed, and chondrocyte-like cell (CLC)-rich nucleus pulposus (NP) from non-chondrodystrophic (NCD) and chondrodystrophic (CD) dogs. * indicates a significant difference between degeneration stages; § indicates a significant difference between NCD and CD dogs. The parameter 'proportion of the NP surface area that stained for caveolin-1' was not divided into NCD and CD dogs because no significant differences were found between breed types. C) Typical examples of NP samples stained for caveolin-1, showing the NC-rich NP, mixed cell population NP with NCs and CLCs, and the CLC-rich NP. In the NC-rich and Mixed groups, membranous (arrow) and cytoplasmic (arrowhead) staining can be observed. Note that caveolin-1 staining is not observed in CLCs. D) Immunofluorescent staining of the NC-rich NP for the proteins caveolin-1 (green) and β -catenin (red), and for DNA (blue). Region of interest (ROI) lines drawn across cell bodies were used to generate profile intensity plots (right) for the signal intensity of the caveolin-1 (green), β -catenin (red), and Topro-3 (blue). The signal intensity peaks for caveolin-1 correspond with the signal peaks of β -catenin at the cell membrane (located at the same distance of the ROI line), indicating co-localization of these proteins. Also, the central β -catenin signal peaks correspond with the Topro-3 signal peaks, indicating nuclear localization of β -catenin.

NC cell membrane (Fig. 6). The expression of caveolin-1 protein per cell was significantly higher on day 4 in culture than on days 0 and 2, but levels decreased thereafter on days 6, 8 and 10.

Parameter	Immunohistochemistry		
	Group	Breed	Group*Breed
Surface Area %	0.006	0.180	0.063
Mean Grey Value	0.967	0.025	0.750
<i>Inter-group comparison per parameter</i>			
	NCR-MX	NCR-CLCR	MX-CLCR
Surface Area %	0.052	<0.001	0.026
Mean Grey Value	-	-	-

Table 5. Linear mixed model results for the caveolin-1 immunohistochemistry analyses of healthy vs. early-degenerated nuclei pulposi. *P* values for the mixed model explanatory factors ‘Group’ (notochordal cell rich (NCR), mixed population (MX), chondrocyte-like cell rich (CLCR), ‘Breed’ (non-chondrodystrophic or chondrodystrophic dog), and their interactions. In case of significant main effects, *P* values for comparisons between groups per parameter and were calculated. $P < 0.05$ was considered statistically significant.

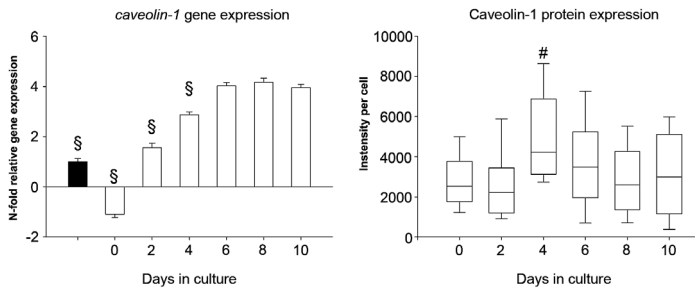


Figure 5. Caveolin-1 gene and protein expression in primary notochordal cells in monolayer culture. A) Relative gene expression of caveolin-1 in notochordal cell (NC) clusters on different days in culture. NC-rich NP tissue served as a reference (black bar; set at 1). §: indicates significant differences with all subsequent time points in culture. B) Boxplots of caveolin-1 protein expression

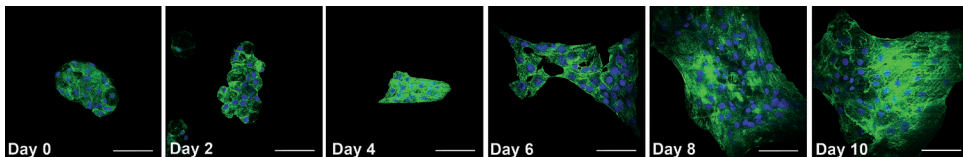


Figure 6. Immunofluorescence of caveolin-1 in primary notochordal cells in monolayer culture. Immunofluorescence images of the notochordal cell clusters on days 0, 2, 4, 6, 8, and 10 in culture. Scale bar: 50 μ m. Nuclear staining (Topro-3) and caveolin-1 staining are depicted in blue and green, respectively. Caveolin-1 protein was located in intracellular membranes, as suggested by the inhomogeneous appearance of the immunolabeled membrane-embedded marker, and in the notochordal cell membrane.

	<i>caveolin-1</i> gene expression	caveolin-1 protein expression
NC tissue vs. Day 0	0.170	-
NC tissue vs. Day 2	<0.001	-
NC tissue vs. Day 4	<0.001	-
NC Tissue vs. Day 6	<0.001	-
NC tissue vs. Day 8	<0.001	-
NC tissue vs. Day 10	<0.001	-
Day 0 vs. 2	<0.001	0.630
Day 0 vs. 4	<0.001	<0.001
Day 0 vs. 6	<0.001	0.248
Day 0 vs. 8	<0.001	0.519
Day 0 vs. 10	<0.001	0.598
Day 2 vs. 4	<0.001	<0.001
Day 2 vs. 6	0.001	0.077
Day 2 vs. 8	0.001	0.999
Day 2 vs. 10	0.006	0.987
Day 4 vs. 6	0.014	0.005
Day 4 vs. 8	0.020	<0.001
Day 4 vs. 10	0.124	<0.001
Day 6 vs. 8	0.534	0.079
Day 6 vs. 10	0.279	0.069
Day 8 vs. 10	0.218	0.958

Table 6. P values for the mixed model analyses of caveolin-1 gene and protein expression of notochordal cells in culture. The explanatory variable used in the mixed model was 'Time point' (days 0, 2, 4, 6, 8 and 10 in culture), and P values for comparisons between time points were calculated. $P < 0.05$ was considered statistically significant (highlighted in bold text).

The physiological role of caveolin-1 in the preservation of NCs was further investigated in caveolin-1 KO mice. The IVD of 3-month-old caveolin-1 KO mice was significantly different from that of wild-type mice of the same age (Fig. 7). The NP of the wild-type IVD consisted of a centrally located area of large cells with highly vacuolated cytoplasm and hyperchromatic nuclei, consistent with the morphological characteristics of viable NCs. A limited amount of chondroid-like intercellular matrix was visible within the area of NCs and there was a large rim of this matrix in the zone between the NCs and the endplate. In contrast, the NP of the caveolin-1 KO mice contained rounded cells, with a smaller amount of cytoplasm lacking the typical vacuolar appearance. Over 75% of these cells did not contain recognizable nuclei and were characterized by cytoplasmic eosinophilia suggestive of necrosis or apoptosis. The NP of caveolin-1 KO mice contained a large amount of chondroid-like intercellular matrix between the cells within the NP.

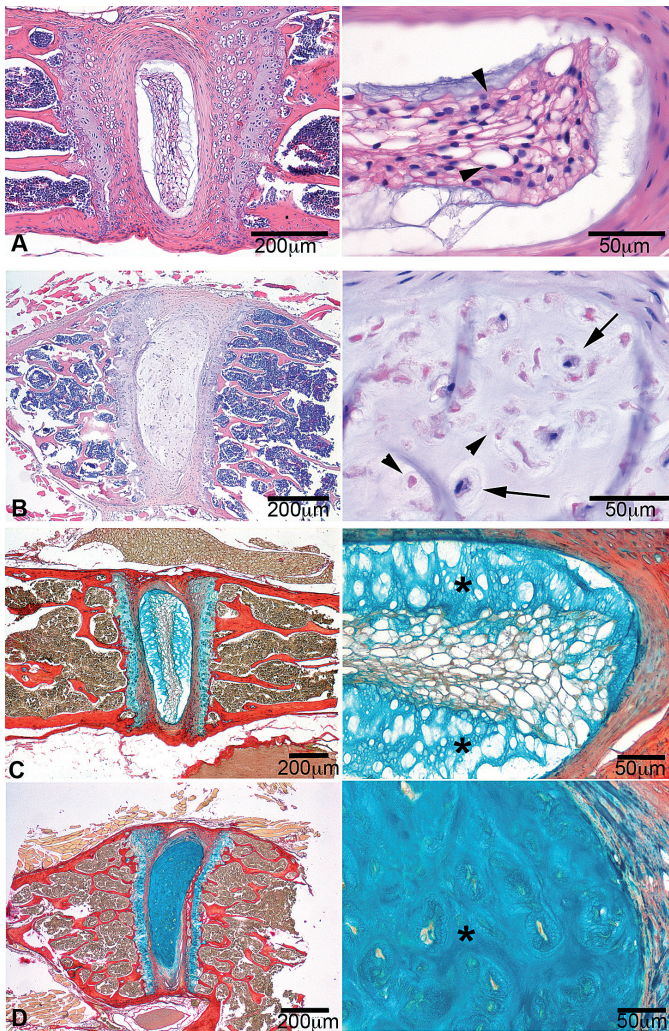


Figure 7. The intervertebral disc phenotype of caveolin-1 knock-out mice. Typical examples of the intervertebral discs from 3-month-old wild-type (A and C) and caveolin-1 knock-out (B and D) mice, stained with hematoxylin/eosin (A and B) and alcian blue/picrosirius red (C and D). The pictures on the right are magnifications of the corresponding pictures on the left. The wild-type nucleus pulposus (NP) consisted of centrally located, viable notochordal cells (arrowhead) and a relatively limited amount of chondroid-like intercellular matrix (*), which stains blue in the sections stained with alcian blue/picrosirius red. The NP of the caveolin-1 KO mice contained apoptotic (arrowheads) and rounded cells, with a smaller amount of cytoplasm lacking the typical vacuolar aspect (arrows), and a relatively large amount of chondroid-like intercellular matrix (*).

Discussion

Gene expression profiling of chondroid metaplasia of the NP, which is seen in physiological aging as well in early (subclinical) degeneration of the IVD, revealed novel genes and pathways involved in the preservation of the NC in the healthy IVD. The results obtained indicate that IVD degeneration in dogs involved significant downregulation of Wnt/ β -catenin signaling and caveolin-1, the latter which seems to be crucial for NC maintenance and an important factor in IVD degeneration. Material was obtained from non-chondrodystrophic and chondrodystrophic dogs, a unique animal model in view of investigating the NC and degeneration/regeneration the IVD: in non-chondrodystrophic dogs, the NC remains the predominant cell type of the NP during the majority of life, with IVD degeneration only occurring at old age and in selected IVDs; conversely, in chondrodystrophic dogs the NC is lost early in life, with concurrent degeneration of all IVDs. Therefore, these two dog types reflect a naturally occurring animal model representing differential maintenance of the NC and associated differences in maintenance of optimal matrix health of the IVD [14, 30].

In the present study the main focus was the transition of a healthy NC-rich into an aging/degenerating CLC-rich NP. However, recent studies have indicated that both the healthy and degenerating NP, apart from NCs and CLCs, contain stem/progenitor cells (approximately 1% of the NP cell population)⁷¹⁻⁷³. These NP progenitor cells express 'stemness' genes and have been shown to functionally differentiate into the adipogenic, osteogenic, chondrogenic, and neurogenic lineage⁷¹. As these progenitor cells are present within the NP, it is very well possible that these cells had a profound effect upon the signaling of NCs and CLCs and on the studied biomolecular signaling events, particularly with respect to the different phenotypes of the non-chondrodystrophic and chondrodystrophic NP investigated. Additional studies are warranted on this specific matter.

The relative expression of the notochordal markers *brachyury* and *cytokeratin 8*^{12,37-39} revealed marked differences between chondrodystrophic and non-chondrodystrophic dogs. In the initial stages of early IVD degeneration (classified as Mixed group), *brachyury* and *cytokeratin 8* gene expression remained constant, indicating the preservation of the NC phenotype in the NP at this stage in both chondrodystrophic and non-chondrodystrophic dogs. However, *brachyury* and *cytokeratin 8* gene expression was significantly decreased in the CLC-rich NP from chondrodystrophic, but not non-chondrodystrophic dogs. Decreased expression of NC markers is also seen in degenerated human IVDs⁷⁴ and is indicative of a significant loss of NCs from the NP^{12,37-39}. The maintenance of high levels of *brachyury* and *cytokeratin 8* gene expression in the non-chondrodystrophic, CLC-rich NP indicates that the NP cells in non-chondrodystrophic dogs undergo significant morphological changes, but can preserve characteristics of NCs on the basis of their gene expression

pattern. These findings are consistent with the observation that there are niches of NCs in degenerated, human CLC-rich NP^{11,12,38,74}. Therefore, based on histopathological assessment and the expression of notochordal marker genes, and in accordance with previous studies^{17,19,75,76}, loss of the notochordal phenotype would appear to be associated with the accelerated IVD degeneration seen in chondrodystrophic dogs, whereas in non-chondrodystrophic dogs the NCs or CLCs retain notochordal characteristics, accounting for the relatively low prevalence of IVD degeneration observed in this breed type^{22,77}.

Canonical Wnt signaling activity is decreased in early IVD degeneration, with a clear differences between non-chondrodystrophic and chondrodystrophic dogs. An increase in canonical Wnt signaling activity results in increased gene expression of *axin2*, which is considered a reliable read-out for the activity of canonical Wnt signaling⁶⁴⁻⁶⁶. *Axin2* gene expression was significantly down-regulated in the CLC-rich NP compared with the NC-rich and Mixed NP in both non-chondrodystrophic and chondrodystrophic dogs, indicating that early (subclinical) IVD degeneration involves a significant reduction in canonical Wnt signaling activity. These results seem contradictory to our previous findings³⁵, showing that the CLC-rich NP had a higher *axin2* gene expression than the NC-rich NP. However, in that particular study CLC-NP tissue from chondrodystrophic dogs was compared with NC-rich NP tissue from non-chondrodystrophic dogs. Indeed, chondrodystrophic NPs exhibit significantly higher levels of *axin2* gene expression than non-chondrodystrophic dogs in all histopathological groups investigated in this study (Fig. 2), which explains the apparently contradictory results between the previous report³⁵ and the present one. The significantly higher *axin2* gene expression found in chondrodystrophic dogs was further sustained by the significantly higher signal intensity for β -catenin-protein expression within the CLC-rich NP tissue as shown by immunohistochemistry and most probably less degraded β -catenin as shown by the western blot analysis (Fig. 3).

The gene expression of *wnt7b*, which activates canonical Wnt signaling through interacting with Wnt receptors LRP5 and Fzd1⁶⁷, was increased during NP chondrification and was consistently higher in all histopathological groups in non-chondrodystrophic dogs than in chondrodystrophic dogs. Increased *wnt7b* gene expression has also been reported in the cartilage of patients with osteoarthritis (OA) and rheumatoid arthritis (RA)⁷⁸. In that respect, the significantly higher gene expression of *wnt7b* may reflect a response to increase canonical Wnt signaling activity and an attempt to preserve NP health. Interestingly, canonical Wnt signaling activity (*axin2* and *fzd1* expression) was markedly higher in chondrodystrophic dogs in all histopathological stages, as was also reported earlier in canine NP cells³⁵. In chondrodystrophic dogs, the decrease in Wnt signaling activity during NP chondrification may be explained by the increased expression of *wif1* and *frizzled-related protein (frzb)* (Wnt inhibitors; Fig. 2, Table 2), and the reduced expression of *r-spondin-3*

(*rspo3*; Wnt activator; Table 2). It is tempting to hypothesize about the potential role of Wnt signaling in the transition from healthy, NC-rich NP to aged or degenerated CLC-rich NP. As Wnt signaling regulates notochord fate and stem cell renewal and apoptosis^{79,80}, decreased Wnt signaling may result in increased apoptosis and decreased self-renewal of NCs or NP stem cells, and ultimately in chondroid metaplasia of the NP. The higher canonical Wnt signaling seen in chondrodystrophic dogs may reflect an ineffective attempt to preserve the notochordal phenotype of NP cells or to regulate stem cell renewal and apoptosis. Conversely, given the involvement of Wnt signaling in tissue degeneration^{81,82}, higher Wnt signaling in chondrodystrophic dogs might reflect a diminished capacity to limit Wnt signaling, resulting in accelerated extracellular matrix breakdown, as is observed in patients with OA or RA^{78,81}. This line of thought may also be in accordance with recent findings showing increased β -catenin protein expression in degenerated human IVD tissue as compared with healthy controls⁸³. Altogether, these data illustrate the dual role of Wnt signaling, which requires further elucidation with respect to the transition from the NC-rich to CLC-rich NP, also with respect to the role played by progenitor cells within the NP in various stages of degeneration⁷¹⁻⁷³.

Loss of NC phenotype involves significant down-regulation of caveolin-1 expression. Caveolin-1 is required for notochord development⁸⁴, and caveolins regulate canonical Wnt signaling by recruiting β -catenin to caveolae membranes, thereby inhibiting Wnt/ β -catenin signaling and reinforcing cell-cell adhesion mechanisms⁴⁹, and by internalizing LRP6 (Wnt receptor), thereby activating canonical Wnt signaling⁵⁰. Furthermore, caveolin-1 stimulates canonical Wnt signaling by activating integrin-linked kinase which inhibits glycogen synthase kinase 3- β , a key enzyme in Wnt/ β -catenin signaling that phosphorylates β -catenin leading to the subsequent degradation of this molecule⁶⁹. Also, caveolin-1 stimulates canonical Wnt signaling through the accumulation of β -catenin to caveolae membranes, thereby preventing degradation of β -catenin by glycogen synthase kinase 3- β ⁴⁹. The performed co-immunofluorescence analysis of caveolin-1 and β -catenin (the effector protein of canonical Wnt signaling) showed protein expression peaks of both proteins localized at the cell membrane, which may indicate an interaction between these proteins within the NC. However, in CLCs no such protein expression/co-localization was observed. It is tempting to hypothesize that, within the NC, caveolae function to regulate β -catenin signaling by preventing its degradation and to reinforce cell-cell clusters, which is a morphological characteristic of NCs³⁶. In line with the decrease in canonical Wnt signaling in early IVD degeneration, *caveolin-1* gene expression was significantly down-regulated in both breed types. Caveolin-1 protein expression was observed almost exclusively in NCs and decreased significantly with chondrification/degeneration of the NP (Fig. 4). However, other authors have reported increased caveolin-1 expression to be associated with senescence of NP cells^{70,85} and chondrocytes, with subsequent

IVD degeneration and OA⁸⁶, respectively. This discrepancy is probably because the other studies investigated advanced stages of degeneration involving CLCs only, whereas we investigated early degeneration, involving the transition from the NC-rich to CLC-rich NP. Apart from cell senescence, caveolin is known to play a significant role various cellular processes, including stem cell regulation and proliferation⁸⁷. Therefore, caveolin-1 may act differently according to the triggering signals and cellular context, such as the stage of IVD degeneration and in different cell types⁸⁸. The relationship between Wnt/ β -catenin signaling and caveolin-1 in the NP in different stages of degeneration and in NCs compared with CLCs requires further investigation. Interestingly, the expression of caveolin-1 protein was consistently lower in chondrodystrophic NP than in non-chondrodystrophic NP regardless of histopathological stage, indicating a direct relationship between the absence of caveolin-1 and the accelerated loss of NCs from the NP in chondrodystrophic dogs.

Caveolin-1 appears to fulfill essential functions in the NC cytoskeleton.

In an attempt to understand the role of caveolin-1 in NC physiology, we studied its distribution in NCs in culture. Caveolin-1 protein was detected in the cell membrane and in intracellular membranes (Fig. 6), as reported previously⁸⁹. As expected, caveolin-1 gene and protein expression increased significantly when the cells adhered to the culture plate (days 4 and 6). Caveolin interacts with actin filaments of the cytoskeleton⁹⁰ and its increased expression may be involved in the formation of the NC cytoskeleton and adherence of NCs to the culture plate. In accordance with these observations, microarray analysis revealed significant changes in cytoskeletal components, supporting a role for caveolin-1 in the NC cytoskeleton. Notochordal cells are known to contain a dense network of intracellular actin, which be involved in the homeostasis of the intracellular vesicles and cluster-formation of these cells³⁶. An important function of caveolin-1 may be to regulate the interaction of caveolae with the actin cytoskeleton, thereby controlling whether caveolae are at the cell surface or traveling to interior sites, or regulating the homeostasis of intracellular vesicles and intercellular clusters⁹¹.

Absence of caveolin-1 coincides with decreased NC preservation and early IVD degeneration.

The essential role of caveolin-1 in NC physiology was corroborated by the IVD phenotype of the caveolin-1 KO mice. Unlike NP from wild-type mice, NP from caveolin-1 KO mice showed relatively few healthy NC clusters; most NP cells lacked the morphological characteristics of NCs and showed signs of apoptosis, and the NP contained an abundance of intercellular chondroid matrix, similar to the CLC-rich NP (Fig. 7). These changes are similar to the histopathological changes observed in the transition from an NC-rich to CLC-rich NP (Fig. 1)^{14,22}. Therefore, these findings suggest that caveolin-1 is essential for NC maintenance, and that decreased caveolin-1 expression is an important factor in NC physiology and IVD degeneration.

To further investigate the role of caveolin-1 and its relationship with Wnt/ β -catenin, future studies need to focus on Wnt/ β -catenin signaling in caveolin-1 KO mice.

Apart from the involvement in IVD degeneration, caveolin proteins are involved in stem cell regulation and proliferation, as well as in the pathogenesis of cancers, pulmonary hypertension, cardiomyopathy, diabetes, and muscular dystrophy⁸⁷. There has been an increasing interest in the application of caveolin-mimetic peptides for the treatment of both cancer and pulmonary hypertension⁸⁷. The findings of this study suggest that caveolin-1 is crucial for NC maintenance and IVD health, and this protein may be regarded an exciting target for developing ways to regenerate the IVD. For example, the degenerated IVD may be treated by locally applying caveolin-1-mimetic peptide or by promoting the expression of caveolin-1 in the cells of the degenerated IVD, thereby promoting regeneration of the degenerated tissue. Also, it should be taken into consideration that caveolin-1 may exert different actions dependent on the cell context and the stage of degeneration⁸⁸, and further *in vitro* mechanistic studies are required to test this concept,

Study limitations

In the present study the main focus was to investigate NCs and CLCs. However, the process of early IVD degeneration may also involve significant changes in NP progenitor/stem cells, and these cells may have a significant influence on the biomolecular signaling events within the NP.

A potential limitation of this study is that relatively few genes were differentially expressed when comparing the NC-rich, Mixed, and CLC-rich NPs in the non-chondrodystrophic dogs, whereas in chondrodystrophic dogs relatively many genes were up- or down-regulated. This might be because of the genetic heterogeneity of the non-chondrodystrophic sample (mongrels of different age and variable size), whereas the chondrodystrophic sample population consisted of Beagle dogs of the same age and standardized size. For the chondrodystrophic breed group (Beagles), an appropriate sample size for the NC-rich, Mixed, and CLC-rich groups could be obtained using young Beagles (25-36 months), as IVD degeneration occurs relatively early in life. In contrast, to obtain an appropriate sample size for the non-chondrodystrophic group IVD material was obtained from young and older dogs, since most IVDs in these non-chondrodystrophic dogs remain rich in NCs and IVD degeneration mainly occurs at older age. Therefore, IVDs graded as Mixed and CLC-rich could only be found in relatively older, non-chondrodystrophic dogs, explaining the relatively large variation in age.

Apart from the distinct IVD phenotype, caveolin-1 KO mice also exhibit a distinct bone phenotype⁹². Since the endplates are proposed to play a role in the pathophysiology of IVD degeneration, endplate changes may also influence IVD and NC physiology.

Conclusion

Early (subclinical) degeneration of the IVD, which is characterized by changes in the NP cell population, involves significant changes in the expression of genes involved in canonical Wnt signaling, ultimately leading to down-regulation of this pathway. The expression of caveolin-1, which regulates canonical Wnt signaling, is decreased in the CLC-rich NP and appears to be essential to NC physiology and preservation. In view of the high resemblance between humans and dogs regarding the biochemistry and molecular biology of IVD degeneration, it is concluded that caveolin-1 may play an important role in IVD aging/degeneration in humans as well. Caveolin-1 may serve as an interesting target for developing novel treatment strategies for IVD degeneration.

Competing interests

The authors declare that there are no conflicts of interest to report.

Acknowledgements

The authors would like to thank Ms. Jane Sykes for language corrections, Mr. Hans Vernooij (Utrecht University) for guidance in statistical analysis, and the Multimedia Department of the Faculty of Veterinary Medicine for technical assistance.

References

1. Luoma K, Riihimaki H, Luukkonen R, et al: Low back pain in relation to lumbar disc degeneration. *Spine* 25:487-492, 2000.
2. Bono CM, Lee CK: Critical analysis of trends in fusion for degenerative disc disease over the past 20 years: influence of technique on fusion rate and clinical outcome. *Spine (Phila Pa 1976)* 29:455-463.
3. Gibson JN, Waddell G: Surgical interventions for lumbar disc prolapse: updated Cochrane Review. *Spine (Phila Pa 1976)* 32:1735-1747, 2007.
4. Brinckmann P, Grootenboer H: Change of disc height, radial disc bulge, and intradiscal pressure from discectomy. An in vitro investigation on human lumbar discs. *Spine* 16:641-646, 1991.
5. Eck JC, Humphreys SC, Hodges SD: Adjacent-segment degeneration after lumbar fusion: a review of clinical, biomechanical, and radiologic studies. *Am J Orthop* 28:336-340, 1999.
6. Frei H, Oxland TR, Rathonyi GC, et al: The effect of nucleotomy on lumbar spine mechanics in compression and shear loading. *Spine* 26:2080-2089, 2001.
7. Goel VK, Nishiyama K, Weinstein JN, et al: Mechanical properties of lumbar spinal motion segments as affected by partial disc removal. *Spine* 11:1008-1012, 1986.
8. Lee CK: Accelerated degeneration of the segment adjacent to a lumbar fusion. *Spine* 13:375-377, 1988.
9. MacDougall J, Perra J, Pinto M: Incidence of adjacent segment degeneration at ten years after lumbar spine fusion. *Spine J* 3:675, 2003.
10. Tow BP, Hsu WK, Wang JC: Disc regeneration: a glimpse of the future. *Clin Neurosurg* 54:122-128, 2007.
11. Erwin WM: The enigma that is the nucleus pulposus cell: the search goes on. *Arthritis Res Ther* 12:118, 2010.
12. Risbud MV, Schaer TP, Shapiro IM: Toward an understanding of the role of notochordal cells in the adult intervertebral disc: from discord to accord. *Dev Dyn* 239:2141-2148, 2010.
13. Risbud MV, Shapiro IM: Notochordal cells in the adult intervertebral disc: new perspective on an old question. *Critical rev eukar gene* 21:29-41, 2011.
14. Bergknut N, Rutges JP, Kranenburg HJ, et al: The dog as an animal model for intervertebral disc degeneration? *Spine*, 2011.
15. Hunter CJ, Matyas JR, Duncan NA: The functional significance of cell clusters in the notochordal nucleus pulposus: survival and signaling in the canine intervertebral disc. *Spine (Phila Pa 1976)* 29:1099-1104, 2004.
16. Trout JJ, Buckwalter JA, Moore KC, et al: Ultrastructure of the human intervertebral disc. I. Changes in notochordal cells with age. *Tissue Cell* 14:359-369, 1982.
17. Erwin WM, Inman RD: Notochord cells regulate intervertebral disc chondrocyte proteoglycan production and cell proliferation. *Spine (Phila Pa 1976)* 31:1094-1099, 2006.
18. Purmessur D, Schek RM, Abbott RD, et al: Notochordal conditioned media from tissue increases proteoglycan accumulation and promotes a healthy nucleus pulposus phenotype in human mesenchymal stem cells. *Arthritis Res Ther* 13:R81, 2011.

19. Erwin WM, Islam D, Inman RD, et al: Notochordal cells protect nucleus pulposus cells from degradation and apoptosis: implications for the mechanisms of intervertebral disc degeneration. *Arthritis Res Ther* 13:R215, 2011.
20. Erwin WM, Las Heras F, Islam D, et al: The regenerative capacity of the notochordal cell: tissue constructs generated in vitro under hypoxic conditions. *J Neurosurg Spine* 10:513-521, 2009.
21. Erwin WM, Inman RD: Notochord cells regulate intervertebral disc chondrocyte proteoglycan production and cell proliferation. *Spine* 31:1094-1099, 2006.
22. Hansen HJ: A pathologic-anatomical study on disc degeneration in dog, with special reference to the so-called enchondrosis intervertebralis. *Acta Orthop Scand Suppl* 11:1-117, 1952.
23. Braund KG, Ghosh P, Taylor TK, et al: Morphological studies of the canine intervertebral disc. The assignment of the beagle to the achondroplastic classification. *Res Vet Sci* 19:167-172, 1975.
24. da Costa RC, Parent JM, Partlow G, et al: Morphologic and morphometric magnetic resonance imaging features of Doberman Pinschers with and without clinical signs of cervical spondylomyelopathy. *Am J Vet Res* 67:1601-1612, 2006.
25. De Decker S, Gielen IM, Duchateau L, et al: Low-field magnetic resonance imaging findings of the caudal portion of the cervical region in clinically normal Doberman Pinschers and Foxhounds. *Am J Vet Res* 71:428-434, 2010.
26. Rossi F, Seiler G, Busato A, et al: Magnetic resonance imaging of articular process joint geometry and intervertebral disk degeneration in the caudal lumbar spine (L5-S1) of dogs with clinical signs of cauda equina compression. *Vet Radiol Ultrasound* 45:381-387, 2004.
27. Seiler GS, Háni H, Busato AR, et al: Facet joint geometry and intervertebral disc degeneration in the L5-S1 region of the vertebral column in German Shepherd Dogs. *Am J Vet Res* 63:86-90, 2002.
28. Johnson JA, da Costa RC, Bhattacharya S, et al: Kinematic motion patterns of the cranial and caudal canine cervical spine. *Vet Surg* 40:720-727, 2011.
29. Breit S, Kunzel W: Shape and orientation of articular facets of cervical vertebrae (C3-C7) in dogs denoting axial rotational ability: an osteological study. *Eur J Morphol* 40:43-51, 2002.
30. Erwin WM: The Notochord, Notochordal cell and CTGF/CCN-2: ongoing activity from development through maturation. *J Cell Commun Signal* 2:59-65, 2008.
31. Vos P, Interma F, van El B, et al: Does loading influence the severity of cartilage degeneration in the canine Groove-model of OA? *J Orthop Res* 27:1332-1338, 2009.
32. Vos PA, Degroot J, Barten-van Rijbroek AD, et al: Elevation of cartilage AGEs does not accelerate initiation of canine experimental osteoarthritis upon mild surgical damage. *J Orthop Res* 30:1398-1404, 2012.
33. Van Meegeren MER, Roosendaal G, Barten-van Rijbroek AD, et al: Coagulation aggravates blood-induced joint damage. *Arthritis Rheum* 64:3231-3239, 2012.
34. van Horssen P, Siebes M, Hoefler I, et al: Improved detection of fluorescently labeled microspheres and vessel architecture with an imaging cryomicrotome. *Med Biol Eng Comput* 48:735-744, 2010.
35. Smolders LA, Meij BP, Riemers FM, et al: Canonical Wnt signaling in the notochordal cell is upregulated in early intervertebral disk degeneration. *J Orthop Res* 30:950-957, 2012.

36. Hunter CJ, Matyas JR, Duncan NA: The three-dimensional architecture of the notochordal nucleus pulposus: novel observations on cell structures in the canine intervertebral disc. *J Anat* 202:279-291, 2003.
37. Herrmann BG, Kispert A: The T genes in embryogenesis. *Trends Genet* 10:280-286, 1994.
38. Gilson A, Dreger M, Urban JP: Differential expression level of cytokeratin 8 in cells of the bovine nucleus pulposus complicates the search for specific intervertebral disc cell markers. *Arthritis Res Ther* 12:R24, 2010.
39. Gotz W, Kasper M, Fischer G, et al: Intermediate filament typing of the human embryonic and fetal notochord. *Cell Tissue Res* 280:455-462, 1995.
40. Opitz L, Salinas-Riester G, Grade M, et al: Impact of RNA degradation on gene expression profiling. *BMC Med Genomics* 3:36, 2010.
41. Ekins S, Nikolsky Y, Bugrim A, et al: Pathway mapping tools for analysis of high content data. *Methods Mol Biol* 356:319-350, 2007.
42. Roepman P, Wessels LF, Kettelarij N, et al: An expression profile for diagnosis of lymph node metastases from primary head and neck squamous cell carcinomas. *Nature genetics* 37:182-186, 2005.
43. Hsieh JC, Kodjabachian L, Rebbert ML, et al: A new secreted protein that binds to Wnt proteins and inhibits their activities. *Nature* 398:431-436, 1999.
44. Cadigan KM, Nusse R: Wnt signaling: a common theme in animal development. *Gene Dev* 11:3286-3305, 1997.
45. Mao J, Wang J, Liu B, et al: Low-density lipoprotein receptor-related protein-5 binds to Axin and regulates the canonical Wnt signaling pathway. *Mol Cell* 7:801-809, 2001.
46. McDonald PC, Fielding AB, Dedhar S: Integrin-linked kinase--essential roles in physiology and cancer biology. *J Cell Sci* 121:3121-3132, 2008.
47. Zhurinsky J, Shtutman M, Ben-Ze'ev A: Plakoglobin and beta-catenin: protein interactions, regulation and biological roles. *J Cell Sci* 113:3127-3139, 2000.
48. Jho EH, Zhang T, Domon C, et al: Wnt/beta-catenin/Tcf signaling induces the transcription of Axin2, a negative regulator of the signaling pathway. *Mol Cell Biol* 22:1172-1183, 2002.
49. Galbiati F, Volonte D, Brown AM, et al: Caveolin-1 expression inhibits Wnt/beta-catenin/Lef-1 signaling by recruiting beta-catenin to caveolae membrane domains. *J Biol Chem* 275:23368-23377, 2000.
50. Yamamoto H, Komekado H, Kikuchi A: Caveolin is necessary for Wnt-3a-dependent internalization of LRP6 and accumulation of beta-catenin. *Dev Cell* 11:213-223, 2006.
51. Nusse R: Developmental biology. Making head or tail of Dickkopf. *Nature* 411:255-256, 2001.
52. Pfaffl MW: A new mathematical model for relative quantification in real-time RT-PCR. *Nucleic Acids Res* 29:e45, 2001.
53. Baroni MG, Cavallo MG, Mark M, et al: Beta-cell gene expression and functional characterisation of the human insulinoma cell line CM. *J Endocrinol* 161:59-68, 1999.
54. Peters IR, Peeters D, Helps CR, et al: Development and application of multiple internal reference (housekeeper) gene assays for accurate normalisation of canine gene expression studies. *Vet Immunol Immunopathol* 117:55-66, 2007.
55. R Development Core Team: R: A language and environment for statistical computing. R Foundation for Statistical Computing. Vienna, Austria, 2010.

56. Pinheiro J, Bates D, DebRoy S, et al: nlme: linear and nonlinear mixed effects models. R package version 3:1-96, 2009.
57. Benjamini Y, Hochberg Y: Controlling the false discovery rate: a practical and powerful approach to multiple testing. *J Roy Stat Soc B* 57:289-300, 1995.
58. Gruber HE, Ingram J, Hanley EN, Jr.: An improved staining method for intervertebral disc tissue. *Biotech Histochem* 77:81-83, 2002.
59. Stosiek P, Kasper M, Karsten U: Expression of cytokeratin and vimentin in nucleus pulposus cells. *Differentiation* 39:78-81, 1988.
60. Salisbury JR, Isaacson PG: Demonstration of cytokeratins and an epithelial membrane antigen in chordomas and human fetal notochord. *Am J Surg Pathol* 9:791-797, 1985.
61. Edgar R, Domrachev M, Lash AE: Gene Expression Omnibus: NCBI gene expression and hybridization array data repository. *Nucleic Acids Res* 30:207-210, 2002.
62. Mudunuri U, Che A, Yi M, et al: bioDBnet: the biological database network. *Bioinformatics* 25:555-556, 2009.
63. Corr M: Wnt-beta-catenin signaling in the pathogenesis of osteoarthritis. *Nat Clin Pract Rheumatol* 4:550-556, 2008.
64. Yan D, Wiesmann M, Rohan M, et al: Elevated expression of axin2 and hnkcd mRNA provides evidence that Wnt/beta -catenin signaling is activated in human colon tumors. *Proceedings of the National Academy of Sciences of the United States of America* 98:14973-14978, 2001.
65. Lustig B, Jerchow B, Sachs M, et al: Negative feedback loop of Wnt signaling through upregulation of conductin/axin2 in colorectal and liver tumors. *Mol Cell Biol* 22:1184-1193, 2002.
66. Jho EH, Zhang T, Domon C, et al: Wnt/beta-catenin/Tcf signaling induces the transcription of Axin2, a negative regulator of the signaling pathway. *Mol Cell Biol* 22:1172-1183, 2002.
67. Wang Z, Shu W, Lu MM, et al: Wnt7b activates canonical signaling in epithelial and vascular smooth muscle cells through interactions with Fzd1, Fzd10, and LRP5. *Mol Cell Biol* 25:5022-5030, 2005.
68. Tesco G, Kim TW, Diehlmann A, et al: Abrogation of the presenilin 1/beta-catenin interaction and preservation of the heterodimeric presenilin 1 complex following caspase activation. *J Biol Chem* 273:33909-33914, 1998.
69. Chun J, Hyun S, Kwon T, et al: The subcellular localization control of integrin linked kinase 1 through its protein-protein interaction with caveolin-1. *Cell Signal* 17:751-760, 2005.
70. Heathfield SK, Le Maitre CL, Hoyland JA: Caveolin-1 expression and stress-induced premature senescence in human intervertebral disc degeneration. *Arthritis Res Ther* 10:R87, 2008.
71. Mark Erwin W, Islam D, Eftekarpour E, et al: Intervertebral Disc-Derived Stem Cells: Implications for Regenerative Medicine and Neural Repair. *Spine*, 2012.
72. Blanco JF, Graciani IF, Sanchez-Guijo FM, et al: Isolation and characterization of mesenchymal stromal cells from human degenerated nucleus pulposus: comparison with bone marrow mesenchymal stromal cells from the same subjects. *Spine* 35:2259-2265, 2010.
73. Risbud MV, Guttapalli A, Tsai TT, et al: Evidence for skeletal progenitor cells in the degenerate human intervertebral disc. *Spine* 32:2537-2544, 2007.

74. Minogue BM, Richardson SM, Zeef LA, et al: Transcriptional profiling of bovine intervertebral disc cells: implications for identification of normal and degenerate human intervertebral disc cell phenotypes. *Arthritis Res Ther* 12:R22, 2010.
75. Aguiar DJ, Johnson SL, Oegema TR: Notochordal cells interact with nucleus pulposus cells: regulation of proteoglycan synthesis. *Exp Cell Res* 246:129-137, 1999.
76. Erwin WM, Ashman K, O'Donnel P, et al: Nucleus pulposus notochord cells secrete connective tissue growth factor and up-regulate proteoglycan expression by intervertebral disc chondrocytes. *Arthritis Rheum* 54:3859-3867, 2006.
77. Cappello R, Bird JL, Pfeiffer D, et al: Notochordal cell produce and assemble extracellular matrix in a distinct manner, which may be responsible for the maintenance of healthy nucleus pulposus. *Spine (Phila Pa 1976)* 31:873-882, 2006.
78. Nakamura Y, Nawata M, Wakitani S: Expression profiles and functional analyses of Wnt-related genes in human joint disorders. *Am J Pathol* 167:97-105, 2005.
79. Ukita K, Hirahara S, Oshima N, et al: Wnt signaling maintains the notochord fate for progenitor cells and supports the posterior extension of the notochord. *Mech Dev* 126:791-803, 2009.
80. Cho HH, Kim YJ, Kim SJ, et al: Endogenous Wnt signaling promotes proliferation and suppresses osteogenic differentiation in human adipose derived stromal cells. *Tissue Eng* 12:111-121, 2006.
81. Corr M: Wnt-beta-catenin signaling in the pathogenesis of osteoarthritis. *Nature Clinical Practice Rheumatology* 4:550-556, 2008.
82. Sen M: Wnt signalling in rheumatoid arthritis. *Rheumatology* 44:708-713, 2005.
83. Wang M, Tang D, Shu B, et al: Conditional activation of beta-catenin signaling in mice leads to severe defects in intervertebral disc tissue. *Arthritis Rheum* 64:2611-2623, 2012.
84. Nixon SJ, Carter A, Wegner J, et al: Caveolin-1 is required for lateral line neuromast and notochord development. *J Cell Sci* 120:2151-2161, 2007.
85. Heathfield SK, Hoyland JA: Interleukin-1 induces caveolin-1 expression in human nucleus pulposus cells. *J Bone Joint Surg Br* 93-B:484, 2011.
86. Dai SM, Shan ZZ, Nakamura H, et al: Catabolic stress induces features of chondrocyte senescence through overexpression of caveolin 1: possible involvement of caveolin 1-induced down-regulation of articular chondrocytes in the pathogenesis of osteoarthritis. *Arthritis Rheum* 54:818-831, 2006.
87. Mercier I, Jasmin JF, Pavlides S, et al: Clinical and translational implications of the caveolin gene family: lessons from mouse models and human genetic disorders. *Lab Invest* 89:614-623, 2009.
88. Boscher C, Nabi IR: Caveolin-1: role in cell signaling. *Adv Exp Med Biol* 729:29-50, 2012.
89. Li WP, Liu P, Pilcher BK, et al: Cell-specific targeting of caveolin-1 to caveolae, secretory vesicles, cytoplasm or mitochondria. *J Cell Sci* 114:1397-1408, 2001.
90. Anderson RG: Caveolae: where incoming and outgoing messengers meet. *Proceedings of the National Academy of Sciences of the United States of America* 90:10909-10913, 1993.
91. Liu P, Rudick M, Anderson RG: Multiple functions of caveolin-1. *J Biol Chem* 277:41295-41298, 2002.
92. Rubin J, Schwartz Z, Boyan BD, et al: Caveolin-1 knockout mice have increased bone size and stiffness. *J Bone Miner Res* 22:1408-1418, 2007.

Appendix I: Top regulated genes for microarray analyses

Results obtained for the microarray comparisons between the notochordal cell (NC)-rich nucleus pulposus (NP), Mixed NP, and chondrocyte-like cell (CLC)-rich NP in non-chondrodystrophic and chondrodystrophic dogs, and between the breed types for each histological stage. When >50 genes were regulated, the top 50 up- and down-regulated genes are displayed. For brevity, only one gene ontology (GO) term is displayed for each gene (obtained with bioDBnet⁶²).

Non-chondrodystrophic dogs: NC-rich NP (reference) vs. Mixed NP					
Gene symbol	Description	GO term: Biological Process	Ensemble Gene ID	N-fold change	P-value
CCL23	Chemokine (C-C motif) ligand 23	Cellular calcium ion homeostasis	ENSG00000167236	3.48	8.27E-03
LYZ	Lysozyme	Cell wall macromolecule catabolic process	ENSG00000090382	3.41	8.92E-03
BMP6	Bone morphogenetic protein 6	SMAD protein signal transduction	ENSG00000153162	3.26	2.98E-02
SRGN	Serglycin	Negative regulation of bone mineralization	ENSG00000122862	2.59	2.98E-02
PLBD1	Phospholipase B domain containing 1	Lipid catabolic process	ENSG00000121316	2.58	8.27E-03
EMP2	Epithelial membrane protein 2	Cell proliferation	ENSG00000213853	2.40	3.65E-02
EMB	Embigin	Cell adhesion	ENSG00000170571	2.34	2.88E-02
VCAM1	Vascular cell adhesion molecule 1	Cell-cell adhesion	ENSG00000162692	2.27	8.53E-03
CD53	CD53 molecule	Signal transduction	ENSG00000143119	2.27	1.35E-02
HPR	Haptoglobin-related protein	Photorespiration	ENSG00000257017	2.00	2.10E-02
HP	Hypothetical protein	Not available	Not available	1.94	2.10E-02
LOC100684963	LOC100684963				
PDE3B	Phosphodiesterase 3B, cGMP-inhibited	Glucose homeostasis	ENSG00000152270	1.89	2.10E-02
STAT5B	Signal transducer and activator of transcription 5B	Regulation of steroid metabolic process	ENSG00000173757	1.63	4.07E-02
CDH8	Cadherin 8, type 2	Cell-cell junction organization	ENSG00000150394	-2.44	3.01E-03

IVD DEGENERATION INVOLVES DECREASED WNT SIGNALING AND CAVEOLIN-1 EXPRESSION

Continued

NUDT19	Nudix (nucleoside diphosphate linked moiety X)-type motif 19	Not available	ENSG00000213965	-2.18	4.65E-02
RINL	Ras and Rab interactor-like	Not available	ENSG00000187994	-2.07	8.27E-03
ST8SIA4	ST8 alpha-N-acetylneuraminide alpha-2, 8-sialyltransferase 4	Protein glycosylation	ENSG00000113532	-1.97	2.10E-02
LAMA4	Laminin, alpha 4	Regulation of cell adhesion	ENSG00000112769	-1.94	8.53E-03
RAB38	RAB38, member RAS oncogene family	Small GTPase mediated signal transduction	ENSG00000123892	-1.90	3.65E-02
ITGA3	Integrin, alpha 3 (antigen CD49C, alpha 3 subunit of VLA-3 receptor)	Cell adhesion	ENSG00000005884	-1.81	2.10E-02
MOSPD2	Motile sperm domain containing 2	Not available	ENSG00000130150	-1.64	3.65E-02
CAV2	Caveolin 2	Vesicle organization	ENSG00000105971	-1.63	4.09E-02

Non-chondrodystrophic dogs: Mixed NP (reference) vs. CLC-rich NP

No significant regulations

Non-chondrodystrophic dogs: NC-rich NP (ref) vs. CLC-rich NP

Gene symbol	Description	GO: Biological Process	Ensemble Gene ID	N-fold change	P-value
FAM63A	Family with sequence similarity 63, member A	Cellular Component	ENSG00000143409	-2.88	3.46E-03

Chondrodystrophic dogs: NC-rich NP (reference) vs. Mixed NP

Total up-regulated genes: 570

Total down-regulated genes: 712

Gene Symbol	Description	GO term: Biological process	Ensemble Gene ID	N-fold change	P-value
SPSB2	SplA/ryanodine receptor domain and SOCS box containing 2	Intracellular signal transduction	ENSG00000111671	7.28	<1.00E-06
ARH-GEF10	Rho guanine nucleotide exchange factor (GEF) 10	Regulation of Rho protein signal transduction	ENSG00000104728	4.88	<1.00E-06
TMEM93	Transmembrane protein 93	Not available	ENSG00000127774	3.73	<1.00E-06
NDUFA7	NADH dehydrogenase (ubiquinone) 1 alpha subcomplex, 7	Oxidation-reduction process	ENSG00000167774	3.57	7.11E-04
SETD5	SET domain containing 5	Not available	ENSG00000168137	3.41	4.02E-05
FOLR4	Folate receptor 4 (delta) homolog	Not available	ENSG00000183560	3.27	3.75E-04
ATM	Ataxia telangiectasia mutated	Reciprocal meiotic recombination	ENSG00000149311	3.25	1.24E-02
DERL2	Der1-like domain family, member 2	Response to unfolded protein	ENSG00000072849	3.23	8.35E-04
BICD1	Bicaudal D homolog 1	Anatomical structure morphogenesis	ENSG00000151746	3.17	1.77E-04
GOLGB1	Golgin B1	Golgi organization	ENSG00000173230	3.06	3.21E-02
SOCS1	Suppressor of cytokine signaling 1	Response to cytokine stimulus	ENSG00000185338	2.98	<1.00E-06
EPHA4	EPH receptor A4	Cell adhesion	ENSG00000116106	2.92	1.14E-05
RBMX2	RNA binding motif protein, X-linked 2	Not available	ENSG00000134597	2.78	2.02E-04
C6orf118	Chromosome 6 open reading frame 118	Not available	ENSG00000112539	2.72	3.05E-06
FAM120A	Family with sequence similarity 120A	Not available	ENSG00000048828	2.63	2.28E-04
PCDH1	Protocadherin 1	Homophilic cell adhesion	ENSG00000156453	2.60	<1.00E-06
C11orf91	Chromosome 11 open reading frame 91	Not available	ENSG00000205177	2.55	<1.00E-06
WNT10B	Wingless-type MMTV integration site family, member 10B	Positive regulation of canonical Wnt receptor signaling pathway	ENSG00000169884	2.54	<1.00E-06

IVD DEGENERATION INVOLVES DECREASED WNT SIGNALING AND CAVEOLIN-1 EXPRESSION

Continued

ACADS	Acyl-CoA dehydrogenase, C-2 to C-3 short chain	Protein homotetramerization	ENSG00000122971	2.46	<1.00E-06
BAZ1B	Bromodomain adjacent to zinc finger domain, 1B	Nucleosome disassembly	ENSG00000009954	2.45	1.61E-04
CCDC33	Coiled-coil domain containing 33	Not available	ENSG00000140481	2.43	9.59E-04
CFC1	Cripto, FRL-1, cryptic family 1	Determination of left/right symmetry	ENSG00000136698	2.42	<1.00E-06
GORASP2	Golgi reassembly stacking protein 2, 55kDa	Organelle organization	ENSG00000115806	2.41	<1.00E-06
DST	Dystonin	Integrin-mediated signaling pathway	ENSG00000151914	2.41	<1.00E-06
HMG20B	High mobility group 20B	Chromatin organization	ENSG00000064961	2.40	1.06E-04
C20orf43	Chromosome 20 open reading frame 43	Biological process	ENSG00000022277	2.38	5.59E-05
PGS1	Phosphatidylglycerophosphate synthase 1	Phospholipid biosynthetic process	ENSG00000087157	2.36	<1.00E-06
FAM63B	Family with sequence similarity 63, member B	Biological process	ENSG00000128923	2.35	2.64E-03
CFL1	Cofilin 1 (non-muscle)	Cytoskeleton organization	ENSG00000172757	2.35	9.76E-04
CAV3	Caveolin 3	Negative regulation of cardiac muscle hypertrophy	ENSG00000182533	2.34	7.26E-03
C6orf103	Chromosome 6 open reading frame 103	Proteolysis	ENSG00000118492	2.33	<1.00E-06
TPCN2	Two pore segment channel 2	Trans membrane transport	ENSG00000162341	2.31	8.65E-03
ASTE1	Asteroid homolog 1 (Drosophila)	DNA repair	ENSG00000034533	2.30	<1.00E-06
MYO3B	Myosin IIIB	Response to stimulus	ENSG00000071909	2.30	3.89E-05
CSDE1	Cold shock domain containing E1, RNA-binding	Regulation of transcription, DNA-dependent	ENSG00000009307	2.29	5.16E-03
NUAK2	NUAK family, SNF1-like kinase, 2	Actin cytoskeleton organization	ENSG00000163545	2.26	1.21E-03
SLC25A4	Solute carrier family 25, member 4	Transmembrane transport	ENSG00000151729	2.22	1.05E-03
TSPAN5	Tetraspanin 5	Not available	ENSG00000168785	2.21	3.90E-02
CCBL1	Cysteine conjugate-beta lyase, cytoplasmic	Kynurenine metabolic process	ENSG00000171097	2.19	9.91E-04

Continued

DPEP3	Dipeptidase 3	Proteolysis	ENSG00000141096	2.19	2.33E-04
SLC7A1	Solute carrier family 7, member 1	Ion transport	ENSG00000139514	2.18	6.58E-03
ATG16L1	ATG16 autophagy related 16-like 1	Autophagic vacuole assembly	ENSG00000085978	2.17	4.74E-05
LAMA2	Laminin, alpha 2	Muscle organ development	ENSG00000196569	2.17	5.87E-04
LTF	Lactotransferrin	Ion transport	ENSG00000012223	2.16	2.17E-03
THR3	Thyroid hormone receptor, beta	Transcription, DNA-dependent	ENSG00000151090	2.15	9.36E-03
YIPF2	Yip1 domain family, member 2	Not available	ENSG00000130733	-7.40	<1.00E-04
CCZ1	CCZ1 vacuolar protein trafficking and biogenesis associated homolog	Vesicle docking	ENSG00000122674	-5.87	<1.00E-04
YPEL4	Yippee-like 4	Not available	ENSG00000166793	-4.83	<1.00E-06
ODAM	Odontogenic, ameloblast associated	Biomaterial tissue development	ENSG00000109205	-4.64	<1.00E-06
SLC39A12	Solute carrier family 39 (zinc transporter), member 12	Zinc ion transport	ENSG00000148482	-4.57	<1.00E-06
TRIM45	Tripartite motif containing 45	Not available	ENSG00000134253	-4.48	<1.00E-06
VPS45	Vacuolar protein sorting 45 homolog	Intracellular protein transport	ENSG00000136631	-4.10	<1.00E-06
SLC44A4	Solute carrier family 44, member 4	Transmembrane transport	ENSG00000204385	-4.05	<1.00E-06
KLHL9	Kelch-like 9 (Drosophila)	Mitosis	ENSG00000198642	-3.98	2.78E-05
WDFY1	WD repeat and FYVE domain containing 1	Biological process	ENSG00000085449	-3.89	1.61E-04
RAB3A	RAB3A, member RAS oncogene family	Regulation of exocytosis	ENSG00000105649	-3.80	<1.00E-06
RTN4RL1	Reticulon 4 receptor-like 1	Axon regeneration	ENSG00000185924	-3.77	<1.00E-06
RTN1	Reticulon 1	Neuron differentiation	ENSG00000139970	-3.65	<1.00E-06
SYN3	Synapsin III	Mitosis	ENSG00000185666	-3.42	<1.00E-06
MAT2A	Methionine adenosyltransferase II, alpha	Methylation	ENSG00000168906	-3.42	<1.00E-06
GPR35	G protein-coupled receptor 35	G-protein coupled receptor signaling pathway	ENSG00000178623	-3.34	1.10E-04
MARCH4	Membrane-associated ring finger (C3HC4) 4	Biological Process	ENSG00000144583	-3.24	<1.00E-06

IVD DEGENERATION INVOLVES DECREASED WNT SIGNALING AND CAVEOLIN-1 EXPRESSION

Continued

FGF13	Fibroblast growth factor 13	MAPKKK cascade	ENSG00000129682	-3.23	<1.00E-06
C5orf4	Chromosome 5 open reading frame 4	Fatty acid biosynthetic process	ENSG00000170271	-2.85	<1.00E-06
STK39	Serine threonine kinase 39	Protein phosphorylation	ENSG00000198648	-2.84	<1.00E-06
VCAN	Versican	Cell adhesion	ENSG00000038427	-2.73	1.58E-05
MT2A	Metallothionein 2A	Cellular response to erythropoietin	ENSG00000125148	-2.70	8.65E-03
SRRM3	Serine/arginine repetitive matrix 3	Not available	ENSG00000177679	-2.66	<1.00E-06
BICD2	Bicaudal D homolog 2 (Drosophila)	microtubule anchoring at microtubule organizing center	ENSG00000185963	-2.65	5.43E-04
IRF6	Interferon regulatory factor 6	Negative regulation of cell proliferation	ENSG00000117595	-2.65	<1.00E-06
IGSF5	Immunoglobulin superfamily, member 5	Cell-cell adhesion	ENSG00000183067	-2.63	<1.00E-06
CLEC3B	C-type lectin domain family 3, member B	Skeletal system development	ENSG00000163815	-2.61	<1.00E-06
MRPS10	Mitochondrial ribosomal protein S10	Translation	ENSG00000048544	-2.56	3.05E-06
OR51V1	Olfactory receptor, family 51, subfamily V, member 1	Detection of chemical stimulus involved in sensory perception of smell	ENSG00000176742	-2.53	3.05E-06
HDHD1	Haloacid dehalogenase-like hydrolase domain containing 1	Nucleotide metabolic process	ENSG00000130021	-2.53	<1.00E-06
ARFGAP2	ADP-ribosylation factor GTPase activating protein 2	Vesicle-mediated transport	ENSG00000149182	-2.52	<1.00E-06
OR10A7	Olfactory receptor, family 10, subfamily A, member 7	Response to stimulus	ENSG00000179919	-2.50	5.37E-03
Cyp2c23	Cytochrome P450, family 2, subfamily c, polypeptide 23	Arachidonic acid metabolic process	ENSR- NOG00000013291	-2.46	<1.00E-06
FAM3D	Family with sequence similarity 3, member D	Negative regulation of insulin secretion	ENSG00000198643	-2.45	5.98E-04
H6PD	Hexose-6-phosphate dehydrogenase (glucose 1-dehydrogenase)	NADP metabolic process	ENSG00000049239	-2.41	<1.00E-06

Continued

SNRNP40	Small nuclear ribonucleoprotein	MRNA processing	ENSG00000060688	-2.34	<1.00E-06
SGSM3	Small G protein signaling modulator 3	Cell cycle arrest	ENSG00000100359	-2.33	<1.00E-06
FLNB	Filamin B, beta	Cytoskeletal anchoring at plasma membrane	ENSG00000136068	-2.33	<1.00E-06
LSM3	LSM3 homolog, U6 small nuclear RNA associated	mRNA processing	ENSG00000170860	-2.25	<1.00E-06
G2E3	G2/M-phase specific E3 ubiquitin protein ligase	Protein polyubiquitination	ENSG00000092140	-2.23	<1.00E-06
APOA1BP	Apolipoprotein A-I binding protein	Biological process	ENSG00000163382	-2.23	3.28E-03
TRIM38	Tripartite motif containing 38	Positive regulation of I-kappaB kinase/NF-kappaB cascade	ENSG00000112343	-2.22	3.59E-04
EEF1A1	Eukaryotic translation elongation factor 1 alpha 1	Regulation of transcription, DNA-dependent	ENSG00000156508	-2.21	3.05E-06
OR6C4	Olfactory receptor, family 6, subfamily C, member 4	Response to stimulus	ENSG00000179626	-2.19	6.38E-05
TTC26	Tetratricopeptide repeat domain 26	Not available	ENSG00000105948	-2.19	3.05E-06

Chondrodystrophic dogs: Mixed NP (ref) vs. CLC-rich NP

Total up-regulated genes: 1121

Total down-regulated genes: 1173

Gene Symbol	Description	GO term: Biological process	Ensemble Gene ID	N-fold change	P-value
MT2A	Metallothionein 2A	Cellular response to erythropoietin	ENSG00000125148	17.75	9.37E-04
PRG4	Proteoglycan 4	Extracellular space	ENSG00000116690	15.63	1.05E-03
FRZB	Frizzled-related protein	Negative regulation of Wnt receptor signaling pathway	ENSG00000162998	14.18	9.11E-03
CPE	Carboxypeptidase E	Protein localization in membrane	ENSG00000109472	11.97	2.80E-03
CDO1	Cysteine dioxygenase, type I	Sulfur amino acid biosynthetic process	ENSG00000129596	11.14	2.35E-03
DCN	Decorin	Peptide cross-linking via chondroitin 4-sulfate glycosaminoglycan	ENSG00000011465	10.59	9.97E-03

IVD DEGENERATION INVOLVES DECREASED WNT SIGNALING AND CAVEOLIN-1 EXPRESSION

Continued

RBP4	Retinol binding protein 4, plasma	Glucose homeostasis	ENSG00000138207	9.73	6.66E-03
LUM	Lumican	Collagen fibril organization	ENSG00000139329	8.90	6.02E-03
CP	Ceruloplasmin (ferroxidase)	Cellular iron ion homeostasis	ENSG00000047457	8.89	9.81E-04
NT5E	5'-nucleotidase, ecto (CD73)	Nucleotide catabolic process	ENSG00000135318	8.84	6.15E-04
ADCY2	Adenylate cyclase 2 (brain)	Activation of adenylate cyclase activity by G-protein signaling pathway	ENSG00000078295	8.45	4.17E-03
TSPAN13	Tetraspanin 13	Not available	ENSG00000106537	8.11	1.35E-02
NPNT	Nephronectin	Cell differentiation	ENSG00000168743	7.88	2.68E-03
RANBP3L	RAN binding protein 3-like	Intracellular transport	ENSG00000164188	7.37	4.24E-02
PID1	Phosphotyrosine interaction domain containing 1	Not available	ENSG00000153823	7.32	1.65E-03
CCDC152	Coiled-coil domain containing 152	Not available	ENSG00000198865	7.01	3.02E-03
PDPN	Podoplanin	Cell morphogenesis	ENSG00000162493	6.91	8.32E-04
SRGN	Serglycin	Negative regulation of bone mineralization	ENSG00000122862	6.17	2.53E-02
BBOX1	Butyrobetaine (gamma), 2-oxoglutarate dioxygenase (gamma-butyrobetaine hydroxylase) 1	Cellular nitrogen compound metabolic process	ENSG00000129151	5.97	4.69E-03
G25L	Glycoprotein 25L Precursor	Not available	Not available	5.95	9.19E-03
CXCL12	Chemokine (C-X-C motif) ligand 12	Collagen fibril organization	ENSG00000107562	4.84	2.69E-03
CPE	Carboxypeptidase E	Nitric oxide mediated signal transduction	ENSG00000109472	4.77	3.38E-03
COL2A1	Collagen, type II, alpha 1	Androgen receptor signaling pathway	ENSG00000168542	4.77	4.02E-04
Mt1	Metallothionein-1-like	Prostaglandin biosynthetic process	N/A	4.73	6.32E-04
PMEPA1	Transmembrane prostate androgen-induced protein	Nervous system development	ENSG00000124225	4.72	2.01E-03
PTGES	Prostaglandin E synthase	Inflammation	ENSG00000148344	4.71	5.35E-03

Continued

SCRG1	Stimulator of chondrogenesis 1	Extracellular space	ENSG00000164106	4.68	8.06E-03
KRT18	Keratin 18	Golgi to plasma membrane CFTR protein transport	ENSG00000111057	-11.57	3.86E-03
AKAP12	A kinase (PRKA) anchor protein 12	G-protein coupled receptor signaling pathway	ENSG00000131016	-8.07	1.90E-03
MYL9	Myosin, light chain 9, regulatory	Regulation of muscle contraction	ENSG00000101335	-7.21	2.00E-02
PCDH15	Protocadherin-related 15	Cell adhesion	ENSG00000150275	-6.57	7.98E-04
PLCL1	Phospholipase C-like 1	Lipid metabolic process	ENSG00000115896	-6.46	8.52E-03
KRT19	Keratin 19	Sarcomere organization	ENSG00000171388	-5.79	3.90E-03
APLN	Apelin	Positive regulation of phosphorylation	ENSG00000143669	-5.65	3.41E-03
LYST	Lysosomal trafficking regulator	Endosome to lysosome transport via multivesicular body sorting pathway	ENSG00000134762	-5.62	3.08E-03
MRPS27	Mitochondrial ribosomal protein S27	Not available	ENSG00000113048	-5.51	3.24E-03
TSPAN7	Tetraspanin 7	Interspecies interaction between organisms	ENSG00000156298	-5.29	5.43E-03
PKP2	Plakophilin 2	Carbohydrate metabolic process	ENSG00000057294	-5.26	5.65E-03
TYW3	tRNA-yW synthesizing protein 3 homolog (S. cerevisiae)	tRNA processing	ENSG00000162623	-5.24	2.90E-03
NLGN4X	Neuroigin 4, X-linked	Cell-cell junction organization	ENSG00000146938	-5.21	4.02E-04
RSPO3	R-spondin 3	Wnt receptor signaling pathway	ENSG00000146374	-5.14	2.03E-04
ENPP2	Ectonucleotide pyrophosphatase/phosphodiesterase 2	Regulation of cell migration	ENSG00000136960	-5.14	8.09E-03
SLC24A5	Solute carrier family 24, member 5	Ion transport	ENSG00000188467	-5.10	5.81E-03
RAB38	RAB38, member RAS oncogene family	Small GTPase mediated signal transduction	ENSG00000123892	-5.02	1.76E-03
PCTP	Phosphatidylcholine transfer protein	Lipid transport	ENSG00000141179	-4.91	2.85E-03
KRT8	Keratin 8	Cytoskeleton organization	ENSG00000170421	-4.90	3.08E-02

IVD DEGENERATION INVOLVES DECREASED WNT SIGNALING AND CAVEOLIN-1 EXPRESSION

Continued

KCNS3	Potassium voltage-gated channel, delayed-rectifier, subfamily S, member 3	Energy reserve metabolic process	ENSG00000170745	-4.75	7.06E-03
SCRN1	Secernin 1	Exocytosis	ENSG00000136193	-4.73	2.13E-02
THY1	Thy-1 cell surface antigen	Cell-cell adhesion	ENSG00000154096	-4.72	4.91E-03
LRRC4	Leucine rich repeat containing 4	Not available	ENSG00000128594	-4.69	2.80E-03
XCL2	Chemokine (C motif) ligand 2	Chemotaxis	ENSG00000143185	-4.50	4.63E-02
RAB20	RAB20, member RAS oncogene family	Small GTPase mediated signal transduction	ENSG00000139832	-4.48	4.07E-03
NAP1L1	Nucleosome assembly protein 1-like 1	Positive regulation of cell proliferation	ENSG00000187109	-4.41	1.76E-03
SORBS2	Sorbin and SH3 domain containing 2	Biological process	ENSG00000154556	-4.39	1.19E-02
NRG1	Neuregulin 1	Transcription, DNA-dependent	ENSG00000157168	-4.33	2.77E-03
SPTLC3	Serine palmitoyltransferase, long chain base subunit 3	Sphingolipid metabolic process	ENSG00000172296	-4.26	1.63E-03
PCDH20	Protocadherin 20	Cell adhesion	ENSG00000197991	-4.25	2.31E-03
VWA5A	Von Willebrand factor A domain containing 5A	Not available	ENSG00000110002	-4.22	1.14E-03
KIAA0368	KIAA0368	ER-associated protein catabolic process	ENSG00000136813	-4.12	4.13E-04
CA8	Carbonic anhydrase VIII	One-carbon metabolic process	ENSG00000178538	-4.12	2.63E-03
CDH2	Cadherin 2, type 1, N-cadherin (neuronal)	Regulation of Rho protein signal transduction	ENSG00000170558	-4.11	6.32E-04
SORL1	Sortilin-related receptor, L (DLR class) A repeats containing	Lipid transport	ENSG00000137642	-4.09	8.69E-03
LAMB4	Laminin, beta 4	Cell adhesion	ENSG00000091128	-4.07	1.14E-03
DSC2	Desmocollin 2	Cell adhesion	ENSG00000134755	-4.02	1.30E-02
C10orf137	Chromosome 10 open reading frame 137	Regulation of transcription, DNA-dependent	ENSG00000107938	-3.98	1.39E-02
CALD1	Coiled-coil domain containing 152	Actin filament bundle assembly	ENSG00000122786	-3.92	9.88E-03
T	T, brachyury homolog (mouse)	Notochord development	ENSG00000164458	-3.89	1.32E-03

Continued

SLC12A2	Solute carrier family 12 (sodium/potassium/chloride transporters), member 2	Ion transport	ENSG00000064651	-3.85	1.66E-02
ADAMTS19	ADAM metallopeptidase with thrombospondin type 1 motif, 19	Proteolysis	ENSG00000145808	-3.75	4.57E-02
CA2	Carbonic anhydrase II	Carbon utilization	ENSG00000104267	-3.75	3.63E-02
DSC3	Desmocollin 3	Cell adhesion	ENSG00000134762	-3.75	2.32E-03
FAM184A	Family with sequence similarity 184, member A	Biological process	ENSG00000111879	-3.68	6.32E-04
PCDH7	Protocadherin-7	Cell adhesion	ENSG00000169851	-3.68	7.22E-03
FJX1	Four-jointed box protein 1	Not available	ENSG00000179431	-3.70	4.40E-03
SPSB2	SplA/ryanodine receptor domain and SOCS box containing 2	Intracellular signal transduction	ENSG00000111671	-3.71	6.80E-03

NC-rich NP: Non-chondrodystrophic (ref) vs. Chondrodystrophic dogs

total up-regulated genes: 1241

Total down-regulated genes: 562

Gene Symbol	Description	GO term: Biological process	Ensemble Gene ID	N-fold change	P-value
BCL2	B-cell CLL/lymphoma 2	Apoptosis	ENSG00000171791	3.03	1.28E-04
BRI3BP	BRI3 binding protein	Not available	ENSG00000184992	2.72	1.03E-04
C5orf4	Chromosome 5 open reading frame 4	Fatty acid biosynthetic process	ENSG00000170271	2.72	2.20E-02
CALN1	Calneuron 1	Not available	ENSG00000183166	2.61	1.50E-03
CCK	Cholecystokinin	Positive regulation of cell proliferation	ENSG00000187094	3.03	1.20E-03
CCZ1	CCZ1 vacuolar protein trafficking and biogenesis associated homolog (<i>S. cerevisiae</i>)	Vesicle docking	ENSG00000122674	3.70	2.84E-02
CILP	Cartilage intermediate layer protein, nucleotide pyrophosphohydrolase	Negative regulation of insulin-like growth factor receptor signaling pathway	ENSG00000138615	4.37	3.12E-02
COL3A1	Collagen, type III, alpha 1	Collagen fibril organization	ENSG00000168542	2.68	2.38E-02

IVD DEGENERATION INVOLVES DECREASED WNT SIGNALING AND CAVEOLIN-1 EXPRESSION

Continued

CP	Ceruloplasmin (ferroxidase)	Ion transport	ENSG00000047457	2.60	4.95E-02
DENND4A	DENN/MADD domain containing 4A	Regulation of transcription, DNA-dependent	ENSG00000174485	2.63	<0.00E-04
FGF13	Fibroblast growth factor 13	MAPKKK cascade	ENSG00000129682	2.91	6.76E-03
FLCN	Folliculin	Regulation of protein phosphorylation	ENSG00000154803	3.10	<0.00E-04
FUT8	Fucosyltransferase 8 (alpha (1,6) fucosyltransferase)	Protein glycosylation in Golgi	ENSG00000033170	4.78	3.81E-04
GNG2	Guanine nucleotide binding protein (G protein), gamma 2	GTP catabolic process	ENSG00000186469	2.65	4.33E-04
GREM1	Gremlin 1	Negative regulation of BMP signaling pathway	ENSG00000166923	2.72	<0.00E-04
GRIK3	Glutamate receptor, ionotropic, kainate 3	Metabotropic glutamate receptor signaling pathway	ENSG00000163873	2.69	1.99E-04
GUCY1B3	Guanylate cyclase 1, soluble, beta 3	Nitric oxide mediated signal transduction	ENSG00000061918	5.20	<0.00E-04
GULP1	GULP, engulfment adaptor PTB domain containing 1	Apoptosis	ENSG00000144366	4.24	<0.00E-04
HSPH1	Heat shock 105kDa/110kDa protein 1	Chaperone mediated protein folding requiring cofactor	ENSG00000120694	3.07	<0.00E-04
KLF4	Kruppel-like factor 4 (gut)	Negative regulation of NF-kappaB transcription factor activity	ENSG00000136826	2.65	1.17E-02
KLHL9	Kelch-like 9 (Drosophila)	Mitosis	ENSG00000198642	3.57	2.77E-02
MRPL23	Mitochondrial ribosomal protein L23	Mitochondrial translation	ENSG00000214026	2.86	3.78E-03
MSMO1	Methylsterol monooxygenase 1	Steroid metabolic process	ENSG00000052802	3.46	<0.00E-04
MYLIP	Myosin regulatory light chain interacting protein	Positive regulation of protein catabolic process	ENSG00000007944	2.69	6.61E-04
NUDT4	Nudix (nucleoside diphosphate linked moiety X)-type motif 4	Cyclic nucleotide metabolic process	ENSG00000173598	3.47	1.57E-04
ODAM	Odontogenic, ameloblast associated	Biomineral tissue development	ENSG00000109205	2.80	4.87E-02

Continued

PDLIM3	PDZ and LIM domain 3	Actin filament organization	ENSG00000154553	2.64	6.61E-04
PDPN	Podoplanin	Cell morphogenesis	ENSG00000162493	3.59	8.15E-03
PNRC2	Proline-rich nuclear receptor coactivator 2	Deadenylation-independent decapping of nuclear-transcribed mRNA	ENSG00000189266	2.68	1.05E-04
PRPF38B	PRP38 pre-mRNA processing factor 38 (yeast) domain containing B	mRNA processing	ENSG00000134186	2.81	<0.00E-04
RFTN2	Raftlin family member 2	Not available	ENSG00000162944	4.28	5.50E-05
RPL13A	Ribosomal protein L13a	Cytoplasmic translation	ENSG00000142541	3.06	2.35E-02
RTN1	Reticulon 1	Protein import into nucleus	ENSG00000139970	2.86	9.50E-03
SERPINI1	Serpin peptidase inhibitor, clade I (neuroserpin), member 1	Negative regulation of endopeptidase activity	ENSG00000163536	3.62	6.68E-04
SFMBT2	Scm-like with four mbt domains 2	Regulation of transcription, DNA-dependent	ENSG00000198879	2.83	3.12E-04
SLC38A2	Solute carrier family 38, member 2	Ion transport	ENSG00000134294	3.45	1.05E-04
SLC39A12	Solute carrier family 39 (zinc transporter), member 12	Ion transport	ENSG00000148482	3.93	1.77E-03
SLC44A4	Solute carrier family 44, member 4	Transmembrane transport	ENSG00000204385	3.06	9.63E-03
SPP1	Secreted phosphoprotein 1	Regulation of transcription, DNA-dependent	ENSG00000118785	3.19	1.25E-02
SQLE	Squalene epoxidase	Cholesterol biosynthetic process	ENSG00000104549	2.64	7.76E-05
TRIM45	Tripartite motif containing 45	Not available	ENSG00000134253	2.66	1.87E-02
VCAN	Versican	Cell adhesion/Extracellular matrix	ENSG00000038427	2.61	9.04E-03
VEGFA	Vascular endothelial growth factor A	Cellular response to hypoxia	ENSG00000112715	2.72	1.05E-04
VPS45	Vacuolar protein sorting 45 homolog (<i>S. cerevisiae</i>)	Golgi to vacuole transport	ENSG00000136631	3.51	1.63E-03
YIPF2	Yip1 domain family, member 2	Not available	ENSG00000130733	4.07	1.23E-03
YPEL4	Yippee-like 4 (<i>Drosophila</i>)	Not available	ENSG00000166793	3.09	1.10E-02

IVD DEGENERATION INVOLVES DECREASED WNT SIGNALING AND CAVEOLIN-1 EXPRESSION

Continued

ARHGEF10	Rho guanine nucleotide exchange factor (GEF) 10	Regulation of Rho protein signal transduction	ENSG00000104728	-4.89	2.79E-03
BICD1	Bicaudal D homolog 1	Minus-end-directed organelle transport along microtubule	ENSG00000151746	-2.38	4.00E-02
C11orf91	Chromosome 11 open reading frame 91	Not available	ENSG00000205177	-2.25	1.12E-02
CCDC33	Coiled-coil domain containing 33	Not available	ENSG00000140481	-2.72	2.82E-04
CDH8	Cadherin 8, type 2	Cell-cell junction organization	ENSG00000150394	-2.25	1.35E-04
CYFIP1	Cytoplasmic FMR1 interacting protein 1	Lamellipodium assembly	ENSG00000068793	-2.73	1.08E-02
DERL2	Der1-like domain family, member 2	Response to unfolded protein	ENSG00000072849	-2.67	1.51E-02
DPP10	Dipeptidyl-peptidase 10 (non-functional)	Proteolysis	ENSG00000175497	-3.20	1.84E-03
ENC1	Ectodermal-neural cortex 1 (with BTB-like domain)	Multicellular organismal development	ENSG00000171617	-2.39	2.89E-02
EPHA4	EPH receptor A4	Cell adhesion	ENSG00000116106	-2.26	4.76E-02
ERRFI1	ERBB receptor feedback inhibitor 1	Regulation of Rho GTPase activity	ENSG00000116285	-3.21	3.66E-02
FAM118A	Family with sequence similarity 118, member A	Not available	ENSG00000100376	-2.39	9.38E-04
FHL2	Four and a half LIM domains 2	Negative regulation of transcription from RNA polymerase II promoter	ENSG00000115641	-2.81	2.86E-03
FYTTD1	Forty-two-three domain containing 1	mRNA export from nucleus	ENSG00000122068	-2.59	1.59E-03
GPN1	GPN-loop GTPase 1	Not available	ENSG00000198522	-3.29	<0.00E-04
GTPBP5	GTP binding protein 5 (putative)	Ribosome biogenesis	ENSG00000101181	-2.42	2.07E-04
H3F3B	H3 histone, family 3B	Nucleosome assembly	ENSG00000132475	-2.41	1.87E-02
HIST1H2BA	Histone cluster 1, H2ba	Nucleosome assembly	ENSG00000146047	-3.94	<0.00E-04
HIST2H2BF	Histone cluster 2, H2bf	Nucleosome assembly	ENSG00000203814	-4.01	<0.00E-04
HS3ST1	Heparan sulfate (glucosamine) 3-O-sulfotransferase 1	Not available	ENSG00000002587	-2.29	3.79E-04
Not available	Hypothetical protein LOC611312	Not available	Not available	-3.71	6.43E-05

Continued

ITGB1BP2	Integrin beta 1 binding protein (melusin) 2	Signal transduction	ENSG00000147166	-3.02	<0.00E-04
JAG1	Jagged 1	Positive regulation of Notch signaling pathway	ENSG00000101384	-2.85	4.98E-04
KCNJ10	Potassium inwardly-rectifying channel, subfamily J, member 10	Ion transport	ENSG00000177807	-2.31	5.07E-06
LNX2	Ligand of numb-protein X 2	Protein homooligomerization	ENSG00000139517	-2.66	<0.00E-04
LRRC4C	Leucine rich repeat containing 4C	Regulation of axonogenesis	ENSG00000148948	-2.79	1.67E-03
NDUFA7	NADH dehydrogenase (ubiquinone) 1 alpha subcomplex	Oxidation-reduction proces	ENSG00000167774	-2.56	2.31E-02
NFIA	Nuclear factor I/A	DNA replication	ENSG00000162599	-2.39	2.79E-03
NFKBIA	Nuclear factor of kappa light polypeptide gene enhancer in B-cells inhibitor, alpha	Activation of NF-kappaB-inducing kinase activity	ENSG00000100906	-2.29	3.55E-02
ODC1	Ornithine decarboxylase 1	Polyamine biosynthetic process	ENSG00000115758	-2.94	9.96E-06
P4HB	Prolyl 4-hydroxylase, beta polypeptide	Lipid metabolic process	ENSG00000185624	-2.37	4.95E-02
PGCP	Plasma glutamate carboxypeptidase	Tissue regeneration	ENSG00000104324	-2.29	5.65E-04
PHLDA1	Pleckstrin homology-like domain, family A, member 1	Induction of apoptosis	ENSG00000139289	-2.76	2.01E-04
PPAP2B	Phosphatidic acid phosphatase type 2B	Canonical Wnt receptor signaling pathway involved in positive regulation of cell-cell adhesion	ENSG00000162407	-4.55	1.82E-05
PRC1	Protein regulator of cytokinesis 1	Vacuolar protein catabolic process	ENSG00000198901	-2.45	5.29E-04
RBM11	RNA binding motif protein 11	Not available	ENSG00000185272	-2.30	3.94E-02
SETD5	SET domain containing 5	Not available	ENSG00000168137	-2.52	1.16E-02
SOCS1	Suppressor of cytokine signaling 1	JAK-STAT cascade	ENSG00000185338	-2.65	2.38E-02
SORBS1	Sorbin and SH3 domain containing 1	Positive regulation of glycogen biosynthetic process	ENSG00000095637	-3.15	5.07E-06

IVD DEGENERATION INVOLVES DECREASED WNT SIGNALING AND CAVEOLIN-1 EXPRESSION

Continued

SPSB2	SplA/ryanodine receptor domain and SOCS box containing 2	Intracellular signal transduction	ENSG00000111671	-6.24	1.10E-02
TGFBR3	Transforming growth factor, beta receptor III	Positive regulation of cell migration	ENSG00000069702	-2.77	3.14E-03
TMEM93	Transmembrane protein 93	Not available	ENSG00000127774	-2.66	1.07E-02
TNFRSF25	Tumor necrosis factor receptor superfamily, member 25	Cell surface receptor linked signaling pathway	ENSG00000215788	-2.32	1.20E-04
TSPAN5	Tetraspanin 5	Not available	ENSG00000168785	-2.53	1.53E-02
TUBB2A	Tubulin, beta 2A	Protein folding	ENSG00000137267	-4.39	6.43E-05

Mixed NP: Non-chondrodystrophic (ref) vs. Chondrodystrophic dogs

Total up-regulated genes: 604

Total down-regulated genes: 248

Gene Symbol	Description	GO term: Biological process	Ensemble Gene ID	N-fold change	P-value
ATG7	ATG7 autophagy related 7 homolog (<i>S. cerevisiae</i>)	Autophagy	ENSG00000197548	2.72	6.15E-03
ATL2	Atlastin GTPase 2	ER to Golgi vesicle-mediated transport	ENSG00000119787	2.84	< 1.00E-6
ATP5A1	ATP synthase, H+ transporting, mitochondrial F1 complex, alpha subunit 1, cardiac muscle	ATP metabolic process	ENSG00000152234	3.00	0.00E+00
CCL24	Chemokine (C-C motif) ligand 24	Positive regulation of cell migration	ENSG00000106178	2.51	4.74E-04
CSTF3	Cleavage stimulation factor, 3' pre-RNA, subunit 3, 77kDa	mRNA processing	ENSG00000176102	2.56	2.06E-04
DSC2	Desmocollin 2	Cell adhesion	ENSG00000134755	2.53	4.74E-04
DSC3	Desmocollin 3	Protein stabilization	ENSG00000134762	2.80	1.10E-02
DSG1	Desmoglein 1	Cell-cell junction assembly	ENSG00000134760	3.91	1.73E-04
EDRF1	Erythroid differentiation-related factor 1-like isoform 1	Not available	Not available	2.30	2.96E-02
EIF4G2	Eukaryotic translation initiation factor 4 gamma, 2	Regulation of translational initiation	ENSG00000110321	2.54	5.90E-04

Continued

FAM84B	Family with sequence similarity 84, member B	Not available	ENSG00000168672	2.75	6.57E-03
FBXO32	F-box protein 32	Protein ubiquitination	ENSG00000156804	2.42	1.24E-04
FLCN	Folliculin	Regulation of protein phosphorylation	ENSG00000154803	2.54	3.56E-05
FUT8	Fucosyltransferase 8 (alpha (1,6) fucosyltransferase)	Protein glycosylation in Golgi	ENSG00000033170	3.75	3.11E-05
GNG2	Guanine nucleotide binding protein (G protein), gamma 2	GTP catabolic process	ENSG00000186469	2.52	3.22E-03
GNRH1	Gonadotropin-releasing hormone 1 (luteinizing-releasing hormone)	Response to steroid hormone stimulus	ENSG00000147437	2.55	1.73E-02
GUCY1B3	Guanylate cyclase 1, soluble, beta 3	Nitric oxide mediated signal transduction	ENSG00000061918	3.33	4.63E-02
GULP1	GULP, engulfment adaptor PTB domain containing 1	Apoptosis	ENSG00000144366	2.79	< 1.00E-6
HCFC2	Host cell factor C2	Regulation of transcription from RNA polymerase II promoter	ENSG00000111727	2.40	2.97E-04
HTRA1	HtrA serine peptidase 1	Negative regulation of BMP signaling pathway	ENSG00000166033	2.46	2.18E-02
KCNK2	Potassium channel, subfamily K, member 2	Potassium ion transmembrane transport	ENSG00000082482	2.57	4.40E-03
LAMB4	Laminin, beta 4	Cell adhesion	ENSG00000091128	2.30	1.52E-02
LDHB	Lactate dehydrogenase B	Glycolysis	ENSG00000111716	2.50	4.74E-04
LRP2	Low density lipoprotein receptor-related protein 2	Endocytosis	ENSG00000081479	2.96	4.10E-03
LYST	Lysosomal trafficking regulator	Endosome to lysosome transport via multivesicular body sorting pathway	ENSG00000143669	3.44	2.57E-02
MUS81	MUS81 endonuclease homolog (<i>S. cerevisiae</i>)	Response to DNA damage stimulus	ENSG00000172732	2.30	2.85E-04
MYL6	Myosin, light chain 6, alkali, smooth muscle and non-muscle	Muscle filament sliding	ENSG00000196465	2.29	< 1.00E-6
NUDT4	Nudix (nucleoside diphosphate linked moiety X)-type motif 4	Cyclic nucleotide metabolic process	ENSG00000173598	2.32	4.98E-05

IVD DEGENERATION INVOLVES DECREASED WNT SIGNALING AND CAVEOLIN-1 EXPRESSION

Continued

PCDH15	Protocadherin-related 15	Cell adhesion	ENSG00000150275	3.24	1.45E-02
PCDH20	Protocadherin 20	Cell adhesion	ENSG00000197991	3.15	2.37E-02
PDGFD	Platelet derived growth factor D	Regulation of peptidyl-tyrosine phosphorylation	ENSG00000170962	2.34	1.66E-04
PKP2	Plakophilin 2	Carbohydrate metabolic process	ENSG00000057294	3.00	5.80E-03
PLCL1	Phospholipase C-like 1	Lipid metabolic process	ENSG00000115896	2.67	1.30E-02
POPDC3	Popeye domain containing 3	Biological process	ENSG00000132429	2.89	6.89E-04
PTER	Phosphotriesterase related	Catabolic process	ENSG00000165983	2.60	1.04E-02
RAB27A	RAB27A, member RAS oncogene family	Protein transport	ENSG00000069974	2.36	7.95E-04
RAB38	RAB38, member RAS oncogene family	Small GTPase mediated signal transduction	ENSG00000123892	2.40	4.50E-02
RSPO3	R-spondin 3	Wnt receptor signaling pathway	ENSG00000146374	2.47	3.29E-02
SPP1	Secreted phosphoprotein 1	Biomaterial tissue development	ENSG00000118785	2.81	4.80E-02
SPTLC3	Serine palmitoyltransferase, long chain base subunit 3	Sphingolipid metabolic process	ENSG00000172296	3.30	4.29E-03
ST8SIA4	ST8 alpha-N-acetylneuraminide alpha-2, 8-sialyltransferase 4	Protein glycosylation	ENSG00000113532	2.67	4.20E-04
T	T, brachyury homolog (mouse)	Notochord development	ENSG00000164458	2.52	7.47E-03
TMEM45A	Transmembrane protein 45A	Not available	ENSG00000181458	2.65	1.96E-03
TRPM7	Transient receptor potential cation channel, subfamily M, member 7	Calcium-dependent cell-matrix adhesion	ENSG00000092439	2.51	2.06E-04
VWA5A	Von Willebrand factor A domain containing 5A	Not available	ENSG00000110002	2.96	2.29E-02
ZCCHC9	Zinc finger, CCHC domain containing 9	Negative regulation of phosphatase activity	ENSG00000131732	2.48	1.66E-02
ZNF323	Zinc finger protein 323	Viral reproduction	ENSG00000235109	2.34	< 1.00E-6
MT2A	Metallothionein 2A	Cellular response to erythropoietin	ENSG00000125148	-7.81	2.93E-02
AK5	Adenylate kinase 5	ADP biosynthetic process	ENSG00000154027	-2.11	3.60E-02

Continued

AT1B1	Sodium/potassium-transporting ATPase subunit beta-1		ENSG00000143153	-2.04	3.24E-02
ATP1A1	ATPase, Na ⁺ /K ⁺ transporting, alpha 1 polypeptide	ATP biosynthetic process	ENSG00000163399	-2.73	2.04E-02
CD53	CD53 molecule	Signal transduction	ENSG00000143119	-2.01	3.22E-03
CKMT2	Creatine kinase, mitochondrial 2 (sarcomeric)	Creatine metabolic process	ENSG00000131730	-2.72	1.56E-03
COL4A1	Collagen, type IV, alpha 1	Cellular response to amino acid stimulus	ENSG00000187498	-2.92	< 1.00E-6
DES	Desmin	Cytoskeleton organization	ENSG00000175084	-4.00	2.21E-02
DUSP6	Dual specificity phosphatase 6	Inactivation of MAPK activity	ENSG00000139318	-2.09	3.56E-05
EMB	Embigin	Cell adhesion	ENSG00000170571	-2.08	1.25E-02
ENC1	Ectodermal-neural cortex 1 (with BTB-like domain)	Nervous system development	ENSG00000171617	-2.41	7.60E-03
EPST11	Epithelial stromal interaction 1 (breast)	Not available	ENSG00000133106	-2.81	4.57E-03
GCKR	Glucokinase (hexokinase 4) regulator	Cellular glucose homeostasis	ENSG00000084734	-2.00	3.47E-02
GDPD2	Glycerophosphodiester phosphodiesterase domain containing 2	Glycerol metabolic process	ENSG00000130055	-2.25	2.71E-02
GLIPR1	GLI pathogenesis-related 1	Cellular lipid metabolic process	ENSG00000139278	-2.05	4.20E-04
GNG11	Guanine nucleotide binding protein (G protein), gamma 11	GTP catabolic process	ENSG00000127920	-2.25	2.74E-02
H3F3A	H3 histone, family 3A	Nucleosome assembly	ENSG00000132475	-2.03	2.85E-03
HLA-DQB2	Major histocompatibility complex, class II, DQ beta 2	Immune response	ENSG00000232629	-2.08	2.41E-02
HPR	Haptoglobin-related protein	Photorespiration	ENSG00000257017	-2.23	7.61E-04
HP	Hypothetical protein	Not available	Not available	-2.00	3.79E-02
LOC100684119	LOC100684119				
IL4	Interleukin 4	Positive regulation of T cell proliferation	ENSG00000113520	-2.05	3.80E-02
KCNJ10	Potassium inwardly-rectifying channel, subfamily J, member 10	Potassium ion transport	ENSG00000177807	-2.15	1.22E-03

IVD DEGENERATION INVOLVES DECREASED WNT SIGNALING AND CAVEOLIN-1 EXPRESSION

Continued

LNX2	Ligand of numb-protein X 2	Protein homooligomerization	ENSG00000139517	-2.20	1.02E-02
LRRC4C	Leucine rich repeat containing 4C	Regulation of axonogenesis	ENSG00000148948	-2.77	7.02E-03
METTL7A	Methyltransferase like 7A	Metabolic process	ENSG00000185432	-2.11	2.08E-02
MN1	Meningioma (disrupted in balanced translocation) 1	Intramembranous ossification	ENSG00000169184	-2.96	2.71E-02
NFIL3	Nuclear factor, interleukin 3 regulated	Transcription from RNA polymerase II promoter	ENSG00000165030	-2.57	1.10E-02
NFKBIA	Nuclear factor of kappa light polypeptide gene enhancer in B-cells inhibitor, alpha	Activation of NF-kappaB-inducing kinase activity	ENSG00000100906	-2.38	9.21E-03
PCK1	Phosphoenolpyruvate carboxykinase 1 (soluble)	Oxaloacetate metabolic process	ENSG00000124253	-2.40	1.39E-03
PDK4	Pyruvate dehydrogenase kinase, isozyme 4	Regulation of acetyl-CoA biosynthetic process from pyruvate	ENSG00000004799	-4.36	5.25E-04
PLBD1	Phospholipase B domain containing 1	Lipid catabolic process	ENSG00000121316	-2.18	3.85E-02
PLP1	Proteolipid protein 1	Protein integrin-mediated signaling pathway	ENSG00000123560	-2.15	3.63E-02
PPAP2B	Phosphatidic acid phosphatase type 2B	Canonical Wnt receptor signaling pathway involved in positive regulation of cell-cell adhesion	ENSG00000162407	-2.78	7.09E-03
PSPH	Phosphoserine phosphatase	Response to mechanical stimulus	ENSG00000146733	-2.39	5.37E-04
PTPRO	Protein tyrosine phosphatase, receptor type, O	Peptidyl-tyrosine dephosphorylation	ENSG00000151490	-2.04	1.99E-02
Q95JD6	Sulfotransferase	Not available	Not available	-2.32	2.10E-03
RTN1	Reticulon 1	Protein import into nucleus	ENSG00000139970	-2.11	4.36E-02
SLC30A1	Solute carrier family 30 (zinc transporter), member 1	Cadmium ion transmembrane transport	ENSG00000170385	-2.16	1.36E-03
SRSF5	Serine/arginine-rich splicing factor 5	mRNA splice site selection	ENSG00000100650	-2.06	3.75E-03

Continued

SVIL	Supervillin	Cytoskeleton organiza- tion	ENSG00000197321	-2.12	9.75E-04
TGFBR3	Transforming growth factor, beta receptor III	Epithelial to mesenchy- mal transition	ENSG00000069702	-2.73	< 1.00E-6
TXNDC11	Thioredoxin domain containing 11	Cell redox homeostasis	ENSG00000153066	-2.34	2.65E-04
VCAM1	Vascular cell adhesion molecule 1	Cell-cell adhesion	ENSG00000162692	-2.14	2.62E-02
ZBTB16	Zinc finger and BTB domain containing 16	Cartilage development	ENSG00000109906	-2.05	3.19E-02

CLC-rich NP: Non-chondrodystrophic (reference) vs. Chondrodystrophic dogs					
Gene Symbol	Description	GO term: Biological Process	Ensemble Gene ID	N-fold change	P-value
SERPINI1	Serpin peptidase inhibitor, clade I (neuroserpin), member 1	Regulation of cell adhesion	ENSG00000163536	5.18	3.08E-03
C1orf63	Chromosome 1 open reading frame 63	Not available	ENSG00000117616	2.72	3.55E-03
PRPF38B	PRP38 pre-mRNA processing factor 38 (yeast) domain containing B	mRNA processing	ENSG00000134186	2.30	1.36E-03
C9orf156	Chromosome 9 open reading frame 156	Interspecies interaction between organisms	ENSG00000136932	2.21	3.55E-03
TOB1	Transducer of ERBB2, 1	Negative regulation of BMP signaling pathway	ENSG00000141232	2.17	2.63E-03
WDR67	WD repeat domain 67	Regulation of Rab GTPase activity	ENSG00000156787	1.98	3.55E-03
HP LOC611312	Hypothetical protein LOC611312	Not available	Not available	-7.03	2.98E-03
ERRFI1	ERBB receptor feedback inhibitor 1	Negative regulation of epidermal growth factor-activated receptor activity	ENSG00000116285	-6.84	1.36E-03
VEGFC	Vascular endothelial growth factor C	Vascular endothelial growth factor receptor signaling pathway	ENSG00000150630	-3.25	2.98E-03
PHYHD1	Phytanoyl-CoA dioxygenase domain containing 1	Not available	ENSG00000175287	-2.16	2.98E-03

GENERAL DISCUSSION

The studies described in this thesis investigated new strategies for the treatment of canine intervertebral disc (IVD) degeneration, focusing on fixation, functional restoration, and regeneration of the degenerated IVD. These strategies are of value to both veterinary and human medicine and have the potential to improve the medical care of both canine and human patients. The General Discussion of this thesis focuses on the treatment strategies available to veterinary medicine.

IVD disease is an important ailment in veterinary medicine and is difficult to diagnose and treat. Ancillary methods for diagnosing canine IVD disease currently used in a clinical setting include radiography, myelography, epidurography, discography, computed tomography, and magnetic resonance imaging (MRI)¹⁻³. Since several factors complicate the diagnosis of IVD disease, such as subclinical IVD degeneration⁴⁻⁷, novel modalities for diagnosing and monitoring patients are valuable, and especially modalities that allow the detection of early stages of IVD degeneration, when functional repair or even regeneration (see below) of the disc is possible. MRI may be particularly suited for this purpose because it allows grading of IVD degeneration on T2-weighted sagittal images, using validated, objective grading schemes^{7,8}. Moreover, the health of the extracellular matrix (ECM) of the IVD can be monitored by means of contrast-enhanced MRI, using contrast media such as gadolinium^{9,10}. The IVD is the largest avascular structure of the body, and contrast medium can only transfer into the disc via diffusion. Because contrast medium diffuses through the endplates into the IVD slowly, the signal intensity of a healthy IVD increases slowly after intravenous administration of contrast medium¹⁰. In contrast, contrast enhancement is more intense and more rapid in degenerating IVDs because diffusion is less restricted owing to the lower glycosaminoglycan content of the degenerated disc¹⁰. In the case of annular tears, contrast enhancement diminishes¹¹. In addition, quantitative MRI techniques allow more accurate evaluation of signal intensity in degenerated IVDs and IVD herniation¹²⁻¹⁴. Recently, the signal of T1_{rho}-weighted MRI, which allows the physicochemical interactions between water and extracellular matrix molecules to be studied, has been shown to be linearly correlated with the sulfated glycosaminoglycan content of the ECM of the IVD and may therefore be used to detect early degenerative changes even before morphological signs are visible¹⁵. In addition to using MRI techniques to investigate degenerative changes of the IVD, genetic and/or molecular screening of breeds susceptible to IVD degeneration would also facilitate the early detection of disease. Chondrodystrophic breeds are appropriate targets for this strategy, as these dogs show early degeneration, and therefore the risk of herniation, of all IVDs⁴.

Evaluation of the ground reaction forces involved in canine locomotion through force plate analysis has been used to assess the functional implications of several diseases and surgical procedures in dogs¹⁶, such as degenerative lumbosacral stenosis (DLSS) and its treatment with dorsal laminectomy and partial discectomy^{17,18}. In addition to the functional analysis of ground reaction

forces (kinetics), three-dimensional motion kinematic gait analysis has been proposed as valuable tool for diagnosing cervical spondylomyelopathy (CSM), DLSS, and nucleus pulposus (NP) herniation. However, the effects of the soft tissue artifact, a commonly recognized, but often neglected, cause of inaccuracy in kinematic gait analysis^{16,19,20} need to be investigated before this technique can be used for canine patients. In the study described in **Chapter 2.2**, the effects of the soft tissue artifact on canine kinematic analysis were assessed. Both kinematic and fluoroscopic investigations revealed significant motion of the markers attached to the skin overlying bony landmarks of interest, which may lead to misinterpretation of results obtained with this technique. These inaccuracies make mathematical correction algorithms necessary for valid kinematic analysis^{21,22}. However, the development of such algorithms, and hence their use in clinical practice, is complicated by differences between dog breeds.

The first aim of the studies reported in this thesis was to develop and test novel surgical treatments for dogs with end-stage IVD disease, such as pedicle screw-rod fixation of the affected segment or a NP prosthesis (NPP) to restore the function of the affected segment.

Salvage of the intervertebral disc

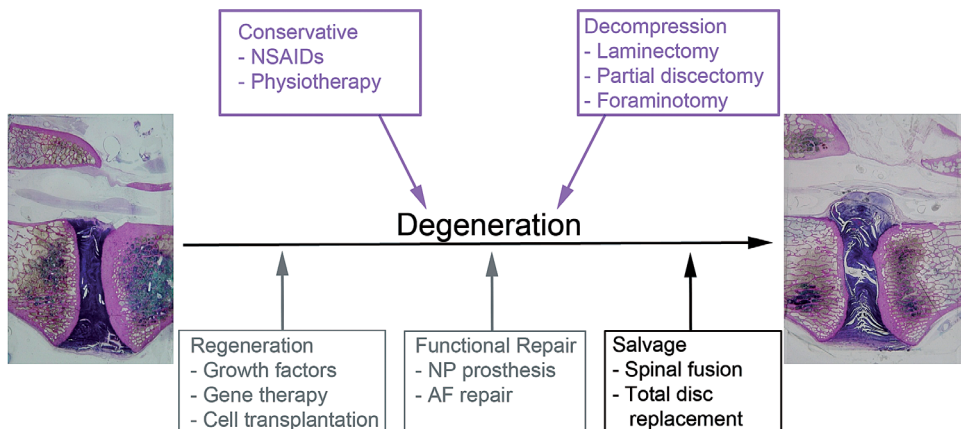


Figure 1. Current and new treatment strategies for intervertebral disc degeneration. Current strategies (purple boxes and letters) consist of conservative measures or surgical decompression. The new treatment strategies (black boxes and letters) can be applied at different stages in the course of intervertebral disc degeneration. In this section, emphasis is on salvage procedures used in late-stage degeneration.

Current surgical strategies for treating dogs with end-stage IVD disease involve decompression of affected neural tissue by removing the dorso-lateral lamina and/or herniated disc material, often combined with nucleotomy of the affected IVD. This involves removing the diseased NP, or foraminotomy, with decompression of spinal nerve roots (Fig. 1) ²³. As has been shown in previous studies of the cervical spine, nucleotomy results in significantly decreased spinal stiffness ²⁴, making, fixation procedures necessary in dogs with CSM and in some dogs with cervical IVD herniation. The studies presented in **Chapters 3.2** and **3.3** showed that nucleotomy alone or combined with dorsal laminectomy results in a significant decrease in disc height and spinal stiffness in the lumbar and lumbosacral canine spine, which may result in spinal instability. Therefore, the second hypothesis of this thesis can be accepted: ***Removal of the nucleus pulposus from the intervertebral disc (nucleotomy) results in a loss of disc height and loss of spinal stability.*** This instability may lead to long-term degenerative changes of the affected segment. In particular, the lumbosacral junction, which is subjected to extreme ranges of mobility and hence considerable workload ^{32,33}, may benefit from additional stabilization, especially in physically active (working) dogs such as German Shepherd dogs, which may be more susceptible to the development of recurrent degenerative changes of the lumbosacral junction.

The study presented in **Chapter 3.1** evaluated fixation and stabilization of the canine lumbosacral junction by way of pedicle screw-rod fixation. This study tested the first hypothesis of this thesis: ***Pedicle screw-rod fixation of the canine lumbosacral junction enables spinal fusion of L7-S1.***

In humans, fixation of the spinal segment, or spinal arthrodesis, was first reported by Hibbs and Albee in 1911 ²⁵ and is now commonly used to treat various spinal disorders, including disc disease, spinal stenosis, and spinal deformities such as spondylolisthesis ²⁶. Different methods to stabilize the spine have been described, applying various approaches and different methods of instrumentation, including wires and cables, hooks, screws, and vertebral interbody cages ²⁷. However, the canine spine is smaller than the human spine and so it is challenging to select appropriately sized material for spinal fixation that provides sufficient implant strength. Pedicle screw-rod fixation is an appropriate method to fix the relatively small canine spine, since pedicle screw fixation is biomechanically superior to other methods for stabilizing the lumbar spinal segment ^{28,29}. In addition, the canine L7 and S1 vertebrae and surrounding soft tissues allow for safe pedicle screw insertion ³⁰. For this reason, stabilization using pedicle screws was chosen to fix the canine lumbosacral junction after spinal decompression.

The *ex vivo* cadaver study described in **Chapter 3.1** showed that pedicle screw-rod fixation can be applied to the lumbosacral junction of middle-sized dogs; however, knowledge of the three-dimensional anatomy of the complete L7-S1 junction is essential for optimal screw anchorage, so that neural structures are not compromised by screw misplacement. ***The in vivo study***

reported in Chapter 3.1 also showed that pedicle screw-rod fixation can be used with clinical success to stabilize the lumbosacral junction of large-breed dogs, and hind limb function, as assessed by force plate analysis, tends to be improved. However, instrumented fixation of the spine is aimed at facilitating bony fusion of the spinal segment³¹⁻³³. Bony fusion of the spinal segment was not observed in any of the operated dogs, so the first hypothesis can be rejected. Bony fusion of the canine lumbar spinal segment has been reported in previous studies assessing spinal fixation techniques, including spinal fixation involving pedicle screw instrumentation, which resulted in fusion in 100% of the surgically treated cases^{32,34}. The absence of spinal fusion in the study described in **Chapter 3.1** may be because thorough decortication of the vertebrae or broaching of the cartilaginous endplates to promote bony spinal fusion was not performed, as reported in studies achieving bony fusion^{32,34}. Although the endplates were curetted in the study reported in **Chapter 3.1**, more extensive preparation of the L7 and S1 endplates may be necessary to achieve bony fusion. An alternative explanation concerns the site of spinal fixation. The studies achieving successful spinal fusion^{32,34} reported fixation of the lumbar spine and not of the lumbosacral junction. The lumbosacral junction allows for extreme flexibility in flexion/extension and axial rotation^{35,36} (sustained by the results reported in Chapter 4 of this thesis), which may complicate lumbosacral junction fusion.

All in all, pedicle screw-rod fixation of the canine lumbosacral junction seems to be a suitable salvage procedure in IVD degenerative disease, as it provides adequate stability, is well tolerated, and may lead to improved hind limb function; however, other aspects need to be assessed in order to obtain fusion of the L7-S1 spinal segment. For example, the surgical procedure described in **Chapter 3.1** should be improved by broaching the endplates down to healthy, bleeding bone instead of superficially curetting them. Bony interbody fusion of the spinal segment may be facilitated by using interbody cages, which are placed in between the L7 and S1 vertebral bodies. Interbody cages are designed to promote spinal fusion in several ways: 1) by creating an optimal environment for spinal fusion in that all intervening soft tissue is removed from the intervertebral space (complete discectomy) and an appropriate cancellous bone graft can be placed within the cage; 2) by providing immediate stiffness to the decompressed segment and by withstanding axial, translational, and rotational forces in all motion directions; and 3) by correcting existing spinal deformities such as spondylolisthesis, resolving the loss of disc height due to IVD degeneration and/or discectomy, and increasing the size of the neuroforaminal space³⁷. Studies of fixation of the canine lumbosacral junction using spinal interbody cages (Synthes, Zeist, the Netherlands) are currently being planned. In addition, bony interbody fusion may be promoted by intradiscal injection of mesenchymal stromal cells (MSCs), derived from either bone marrow or adipose tissue³⁸⁻⁴¹. This technique could potentially be improved by injecting growth factors, such as bone morphogenetic protein (BMP)-2 and fibroblast

growth factor (FGF), or by seeding the cells in specifically designed scaffolds^{38,40,42}. Also, MSCs could be primed toward osteogenic differentiation before injection into the IVD space, to accelerate the fusion process⁴³. These potential strategies to accelerate and promote spinal fusion constitute exciting topics for future research in dogs.

Functional repair of the intervertebral disc

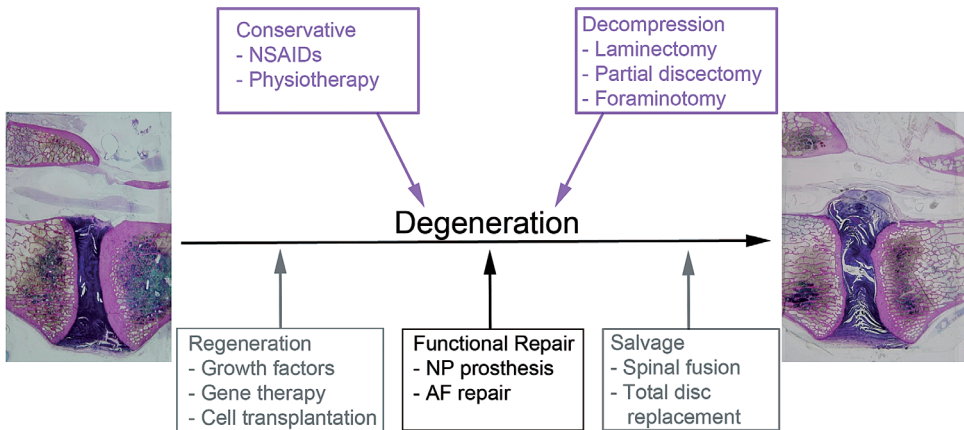


Figure 2. Current and new treatment strategies for intervertebral disc degeneration. Current strategies (purple boxes and letters) consist of conservative measures or surgical decompression. The new treatment strategies (black boxes and letters) can be applied at different stages in the course of intervertebral disc degeneration. In this section, emphasis is on functional repair of the disc, applicable in intermediate-stage degeneration.

Although decompression combined with spinal stabilization can lead to resolution of clinical signs, this approach is suboptimal. Spinal fixation stabilizes the spinal segment, but the resulting spinal stiffness has its downside^{44,45}. Fixation of the decompressed segment increases the workload on adjacent IVDs and facet joints, which in turn may lead to degenerative changes of adjacent spinal segments, the so-called adjacent segment disease (or domino effect)⁴⁶⁻⁴⁹. A radiographic study reported the incidence of adjacent segment degeneration in humans during a follow-up of 36 to 369 months to range from 5.2% to 100%, and the incidence of symptomatic adjacent segment disease to range from 5.2% to 18.5% during 45 to 164 months of follow-up⁴⁹. Stabilization of the spinal segment may significantly restrict the functionality of the canine spine. Working dogs with degenerative lumbosacral stenosis may benefit from a functional lumbosacral junction rather than a fixed lumbosacral junction. This makes restoration of IVD function and prevention of the complications

associated with spinal fusion a more appropriate strategy for dogs with IVD disease⁵⁰.

Partial disc replacement can lead to functional recovery (Fig. 2). This technique, which involves replacement of the NP, has several advantages over total disc replacement: the endplates and annulus fibrosus are preserved, the surgical technique is less invasive and less complicated, and different approaches (dorsal, lateral, ventral) can be used⁵⁰⁻⁵². Many partial disc replacement devices have been designed and tested⁵². The NPP tested in the studies reported in **Chapters 3.2 and 3.3** had several distinctive and specialized qualities relative to those of other NP replacement devices. The NPP consisted of a specially designed hydrogel material (N-vinyl-2-pyrrolidinone copolymerized with 2-(4'-iodobenzoyl)-oxo-ethyl methacrylate). The intrinsic radiopacity of this material makes accurate placement and evaluation of the NPP possible. The NPP was specifically designed to swell *in situ* to fill the nucleus cavity and restore disc height. This is important because nucleotomy of the IVD results in a significant decrease in disc height and spinal stiffness. After insertion of the NPP, IVD height was restored in 80% of the spinal segments, and biomechanical testing showed that the NPP restored spinal stiffness, and thereby functionality, to the spinal segment. Therefore the third hypothesis of this thesis can be accepted: ***Spinal stability can be restored by inserting a nucleus pulposus prosthesis (NPP) into the excavated intervertebral disc.***

However, although the NPP was able to restore disc height and functionality, short-term biomechanical loading of the NPP *in situ* caused NPP fragmentation and consequent implant extrusion in a large percentage of cases. NPP integrity is essential to its functionality, and NPP fragmentation may lead to clinical signs similar to those caused by herniation/bulging of natural IVD tissue. Therefore, **this first-generation NPP should not be used in vivo because it is unsafe**; however, several aspects of the NPP can be improved. First, the material properties of the NPP should be altered so that the prosthesis does not fragment during long-term cyclic loading *in situ*. A second-generation NPP with a peripheral-to-central softness gradient and altered material properties is currently under investigation⁵³. Second, adequate closure of the annulus fibrosus, involving both the inner and outer annular layers, is essential for the functionality of the NPP, so it is important to ensure that there is adequate closure of the inner and outer layers of the annulus fibrosus after prosthesis placement. Failure to achieve this, which is likely when the annulus fibrosus is closed with sutures, cyanoacrylate glue, or polypropylene mesh, may mean that the nuclear space is larger than originally measured, so that the fit of the NPP is suboptimal. This could lead to implant migration inside the nuclear cavity, predisposing the NPP to fragmentation and leading to suboptimal restoration of IVD functionality. Thus, **even though alterations to the NPP material properties are promising, adequate annulus fibrosus closure is also of fundamental importance**. An ideal annular closure maintains the NPP within the nuclear cavity, replaces the annular tissue lost due to surgery, and restores

biomechanical functionality to the annulus fibrosus⁵⁴. Strategies for annulus closure include annulus regeneration, which can consist of gene and/or cell therapy in combination with scaffolds, and surgical repair of the annulus with specialized sutures, seals, and barriers⁵⁴. Future studies involving long-term cyclic biomechanical testing of the upgraded version of the NPP in combination with appropriate closure of the annulus fibrosus are warranted to assess the full potential of this concept before the device is tested *in vivo*.

Once the NPP has been optimized, it might form a valuable surgical option for dogs with IVD disease. Dogs eligible for such treatment should meet the following criteria: 1) disc degeneration manifest by morphological changes of the NP, 2) a repairable/competent annulus fibrosus, and 3) incomplete collapse of the IVD height (humans: disc height ≥ 5 mm)^{55,56}. The NPP can be used to replace the degenerated NP in dogs with NP herniation that are routinely treated by hemilaminectomy and partial discectomy; in dogs with DLSS treated by dorsal laminectomy and partial discectomy; in chondrodystrophic dogs at high risk of NP herniation treated prophylactically with IVD fenestration; and in dogs that have undergone spinal fusion, which often results in degeneration of IVDs adjacent to the fixed segment, such that NPP insertion may restore segment functionality.

Insertion of the NPP will improve the quality of treatment for dogs with IVD disease by restoring functionality to the degenerated spinal segment, thereby reducing the risk of exacerbation of degenerative changes as a result of spinal instability. Restoration of IVD function might be an alternative and better treatment strategy for dogs with CSM and DLSS. However, NP replacement can only be applied in selected cases, and stabilization by way of fusion will probably remain the best possible surgical option for segments with such severe degeneration that functional restoration is not possible.

Regeneration of the intervertebral disc

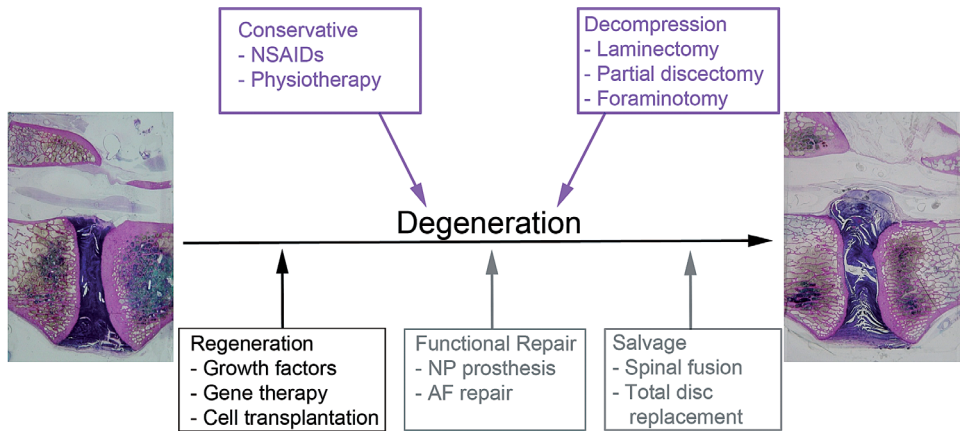


Figure 3. Current and new treatment strategies for intervertebral disc degeneration. Current strategies (purple boxes and letters) consist of conservative measures or surgical decompression. The new treatment strategies (black boxes and letters) can be applied at different stages in the course of intervertebral disc degeneration. In this section, emphasis is regeneration of the disc, applicable in early-stage degeneration.

Although restoration of the IVD by partial or total disc replacement can restore functionality and stability to the spinal segment, the best replacement material remains natural IVD tissue (Fig. 3). For this reason, IVD regeneration is the ideal scenario for treating early-stage IVD-degenerative disease, a treatment option that has received interest in recent years⁵⁷⁻⁶¹. Regeneration of the IVD can be defined as the prevention, inhibition, and/or reversal of degenerative processes by concomitantly stimulating the synthesis of ECM and by decreasing, and ideally, reversing the process of ECM degradation^{62,63}. Different strategies for IVD regeneration are available, including the use of growth factors and anti-catabolic agents, gene therapy, and cell-based strategies⁵⁷⁻⁶⁰. The optimal strategy will depend on a number of factors, such as the integrity of the IVD structure, the physiological status, the quality of the matrix, and the viability and activity of the native IVD cells. If the native cells of the disc are still metabolically active, then growth factors could be injected to stimulate matrix anabolism. If a longer effect is needed, then gene therapy, to produce the sustained synthesis of relevant growth factors, can be used. If the cells of the IVD have lost their ability to synthesize a functionally healthy matrix, cell-based strategies may be the best option for achieving IVD regeneration⁵⁸⁻⁶⁰.

The focus of cell-based strategies for IVD regeneration has been on the use of MSCs and/or chondrocyte-like cells (CLCs)^{59,64-68}. During IVD degeneration, the notochordal cells (NCs) of the healthy, juvenile NP are gradually replaced

by CLCs. It has been much debated whether CLCs are of mesenchymal (endplate-derived) or notochordal origin,⁶⁹⁻⁷² but recent findings suggest that both NCs and CLCs are of notochordal lineage⁷³⁻⁷⁷. The transition from a NC-rich NP to a CLC-rich NP, also referred to as *chondrification*, involves significant changes in the cellular and matrix composition of the NP. Unlike the proteoglycans of the NC-rich NP, which are rich in chondroitin sulfate, the proteoglycans of the CLC-rich NP are rich in the relatively shorter keratan sulfate side chains⁷⁸⁻⁸⁰, the presence of which is thought to be related to the appearance of CLCs, as keratan sulfate has not been detected in the notochord itself^{81,82}. Chondrification of the NP results in an increase in its collagen content, imparting a more fibrocartilaginous, and less hydrated, character to the NP⁸³. The ECM produced by NCs is more hydrated because proteoglycan synthesis is higher in NCs than in CLCs. NCs are more efficient in filling the pericellular (territorial) and the intercellular (interterritorial) phases of the ECM (further away from the cell) than are CLCs⁸⁴. NCs regulate the physiology of CLCs by suppressing apoptosis through inhibition of caspase-9 and caspase 3/7, and by stimulating ECM production by CLCs through secretion of connective tissue growth factor-2 and by up-regulation of the expression of genes that promote matrix anabolism, such as aggrecan and TIMP-1⁸⁵⁻⁸⁸. All in all, NCs exert beneficial effects on ECM quality and production, characteristics that make these cells interesting targets for regenerative strategies.

As the NPs from non-chondrodystrophic and chondrodystrophic dogs have a different biochemical composition and cell population, the study in **Chapter 4** investigated whether these differences affect the biomechanical properties of the spinal segment and the composition of the ECM. It was not possible to compare the relatively larger non-chondrodystrophic and smaller chondrodystrophic spine directly, because of differences in spine size, facet joint orientation, IVD dimensions, and other factors affecting spinal biomechanical properties; however, **comparison of the effects of decompressive surgery in these two types of dog breed revealed significant differences, with instability being greater at L2-L3 in chondrodystrophic dogs and at L7-S1 in non-chondrodystrophic dogs.** The results indicate that the NC-rich NP may be biomechanically different from the CLC-rich NP, suggesting that the biomechanical function of the ECM is different too. The apparent discrepancy between the findings for L2-L3 and for L7-S1 warrants further investigation of anatomical and biomechanical differences between the chondrodystrophic and non-chondrodystrophic spine regarding the dimensions and orientation of the facet joints, IVDs, and other biomechanically significant structures. In addition to providing a valid explanation for the results obtained in **Chapter 4**, such studies may explain why IVD disease occurs at distinct spinal levels in both chondrodystrophic and non-chondrodystrophic dogs. The orientation of the facet joints, which is decisive for the degree of axial rotation within a spinal segment^{89,90}, has already been mentioned as a potential risk factor for cervical and lumbosacral IVD degeneration in non-chondrodystrophic dogs⁹¹⁻⁹⁵.

In addition, comparison of the axial compression biomechanics⁹⁶ in NC-rich and CLC-rich IVDs and studies of more advanced stages of IVD degeneration (Thompson I-V) will provide increased insight into the biomechanical effects of canine IVD degeneration and the potential use of the dog as a model for human spinal research.

Differences in the composition of the ECM in NC-rich and CLC-rich NP are the result of differences in gene and protein expression in the two cell types. The studies reported in **Chapter 5** investigated the changes in the biomolecular signaling pathways involved in the chondrification of the IVD in early IVD degeneration. Numerous biomolecular signaling pathways were found to be significantly changed in early IVD degeneration, which supports the fourth hypothesis of this thesis: *Significant loss of the notochordal cells from the nucleus pulposus results in significant alterations in the biomolecular signaling pathways involved in intervertebral disc matrix health and degeneration.*

The biomolecular signaling pathways investigated, namely, those involving ECM remodeling, plasmin signaling, plasminogen activator, urokinase (PLAU) signaling, bone morphogenetic protein (BMP) signaling, and Wnt signaling/cytoskeletal remodeling, provided insight into fundamental processes associated with IVD degeneration. Of 180 pathways that were identified by microarray analysis to be different, only 5 were investigated in depth. Therefore, the data presented in **Chapter 5.2** should be considered preliminary, because the data require validation and other pathways should be investigated. The gene material is stored in a database and is available for studies investigating various scientific questions, such as finding NC-specific markers that can be used to distinguish NCs from CLCs and to explore the fate of NCs during degeneration; investigating the regenerative potential of the NC; determining the function and content of the intracellular vesicles that are morphologically characteristic of NCs; and elucidating the factors responsible for the change in NP cell population observed early in the degenerative cascade^{71,72,75}.

To further characterize NCs and the fundamental processes involved in the degenerative cascade, canonical Wnt signaling, a pathway involved in the differentiation or maintenance of stem cells in a self-renewing state⁹⁷, was investigated. The study described in **Chapter 5.1** investigated which set of reference genes would be best for quantitative gene expression analysis using canine IVD tissue. As the expression stability of commonly used reference genes differed by type of breed and animal age, customized sets of reference genes were designed for all gene expression analysis experiments (discussed below). Other substudies concerned the investigation of well-known Wnt-associated genes and its effector protein β -catenin (**Chapter 5.2**), and microarray analysis of genes involved in early IVD degeneration in non-chondrodystrophic and chondrodystrophic dogs, the results of which supported the investigation of canonical Wnt signaling and detected other gene targets in this biomolecular pathway (**Chapter 5.4**). Overall, the results reported in **Chapter 5** show that

NCs express various biomolecular components indicative of active canonical Wnt signaling, including Wnt ligands *wnt7b* and *wnt10b*, intracellular components *r-spondin 3* and *caveolin-1*, and nuclear components *axin2* and β -catenin. **The presence of active canonical Wnt signaling in notochordal cells supports the role of this cell as a NP progenitor cell, which makes notochordal cells an attractive target for IVD regenerative strategies.**

In addition to active canonical Wnt signaling, NCs, but not CLCs, were found to express high levels of *caveolin-1* and 2 (Chapter 5.3). Moreover, the NPs of 3-month-caveolin-1 knockout mice showed signs of early IVD degeneration, which suggests that caveolin proteins are essential to the function and preservation of NCs. Caveolin-1 is the main constituent of caveolae. Caveolin-2 is tightly co-expressed with caveolin-1, which is required for proper membrane localization of caveolin-2. One of the main functions of caveolae is the regulation of vesicle trafficking, formation, docking, and fusion^{98,99}. In this respect, it is tempting to postulate that caveolin proteins have a function in the intracellular vesicles that are characteristic of NCs, and that down-regulation or knockout of these proteins induces NC apoptosis and consequently IVD degeneration. In relation to canonical Wnt signaling, caveolae have been shown to regulate the effects of β -catenin: independent of β -catenin/Tcf-Lef transcription activity, up-regulation of caveolin-1 expression results in the recruitment of β -catenin to caveolae membranes, inhibiting β -catenin/Tcf-Lef signaling¹⁰⁰. In contrast, caveolin-1 has been shown to induce the internalization of LRP-6 and the accumulation of β -catenin, thereby activating canonical Wnt signaling¹⁰¹. Also, caveolin-1 stimulates canonical Wnt signaling by inhibiting glycogen synthase kinase 3- β through activation of integrin linked kinase¹⁰². The activation of canonical Wnt signaling through caveolin-1 seems plausible because NCs express high levels of caveolin-1 and higher levels of Wnt/ β -catenin expression than do CLCs. However, the exact mechanisms by which caveolin-1 functions in NCs need to be clarified, for example, by studying the gene and protein expression of Wnt/ β -catenin/caveolin-1 in IVDs collected from caveolin-1 knockout mice of different ages (from birth to adulthood) and subsequently in the canine IVD, with a view to identifying therapeutic targets for IVD regeneration.

NCs could be used clinically in several cell-based treatment strategies to promote IVD regeneration. For example, autologous, cultured NCs isolated from a healthy disc could be injected into a degenerating IVD, although several practical obstacles need to be overcome before this can be realized. First, the harvesting of NCs from a healthy IVD may prompt degeneration of the donor disc¹⁰³. Secondly, environmental factors, such as the nutritional supply in the degenerated IVD, may have deteriorated significantly, adversely affecting the health and functionality of NCs. Thirdly, it might not be possible to harvest NCs from adult chondrodystrophic dogs suffering from IVD disease because these cells have largely been replaced by CLCs^{4,84}. As NCs have a beneficial effect on the regenerative potential of MSCs and CLC,¹⁰⁴⁻¹⁰⁷ it may be relevant to try

to identify factors secreted by NCs, with a view to developing an injectable solution of matrix-anabolizing agents and factors that could stimulate native CLCs to produce ECM 85,87.

The results of the studies described in **Chapter 5** show that active canonical Wnt signaling is essential for the preservation of NC-like characteristics in NCs in culture. Under standard culture conditions, NCs showed basal levels of canonical Wnt signaling, comparable to those seen *in vivo*. Although the cultured NCs retained their cytoplasmic vesicles up to 10 days in culture, culture conditions may have been suboptimal in preserving the natural NC phenotype, as indicated by the significant decrease in *brachyury* and *cytokeratin 8* gene expression. The culture of NCs under hypoxic conditions in three-dimensional culture has been proposed as being more representative of the *in vivo* situation, as NCs have been shown to produce a more complex three-dimensional cellular construct with a complex matrix containing high levels of aggrecan and collagen II under hypoxic conditions as compared with normoxic culture conditions¹⁰⁸. This culture set-up should be investigated further as it is essential to identify the optimal culture conditions for NCs if their regenerative potential is to be harnessed to treat IVD degenerative diseases^{108, 109}.

Early IVD degeneration seems to involve the up-regulation of canonical Wnt/ β -catenin signaling (**Chapter 5.2**), as indicated by the significantly higher expression of *axin2*, *c-myc*, and *cyclin D1* and higher β -catenin protein staining intensity in chondrodystrophic, CLC-rich NP compared with the non-chondrodystrophic, NC-rich NP. In contrast, the studies reported in **Chapters 5.3** and **5.4** showed that canonical Wnt signaling was significantly down-regulated in early NP degeneration in both chondrodystrophic and non-chondrodystrophic dog breeds, involving changes in the expression of various canonical Wnt signaling components, including *axin2*, *caveolin-1* and *-2*, *wnt inhibitory factor*, and *wnt 7b*. The apparently contradictory findings of these studies may be explained by intracrine differences in this signaling pathway between non-chondrodystrophic and chondrodystrophic dogs, as evidenced by the findings of **Chapter 5.4**, which showed that the expression of *axin2* was significantly higher in chondrodystrophic dogs than in non-chondrodystrophic dogs.

The significantly higher canonical Wnt signaling activity observed in chondrodystrophic dogs, as well as the trend toward significantly higher Wnt signaling activity in the Mixed NP (containing both NCs and CLCs) compared with the NC-rich NP, could suggest that NP cells can decelerate or reverse the degenerative cascade. Conversely, given the involvement of Wnt signaling in tissue degeneration, the significantly higher Wnt signaling activity observed in tissue from chondrodystrophic dogs could indicate that the capacity to limit Wnt signaling may be limited in these breeds, resulting in accelerated ECM breakdown¹¹⁰. All in all, it remains to be ascertained whether Wnt/ β -catenin signaling promotes IVD regeneration through increased cell proliferation and optimal matrix production or

promotes the loss of NCs from the NP and thereby IVD degeneration.

Depending on the exact role of Wnt signaling in IVD degeneration, several approaches can be used to influence this pathway with a view to inducing IVD regeneration. Wnt/ β -catenin signaling can be targeted at an extracellular, cytoplasmic, or nuclear level, thereby influencing different steps in the pathway¹¹¹. Current therapeutic strategies targeting Wnt signaling have mostly focused on anticancer therapies¹¹². For example, targeted suppression of β -catenin expression can be achieved with antisense oligonucleotides, RNA interference, and protein knockdown strategies¹¹². Antisense oligonucleotides directed against β -catenin effectively decrease β -catenin expression in tumors, resulting in complete tumor regression, which suggests that these strategies could be of therapeutic value¹¹². In addition to inhibiting Wnt/ β -catenin signaling and consequent cell proliferation, as described above, another potential strategy is to activate Wnt signaling with Wnt ligands, as has been suggested for the treatment of osteoporosis and which results in the stimulation of osteoblast differentiation and bone formation¹¹¹. Similar strategies could be used to promote IVD regeneration, and findings described in **Chapter 5.4** indicate that Wnt7b and Wnt10b may be interesting agents in this respect.

In addition to canonical Wnt signaling, caveolin-1 was abundantly expressed in NCs, and levels decreased significantly during IVD degeneration. As caveolin-1 expression was higher in non-chondrodystrophic dogs than in chondrodystrophic dogs, the protein would appear to be crucial for IVD health, and could be an exciting target for IVD regenerative strategies. Apart from their involvement in IVD degeneration, caveolin proteins are involved in the pathogenesis of cancers, pulmonary hypertension, cardiomyopathy, diabetes, and muscular dystrophy¹¹³. There has been increasing interest in the use of caveolin-mimetic peptides for the treatment of both cancer and pulmonary hypertension¹¹³, and these peptides might also prove useful in IVD regeneration.

Although intriguing information can be obtained by investigating fundamental biomolecular process, scientific hypotheses and knowledge need to be applied in clinical practice. While functional and mechanistic studies can provide insight into the effects of targeting biomolecular signaling on ECM health, it is important to ensure that the experimental set-up mimics *in vivo* conditions as well as possible. For example, three-dimensional cultures of NCs should be used instead of monolayer cultures,^{108,114} or NP explant systems, which maintain *in vitro* NP tissue explants under simulated physiological conditions (osmolarity, hypoxia, glucose, cyclic hydraulic pressure), could be used^{115,116}. Biomolecular pathways could be investigated in *ex vivo* loaded disc culture systems, in which complete IVDs (endplate-IVD-endplate) can be tested under physiological circumstances and under controlled loading conditions¹¹⁷.

Once research findings have been evaluated, they could be used to develop new treatment modalities for IVD disease, such as the NPP and regeneration of the degenerated IVD by targeting one of the biomolecular pathways mentioned above. The use of veterinary patients in research not only helps

improve veterinary care, but also provides information potentially relevant to human medicine. It also reduces the use of laboratory dogs. In addition, it is highly probable that the spontaneous IVD degeneration seen in canine patients resembles the disease process occurring in humans better than does IVD degeneration induced in laboratory animals, so that results would be more reliable and could be extrapolated better to the human situation ¹¹⁸.

In conclusion, current surgical treatments for IVD disease in dogs are suboptimal, and the new strategies described here to stabilize or restore the functionality of the canine spinal segment could constitute promising improvements to the surgical treatment of these patients in the near future. Tissue regeneration is the ideal road toward optimal restoration of the degenerated disc, and this is where the biggest challenge lies. The data discussed above show that we have merely scratched the surface regarding the fundamental biomolecular processes involved in canine IVD degeneration. Although the gap between fundamental research and clinical application is considerable, the data from the studies described in this thesis are a promising start to the development of regenerative treatment modalities for dogs affected by IVD disease.

Key points

- Surgical treatments for canine intervertebral disc disease that involve partial removal of the intervertebral disc (partial discectomy/nuclectomy) result in a significant loss of disc height and spinal stability. Additional stabilization and restoration of intervertebral disc functionality are required for optimal treatment of dogs with intervertebral disc degenerative diseases.
- Pedicle screw-rod fixation of the lumbosacral junction can successfully stabilize spinal segments affected by intervertebral disc degeneration in middle-sized and large-breed dogs. Although this procedure does not result in interbody fusion of the spinal segment, the surgical outcome is successful and appears to restore the propulsive function of the hind limbs in patients affected by degenerative lumbosacral stenosis. Ways to improve the surgical technique to achieve spinal fusion have been identified.
- Functional repair of the nuclectomized intervertebral disc can be achieved by inserting a nucleus pulposus prosthesis into the nuclear cavity created after nuclectomy. The success of prosthesis insertion can be evaluated by radiography, computed tomography, and magnetic resonance imaging. When intact, *in situ*, and with adequate closure of the annulus fibrosus, the prosthesis significantly restores disc height and spinal stiffness to the nuclectomized spinal segment, and therefore may serve as a valuable future treatment for dogs with intervertebral disc disease.
- Intervertebral disc degeneration alters the biomechanics of the spine. The spinal biomechanics of chondrodystrophic dogs (with nucleus pulposus rich in chondrocyte-like cells) and non-chondrodystrophic dogs (with nucleus pulposus rich in notochordal cells) are markedly different, probably as a result of differences in the cell population and the extracellular matrix of the nucleus pulposus, and other biomechanical factors.
- The notochordal cell, the main cell type of the healthy canine nucleus pulposus, exhibits basal canonical Wnt signaling, which supports its potential role as a progenitor cell of the nucleus pulposus.
- Early intervertebral disc degeneration, which involves the replacement/differentiation of notochordal cells by/into chondrocyte-like cells, is associated with down-regulation of canonical Wnt signaling and with a decreased expression of caveolin-1, a protein that appears to be fundamental to the preservation of notochordal cells.
- Early intervertebral disc degeneration is accompanied by significant changes in the expression of genes involved in numerous biomolecular signaling pathways, including extracellular matrix remodeling and bone morphogenetic protein signaling. The findings might facilitate the design of strategies for intervertebral disc regeneration and help clarify several points debated in the current scientific literature.

References

1. Brisson BA: Intervertebral disc disease in dogs. *Vet Clin N Am-Small* 40:829-858, 2010.
2. da Costa RC: Cervical spondylomyelopathy (wobbler syndrome) in dogs. *Vet Clin N Am-Small* 40:881-913, 2010.
3. Meij BP, Bergknot N: Degenerative lumbosacral stenosis in dogs. *Vet Clin N Am-Small* 40:983-1009, 2010.
4. Hansen HJ: A pathologic-anatomical study on disc degeneration in dog, with special reference to the so-called enchondrosis intervertebralis. *Acta Orthop Scand Suppl* 11:1-117, 1952.
5. Bergknot N, Auriemma E, Wijsman S, et al: Evaluation of intervertebral disk degeneration in chondrodystrophic and nonchondrodystrophic dogs by use of Pfirrmann grading of images obtained with low-field magnetic resonance imaging. *Am J Vet Res* 72:893-898, 2011.
6. da Costa RC, Parent J, Dobson H, et al: Comparison of magnetic resonance imaging and myelography in 18 Doberman pinscher dogs with cervical spondylomyelopathy. *Vet Radiol Ultrasound* 47:523-531, 2006.
7. Bergknot N, Grinwis G, Pickee E, et al: Reliability of macroscopic grading of canine intervertebral disc degeneration according to Thompson and comparison with low-field magnetic resonance imaging findings *Am J Vet Res* 72:899-904, 2011.
8. Pfirrmann CW, Metzendorf A, Zanetti M, et al: Magnetic resonance classification of lumbar intervertebral disc degeneration. *Spine (Phila Pa 1976)* 26:1873-1878, 2001.
9. Ibrahim MA, Houghton VM, Hyde JS: Effect of disk maturation on diffusion of low-molecular-weight gadolinium complexes: an experimental study in rabbits. *Am J Neuroradiol* 16:1307-1311, 1995.
10. Houghton V: Medical imaging of intervertebral disc degeneration: current status of imaging. *Spine* 29:2751-2756, 2004.
11. Nguyen-minh C, Riley L, 3rd, Ho KC, et al: Effect of degeneration of the intervertebral disk on the process of diffusion. *Am J Neuroradiol* 18:435-442, 1997.
12. Boos N, Dreier D, Hilfiker E, et al: Tissue characterization of symptomatic and asymptomatic disc herniations by quantitative magnetic resonance imaging. *J Orthop Res* 15:141-149, 1997.
13. Boos N, Boesch C: Quantitative magnetic resonance imaging of the lumbar spine. Potential for investigations of water content and biochemical composition. *Spine* 20:2358-2365, 1995.
14. Boos N, Wallin A, Schmucker T, et al: Quantitative MR imaging of lumbar intervertebral disc and vertebral bodies: methodology, reproducibility, and preliminary results. *Magn Reson Imaging* 12:577-587, 1994.
15. Johannessen W, Auerbach JD, Wheaton AJ, et al: Assessment of human disc degeneration and proteoglycan content using T1rho-weighted magnetic resonance imaging. *Spine* 31:1253-1257, 2006.
16. Gillette RL, Angle TC: Recent developments in canine locomotor analysis: A review. *Vet J*, 2008.
17. Suwankong N, Meij BP, Van Klaveren NJ, et al: Assessment of decompressive surgery in dogs with degenerative lumbosacral stenosis using force plate analysis and questionnaires. *Vet Surg* 36:423-431, 2007.

18. van Klaveren NJ, Suwankong N, De Boer S, et al: Force plate analysis before and after dorsal decompression for treatment of degenerative lumbosacral stenosis in dogs. *Vet Surg* 34:450-456, 2005.
19. Bockstahler BB, Gesky R, Mueller M, et al: Correlation of surface electromyography of the vastus lateralis muscle in dogs at a walk with joint kinematics and ground reaction forces. *Vet Surg* 38:754-761, 2009.
20. Gradner G, Bockstahler B, Peham C, et al: Kinematic study of back movement in clinically sound malinois dogs with consideration of the effect of radiographic changes in the lumbosacral junction. *Vet Surg* 36:472-481, 2007.
21. van den Bogert AJ, van Weeren PR, Schamhardt HC: Correction for skin displacement errors in movement analysis of the horse. *J Biomech* 23:97-101, 1990.
22. van Weeren PR, van den Bogert AJ, Barneveld A: Correction models for skin displacement in equine kinematic gait analysis. *J Equine Vet Sc* 12:178-192, 1990.
23. Sharp NJH, Wheeler SJ: Thoracolumbar and Lumbosacral disease, in Sharp NJH, Wheeler SJ (eds): *Small Animal Spinal Disorders. Diagnosis and Surgery* (ed 2). Edinburgh, Elsevier Mosby, 2005, pp 121-209.
24. Macy NB, Les CM, Stover SM, et al: Effect of disk fenestration on sagittal kinematics of the canine C5-C6 intervertebral space. *Vet Surg* 28:171-179, 1999.
25. Bick EM: An essay on the history of spine fusion operations. *Clin Orthop Relat R* 35:9-15, 1964.
26. Deyo RA, Nachemson A, Mirza SK: Spinal-fusion surgery - the case for restraint. *N Engl J Med* 350:722-726, 2004.
27. Lenke LG: Basic Techniques of Posterior Segmental Spine Internal Fixation, in Bridwell KH, DeWald RL (eds): *The Textbook of Spinal Surgery*, Vol 1. Philadelphia, Lippincott-Raven, 1997, pp 121-138.
28. Gurr KR, McAfee PC, Shih CM: Biomechanical analysis of posterior instrumentation systems after decompressive laminectomy. An unstable calf-spine model. *J Bone Joint Surg Am* 70:680-691, 1988.
29. Ferguson RL, Tencer AF, Woodard P, et al: Biomechanical comparisons of spinal fracture models and the stabilizing effects of posterior instrumentations. *Spine (Phila Pa 1976)* 13:453-460, 1988.
30. Watine S, Cabassu JP, Catheland S, et al: Computed tomography study of implantation corridors in canine vertebrae. *J Small Anim Pract* 47:651-657, 2006.
31. Lorenz M, Zindrick M, Schwaegler P, et al: A comparison of single-level fusions with and without hardware. *Spine (Phila Pa 1976)* 16:S455-458, 1991.
32. McAfee PC, Farey ID, Sutterlin CE, et al: 1989 Volvo Award in basic science. Device-related osteoporosis with spinal instrumentation. *Spine (Phila Pa 1976)* 14:919-926, 1989.
33. Zdeblick TA: A prospective, randomized study of lumbar fusion. Preliminary results. *Spine (Phila Pa 1976)* 18:983-991, 1993.
34. Thomas I, Kirkaldy-Willis WH, Singh S, et al: Experimental spinal fusion in guinea pigs and dogs: the effect of immobilization. *Clin Orthop Relat Res*:363-375, 1975.
35. Benninger MI, Seiler GS, Robinson LE, et al: Three-dimensional motion pattern of the caudal lumbar and lumbosacral portions of the vertebral column of dogs. *Am J Vet Res* 65:544-551, 2004.

36. Hediger KU, Ferguson SJ, Gedet P, et al: Biomechanical analysis of torsion and shear forces in lumbar and lumbosacral spine segments of nonchondrodystrophic dogs. *Vet Surg* 38:874-880, 2009.
37. Weiner BK, Fraser RD: Spine update lumbar interbody cages. *Spine* 23:634-640, 1998.
38. Cinotti G, Patti AM, Vulcano A, et al: Experimental posterolateral spinal fusion with porous ceramics and mesenchymal stem cells. *J Bone Joint Surg BR* 86:135-142, 2004.
39. Gan Y, Dai K, Zhang P, et al: The clinical use of enriched bone marrow stem cells combined with porous beta-tricalcium phosphate in posterior spinal fusion. *Biomaterials* 29:3973-3982, 2008.
40. Miyazaki M, Zuk PA, Zou J, et al: Comparison of human mesenchymal stem cells derived from adipose tissue and bone marrow for ex vivo gene therapy in rat spinal fusion model. *Spine* 33:863-869, 2008.
41. Hoogendoorn RJ, Lu ZF, Kroeze RJ, et al: Adipose stem cells for intervertebral disc regeneration: current status and concepts for the future. *J Cell Mol Med* 12:2205-2216, 2008.
42. Minamide A, Yoshida M, Kawakami M, et al: The effects of bone morphogenetic protein and basic fibroblast growth factor on cultured mesenchymal stem cells for spine fusion. *Spine* 32:1067-1071, 2007.
43. Nakajima T, Iizuka H, Tsutsumi S, et al: Evaluation of posterolateral spinal fusion using mesenchymal stem cells: differences with or without osteogenic differentiation. *Spine* 32:2432-2436, 2007.
44. Meij BP, Suwankong N, Van der Veen AJ, et al: Biomechanical flexion-extension forces in normal canine lumbosacral cadaver specimens before and after dorsal laminectomy-discectomy and pedicle screw-rod fixation. *Vet Surg* 36:742-751, 2007.
45. Walker TM, Pierce WA, Welch RD: External fixation of the lumbar spine in a canine model. *Vet Surg* 31:181-188, 2002.
46. Eck JC, Humphreys SC, Hodges SD: Adjacent-segment degeneration after lumbar fusion: a review of clinical, biomechanical, and radiologic studies. *Am J Orthop* 28:336-340, 1999.
47. Lee CK: Accelerated degeneration of the segment adjacent to a lumbar fusion. *Spine* 13:375-377, 1988.
48. MacDougall J, Perra J, Pinto M: Incidence of adjacent segment degeneration at ten years after lumbar spine fusion. *Spine J* 3:675, 2003.
49. Park P, Garton HJ, Gala VC, et al: Adjacent segment disease after lumbar or lumbosacral fusion: review of the literature. *Spine* 29:1938-1944, 2004.
50. Di Martino A, Vaccaro AR, Lee JY, et al: Nucleus pulposus replacement: basic science and indications for clinical use. *Spine* 30:S16-22, 2005.
51. Bao QB, McCullen GM, Higham PA, et al: The artificial disc: theory, design and materials. *Biomaterials* 17:1157-1167, 1996.
52. Coric D, Mummaneni PV: Nucleus replacement technologies. *J Neurosurg Spine* 8:115-120, 2008.
53. Kranenburg HC, Onis D, van der Veen AJ, et al: Design, synthesis, imaging and biomechanics of a softness-gradient hydrogel nucleus pulposus prosthesis in a canine lumbar spine model. *J Biomed Mater Res B*, accepted for publication, 2012.
54. Bron JL, Helder MN, Meisel HJ, et al: Repair, regenerative and supportive therapies of the annulus fibrosus: achievements and challenges. *Eur Spine J* 18:301-313, 2009.

55. Boelen EJH, van Hooy-Corstjens CSJ, Gijbels MJJ, et al: Preliminary evaluation of new intrinsically radiopaque hydrogels for replacing the nucleus pulposus. *J Mater Chem* 16:824-828, 2006.
56. Guyer RD, Ohnmeiss DD: Intervertebral disc prostheses. *Spine* 28:S15-23, 2003.
57. An HS, Masuda K: Relevance of in vitro and in vivo models for intervertebral disc degeneration. *J Bone Joint Surg Am* 88 Suppl 2:88-94, 2006.
58. Masuda K: Biological repair of the degenerated intervertebral disc by the injection of growth factors. *Eur Spine J* 17 Suppl 4:441-451, 2008.
59. Sakai D: Future perspectives of cell-based therapy for intervertebral disc disease. *Eur Spine J* 17 Suppl 4:452-458, 2008.
60. Tow BP, Hsu WK, Wang JC: Disc regeneration: a glimpse of the future. *Clin Neur* 54:122-128, 2007.
61. Lewis G: Nucleus pulposus replacement and regeneration/repair technologies: Present status and future prospects. *J Biomed Mater Res B*, epub ahead of print, 2012.
62. Guyer RD, Ohnmeiss DD: Lumbar discography. *Spine J* 3:11S-27S, 2003.
63. Chang YS, Guyer RD, Ohnmeiss DD, et al: Case report: intraoperative left common iliac occlusion in a scheduled 360-degree spinal fusion. *Spine* 28:E316-319, 2003.
64. Ganey T, Hutton WC, Moseley T, et al: Intervertebral disc repair using adipose tissue-derived stem and regenerative cells: experiments in a canine model. *Spine* 34:2297-2304, 2009.
65. Ganey T, Libera J, Moos V, et al: Disc chondrocyte transplantation in a canine model: a treatment for degenerated or damaged intervertebral disc. *Spine* 28:2609-2620, 2003.
66. Meisel HJ, Ganey T, Hutton WC, et al: Clinical experience in cell-based therapeutics: intervention and outcome. *Eur Spine J* 15 Suppl 3:S397-405, 2006.
67. Meisel HJ, Siodla V, Ganey T, et al: Clinical experience in cell-based therapeutics: disc chondrocyte transplantation A treatment for degenerated or damaged intervertebral disc. *Biomol Eng* 24:5-21, 2007.
68. Longo UG, Papapietro N, Petrillo S, et al: Mesenchymal stem cell for prevention and management of intervertebral disc degeneration. *Stem cells International* 2012:921053, 2012.
69. Kim KW, Kim YS, Ha KY, et al: An autocrine or paracrine Fas-mediated counterattack: a potential mechanism for apoptosis of notochordal cells in intact rat nucleus pulposus. *Spine* 30:1247-1251, 2005.
70. Kim KW, Lim TH, Kim JG, et al: The origin of chondrocytes in the nucleus pulposus and histologic findings associated with the transition of a notochordal nucleus pulposus to a fibrocartilaginous nucleus pulposus in intact rabbit intervertebral discs. *Spine (Phila Pa 1976)* 28:982-990, 2003.
71. Risbud MV, Schaer TP, Shapiro IM: Toward an understanding of the role of notochordal cells in the adult intervertebral disc: from discord to accord. *Dev Dynam* 239:2141-2148, 2010.
72. Erwin WM: The enigma that is the nucleus pulposus cell: the search goes on. *Arthritis Res Ther* 12:118, 2010.
73. Minogue BM, Richardson SM, Zeef LA, et al: Transcriptional profiling of bovine intervertebral disc cells: implications for identification of normal and degenerate human intervertebral disc cell phenotypes. *Arthritis Res Ther* 12:R22, 2010.

74. Kim JH, Deasy BM, Seo HY, et al: Differentiation of intervertebral notochordal cells through live automated cell imaging system in vitro. *Spine (Phila Pa 1976)* 34:2486-2493, 2009.
75. Shapiro IM, Risbud MV: Transcriptional profiling of the nucleus pulposus: say yes to notochord. *Arthritis Res Ther* 12:117, 2010.
76. Choi KS, Cohn MJ, Harfe BD: Identification of nucleus pulposus precursor cells and notochordal remnants in the mouse: implications for disk degeneration and chordoma formation. *Dev Dynam* 237:3953-3958, 2008.
77. McCann MR, Tamplin OJ, Rossant J, et al: Tracing notochord-derived cells using a Noto-cre mouse: implications for intervertebral disc development. *Dis Model Mech* 5: 73-82, 2012.
78. Ghosh P, Bushell GR, Taylor TF, et al: Collagens, elastin and noncollagenous protein of the intervertebral disk. *Clin Orthop Relat Res*:124-132, 1977.
79. Ghosh P, Taylor TK, Braund KG: The variation of the glycosaminoglycans of the canine intervertebral disc with ageing. I. Chondrodystrophoid breed. *Gerontology* 23:87-98, 1977.
80. Ghosh P, Taylor TK, Braund KG: Variation of the glycosaminoglycans of the intervertebral disc with ageing. II. Non-chondrodystrophoid breed. *Gerontology* 23:99-109, 1977.
81. Salisbury JR, Watt FM: Lack of keratan sulphate in the human notochord. *J Anat* 157:175-179, 1988.
82. Roughley PJ: Biology of intervertebral disc aging and degeneration: involvement of the extracellular matrix. *Spine* 29:2691-2699, 2004.
83. Ghosh P, Taylor TK, Braund KG, et al: The collagenous and non-collagenous protein of the canine intervertebral disc and their variation with age, spinal level and breed. *Gerontology* 22:124-134, 1976.
84. Cappello R, Bird JL, Pfeiffer D, et al: Notochordal cell produce and assemble extracellular matrix in a distinct manner, which may be responsible for the maintenance of healthy nucleus pulposus. *Spine* 31:873-882, 2006.
85. Aguiar DJ, Johnson SL, Oegema TR: Notochordal cells interact with nucleus pulposus cells: regulation of proteoglycan synthesis. *Exp Cell Res* 246:129-137, 1999.
86. Erwin WM, Ashman K, O'Donnell P, et al: Nucleus pulposus notochord cells secrete connective tissue growth factor and up-regulate proteoglycan expression by intervertebral disc chondrocytes. *Arthritis Rheum* 54:3859-3867, 2006.
87. Erwin WM, Inman RD: Notochord cells regulate intervertebral disc chondrocyte proteoglycan production and cell proliferation. *Spine* 31:1094-1099, 2006.
88. Erwin WM, Islam D, Inman RD, et al: Notochordal cells protect nucleus pulposus cells from degradation and apoptosis: implications for the mechanisms of intervertebral disc degeneration. *Arth Res Ther* 13:R215, 2011.
89. Ahmed AM, Duncan NA, Burke DL: The effect of facet geometry on the axial torque-rotation response of lumbar motion segments. *Spine* 15:391-401, 1990.
90. Hofstetter M, Gedet P, Doherr M, et al: Biomechanical analysis of the three-dimensional motion pattern of the canine cervical spine segment C4-C5. *Vet Surg* 38:49-58, 2009.
91. Breit S, Kunzel W: Shape and orientation of articular facets of cervical vertebrae (C3-C7) in dogs denoting axial rotational ability: an osteological study. *European J Morphol* 40:43-51, 2002.

92. Johnson JA, da Costa RC, Allen MJ: Kinematics of the cranial and caudal cervical spine in large breed dogs. American College of Veterinary Internal Medicine Forum Proceedings, Lakewood (CO), 2010.
93. Farfan HF, Cossette JW, Robertson GH, et al: The effects of torsion on the lumbar intervertebral joints: the role of torsion in the production of disc degeneration. *J Bone Joint Surg Am* 52:468-497, 1970.
94. Seiler GS, Hani H, Busato AR, et al: Facet joint geometry and intervertebral disk degeneration in the L5-S1 region of the vertebral column in German Shepherd dogs. *Am J Vet Res* 63:86-90, 2002.
95. Rossi F, Seiler G, Busato A, et al: Magnetic resonance imaging of articular process joint geometry and intervertebral disk degeneration in the caudal lumbar spine (L5-S1) of dogs with clinical signs of cauda equina compression. *Vet Radiol Ultrasound* 45:381-387, 2004.
96. Boxberger JI, Sen S, Yerramalli CS, et al: Nucleus pulposus glycosaminoglycan content is correlated with axial mechanics in rat lumbar motion segments. *J Orthop Res* 24:1906-1915, 2006.
97. Nusse R: Wnt signaling and stem cell control. *Cell research* 18:523-527, 2008.
98. Pelkmans L, Helenius A: Endocytosis via caveolae. *Traffic* 3:311-320, 2002.
99. Schnitzer JE, Liu J, Oh P: Endothelial caveolae have the molecular transport machinery for vesicle budding, docking, and fusion including VAMP, NSF, SNAP, annexins, and GTPases. *J Biol Chem* 270:14399-14404, 1995.
100. Galbiati F, Volonte D, Brown AM, et al: Caveolin-1 expression inhibits Wnt/beta-catenin/Lef-1 signaling by recruiting beta-catenin to caveolae membrane domains. *J Biol Chem* 275:23368-23377, 2000.
101. Yamamoto H, Komekado H, Kikuchi A: Caveolin is necessary for Wnt-3a-dependent internalization of LRP6 and accumulation of beta-catenin. *Dev Cell* 11:213-223, 2006.
102. Chun J, Hyun S, Kwon T, et al: The subcellular localization control of integrin linked kinase 1 through its protein-protein interaction with caveolin-1. *Cell Signal* 17:751-760, 2005.
103. Kim KS, Yoon ST, Li J, et al: Disc degeneration in the rabbit: a biochemical and radiological comparison between four disc injury models. *Spine* 30:33-37, 2005.
104. Korecki CL, Taboas JM, Tuan RS, et al: Notochordal cell conditioned medium stimulates mesenchymal stem cell differentiation toward a young nucleus pulposus phenotype. *Stem Cell Research & Therapy* 1:18, 2010.
105. Le Maitre CL, Baird P, Freemont AJ, et al: An in vitro study investigating the survival and phenotype of mesenchymal stem cells following injection into nucleus pulposus tissue. *Arthritis Res Ther* 11:R20, 2009.
106. Strassburg S, Richardson SM, Freemont AJ, et al: Co-culture induces mesenchymal stem cell differentiation and modulation of the degenerate human nucleus pulposus cell phenotype. *Regen Med* 5:701-711, 2010.
107. Svanvik T, Henriksson HB, Karlsson C, et al: Human disk cells from degenerated disks and mesenchymal stem cells in co-culture result in increased matrix production. *Cells Tissues Organs* 191:2-11, 2010.
108. Erwin WM, Las Heras F, Islam D, et al: The regenerative capacity of the notochordal cell: tissue constructs generated in vitro under hypoxic conditions. *J Neurosurg Spine* 10:513-521, 2009.

109. Risbud MV, Schipani E, Shapiro IM: Hypoxic regulation of nucleus pulposus cell survival: from niche to notch. *Am J Pathol* 176:1577-1583, 2010.
110. Corr M: Wnt-beta-catenin signaling in the pathogenesis of osteoarthritis. *Nat Clin Pract Rheum* 4:550-556, 2008.
111. Luo J, Chen J, Deng ZL, et al: Wnt signaling and human diseases: what are the therapeutic implications? *Lab Invest* 87:97-103, 2007.
112. Luu HH, Zhang R, Haydon RC, et al: Wnt/beta-catenin signaling pathway as a novel cancer drug target. *Curr Cancer Durg Targ* 4:653-671, 2004.
113. Mercier I, Jasmin JF, Pavlides S, et al: Clinical and translational implications of the caveolin gene family: lessons from mouse models and human genetic disorders. *Lab Invest* 89:614-623, 2009.
114. Rastogi A, Thakore P, Leung A, et al: Environmental regulation of notochordal gene expression in nucleus pulposus cells. *J Cell Physiol* 220:698-705, 2009.
115. Hendriks JAA: Co-culture or co-implantation of primary chondrocytes with expanded chondrocytes or bone marrow mesenchymal stem cells enhances cartilage tissue formation; a powerful tool in cartilage cell therapy. In: *The influence of cellular interactions in tissue engineering for cartilage repair*. PhD Thesis; Twente Univeristy. 2006.
116. van Dijk BGM: The effect of osmolarity on cultured nucleus pulposus explants, *Proc World Forum for Spine Research*, 2010.
117. Paul CP, Zuiderbaan HA, Zandieh Doulabi B, et al: Simulated-physiological loading conditions preserve biological and mechanical properties of caprine lumbar intervertebral discs in ex vivo culture. *PloS One* 7:e33147, 2012.
118. Bergknut N, Rutges JP, Kranenburg HJ, et al: The dog as an animal model for intervertebral disc degeneration? *Spine* 37, 351-358, 2012.

SUMMARY

The intervertebral disc (IVD) is an essential component of the spine, as it simultaneously provides the spinal column with stability and mobility, characteristics that are vital for movement and spinal function. IVD degeneration is a common problem in dogs and involves cellular and physical/metabolic changes within the IVD and concurrent degeneration of the IVD matrix. IVD degeneration can result in bulging or herniation of the IVD with subsequent compression of the neural structures overlying the IVD, resulting in neurological deficits. Common IVD degenerative diseases in dogs are cervical and thoracolumbar IVD herniation, cervical spondylomyelopathy, and degenerative lumbosacral stenosis.

The canine species can be divided into two types of breed based on the predisposition to chondrodystrophy, i.e. chondrodystrophic breeds which have short long bones relative to the length of the spine, and non-chondrodystrophic breeds, with normal length of the long bones. This trait is, to a high extent, linked to IVD degeneration, making the types of breed characteristically different regarding various aspects of IVD degeneration and IVD degenerative diseases. All chondrodystrophic breeds suffer from IVD degeneration and associated IVD disease relatively early in life. In contrast, in non-chondrodystrophic breeds, IVD degeneration and disease typically occur at an older age. The fundamental difference between the IVDs of these two breed types is linked to the preservation of notochordal cells in the nucleus pulposus of the IVD. Notochordal cells are thought to be essential to the health of the IVD, and therefore can be regarded as an interesting focus of research into regeneration of the degenerated IVD.

Current treatment of IVD disease is conservative or surgical. Conservative therapy consists of anti-inflammatory drugs, exercise restriction, and physical therapy. Surgical therapy consists of decompression of neural tissue, often combined with removal of degenerated disc tissue. However, therapies involving removal of the nucleus pulposus are far from optimal, as these techniques do not restore health or functionality to the IVD and may lead to spinal instability and recurrence of clinical signs. Therefore, it was decided to perform studies on new treatment strategies for dogs with IVD degenerative disease, as well as for humans with IVD degenerative disease using the dog as a research model for translational research purposes.

The first aim of the studies described in this thesis was to develop and test novel surgical techniques involving fixation of the degenerated spinal segment, using pedicle screw-rod fixation.

The second aim was to investigate functional restoration of the degenerated IVD by insertion of a nucleus pulposus prosthesis.

The third aim was to investigate the processes and effects of early IVD degeneration from a biomechanical and biomolecular perspective, in order to identify key components of the degenerative process. This information could help identify novel targets for treatment strategies aimed at regenerating the degenerated IVD at an early stage.

The studies of this thesis investigated four hypotheses:

- 1) *Pedicle screw-rod fixation of the canine lumbosacral junction enables spinal fusion of L7-S1.*
- 2) *Removal of the nucleus pulposus from the intervertebral disc (nuclectomy) results in a loss of disc height and loss of spinal stability.*
- 3) *Spinal stability can be restored by inserting a nucleus pulposus prosthesis (NPP) into the excavated intervertebral disc.*
- 4) *Significant loss of the notochordal cells from the nucleus pulposus results in significant alterations in biomolecular signaling pathways involved in intervertebral disc matrix health and degeneration.*

The specific aims and conclusions of the studies presented in the chapters of this thesis are described below.

Chapter 2.1 reviewed the current literature on canine IVD degeneration and IVD disease, in order to establish what is known about the degenerative process in dogs and currently used diagnostic methods and treatments.

The study described in **Chapter 2.2** investigated the applicability of kinematic gait analysis in dogs, with special attention being paid to the soft tissue artifact. It was found that markers attached to the skin move considerably relative to the underlying skeletal structures, which introduces artifacts to the measurement of canine gait.

The aim of the study described in **Chapter 3.1** was to evaluate whether surgical pedicle screw-rod fixation of the canine lumbosacral junction could be used as a new surgical option for the treatment of canine IVD disease. Pedicle screw-rod fixation of the lumbosacral junction of middle-sized and large-breed dogs is technically possible and appears to result in improved hind limb function compared with that achieved with decompressive surgery alone. Pedicle screw-rod fixation may become a valuable addition to decompressive surgery in patients with degenerative lumbosacral stenosis, but the surgical

technique should be improved to induce spinal interbody fusion and should be assessed in more patients.

The study described in **Chapter 3.2** evaluated the feasibility of implanting a nucleus pulposus prosthesis, using canine lumbosacral segments *ex vivo*. A clinically adapted method for implanting the prosthesis in the nuclear cavity of the L7-S1 IVD was evaluated. Both on imaging (radiography, computed tomography, and magnetic resonance imaging) and macroscopically, the prosthesis appeared to have a near perfect fit and restored disc height in most spinal segments after inserting the prosthesis after nucleotomy.

The study reported in **Chapter 3.3** further investigated the nucleus pulposus prosthesis *in situ* during biomechanical loading, to assess the potential of the prosthesis to restore the biomechanical function of the L2-L3 and L7-S1 IVD. To this end, canine cadaveric spinal segments were used. After spinal decompression (dorsal laminectomy and nucleotomy), implantation of the nucleus pulposus prosthesis resulted in significant restoration of spinal stability; however, biomechanical testing resulted in fragmentation/herniation of the prosthesis in half of the cases. While the nucleus pulposus prosthesis has the ability to restore disc height and to improve the functionality of the canine IVD, the high rate of prosthesis failure requires further modification, to maintain integrity of the NPP and to ensure that the prosthesis remains confined to the nuclear cavity.

The aim of the study reported in **Chapter 4** was to investigate the biomechanical properties of the non-chondrodystrophic (healthy, notochordal cell-rich IVDs) and chondrodystrophic (degenerated, IVDs devoid of notochordal cells) spine, before and after decompressive surgery, to assess the effects of IVD degeneration and breed type on spinal biomechanics. In both non-chondrodystrophic and chondrodystrophic dogs, the biomechanics of the native spine differed by spinal level, and decompressive surgery resulted in a significant decrease in spinal stiffness. Spinal biomechanics and the effects of spinal surgery differed significantly between non-chondrodystrophic and chondrodystrophic dogs as a result of existing IVD degeneration in chondrodystrophic dogs.

The studies reported in **Chapter 5** investigated the biomolecular processes that occur during early IVD degeneration. The aim of the study described in **Chapter 5.1** was to determine which reference genes are optimal for performing quantitative gene expression analysis with canine IVD tissue. It was found that, for quantitative PCR analysis of healthy and mildly degenerated nucleus pulposus tissue, the use of 2 to 3 reference genes was sufficient for accurate normalization in dogs. However, the expression stability of commonly used reference genes can differ by type of breed and animal age, which means that the ideal set of reference genes needs to be determined in each individual experiment.

The study described in **Chapter 5.2** investigated the role of Wnt/ β -catenin signaling in notochordal cells *in vivo* and *in vitro*, and in early IVD degeneration.

Both notochordal cells and chondrocyte-like cells (early degenerated nucleus pulposus) showed nuclear and cytoplasmic expression of the Wnt effector protein β -catenin, and showed gene expression of the Wnt target gene *axin2*. β -catenin signal intensity and Wnt target gene expression were higher in the nucleus pulposus rich in chondrocyte-like cells derived from chondrodystrophic dogs than in the nucleus pulposus rich in notochordal cells derived from non-chondrodystrophic dogs.

With the aim of identifying additional pathways and genes involved in early IVD degeneration, the study described in **Chapter 5.3** investigated gene expression profiles associated with early IVD degeneration in non-chondrodystrophic and chondrodystrophic dog breeds.

The biomolecular pathways involved in extracellular matrix synthesis, cell-matrix interactions, and cytoskeletal remodeling were found to be altered in early IVD degeneration. One of these pathways was Wnt/ β -catenin signaling. The study reported in **Chapter 5.4** explored the differences between non-chondrodystrophic and chondrodystrophic dogs with regard to Wnt/ β -catenin signaling in notochordal cells and in early IVD degeneration. Functional studies investigated the relevance of caveolin-1 to the preservation of a healthy IVD. On the basis of the studies reported in **Chapter 5**, it can be concluded that notochordal cells express abundant Wnt/ β -catenin signaling activity, both *in vivo* and *in vitro*, supporting the potential role of this cell as a progenitor cell of the nucleus pulposus. Also, notochordal cells abundantly express caveolin-1, a protein involved in intracellular vesicle trafficking. Early IVD degeneration involves down-regulation of canonical Wnt signaling and caveolin-1 expression, which appear to be essential to the physiology and preservation of notochordal cells. In the course of early IVD degeneration, there are distinct differences in Wnt/ β -catenin signaling between chondrodystrophic and non-chondrodystrophic dogs.

The results of all studies were summarized and discussed in **Chapter 6**, and the thesis was concluded with summaries in English (**Chapter 7**) and Dutch (**Chapter 8**).

Key findings

- Surgical treatments for canine intervertebral disc disease that involve partial removal of the intervertebral disc (partial discectomy/nuclectomy) result in a significant loss of disc height and spinal stability. Additional stabilization and restoration of intervertebral disc functionality are required for optimal treatment of dogs with intervertebral disc degenerative diseases.
- Pedicle screw-rod fixation of the lumbosacral junction can successfully stabilize spinal segments affected by intervertebral disc degeneration in middle-sized and large-breed dogs. Although this procedure does not result in interbody fusion of the spinal segment, the surgical outcome is successful and appears to restore the propulsive function of the hind limbs in patients affected by degenerative lumbosacral stenosis. Ways to improve the surgical technique to achieve spinal fusion have been identified.
- Functional repair of the nuclectomized intervertebral disc can be achieved by inserting a nucleus pulposus prosthesis into the nuclear cavity created after nuclectomy. The success of prosthesis insertion can be evaluated by radiography, computed tomography, and magnetic resonance imaging. When intact, *in situ*, and with adequate closure of the annulus fibrosus, the prosthesis significantly restores disc height and spinal stiffness to the nuclectomized spinal segment, and therefore may serve as a valuable future treatment for dogs with intervertebral disc disease.
- Intervertebral disc degeneration alters the biomechanics of the spine. The spinal biomechanics of chondrodystrophic dogs (with nucleus pulposus rich in chondrocyte-like cells) and non-chondrodystrophic dogs (with nucleus pulposus rich in notochordal cells) are markedly different, probably as a result of differences in the cell population and the extracellular matrix of the nucleus pulposus, and other biomechanical factors.
- The notochordal cell, the main cell type of the healthy canine nucleus pulposus, exhibits basal canonical Wnt signaling, which supports its potential role as a progenitor cell of the nucleus pulposus.
- Early intervertebral disc degeneration, which involves the replacement/differentiation of notochordal cells by/into chondrocyte-like cells, is associated with down-regulation of canonical Wnt signaling and with a decreased expression of caveolin-1, a protein that appears to be fundamental to the preservation of notochordal cells.
- Early intervertebral disc degeneration is accompanied by significant changes in the expression of genes involved in numerous biomolecular signaling pathways, including extracellular matrix remodeling and bone morphogenetic protein signaling. The findings might facilitate the design of strategies for intervertebral disc regeneration and help clarify several points debated in the current scientific literature.

Conclusion

Although pedicle screw-rod fixation can be applied to stabilize the canine lumbosacral junction, it does not result in spinal interbody fusion. Therefore, the first hypothesis of this thesis is rejected.

Removal of the nucleus pulposus from the intervertebral disc (nucleotomy) results in a loss of disc height and loss of spinal stability, which can be restored by inserting a nucleus pulposus prosthesis into the excavated intervertebral disc. Therefore, the second and third hypothesis of this thesis are accepted.

Last, the studies reported in this thesis showed that significant loss of the notochordal cells from the nucleus pulposus result in significant alterations in the biomolecular signaling pathways involved in intervertebral disc matrix health and degeneration. Therefore, the fourth hypothesis of this thesis is accepted.

Therefore, new strategies for treating IVD degenerative disease investigated in this thesis are promising improvements to the current surgical treatments of these patients. Theoretically, tissue regeneration would be the optimal treatment strategy for restoration of the degenerated IVD but to date, this remains a challenge. The data reported in this thesis show that we have merely scratched the surface of the fundamental biomolecular processes involved in canine IVD degeneration. Although the gap between fundamental research and clinical application is considerable, the findings of this thesis provide new insights to support the further development of regenerative treatment modalities for humans and dogs affected by IVD degenerative disease.

SAMENVATTING

De wervelkolom van gewervelde dieren, zoals de hond en de mens, is opgebouwd uit wervels die verbonden zijn door een tussenwervelschijf (TWS). De TWS bestaat uit bindweefsel (collageen), cellen en grondstof die veel water bevat.

De TWS is een essentieel onderdeel van de wervelkolom, aangezien het zorg draagt voor zowel stabiliteit als mobiliteit, kenmerken die essentieel zijn voor de beweging en functie van de wervelkolom. TWS degeneratie is een veel voorkomend probleem bij de hond en het betreft mobiele, fysieke, en veranderingen in de stofwisseling van de TWS met gelijktijdige degeneratie van de TWS-matrix. TWS-degeneratie kan leiden tot uitpuiling (hernia) van de TWS met als gevolg druk op zenuwen en ruggenmerg, hetgeen kan resulteren in zenuwpijn en/of -uitval. Veel voorkomende ziekten bij de hond die gevolg zijn van TWS-degeneratie zijn de cervicale (hals) en de thoracolumbale (rug) hernia, cervicale spondylomyelopathie (halswervel instabiliteit) en degeneratieve lumbosacrale stenose (lage rugpijn).

Hondenrassen kunnen worden onderverdeeld in twee typen op basis van predispositie voor chondrodystrofie, namelijk de chondrodystrofe rassen, met relatief korte pijpbeenderen in relatie tot de lengte van de rug, en de niet-chondrodystrofe rassen, die een normale lengte hebben van de pijpbeenderen. Deze raseigenschap is in sterke mate gerelateerd aan degeneratie van de TWS, waardoor deze rastypen karakteristiek verschillend zijn voor wat betreft verschillende aspecten van TWS-degeneratie. Alle chondrodystrofe rassen ontwikkelen op jonge leeftijd al TWS-degeneratie. Bij niet-chondrodystrofe rassen ontwikkelt TWS-degeneratie en ziekte zich meestal op oudere leeftijd. Het fundamentele verschil tussen de TWS van deze twee rasgroepen is het verlies (chondrodystrofe rassen) en het behoud (niet-chondrodystrofe rassen) van notochordale cellen (een soort stamcellen) in het centrum (de nucleus pulposus) van de TWS. Notochordale cellen worden als essentieel beschouwd voor de gezondheid van de TWS en worden daarom gezien als een interessante focus van onderzoek naar regeneratie van de gedegenererde TWS.

De huidige behandeling voor TWS-ziekten is conservatief of chirurgisch. Conservatieve behandeling bestaat uit anti-inflammatoire geneesmiddelen, bewegingsadvies, en fysiotherapie. Chirurgische therapie bestaat uit decompressie van het zenuwweefsel, vaak gecombineerd met het verwijderen van het zieke TWS-weefsel. Echter, therapieën waarbij de nucleus pulposus van de TWS geheel of gedeeltelijk verwijderd wordt, zijn verre van optimaal, omdat deze technieken de functionaliteit van de TWS niet herstellen en kunnen leiden tot instabiliteit en recidief van klinische symptomen.

Het eerste doel van dit proefschrift was het ontwikkelen en testen van een nieuwe chirurgische fixatietechniek waarmee het gedegeneerde spinale segment wordt vastgezet met een pedikelschroef-staaf fixatie.

Het tweede doel was onderzoek naar het functionele herstel van de gedegeneerde TWS door het inbrengen van een nucleus pulposus prothese.

Het derde doel was de processen en effecten van vroege TWS-degeneratie te onderzoeken vanuit een biomechanisch en biomoleculair perspectief met het oog op identificatie van nieuwe doelwitten voor behandelingsstrategieën die gericht zijn op regeneratie van de gedegeneerde TWS in een vroeg stadium.

In dit proefschrift werden vier hypothesen getoetst:

- 1) *Pedikelschroef-staaf fixatie van de lumbosacrale overgang bij de hond resulteert in spinale fusie van L7-S1.*
- 2) *Het verwijderen van de nucleus pulposus van de tussenwervelschijf (nuclectomie) resulteert in verlies van de tussenwervelschijfhoogte en verlies van spinale stabiliteit.*
- 3) *Spinale stabiliteit kan worden hersteld door het inbrengen van een nucleus pulposus prothese (NPP) na nuclectomie.*
- 4) *Significant verlies van notochordale cellen van de nucleus pulposus resulteert in significante veranderingen in biomoleculaire signaalwegen die betrokken zijn bij de gezondheid en degeneratie van de tussenwervelschijfmatrix.*

In **Hoofdstuk 2.1** werd de huidige literatuur over TWS-degeneratie en TWS-ziekten, om vast te stellen wat er momenteel bekend is over het degeneratieve proces en de momenteel gebruikte diagnostische methoden en behandelingen bij de hond.

De studie beschreven in **Hoofdstuk 2.2** onderzocht de toepasbaarheid van kinematische ganganalyse bij honden, met speciale aandacht voor het zogeheten ‘weke delen artefact’. De markers verbonden aan de huid bewogen significant ten opzichte van de onderliggende skeletstructuren, hetgeen significante artefacten introduceerde bij kinematische ganganalyse bij de hond.

Het doel van de studie beschreven in **Hoofdstuk 3.1** was om te evalueren of chirurgische pedikelschroef-staaffixatie van de lumbosacrale overgang bij de hond kan worden gebruikt als een nieuwe chirurgische optie voor de behandeling van TWS-ziekte. Pedikelschroef-staaffixatie van de lumbosacrale overgang bleek technisch mogelijk bij grote hondenrassen en leek een betere voortstuwing van de achterpoten tot gevolg te hebben in vergelijking met chirurgische decompressie zonder fixatie. Pedikelschroef-staaffixatie kan een waardevolle aanvulling gaan vormen op chirurgische decompressie voor

patiënten met degeneratieve lumbosacrale stenose, maar de chirurgische techniek moet worden verfijnd om spinale fusie met botdoorgroei te bewerkstelligen.

De studie beschreven in **Hoofdstuk 3.2** onderzocht de haalbaarheid van het implanteren van een nucleus pulposus prothese in postmortale lumbosacrale segmenten van honden. Een klinisch aangepaste methode voor het implanteren van de prothese in de nucleus pulposus holte van de L7-S1 TWS werd geëvalueerd. Zowel bij beeldvorming (radiografie, computer tomografie en kernspintomografie) als op macroscopisch niveau bleek de prothese een bijna perfecte pasvorm te hebben en bleek de hoogte van de TWS in de meeste spinale segmenten hersteld te zijn nadat de prothese werd ingebracht na nucleotomie.

In de studie beschreven in **Hoofdstuk 3.3** is nader biomechanisch onderzoek gedaan naar de belastbaarheid van de nucleus pulposus prothese in de L2-L3 en L7-S1 TWS. Daartoe zijn postmortale spinale segmenten van honden gebruikt. Na chirurgische decompressie (dorsale laminectomie en nucleotomie) resulteerde implantatie van de nucleus pulposus prothese in een significant herstel van de stabiliteit van de wervelkolom. Echter, de prothese fragmenteerde of hernieerde in de helft van de gevallen. De nucleus pulposus prothese kan potentieel de hoogte en de functionaliteit van de TWS herstellen, maar de kwaliteit dient verder verbeterd te worden om fragmentatie te voorkomen en om ervoor te zorgen dat de prothese gepositioneerd blijft in de nucleus pulposus holte gecreëerd na nucleotomie.

Het doel van de studie beschreven in **Hoofdstuk 4** was om de biomechanische eigenschappen van de wervelkolom van non-chondrodystrofe honden (met gezonde, notochordale cel-rijke TWS'en) en van chondrodystrofe honden (gedegeneerde, TWS'en zonder notochordale cellen) te onderzoeken, vóór en na chirurgische decompressie. In zowel non-chondrodystrofe als chondrodystrofe honden verschilden de spinale biomechanica per spinaal niveau en chirurgische decompressie resulteerde in een significante afname van de spinale stijfheid. De spinale biomechanica en de effecten van spinale chirurgie verschilden significant tussen non-chondrodystrofe en chondrodystrofe honden als gevolg van pre-existente TWS-degeneratie in chondrodystrofe honden.

De studies beschreven in **Hoofdstuk 5** onderzochten de biomoleculaire processen die optreden tijdens vroege TWS-degeneratie. Het doel van de studie beschreven in **Hoofdstuk 5.1** was om te bepalen welke referentie-genen optimaal zijn voor het uitvoeren van kwantitatieve analyse van genexpressie van TWS-weefsel van de hond. Gebleken is dat, voor de kwantitatieve PCR analyse van gezond en matig gedegeneerd nucleus pulposus weefsel, het gebruik van 2 tot 3 referentiegenen voldoende was voor een accurate normalisatie in honden. De expressiestabiliteit van gebruikelijke referentiegenen verschilden per rasstype en leeftijd, hetgeen betekent dat de ideale set referentiegenen bepaald moet worden voor elk verschillend onderzoek.

De studie beschreven in **Hoofdstuk 5.2** onderzocht de rol van de Wnt/ β -catenine signalering in notochordale cellen *in vivo* en *in vitro* en in vroege TWS-degeneratie. Zowel notochordale cellen als chondrocyt-achtige cellen

(aanwezig in de vroeg gedegeneerde nucleus pulposus) lieten nucleaire en cytoplasmatische expressie zien van het Wnt-effector eiwit β -catenine en het Wnt-doelwitgen *axin2*. De signaalintensiteit van β -catenine en de genexpressie van Wnt-doelwitgenen waren hoger in de nucleus pulposus die rijk was aan chondrocyt-achtige cellen (afkomstig van chondrodystrofe honden) dan in de nucleus pulposus die rijk was aan notochordale cellen (afkomstig van non-chondrodystrofe honden).

Met het oog op het identificeren van aanvullende biomoleculaire paden en genen die betrokken zijn bij vroege TWS-degeneratie, onderzocht **Hoofdstuk 5.3** de genexpressieprofielen geassocieerd met vroege TWS-degeneratie in non-chondrodystrofe en chondrodystrofe hondensassen.

De biomoleculaire signaalcascades betrokken bij extracellulaire matrixsynthese, cel-matrix interacties en remodelering van het cytoskelet, bleken te zijn veranderd in vroege TWS-degeneratie. Eén van deze paden was Wnt/ β -catenine signalering. De studie beschreven in **Hoofdstuk 5.4** onderzocht de verschillen tussen niet-chondrodystrofe en chondrodystrofe honden met betrekking tot Wnt/ β -catenine signalering in notochordale cellen en bij vroege TWS-degeneratie. Functionele studies onderzochten de relevantie van caveoline-1, een belangrijk eiwit betrokken in Wnt/ β -catenine signalering, voor het behoud van een gezonde TWS. Op basis van de studies in **Hoofdstuk 5** kan worden geconcludeerd dat notochordale cellen overvloedige Wnt/ β -catenine signalering tot expressie brengen, zowel *in vivo* als *in vitro*, hetgeen de potentiële rol van deze cel als progenitorcel van de nucleus pulposus ondersteunt. Daarnaast brengen notochordale cellen caveoline-1 tot expressie, een eiwit dat betrokken is bij intracellulaire mobilisatie en transport van vesikels. Vroege TWS-degeneratie gaat gepaard met een verminderde activiteit van Wnt signalering en verminderde caveoline-1 expressie. Actieve Wnt signalering en caveoline-1 lijken daarom van essentieel belang te zijn voor de fysiologie en het behoud van notochordale cellen. Er bestaan duidelijke verschillen in Wnt/ β -catenine signalering voor wat betreft vroege TWS-degeneratie tussen chondrodystrofe en niet-chondrodystrofe honden.

De resultaten van alle studies zijn samengevat en bediscussieerd in **Hoofdstuk 6**, en het proefschrift is afgesloten met samenvattingen in Engels (**Hoofdstuk 7**) en Nederlands (**Hoofdstuk 8**).

Belangrijkste bevindingen

- Chirurgische interventies voor tussenwervelschijfziekte bij de hond waarbij de tussenwervelschijf gedeeltelijk verwijderd wordt (gedeeltelijke discectomie/nuclectomie) resulteren in een aanzienlijk verlies van de hoogte van de tussenwervelschijf en de stabiliteit van de wervelkolom. Aanvullende stabilisatie en herstel van de tussenwervelschijffunctionaliteit zijn nodig voor een optimale behandeling van honden met degeneratieve ziekten van de tussenwervelschijf.
- Pedikelschroef-staaffixatie van de lumbosacrale overgang kan succesvolle stabilisatie geven van spinale segmenten met tussenwervelschijfdegeneratie bij middelgrote en grote hondenrassen. Hoewel deze procedure niet leidt tot benige fusie van het spinale segment, lijkt deze de voortstuwende functie van de achterste ledematen te herstellen in patiënten die getroffen zijn door degeneratieve lumbosacrale stenose. Manieren ter verbetering van de chirurgische techniek om benige spinale fusie te bereiken zijn geïdentificeerd.
- Functioneel herstel van de tussenwervelschijf na nuclectomie kan worden bereikt door het inbrengen van een nucleus pulposus prothese in de nucleaire holte gecreëerd door middel van nuclectomie. De plaatsing van de prothese kan worden beoordeeld aan de hand van radiografie, computer tomografie en kernspintomografie. Wanneer de prothese intact en op zijn plaats blijft, herstelt de prothese de discusshoogte en stijfheid van de wervelkolom en is in potentie een waardevolle, toekomstige behandelingsmethode voor honden met tussenwervelschijfziekte.
- Tussenwervelschijfdegeneratie verandert de biomechanica van de wervelkolom. Chondrodystrofe honden (met nucleus pulposus rijk aan chondrocyt-achtige cellen) en non-chondrodystrofe honden (met nucleus pulposus rijk aan notochordale cellen) verschillen ook in biomechanisch opzicht van elkaar, mogelijk als gevolg van verschillen in de celpopulatie, de extracellulaire matrix van de nucleus pulposus en andere biomechanische factoren.
- De notochordale cel, de voornaamste cel van de gezonde nucleus pulposus bij de hond, vertoont basale Wnt-signalering, hetgeen de potentiële rol van deze cel als een nucleus pulposus progenitor cel ondersteunt.
- Vroege tussenwervelschijfdegeneratie, gekarakteriseerd door de vervanging/differentiatie van notochordale cellen naar chondrocyt-achtige cellen, wordt geassocieerd met verlaagde expressie van Wnt signalering en met een verminderde expressie van caveoline-1, een eiwit dat van fundamenteel belang lijkt te zijn voor het behoud van notochordale cellen.
- Vroege tussenwervelschijfdegeneratie gaat gepaard met significante veranderingen in de expressie van genen betrokken bij tal van biomoleculaire signaalwegen, met inbegrip van extracellulaire matrixremodelering en boteiwitsignalering. Bevindingen van deze studie kunnen aanknopingspunten

geven voor toekomstige strategieën voor tussenwervelschijfregeneratie en punten bediscussieerd in de huidige wetenschappelijke literatuur helpen ophelderen.

Conclusie

Alhoewel pedikelschroef-staaffixatie toegepast kan worden om de lumbosacrale overgang bij de hond te stabiliseren, resulteert het niet in benige doorgroei van het lumbosacrale segment. Daarom wordt de eerste hypothese van dit proefschrift verworpen.

Het verwijderen van de nucleus pulposus van de tussenwervelschijf (nuclectomie) resulteert in een verlies van tussenwervelschijfhoogte en verlies van spinale stijfheid, hetgeen hersteld kan worden door het inbrengen van een nucleus pulposus prothese na nuclectomie. Daarom worden de tweede en derde hypothese van dit proefschrift geaccepteerd.

De onderzoeken in dit proefschrift tonen dat een significant verlies van notochordale cellen van de nucleus pulposus resulteert in significante veranderingen in biomoleculaire signaalwegen die betrokken zijn bij de gezondheid en degeneratie van de tussenwervelschijfmatrix. Daarom wordt de vierde hypothese van dit proefschrift geaccepteerd.

Op basis van dit proefschrift kan geconcludeerd worden dat nieuwe behandelstrategieën van tussenwervelschijfziekten bij de hond de wervelkolom kunnen stabiliseren of de functie van de wervelkolom kunnen herstellen. De beschreven technieken zijn veelbelovende verbeteringen van de chirurgische interventies die op dit moment toegepast worden. Regeneratie van de tussenwervelschijf is theoretisch gezien de optimale behandeling voor gedegenererde tussenwervelschijven en de toepassing hiervan is een uitdaging voor de toekomst. De gegevens gerapporteerd in dit proefschrift laten zien dat de fundamentele, biomoleculaire processen betrokken bij tussenwervelschijfdegeneratie nog grotendeels onbekend zijn. Alhoewel de kloof tussen fundamenteel onderzoek en klinische toepassing nog aanzienlijk is, levert het huidige proefschrift nieuwe inzichten voor therapeutische mogelijkheden voor de behandeling van degeneratieve tussenwervelschijfaandoeningen voor de mens en de hond.

Addendum

Dankwoord

Curriculum Vitae

List of peer-reviewed publications

Dankwoord

Deze promotie is tot stand gekomen dankzij de hulp, inzet en interesse van velen. Zij hebben bijgedragen aan mijn ontwikkeling, leerproces en vreugde tijdens deze periode. Middels dit dankwoord zal ik pogen hen specifiek te benoemen.

Professor dr. Herman Hazewinkel, waarde promotor. Aan het begin van mijn Excellent Tracé (ET) heb ik u leren kennen. U hebt tijdens mijn tijd als promovendus constant gefungeerd als een begeleider met een duidelijk overzicht en op wiens behulpzaamheid ik altijd heb kunnen bouwen. Ik heb altijd op zeer prettige wijze met u samengewerkt, waarbij u uw structurele sturing regelmatig afwisselde met humoristische gesprekken. Ik heb uw wijsheid en begeleiding altijd als zeer enthousiasmerend en motiverend ervaren, waarvoor mijn hartelijke dank.

Dr. Björn Meij, waarde co-promotor. Ik leerde je voor het eerst kennen toen ik op zoek was naar een onderwerp voor mijn ET. Ik heb geen enkel moment spijt gehad van mijn keuze voor jou als begeleider. Jouw begeleiding, expertise en kritisch denken als wetenschapper en clinicus zijn van onschatbare waarde voor mij geweest. Je hebt me zowel daadkrachtig weten te sturen als de vrijheid gegeven om te excelleren in allerlei aspecten, afgewisseld met jouw karakteristieke humor. Ik heb een diep respect voor jou als persoon en beschouw je als een ware mentor.

Dr. Niklas Bergknut, waarde co-promotor. We kunnen allebei lachend terugkijken op de eerste indruk die op jou maakte. Snel daarna is deze indruk veranderd en hebben we dankzij jouw kwaliteiten als manager een heuse artikelmachine op de rails weten te zetten. Dankzij jouw begeleiding en bereidheid om anderen te laten floreren heb je mij de mogelijkheid gegeven om mijn promotie te starten. Zonder jouw supervisie en positieve aansporing zou dit nooit gelukt zijn. De geweldige tijd als ‘men behaving badly’ mag zeker niet vergeten worden. De samenwerking met jou was zeer stimulerend. Ik hoop onze interacties en waardevolle gesprekken nog lang te kunnen voortzetten.

Dr. Marianna Tryfonidou, waarde co-promotor. Ik heb zelden iemand gezien met zo'n hart voor de wetenschap. Je enthousiasme, discipline, inventiviteit en oog voor detail zijn ongekend. Je capaciteiten als begeleider hebben mijn promotie en het ‘Canine Spine Investigation’ (CSI) onderzoek naar een aanzienlijk hoger niveau weten te tillen. Dankzij jouw inzet doet het veterinaire CSI onderzoek zeker niet onder voor de humane onderzoekswereld, en een publicatie in Nature lijkt me op de lange termijn onvermijdelijk. Ik ben zeer dankbaar voor je stimulerende samenwerking en coaching.

Dr. Hendrik-jan Kranenburg, waarde paranimf. Ikzelf had de eer om als jouw paranimf te fungeren, en nu is het uiteraard jouw beurt. Naast mede-AIO ben

je uitgegroeid tot een goede vriend. Onze flauwe en belachelijke humor, met name ook met andere personen als doelwit, hebben geleid tot aanzienlijk vermaak. Ik heb met name veel van je geleerd op sociaal en organisatorisch vak, zaken waar jij een ‘natural’ in bent. Ik heb respect voor het feit dat je je sociale hobby’s, promotie/specialisatie en een gezin op succesvolle wijze hebt weten te combineren. Ik twijfel er geen moment aan dat je dat met succes zult blijven doen.

Dr. Guy Grinwis. Als CSI patholoog ben jij onontbeerlijk geweest voor het onderzoek. Je expertise, enthousiasme en benaderbaarheid heb ik altijd gewaardeerd. Ik ben nog regelmatig onder de indruk van je visie als patholoog en persoon.

Frank Riemers. Jouw enthousiasme, vakkundigheid in het lab, en kwaliteiten wat betreft de verwerking van gigantische hoeveelheden data hebben ervoor gezorgd dat labwerk van hoge kwaliteit in dit proefschrift terecht gekomen is.

Dr. Louis Penning. Dr. Papi. Door je gezelligheid en kennis heb je waardevolle input geleverd in het onderzoek. We kunnen lachend terugkijken op de tijd in Zweden. Gesprekken met jou zijn altijd bijzonder en vol input uit onverwachtse hoeken. Ik hoop dat je nog veel successen zult boeken als wetenschapper

Hans Vernooij. Als statisticus heb jij een fundamentele ondersteuning gegeven aan het onderzoek in dit proefschrift. Statistiek wordt door velen beschouwd als een kwelling, maar door jouw begeleiding heb ik dit als zeer prettig ervaren.

Dr. Richard Wubbolts. Jouw kritische blik en wetenschappelijke visie met betrekking tot de imaging van cellen zijn essentieel geweest voor een aantal van de studies in mijn proefschrift. Ik wil je bedanken voor de gezellige, waardevolle samenwerking

Prof. dr. George Voorhout, hartelijk dank voor uw positieve begeleiding en advies wat betreft de beeldvorming van de pedikelschroevenstudie.

Mirjam Duijvestijn. Als tutor heb je mij een aanzet gegeven tot het doen van onderzoek en mijn progressie vol interesse gevolgd, waarvoor ik je zeer dankbaar ben.

Monique Schwencke, we hebben samen ervaren dat onderzoek niet altijd van een leien dakje gaat. Desondanks hebben we toch een mooie publicatie weten neer te zetten.

Harry van Engelen, jij bent een gouden kracht binnen de UKG. Je staat altijd klaar voor anderen, en dat wordt zeer gewaardeerd. Bovendien ben je een

leermeester geweest in het hanteren van de Black & Decker zaag, een kunst die niet vergeten mag worden.

De afdeling Diagnostische Beeldvorming van de UKG. Elise Petersen en Monique Jacobs, Anke Wassink, en Joris Brouwer. Hartelijk dank voor jullie hulp en gezelligheid.

De afdeling Multimedia van de Faculteit Diergeneeskunde: Joop Fama, Anneke Jansen, Anjolieke Dertien. Hartelijk dank voor jullie vakkundigheid wat betreft de fotografie, afbeeldingen en vormgeving van dit proefschrift. 'Pictures say a thousand words', en dat is ook zeker hier van toepassing.

Carolien Kolijn en Marylene Paes, Dames van de sterilisatie. Hartelijk dank voor jullie hulp met tal van instrumentaria.

Arie Doornenbal en Ank van Wees, hartelijk dank voor jullie inzicht en hulp bij de force plate metingen en het kinematica onderzoek.

Prof. dr. Jolle Kirpensteijn, tijdens mijn zoektocht naar een gepast ET onderwerp hebt u mij voorgesteld aan Björn Meij, waarvoor hartelijk dank.

Onderzoekers van het Skeletal Tissue Engineering Group Amsterdam (STEGA) en Research Institute MOVE, Albert van der Veen, Idsart Kingma, Jaap van Dieën, Theo Smit. Als team van de Vrije Universiteit Amsterdam hebben wij een zeer prettige samenwerking gehad. Jullie expertise hebben zaken mogelijk gemaakt die anders nooit gelukt waren.

Collega onderzoekers van het Departement Orthopedie binnen het Universitair Medisch Centrum (UMC) Utrecht. Ruud Licht, dankzij jouw ongeremde enthousiasme voor de wetenschap en persoonlijke interesses hebben wij samen een start gemaakt met het onderzoek naar de notochordale cellen. Zonder jou had het onderzoek niet deze sprong gemaakt. Prof. dr. Wouter Dhert en Dr. Laura Creemers, de samenwerking met jullie heeft dit onderzoek aanzienlijk gestimuleerd en naar nieuwe hoogten gebracht.

Prof. dr. Leo Koole van de Universiteit Maastricht. Het project van de nucleus pulposus prothese heb ik als zeer interessant ervaren. Onze samenwerking met betrekking tot dit onderwerp vond ik zeer prettig.

Fellow researchers from the University of Uppsala, Sweden. Anne-Sofie Lagerstedt, Ragnvi Hagman, Pia Gustås, and Odd Höglund. Thank you for your coöperation and the good times in Sweden.

Ik wil de gehele 2^o verdieping van het JDV gebouw bedanken voor de leuke tijd, met in het bijzonder: De 'Bone Room'. Gaya, Lau and Ineke, on multiple occasions the three of you needed ear plugs when sounds of masculin discussion filled the room. During the 'golden days' you have had the pleasure of experiencing loud CSI humor, and although you may deny this, I'm sure you enjoyed these 'male' additions to the room (as women don't really have humor). Gaya, I enjoyed our discussions regarding various topics and your sunny charisma. Lau, I'm sure you will publish some high quality articles on canine elbow dysplasia, and after that I hope you will actually compete in a

triathlon of some sort. Ineke, ik weet zeker dat jouw harde werk zal resulteren in een prachtig proefschrift.

De ‘Liver Room’ ofwel ‘Room #2’: Frank van Steenbeek, Baukje Schotanus, Bart Spee, Hedwig Kruitwagen, Kim Boerkamp en Hille Fieten. Dankje voor de gezelligheid, samenwerking, en een gezonde vorm van competitie (welke wij vanzelfsprekend gewonnen hebben).

Het werk tijdens de promotie is ook tot stand gekomen middels de inzet van mijn collega veterinaire studenten. David Onis, tijdens jouw ET heb jij aanzienlijk bijgedragen aan de grootste studie van dit proefschrift, en dat waardeer ik zeer. Discussies hierover op de WSB waren ook zeer nuttig. Douwe Heuvel, dankje voor je inzet wat betreft het onderzoek naar de referentiegenen. Renée van de Ven, bedankt voor je enthousiasme en productieve houding in het manuscript over de pedikelschroeven. Floor Bonestroo, ook al heb je niet direct te maken gehad met mijn onderzoek, toch heb je op jouw manier gezorgd voor het nodige vermaak.

Mijn co-maatjes Laura, Hilde, Robert, Vera, Steffie en Kyra. Ik ben blij dat wij een erg gezellige tijd hebben gehad tijdens de coschappen.

Mijn vrienden, altijd geïnteresseerd in de vooruitgang van mijn werk, en wie hebben gezorgd voor de broodnodige afleiding. Waarde Mannen, Tristan, Mark, Joost, Gertjan, Arie, hartelijk dank voor de geweldige, testosteron-gevulde gezelligheid. Denk ook aan de weekenden, welke ervoor gezorgd hebben dat ik mijn verworven kennis binnen drie dagen weer compleet verloren was. De meiden, Roos, Marjon (bedankt voor de mond), Mendy, Stephany, Saffiera, Anna, Sandy, Annelies. Heel erg bedankt voor vele dramatische, komische, en belachelijke gebeurtenissen. Daarnaast wil ik graag alle andere vrienden en vriendinnen bedanken voor hun interesse, enthousiasme en gezellige tijd

Mijn familie. Kees, waarde paranimf, grote broer. Jij hebt tijdens deze promotie alles van mij meegekregen op persoonlijk gebied. Jij kent me als geen ander, en dat is uniek. Je frisse blik en advies hebben me aanzienlijk geholpen op allerlei fronten. Ik hoop dat we elkaar als broers continu zullen blijven helpen hogere niveaus te bereiken.

Pap en Mam, jullie zijn van essentieel belang in mijn leven. Jullie enthousiasme, vertrouwen, motivatie en advies zijn erg belangrijk voor mij geweest en dat zullen ze altijd blijven. Jullie liefde en steun hebben mij gevormd tot de persoon die ik ben. Ik ben jullie hiervoor ongelofelijk dankbaar.

Luc

Utrecht, december 2012

Curriculum Vitae

Lucas Adam Smolders was born on January 28, 1986 in Geldrop, the Netherlands. After graduating cum laude from secondary school (Augustinianum, Eindhoven) in 2004, he started to study Veterinary Medicine at the Faculty of Veterinary Medicine of Utrecht University, the Netherlands. During his studies, from 2008 to 2009 he participated in the Honours Program (Excellent Track) of the Faculty of Veterinary Medicine. At the Department of Clinical Sciences of Companion Animals of Utrecht University, he performed research on the topic of intervertebral disc degeneration in dogs for one year. Thereafter, he continued this research as a PhD candidate, performing full-time research for 15 months. During this research period, he has won several prizes for best oral presentation at international veterinary and human congresses. Thereafter, he continued to complete his veterinary studies while simultaneously finishing his PhD research. From June to August 2012, he participated in the Veterinary Leadership Program for Veterinary Students at Cornell University, NY, the United States. In this program, he performed a short-term research project on 'cerebral microglial response to cortical microhemorrhages' at the Department of Biomedical Engineering. His participation was awarded with the Integrative Biology Prize. At this time, Luc is continuing his veterinary studies and he is expected to graduate in March 2013.

Lucas Adam Smolders werd op 28 januari 1986 geboren in Geldrop, Nederland. Na het behalen van het VWO-diploma aan het Augustinianum te Eindhoven in 2004, startte hij met de studie Diergeneeskunde aan de Faculteit Diergeneeskunde van de Universiteit Utrecht. Tijdens zijn studie nam hij deel aan het Excellent Tracé van de Faculteit Diergeneeskunde, waarbij hij gedurende één jaar onderzoek verrichtte naar tussenwervelschijfdegeneratie bij de hond aan het Departement Geneeskunde van Gezelschapsdieren, Universiteit Utrecht. Hierna werd hij aan dit Departement gedurende 15 maanden aangesteld als promovendus op hetzelfde onderzoeksonderwerp. Tijdens deze onderzoeksperiode heeft hij meerdere prijzen weten te behalen op internationale veterinaire en humane congressen. Hierna heeft hij de studie Diergeneeskunde voortgezet en tegelijkertijd het promotieonderzoek afgerond. In de periode van juni tot en met augustus 2012 heeft hij deelgenomen aan het 'Veterinary Leadership Program for Veterinary Students' aan de Universiteit van Cornell, New York, de Verenigde Staten. Hier verrichtte hij onderzoek naar 'de respons van microglia op corticale microbloedingen' aan het Departement van Biomedische Wetenschappen. Zijn deelname was beloond met de prijs voor 'geïntegreerde biologie'. Op dit moment voltooit Luc zijn studie Diergeneeskunde en wordt verwacht af te studeren in maart 2013.

List of peer-reviewed publications

Smolders LA, Meij BP, Onis D, Riemers FM, Bergknut N, Wubbolts R, Grinwis GCM, Houweling M, Groot Koerkamp MJA, van Leenen D, Holstege FCP, Hazewinkel HAW, Creemers LB, Penning LC, Tryfonidou MA. Gene expression profiling of early intervertebral disc degeneration reveals a down-regulation of canonical Wnt signaling and caveolin-1 expression: implications for development of regenerative strategies. *Arthritis Research & Therapy*, pending acceptance, resubmitted after revision.

Smolders LA, Bergknut N, Grinwis GC, Hagman R, Lagerstedt AS, Hazewinkel HA, Tryfonidou MA, Meij BP. Intervertebral disc degeneration in the dog. Part 2: Chondrodystrophic and non-chondrodystrophic breeds. *The Veterinary Journal*, 2012 Nov 12. Accepted for publication. doi:10.1016/j.tvjl.2012.10.011. Epub ahead of print.

Smolders LA, Bergknut N, Grinwis GC, Hagman R, Lagerstedt AS, Hazewinkel HA, Tryfonidou MA, Meij BP. Intervertebral disc degeneration in the dog. Part 1: Anatomy and physiology of the intervertebral disc and characteristics of intervertebral disc degeneration. *The Veterinary Journal*, 2012 Nov 20. Accepted for publication. doi: 10.1016/j.tvjl.2012.10.024. Epub ahead of print.

Smolders LA, Kingma I, Bergknut N, van der Veen AJ, Dhert WJ, Hazewinkel HA, van Dieën JH, Meij BP. Biomechanical assessment of the non-chondrodystrophic and chondrodystrophic canine multisegmented lumbar spine. *European Spine Journal*. 2012 Sep; 21(9): 1692-9.

Smolders LA, Voorhout G, van de Ven R, Bergknut N, Grinwis GC, Hazewinkel HA, Meij BP. Pedicle screw-rod fixation of the canine lumbosacral junction. *Veterinary Surgery*. 2012 Aug; 41(6):720-32.

Smolders LA, Meij BP, Riemers FM, Licht R, Wubbolts R, Heuvel D, Grinwis GC, Vernooij HC, Hazewinkel HA, Penning LC, Tryfonidou MA. Canonical Wnt signalling in the notochordal cell is upregulated in early intervertebral disc degeneration. *Journal of Orthopedic Research*. 2012, Jun; 30(6): 950-7.

Smolders LA, Bergknut N, Kingma I, van der Veen AJ, Smit TH, Koole LH, Hazewinkel HA, Meij BP. Biomechanical evaluation of a novel nucleus pulposus prosthesis in canine cadaveric spines. *The Veterinary Journal*. 2012 May; 192(2): 199-205.

Schwencke M, **Smolders LA**, Bergknut N, Gustås P, Meij BP, Hazewinkel HAW. Soft tissue artifact in canine kinematic gait analysis. *Veterinary Surgery*. 2012 Oct;41(7):829-37

Bergknut N, **Smolders LA**, Koole LH, Voorhout G, Hagman RE, Lagerstedt AS, Saralidze K, Hazewinkel HA, van der Veen AJ, Meij BP. The performance of a hydrogel nucleus pulposus prosthesis in an ex vivo canine model. *Biomaterials*. 2010 Sep;31(26):6782-8.

Kranenburg HJ, Meij BP, Onis D, van der Veen AJ, Saralidze K, **Smolders LA**, Huizinga JG, Knetsch ML, Luijten PR, Visser F, Voorhout G, Dhert WJ, Hazewinkel HA, Koole LH. Design, synthesis, imaging, and biomechanics of a softness-gradient hydrogel nucleus pulposus prosthesis in a canine lumbar spine model. *Journal of Biomedical Materials Research Part B: Applied Biomaterials*. 2012 Nov;100(8):2148-55.

Bergknut N, Meij BP, Hagman R, de Nies KS, Rutges JP, **Smolders LA**, Creemers LB, Lagerstedt AS, Hazewinkel HA, Grinwis GC. Intervertebral disc disease in dogs - Part 1: A new histological grading scheme for classification of intervertebral disc degeneration in dogs. *The Veterinary Journal*. 2012 Jul 10. Epub ahead of print.

Bergknut N, Rutges JP, Kranenburg HJ, **Smolders LA**, Hagman R, Smidt HJ, Lagerstedt AS, Voorhout G, Hazewinkel HH, Grinwis GC, Creemers LB, Meij BP, Dhert WJ. The dog as an animal model for intervertebral disc degeneration? *Spine (Phila Pa 1976)*. 2012 Mar 1;37(5):351-8.